NASA/TM-2006-214312 (CORRECTED COPY)

Low Reynolds Number Aerodynamic Characteristics of Several Airplane Configurations Designed to Fly in the Mars Atmosphere at Subsonic Speeds

Richard J. Re, Odis C. Pendergraft, Jr., and Richard L. Campbell
Langley Research Center, Hampton, Virginia

August 2006

The NASA STI Program Office . . . in Profile

Since its founding, NASA has been dedicated to the advancement of aeronautics and space science. The NASA Scientific and Technical Information (STI) Program Office plays a key part in helping NASA maintain this important role.

The NASA STI Program Office is operated by Langley Research Center, the lead center for NASA's scientific and technical information. The NASA STI Program Office provides access to the NASA STI Database, the largest collection of aeronautical and space science STI in the world. The Program Office is also NASA's institutional mechanism for disseminating the results of its research and development activities. These results are published by NASA in the NASA STI Report Series, which includes the following report types:

- TECHNICAL PUBLICATION. Reports of completed research or a major significant phase of research that present the results of NASA programs and include extensive data or theoretical analysis. Includes compilations of significant scientific and technical data and information deemed to be of continuing reference value. NASA counterpart of peer-reviewed formal professional papers, but having less stringent limitations on manuscript length and extent of graphic presentations.

- TECHNICAL MEMORANDUM. Scientific and technical findings that are preliminary or of specialized interest, e.g., quick release reports, working papers, and bibliographies that contain minimal annotation. Does not contain extensive analysis.

- CONTRACTOR REPORT. Scientific and technical findings by NASA-sponsored contractors and grantees.

- CONFERENCE PUBLICATION. Collected papers from scientific and technical conferences, symposia, seminars, or other meetings sponsored or co-sponsored by NASA.

- SPECIAL PUBLICATION. Scientific, technical, or historical information from NASA programs, projects, and missions, often concerned with subjects having substantial public interest.

- TECHNICAL TRANSLATION. English-language translations of foreign scientific and technical material pertinent to NASA's mission.

Specialized services that complement the STI Program Office's diverse offerings include creating custom thesauri, building customized databases, organizing and publishing research results ... even providing videos.

For more information about the NASA STI Program Office, see the following:

- Access the NASA STI Program Home Page at ***http://www.sti.nasa.gov***

- E-mail your question via the Internet to help@sti.nasa.gov

- Fax your question to the NASA STI Help Desk at (301) 621-0134

- Phone the NASA STI Help Desk at (301) 621-0390

- Write to:
  NASA STI Help Desk
  NASA Center for AeroSpace Information
  7121 Standard Drive
  Hanover, MD 21076-1320

NASA/TM-2006-214312 (CORRECTED COPY)

Low Reynolds Number Aerodynamic Characteristics of Several Airplane Configurations Designed to Fly in the Mars Atmosphere at Subsonic Speeds

Richard J. Re, Odis C. Pendergraft, Jr., and Richard L. Campbell
Langley Research Center, Hampton, Virginia

National Aeronautics and
Space Administration

Langley Research Center
Hampton, Virginia 23681-2199

August 2006

Available from:

NASA Center for AeroSpace Information (CASI)
7121 Standard Drive
Hanover, MD 21076-1320
(301) 621-0390

National Technical Information Service (NTIS)
5285 Port Royal Road
Springfield, VA 22161-2171
(703) 605-6000

ERRATA

NASA/TM-2006-214312

Low Reynolds Number Aerodynamic Characteristics of Several Airplane Configurations Designed to Fly in the Mars Atmosphere at Subsonic Speeds

Richard J. Re, Odis C. Pendergraft, Jr., and Richard L. Campbell

August 2006

Issued: 09/29/2006

Page 47, Figure 1 (e): Bottom view of model MA-SC-1 with tails inverted and lower fuselage fairing removed.

Summary

A 1/4-scale wind tunnel model of an airplane configuration developed for short duration flight at subsonic speeds in the Mars atmosphere has been tested in the Langley Research Center Transonic Dynamics Tunnel. This continuous-flow closed-circuit tunnel was pumped down to extremely low pressures to represent Martian Mach/Reynolds number conditions. Three unswept wings having the same planform but different airfoil sections were investigated. A sweptback wing incorporating one of the three airfoil sections was also tested. One unswept wing configuration was tested with the lower part of the fuselage removed and the vertical/horizontal tail assembly inverted and mounted from beneath the fuselage. Horizontal tail incidence was varied on an unswept wing configuration as was the deflection of plain and split flaps on the trailing-edge. Aerodynamic data were obtained with a force balance. Upper and lower surface wing pressures were measured at one spanwise station on some configurations.

Most of the testing was conducted at Mach numbers of 0.65 and 0.80 but some data were obtained at other Mach numbers in the range 0.50 to 0.90. Wing chord Reynolds number was varied from 40,000 to 100,000 and angles of attack and sideslip were varied from –10° to 20° and –10° to 10°, respectively.

Introduction

An airplane configuration has been developed for short duration cruise flight at subsonic speeds in the Mars atmosphere. The airplane would travel to Mars as an undeployed (folded) rocket payload and would assume its airplane configuration after entry into the Mars atmosphere and release from an aeroshell. Program economics, packaging,and timing necessitated that the airplane be small in size with the consequence of very low Reynolds numbers flight in the Martian atmosphere (which is primarily carbon dioxide with pressure at the surface of Mars approximately 0.6 percent of the sea level pressure on Earth). The range of Martian flight Reynolds numbers approximate those of model airplanes (or very small pilotless air vehicles) in the Earth's atmosphere at very low speeds. The airfoil Reynolds numbers are below the threshold for which most experimental airfoil data are considered applicable (reliable) because of laminar separation/reattachment phenomena.

Four wing geometries were selected for investigation. They consisted of three different airfoil sections for the same unswept wing planform and a sweptback wing planform incorporating the same airfoil section design approach as one of the unswept airfoils. One unmodified existing airfoil design, the Eppler 387, was selected for investigation with the unswept wing configuration. Two outer panel airfoils were developed for the unswept and swept wing configurations (MA-SC-1 and MA-SC-1t, respectively) using the CDISC (ref. 1) knowledge-based design method coupled with the MSES (ref. 2) 2-D interacted Euler/boundary-layer flow solver. Flow constraints were selected to give an upper surface rooftop pressure distribution and aft-loading similar to supercritical airfoils for the cruise condition, and a geometry constraint was applied to maintain the original maximum thickness. A 30-percent chord simple flap was also defined for the MA-SC-1 wing panel to allow higher lift coefficients to be obtained during the pull-out phase of the flight. The fourth airfoil geometry (MA-SF-1) was derived from a NACA 67(.5)-406 airfoil by dividing the aft 20-percent chord along the mean line to create a split flap. This wing was expected to obtain the highest maximum lift coefficients with the flaps deflected. The FUN2D (refs. 3 and 4) 2-D unstructured grid Navier-Stokes flow solver was used to assess the performance of this airfoil with various split flap deflections. An attempt was made to reduce the high leading edge velocity peak on the airfoil using the optimization capability in FUN2D, but it was abandoned because of convergence difficulties. The airplane configuration geometric details reflect some shaping compomises made necessary by the space available in the aeroshell.

There was a concern, especially at the lowest Reynolds numbers planned for the test, that if a laminar separation bubble occurred on the wing, it would not close before the trailing edge, leading to a loss of lift and an increase in drag. This would be more likely to occur at the higher Mach numbers, where compressibility effects tend to suppress transition. As there was some doubt as to the effectiveness of traditional transition-inducing devices such as grit, disks, or turbulators at these conditions, a new concept known as a transition bump was proposed.

This concept grew out of the observation that at low Reynolds numbers and moderate angles of attack, a laminar separation bubble would close in a

short distance once the leading-edge pressure peak provided a strong enough adverse gradient. The idea then was to add a bump to the upper surface that had sufficient curvature to create a "2nd leading edge" pressure peak at cruise angles of attack that would be similar in magnitude to the leading edge peak at higher angles. This requires that the bump be thicker than the boundary layer at the cruise conditions, but small enough to be submerged in the boundary layer at the higher angles where the leading edge peak is effective. This differs from normal transition devices that would be submerged in the boundary layer at all times and ideally would produce almost no perturbation to the surface pressures. A parametric study was conducted using the MSES code to select the best chord-wise location and radius for a semicircular bump on the MA-SC-1 airfoil. It was determined that a bump with a radius of 0.7 percent of chord, located at 15 percent chord, gave the desired characteristics at the lowest test Reynolds number.

A 1/4-scale wind tunnel model of this configuration has been fabricated for testing in the Langley Research Center Transonic Dynamics Tunnel. This continuous-flow closed-circuit tunnel can be pumped down to extremely low pressures so that Martian Mach/Reynolds number conditions can be represented using air as a flow medium. The model was supported in the tunnel test section by a rear sting. Aerodynamic force and moment data were obtained with an internal force balance and wing upper and lower surface (chordwise) static pressures were measured at one spanwise station. Horizontal tail incidence was varied on an unswept wing configuration with the tails mounted above the model. Some wing configurations were tested with a transition bump modelled by a cylindrical wire cemented to the wing upper surface at 15 percent chord to force. Some data were obtained with deflected plain or split trailing-edge flaps on two unswept wings. The swept wing configuration was tested without any flap deflection. The effect of removing the lower fuselage fairing and mounting the horizontal and vertical tails inverted from the bottom of the model on the lift and stability and control were determined for one of the unswept wing configurations as a separate tunnel test entry.

The investigations were conducted in the wing chord Reynolds number range from 40,000 to 100,000 at Mach numbers from 0.50 to 0.90 (a single run was made at a Mach number of 0.25). Angles of attack and sideslip were varied from -10° to 20° and -10° to 10°, respectively.

Symbols and Abbreviations

Force and moment data are presented in coefficient form with the longitudinal aerodynamic characteristics referred to the stability axis system and lateral/directional characteristics in the body axis system. The reference center for the computation of aerodynamic moment coefficients was located at Model Station 1.876, Waterline 0, and Buttock Line 0. The symbols and abbreviations used in this report are defined as follows:

Symbols:

b	wing reference span (See Data Reduction and Accuracy Section)
c	local streamwise chord of outboard wing panel c = 3.451 in. for unswept wings c = 3.438 in. for swept wing
C_A	axial-force coefficient, Axial force/($q_\infty S$)
cbar	wing reference chord (See Data Reduction and Accuracy Section)
C_D	drag coefficient, Drag/($q_\infty S$)
C_{Db}	base drag coefficient (upper fuselage fairing), Base drag/($q_\infty S$)
C_L	lift coefficient, Lift/($q_\infty S$)
C_l	rolling-moment coefficient, Rolling moment/($q_\infty Sb$)
C_m	pitching-moment coefficient, Pitching moment/($q_\infty Scbar$)
C_N	normal-force coefficient, Normal force/($q_\infty S$)
C_n	yawing-moment coefficient, Yawing moment/($q_\infty Sb$)
C_p	pressure coefficient, $(p_l - p_\infty)/q_\infty$
C_y	side-force coefficient, Side force/($q_\infty S$)
l	fuselage reference length, 5.841 in.
L/D	lift to drag ratio, Lift/Drag

M_∞	test section free-stream Mach number
p_l	local static pressure
p_∞	free-stream static pressure
$p_{t,\infty}$	free-stream total pressure
q_∞	free-stream dynamic pressure
R_c	model Reynolds number based on wing reference chord
S	wing reference area (See Data Reduction and Accuracy Section)
x	streamwise airfoil coordinate measured from outer wing panel leading edge
z	vertical coordinate measured relative to horizontal line through the airfoil leading edge
α	model angle of attack, deg
β	model angle of sideslip, deg
Δ	± incremental value
δ_f	wing flap deflection angle, deg
δ_h	horizontal tail incidence angle, deg

Abbreviations:

atms	atmospheres
BL	Buttock Line, in.
Eppler 387	wing configuration with Eppler 387 airfoil
MA-SC-1	wing configuration with CDISC airfoil design and supercritical flow technology
MA-SC-1t	sweptback wing configuration with MA-SC-1 airfoil
MA-SF-1	split flap wing configuration with FUN2D numerically optimized airfoil design
MS	Model Station, in.
TDT	Transonic Dynamics Tunnel
WL	Waterline, in.

Description of Test

Model

The geometry of the 1/4-scale model consisted of a fuselage made up of fairings attached above and below the central portion of a one-piece wing and a twin-boom arrangement for the support of the horizontal and vertical tails (figs. 1 and 2). There were three unswept wings of the same planform geometry (fig. 2) having outboard wing panels with different airfoil sections and a sweptback wing (fig. 3) having the same airfoil section as one of the unswept wings. The wings were made of aluminum and were specified to have a surface finish of 32 microinches and a contour tolerance of ±0.005 inches. After the testing of the four original configurations (Test 540) was completed one of the unswept wing configurations was modified so that the tail support booms could be mounted from beneath the model with the tails inverted and the lower fuselage fairing removed (fig. 1(e), Test 541). A 0.020 inch diameter wire was cemented to the upper surface of the outer wing panel at 15 percent chord on one unswept wing configuration (fig. 2(a)) and the swept wing configuration (fig. 3) to act as a transition bump. Presence or absence on the wing of the wire is indicated in the report as “bump on” or “bump off”.

The upper fuselage fairing (fabricated from fiberglass and graphite plies) was not representative of the top of the airplane configuration but was necessary for housing the internal force balance. The lower fuselage fairing (also fiberglass and graphite plies) represented a shape for housing the mission instrumentation in a geometry suitable for packaging the undeployed (folded) airplane in the payload space of the Mars entry aeroshell.

The unswept MA-SC-1 wing configuration had a plain trailing-edge flap on the right wing panel (fig. 4(a)). The unswept MA-SF-1 wing configuration had a split trailing-edge flap on both wing panels, represented by solid wedge-shaped pieces that bolted to the wing lower surface, (fig. 4(b)). The MA-SF-1 wing was designed so that with a split flap deflection of 10° it would have about the same amount of camber as the MA-SC-1 wing. The Eppler 387 wing (unswept) and the MA-SC-1t (swept) had no provision for flap deflections. The single vertical tail was mounted directly to the horizontal tail in the centerline plane of the model and when the horizontal tail incidence was changed

the entire empennage moved. The planform shapes of the horizontal and vertical tails (fig. 2(b)) were selected for efficient packaging of the folded airplane (payload) in the aeroshell.

Upper and lower surface static pressure orifices were installed in the outer wing panel at one spanwise station (table 1). At one point in the test a row of model centerline pressure orifices on the lower fuselage fairing and the wing ahead of it were recorded in place of the wing pressure orifices. The wing surface and base pressure scanning unit was installed on the support sting far enough downstream of the model base to avoid pressurizing affects on the tails and aft part of the fuselage. The design airfoil ordinates of the outer panels of the various wing configurations are presented in nondimensional form in table 2. A thin sheet of hot-film sensors was wrapped around the left panel of some of the wings and remained on the model during all the tests (fig. 1).

After completion of testing, the model was assembled with the Eppler 387 wing, both fuselage fairings, and the empennage upright (at 0° incidence) and was scanned to obtain accurate as-built as-assembled dimensions of the right hand half of the model. These measurements were made as cross-sections in the MS, WL, and BL system and are presented in tables 3 through 6. The empennage support struts which were not of constant diameter were not measured during the scanning process. However, three representative diameters (perpendicular to the support strut centerline) are given in figure 3.

Wind Tunnel

The transonic Dynamics Tunnel is a continuous flow, variable pressure wind tunnel with a slotted 16 foot square test section with filleted corners. The contraction ratio (settling chamber area/test section entrance area) is 8.9. The test section is slotted with three longitudinal slots in both the floor and ceiling to provide 2.1 percent open area and with two longitudinal slots on each sidewall to provide an additional 2.3 percent open area. The tunnel is capable of using either air or R-134a as the test medium. Testing in R-134a,which is a heavy gas, has important advantages for flutter testing of aeroelastic models. These advantages include improved model to full-scale similitude, higher Reynolds number, and reduced power requirements. The tunnel is specially configured with safety screens, bypass valves, and an airstream oscillation system for flutter tests of fixed-wing models. The tunnel can operate up to a Mach number of 1.2 and is capable of maximum Reynolds numbers of about 3×10^6 per foot in air and 10×10^6 per foot in R-134a. The tunnel may be operated at stagnation pressures from near vacuum (0.025 atms) to atmospheric.

Model support systems include a sidewall turntable for semispan models, a two cable suspension system for “flying” models, a floor mounted turntable for ground-wind loads studies, a sidewall mount for semispan tilt rotor models, a floor-mounted post for a rotorcraft testbed, and a sting support system for full span models. The sting support system for full span models, which was used for the present investigation, is in the vertical plane downstream of the test section and supports models in the test section by means of cantilever stings. This support system may be traversed up or down about five feet from the test section centerline in the vertical plane. In addition the support sting may be pitched in the vertical plane through an angle range of ±15°. This combination of support system movements allows the model to be positioned near the test section centerline through a large angle of attack range. A prebent pitch coupling (+5°) was installed to bias the support system pitch range so that the model could be pitched in from -10° to +20°. A remotely controlled roll mechanism was installed between the prebent pitch coupling and model sting to provide the on-line combined model pitch and roll angles necessary for setting model angle of attack and sideslip combinations.

Test Conditions and Configurations

The extremely low tunnel pressure required to set free-stream test conditions resulted in noticeable variations in test conditions during angle sweeps that were caused by small leaks through the tunnel shell. Pumping to maintain a constant pressure to compensate for the leaks while taking data during an angle sweep was not considered viable because of the expectation that flow quality would be affected. Tunnel free-stream stagnation pressure was within 1°F or 2°F of being constant during a given tunnel run and was in the range from 77°F to 89°F for the tests.

As is evident from the tables and figures presented the word “Run” is used in this document to identify a sweep through an angle of attack range

or through an angle of sideslip range for a given model configuration at a "constant" set of tunnel conditions. Tables of the configuration geometric and test variables and relevant Run numbers are presented in Appendix A for Tests 540 and 541. The Test and Run numbers are presented in Appendix A to indicate that a specific configuration was tested as well as to give an identifier so that the actual range of tunnel flow conditions can be obtained from Appendix B if other than the averaged or nominal values are presented in the text, figure keys, or figure titles are desired.

Most of the data were obtained with the vertical tails mounted from the top of the model and with both the upper and lower fuselage fairings on (Test 540). The top fuselage fairing was not representative of the airplane fuselage configuration but was necessary to shield the force balance from the tunnel airflow and to allow the support sting to pass through the model base. The model was modified after Test 540 to assess the effect on the aerodynamic characteristics of having the tails inverted and below the the plane of the wing (fig. 1(e)). The lower fuselage fairing was removed and modifications were made to permit attachment of the struts that support the tail booms to the lower surface of the wing (Test 541). The leading edges of the exposed struts were aerodynamically faired as were wing lower surface protrusions (attachment points for lower fuselage fairing).

Data Reduction and Accuracy

Prior to the start of each of the two tests the assembled model support hardware (installed in the tunnel test section) was loaded with calibrated weights to verify balance installation integrity, the restraint effects of hot film electrical leads, and to determine the angular deflection characteristics of the support hardware under loaded conditions.

The longitudinal aerodynamic data presented are in the stability axis system and the lateral/directional aerodynamic data are in the body axis system. The base (sting cavity) pressure at the rear of the fairing was measured so that the balance axial force measurement at each test point could be adjusted to the condition of freestream static pressure acting on the projected area of the upper fuselage fairing base. The location of the model moment reference center was the same for both the unswept and swept wing configurations (fig. 2(a) or 3). The reference constants used in the computation of the aerodynamic data for the two wing sweeps are listed in the followimg table.

Reference constants	Wing	
	Unswept	Swept
Wing area (S)	64.55 in^2	53.76 in^2
Wing span (b)	17.01 in.	14.71 in.
Wing chord (cbar)	3.91 in.	4.15 in.
Fuselage base area	2.64 in^2 (axially projected area)	
Moment center	3.298 in. (aft of fuselage leading edge)	

The pitch attitude of the tunnel support system was measured using an attitude transmitter. Sting roll angle was also measured by a transmitter in the roll coupling aft of the model sting but forward of the tunnel support system. Model angles of attack and sideslip at each test point were computed using the support system pitch and roll coupling attitude transmitter measurements and the calculated deflection characteristics of the assembled support hardware due to model aerodynamic loads. No corrections were made to the data for tunnel flow angularity which is believed to be small at these test conditions. Model size relative to the test section cross-sectional area was small so blockage effects are negligible for the range of subsonic Mach numbers tested.

In order to permit testing with one force balance over the range of static forces and moments anticipated, the static balance loads were estimated for testing at the highest freestream dynamic pressures at the extremes of model attitude. These static forces and moments were small but an increase in balance component capacity was necessary to allow for unsteady loads due to flow separation that would be additive at the extremes of model attitude and free-stream dynamic pressure. This resulted in installing a balance that was oversized at low Mach numbers and dynamic pressures as indicated by the aerodynamic coefficient accuracies shown in figure 5. These values were calculated using the unswept wing reference constants and the balance component accuracies cited below, transferred to the model

moment reference center for the highest and lowest dynamic pressures encountered at each Reynolds number (Appendix B).

Based on primary and combined loadings in a calibration laboratory the force balance used in the investigation had the following component accuracies:

Balance component	Component capacity	Accuracy 95% confidence level (% full scale)
Normal force	±100 lbs	±0.08
Axial force	±15 lbs	±0.19
Pitching moment	±300 in. lbs	±0.07
Rolling moment	±50 in. lbs	±0.25
Yawing moment	±150 in. lbs	±0.07
Side force	±50 lbs	±0.10

In order to take some account of the restraint effect on the balance readings of hot film wires and soft pressure tubes crossing from the model (metric) to the sting (non-metric) a series of primary loadings were applied to the assembled model on each balance component. The load series were applied separately to each balance component and restraint factors were calculated and applied (for data reduction) to each laboratory determined balance component sensitivity. The loadings were done only for the first configuration built up for testing at the ambient temperature of the test section with the tunnel open and no attempt was made to consider the effect of the relatively small temperature difference that would exist when the tunnel was running. Each time a wing configuration change was made the hot film wires and soft pressure tubes had to be reconnected and secured. This was done without recalibration of the model/balance assembly. The combined effect of reconnecting and securing the wires and tubes and the temperature difference may affect the balance sensitivity correction factors applied, primarily in axial force. However, the wires and tubes were consistently secured so that they were relatively slack to minimize any variation in restraint. The effect on axial force measurement may be significant at times but balance zero returns after each run series were good so that axial force balance readings within a run series are believed, in general, to be consistent.

Tunnel free-stream pressures were measured on precision instruments which at the conditions of this test have an accuracy of ±0.0013 psi. Wing and fuselage base (sting cavity) pressures were measured on a 1 psi differential pressure scanning unit which was calibrated in place during the test as necessary and checked frequently by applying a known pressure. The pressure module has a manufacturer's stated accuracy of ±0.1 percent of the full scale pressure reading, and that, in combination with the accuracy of the free-stream static reference pressure measurement, is estimated to yield an accuracy in pressure readings of about ±0.002 psi.

Presentation of Results

Force balance and fuselage base pressure data were obtained for all the test runs and reduced to coefficient form. At the end of Test 540 a few runs with the Eppler 387 wing configuration were made with lower fuselage centerline pressures hooked up in place of some of the wing pressures. No wing pressures were measured during Test 541 (tails inverted and lower fuselage fairing removed). The presence or absence of the transition bump on the upper surface of the wing at 15 percent chord is indicated in the figure titles, keys, and tables by the phrases "bump on" or "bump off", respectively.

Some values of the test variables given as constants in the keys for graphical data presentation in this document are averaged for all the points shown for the given Run. This is most evident for Reynolds number which increased slowly during each Run due to small leaks to atmospheric pressure through the tunnel shell. The actual range of Reynolds numbers for a given Run is shown in the tables of Appendix B along with the freestream static and dynamic pressure ranges. Other variables that appear in figure keys that were averaged are Mach number and angle of attack (when sideslip angle was the variable). However, both of these variables were adjusted from point-to-point during a Run so that deviations from the average are minor. Nominal values of variables are used in figure and table titles.

The basic aerodynamic force and moment coefficient data for the model with each wing configuration are presented graphically to illustrate

the effect of the various tunnel or model geometry variables in the following figures. Unless the words "inverted tails" are used to indicate configurations with the lower fuselage fairing removed, and the tails inverted and mounted from the bottom of the model (Test 541), the data are from Test 540 where the lower fuselage fairing was always on, and when installed, the tails were upright and supported from the top of the model.

Pressure coefficient distributions on the four wing outer panel configurations (at one spanwise station) and on the centerline of the lower fuselage fairing (Eppler 387 configuration only) are presented in the following figures.

Results

Effect of Reynolds Number

The effects of Reynolds number on the aerodynamic characteristics of the model with the different wing configurations at Mach numbers of 0.65 and 0.80 are shown in figures 6 through 25. Testing at other Mach numbers was done only at a Reynolds number of 40,000.

Lift coefficient. In general, at a given angle of attack in the range from -6° to 10°, lift coefficient increased with Reynolds number for the unswept and swept wing configurations. At a Mach number of 0.65 and Reynolds number of 40,000 there was a break in the lift curve for the unswept wing configurations somewhere between 0° and 6° angle of attack (except with the tails inverted and the lower fuselage fairing removed) that either did not occur or was much less severe at the two higher Reynolds numbers (e.g. fig. 8(a)). At a Mach number of 0.80 the break in the lift curve often occurred at a Reynolds number of 40,000 and sometimes at a Reynolds number of 60,000 (figs. 9(a) and 19(a)). Based on the data obtained at a Reynolds number of 40,000 at Mach number 0.65 with the lower fuselage fairing removed and the tails inverted (fig. 12(a), 13(a), 14(a), and 16(a), and the same unswept wing configuration as figs. 8(a) through 11(a)) it appears that the lower surface fuselage fairing and/or its flow field effect on the horizontal tail is the primary cause of the break in the lift curve and the subsequent lift loss. At Mach number 0.65 and a Reynolds numbers of 40,000 the lift curve break for the sweptback wing configuration was less abrupt and the subsequent lift loss was smaller (fig. 24(a)) than for the unswept configurations. However at this Mach number at a Reynolds number of 100,000 the lift curve break was abrupt and the subsequent lift loss was large.

Pitching-moment coefficient. The unswept wing configurations MA-SC-1 (with tails in the upright position) and MA-SF-1 were either longitudinally unstable or neutrally stable at positive lift coefficients and only slightly affected by changes in Reynolds number (figs. 8(a) through 11(a) and figs. 18(a) through 23(a)). At negative lift coefficients these configurations were either marginally stable or neutrally stable. Removal of the lower fuselage fairing and mounting the tails inverted from below the model on the unswept MA-SC-1 configuration resulted in a negative pitching-moment coefficient shift (e.g. figs. 10(a) and 12(a)) and increased instability with increasing Reynolds number at moderate lift coefficients at Mach number 0.65 (fig. 12(a)). The swept wing configuration was longitudinally stable over most of the lift coefficient range (figs. 24(a) and 25(a)) and it's stability was only slightly affected by changes in Reynolds number. Although there were no large incremental displacements in the pitching-moment coefficient curves due to Reynolds number there usually was an irregularity coincident with the first lift curve break (e.g. 24(a)).

Drag coefficient. As would be expected drag coefficient generally decreased with increasing Reynolds number with an indication of a small increase in the lift coefficient for minimum drag for some configurations. With the unswept wing MA-SC-1 and the tails inverted and lower fuselage fairing removed there was little effect of Reynolds number on model drag coefficient at zero lift coefficient but there was a beneficial rotation of the drag polars with increasing Reynolds number (figs.12(b), 13(b), 14(b), and 16(b)). When the wing split trailing edge flaps were deflected (MA-SF-1) there was a more significant increase in the lift coefficient for minimum drag resulting from rotation of the drag polar as Reynolds number increased (figs. 18(b) through 23(b)). For the swept wing configuration (MA-SC-1t) the decrease in drag coefficient with increasing Reynolds number was negligible at zero lift at both Mach numbers but there was significant rotation of the drag polar with increasing Reynolds number so that minimum drag coefficient occurred at a lift coefficient about 0.1 higher at the highest Reynolds number (e.g. fig. 24(b)).

Lift-drag ratio. As a result of drag coefficient decreases and drag polar rotation with increasing Reynolds number maximum lift-drag ratio generally increased with Reynolds number, as would be expected, and was greater at Mach number 0.65 than at Mach number 0.80.

Lateral-directional characteristics. Reynolds number effects on the lateral directional characteristics at Mach numbers 0.65 and 0.80 which were determined for the unswept wing configuration (MA-SC-1) with inverted tails and lower fuselage fairing removed were

small (figs. 15(a) and 17(a)). There was a small Reynolds number effect on rolling-moment coefficient at a Mach number of 0.65 (fig. 15(a)) that may be associated with the hysteresis of asymmetric separation as the sideslip angle settings were made incrementally from -10° to +10°.

Effect of Mach Number

The effect of Mach number on the longitudinal aerodynamic characteristics of the model with the four wing configurations is presented in figures 26 through 45. Most of the data were obtained at Mach numbers of 0.65 and 0.80 but some configurations were tested over the Mach number range from 0.50 to 0.90 at a Reynolds number of 40,000 (figs. 28, 29, 34, 35, 36, and 43). A single angle of attack sweep at a Mach number of 0.25 at 40,000 Reynolds number (included in figure 26) was made with the configuration with the Eppler 387 airfoil.

Lift coefficient. In general, when Mach number was increased at Reynolds numbers of 40,000 and 60,000, lift coefficient at a given angle of attack decreased between the angles of attack of about –6° and 10°. At a Mach number of 0.50 the break in the lift curve at low angle of attack at a Reynolds number of 40,000 did not occur for the unswept wing configuration (figs. 28(a) and 34(a)). At Mach numbers above 0.50 the combined effect of the decrease in lift coefficient with increasing Mach number and the lift curve break resulted in much lower lift coefficients at low to moderate angles of attack for the higher Mach numbers (e.g. fig. 29(a)). The lift curve slope of the configuration with the swept wing (MA-SC-1t) decreased significantly with increasing Mach number at lift coefficients below the break in the lift curve at low angle of attack (figs. 43(a) through 45(a)).

Pitching-moment coefficient. The effect of increasing Mach number on pitching-moment coefficient was generally small and consisted of a stabilizing effect over most of the lift coefficient range for both unswept and swept wing configurations. The changes in stability did not result in a shift in level of the pitching-moment curves but tended in most cases to be a small slope change centered at low positive lift coefficients. The most significant Mach number effect occurred on the swept wing configuration at a Reynolds number of 40,000 where above a Mach number of 0.70 there was an increase in pitching-moment curve slope at the break in the lift curve that persisted up to a lift coefficient of about 0.40 (fig. 43(a)).

Drag coefficient. Minimum drag coefficient generally increased with Mach number but the effect was inconsistent in that for some of the unswept wing configurations drag coefficient at a Mach number of 0.70 was lower than at Mach numbers 0.50 and 0.65 (figs. 28(b), 34(b), and 35(b)). The axial force restraint effect of the wires and tubes crossing from the model to the support sting may have an influence on the differences observed in minimum drag coefficient measurements. A detailed discussion of the measures taken to reduce the effect of the tubes and wires crossing from the model to the sting is contained in the Data Reduction and Accuracy section of this report.

The drag due to lift at moderate lift coefficients increased with increasing Mach number so that the drag coefficient increment at lifting conditions was greater than the increment at minimum drag, that is, there was a rotation of the drag polars (e.g. fig. 36(b)). As would be expected drag coefficient for the configuration with the swept wing was less affected by Mach number increases (figs 43(b), 44(b), and 45(b)).

Lift-drag ratio. Lift-drag ratio generally decreased with increasing Mach number due to decreases in lift coefficient, increases in minimum drag coefficient, and adverse rotation of the drag polars.

Effect of Tails and Horizontal Tail Incidence

The effect of tails and horizontal tail incidence on the longitudinal aerodynamic characteristics of the model are presented in figures 46 through 59. Tail and tail incidence effects were obtained for unswept wing configuration MA-SC-1 with the tails mounted in the upright position at Mach numbers of 0.65 and 0.80 at Reynolds numbers of 40,000 and 60,000 (figs. 46 through 49). Data were obtained with this wing configuration at Reynolds numbers up to 100,000 with the tails inverted and the lower fuselage fairing removed (figs. 50 through 55). Horizontal tail incidence effects were not obtained for the model with the sweptback wing (MA-SC-1t) but it was tested

tail-on and tail-off at Reynolds numbers of 40,000 and 60,000 (figs. 56 through 59).

Lift coefficient. Increases in horizontal tail incidence on the model with the unswept wing (MA-SC-1) and the tails in the upright position increased lift coefficient at angles of attack up to the break in the lift curve (fig. 46(a)). Above the break in the lift curve the lift contribution due to changes in tail incidence decreased significantly and at a Reynolds number of 40,000 the lift coefficient data nearly collapsed to a single line for Mach numbers of 0.65 and 0.80. At a Reynolds number of 60,000 horizontal tail lift effectiveness was maintained to some extent above the lift curve break at a Mach number of 0.65 (fig. 48(a)) but lift coefficients collapsed to nearly a single line at 0.80 Mach number (fig. 49(a)). When the tails were inverted and the lower fuselage fairing removed horizontal tail lift effectiveness was maintained over the angle of attack range at both Mach numbers and at all three Reynolds numbers (figs. 50(a) through 55(a)). Since the wing (MA-SC-1) is the same for both the upright and inverted tail configurations the only possible explanation for the improved lift effectiveness with inverted tails is the elimination of the low angle of attack break in the lift curves. The model was tested (lower fuselage fairing still on) with the upright tails on and the tails removed. The tails off data showed a break in the lift curve at Mach number 0.65 and a Reynolds number of 40,000 (fig. 46(a)) at about the same low angle of attack as with the tails on. However, the break in the tails-off lift curve was less noticeable at other Mach and Reynolds numbers. Therefore, it appears that the breaks in the lift curves are due to the flow over the fuselage fairings and to the fuselage wake interaction on the tail lift effectiveness at angle of attack.

The effect of horizontal tail incidence on the model with the swept wing configuration (MA-SC-1t) was not obtained. But with the tails off there was an increase in lift coefficient at negative angles of attack which decreased in magnitude with increasing angle of attack (figs. 56(a) through 59(a)). Above 0° or 1° angle of attack there was almost no lift coefficient contribution from the horizontal tail (δ_h = 0°) at a Reynolds number of 40,000. At a Reynolds number of 60,000 there was essentially no effect of the tails above an angle of attack of 2° at a Mach number of 0.65, but at a Mach number of 0.80 tails on lift coefficient, which was less at angles of attack below 0°, was greater at angles of attack up to 7° (fig. 59(a)).

Pitching-moment coefficient. For the unswept wing configuration (MA-SC-1) with the tails in the upright position horizontal tail pitch effectiveness decreased sharply at lift coeffficients above the break in the lift curve at a Reynolds number of 40,000 at Mach numbers 0.65 and 0.80 (figs. 46(a) and 47(a)). At a Reynolds number of 60,000 the break in the lift curve was less pronounced at a Mach number of 0.65 (fig. 48(a)) and horizontal tail pitch effectiveness was maintained to a lift coefficient of 0.70. But at Mach number 0.80 at this Reynolds number (fig. 49(a)) the lift curve break occurred at a lower angle of attack and was more pronounced causing horizontal tail pitch effectiveness to decrease greatly above 0.30 lift coefficient. With the tails inverted and the lower fuselage fairing removed the horizontal tail pitch effectiveness was maintained up to a lift coefficient of about 0.8 (figs. 50(a) through 55(a)). For the model with the sweptback wing (MA-SC-1t) addition of the tails (δ_h = 0°) increased stability at Mach numbers of 0.65 and 0.80 at Reynolds numbers of 40,000 and 60,000 and trimmed the model at low positive lift coefficients (figs. 56(a) through 59(a)).

Drag coefficient. In general, for the unswept wing configuration, drag coefficient decreased with increasing horizontal tail incidence up to 5° incidence angle with the tails in either the upright or inverted location. With the tails in the upright position, for all tail incidence angles or with the tails off, there was a discontinuity in the lift curves and drag polars in the vicinity of maximum lift-drag ratio (e.g. fig. 46). The discontinuities did not occur when the tails were inverted and the lower fuselage fairing was removed (figs. 50 through 55).

Lift-drag ratio. The largest maximum lift-drag ratio for the unswept wing configurations with the tails on was obtained with a horizontal tail incidence of 5°. With the inverted tails and the lower fuselage fairing removed discontinuities in the lift-drag ratio curves did not occur and maximum lift-drag ratio occurred at higher lift coefficients and was greater than with the tails upright and the fuselage fairing on. It is likely that the configurations with the upright tails would have

had higher maximum lift-drag ratios if they also had been tested without the lower fuselage fairing.

Effect of Wing Trailing-Edge Flap Deflection

Two of the unswept wing configurations were tested with wing trailing-edge flap deflections. The MA-SC-1 wing had a plain trailing-edge flap on the right wing (only) capable of being deflected –10°, 0°, 10°, and 20°. Therefore when flap deflection was other than 0° force and moment increments in the lateral plane were also generated (figs. 60 through 63). The MA-SF-1 wing configuration, designed to obtain the highest maximum lift coefficients with deflected trailing-edge flaps, had a split flap on each wing capable of deflections of 0°, 10°, and 30° (figs 64 through 73).

Plain flap configuration. Since the wing (MA-SC-1) with the plain flap had only a right wing flap the incremental effect of flap deflection on the longitudinal aerodynamic characteristics data of figures 60 through 63 should be doubled to obtain the total flap effect (assuming cross-flow effects due to flap deflection asymmetry are small). At Mach numbers of 0.65 and 0.80 lift was increased for downward flap deflections as would be expected and at some conditions there was a tendency for the break in the lift curves to shift to a lower angle of attack with increasing flap deflection. There was little effect of flap deflection on longitudinal stability and at positive flap deflections only small changes in pitching-moment coefficient level. At a Reynolds number of 40,000 maximum lift-drag ratio was obtained with 0° flap deflection but at a Reynolds number of 60,000 there was some drag polar rotation and maximum lift-drag ratio was obtained with 10° flap deflection. Since the flap extended relatively far outboard on the wing (there are no separate ailerns on these wings), flap deflection produced significant rolling and yawing moments over most of the angle of attack range at both Mach numbers and Reynolds numbers (figs. 60(c) through 63(c)). At a Reynolds number of 40,000 and a Mach number 0.65 (fig. 60(c)) there was a loss of rolling moment coefficient at an angle of attack of 14° with 20° flap deflection which was recovered at the higher angles of attack. Rolling moment coefficient became very irregular between 10° and 16° angle of attack at this Mach number at a Reynolds number of 60,000 (fig. 62(c)) with flap deflections of 10° and 20°. Since the flap hinge line was unswept negligible side force was generated by flap deflection.

Split flap configuration. The wing configuration with the split flaps (MA-SF-1) was tested over a range of Mach numbers at a Reynolds number of 40,000 (figs. 64 through 69) and at Mach numbers of 0.65 and 0.80 at Reynolds numbers of 60,000 and 100,000 (figs. 70 through 73). At all Mach and Reynolds numbers flap deflection had a stabilizing effect on the model at negative and low positive lift coefficients while at moderate positive lift coefficients the flap effect was more like adownward shift in pitching moment level. At a Reynolds number of 40,000 with 30° flap deflection the model trimmed at a lift coefficient of 0.48 at Mach number 0.50 (fig. 64(a)). As Mach number was increased the lift coefficient for trim with 30° flap deflection increased and was about 0.89 at Mach number 0.90. Minimum drag coefficient decreased when flap deflection was increased from 10° to 30° at Mach numbers through 0.80 and maximum lift-drag ratio was the greatest with 30° flap deflection (figs. 64(b) through 67(b)). Minimum drag coefficient was nearly constant with increasing flap deflection at Mach numbers 0.85 and 0.90 but with 30° flap deflection rotation of the drag polars resulted in the largest maximum lift-drag ratio (figs. 68(b) through 69(b)). At a Reynolds number of 60,000 minimum drag coefficient at Mach number 0.80 was lowest with undeflected flaps (fig. 71(b)) but maximum lift-drag ratio again occurred with 30° flap deflection. However, at a Reynolds number of 100,000, the model with 30° flap deflection had the highest drag and the largest maximum lift-drag ratio was obtained with 10° flap deflection at 0.65 and 0.80 Mach number (figs. 72(b) and 73(b)).

Effect of Sideslip Angle

The effect of sideslip angle on the aerodynamic characteristics of the model at five angles of attack with the tails upright ($\delta_h = 0°$) was determined with one unswept wing configuration (MA-SC-1, figs. 74 through 77) and the swept wing configuration (MA-SC-1t, figs 79 through 82) at Mach numbers 0.65 and 0.80 at Reynolds numbers of 40,000 and 60,000. The unswept wing configuration was also tested in sideslip with the tails and tail supports

removed at a Mach number of 0.65 and Reynolds number of 40,000 (fig. 78). With the tails inverted (mounted from the bottom of the model) and the lower fuselage fairing removed, the unswept wing configuration (MA-SC-1) was tested through the sideslip angle range at Mach numbers of 0.65 and 0.80 at 4° angle of attack with a horizontal tail incidence of -5° (figs. 15 and 17).

Unswept wing configuration. With the tails on, the model was stable in the lateral-directional plane in the range of sideslip angles from -10° to 10° at both Mach numbers and Reynolds numbers tested (figs. 74(a) through 77(a)). Dihedral effect (geometrically the wings and tails were at 0° dihedral angle) generally increased with angle of attack at both Mach numbers and Reynolds numbers. With the tails off (fig. 78(a)) the model had decreased directional stability and had lower dihedral effect at lower angles of attack. Side force was small over the sideslip angle range with the tails off. There were no significant variations in the longitudinal aerodynamic coefficients with sideslip angle for either the tails-on or tails-off configurations(figs. 74(b) through 78(b)). Aerodynamic coefficient offsets at 0° sideslip angle may be attributed to model or tunnel flow assymetries or to the small increase in local thickness on the left wing panel from a thin sheet of hot film sensors wrapped around the wing (figs. 1(a) through (d)).

Swept wing configuration. The configuration with the swept wing generally had similar levels of lateral-directional stability as the unswept wing configuration although the dihedral effect at angles of attack of 10° and 16° was less than at 5° (figs. 79(a) through 82(a)). At Mach number 0.65 at a Reynolds number of 60,000 (fig. 81(a)) hysteresis was evident in the variation of rolling-moment coefficient with sideslip angle at 10° angle of attack. An explanation for this rolling moment behavior is available since some extra aerodyhamic data were taken at $\beta = 0°$ and chordwise pressure measurements (at one span station) were made on the right wing simultaneously with the aerodynamic force and moment measurements. The pressure data at 10° angle of attack (fig. 127(a)) show that at positive angles of sideslip the flow on the upper surface of the right wing (upwind wing) was separated while at negative angles of sideslip the flow was mostly attached. The rolling-moment coefficient data of figure 81(a) indicate that the flow on the downwind wing in both cases is at least partially attached. The positive rolling-moment coefficient at -10° sideslip angle is due to a partial flow separation on the right wing as shown by the pressure coefficients of figure 127(a). The discontinuity in the rolling-moment coefficient data (at $\alpha = 10°$) between 0° and 2° sideslip angles is related to how the 0° sideslip angle setting is approached and this is illustrated in figure 127(a) by the pressure coefficient data of two additional 0° sideslip angle points. The three 0° sideslip angle pressure data points at 10° angle of attack were recorded in the order shown in the key of figure 127(a). The first 0° sideslip data point, which shows attached upper surface flow, was recorded after the model (at 0° sideslip angle) was brought up to 10° angle of attack from 5° angle of attack. The second 0° sideslip angle data point was taken at mid sideslip angle sweep (from -10° to 10°) and indicates attached flow on the right wing also. The third data point was taken after the sideslip angle sweep was completed and the model was brought back from 10° to 0° sideslip angle. The force balance rolling-moment coefficient data taken for the first and third 0° sideslip angle settings are shown in figure 81(a) and when considered with the pressure data of figure 127(a) indicate that the flow was attached on both wings for the first point (zero rolling moment) and remained separated on the right wing for the third 0° sideslip angle point (positive rolling moment). These three different rolling moment results at the same sideslip angle setting indicate a wing upper surface flow separation hysteresis related to how the 0° sideslip angle is approached. At 16° angle of attack the pressure data indicate that the flow on the right wing is separated for all sideslip angles and the well behaved but reduced rolling moment coefficient data indicate that the flow on the left wing is apparently also separated since there is no hysteresis effect. At a Reynolds number of 40,000 the right wing pressure distributions (fig. 125(a)) also indicate upper surface separation hysteresis effects at 0° sideslip angle but the variation of rolling-moment coefficient with sideslip angle (fig. 79(a)) indicates that, within the range of data taken, when the flow separated it apparently did so on both wings.

Wing Configuration Comparisons

There were five wing geometry related configurations investigated. Four wing configurations involved different airfoil sections or wing sweep and the fifth wing variation was a spanwise cylindrical bump (wire) cemented to the wing upper surface at the 15 percent chord on one of the unswept wing configurations (MA-SC-1). The intent of the bump was to energize an early transition and thereby increase the extent of flow attachment on the aft portion of the wing. The MA-SF-1 wing was designed so that with a split flap deflection of 10° it would have about the same amount of camber as the MA-SC-1 wing. To reduce the number of wing configurations compared only the 0° split flap MA-SF-1 configuration will be included. However, to compare coefficient levels of this configuration, which is designed to operate with deflected trailing-edge flaps, it would be necessary to refer to figures 65, 67, 70, 71, 72, and 73 where data are presented for the various split flap deflections. The configuration with the lower fuselage fairing removed and the tails inverted is not included in the wing comparison figures because the wing is identical to one of the other unswept wing configurations (MA-SC-1) and the fuselage configuration and tail installation are different. To consider removal of the lower fuselage fairing as a wing modification for comparison purposes it's effect would have to have been isolated by testing without the inverted tails, or conversely, the model with the upright tails should have been tested without the lower fuselage fairing. Neither was done. Performance comparisons can be made at Mach numbers of 0.65 and 0.80 at Reynolds numbers of 40,000, 60,000, and 100,000 for most configurations. Sideslip angle was varied at constant angles of attack to obtain lateral-directional data only for the MA-SC-1 (unswept) and MA-SC-1t (swept) wing configurations.

Reynolds number 40,000. At a Mach number of 0.65 the unswept wing (MA-SC-1) with the bump had the highest lift curve slope at angles of attack below the break in the lift curve and higher lift at all angles of attack (fig. 83(a)). The configuration designed to operate with a deflected split flap (MA-SF-1, $\delta_f = 0°$) had a lift curve that was very similar to that of the configuration with the Eppler 387 airfoil up to 8° angle of attack. Below the break in the lift curve the swept wing configuration (MA-SC-1t) lift curve slope was about the same as the two aforementioned configurations. At Mach number 0.80 the unswept wing configuration (MA-SC-1) with the bump had about the same lift curve slope as without the bump at negative angles of attack, but at angles of attack between 0° and 8° it developed more lift (fig. 85(a)). The four unswept wing configurations (with tails on) had about the same level of longitudinal instability at higher positive lift coefficients at Mach number of 0.65 while the swept wing configuration was stable over the range of lift coefficients . At a Mach number of 0.80 the four unswept wing configurations were essentially neutrally stable at negative lift coefficients and all were slightly unstable at positive lift coefficients above 0.30. The configuration with the Eppler 387 airfoil had the lowest drag coefficient of the four unswept configurations at both Mach numbers (figs. 83(b) and 85(b)) but had higher drag due to lift so that its maximum lift-drag ratio was about the same as the MA-SC-1 wing configuration with the bump. The swept wing configuration had the lowest drag coefficient at Mach number 0.80 and its drag due to lift characteristics were such that it had the largest maximum lift-drag ratio. The swept and unswept wing configurations were both stable in the lateral-directional plane over the range of sideslip angles at both Mach numbers at the angles of attack tested (figs. 84(a) and 86(a)).

Reynolds number 60,000. At a Mach number of 0.65 the lift curve slopes of the five configurations did not differ significantly at low positive lift coefficients (fig. 87(a)). The split flap wing configuration with 0° flap deflection had no lift curve break at low angle of attack at this Mach number. At Mach number 0.80 (fig. 89(a)) there was little difference in the lift curve levels or slopes of the two MA-SC-1 configurations (with and without bump). The trends in pitching-moment coefficient at both Mach numbers were much the same at this Reynolds number as at 40,000. At a Mach number of 0.65, drag coefficient for all four unswept wing configurations decreased relative to that measured at 40,000 Reynolds number with the largest decreases occurring for the Eppler 387 and MA-SC-1 (no bump) wing configurations (figs. 83(b) and 87(b)). There was only a small decrease in minimum drag coefficient for the swept wing configuration but at lift coefficients near maximum lift-drag ratio the drag coefficient decrease was large. At a Mach number of 0.80 minimum drag coefficient for the MA-SC-1 (bump on) wing configuration

increased slightly with Reynolds number but at lift coefficients near maximum lift-drag ratio drag coefficient decreased (figs. 85(b) and 89(b)). Minimum drag coefficient for the swept wing configuration remained unchanged with Reynolds number but at lift coefficients in the vicinity of maximum lift-drag ratio drag coefficient decreased so the swept wing configuration had the largest maximum lift-drag ratio at this Mach number also.

Reynolds number 100,000. Data were not obtained with the Eppler 387 wing configuration at a Reynolds number of 100,000. At this Reynolds number only the swept wing configuration had a sharp lift curve break at Mach number 0.65 (fig. 91(a)). As a result, the two MA-SC-1 wing configurations had significantly more lift above 3° angle of attack. None of the lift curves had a noticeable break in the low positive angle of attack range at 0.80 Mach number (fig. 92(a)). For the moment reference centers chosen, the swept wing configuration was the only longitudinally stable configuration at positive angles of attack at both Mach numbers. At a Reynolds number of 100,000 drag coefficient was not affected as much by increasing Mach number as it was at the lower Reynolds numbers, with the largest reduction occurring for the MA-SC-1 bump on wing configuration. Once again the swept wing configuration had the largest maximum lift-drag ratio (fig. 92(b)).

Fuselage Base Pressure and Drag Coefficients

As is typically done for aerodynamic models modified for a rear sting support the drag coefficient data presented have been adjusted to the condition of freestream static pressure acting on the total axially projected area of the upper fuselage base as modified for passage of the support sting. Some examples of the magnitude and variation of the base pressure and drag coefficients with angles of attack and sideslip at each Reynolds number are presented in figures 93 through 96. Figures 93 through 95 contain data measured during the first tunnel entry (Test 540) when the lower fuselage fairing was on for all configurations and, when installed, the tails were in the upright position. Figure 96 contains data obtained during the tests with the lower fuselage fairing removed and the tails inverted and mounted from the bottom of the model (Test 541).

Test 540. As can be seen in figure 93(a) base drag coefficient increased with Mach number at a Reynolds number of 40,000 with the largest changes occurring between Mach numbers of 0.50 and 0.65 between angles of attack of 4° and 14°. The beginning of this base pressure difference coincides with the angle of attack of the lift curve break at a Mach number of 0.65 (figs. 28(a) and 29(a)). At the higher Reynolds numbers at Mach number 0.65 (figs. 94(a) and 95) the variation of the base drag coefficient with angle of attack in the low angle of attack range more closely resembles that of the Mach number 0.50 data at 40,000 Reynolds number. There was no significant variation of base drag coefficient with angle of sideslip at constant angles of attack at Reynolds numbers of 40,000 and 60,000 (figs. 93(b) and 94(b)).

Test 541. With the tails inverted and the lower fuselage fairing removed longitudinal aerodynamic data were obtained at Mach numbers of 0.65 and 0.80 over the angle of attack range and lateral aerodynamic data were obtained over the angle of sideslip range with the model at 4° angle of attack. At these Mach numbers there were similar effects of Reynolds number on base drag coefficient over the angle of attack and sideslip ranges (fig. 96).

Wing and Fuselage Lower Surface Pressure Coefficients

During Test 540, which included all the different wing and flap configuration variables, pressure measurements were made at the same time as the force balance measurements. The small size of the model limited the amount of instrumentation that could be installed. A single chordwise row of upper and lower surface static pressure orifices were installed in the right outboard panel of each wing configuration except for the MA-SF-1 wing where the wing lower surface pressure orifices were on the left wing panel. An additional row of static pressure orifices was installed on the fuselage centerline from the underside of the wing leading edge extending aft over the fairing that made up the lower fuselage shape. These fuselage pressures were measured only briefly (with the Eppler 387 wing configuration) since when connected they replaced some of the wing pressures on the recording instrumentation. The fuselage pressures were obtained over the angle of attack

range only at Reynolds numbers of 40,000 and 60,000 at zero degrees sideslip angle. No external static pressure data on the wing or model centerline lower surface were obtained during Test 541 (unswept MA-SC-1 wing with lower fuselage fairing not installed and tails inverted).

Eppler 387. The configuration with the Eppler 387 wing was the only one tested at a Mach number of 0.25 (at 40,000 Reynolds number). The pressure coefficient distributions at this Mach number (fig. 97(a)) show that the negative leading-edge pressure coefficient peaked at an angle of attack of 14° and that pressure recovery occurred as far aft as measurements were made (x/c = 0.95). Above 14° angle of attack the pressure peak decreased and upper surface flow was completely separated at 20° angle of attack. At a Mach number of 0.65 (fig. 97(b)) the pressure distributions were similar to those at 0.25 Mach number up to about 5° angle of attack above which the pressure peak decreased with eventual separation aft of the 20 percent chord. The Mach number effect on the pressure distributions resulted in a lift coefficient 0.2 greater at Mach number 0.25 than at Mach number 0.65 at 14° angle of attack (fig. 26(a)). At a Mach number of 0.80 (fig. 97(c)) the pressure peak at the leading edge was suppressed relative to that at Mach number 0.65 as was the pressure over the forward 20 percent chord in the angle of attack range from about 0° to 10°. Increasing Reynolds number to 60,000 at a Mach number 0.65 (fig. 98(a)) did not significantly change the pressure distributions up to an angle of attack of about 10°. Between 10° and 20° angle of attack the upper surface pressures were lower at 60,000 Reynolds number and higher lift coefficients were obtained before the upper surface flow became completely separated at 20° angle of attack. At 0.80 Mach number (fig. 98(b)) there was no significant effect of increasing Reynolds number on the pressure distributions.

Fuselage lower surface centerline pressures measured at Reynolds numbers of 40,000 and 60,000 at Mach numbers of 0.65 and 0.80 (figs. 99 and 100) indicate that there is an increase in the magnitude of the negative pressure coefficient level over the aft 50 percent of the fairing at angles of attack that coincide with the break in the lift curves (figs. 6(a) and 7(a)). Although these lower surface fuselage pressures were recorded only with the Eppler 387 wing configuration it is likely that the same flow conditions exist with the other wings since the lower fuselage shape is the same and the same lift curve break occurs. Comparison of the lift coefficient results from Test 540 with those of Test 541 (MA-SC-1 wing, lower fuselage fairing not installed) shows that the lift curve break did not occur when the fuselage lower surface fairing was absent at a Reynolds number of 40,000 (compare fig. 10(a) with 12(a) or 14(a)).

MA-SC-1. The MA-SC-1 wing configuration with and without the 15 percent chord upper surface bump (with $\delta_f = 0°$) was tested at three Reynolds numbers and with flap deflections at Reynolds numbers of 40,000 and 60,000. At a Reynolds number of 40,000 the bump ($\delta_f = 0°$) was effective in increasing lift by a moderate amount at angles of attack between 0° and 9° at Mach numbers from 0.50 to 0.80 (e.g. figs. 83(a) and 85(a)). The portion of the wing upper surface flow field affected at these Mach numbers and angles of attack by addition of the bump is shown by comparison of the pressure coefficients of figures 101(a) through (d) with figures 103(a) through (d), respectively. At the high angles of attack, above approximately 9°, the bump, as planned, has no significant effect on the wing upper surface flow. At Mach numbers 0.85 and 0.90 the increase in lift coefficient due to addition of the bump was insignificant and the pressure coefficient distributions were similar (compare the data of figures 101(e) and (f) with figures 103(e) and (f), respectively). At a Reynolds number of 60,000 the lift coefficient was also increased by addition of the bump by a moderate amount between angles of attack of about -2° and 6° at Mach numbers 0.65 and 0.80 (figs. 87(a) and 89(a)) and the pressure coefficient data (figs. 107 and 109) show the affected portion of the wing. At a Reynolds number of 100,000 the addition of the bump increased lift coefficient at angles of attack from –10° up to at least 4° at Mach numbers 0.65 and 0.80 (figs. 91(a) and 92(a)), with changes in pressure occurring in the vicinity of the bump (figs. 113 and 114). Variation of sideslip angle at constant angle of attack had only a small effect on the pressure distributions ($\delta_f = 0°$) at Reynolds numbers of 40,000 and 60,000 at Mach numbers of 0.65 and 0.80 (figs 106 and 112).

The model was tested with the right wing flap deflected at Mach numbers of 0.65 and 0.80 at Reynolds numbers of 40,000 and 60,000 with

the bump on. At both Reynolds numbers flap deflection increased the pressure on the lower surface of the wing caused a slight decrease in pressure on the upper surface (figs. 102 through 105 and 108); and produced positive lift increments for positive flap deflections over most of the angle of attack range (figs. 60(a) to 63(a)). It should be remembered that since only the right wing flap was deflected any longitudinal aerodynamic coefficient change indicated due to flap deflection should be doubled.

MA-SF-1. The MA-SF-1 wing configuration, expected to obtain a higher maximum lift coefficient with deflected split trailing-edge flaps, was tested at three Reynolds numbers with the flaps deflected up to 30° (figs. 115 through 123). At a Reynolds number of 40,000 Mach number was varied from 0.50 to 0.90 for flap deflections of 0°, 10°, and 30° while at the two higher Reynolds numbers only Mach numbers of 0.65 and 0.80 were investigated. Deflection of the flaps increased the pressure on the lower surface of the wing aft of about the 30 percent chord at all Mach and Reynolds numbers producing large increases in lift coefficient (figs. 64(a) through 73(a)). The increase in lower surface pressure on the aft portion of the wing produced a stabilizing pitching-moment increment (since most of the affected wing area was aft of the moment reference center) and this resulted in a large shift in the trim point with flap deflection. As Mach number was increased the leading edge negative pressure coefficient peak decreased and the upper surface flow separated at lower angles of attack regardless of flap deflection (e.g. figs. 115, 116, or 117). As Reynolds number was increased, at a given Mach number and flap deflection angle, the forward portion of the wing sustained higher pressure peaks (e.g. compare figs. 115(b) and 121(a)) and higher lift coefficients were obtained (figs. 65(a) and 73 (a)).

MA-SC-1t. The swept wing configuration (MA-SC-1t) was tested in the longitudinal plane at all three Reynolds numbers with the bump on. At a Reynolds number of 40,000 the model was tested at Mach numbers from 0.50 to 0.90 in the longitudinal plane and over a sideslip angle range at Reynolds numbers of 40,000 and 60,000 at Mach numbers 0.65 and 0.80. At a Reynolds number of 40,000 the angle of attack for wing upper surface flow separation was about 16° from Mach number 0.65 to 0.85 (figs. 124(b) through (e)). At a Mach number of 0.65 the lowest angle of attack at which the flow on the wing upper surface was separated decreased from 16° at 40,000 Reynolds number to 10° at 100,000 Reynolds number (figs. 124(b) and 128(a)). However, at a Mach number of 0.80 the upper surface flow was separated at 8° angle of attack at a Reynolds number of 60,000 (fig. 126(b)) while at a Reynolds number of 100,000 it was not separated until 12° angle of attack (fig. 128(b)).

As indicated in the discussion on the effect of sideslip on the aerodynamic characteristics of the model with the swept wing, the rolling-moment coefficient and pressure data indicate that at Mach number 0.65 at a Reynolds number of 60,000 the windward wing separates at 10° angle of attack and extra aerodynamic data taken indicate that there is separation hysteresis dependent on how the zero degrees sideslip angle is approached. At a Mach number of 0.80 (fig. 127(b)) the initial 0° sideslip angle data at 10° angle of attack also indicates that the upper surface flow is separated while the midsweep and final 0° sideslip pressure data does not indicate separation. This hysteresis effect is not shown in the rolling moment data of figure 82(a) since only the midsweep $\beta = 0°$ force balance data are presented, however the rolling-moment coefficient data for that point are offset from zero by a large amount indicating flow separation on one wing panel.

Concluding Remarks

An investigation of the aerodynamic characteristics of a 1/4-scale model of an airplane designed to cruise in the Mars atmosphere has been conducted in the Langley Research Center Transonic Dynamics Tunnel. The tests were conducted at Mach numbers from 0.50 to 0.90 and at Reynolds numbers of 40,000, 60,000, and 100,000. The model configurations included unswept wings with three different airfoil sections and a swept wing having the same airfoil section as one of the unswept wings. Aerodynamic force and moment and wing pressure data were obtained to show the effects of angle of attack and sideslip, tails, tail location, horizontal tail incidence, wing flaps, and a wing upper surface flow transition bump. The investigation has led to the following conclusions.

Lift coefficient at a given angle of attack increased with Reynolds number and a break in the lift curve at low angles of attack lessened in severity, or disappeared completely with increasing Reynolds number. When the lower fuselage fairing was removed and the tails inverted the break in the lift curve did not occur and there was a beneficial rotation of the drag polar with increasing Reynolds number. Unswept wing configurations were either marginally stable longitudinally or unstable over the angle of attack range with stability only slightly affected by Reynolds number changes. The swept wing configuration was longitudinally stable and trimmed at low positive lift coefficients.

Lift coefficient decreased with increasing Mach number in the angle of attack range from –6° to 10°. At a Reynolds number of 40,000 the break in the lift curve that occurred at Mach number 0.65 for the model with the unswept wing diminished as Mach number increased. The lift curve slope for the configuration with the swept wing decreased with increasing Mach number at lift coefficients below that for the break in the lift curve, and minimum drag coefficient and drag due to lift generally increased with Mach number. The effect of increasing Mach number on longitudinal stability for both unswept and swept wing configurations was small and consisted of a stabilizing effect over most of the lift coefficient range.

Increasing horizontal tail incidence on an unswept wing configuration increased lift coefficient at angles of attack below that for the break in the lift curve. Above the break in the lift curve lift coefficient was nearly constant for all tail incidences. The break in the lift curve was weaker but still present with the tails removed. When the lower fuselage fairing was removed and the tails inverted and mounted from beneath the wing the break in the lift curve disappeared and lift increased with horizontal tail incidence over the angle of attack range. Horizontal tail pitch effectiveness for the model with the tails in the upright position was greatly reduced above the break in the lift curve. With the lower fuselage fairing removed and the tails inverted and mounted from beneath the wing the break in the lift curve disappeared and pitch effectiveness was maintained up to a lift coefficient of about 0.8.

Downward deflection of trailing-edge split flaps on an unswept wing configuration had a stabilizing effect on the model at negative and low positive lift coefficients. Increasing flap deflection shifted the pitching-moment curves downward at moderate positive lift coefficients.

An unswept wing configuration with tails on was stable in the lateral-directional plane over the sideslip angle range from –10° to 10° at Mach numbers 0.65 and 0.80 and Reynolds numbers of 40,000 and 60,000. The swept wing configuration was also stable in the lateral-directional plane but at 10° angle of attack experienced wing upper surface flow separation hysteresis in sideslip on the windward wing at a Mach number of 0.65 and a Reynolds number of 60,000.

References

1. Campbell, R.: *Efficient Viscous Design of Realistic Aircraft Configurations,* AIAA Paper 98-2539.

2. Drela, M.: *Design and Optimization Method for Multi-Element Airfoils,* AIAA Paper 93-0969.

3. Anderson, W.; and Bonhaus D.: *An Implicit Upwind Algorithm for Computing Turbulent Flows on Unstructured Grids,* Computers and Fluids, Vol. 23, 1994, pp. 1-21.

4. Anderson, W.; and Bonhaus D.: *Aerodynamic Design on Unstructured Grids for Turbulent Flows,* NASA Technical Memorandum 112867, June, 1997

Table 1. Model Pressure Orifice Locations

Eppler 387 and MA-SC-1 wing outer panel orifice locations

Upper surface		Lower surface	
x/c	BL/(b/2)	x/c	BL/(b/2)
0	0.667	0.01	0.679
.01	.655	.02	.690
.02	.643	.03	.702
.03	.632	.05	.667
.05	.667	.10	↓
.10	↓	.20	
.20		.30	
.30		.40	
.40		.50	
.50		.60	↓
.60		.70	.655
.70		.80	↓
.80		.90	
.90			
.95	↓		

MA-SF-1 wing outer panel orifice locations

Right wing		Left wing	
Upper surface		Lower surface	
x/c	BL/(b/2)	x/c	BL/(b/2)
0	0.667	0.01	0.655
.01	.655	.02	.643
.02	.643	.03	.632
.03	.667	.05	.667
.05	↓	.10	↓
.10		.20	
.20		.30	
.30		.40	
.40		.50	
.50		.60	
.60		.70	
.70		.80	
.80		.90	↓
.90			
.95	↓		

MA-SC-1t wing outer panel pressure orifice locations

Upper surface		Lower surface	
x/c	BL/(b/2)	x/c	BL/(b/2)
0	0.540	0.0122	0.552
.0102	.526	.0215	.567
.0204	.513	.0306	.582
.0308	.499	.0481	.540
.0514	.540	.0969	↓
.1007	↓	.1998	
.2015		.2996	
.2999		.4013	
.4012		.4957	
.5003		.5946	↓
.6026		.7033	.552
.7015		.8001	.554
.8029		.8976	.554
.9000			
.9533	↓		

Pressure orifice locations on centerlines of wing lower surface and lower fuselage fairing

x/l	BL/(b/2)	Location
0	0	wing
.05	↓	wing
.10		fuselage fairing
.20		↓
.30		
.40		
.50		
.60		
.70		
.80		
.90		
.95	↓	↓

Table 2. Streamwise Outer Wing Panel Non-Dimensionalized Airfoil Ordinates

(a) Wing Configurations: Eppler 387, MA-SC-1, and MA-SC-1t

Eppler 387			MA-SC-1			MA-SC-1t		
	Upper surface	Lower surface		Upper surface	Lower surface		Upper surface	Lower surface
x/c	z/c	z/c	x/c	z/c	z/c	x/c	z/c	z/c
0.00000	0.0000000	0.0000000	0.00000	0.0420357	0.0420357	0.00000	0.0420357	0.0420357
0.00107	0.0034084	-0.0028322	0.00107	0.0461225	0.0364536	0.00107	0.0454790	0.0370971
0.00428	0.0081929	-0.0055322	0.00428	0.0497618	0.0331445	0.00428	0.0486558	0.0342505
0.00961	0.0132968	-0.0077293	0.00961	0.0532566	0.0305476	0.00961	0.0517452	0.0320590
0.01704	0.0191197	-0.0099203	0.01704	0.0566782	0.0282004	0.01704	0.0547829	0.0300957
0.02653	0.0252076	-0.0114917	0.02653	0.0600385	0.0260040	0.02653	0.0577733	0.0282692
0.03806	0.0310310	-0.0128569	0.03806	0.0633457	0.0239414	0.03806	0.0607232	0.0265639
0.05156	0.0367627	-0.0139416	0.05156	0.0665637	0.0220337	0.05156	0.0636000	0.0249974
0.06699	0.0424885	-0.0146232	0.06699	0.0696612	0.0203130	0.06699	0.0663768	0.0235974
0.08427	0.0480120	-0.0150100	0.08427	0.0725993	0.0188146	0.08427	0.0690197	0.0223942
0.10332	0.0533642	-0.0150730	0.10332	0.0753461	0.0175653	0.10332	0.0715005	0.0214109
0.12408	0.0584247	-0.0149019	0.12408	0.0778798	0.0165817	0.12408	0.0738001	0.0206614
0.14645	0.0630278	-0.0145405	0.14645	0.0801809	0.0158732	0.14645	0.0759009	0.0201532
0.17033	0.0672437	-0.0139533	0.17033	0.0822370	0.0154415	0.17033	0.0777914	0.0198871
0.19562	0.0711200	-0.0132117	0.19562	0.0840419	0.0152821	0.19562	0.0794656	0.0198584
0.22221	0.0745528	-0.0123303	0.22221	0.0855930	0.0153843	0.22221	0.0809203	0.0200570
0.25000	0.0774584	-0.0113299	0.25000	0.0868731	0.0157425	0.25000	0.0821390	0.0204766
0.27886	0.0797841	-0.0102509	0.27886	0.0878643	0.0163443	0.27886	0.0831043	0.0211043
0.30866	0.0814413	-0.0091149	0.30866	0.0885531	0.0171700	0.30866	0.0838022	0.0219209
0.33928	0.0823341	-0.0079451	0.33928	0.0889284	0.0181925	0.33928	0.0842206	0.0229003
0.37059	0.0824047	-0.0067774	0.37059	0.0889798	0.0193779	0.37000	0.0843475	0.0240102
0.40245	0.0816592	-0.0056067	0.40245	0.0886967	0.0206851	0.40200	0.0841702	0.0252116
0.43474	0.0801289	-0.0044466	0.43474	0.0880677	0.0220697	0.43400	0.0836752	0.0264622
0.46730	0.0778440	-0.0033131	0.46730	0.0870817	0.0234808	0.46700	0.0828488	0.0277137
0.50000	0.0749014	-0.0022565	0.50000	0.0857269	0.0248651	0.50000	0.0816763	0.0289157
0.53270	0.0714091	-0.0012893	0.53270	0.0839924	0.0261657	0.53200	0.0801437	0.0300143
0.56526	0.0674303	-0.0003958	0.56526	0.0818692	0.0273239	0.56500	0.0782389	0.0309542
0.59755	0.0631312	0.0004336	0.59755	0.0793504	0.0282809	0.59700	0.0759515	0.0316798
0.62941	0.0586289	0.0011751	0.62941	0.0764362	0.0289796	0.62941	0.0732777	0.0321381
0.66072	0.0540103	0.0017973	0.66072	0.0731291	0.0293693	0.66072	0.0702167	0.0322817
0.69134	0.0493381	0.0023103	0.69134	0.0694411	0.0294073	0.69134	0.0667767	0.0320717
0.72114	0.0446601	0.0027241	0.72114	0.0653921	0.0290634	0.72114	0.0629742	0.0314812
0.75000	0.0401147	0.0030430	0.75000	0.0610106	0.0283223	0.75000	0.0588350	0.0304979
0.77779	0.0357161	0.0032567	0.77779	0.0563376	0.0271866	0.77779	0.0543975	0.0291267
0.80438	0.0314387	0.0033583	0.80438	0.0514258	0.0256770	0.80438	0.0497121	0.0273907
0.82967	0.0273681	0.0033741	0.82967	0.0463339	0.0238313	0.82967	0.0448362	0.0253290
0.85355	0.0235242	0.0032916	0.85355	0.0411332	0.0217047	0.85355	0.0398401	0.0229978
0.87592	0.0199281	0.0031140	0.87592	0.0359018	0.0193638	0.87592	0.0348011	0.0204645
0.89668	0.0165964	0.0028440	0.89668	0.0307254	0.0168840	0.89668	0.0298042	0.0178052
0.91573	0.0135412	0.0025349	0.91573	0.0256956	0.0143470	0.91573	0.0249403	0.0151023
0.93301	0.0107741	0.0022374	0.93301	0.0208964	0.0118292	0.93301	0.0202929	0.0124327
0.94844	0.0083276	0.0019219	0.94844	0.0164175	0.0094066	0.94844	0.0159509	0.0098732
0.96194	0.0062416	0.0014819	0.96194	0.0123467	0.0071516	0.96194	0.0120009	0.0074974
0.97347	0.0045463	0.0008941	0.97347	0.0087561	0.0051242	0.97347	0.0085144	0.0053659
0.98296	0.0031955	0.0003033	0.98296	0.0057228	0.0033850	0.98296	0.0055672	0.0035406
0.99039	0.0021575	-0.0002059	0.99039	0.0032843	0.0019646	0.99039	0.0031965	0.0020524
0.99572	0.0014198	-0.0005876	0.99572	0.0014885	0.0009003	0.99572	0.0014494	0.0009394
0.99893	0.0009773	-0.0008216	0.99893	0.0003782	0.0002299	0.99893	0.0003683	0.0002398
1.00000	0.0008300	-0.0009000	1.00000	0.0000000	0.0000000	1.00000	0.0000000	0.0000000

Table 2. Concluded

(b) Wing Configuration MA-SF-1

MA-SF-1		0° flaps	10° flaps	30° flaps
	Upper surface	Lower surface	Lower surface	Lower surface
x/c	z/c	z/c	z/c	z/c
0.00000	0.0012120	0.0012120		
0.00107	0.0034344	-0.0015459		
0.00428	0.0063922	-0.0029669		
0.00961	0.0094444	-0.0038820		
0.01704	0.0126613	-0.0044308		
0.02653	0.0159256	-0.0045979		
0.03806	0.0192885	-0.0045236		
0.05156	0.0227393	-0.0043112		
0.06699	0.0262612	-0.0040290		
0.08427	0.0297763	-0.0036794		
0.10332	0.0332327	-0.0032596		
0.12408	0.0366172	-0.0028063		
0.14645	0.0398922	-0.0023431		
0.17033	0.0430203	-0.0018789		
0.19562	0.0459714	-0.0014298		
0.22200	0.0487116	-0.0010041		
0.25000	0.0512150	-0.0006182		
0.27800	0.0534553	-0.0002842		
0.30800	0.0554078	-0.0000172		
0.33900	0.0570473	0.0001712		
0.37059	0.0583364	0.0002781		
0.40245	0.0592503	0.0002848		
0.43474	0.0597682	0.0001661		
0.46730	0.0598463	-0.0001030		
0.50000	0.0594093	-0.0005711		
0.53270	0.0583470	-0.0013549		
0.56526	0.0567849	-0.0022904		
0.59755	0.0547970	-0.0032729		
0.62941	0.0524349	-0.0042291		
0.66072	0.0497362	-0.0050980		
0.69134	0.0467337	-0.0058216		
0.72114	0.0434154	-0.0063035		
0.75000	0.0397600	-0.0064592		
0.77779	0.0357915	-0.0062569	-0.0062569	-0.0062569
0.80438	0.0316181	-0.0057734	-0.0067587	-0.0109333
0.82967	0.0274499	-0.0051623	-0.0105777	-0.0246582
0.85355	0.0234075	-0.0044807	-0.0140699	-0.0374373
0.87592	0.0195201	-0.0037227	-0.0172145	-0.0492285
0.89668	0.0158371	-0.0029141	-0.0200281	-0.0600623
0.91573	0.0124342	-0.0021052	-0.0225519	-0.0700062
0.93301	0.0093832	-0.0013577	-0.0248404	-0.0791745
0.94844	0.0067610	-0.0007344	-0.0269474	-0.0876268
0.96194	0.0046080	-0.0002745	-0.0289016	-0.0953936
0.96659	-	-	-	-0.0982269
0.97347	0.0029303	0.0000122	-0.0306933	-
0.98296	0.0016883	0.0001540	-0.0322847	-
0.98320	-	-	-	-0.0490000
0.99039	0.0008412	0.0001736	-0.0336649	-
0.99466	-	-	-0.0345284	-
0.99490	-	-	-0.0174000	-
0.99572	0.0003373	0.0001066	-	-
0.99893	0.0000798	0.0000301	0.0000301	0.0000301
1.00000	0.0000000	0.0000000	0.0000000	0.0000000

Table 3. Measured Longitudinal Coordinates of the Body-Eppler Wing Combination

1. BL = 0.0, 0.35, 0.70, and 1.05

BL = 0.0			
Upper surface		Lower surface	
MS	WL	MS	WL
-0.4247	-0.4108	-0.4238	-0.4173
-0.4243	-0.4040	-0.4217	-0.4235
-0.4227	-0.3969	-0.4184	-0.4295
-0.4198	-0.3894	-0.4139	-0.4352
-0.4156	-0.3817	-0.4081	-0.4407
-0.4102	-0.3736	-0.4012	-0.4459
-0.3954	-0.3565	-0.3931	-0.4508
-0.3753	-0.3379	-0.3735	-0.4601
-0.3498	-0.3178	-0.3493	-0.4685
-0.3189	-0.2961	-0.3206	-0.4761
-0.2503	-0.2146	-0.2875	-0.4831
-0.1808	-0.1367	-0.2501	-0.4894
-0.1102	-0.0623	-0.2085	-0.4952
-0.0386	0.0087	0.0441	-0.5979
0.0340	0.0764	0.1700	-0.6479
0.1077	0.1408	0.3396	-0.7140
0.1824	0.2020	0.4847	-0.7696
0.2582	0.2601	0.8236	-0.8974
0.3350	0.3151	1.0199	-0.9706
0.4128	0.3672	1.3339	-1.0864
0.4917	0.4164	1.5162	-1.1527
0.5717	0.4628	1.7831	-1.2479
0.6526	0.5064	1.9733	-1.3138
0.7345	0.5473	2.0240	-1.3308
0.8174	0.5856	2.1610	-1.3750
0.9013	0.6214	2.2477	-1.4007
0.9861	0.6547	2.3350	-1.4243
1.0719	0.6855	2.3789	-1.4350
1.1585	0.7141	2.4229	-1.4449
1.2460	0.7404	2.4843	-1.4573
1.3343	0.7645	2.5459	-1.4679
1.4235	0.7865	2.6079	-1.4766
1.5134	0.8064	2.6701	-1.4832
1.6041	0.8244	2.7234	-1.4872
1.6955	0.8404	2.7768	-1.4896
1.7876	0.8546	2.8303	-1.4904
1.8804	0.8670	2.8839	-1.4895
1.9737	0.8777	2.9531	-1.4861
2.0677	0.8868	3.0222	-1.4803
2.1622	0.8943	3.0911	-1.4722
2.2572	0.9003	3.1598	-1.4622
2.3528	0.9048	3.2267	-1.4507
2.4487	0.9080	3.2932	-1.4374
2.5451	0.9099	3.3594	-1.4224
2.6419	0.9105	3.4251	-1.4055
2.7390	0.9100	3.4860	-1.3880
2.8364	0.9084	3.5466	-1.3690
2.9341	0.9057	3.6068	-1.3488
3.0320	0.9020	3.6666	-1.3276
3.1301	0.8975	3.7718	-1.2880
3.3268	0.8858	3.8764	-1.2461
3.5238	0.8713	3.9808	-1.2023
3.7207	0.8543	4.1459	-1.1300
3.9173	0.8352	4.4098	-1.0121
4.1132	0.8145	4.5745	-0.9400
4.3081	0.7926	4.8757	-0.8111
4.6928	0.7465	5.1142	-0.7107
5.0680	0.6993	5.3895	-0.5960
5.4292	0.6523		

BL = 0.35			
Upper surface		Lower surface	
MS	WL	MS	WL
-0.3724	-0.4155	-0.3711	-0.4224
-0.3722	-0.4081	-0.3686	-0.4289
-0.3705	-0.4002	-0.3648	-0.4349
-0.3673	-0.3918	-0.3599	-0.4406
-0.3624	-0.3828	-0.3538	-0.4458
-0.3558	-0.3733	-0.3389	-0.4552
-0.3474	-0.3632	-0.3206	-0.4633
-0.3371	-0.3525	-0.2995	-0.4702
-0.3249	-0.3411	-0.2765	-0.4762
-0.3106	-0.3291	-0.2267	-0.4859
-0.2713	-0.2627	-0.1765	-0.4938
-0.2634	-0.2477	-0.1504	-0.5136
-0.2517	-0.2314	-0.1324	-0.5252
-0.2377	-0.2144	-0.1078	-0.5385
-0.2227	-0.1976	-0.0821	-0.5503
-0.1665	-0.1382	0.1296	-0.6350
-0.0529	-0.0257	0.1520	-0.6432
0.0083	0.0322	0.2890	-0.6932
0.0558	0.0744	0.5613	-0.7953
0.1042	0.1154	0.7197	-0.8535
0.1534	0.1555	1.5848	-1.1688
0.2464	0.2292	1.6644	-1.1975
0.3343	0.2958	1.8307	-1.2561
0.3789	0.3279	2.0048	-1.3149
0.4342	0.3655	2.0923	-1.3431
0.4903	0.4015	2.1795	-1.3699
0.5474	0.4361	2.2672	-1.3951
0.6054	0.4695	2.3554	-1.4182
0.6616	0.5003	2.4444	-1.4387
0.7187	0.5299	2.4913	-1.4482
0.7765	0.5580	2.5384	-1.4567
0.8351	0.5845	2.5857	-1.4641
0.8904	0.6074	2.6331	-1.4705
0.9461	0.6289	2.6806	-1.4755
1.0023	0.6491	2.7283	-1.4792
1.0587	0.6683	2.7760	-1.4814
1.1424	0.6952	2.8237	-1.4821
1.2264	0.7204	2.8915	-1.4803
1.3110	0.7438	2.9592	-1.4757
1.3964	0.7654	3.0268	-1.4691
1.4636	0.7810	3.0944	-1.4609
1.5311	0.7954	3.1651	-1.4513
1.5990	0.8087	3.2355	-1.4400
1.6669	0.8209	3.3054	-1.4268
1.7623	0.8361	3.3746	-1.4109
1.8578	0.8492	3.4123	-1.4009
1.9534	0.8604	3.4498	-1.3901
2.0494	0.8701	3.5241	-1.3662
2.1412	0.8780	3.5977	-1.3402
2.2334	0.8845	3.6709	-1.3128
2.3258	0.8899	3.7726	-1.2734
2.4909	0.8963	3.8737	-1.2329
2.6362	0.8987	3.9745	-1.1915
2.7910	0.8983	4.0749	-1.1492
2.8732	0.8968	4.2127	-1.0899
2.9552	0.8946	4.6255	-0.9094
3.0373	0.8915	4.8558	-0.8116
3.3667	0.8714	5.0874	-0.7166
3.5863	0.8522	5.3164	-0.6247
3.8060	0.8302	5.3940	-0.5928
3.9759	0.8122		
4.2610	0.7807		
4.4926	0.7540		
4.8226	0.7152		
5.2324	0.6655		
5.4461	0.6370		

BL = 0.70			
Upper surface		Lower surface	
MS	WL	MS	WL
-0.3211	-0.4095	-0.3207	-0.4165
-0.3204	-0.4022	-0.3190	-0.4232
-0.3183	-0.3945	-0.3162	-0.4296
-0.3150	-0.3865	-0.3123	-0.4357
-0.3102	-0.3782	-0.3073	-0.4414
-0.3040	-0.3695	-0.2944	-0.4520
-0.2964	-0.3605	-0.2778	-0.4615
-0.2873	-0.3512	-0.2580	-0.4697
-0.2643	-0.3315	-0.2352	-0.4768
-0.2347	-0.3103	-0.2098	-0.4828
-0.1981	-0.2877	-0.1823	-0.4877
-0.1843	-0.2498	-0.1529	-0.4916
-0.1681	-0.2202	-0.1421	-0.5028
-0.1574	-0.2055	-0.1339	-0.5093
-0.1152	-0.1555	-0.0956	-0.5309
-0.0837	-0.1207	-0.0532	-0.5483
-0.0515	-0.0868	0.0435	-0.5847
-0.0187	-0.0538	0.1478	-0.6229
0.0149	-0.0216	0.4761	-0.7407
0.0489	0.0099	0.6027	-0.7853
0.1186	0.0710	1.1274	-0.9681
0.1855	0.1263	1.4024	-1.0630
0.2538	0.1799	1.8507	-1.2165
0.3234	0.2318	2.0092	-1.2690
0.3943	0.2821	2.0889	-1.2940
0.4432	0.3155	2.1631	-1.3161
0.4928	0.3482	2.2378	-1.3369
0.5936	0.4107	2.3129	-1.3562
0.6449	0.4404	2.3886	-1.3737
0.6968	0.4691	2.4373	-1.3838
0.7493	0.4965	2.4862	-1.3930
0.8025	0.5226	2.5352	-1.4013
0.8688	0.5530	2.5845	-1.4084
0.9360	0.5813	2.6338	-1.4144
1.0040	0.6078	2.6833	-1.4192
1.0727	0.6325	2.7329	-1.4226
1.1419	0.6554	2.7825	-1.4247
1.2117	0.6767	2.8279	-1.4253
1.2819	0.6964	2.8733	-1.4248
1.3524	0.7147	2.9187	-1.4231
1.4475	0.7372	2.9640	-1.4204
1.5430	0.7573	3.0093	-1.4168
1.6389	0.7751	3.0546	-1.4122
1.7351	0.7909	3.1448	-1.4006
1.8317	0.8046	3.1979	-1.3924
1.9287	0.8165	3.2509	-1.3831
2.0261	0.8267	3.3036	-1.3729
2.1238	0.8353	3.3560	-1.3616
2.2552	0.8444	3.4082	-1.3493
2.3871	0.8510	3.4602	-1.3361
2.5191	0.8553	3.5119	-1.3218
2.6511	0.8575	3.5632	-1.3066
2.7766	0.8578	3.6271	-1.2860
2.9020	0.8563	3.6906	-1.2641
3.0272	0.8529	3.7536	-1.2410
3.1522	0.8478	3.8162	-1.2168
3.2702	0.8412	3.9406	-1.1659
3.3880	0.8331	4.1373	-1.0809
3.5057	0.8236	4.3564	-0.9849
3.6233	0.8127	4.5493	-0.9030
3.7408	0.8007	4.7432	-0.8241
3.9748	0.7743	4.9045	-0.7611
4.4617	0.7151	5.1051	-0.6858
4.9714	0.6502	5.2596	-0.6282
5.2456	0.6131	5.3124	-0.6076
5.3823	0.5931	5.3456	-0.5943

BL = 1.05			
Upper surface		Lower surface	
MS	WL	MS	WL
-0.2189	-0.4094	-0.2167	-0.4195
-0.2183	-0.3987	-0.2119	-0.4291
-0.2150	-0.3877	-0.2043	-0.4382
-0.2089	-0.3761	-0.1941	-0.4468
-0.2001	-0.3642	-0.1811	-0.4547
-0.1885	-0.3518	-0.1655	-0.4621
-0.1741	-0.3391	-0.1473	-0.4689
-0.1568	-0.3260	-0.1264	-0.4751
-0.1139	-0.2988	-0.1029	-0.4806
-0.0597	-0.2704	-0.0768	-0.4854
0.0061	-0.2409	-0.0481	-0.4895
0.0834	-0.2106	-0.0168	-0.4930
0.1265	-0.1951	0.0170	-0.4957
0.1704	-0.1614	0.0534	-0.4976
0.1714	-0.1436	0.0924	-0.4988
0.1735	-0.1332	0.1140	-0.5178
0.1808	-0.1131	0.1313	-0.5290
0.1940	-0.0929	0.1497	-0.5381
0.2438	-0.0373	0.1715	-0.5469
0.2856	0.0071	0.2163	-0.5617
0.3286	0.0504	0.2969	-0.5872
0.3729	0.0922	0.4931	-0.6527
0.4309	0.1428	0.6933	-0.7177
0.4910	0.1910	1.4113	-0.9491
0.5529	0.2371	1.5867	-1.0047
0.6162	0.2813	1.8125	-1.0755
0.6712	0.3177	1.9489	-1.1175
0.7839	0.3860	2.0859	-1.1582
0.8418	0.4175	2.2004	-1.1901
0.8887	0.4410	2.2579	-1.2050
0.9846	0.4843	2.3156	-1.2189
1.0825	0.5229	2.4068	-1.2384
1.1822	0.5572	2.4984	-1.2549
1.2873	0.5889	2.5711	-1.2657
1.3978	0.6181	2.6441	-1.2744
1.4533	0.6312	2.6922	-1.2789
1.5650	0.6550	2.7404	-1.2824
1.6773	0.6757	2.7886	-1.2849
1.7957	0.6945	2.8369	-1.2863
1.9146	0.7105	2.8991	-1.2867
2.0339	0.7239	2.9612	-1.2853
2.1533	0.7349	3.0233	-1.2822
2.2450	0.7418	3.0852	-1.2774
2.3367	0.7475	3.1350	-1.2723
2.4285	0.7521	3.1846	-1.2662
2.5203	0.7554	3.2834	-1.2508
2.6122	0.7577	3.3843	-1.2310
2.7041	0.7589	3.4844	-1.2072
2.7960	0.7591	3.5993	-1.1747
2.8879	0.7582	3.7127	-1.1372
3.0288	0.7550	3.8546	-1.0827
3.1695	0.7495	3.9248	-1.0534
3.3101	0.7413	4.0563	-0.9956
3.4506	0.7304	4.3480	-0.8619
3.5650	0.7193	4.4549	-0.8120
3.6792	0.7063	4.6777	-0.7064
3.7932	0.6915	4.7195	-0.6846
4.0237	0.6560	4.7600	-0.6609
4.2567	0.6171	4.7883	-0.6420
4.3735	0.5992	4.8151	-0.6213
4.6556	0.5610	4.8399	-0.5979
4.7972	0.5386	4.8624	-0.5716
4.9382	0.5130	4.8726	-0.5567
5.1089	0.4780	4.8854	-0.5336
5.1939	0.4589	5.0714	-0.5459
5.2787	0.4387	5.2610	-0.5570

Table 3. Continued

(b) BL = 1.4, 1.75 2.00, and 2.272

BL = 1.40			
Upper surface		Lower surface	
MS	WL	MS	WL
0.1693	-0.3681	0.1712	-0.3769
0.1701	-0.3601	0.1758	-0.3850
0.1730	-0.3517	0.1826	-0.3924
0.1840	-0.3346	0.1915	-0.3991
0.1998	-0.3177	0.2019	-0.4052
0.2176	-0.3021	0.2137	-0.4107
0.2388	-0.2859	0.2398	-0.4203
0.2595	-0.2724	0.2619	-0.4267
0.2997	-0.2499	0.2846	-0.4322
0.3564	-0.2218	0.3313	-0.4408
0.4141	-0.1972	0.3788	-0.4470
0.4807	-0.1742	0.4259	-0.4515
0.6298	-0.1322	0.5175	-0.4581
0.7908	-0.0955	0.6890	-0.4646
0.9506	-0.0666	0.8784	-0.4664
1.0711	-0.0492	0.9850	-0.4664
1.2384	-0.0308	1.2216	-0.4650
1.3418	-0.0007	1.4849	-0.4623
1.3424	-0.0228	1.7908	-0.4581
1.3440	0.0358	2.3520	-0.4495
1.3503	0.0640	2.3538	-0.4941
1.3595	0.0862	2.3555	-0.5107
1.3718	0.1060	2.3576	-0.5243
1.3948	0.1324	2.3602	-0.5355
1.4113	0.1471	2.3632	-0.5447
1.4452	0.1734	2.3703	-0.5597
1.4803	0.1977	2.3781	-0.5723
1.5375	0.2292	2.3867	-0.5841
1.6236	0.2663	2.4064	-0.6054
1.6678	0.2824	2.4286	-0.6240
1.7289	0.3020	2.4525	-0.6403
1.7883	0.3178	2.4994	-0.6657
1.8501	0.3311	2.5489	-0.6858
1.9126	0.3416	2.6002	-0.7017
1.9761	0.3498	2.6528	-0.7142
2.0409	0.3558	2.6863	-0.7207
2.1520	0.3621	2.7540	-0.7310
2.2542	0.3644	2.7880	-0.7349
2.3183	0.3642	2.8563	-0.7404
2.3820	0.3629	2.9251	-0.7433
2.5319	0.3561	2.9916	-0.7438
2.7074	0.3436	3.0582	-0.7423
2.8501	0.3305	3.1246	-0.7385
3.0120	0.3126	3.2454	-0.7258
3.1216	0.2981	3.3554	-0.7059
3.2304	0.2800	3.4549	-0.6784
3.3406	0.2563	3.4981	-0.6612
3.4505	0.2264	3.5192	-0.6507
3.5066	0.2081	3.5398	-0.6385
3.5335	0.1976	3.5598	-0.6244
3.5590	0.1858	3.5790	-0.6083
3.5841	0.1717	3.5910	-0.5964
3.6073	0.1560	3.6026	-0.5831
3.6489	0.1197	3.6136	-0.5679
3.6747	0.0902	3.6241	-0.5503
3.6983	0.0532	3.6338	-0.5299
3.7157	0.0155	3.6428	-0.5061
3.7296	-0.0250	3.6510	-0.4785
3.7361	-0.0517	3.6583	-0.4466
3.7362	-0.2353	3.9948	-0.4537
3.7400	-0.2055	4.1738	-0.4586
3.7403	-0.0777	4.5111	-0.4703
3.7424	-0.1782	4.7799	-0.4818
3.7436	-0.1527	4.9563	-0.4915
3.7437	-0.1278	5.1076	-0.5024
5.1621	-0.4928	5.1581	-0.5070

BL = 1.75			
Upper surface		Lower surface	
MS	WL	MS	WL
0.5615	-0.3184	0.5615	-0.3255
0.5630	-0.3124	0.5641	-0.3342
0.5657	-0.3073	0.5693	-0.3419
0.5690	-0.3025	0.5763	-0.3487
0.5836	-0.2861	0.5843	-0.3549
0.6021	-0.2696	0.5959	-0.3623
0.6222	-0.2543	0.6076	-0.3688
0.6538	-0.2333	0.6308	-0.3788
0.6740	-0.2218	0.6520	-0.3852
0.7073	-0.2052	0.6725	-0.3897
0.7310	-0.1946	0.7060	-0.3956
0.7794	-0.1755	0.7394	-0.4001
0.8231	-0.1604	0.8072	-0.4066
0.8671	-0.1463	0.9032	-0.4129
0.9616	-0.1188	0.9933	-0.4160
1.0304	-0.1014	1.0693	-0.4171
1.1050	-0.0850	1.1947	-0.4181
1.1808	-0.0706	1.4063	-0.4170
1.2577	-0.0581	2.3564	-0.4061
1.3690	-0.0431	2.5627	-0.4044
1.4418	-0.0349	2.9490	-0.4026
1.5140	-0.0277	3.0870	-0.4025
1.5864	-0.0214	3.3829	-0.4033
1.6926	-0.0139	3.6069	-0.4051
1.7991	-0.0083	3.7923	-0.4075
1.9092	-0.0045	3.9318	-0.4099
2.0193	-0.0029	4.1609	-0.4150
2.1443	-0.0035	4.3438	-0.4201
2.2779	-0.0072	4.5836	-0.4281
2.4042	-0.0134	4.6903	-0.4323
2.4727	-0.0179	4.8086	-0.4377
2.6090	-0.0294	4.9024	-0.4430
2.7571	-0.0452	4.9906	-0.4492
2.8958	-0.0628	5.0284	-0.4527
3.0063	-0.0783	5.0637	-0.4566
3.1168	-0.0951		
3.2125	-0.1102		
3.3737	-0.1370		
3.5697	-0.1708		
3.7601	-0.2044		
5.0637	-0.4382		

BL = 2.00			
Upper surface		Lower surface	
MS	WL	MS	WL
0.8192	-0.2994	0.8201	-0.3046
0.8201	-0.2951	0.8223	-0.3094
0.8224	-0.2905	0.8258	-0.3139
0.8307	-0.2810	0.8303	-0.3180
0.8420	-0.2714	0.8414	-0.3254
0.8684	-0.2514	0.8537	-0.3317
0.9051	-0.2252	0.8757	-0.3414
0.9365	-0.2058	0.8966	-0.3489
0.9694	-0.1879	0.9173	-0.3546
1.0035	-0.1717	0.9386	-0.3592
1.0383	-0.1571	0.9862	-0.3668
1.0853	-0.1399	1.0382	-0.3724
1.1329	-0.1250	1.0924	-0.3764
1.1811	-0.1119	1.1466	-0.3790
1.2298	-0.1003	1.2419	-0.3816
1.2874	-0.0879	1.4851	-0.3827
1.3455	-0.0768	1.7466	-0.3823
1.4623	-0.0571	1.9421	-0.3812
1.5668	-0.0414	2.3538	-0.3777
1.6713	-0.0276	2.5901	-0.3749
1.7538	-0.0181	3.0577	-0.3687
1.8365	-0.0102	3.2036	-0.3676
1.9193	-0.0041	3.4758	-0.3669
2.0022	0.0000	3.6002	-0.3672
2.0772	0.0018	3.8400	-0.3691
2.1522	0.0020	4.0127	-0.3728
2.2272	0.0013	4.1261	-0.3764
2.3707	-0.0014	4.3781	-0.3856
2.5079	-0.0057	4.5902	-0.3945
2.5764	-0.0091	4.7537	-0.4020
2.6598	-0.0149	4.8465	-0.4072
2.7431	-0.0223	4.9217	-0.4122
2.8263	-0.0311	4.9972	-0.4180
2.9704	-0.0489		
3.1534	-0.0751		
3.3380	-0.1046		
3.5223	-0.1360		
3.8788	-0.1995		
4.3156	-0.2808		
4.3649	-0.2895		
4.5128	-0.3150		
4.8003	-0.3636		
4.9972	-0.3987		

BL = 2.272			
Upper surface		Lower surface	
MS	WL	MS	WL
1.1427	-0.2665	1.1431	-0.2723
1.1437	-0.2553	1.1444	-0.2775
1.1470	-0.2466	1.1465	-0.2821
1.1519	-0.2397	1.1492	-0.2863
1.1579	-0.2336	1.1565	-0.2934
1.1747	-0.2196	1.1654	-0.2994
1.1940	-0.2061	1.1802	-0.3067
1.2154	-0.1933	1.1967	-0.3127
1.2383	-0.1812	1.2146	-0.3176
1.2623	-0.1696	1.2336	-0.3216
1.2870	-0.1587	1.2732	-0.3274
1.3366	-0.1389	1.3482	-0.3341
1.3953	-0.1178	1.4450	-0.3399
1.4511	-0.1002	1.5479	-0.3434
1.5050	-0.0854	1.6254	-0.3446
1.5582	-0.0728	1.7553	-0.3450
1.6117	-0.0618	1.9219	-0.3443
1.6657	-0.0522	2.1028	-0.3426
1.7199	-0.0437	2.3077	-0.3397
1.7742	-0.0361	2.4762	-0.3363
1.8410	-0.0277	2.7447	-0.3313
1.9078	-0.0203	2.8825	-0.3294
1.9748	-0.0138	3.1499	-0.3268
2.0418	-0.0081	3.2797	-0.3264
2.1564	-0.0005	3.4920	-0.3273
2.2712	0.0042	3.6408	-0.3288
2.3387	0.0057	3.7833	-0.3310
2.4063	0.0060	4.0259	-0.3359
2.4738	0.0054	4.1079	-0.3381
2.5413	0.0037	4.4003	-0.3479
2.6249	0.0002	4.7449	-0.3630
2.7085	-0.0048	4.8861	-0.3701
2.7920	-0.0112	4.9248	-0.3722
2.8754	-0.0189		
2.9633	-0.0285		
3.0511	-0.0393		
3.1388	-0.0511		
3.2263	-0.0639		
3.3936	-0.0900		
3.6160	-0.1269		
3.7823	-0.1552		
4.0373	-0.1998		
4.5312	-0.2888		
4.7961	-0.3332		
4.9248	-0.3563		

Table 3. Measured Longitudinal Coordinates of the Body-Eppler Wing Combination

1. BL = 0.0, 0.35, 0.70, and 1.05

BL = 0.0			
Upper surface		Lower surface	
MS	WL	MS	WL
-0.4247	-0.4108	-0.4238	-0.4173
-0.4243	-0.4040	-0.4217	-0.4235
-0.4227	-0.3969	-0.4184	-0.4295
-0.4198	-0.3894	-0.4139	-0.4352
-0.4156	-0.3817	-0.4081	-0.4407
-0.4102	-0.3736	-0.4012	-0.4459
-0.3954	-0.3565	-0.3931	-0.4508
-0.3753	-0.3379	-0.3735	-0.4601
-0.3498	-0.3178	-0.3493	-0.4685
-0.3189	-0.2961	-0.3206	-0.4761
-0.2503	-0.2146	-0.2875	-0.4831
-0.1808	-0.1367	-0.2501	-0.4894
-0.1102	-0.0623	-0.2085	-0.4952
-0.0386	0.0087	0.0441	-0.5979
0.0340	0.0764	0.1700	-0.6479
0.1077	0.1408	0.3396	-0.7140
0.1824	0.2020	0.4847	-0.7696
0.2582	0.2601	0.8236	-0.8974
0.3350	0.3151	1.0199	-0.9706
0.4128	0.3672	1.3339	-1.0864
0.4917	0.4164	1.5162	-1.1527
0.5717	0.4628	1.7831	-1.2479
0.6526	0.5064	1.9733	-1.3138
0.7345	0.5473	2.0240	-1.3308
0.8174	0.5856	2.1610	-1.3750
0.9013	0.6214	2.2477	-1.4007
0.9861	0.6547	2.3350	-1.4243
1.0719	0.6855	2.3789	-1.4350
1.1585	0.7141	2.4229	-1.4449
1.2460	0.7404	2.4843	-1.4573
1.3343	0.7645	2.5459	-1.4679
1.4235	0.7865	2.6079	-1.4766
1.5134	0.8064	2.6701	-1.4832
1.6041	0.8244	2.7234	-1.4872
1.6955	0.8404	2.7768	-1.4896
1.7876	0.8546	2.8303	-1.4904
1.8804	0.8670	2.8839	-1.4895
1.9737	0.8777	2.9531	-1.4861
2.0677	0.8868	3.0222	-1.4803
2.1622	0.8943	3.0911	-1.4722
2.2572	0.9003	3.1598	-1.4622
2.3528	0.9048	3.2267	-1.4507
2.4487	0.9080	3.2932	-1.4374
2.5451	0.9099	3.3594	-1.4224
2.6419	0.9105	3.4251	-1.4055
2.7390	0.9100	3.4860	-1.3880
2.8364	0.9084	3.5466	-1.3690
2.9341	0.9057	3.6068	-1.3488
3.0320	0.9020	3.6666	-1.3276
3.1301	0.8975	3.7718	-1.2880
3.3268	0.8858	3.8764	-1.2461
3.5238	0.8713	3.9808	-1.2023
3.7207	0.8543	4.1459	-1.1300
3.9173	0.8352	4.4098	-1.0121
4.1132	0.8145	4.5745	-0.9400
4.3081	0.7926	4.8757	-0.8111
4.6928	0.7465	5.1142	-0.7107
5.0680	0.6993	5.3895	-0.5960
5.4292	0.6523		

BL = 0.35			
Upper surface		Lower surface	
MS	WL	MS	WL
-0.3724	-0.4155	-0.3711	-0.4224
-0.3722	-0.4081	-0.3686	-0.4289
-0.3705	-0.4002	-0.3648	-0.4349
-0.3673	-0.3918	-0.3599	-0.4406
-0.3624	-0.3828	-0.3538	-0.4458
-0.3558	-0.3733	-0.3389	-0.4552
-0.3474	-0.3632	-0.3206	-0.4633
-0.3371	-0.3525	-0.2995	-0.4702
-0.3249	-0.3411	-0.2765	-0.4762
-0.3106	-0.3291	-0.2267	-0.4859
-0.2713	-0.2627	-0.1765	-0.4938
-0.2634	-0.2477	-0.1504	-0.5136
-0.2517	-0.2314	-0.1324	-0.5252
-0.2377	-0.2144	-0.1078	-0.5385
-0.2227	-0.1976	-0.0821	-0.5503
-0.1665	-0.1382	0.1296	-0.6350
-0.0529	-0.0257	0.1520	-0.6432
0.0083	0.0322	0.2890	-0.6932
0.0558	0.0744	0.5613	-0.7953
0.1042	0.1154	0.7197	-0.8535
0.1534	0.1555	1.5848	-1.1688
0.2464	0.2292	1.6644	-1.1975
0.3343	0.2958	1.8307	-1.2561
0.3789	0.3279	2.0048	-1.3149
0.4342	0.3655	2.0923	-1.3431
0.4903	0.4015	2.1795	-1.3699
0.5474	0.4361	2.2672	-1.3951
0.6054	0.4695	2.3554	-1.4182
0.6616	0.5003	2.4444	-1.4387
0.7187	0.5299	2.4913	-1.4482
0.7765	0.5580	2.5384	-1.4567
0.8351	0.5845	2.5857	-1.4641
0.8904	0.6074	2.6331	-1.4705
0.9461	0.6289	2.6806	-1.4755
1.0023	0.6491	2.7283	-1.4792
1.0587	0.6683	2.7760	-1.4814
1.1424	0.6952	2.8237	-1.4821
1.2264	0.7204	2.8915	-1.4803
1.3110	0.7438	2.9592	-1.4757
1.3964	0.7654	3.0268	-1.4691
1.4636	0.7810	3.0944	-1.4609
1.5311	0.7954	3.1651	-1.4513
1.5990	0.8087	3.2355	-1.4400
1.6669	0.8209	3.3054	-1.4268
1.7623	0.8361	3.3746	-1.4109
1.8578	0.8492	3.4123	-1.4009
1.9534	0.8604	3.4498	-1.3901
2.0494	0.8701	3.5241	-1.3662
2.1412	0.8780	3.5977	-1.3402
2.2334	0.8845	3.6709	-1.3128
2.3258	0.8899	3.7726	-1.2734
2.4909	0.8963	3.8737	-1.2329
2.6362	0.8987	3.9745	-1.1915
2.7910	0.8983	4.0749	-1.1492
2.8732	0.8968	4.2127	-1.0899
2.9552	0.8946	4.6255	-0.9094
3.0373	0.8915	4.8558	-0.8116
3.3667	0.8714	5.0874	-0.7166
3.5863	0.8522	5.3164	-0.6247
3.8060	0.8302	5.3940	-0.5928
3.9759	0.8122		
4.2610	0.7807		
4.4926	0.7540		
4.8226	0.7152		
5.2324	0.6655		
5.4461	0.6370		

BL = 0.70			
Upper surface		Lower surface	
MS	WL	MS	WL
-0.3211	-0.4095	-0.3207	-0.4165
-0.3204	-0.4022	-0.3190	-0.4232
-0.3183	-0.3945	-0.3162	-0.4296
-0.3150	-0.3865	-0.3123	-0.4357
-0.3102	-0.3782	-0.3073	-0.4414
-0.3040	-0.3695	-0.2944	-0.4520
-0.2964	-0.3605	-0.2778	-0.4615
-0.2873	-0.3512	-0.2580	-0.4697
-0.2643	-0.3315	-0.2352	-0.4768
-0.2347	-0.3103	-0.2098	-0.4828
-0.1981	-0.2877	-0.1823	-0.4877
-0.1843	-0.2498	-0.1529	-0.4916
-0.1681	-0.2202	-0.1421	-0.5028
-0.1574	-0.2055	-0.1339	-0.5093
-0.1152	-0.1555	-0.0956	-0.5309
-0.0837	-0.1207	-0.0532	-0.5483
-0.0515	-0.0868	0.0435	-0.5847
-0.0187	-0.0538	0.1478	-0.6229
0.0149	-0.0216	0.4761	-0.7407
0.0489	0.0099	0.6027	-0.7853
0.1186	0.0710	1.1274	-0.9681
0.1855	0.1263	1.4024	-1.0630
0.2538	0.1799	1.8507	-1.2165
0.3234	0.2318	2.0092	-1.2690
0.3943	0.2821	2.0889	-1.2940
0.4432	0.3155	2.1631	-1.3161
0.4928	0.3482	2.2378	-1.3369
0.5936	0.4107	2.3129	-1.3562
0.6449	0.4404	2.3886	-1.3737
0.6968	0.4691	2.4373	-1.3838
0.7493	0.4965	2.4862	-1.3930
0.8025	0.5226	2.5352	-1.4013
0.8688	0.5530	2.5845	-1.4084
0.9360	0.5813	2.6338	-1.4144
1.0040	0.6078	2.6833	-1.4192
1.0727	0.6325	2.7329	-1.4226
1.1419	0.6554	2.7825	-1.4247
1.2117	0.6767	2.8279	-1.4253
1.2819	0.6964	2.8733	-1.4248
1.3524	0.7147	2.9187	-1.4231
1.4475	0.7372	2.9640	-1.4204
1.5430	0.7573	3.0093	-1.4168
1.6389	0.7751	3.0546	-1.4122
1.7351	0.7909	3.1448	-1.4006
1.8317	0.8046	3.1979	-1.3924
1.9287	0.8165	3.2509	-1.3831
2.0261	0.8267	3.3036	-1.3729
2.1238	0.8353	3.3560	-1.3616
2.2552	0.8444	3.4082	-1.3493
2.3871	0.8510	3.4602	-1.3361
2.5191	0.8553	3.5119	-1.3218
2.6511	0.8575	3.5632	-1.3066
2.7766	0.8578	3.6271	-1.2860
2.9020	0.8563	3.6906	-1.2641
3.0272	0.8529	3.7536	-1.2410
3.1522	0.8478	3.8162	-1.2168
3.2702	0.8412	3.9406	-1.1659
3.3880	0.8331	4.1373	-1.0809
3.5057	0.8236	4.3564	-0.9849
3.6233	0.8127	4.5493	-0.9030
3.7408	0.8007	4.7432	-0.8241
3.9748	0.7743	4.9045	-0.7611
4.4617	0.7151	5.1051	-0.6858
4.9714	0.6502	5.2596	-0.6282
5.2456	0.6131	5.3124	-0.6076
5.3823	0.5931	5.3456	-0.5943

BL = 1.05			
Upper surface		Lower surface	
MS	WL	MS	WL
-0.2189	-0.4094	-0.2167	-0.4195
-0.2183	-0.3987	-0.2119	-0.4291
-0.2150	-0.3877	-0.2043	-0.4382
-0.2089	-0.3761	-0.1941	-0.4468
-0.2001	-0.3642	-0.1811	-0.4547
-0.1885	-0.3518	-0.1655	-0.4621
-0.1741	-0.3391	-0.1473	-0.4689
-0.1568	-0.3260	-0.1264	-0.4751
-0.1139	-0.2988	-0.1029	-0.4806
-0.0597	-0.2704	-0.0768	-0.4854
0.0061	-0.2409	-0.0481	-0.4895
0.0834	-0.2106	-0.0168	-0.4930
0.1265	-0.1951	0.0170	-0.4957
0.1704	-0.1614	0.0534	-0.4976
0.1714	-0.1436	0.0924	-0.4988
0.1735	-0.1332	0.1140	-0.5178
0.1808	-0.1131	0.1313	-0.5290
0.1940	-0.0929	0.1497	-0.5381
0.2438	-0.0373	0.1715	-0.5469
0.2856	0.0071	0.2163	-0.5617
0.3286	0.0504	0.2969	-0.5872
0.3729	0.0922	0.4931	-0.6527
0.4309	0.1428	0.6933	-0.7177
0.4910	0.1910	1.4113	-0.9491
0.5529	0.2371	1.5867	-1.0047
0.6162	0.2813	1.8125	-1.0755
0.6712	0.3177	1.9489	-1.1175
0.7839	0.3860	2.0859	-1.1582
0.8418	0.4175	2.2004	-1.1901
0.8887	0.4410	2.2579	-1.2050
0.9846	0.4843	2.3156	-1.2189
1.0825	0.5229	2.4068	-1.2384
1.1822	0.5572	2.4984	-1.2549
1.2873	0.5889	2.5711	-1.2657
1.3978	0.6181	2.6441	-1.2744
1.4533	0.6312	2.6922	-1.2789
1.5650	0.6550	2.7404	-1.2824
1.6773	0.6757	2.7886	-1.2849
1.7957	0.6945	2.8369	-1.2863
1.9146	0.7105	2.8991	-1.2867
2.0339	0.7239	2.9612	-1.2853
2.1533	0.7349	3.0233	-1.2822
2.2450	0.7418	3.0852	-1.2774
2.3367	0.7475	3.1350	-1.2723
2.4285	0.7521	3.1846	-1.2662
2.5203	0.7554	3.2834	-1.2508
2.6122	0.7577	3.3843	-1.2310
2.7041	0.7589	3.4844	-1.2072
2.7960	0.7591	3.5993	-1.1747
2.8879	0.7582	3.7127	-1.1372
3.0288	0.7550	3.8546	-1.0827
3.1695	0.7495	3.9248	-1.0534
3.3101	0.7413	4.0563	-0.9956
3.4506	0.7304	4.3480	-0.8619
3.5650	0.7193	4.4549	-0.8120
3.6792	0.7063	4.6777	-0.7064
3.7932	0.6915	4.7195	-0.6846
4.0237	0.6560	4.7600	-0.6609
4.2567	0.6171	4.7883	-0.6420
4.3735	0.5992	4.8151	-0.6213
4.6556	0.5610	4.8399	-0.5979
4.7972	0.5386	4.8624	-0.5716
4.9382	0.5130	4.8726	-0.5567
5.1089	0.4780	4.8854	-0.5336
5.1939	0.4589	5.0714	-0.5459
5.2787	0.4387	5.2610	-0.5570

Table 3. Continued

(d) BL = 3.185, 3.399, 6.00, and 7.927

BL = 3.185			
Upper surface		Lower surface	
MS	WL	MS	WL
1.4690	-0.2433	1.4695	-0.2474
1.4706	-0.2333	1.4727	-0.2545
1.4755	-0.2243	1.4803	-0.2638
1.4806	-0.2180	1.4864	-0.2688
1.4938	-0.2056	1.4926	-0.2724
1.5097	-0.1939	1.5065	-0.2780
1.5264	-0.1832	1.5311	-0.2840
1.5642	-0.1620	1.5593	-0.2879
1.6102	-0.1404	1.5930	-0.2907
1.6451	-0.1260	1.6626	-0.2933
1.6807	-0.1127	1.7110	-0.2937
1.7168	-0.1005	1.7570	-0.2931
1.7602	-0.0872	1.9180	-0.2885
1.8036	-0.0752	1.9491	-0.2872
1.8470	-0.0644	2.2028	-0.2751
1.9272	-0.0468	2.8540	-0.2397
2.0010	-0.0327	3.0556	-0.2299
2.0925	-0.0179	3.3035	-0.2187
2.1471	-0.0104	3.4534	-0.2128
2.2018	-0.0039	3.6328	-0.2067
2.2566	0.0018	3.7100	-0.2045
2.3135	0.0067	3.8931	-0.2010
2.3705	0.0108	3.9985	-0.1998
2.4275	0.0140	4.1370	-0.1992
2.4846	0.0163	4.2677	-0.1997
2.5477	0.0180	4.4012	-0.2011
2.6108	0.0186	4.4722	-0.2026
2.6740	0.0183	4.5335	-0.2042
2.7371	0.0171		
2.8306	0.0138		
2.9241	0.0088		
3.0176	0.0023		
3.1109	-0.0055		
3.2367	-0.0179		
3.3623	-0.0321		
3.4728	-0.0459		
3.5833	-0.0604		
4.5335	-0.1897		

BL = 3.399			
Upper surface		Lower surface	
MS	WL	MS	WL
1.4640	-0.2809	1.4648	-0.2857
1.4644	-0.2751	1.4668	-0.2895
1.4656	-0.2703	1.4728	-0.2951
1.4674	-0.2661	1.4850	-0.3031
1.4769	-0.2535	1.4993	-0.3094
1.4857	-0.2445	1.5132	-0.3133
1.4958	-0.2356	1.5457	-0.3190
1.5157	-0.2204	1.5984	-0.3245
1.5337	-0.2085	1.6098	-0.3253
1.5479	-0.2000	1.6869	-0.3279
1.5892	-0.1779	1.7342	-0.3285
1.6153	-0.1653	1.8295	-0.3268
1.6422	-0.1533	1.9703	-0.3223
1.6922	-0.1333	2.1046	-0.3162
1.7377	-0.1173	2.7565	-0.2804
1.8003	-0.0977	3.0252	-0.2669
1.8403	-0.0865	3.2594	-0.2560
1.9141	-0.0677	3.5097	-0.2452
1.9885	-0.0513	3.7062	-0.2376
2.0681	-0.0358	3.8719	-0.2322
2.1481	-0.0224	4.0002	-0.2286
2.2151	-0.0127	4.1810	-0.2247
2.3242	0.0003	4.3385	-0.2224
2.4081	0.0081	4.5184	-0.2208
2.4878	0.0138	4.6341	-0.2204
2.6008	0.0192	4.7054	-0.2208
2.7192	0.0217	4.8204	-0.2228
2.8259	0.0214	4.8832	-0.2253
2.8931	0.0200	4.9248	-0.2279
2.9603	0.0178		
3.0778	0.0121		
3.1784	0.0053		
3.2963	-0.0045		
3.3639	-0.0110		
3.4855	-0.0238		
3.5827	-0.0349		
3.7357	-0.0539		
3.8320	-0.0665		
4.0650	-0.0988		
4.3583	-0.1399		
4.6065	-0.1736		
4.7019	-0.1859		
4.8652	-0.2055		
4.9248	-0.2111		

BL = 6.0			
Upper surface		Lower surface	
MS	WL	MS	WL
1.4625	-0.2697	1.4639	-0.2788
1.4633	-0.2630	1.4681	-0.2867
1.4656	-0.2572	1.4758	-0.2947
1.4691	-0.2519	1.4854	-0.3007
1.4736	-0.2469	1.4931	-0.3040
1.4828	-0.2387	1.5108	-0.3097
1.5047	-0.2226	1.5404	-0.3169
1.5353	-0.2031	1.5557	-0.3194
1.5534	-0.1925	1.5925	-0.3228
1.5988	-0.1688	1.6313	-0.3246
1.6461	-0.1473	1.6953	-0.3265
1.6808	-0.1334	1.7397	-0.3271
1.7157	-0.1206	1.8429	-0.3261
1.7510	-0.1087	1.9195	-0.3240
1.7864	-0.0977	2.1061	-0.3161
1.8322	-0.0844	2.2248	-0.3100
1.8782	-0.0722	3.1432	-0.2590
1.9245	-0.0608	3.3336	-0.2492
1.9709	-0.0502	3.5625	-0.2385
2.0367	-0.0366	3.6388	-0.2353
2.1027	-0.0244	3.9146	-0.2257
2.1689	-0.0136	4.1906	-0.2191
2.2354	-0.0042	4.4238	-0.2159
2.3048	0.0043	4.6190	-0.2146
2.3743	0.0115	4.7407	-0.2148
2.4439	0.0174	4.8246	-0.2155
2.5136	0.0220	4.9248	-0.2173
2.5917	0.0259		
2.6699	0.0283		
2.7482	0.0294		
2.8266	0.0292		
2.9036	0.0278		
2.9806	0.0253		
3.0576	0.0218		
3.1344	0.0173		
3.2267	0.0107		
3.3189	0.0028		
3.4108	-0.0060		
3.5813	-0.0248		
3.7385	-0.0443		
3.8923	-0.0648		
4.2694	-0.1176		
4.4844	-0.1472		
4.6123	-0.1639		
4.8462	-0.1926		
4.9248	-0.2038		

BL = 7.927			
Upper surface		Lower surface	
MS	WL	MS	WL
1.4720	-0.2738	1.4726	-0.2790
1.4728	-0.2657	1.4743	-0.2838
1.4753	-0.2578	1.4768	-0.2880
1.4791	-0.2501	1.4822	-0.2936
1.4844	-0.2426	1.4871	-0.2969
1.4908	-0.2352	1.4897	-0.2982
1.4984	-0.2279	1.4995	-0.3022
1.5162	-0.2136	1.5099	-0.3052
1.5446	-0.1948	1.5317	-0.3091
1.5772	-0.1763	1.5583	-0.3126
1.6131	-0.1586	1.5849	-0.3153
1.6513	-0.1420	1.6210	-0.3178
1.6975	-0.1243	1.6572	-0.3192
1.7449	-0.1083	1.7127	-0.3197
1.7932	-0.0936	1.7681	-0.3189
1.8418	-0.0803	1.9375	-0.3134
1.9122	-0.0626	2.0705	-0.3077
1.9818	-0.0470	2.3828	-0.2931
2.0505	-0.0332	2.6320	-0.2804
2.1180	-0.0213	3.2979	-0.2457
2.1661	-0.0136	3.3985	-0.2410
2.2608	-0.0006	3.7304	-0.2271
2.3736	0.0118	3.9599	-0.2194
2.4394	0.0175	4.1981	-0.2135
2.5053	0.0221	4.4091	-0.2103
2.5713	0.0258	4.5932	-0.2093
2.6386	0.0286	4.7286	-0.2097
2.7061	0.0304	4.8415	-0.2123
2.7736	0.0313	4.9248	-0.2155
2.8412	0.0312		
2.9180	0.0299		
2.9947	0.0274		
3.0714	0.0238		
3.1481	0.0189		
3.2546	0.0104		
3.4249	-0.0066		
3.5527	-0.0212		
3.7016	-0.0392		
3.8715	-0.0606		
4.0058	-0.0782		
4.4168	-0.1344		
4.6327	-0.1637		
4.7289	-0.1760		
4.8453	-0.1896		
4.9248	-0.1970		

Table 3. Concluded

(e) BL = 8.14, 8.34, and 8.43

BL = 8.14			
Upper surface		Lower surface	
MS	WL	MS	WL
1.4762	-0.2481	1.4770	-0.2521
1.4776	-0.2367	1.4791	-0.2558
1.4816	-0.2260	1.4858	-0.2620
1.4878	-0.2160	1.4924	-0.2661
1.4958	-0.2066	1.5066	-0.2717
1.5053	-0.1978	1.5279	-0.2769
1.5157	-0.1895	1.5418	-0.2794
1.5382	-0.1745	1.5746	-0.2835
1.5673	-0.1577	1.6261	-0.2866
1.5963	-0.1429	1.6815	-0.2870
1.6377	-0.1242	1.8190	-0.2848
1.6800	-0.1074	1.9518	-0.2804
1.7229	-0.0923	2.1260	-0.2725
1.7660	-0.0788	2.7628	-0.2369
1.8106	-0.0663	2.8844	-0.2308
1.8551	-0.0550	3.2167	-0.2156
1.8999	-0.0449	3.5226	-0.2038
1.9449	-0.0356	3.7161	-0.1977
1.9716	-0.0305	3.8269	-0.1949
2.0253	-0.0211	4.0047	-0.1915
2.1102	-0.0080	4.2056	-0.1899
2.1681	-0.0004	4.3107	-0.1901
2.2262	0.0063	4.5041	-0.1910
2.2844	0.0121	4.5335	-0.1905
2.3819	0.0197		
2.4796	0.0250		
2.5827	0.0280		
2.6859	0.0285		
2.7578	0.0274		
2.8296	0.0252		
2.9014	0.0219		
2.9731	0.0176		
3.0769	0.0095		
3.1807	-0.0004		
3.3520	-0.0202		
3.4779	-0.0362		
3.8367	-0.0846		
4.2229	-0.1365		
4.3126	-0.1479		
4.5335	-0.1743		

BL = 8.34			
Upper surface		Lower surface	
MS	WL	MS	WL
1.4782	-0.2176	1.4795	-0.2254
1.4790	-0.2089	1.4832	-0.2308
1.4814	-0.2007	1.4886	-0.2346
1.4851	-0.1928	1.4949	-0.2373
1.4900	-0.1853	1.5055	-0.2405
1.4957	-0.1782	1.5172	-0.2429
1.5022	-0.1715	1.5450	-0.2461
1.5166	-0.1593	1.6024	-0.2490
1.5339	-0.1473	1.6514	-0.2500
1.5519	-0.1369	1.7116	-0.2501
1.5705	-0.1276	1.8089	-0.2484
1.5898	-0.1190	1.9376	-0.2433
1.6237	-0.1052	2.6943	-0.2028
1.6593	-0.0921	2.8791	-0.1938
1.6966	-0.0797	3.0952	-0.1842
1.7357	-0.0680	3.2336	-0.1789
1.7828	-0.0553	3.3631	-0.1746
1.8313	-0.0436	3.5149	-0.1706
1.8801	-0.0330	3.7373	-0.1669
1.9284	-0.0235	3.9581	-0.1651
1.9754	-0.0152	4.1655	-0.1643
2.0213	-0.0079		
2.1113	0.0039		
2.1942	0.0123		
2.2771	0.0185		
2.3429	0.0219		
2.4087	0.0242		
2.4745	0.0253		
2.5403	0.0254		
2.6361	0.0238		
2.7320	0.0201		
2.8543	0.0121		
2.9845	0.0002		
3.0739	-0.0095		
3.2324	-0.0285		
3.3906	-0.0491		
3.8369	-0.1105		
3.9682	-0.1281		
4.0799	-0.1414		
4.1046	-0.1443		
4.1655	-0.1486		

BL = 8.43			
Upper surface		Lower surface	
MS	WL	MS	WL
1.6414	-0.1670	1.6416	-0.1774
1.6438	-0.1595	1.6428	-0.1833
1.6511	-0.1486	1.6449	-0.1891
1.6579	-0.1418	1.6477	-0.1942
1.6654	-0.1357	1.6539	-0.2012
1.6843	-0.1231	1.6615	-0.2062
1.7172	-0.1049	1.6701	-0.2097
1.7551	-0.0872	1.6790	-0.2122
1.7941	-0.0718	1.6926	-0.2149
1.8339	-0.0582	1.7193	-0.2179
1.8743	-0.0463	1.7597	-0.2196
1.9288	-0.0323	1.8424	-0.2198
1.9838	-0.0203	1.9523	-0.2170
2.0474	-0.0086	2.1023	-0.2107
2.1112	0.0011	2.1919	-0.2062
2.1836	0.0100	2.4158	-0.1930
2.2563	0.0169	2.6887	-0.1771
2.3559	0.0233	2.8275	-0.1698
2.4553	0.0268	3.0025	-0.1618
2.5214	0.0276	3.1209	-0.1572
2.5875	0.0273	3.2474	-0.1531
2.6536	0.0259	3.3804	-0.1496
2.7607	0.0213	3.5815	-0.1458
2.8676	0.0140	3.6680	-0.1446
2.9545	0.0061	3.7677	-0.1441
3.0787	-0.0079	3.9695	-0.1466
3.1162	-0.0126	3.9999	-0.1479
3.3892	-0.0502		
3.4694	-0.0612		
3.8837	-0.1137		
3.9999	-0.1299		

Table 4. Measured Lateral Coordinates of the Body-Eppler Wing Combination

(a) MS = -0.288, -0.125, 0.375, 0.875

MS = -0.288	
BL	WL
-3E-14	-0.2828
0.0596	-0.2842
0.1274	-0.2879
0.2017	-0.2936
0.2805	-0.3009
0.3620	-0.3095
0.4444	-0.3189
0.6046	-0.3391
0.7487	-0.3594
0.8106	-0.3692
0.8642	-0.3788
0.9082	-0.3880
0.9414	-0.3970
0.9536	-0.4014
0.9627	-0.4056
0.9685	-0.4098
0.9708	-0.4138
0.9706	-0.4158
0.9695	-0.4178
0.9648	-0.4217
0.9568	-0.4254
0.9457	-0.4291
0.9143	-0.4361
0.8719	-0.4426
0.8195	-0.4487
0.7584	-0.4544
0.6894	-0.4596
0.6139	-0.4643
0.4512	-0.4722
0.2836	-0.4780
0.1277	-0.4816
-1E-15	-0.4827

MS = -0.125	
BL	WL
4.1E-17	-0.0791
0.1161	-0.0808
0.2178	-0.0845
0.2801	-0.0881
0.3436	-0.0933
0.4104	-0.1006
0.4827	-0.1108
0.5289	-0.1185
0.5767	-0.1279
0.6251	-0.1399
0.6728	-0.1548
0.7189	-0.1735
0.7621	-0.1963
0.8015	-0.2241
0.8358	-0.2574
0.8675	-0.2591
0.8981	-0.2618
0.9274	-0.2658
0.9555	-0.2711
0.9821	-0.2777
1.0072	-0.2856
1.0306	-0.2947
1.0521	-0.3048
1.0715	-0.3159
1.0887	-0.3278
1.1035	-0.3403
1.1156	-0.3532
1.1251	-0.3664
1.1317	-0.3795
1.1354	-0.3926
1.1361	-0.4053
1.1337	-0.4175
1.1282	-0.4290
1.1197	-0.4398
1.1082	-0.4497
1.0938	-0.4587
1.0766	-0.4666
1.0567	-0.4735
1.0343	-0.4793
1.0096	-0.4840
0.9827	-0.4877
0.9540	-0.4905
0.9235	-0.4925
0.8585	-0.4944
0.7893	-0.4948
0.7837	-0.5043
0.7704	-0.5116
0.7506	-0.5169
0.7257	-0.5206
0.6970	-0.5231
0.6657	-0.5245
0.4302	-0.5279
0.2822	-0.5290
5.3E-19	-0.5286

MS = 0.375			
Upper surface		Lower surface	
BL	WL	BL	WL
1.2E-16	0.3421	1.2E-16	-0.7291
0.1142	0.3409	0.0286	-0.7291
0.1916	0.3383	0.1424	-0.7288
0.2703	0.3336	0.3164	-0.7265
0.3501	0.3268	0.4308	-0.7229
0.4333	0.3172	0.5335	-0.7175
0.5200	0.3046	0.6248	-0.7104
0.6058	0.2892	0.7107	-0.7012
0.6483	0.2804	0.7909	-0.6898
0.6906	0.2707	0.8309	-0.6830
0.7324	0.2598	0.8972	-0.6695
0.7638	0.2508	0.9300	-0.6616
0.7949	0.2409	0.9625	-0.6527
0.8257	0.230	1.0015	-0.6399
0.8562	0.2179	1.0204	-0.6322
0.8857	0.2048	1.0388	-0.6230
0.9147	0.1903	1.0562	-0.6124
0.9430	0.1746	1.0726	-0.6002
0.9705	0.1576	1.0875	-0.5863
0.9941	0.1414	1.1007	-0.5707
1.0168	0.1240	1.1078	-0.5602
1.0385	0.1054	1.1139	-0.5491
1.0591	0.0855	1.1188	-0.5376
1.0848	0.0568	1.1236	-0.5194
1.1077	0.0256	1.1251	-0.5003
1.1270	-0.0078	1.2111	-0.4861
1.1420	-0.0431	1.2928	-0.4717
1.1490	-0.0668	1.3679	-0.4566
1.1542	-0.0911	1.4022	-0.4487
1.1577	-0.1156	1.4342	-0.4405
1.1599	-0.1443		
1.2133	-0.1573		
1.2635	-0.1707		
1.3104	-0.1845		
1.3540	-0.1986		
1.3939	-0.2127		
1.4303	-0.2270		
1.4629	-0.2412		
1.4916	-0.2554		
1.5165	-0.2695		
1.5375	-0.2834		
1.5546	-0.2970		
1.5676	-0.3104		
1.5768	-0.3235		
1.5799	-0.3299		
1.5820	-0.3362		
1.5831	-0.3424		
1.5833	-0.3485		
1.5825	-0.3545		
1.5808	-0.3604		
1.5781	-0.3662		
1.5745	-0.3719		
1.5645	-0.3830		
1.5509	-0.3936		
1.5339	-0.4038		
1.5136	-0.4136		
1.4901	-0.4229		
1.4636	-0.4319		

MS = 0.875			
Upper surface		Lower surface	
BL	WL	BL	WL
0	0.6087	0	-0.916
0.1886	0.6076	0.1028	-0.916
0.2954	0.6045	0.1770	-0.916
0.3654	0.6007	0.2852	-0.914
0.4514	0.5937	0.3415	-0.912
0.5023	0.5882	0.4247	-0.908
0.5531	0.5816	0.5055	-0.902
0.6038	0.5739	0.5676	-0.896
0.6457	0.5665	0.6208	-0.890
0.6875	0.5584	0.6533	-0.886
0.7291	0.5493	0.7319	-0.873
0.7706	0.5393	0.8020	-0.858
0.8129	0.5281	0.8701	-0.841
0.8548	0.5157	0.9182	-0.827
0.8961	0.5021	0.9645	-0.811
0.9367	0.4871	1.0087	-0.792
0.9631	0.4763	1.0433	-0.776
0.9892	0.4648	1.0686	-0.761
1.0149	0.4523	1.0944	-0.744
1.0405	0.4388	1.1075	-0.733
1.0712	0.4209	1.1200	-0.722
1.1012	0.4014	1.1321	-0.711
1.1301	0.3802	1.1453	-0.696
1.1577	0.3576	1.1575	-0.681
1.1839	0.3328	1.1687	-0.665
1.1961	0.3198	1.1786	-0.649
1.2078	0.3061	1.1869	-0.632
1.2249	0.2836	1.1941	-0.614
1.2404	0.2599	1.2003	-0.597
1.2544	0.2352	1.2056	-0.579
1.2669	0.2099	1.2123	-0.549
1.2771	0.1866	1.2164	-0.520
1.2861	0.1629	1.2172	-0.493
1.2941	0.1389	1.3881	-0.469
1.3011	0.1145	1.4841	-0.455
1.3072	0.0895	1.5827	-0.439
1.3125	0.0643	1.6807	-0.422
1.3168	0.0388	1.7747	-0.404
1.3214	0.0012	1.8192	-0.394
1.3228	-0.0382	1.8615	-0.384
1.3229	-0.0736	1.9011	-0.374
1.3851	-0.0788	1.9377	-0.363
1.4539	-0.0862	1.9740	-0.351
1.5272	-0.0961	1.9897	-0.344
1.6031	-0.1086	2.0036	-0.337
1.6793	-0.1239	2.0152	-0.330
1.7170	-0.1327	2.0243	-0.323
1.7540	-0.1422	2.0306	-0.314
1.7901	-0.1525	2.0326	-0.310
1.8250	-0.1636	2.0338	-0.306
1.8585	-0.1755		
1.8902	-0.1883		
1.9213	-0.2025		
1.9498	-0.2174		
1.9750	-0.2328		
1.9964	-0.2482		
2.0136	-0.2635		
2.0204	-0.2710		
2.0259	-0.2784		
2.0301	-0.2855		
2.0328	-0.2925		
2.0341	-0.2992		

Table 4. Continued

(b) MS =1.875 and 2.875

MS = 1.875							
Upper surface				Lower surface			
BL	WL	BL	WL	BL	WL	BL	WL
0	0.8658	3.4314	-0.0779	0.0007	-1.2799	3.5488	-0.3295
0.1099	0.8646	3.4656	-0.0787	0.1485	-1.2803	3.5823	-0.3296
0.2197	0.8608	3.5881	-0.0790	0.2287	-1.2784	6.1730	-0.3256
0.3274	0.8545	4.5254	-0.0744	0.3069	-1.2745	7.2240	-0.3228
0.4059	0.8483	6.0610	-0.0713	0.3829	-1.2687	7.7565	-0.3207
0.4935	0.8395	7.4152	-0.0700	0.4685	-1.2598	7.8665	-0.3187
0.5754	0.8295	7.8734	-0.0696	0.5161	-1.2536	7.9361	-0.3153
0.6513	0.8183	7.9148	-0.0691	0.5635	-1.2466	7.9786	-0.3109
0.7240	0.8056	7.9607	-0.0674	0.6108	-1.2386	8.0171	-0.3053
0.7932	0.7912	8.0440	-0.0598	0.6696	-1.2273	8.0820	-0.2944
0.8568	0.7754	8.1892	-0.0459	0.7280	-1.2142	8.1672	-0.2791
0.9149	0.7583	8.2701	-0.0389	0.7733	-1.2026	8.2859	-0.2563
0.9689	0.7397	8.3327	-0.0321	0.8182	-1.1897	8.3487	-0.2426
1.0190	0.7201	8.3525	-0.0320	0.8627	-1.1754	8.3818	-0.2342
1.0437	0.7093	8.3625	-0.0327	0.9068	-1.1598	8.4347	-0.2186
1.0746	0.6949	8.3872	-0.0362	0.9446	-1.1450	8.4638	-0.2082
1.1049	0.6794	8.4224	-0.0443	0.9819	-1.1289	8.4821	-0.1996
1.1345	0.6628	8.4449	-0.0514	1.0184	-1.1112	8.4924	-0.1925
1.1631	0.6450	8.4706	-0.0618	1.0540	-1.0917	8.4963	-0.1873
1.1855	0.6297	8.4833	-0.0685	1.0845	-1.0729	8.4983	-0.1818
1.2070	0.6134	8.4932	-0.0757	1.1139	-1.0524	8.4990	-0.1761
1.2278	0.5962	8.4985	-0.0832	1.1419	-1.0302		
1.2478	0.5780	8.4991	-0.1074	1.1684	-1.0062		
1.2683	0.5575			1.1937	-0.9798		
1.2876	0.5358			1.2171	-0.9517		
1.3058	0.5132			1.2385	-0.9221		
1.3227	0.4896			1.2579	-0.8912		
1.3368	0.4678			1.2747	-0.8603		
1.3498	0.4455			1.2897	-0.8286		
1.3617	0.4225			1.3030	-0.7961		
1.3727	0.3989			1.3145	-0.7628		
1.3832	0.3735			1.3225	-0.7356		
1.3928	0.3477			1.3294	-0.7081		
1.4013	0.3216			1.3353	-0.6803		
1.4143	0.2737			1.3402	-0.6522		
1.4234	0.2300			1.3440	-0.4666		
1.4316	0.1762			1.3442	-0.6224		
1.4379	0.1119			1.3471	-0.5926		
1.4405	0.0693			1.3483	-0.5032		
1.4407	-0.0078			1.3488	-0.5627		
1.6622	-0.0044			1.3493	-0.5328		
1.7618	-0.0042			1.3899	-0.4602		
1.8357	-0.0048			1.5786	-0.4368		
1.9611	-0.0070			1.6682	-0.4258		
2.0941	-0.0118			2.1803	-0.3588		
2.3727	-0.0268			2.2453	-0.3479		
2.4768	-0.0323			2.2777	-0.3412		
2.5663	-0.0390			2.3422	-0.3263		
2.6211	-0.0442			2.4825	-0.2928		
2.6459	-0.0470			2.7935	-0.2088		
2.6950	-0.0542			2.8187	-0.2035		
2.7898	-0.0727			2.8314	-0.2024		
2.8272	-0.0769			2.8460	-0.2029		
2.8380	-0.0771			2.8603	-0.2054		
2.8433	-0.0768			2.8731	-0.2092		
2.8591	-0.0735			2.8941	-0.2173		
2.8746	-0.0680			2.9526	-0.2401		
2.9056	-0.0553			2.9860	-0.2505		
2.9209	-0.0507			3.0104	-0.2564		
2.9365	-0.0475			3.0849	-0.2703		
2.9524	-0.0454			3.1874	-0.2913		
2.9810	-0.0437			3.2551	-0.3036		
3.0189	-0.0442			3.3392	-0.3170		
3.0717	-0.0475			3.3896	-0.3232		
3.3048	-0.0702			3.4293	-0.3263		
3.3664	-0.0750			3.4691	-0.3282		

MS = 2.875							
Upper surface				Lower surface			
BL	WL	BL	WL	BL	WL	BL	WL
-5E-04	0.9076	3.9710	0.0256	0.2158	-1.4876	3.0899	-0.2223
0.1075	0.9065	4.4989	0.0258	0.3178	-1.4812	3.1916	-0.2419
0.1835	0.9045	5.1017	0.0262	0.3882	-1.4749	3.2632	-0.2549
0.2578	0.9014	6.1645	0.0308	0.4584	-1.4669	3.3480	-0.2692
0.3403	0.8969	6.7148	0.0318	0.4894	-1.4628	3.3925	-0.2751
0.3678	0.8951	7.6185	0.0330	0.5510	-1.4534	3.4428	-0.2788
0.4819	0.8858	7.8658	0.0324	0.6219	-1.4403	3.4932	-0.2801
0.5389	0.8799	7.9631	0.0316	0.6620	-1.4318	4.5175	-0.2775
0.6366	0.8677	8.0746	0.0290	0.7019	-1.4224	4.8930	-0.2764
0.7180	0.8549	8.1331	0.0264	0.7416	-1.4123	7.2908	-0.2741
0.7585	0.8473	8.1841	0.0234	0.7830	-1.4007	7.5971	-0.2732
0.8031	0.8379	8.2366	0.0193	0.8244	-1.3880	7.7323	-0.2720
0.8474	0.8273	8.2877	0.0144	0.8658	-1.3739	7.8635	-0.2698
0.8914	0.8154	8.3169	0.0119	0.9076	-1.3583	7.9091	-0.2676
0.9349	0.8020	8.3486	0.0108	0.9436	-1.3435	7.9453	-0.2637
0.9774	0.7874	8.3963	0.0115	0.9794	-1.3275	7.9633	-0.2612
1.0193	0.7711	8.4767	0.0131	1.0144	-1.3104	8.0331	-0.2500
1.0605	0.7530	8.4853	0.0124	1.0481	-1.2923	8.2016	-0.2233
1.1007	0.7329	8.4900	0.0111	1.0751	-1.2763	8.2794	-0.2088
1.1420	0.7092	8.4937	0.0089	1.1009	-1.2596	8.3242	-0.1988
1.1621	0.6964	8.4963	0.0045	1.1254	-1.2421	8.3619	-0.1894
1.1816	0.6829	8.4980	-0.0061	1.1488	-1.2237	8.3920	-0.1811
1.2006	0.6686	8.4984	-0.0220	1.1711	-1.2043	8.4259	-0.1709
1.2189	0.6536			1.1923	-1.1839	8.4751	-0.1542
1.2366	0.6377			1.2126	-1.1623	8.4881	-0.1485
1.2534	0.6211			1.2320	-1.1396	8.4932	-0.1442
1.2674	0.6059			1.2513	-1.1145	8.4961	-0.1377
1.2808	0.5901			1.2696	-1.0882	8.4979	-0.1219
1.2934	0.5738			1.2868	-1.0609		
1.3055	0.5570			1.3028	-1.0327		
1.3168	0.5396			1.3236	-0.9912		
1.3274	0.5219			1.3419	-0.9486		
1.3466	0.4852			1.3579	-0.9051		
1.3567	0.4630			1.3718	-0.8608		
1.3658	0.4403			1.3809	-0.8270		
1.3741	0.4173			1.3888	-0.7930		
1.3815	0.3941			1.3958	-0.7587		
1.3894	0.3657			1.4018	-0.7243		
1.3964	0.3370			1.4107	-0.6585		
1.4077	0.2789			1.4165	-0.5925		
1.4173	0.2133			1.4191	-0.5434		
1.4240	0.1474			1.4197	-0.4466		
1.4277	0.0901			1.4202	-0.4943		
1.4300	0.0124			1.5763	-0.4275		
1.4301	-0.0283			1.7102	-0.4103		
1.4294	-0.0897			2.1477	-0.3519		
1.4814	-0.0823			2.2114	-0.3422		
1.7125	-0.0606			2.2401	-0.3368		
1.8414	-0.0496			2.3000	-0.3230		
1.9777	-0.0389			2.3771	-0.3020		
2.1100	-0.0295			2.4406	-0.2832		
2.2409	-0.0213			2.5485	-0.2496		
2.3425	-0.0156			2.6089	-0.2300		
2.4584	-0.0100			2.7133	-0.1946		
2.5906	-0.0046			2.7434	-0.1842		
2.7011	-0.0009			2.7869	-0.1707		
2.7374	-9E-05			2.8133	-0.1650		
2.8100	0.0002			2.8267	-0.1635		
2.9031	-0.0019			2.8396	-0.1630		
2.9341	-0.0020			2.8525	-0.1635		
2.9974	0.0005			2.8754	-0.1664		
3.1472	0.0095			2.8978	-0.1719		
3.2962	0.0157			2.9422	-0.1883		
3.4825	0.0207			2.9574	-0.1932		
3.5939	0.0227			2.9825	-0.1998		
3.7939	0.0248			3.0078	-0.2054		

Table 4. Concluded

(c) MS = 3.875 and 4.875

MS = 3.875							
Upper surface				Lower surface			
BL	WL	BL	WL	BL	WL	BL	WL
0	0.8350	3.2831	-0.0864	0	-1.2467	4.0333	-0.2331
0.1161	0.8334	3.3517	-0.0786	0.0436	-1.2465	4.6252	-0.2316
0.1655	0.8321	3.4145	-0.0730	0.1430	-1.2449	5.9938	-0.2289
0.2717	0.8276	3.4721	-0.0698	0.1987	-1.2432	7.4897	-0.2265
0.3271	0.8243	3.5346	-0.0688	0.3250	-1.2374	7.7528	-0.2254
0.4169	0.8177	3.9043	-0.0696	0.4212	-1.2307	7.8597	-0.2236
0.5201	0.8079	4.2125	-0.0685	0.4752	-1.2258	7.9437	-0.2207
0.5519	0.8044	5.4544	-0.0643	0.5292	-1.2200	7.9835	-0.2169
0.6470	0.7922	7.4865	-0.0591	0.5831	-1.2131	8.0784	-0.2015
0.7404	0.7772	7.7466	-0.0576	0.6466	-1.2032	8.1321	-0.1934
0.7990	0.7657	7.8329	-0.0575	0.7098	-1.1913	8.2653	-0.1757
0.8541	0.7529	7.9014	-0.0598	0.7574	-1.1808	8.3178	-0.1686
0.8815	0.7457	7.9640	-0.0648	0.8046	-1.1688	8.3758	-0.1589
0.9191	0.7347	7.9945	-0.0681	0.8514	-1.1553	8.4273	-0.1478
0.9565	0.7223	8.0792	-0.0790	0.8976	-1.1403	8.4651	-0.1374
0.9933	0.7084	8.1253	-0.0855	0.9388	-1.1252	8.4826	-0.1309
1.0294	0.6929	8.2932	-0.1106	0.9793	-1.1088	8.4886	-0.1267
1.0596	0.6782	8.3186	-0.1136	1.0193	-1.0908		
1.0890	0.6623	8.3643	-0.1170	1.0586	-1.0712		
1.1177	0.6450	8.3808	-0.1172	1.0894	-1.0544		
1.1454	0.6266	8.4087	-0.1157	1.1192	-1.0361		
1.1669	0.6110	8.4428	-0.1126	1.1478	-1.0161		
1.1876	0.5946	8.4672	-0.1130	1.1747	-0.9939		
1.2076	0.5773	8.4814	-0.1148	1.1965	-0.9726		
1.2269	0.5590	8.4862	-0.1161	1.2168	-0.9496		
1.2453	0.5396	8.4896	-0.1183	1.2357	-0.9253		
1.2628	0.5192	8.4909	-0.1217	1.2531	-0.8999		
1.2793	0.4978			1.2725	-0.8679		
1.2946	0.4756			1.2900	-0.8349		
1.3077	0.4543			1.3056	-0.8010		
1.3197	0.4325			1.3193	-0.7663		
1.3306	0.4100			1.3282	-0.7407		
1.3403	0.3871			1.3360	-0.7147		
1.3506	0.3587			1.3430	-0.6885		
1.3593	0.3298			1.3490	-0.6620		
1.3665	0.3004			1.3546	-0.6324		
1.3725	0.2708			1.3591	-0.6026		
1.3791	0.2272			1.3625	-0.5726		
1.3839	0.1834			1.3648	-0.5426		
1.3881	0.1250			1.3658	-0.4596		
1.3915	0.0355			1.3661	-0.5063		
1.3922	-0.0577			1.4109	-0.4531		
1.3914	-0.1361			1.8285	-0.3970		
1.3892	-0.2304			2.0553	-0.3665		
1.3881	-0.2653			2.1304	-0.3557		
1.4989	-0.2505			2.2055	-0.3438		
1.5585	-0.2434			2.2570	-0.3342		
1.7308	-0.2246			2.3117	-0.3215		
1.9146	-0.2057			2.3694	-0.3048		
2.0267	-0.1946			2.4231	-0.2872		
2.1390	-0.1843			2.6337	-0.2120		
2.2416	-0.1760			2.7152	-0.1833		
2.3854	-0.1668			2.7965	-0.1561		
2.5093	-0.1597			2.8199	-0.1506		
2.5909	-0.1533			2.8385	-0.1485		
2.6316	-0.1491			2.8573	-0.1484		
2.7024	-0.1399			2.8762	-0.1499		
2.7899	-0.1275			2.8948	-0.1529		
2.8369	-0.1231			2.9565	-0.1679		
2.8595	-0.1223			2.9896	-0.1742		
2.8818	-0.1227			3.0442	-0.1819		
2.9618	-0.1288			3.3031	-0.2192		
2.9920	-0.1285			3.3529	-0.2264		
3.0158	-0.1265			3.4054	-0.2324		
3.0662	-0.1192			3.4444	-0.2345		
3.1715	-0.1019			3.5193	-0.2353		

MS = 4.875			
Upper surface		Lower surface	
BL	WL	BL	WL
0	0.7217	0	-0.8120
0.0970	0.7207	0.1438	-0.8114
0.1583	0.7190	0.2307	-0.8102
0.2453	0.7152	0.3469	-0.8066
0.3673	0.7071	0.4061	-0.8035
0.4747	0.6971	0.4998	-0.7967
0.5413	0.6892	0.5991	-0.7865
0.6152	0.6787	0.6696	-0.7768
0.6888	0.6658	0.7311	-0.7661
0.7481	0.6533	0.7836	-0.7548
0.7777	0.6459	0.8255	-0.7438
0.8074	0.6375	0.8727	-0.7284
0.8475	0.6245	0.9038	-0.7161
0.8871	0.6095	0.9360	-0.7012
0.9257	0.5927	0.9575	-0.6897
0.9627	0.5742	0.9762	-0.6781
0.9940	0.5563	0.9936	-0.6646
1.0236	0.5370	1.0083	-0.6499
1.0516	0.5164	1.0206	-0.6333
1.0781	0.4942	1.0261	-0.6237
1.1034	0.4702	1.0307	-0.6138
1.1270	0.4446	1.0377	-0.5930
1.1486	0.4171	1.0392	-0.5866
1.1682	0.3879	1.0424	-0.5671
1.1795	0.3682	1.0440	-0.5378
1.1898	0.3477	1.0553	-0.5362
1.1992	0.3263	1.2379	-0.5111
1.2076	0.3040	1.6106	-0.4620
1.2146	0.2821	1.9178	-0.4216
1.2208	0.2596	2.0941	-0.3978
1.2262	0.2366	2.2455	-0.3761
1.2308	0.2136	2.2815	-0.3685
1.2351	0.1874	2.2924	-0.3646
1.2413	0.1356	2.2959	-0.3616
1.2461	0.0754	2.2972	-0.3574
1.2509	-0.0268	3.3840	-0.2147
1.2539	-0.1548	3.3862	-0.2198
1.2552	-0.2839	3.3919	-0.2225
1.2552	-0.3742	3.4000	-0.2235
3.3840	-0.2147	3.4090	-0.2237
3.3849	-0.2094	4.8392	-0.2214
3.3875	-0.2066	6.1403	-0.2180
3.3911	-0.2054	7.7984	-0.2144
3.4491	-0.2040	7.9110	-0.2137
3.7132	-0.2028	7.9214	-0.2132
7.9096	-0.1888	7.9309	-0.2113
7.9206	-0.1893	7.9348	-0.2082
7.9310	-0.1910	7.9360	-0.2053
7.9330	-0.1918		
7.9348	-0.1933		
7.9360	-0.1962		
7.9364	-0.2011		

Table 5. Measured Horizontal Tail Upper Surface Coordinates at Several Spanwise Stations

BL = 0.25	
Upper surface	
MS	WL
7.8925	1.5000
7.8937	1.5038
7.8989	1.5099
7.9044	1.5145
7.9146	1.5213
7.9223	1.5252
7.9385	1.5304
7.9440	1.5317
7.9810	1.5384
8.0108	1.5423
8.0785	1.5489
8.1240	1.5519
8.1721	1.5540
8.2307	1.5556
8.3072	1.5566
8.4169	1.5570
8.5221	1.5566
8.6770	1.5547
8.7672	1.5531
8.9546	1.5484
9.1208	1.5430
9.2956	1.5362
9.4671	1.5286
9.5832	1.5227
9.6333	1.5196
9.6843	1.5155
9.7389	1.5095
9.7676	1.5050

BL = 0.50	
Upper surface	
MS	WL
7.7201	1.5000
7.7219	1.5061
7.7261	1.5116
7.7334	1.5179
7.7466	1.5251
7.7561	1.5286
7.7758	1.5335
7.8198	1.5414
7.8640	1.5473
7.9331	1.5535
8.0107	1.5573
8.1323	1.5602
8.2891	1.5616
8.4691	1.5613
8.5960	1.5598
8.7244	1.5574
8.8544	1.5540
9.0414	1.5479
9.2080	1.5411
9.3419	1.5349
9.4908	1.5271
9.5690	1.5224
9.6264	1.5181
9.6926	1.5112
9.7299	1.5050

BL = 0.75	
Upper surface	
MS	WL
7.5476	1.5000
7.5492	1.5056
7.5529	1.5104
7.5577	1.5144
7.5657	1.5195
7.5826	1.5273
7.6158	1.5381
7.6417	1.5441
7.6595	1.5473
7.6908	1.5519
7.7222	1.5556
7.7854	1.5608
7.8682	1.5643
8.0101	1.5672
8.1431	1.5684
8.2847	1.5684
8.3963	1.5676
8.5462	1.5655
8.6789	1.5626
8.7944	1.5593
8.9286	1.5546
9.0954	1.5477
9.2524	1.5400
9.3696	1.5334
9.5022	1.5246
9.5988	1.5159
9.6436	1.5096
9.6658	1.5050

BL = 1.00	
Upper surface	
MS	WL
7.3751	1.5000
7.3762	1.5046
7.3787	1.5087
7.3857	1.5152
7.3966	1.5211
7.4133	1.5277
7.4396	1.5364
7.4691	1.5443
7.5018	1.5511
7.5332	1.5558
7.5632	1.5589
7.6202	1.5630
7.6639	1.5652
7.7732	1.5693
7.8495	1.5712
7.9628	1.5729
8.0300	1.5733
8.1729	1.5729
8.2609	1.5719
8.4243	1.5688
8.5321	1.5659
8.7009	1.5604
8.8368	1.5552
8.9743	1.5492
9.0987	1.5430
9.2551	1.5340
9.3672	1.5268
9.4815	1.5186
9.5061	1.5164
9.5305	1.5135
9.5520	1.5100
9.5731	1.5050

BL = 1.25	
Upper surface	
MS	WL
7.2027	1.5000
7.2039	1.5048
7.2082	1.5116
7.2128	1.5160
7.2198	1.5199
7.2602	1.5357
7.2904	1.5446
7.3311	1.5531
7.3571	1.5571
7.4094	1.5627
7.4840	1.5674
7.5323	1.5691
7.6487	1.5718
7.7407	1.5729
7.8661	1.5734
7.9883	1.5729
8.1059	1.5716
8.2122	1.5697
8.3900	1.5653
8.5301	1.5610
8.7288	1.5537
8.8973	1.5466
9.0568	1.5391
9.1548	1.5339
9.2418	1.5288
9.3181	1.5231
9.3794	1.5171
9.4025	1.5140
9.4255	1.5101
9.4481	1.5050

BL =1.50	
Upper surface	
MS	WL
7.0302	1.5000
7.0318	1.5058
7.0356	1.5102
7.0459	1.5161
7.0710	1.5282
7.0881	1.5352
7.1153	1.5434
7.1472	1.5502
7.1986	1.5575
7.2566	1.5632
7.3270	1.5678
7.4377	1.5717
7.5929	1.5737
7.6973	1.5738
7.8431	1.5730
7.9851	1.5713
8.1227	1.5687
8.2555	1.5655
8.4211	1.5603
8.5763	1.5546
8.7332	1.5480
8.9044	1.5399
9.0120	1.5340
9.1195	1.5259
9.2027	1.5171
9.2440	1.5115
9.2849	1.5050

BL = 1.75	
Upper surface	
MS	WL
6.8578	1.5000
6.8593	1.5049
6.8646	1.5111
6.8668	1.5129
6.8744	1.5179
6.8908	1.5252
6.9342	1.5393
6.9580	1.5453
6.9946	1.5517
7.0398	1.5577
7.0803	1.5617
7.1566	1.5669
7.1959	1.5686
7.2628	1.5704
7.3776	1.5717
7.5024	1.5719
7.6306	1.5712
7.7543	1.5698
7.9370	1.5665
8.0676	1.5632
8.2288	1.5583
8.3896	1.5523
8.5680	1.5446
8.7060	1.5378
8.8553	1.5297
8.9163	1.5257
8.9572	1.5226
8.9977	1.5184
9.0368	1.5128
9.0733	1.5050

BL = 2.00	
Upper surface	
MS	WL
6.6853	1.5000
6.6860	1.5035
6.6876	1.5056
6.6969	1.5128
6.7082	1.5195
6.7319	1.5309
6.7528	1.5383
6.7742	1.5438
6.8036	1.5488
6.8911	1.5588
6.9579	1.5641
7.0314	1.5678
7.1430	1.5704
7.3278	1.5703
7.4361	1.5692
7.5950	1.5667
7.7380	1.5636
7.9189	1.5585
8.0691	1.5534
8.2716	1.5455
8.4114	1.5393
8.5973	1.5300
8.6691	1.5253
8.7006	1.5226
8.7320	1.5189
8.7629	1.5133
8.7931	1.5050

BL = 2.25	
Upper surface	
MS	WL
6.5128	1.5000
6.5141	1.5045
6.5204	1.5115
6.5327	1.5196
6.5526	1.5284
6.5732	1.5349
6.6055	1.5417
6.6574	1.5487
6.6924	1.5524
6.7331	1.5557
6.7644	1.5574
6.8608	1.5609
6.9544	1.5628
7.0575	1.5639
7.1421	1.5640
7.2527	1.5632
7.3529	1.5616
7.4810	1.5584
7.6195	1.5542
7.8478	1.5460
8.0209	1.5390
8.0893	1.5358
8.1675	1.5315
8.2455	1.5254
8.3203	1.5170
8.3576	1.5116
8.3947	1.5054

BL = 2.35	
Upper surface	
MS	WL
6.4438	1.5000
6.4451	1.5054
6.4482	1.5098
6.4545	1.5153
6.4620	1.5197
6.4788	1.5257
6.5046	1.5317
6.5468	1.5379
6.5976	1.5435
6.6700	1.5489
6.7528	1.5524
6.8173	1.5540
6.9067	1.5553
7.0241	1.5558
7.1515	1.5551
7.2422	1.5538
7.3739	1.5510
7.5256	1.5468
7.6526	1.5424
7.7564	1.5381
7.8580	1.5330
7.9595	1.5264
8.0648	1.5172
8.1174	1.5116
8.1699	1.5050

Table 6. Measured Vertical Tail Coordinates in Several Horizontal Planes

WL = 1.75	
Right surface	
MS	BL
7.8966	0.0000
7.8975	0.0074
7.9002	0.0139
7.9053	0.0197
7.9117	0.0244
7.9225	0.0298
7.9337	0.0337
7.9499	0.0380
7.9663	0.0413
7.9998	0.0456
8.0733	0.0517
8.1576	0.0561
8.2452	0.0589
8.3291	0.0607
8.4981	0.0623
8.6077	0.0621
8.8176	0.0595
8.9686	0.0563
9.0843	0.0530
9.2778	0.0461
9.3911	0.0412
9.4975	0.0357
9.5619	0.0318
9.6420	0.0258
9.6732	0.0227
9.7050	0.0187
9.7211	0.0159
9.7370	0.0123
9.7524	0.0075

WL = 2.00	
Right surface	
MS	BL
7.7282	0.0000
7.7286	0.0045
7.7315	0.0119
7.7373	0.0184
7.7457	0.0239
7.7646	0.0317
7.7871	0.0379
7.8110	0.0427
7.8333	0.0460
7.8833	0.0519
7.9214	0.0555
7.9929	0.0605
8.0549	0.0634
8.1498	0.0662
8.2152	0.0673
8.3455	0.0683
8.4867	0.0681
8.5952	0.0671
8.7340	0.0648
8.8386	0.0624
8.9965	0.0575
9.0923	0.0539
9.2671	0.0460
9.3895	0.0396
9.5148	0.0320
9.5944	0.0264
9.6366	0.0230
9.6673	0.0190
9.6876	0.0142
9.6977	0.0103
9.7025	0.0075

WL = 2.25	
Right surface	
MS	BL
7.5598	0.0000
7.5603	0.0042
7.5634	0.0114
7.5711	0.0197
7.5775	0.0241
7.5918	0.0309
7.6109	0.0371
7.6496	0.0457
7.6891	0.0526
7.7369	0.0586
7.7649	0.0611
7.8227	0.0652
7.9002	0.0692
7.9606	0.0716
8.0924	0.0752
8.1764	0.0766
8.2792	0.0774
8.3934	0.0772
8.5056	0.0759
8.6532	0.0730
8.7746	0.0697
8.9218	0.0648
9.0541	0.0595
9.2054	0.0525
9.3222	0.0463
9.4389	0.0391
9.5031	0.0342
9.5712	0.0270
9.6067	0.0207
9.6254	0.0157
9.6343	0.0121
9.6429	0.0075

WL = 2.50	
Right surface	
MS	BL
7.3919	0.0008
7.3923	0.0059
7.3936	0.0104
7.3982	0.0181
7.4028	0.0225
7.4142	0.0292
7.4355	0.0366
7.4508	0.0402
7.4762	0.0451
7.5282	0.0525
7.6025	0.0599
7.6984	0.0666
7.7986	0.0709
7.9563	0.0743
8.1471	0.0748
8.3840	0.0720
8.5052	0.0696
8.7340	0.0636
8.9044	0.0582
9.0927	0.0513
9.2095	0.0461
9.3245	0.0395
9.3611	0.0369
9.4354	0.0304
9.4953	0.0234
9.5165	0.0199
9.5372	0.0150
9.5570	0.0083

WL = 2.75	
Right surface	
MS	BL
7.2231	0.0000
7.2246	0.0075
7.2283	0.0141
7.2339	0.0203
7.2407	0.0256
7.2560	0.0339
7.2731	0.0402
7.2904	0.0446
7.3256	0.0498
7.3910	0.0566
7.4628	0.0621
7.5112	0.0649
7.6057	0.0689
7.6698	0.0706
7.7675	0.0720
7.8674	0.0724
8.0095	0.0718
8.1022	0.0707
8.2829	0.0671
8.3709	0.0647
8.6358	0.0560
8.8181	0.0491
9.0528	0.0394
9.1503	0.0348
9.2327	0.0303
9.3019	0.0254
9.3651	0.0191
9.4203	0.0118
9.4470	0.0075

WL = 3.00	
Right surface	
MS	BL
7.0547	0.0000
7.0551	0.0053
7.0565	0.0101
7.0586	0.0144
7.0615	0.0181
7.0669	0.0227
7.0733	0.0262
7.0877	0.0313
7.1230	0.0405
7.1607	0.0471
7.2240	0.0545
7.2608	0.0578
7.3329	0.0626
7.3890	0.0650
7.4532	0.0667
7.5301	0.0676
7.6195	0.0675
7.7534	0.0663
7.9446	0.0633
8.1265	0.0594
8.3539	0.0533
8.5290	0.0478
8.8410	0.0369
8.9950	0.0309
9.0767	0.0270
9.1642	0.0216
9.2105	0.0178
9.2568	0.0131
9.3025	0.0075

WL = 3.25	
Right surface	
MS	BL
6.8863	0.0000
6.8868	0.0043
6.8881	0.0082
6.8928	0.0148
6.8984	0.0193
6.9049	0.0228
6.9192	0.0277
6.9538	0.0359
7.0217	0.0468
7.0389	0.0490
7.0861	0.0536
7.1160	0.0555
7.1844	0.0585
7.2738	0.0606
7.3405	0.0612
7.5111	0.0605
7.6368	0.0586
7.9867	0.0513
8.2078	0.0458
8.5393	0.0365
8.7123	0.0311
8.8536	0.0258
8.9373	0.0217
9.0310	0.0155
9.1247	0.0075

WL = 3.50	
Right surface	
MS	BL
6.7179	0.0000
6.7191	0.0078
6.7224	0.0143
6.7272	0.0191
6.7333	0.0229
6.7473	0.0284
6.7756	0.0356
6.8033	0.0403
6.8534	0.0461
6.9055	0.0503
6.9933	0.0547
7.1000	0.0575
7.1659	0.0580
7.2871	0.0576
7.4008	0.0562
7.5680	0.0531
7.7860	0.0478
8.1494	0.0377
8.5326	0.0264
8.6348	0.0229
8.7503	0.0179
8.8049	0.0147
8.8871	0.0075

WL = 3.70	
Right surface	
MS	BL
6.5832	0.0000
6.5837	0.0053
6.5852	0.0102
6.5876	0.0146
6.5906	0.0184
6.5972	0.0237
6.6052	0.0276
6.6229	0.0328
6.6566	0.0396
6.6894	0.0441
6.7337	0.0483
6.7786	0.0510
6.8823	0.0549
6.9852	0.0569
7.0791	0.0577
7.1949	0.0575
7.2884	0.0565
7.4257	0.0537
7.5811	0.0494
7.9073	0.0391
8.2103	0.0288
8.3413	0.0236
8.4791	0.0172
8.5484	0.0131
8.6175	0.0075

WL = 3.90	
Right surface	
MS	BL
6.4704	0.0000
6.4715	0.0074
6.4735	0.0112
6.4764	0.0147
6.4803	0.0179
6.4903	0.0233
6.5021	0.0276
6.5295	0.0343
6.5579	0.0385
6.5932	0.0420
6.6362	0.0452
6.6781	0.0474
6.7630	0.0498
6.8352	0.0511
6.9226	0.0519
7.0055	0.0517
7.0943	0.0505
7.1999	0.0481
7.4077	0.0417
7.6189	0.0344
7.8317	0.0261
7.9248	0.0220
7.9898	0.0185
8.0361	0.0151
8.1097	0.0075

Appendix A

Run Number Summaries for Various Model Configurations

Table A1. Test 540 - Eppler 387 Wing

Longitudinal aerodynamic characteristics, $\delta_h = \delta_f = 0°$, bump off

R_c	Pressures	Run		
		M_∞ =		
		0.25	0.65	0.80
40,000	Wing	218	215	213
	Lower fuselage	-	222	221
60,000	Wing	-	217	216
	Lower fuselage	-	224	223

Table A2. Test 540 - MA-SC-1 Wing

Longitudinal aerodynamic characteristics, $\delta_h = \delta_f = 0°$

R_c	Bump	Run					
		M_∞ =					
		0.50	0.65	0.70	0.80	0.85	0.90
40,000	Off	21	20	16	15	14	12
	On	29	35	28	33	34	27
60,000	Off	-	18	-	17	-	-
	On	-	30	-	36	-	-
100,000	Off	-	22	-	11	-	-
	On	-	37	-	31	-	-

Table A2. Concluded.

Horizontal tail effectiveness, $\delta_f = 0°$, bump on

R_c	δ_h, deg	Run, M_∞ = 0.65	Run, M_∞ = 0.80
40,000	-5	40	39
	0	35	33
	5	44	43
	10	51	50
	15	56	55
	Off	106	105
60,000	-5	42	41
	0	30	36
	5	47	46
	10	53	52
	15	58	57
	Off	113	107

Right wing trailing-edge flap (plain) effectiveness, $\delta_h = 0°$, bump on

R_c	δ_f, deg	Run, M_∞ = 0.65	Run, M_∞ = 0.80
40,000	-10	62	61
	0	35	33
	10	69	68
	20	75	74
60,000	-10	65	64
	0	30	36
	10	71	70
	20	77	76

Lateral aerodynamic characteristics, bump on

$\delta_h = \delta_f = 0°$

R_c	α, deg	Run, M_∞ = 0.65	Run, M_∞ = 0.80
40,000	1	86	81
	3	87	82
	5	88	83
	10	89	84
	16	90	85
60,000	1	97	91
	3	98	92
	5	99	93
	10	100	94
	16	101	95

Tails off, $\delta_f = 0°$

R_c	α, deg	Run, M_∞ = 0.65
40,000	1	108
	3	109
	5	110
	10	111
	16	112

Table A3. Test 540 - MA-SF-1 Wing

Longitudinal aerodynamic characteristics and trailing-edge flap effectiveness (split flaps on both wings), $\delta_h = 0°$, bump off

R_c	δ_f, deg	Run					
		M_∞ =					
		0.50	0.65	0.70	0.80	0.85	0.90
40,000	0	131	122	129	130	128	127
	10	138	137	140	136	142	135
	30	150	155	149	154	148	153
60,000	0	-	124	-	123	-	-
	10	-	141	-	143	-	-
	30	-	152	-	156	-	-
100,000	0	-	126	-	125	-	-
	10	-	145	-	144	-	-
	30	-	158	-	157	-	-

Table A4. Test 540 - MA-SC-1t Wing

Longitudinal aerodynamic characteristics, $\delta_h = \delta_f = 0°$, bump on

R_c	Run					
	M_∞ =					
	0.50	0.65	0.70	0.80	0.85	0.90
40,000	170	169	172	168	175	171
60,000	-	174	-	173	-	-
100,000	-	177	-	176	-	-

Tails off

R_c	Run	
	M_∞ =	
	0.65	0.80
40,000	205	203
60,000	207	206

Table A4. Concluded.

Lateral aerodynamic characteristics, $\delta_h = \delta_f = 0°$, bump on

R_c	α, deg	Run	
		M_∞ =	
		0.65	0.80
40,000	1	185	180
	3	186	181
	5	187	182
	10	188	183
	16	189	184
60,000	1	195	190
	3	196	191
	5	197	192
	10	198	193
	16	199	194

Table A5. Test 541 – MA-SC-1 Wing (inverted tails and lower fuselage fairing removed)

Longitudinal aerodynamic characteristics, $\delta_f = 0°$, bump on

R_c	Run						Run					
	$M_\infty = 0.65$						$M_\infty = 0.80$					
	δ_h, deg =						δ_h, deg =					
	-15	-5	0	5	10	15	-15	-5	0	5	10	15
40,000	20	27	12	34	41	49	19	26	11	33	40	48
60,000	22	29	14	36	43	51	21	28	13	35	42	50
100,000	24	31	17	38	46	53	23	30	16	37	45	52

Lateral aerodynamic characteristics at $\alpha = 4°$ with $\delta_h = -5°$, $\delta_f = 0°$, bump on

R_c	Run	
	M_∞ =	
	0.65	0.80
40,000	57	56
60,000	59	58
100,000	61	60

Appendix B

Tunnel Condition Ranges

Table B1. Test 540

Test	Run	Mach	R_c		q_∞, psf		$p_{t,\infty}$, psf	
			Lower	Upper	Lower	Upper	Lower	Upper
540	11	0.80	89,200	103,200	47.27	50.49	160.65	171.16
	12	.90	41,050	47,390	20.60	23.98	61.60	71.49
	14	.85	40,340	43,460	19.49	21.10	62.00	66.90
	15	.80	39,420	42,760	18.38	19.99	62.50	67.70
	16	.70	39,040	41,560	16.55	17.49	66.31	71.02
	17	.80	58,230	62,510	27.24	29.42	92.48	99.21
	18	.65	58,370	62,660	23.40	25.11	104.59	111.98
	20	.65	38,400	40,740	15.38	16.38	68.40	73.70
	21	.50	38,120	40,350	12.24	13.05	83.04	87.58
	22	.65	98,000	100,460	40.22	41.47	180.50	185.77
	27	.90	39,410	43,210	20.32	22.64	60.40	67.00
	28	.70	38,020	41,250	16.45	17.81	66.69	71.85
	29	.50	37,910	40,380	12.29	13.07	83.56	88.49
	30	.65	58,120	60,910	23.64	24.76	105.70	110.60
	31	.80	97,940	100,710	47.58	49.45	161.89	168.06
	33	.80	39,300	44,250	18.24	20.65	62.02	70.09
	34	.85	38,300	43,150	18.48	20.90	58.37	66.35
	35	.65	38,660	42,220	15.46	16.85	68.69	75.40
	36	.80	58,380	63,180	27.19	29.64	92.49	100.30
	37	.65	98,260	101,110	39.58	40.70	176.30	181.90
	39	.80	39,980	44,440	18.56	20.77	63.16	70.52
	40	.65	38,690	42,240	15.39	16.82	69.28	75.61
	41	.80	58,560	61,860	27.36	28.96	93.20	98.29
	42	.65	58,610	61,310	23.35	24.46	104.96	109.69
	43	.80	38,030	41,020	17.77	19.20	60.21	65.07
	44	.65	37,980	40,150	15.16	15.92	67.80	72.00
	46	.80	58,940	62,480	27.51	29.18	93.40	99.27
	47	.65	58,360	60,880	23.25	24.26	104.23	108.74
	50	.80	38,670	41,430	18.50	19.92	62.74	67.42
	51	.65	38,670	40,670	15.79	16.66	70.60	74.21
	52	.80	58,500	61,200	28.09	29.37	95.12	99.58
	53	.65	58,310	60,550	23.71	24.64	106.69	110.37
	55	.80	38,040	42,375	17.39	19.38	59.10	65.80
	56	.65	38,300	41,170	14.96	16.13	66.90	71.80
	57	.80	58,500	61,730	26.83	28.35	91.08	96.53
	58	.65	58,330	61,700	22.95	24.36	102.60	108.36
	61	.80	38,070	41,290	17.56	19.26	59.80	65.36
	62	.65	39,320	41,710	15.65	16.71	69.90	74.20
	64	.80	58,750	62,430	27.00	29.00	91.90	97.90
	65	.65	58,030	60,540	22.93	23.95	102.56	108.06
	68	.80	39,120	43,030	18.52	20.49	63.10	69.50
	69	.65	39,190	41,320	15.84	16.76	71.10	74.92

Table B1. Continued.

Test	Run	Mach	R_c		q_∞, psf		$p_{t,\infty}$, psf	
			Lower	Upper	Lower	Upper	Lower	Upper
540	70	0.80	59,110	61,850	28.04	29.51	95.50	99.91
	71	.65	58,760	60,490	23.82	24.50	106.68	109.81
	74	.80	38,850	41,880	18.03	19.50	61.38	66.40
	75	.65	38,450	41,450	15.27	16.52	68.61	73.82
	76	.80	58,040	61,050	27.17	28.57	91.91	96.95
	77	.65	58,020	60,310	23.08	24.01	103.90	107.90
	81	.80	36,250	42,620	16.88	19.91	57.44	67.32
	82	↓	40,192	42,618	18.86	19.87	63.60	67.31
	83	↓	42,700	45,210	19.86	21.19	67.71	71.54
	84	↓	37,320	39,750	17.48	18.57	59.00	62.78
	85	↓	39,900	41,420	18.63	19.35	63.06	65.47
	86	.65	35,900	37,890	14.30	15.16	63.90	67.46
	87	↓	38,010	39,820	15.16	15.81	67.87	71.06
	88	↓	39,910	41,530	15.86	16.55	71.30	73.99
	89	↓	41,850	43,350	16.72	17.29	74.32	76.88
	90	↓	39,670	40,860	15.78	16.30	70.56	72.50
	91	.80	57,390	59,630	26.81	27.81	90.52	94.38
	92	↓	59,820	62,660	27.90	29.27	94.63	99.39
	93	↓	57,210	59,010	26.75	27.59	90.81	93.69
	94	↓	59,170	60,640	27.68	28.40	93.91	96.22
	95	↓	60,730	62,040	28.37	29.05	96.50	98.55
	97	.65	57,090	59,600	22.73	23.77	101.60	106.00
	98	↓	59,560	61,450	23.69	24.49	106.20	109.45
	99	↓	61,370	62,640	24.37	24.96	109.56	111.64
	100	↓	58,260	59,277	23.24	23.66	103.86	105.72
	101	↓	59,420	60,290	23.70	24.05	105.96	107.50
	105	.80	37,940	41,480	17.67	19.32	59.99	65.70
	106	.65	39,660	42,200	15.76	16.79	70.70	75.30
	107	.80	57,840	60,080	26.93	28.09	91.70	95.06
	108	.65	38,170	40,870	15.14	16.28	68.09	72.70
	109	↓	40,880	42,700	16.23	16.88	72.92	76.34
	110	↓	37,290	38,900	14.84	15.43	66.41	69.50
	111	↓	39,280	40,900	15.65	16.29	69.92	72.80
	112	↓	41,060	42,400	16.35	16.94	73.07	75.50
	113	↓	58,390	60,750	23.25	24.20	103.96	106.50
	122	↓	38,450	41,430	15.07	16.36	67.52	73.62
	123	.80	57,270	61,520	26.74	28.72	90.58	97.49
	124	.65	56,990	60,100	22.76	23.88	101.39	107.40
	125	.80	97,100	99,840	45.56	47.07	155.41	155.91
	126	.65	97,620	99,660	39.20	40.13	175.80	179.30
	127	.90	36,400	39,230	18.47	19.91	54.92	59.20
	128	.85	39,700	42,660	19.38	20.80	61.27	65.81

Table B1. Continued.

Test	Run	Mach	R_c		q_∞, psf		$p_{t,\infty}$, psf	
			Lower	Upper	Lower	Upper	Lower	Upper
540	129	0.70	37,990	40,030	16.09	16.91	64.77	68.34
	130	.80	38,990	41,860	18.23	19.59	61.73	66.30
	131	.50	38,550	40,030	12.38	12.80	82.50	85.75
	135	.90	38,020	40,950	19.19	20.59	57.10	61.49
	136	.80	39,740	42,670	18.48	19.84	62.74	67.16
	137	.65	38,330	40,420	15.20	15.91	67.66	71.60
	138	.50	38,150	40,040	12.04	12.72	81.40	85.42
	140	.70	39,090	42,320	16.45	17.64	66.70	71.22
	141	.65	57,000	59,660	22.42	23.60	100.80	105.20
	142	.85	39,260	43,060	18.87	20.71	60.00	65.82
	143	.80	57,710	60,650	26.67	28.15	90.89	95.50
	144	.80	97,470	99,670	45.72	46.94	155.20	159.27
	145	.65	97,530	99,360	39.03	39.91	175.50	178.60
	148	.85	37,290	40,070	17.90	19.71	56.59	62.58
	149	.70	38,260	41,490	16.18	17.34	64.88	70.00
	150	.50	37,700	39,560	11.87	12.48	80.93	84.77
	152	.65	57,970	60,140	23.05	23.95	103.10	107.00
	153	.90	38,440	41,360	19.42	20.95	57.70	62.30
	154	.80	40,440	43,140	18.89	20.12	64.09	68.45
	155	.65	38,590	40,480	15.39	16.14	68.90	72.22
	156	.80	59,100	61,690	27.56	28.85	93.82	97.88
	157	.80	99,040	100,720	46.78	47.58	158.30	161.50
	158	.65	98,780	100,870	39.73	40.55	177.59	181.80
	168	.80	39,470	43,210	16.99	18.79	57.95	63.51
	169	.65	39,090	42,330	14.43	15.72	65.10	70.16
	170	.50	37,360	40,720	11.09	12.11	74.96	81.30
	171	.90	36,440	39,760	17.23	18.83	51.21	55.80
	172	.70	39,430	41,890	15.59	16.52	62.60	66.64
	173	.80	58,850	62,250	25.76	27.40	87.08	93.00
	174	.65	58,470	60,370	21.95	22.69	98.21	101.41
	175	.85	38,170	41,210	17.55	18.93	55.40	59.89
	176	.80	97,850	101,590	43.35	45.12	147.30	152.86
	177	.65	98,190	100,380	37.17	38.06	166.12	169.31
	180	.80	37,760	40,860	16.33	17.68	55.25	60.18
	181	↓	41,490	43,060	18.02	18.71	61.00	63.40
	182	↓	36,980	38,800	16.11	16.91	54.56	57.30
	183	↓	39,050	40,570	16.99	17.68	57.75	60.00
	184	↓	40,860	42,420	17.83	18.47	60.41	62.89
	185	.65	36,910	40,030	13.77	14.91	61.54	66.46
	186	↓	40,260	41,850	15.02	15.61	66.79	69.48
	187	↓	36,890	38,210	13.68	14.18	61.51	63.69
	188	↓	38,380	39,460	14.29	14.69	63.90	65.68

Table B1. Concluded.

Test	Run	Mach	R_c		q_{∞}, psf		$p_{t,\infty}$, psf	
			Lower	Upper	Lower	Upper	Lower	Upper
540	189	0.65	39,560	40,960	14.68	15.30	66.08	68.10
	190	.80	57,370	59,640	25.07	26.08	85.06	88.81
	191	↓	60,160	63,280	26.33	27.82	89.59	94.35
	192		56,570	58,730	24.85	25.82	84.50	87.87
	193		59,000	60,780	25.98	26.74	88.20	90.99
	194		60,940	62,070	26.83	27.33	91.22	92.96
	195	.65	57,210	59,090	21.53	22.18	96.29	99.18
	196	↓	59,200	61,220	22.23	23.04	99.32	102.70
	197		56,820	58,840	21.35	22.16	95.50	98.80
	198		59,200	60,560	22.26	22.73	99.50	102.00
	199		60,950	62,470	22.83	23.43	102.67	105.10
	203	.80	37,380	40,940	16.23	17.85	54.86	60.26
	205	.65	37,820	40,460	13.94	14.94	62.38	66.90
	206	.80	57,180	60,360	24.70	26.27	84.32	89.13
	207	.65	57,430	60,380	21.36	22.49	95.53	100.78
	213	.80	37,850	41,700	17.45	19.33	59.24	65.63
	215	.65	37,660	39,670	14.81	15.73	66.30	69.98
	216	.80	57,040	59,050	26.47	27.51	89.99	93.65
	217	.65	57,970	59,530	23.10	23.65	103.27	106.27
	218	.25	39,440	39,960	6.63	6.67	154.67	157.28
	221	.80	39,930	43,110	18.28	19.83	62.20	67.21
	222	.65	37,790	41,000	14.85	16.14	66.38	72.06
	223	.80	58,280	62,080	26.85	28.74	91.20	97.03
	224	.65	58,140	61,060	22.94	24.01	102.49	108.12

Table B2. Test 541.

Test	Run	Mach	R_c		q_∞, psf		$p_{t,\infty}$, psf	
			Lower	Upper	Lower	Upper	Lower	Upper
541	11	0.80	37,440	43,270	17.14	19.73	57.73	66.58
	12	.65	38,620	41,910	14.98	16.27	67.29	73.05
	13	.80	58,610	64,280	26.64	29.38	90.61	99.84
	14	.65	57,620	60,140	22.61	23.47	100.29	105.07
	16	.80	97,270	99,970	44.78	46.08	151.75	156.55
	17	.65	98,590	100,930	38.88	40.03	173.52	178.31
	19	.80	38,330	41,350	17.86	19.30	60.70	65.48
	20	.65	38,320	41,720	15.26	16.56	68.22	74.25
	21	.80	57,950	60,510	27.07	28.37	91.39	95.86
	22	.65	58,400	60,860	23.33	24.19	104.23	108.65
	23	.80	98,780	100,540	46.94	48.24	159.35	163.87
	24	.65	98,370	100,340	40.03	41.04	179.42	182.95
	26	.80	40,070	43,150	18.43	19.87	61.67	67.05
	27	.65	37,730	40,170	14.69	15.84	65.89	70.24
	28	.80	58,940	62,650	27.22	29.23	91.92	99.29
	29	.65	58,360	60,400	23.18	24.05	103.94	107.59
	30	.80	98,710	101,120	46.22	47.66	157.53	161.29
	31	.65	98,600	100,790	39.46	40.32	176.77	180.66
	33	.80	39,530	41,950	18.14	19.58	61.91	66.63
	34	.65	38,370	40,520	15.26	16.27	68.53	72.28
	35	.80	58,220	60,810	27.36	28.66	93.16	97.81
	36	.65	58,530	60,890	23.62	24.62	105.73	109.88
	37	.80	97,970	101,700	47.23	49.68	160.36	168.04
	38	.65	97,970	101,700	40.32	41.18	181.04	184.61
	40	.80	37,640	41,360	17.71	19.58	60.10	66.33
	41	.65	37,450	39,950	15.12	15.98	67.38	71.67
	42	.80	57,030	60,480	26.78	28.66	91.15	96.57
	43	.65	57,150	59,730	23.04	23.90	102.90	107.03
	45	.80	98,320	102,280	45.50	48.10	154.26	163.10
	46	.65	98,000	99,680	39.17	39.89	175.63	178.76
	48	.80	37,240	39,920	17.57	18.64	59.76	64.28
	49	.65	37,680	39,810	15.26	16.13	68.07	71.86
	50	.80	57,480	60,110	27.22	28.51	92.38	96.85
	51	.65	57,220	59,780	23.18	24.19	103.89	108.05
	52	.80	97,150	99,480	46.66	48.24	158.75	163.89
	53	.65	98,070	99,400	40.18	40.90	180.38	183.33
	56	.80	38,810	40,330	18.14	19.01	61.74	64.57
	57	.65	39,500	41,280	15.84	16.56	71.41	74.44
	58	.80	59,480	61,250	28.08	29.09	95.61	98.39
	59	.65	59,370	60,590	24.04	24.48	107.26	109.73
	60	.80	98,960	100,360	47.81	48.82	162.06	165.53
	61	.65	99,060	99,620	40.75	40.90	182.53	184.53

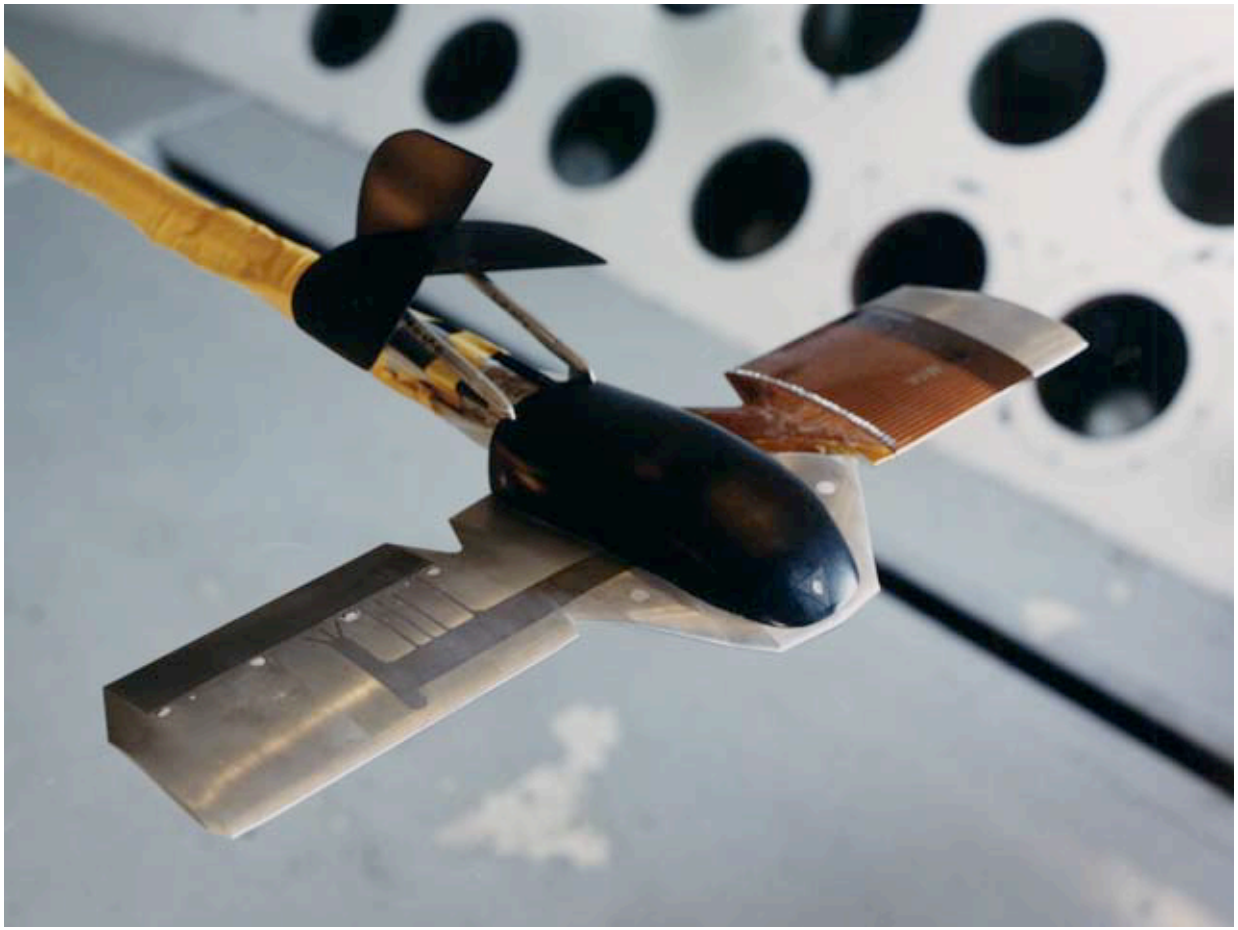

L99-1672

(a) Model with unswept wing and tails in the upright position.

Figure 1. Photographs showing model installed in the Transonic Dynamics Tunnel test section.

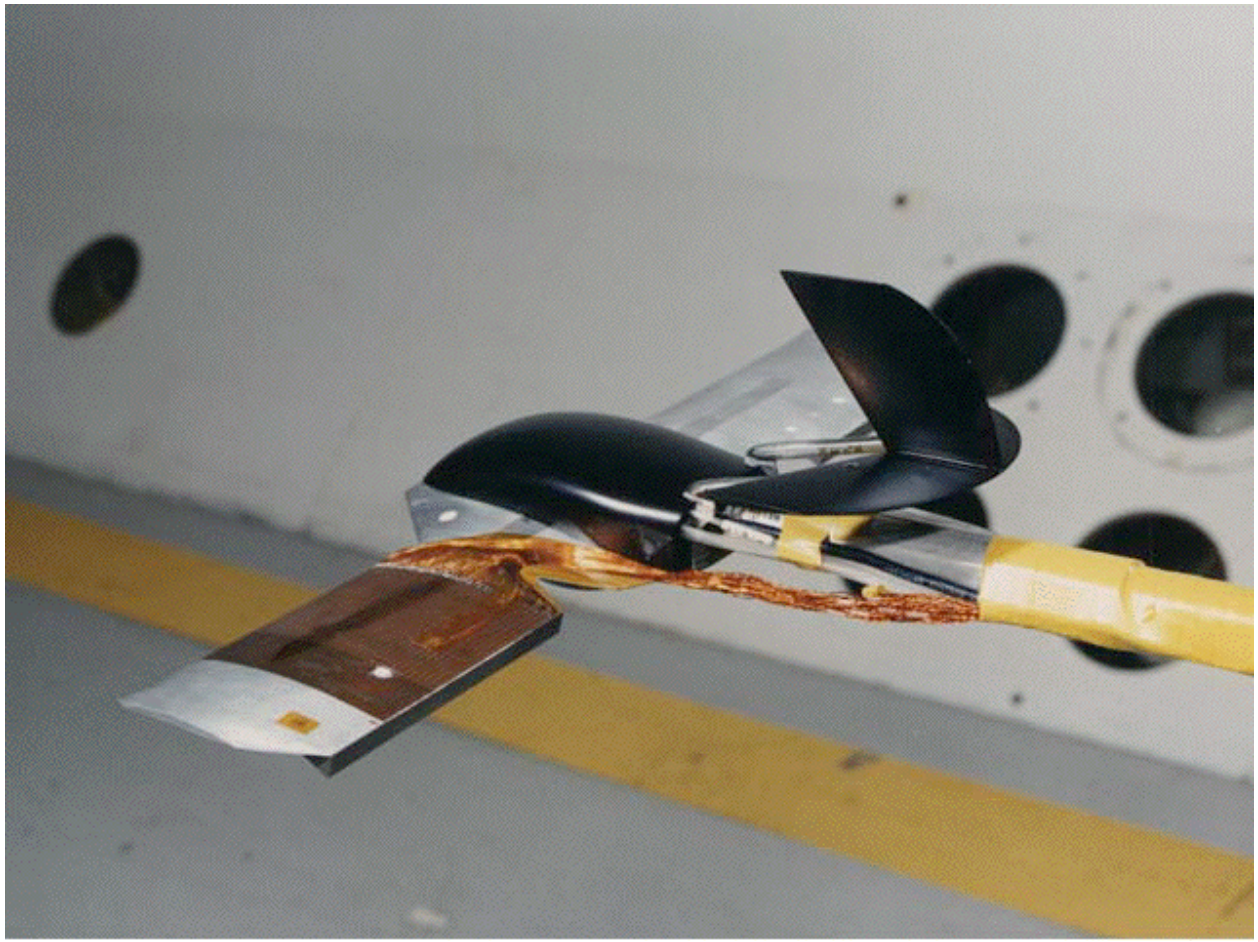

L99-01780

(b) MA-SF-1 configuration with wing trailing edge flaps deflected.

Figure 1. Continued.

L99-01957

(c) Model with sweptback wing and tails off.

Figure 1. Continued.

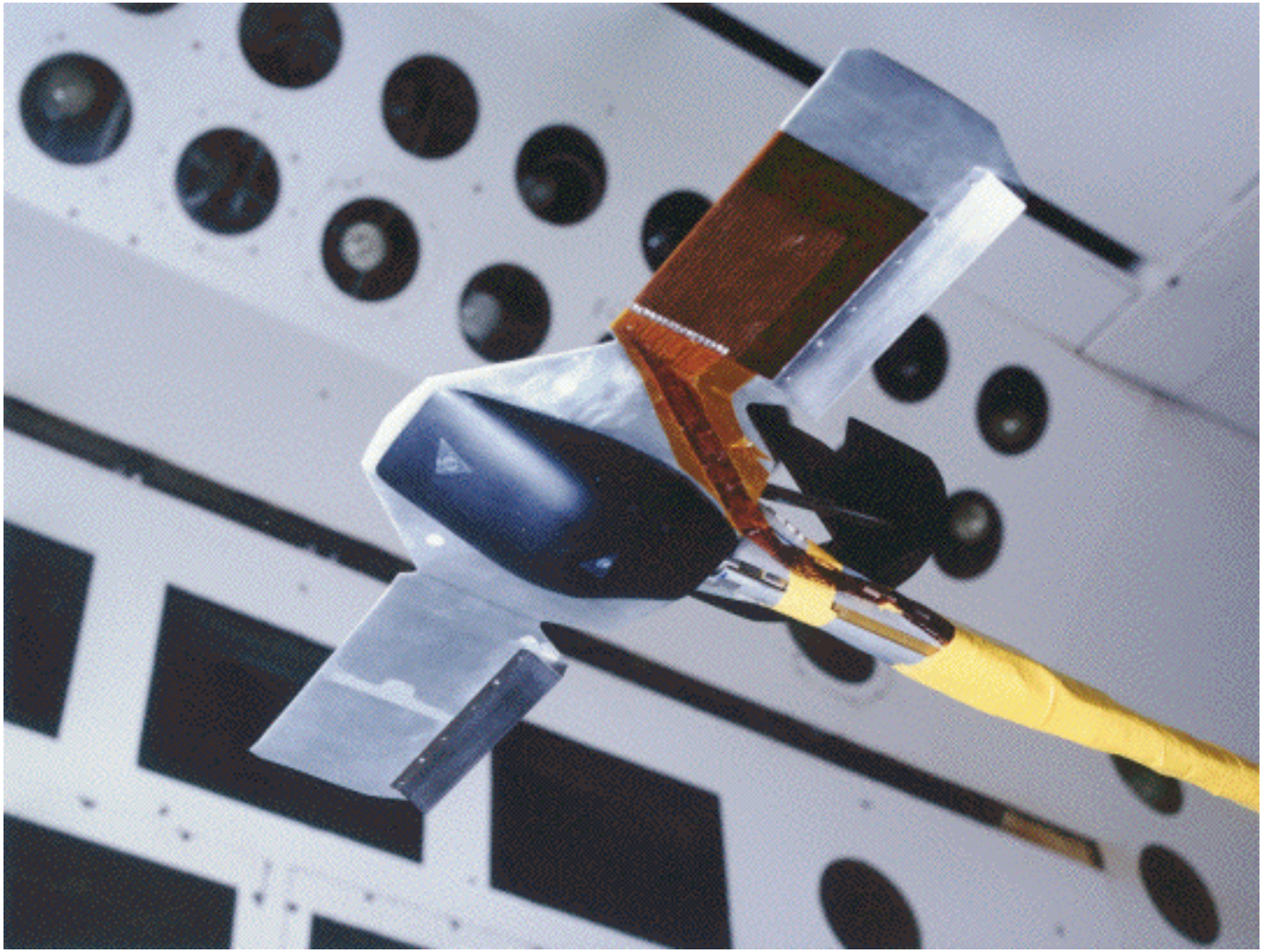

L99-01779

(d) Bottom view of model MA-SF-1 with split flaps deflected.

Figure 1. Continued.

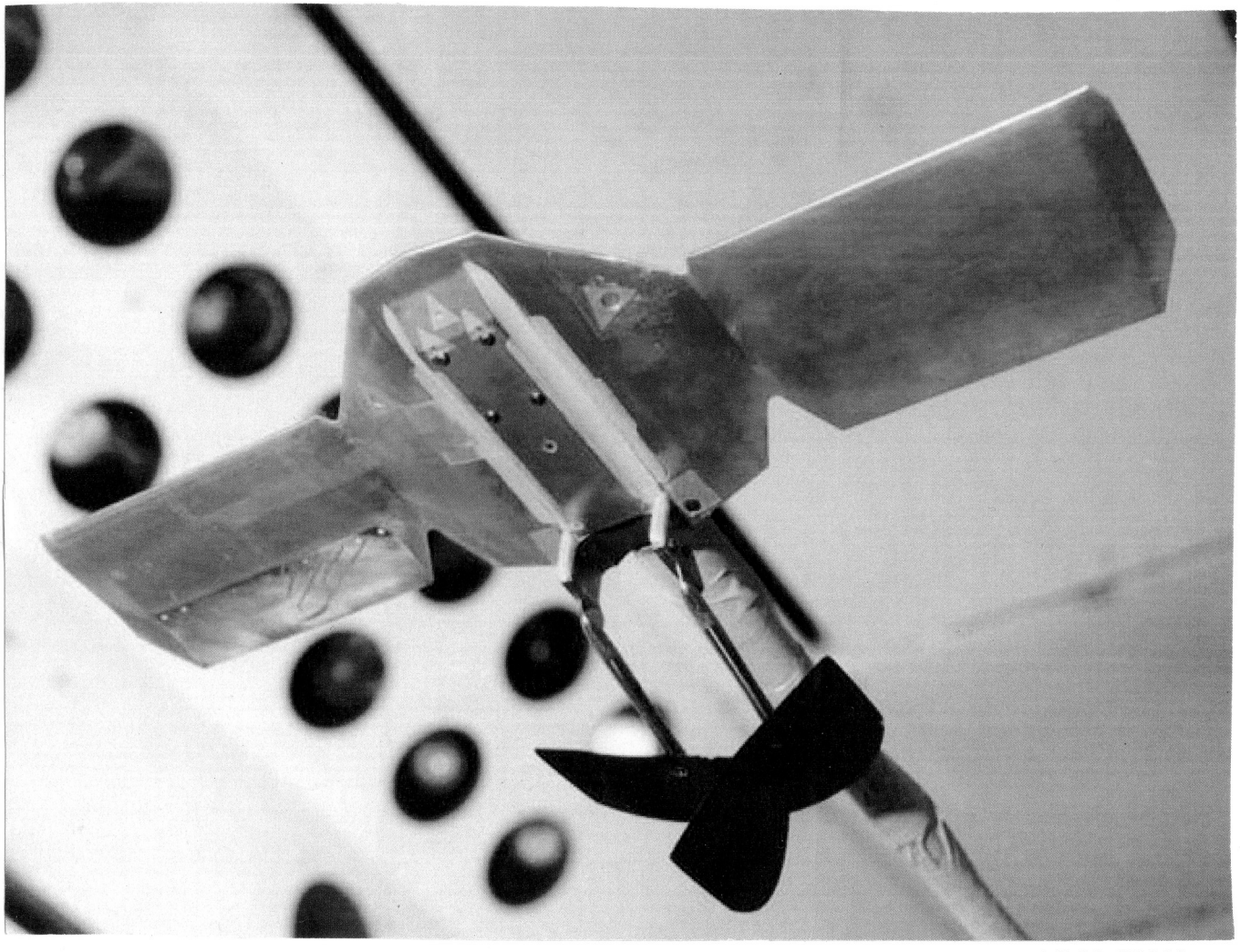

L99-02392

(e) Bottom view of model MA-SC-1 with tails inverted and lower fuselage fairing removed.

Figure 1. Concluded.

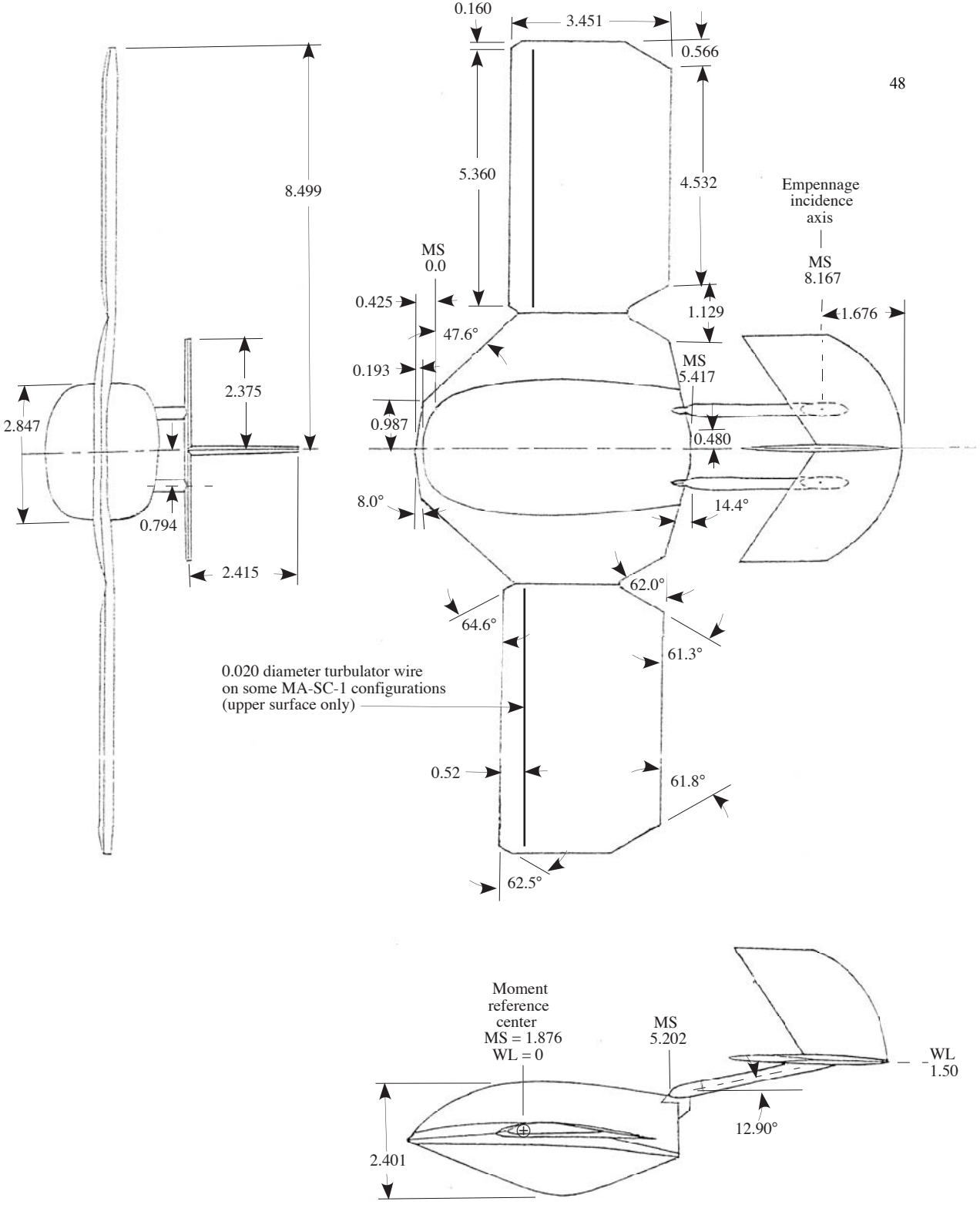

(a) Model assembled with unswept wings.

Figure 2. Geometry of assembled model with unswept wings and tails in the upright position. All dimensions are in inches unless otherwise indicated.

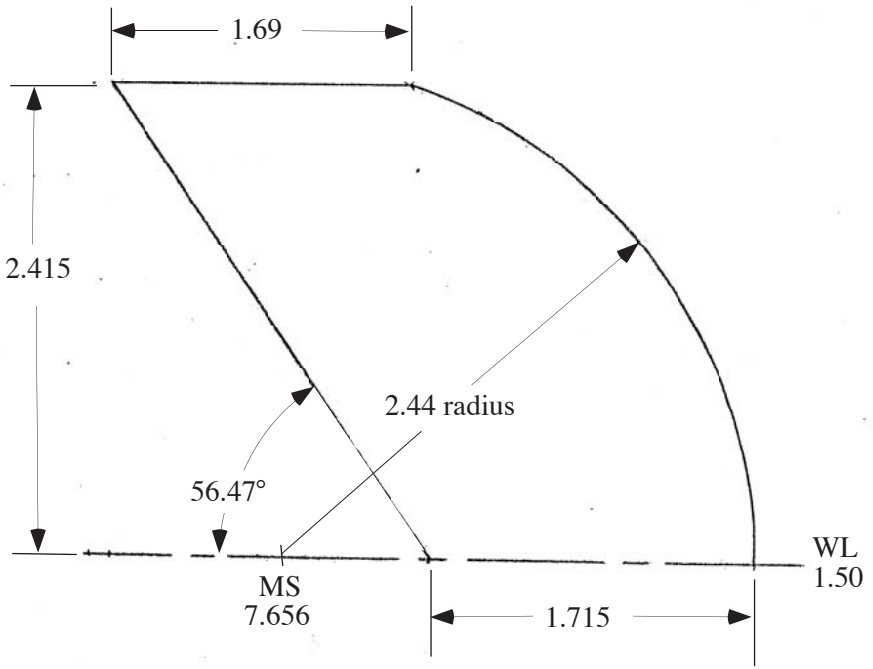

Vertical tail

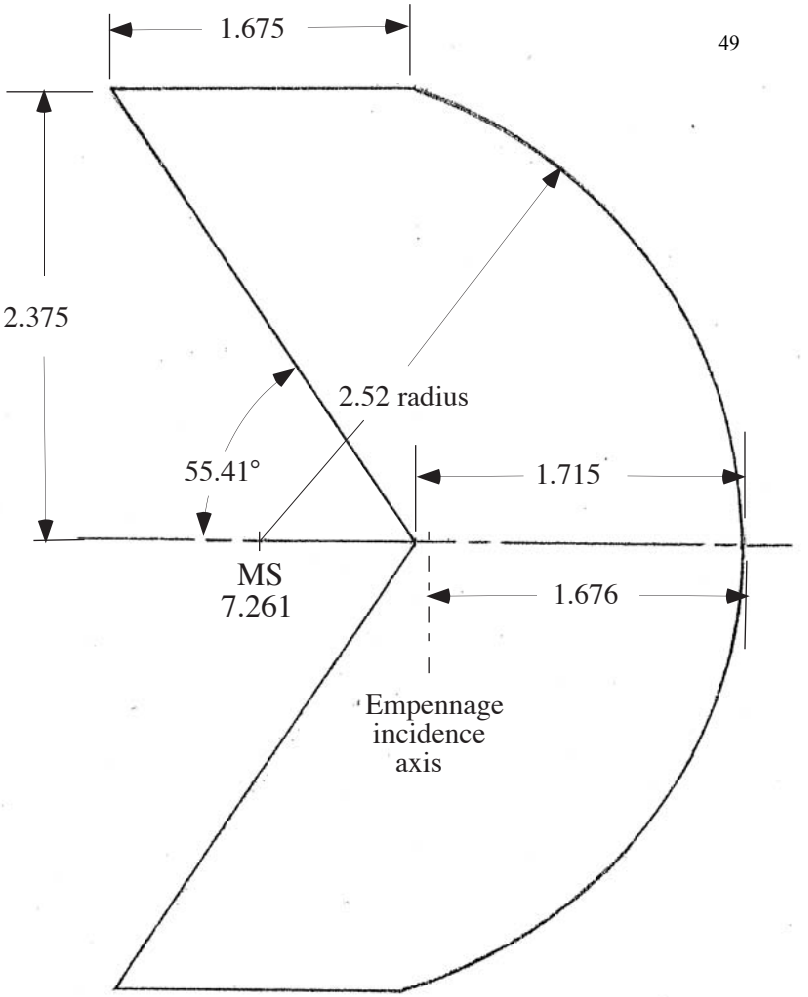

Horizontal tail

(b) Horizontal and vertical tail geometry.

Figure 2. Concluded.

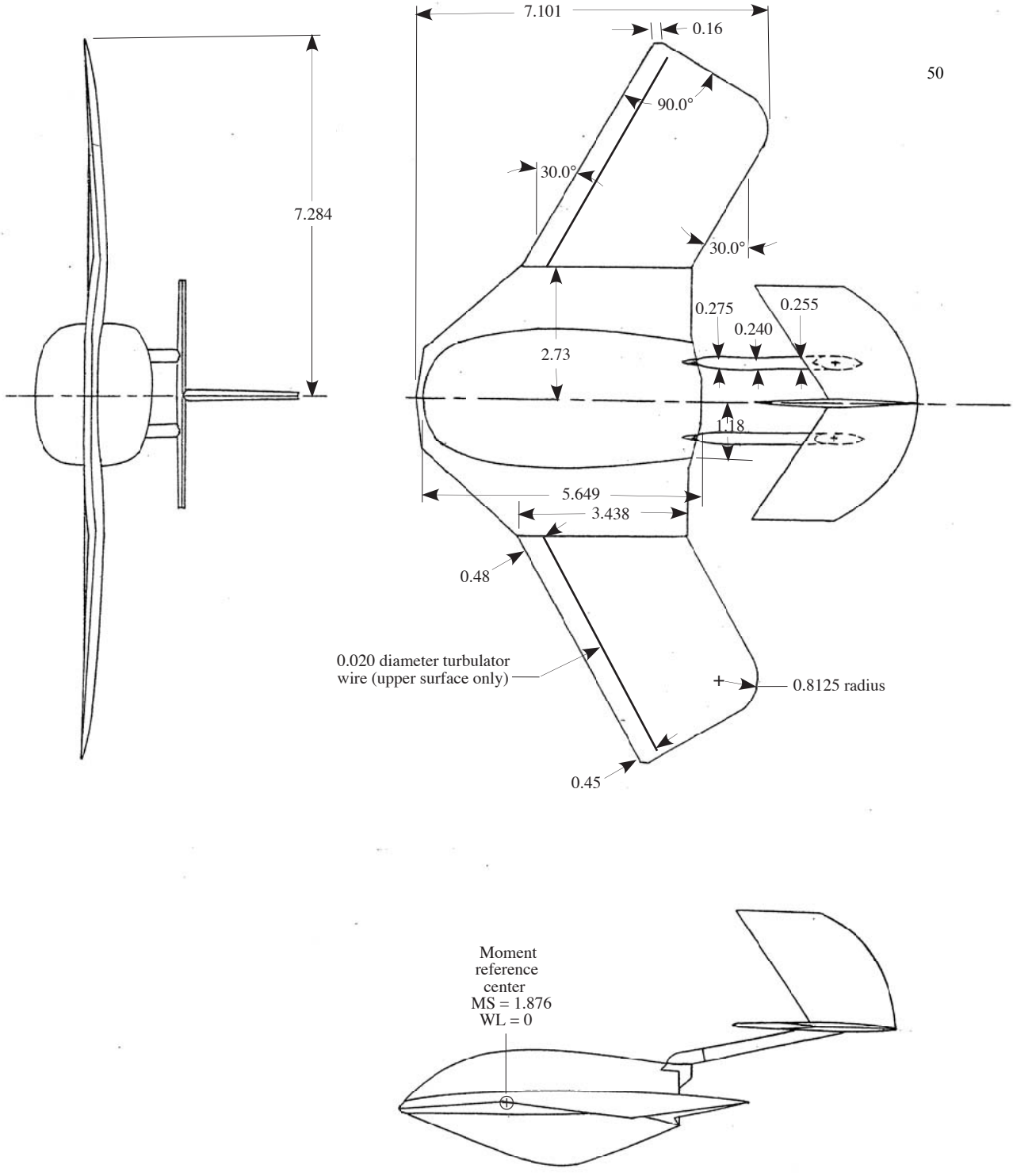

Figure 3. Geometry of swept wing model configuration. All dimensions in inches unless otherwise indicated.

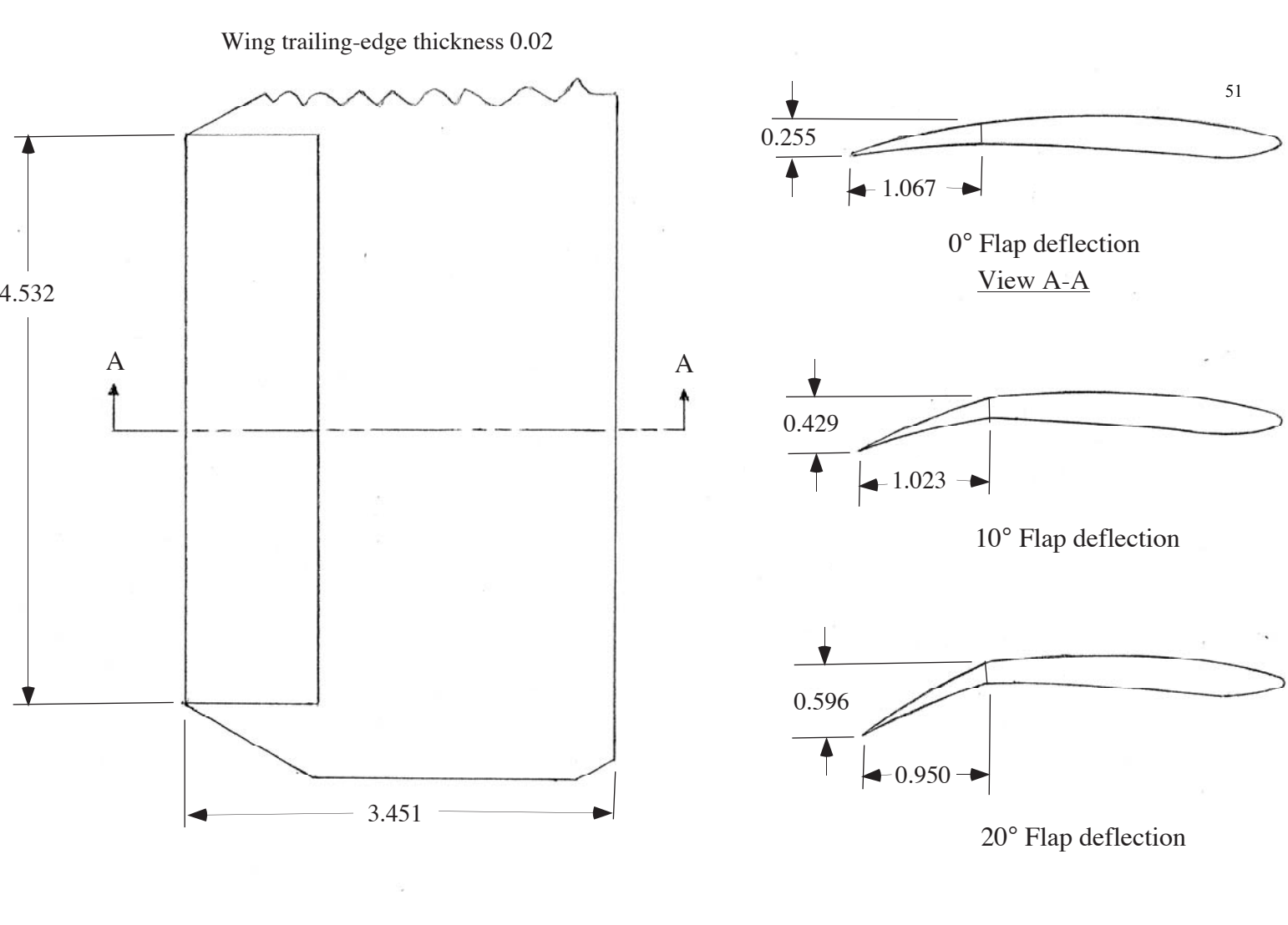

(a) Flap details on MA-SC-1.

Figure 4. Flap deflection and geometry details for unswept wings MA-SC-1 and MA-SF-1. All dimensions are in inches unless otherwise indicated. Wing trailing-edge thickness 0.02.

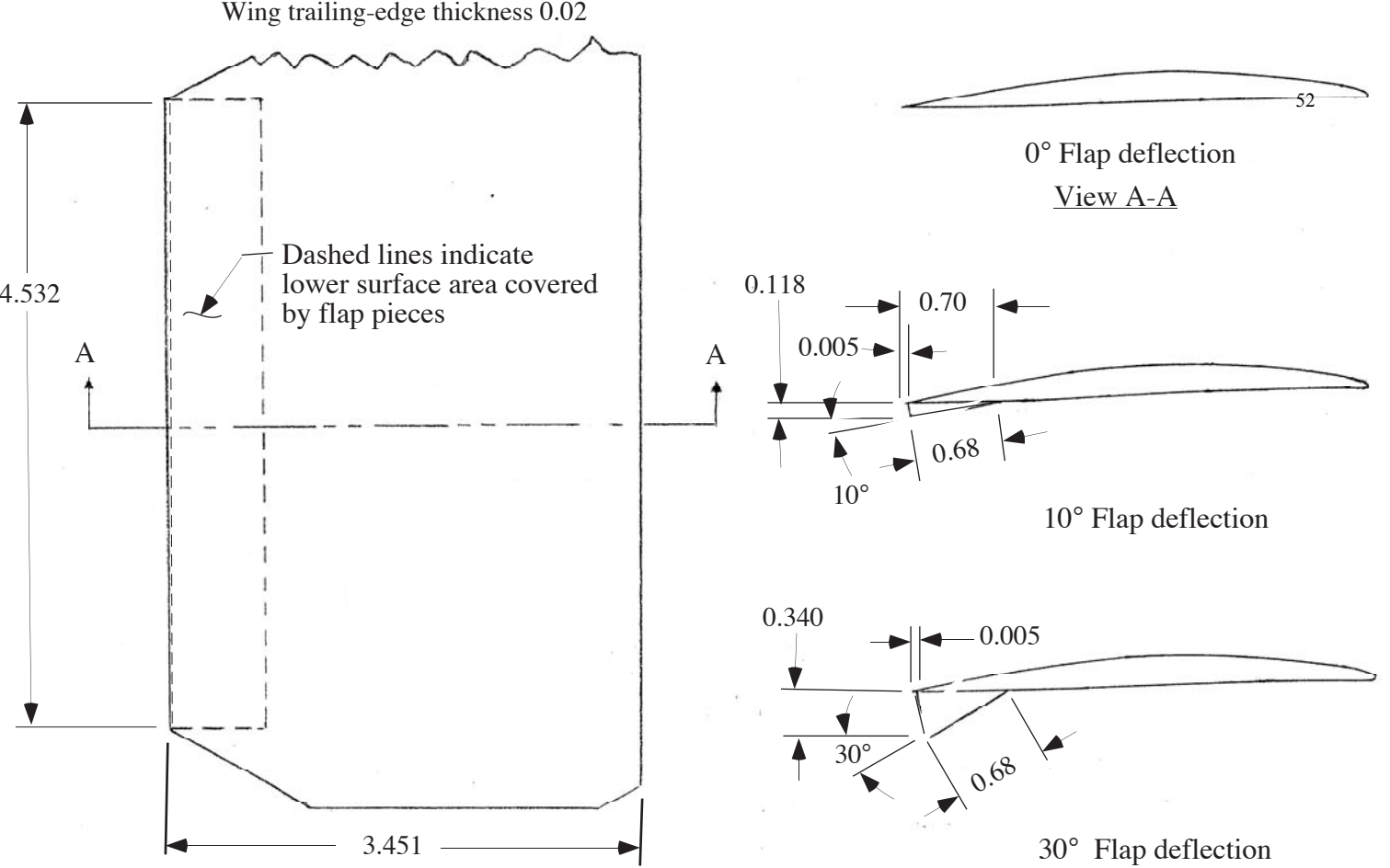

(b) Flap details on MA-SF-1.

Figure 4. Concluded.

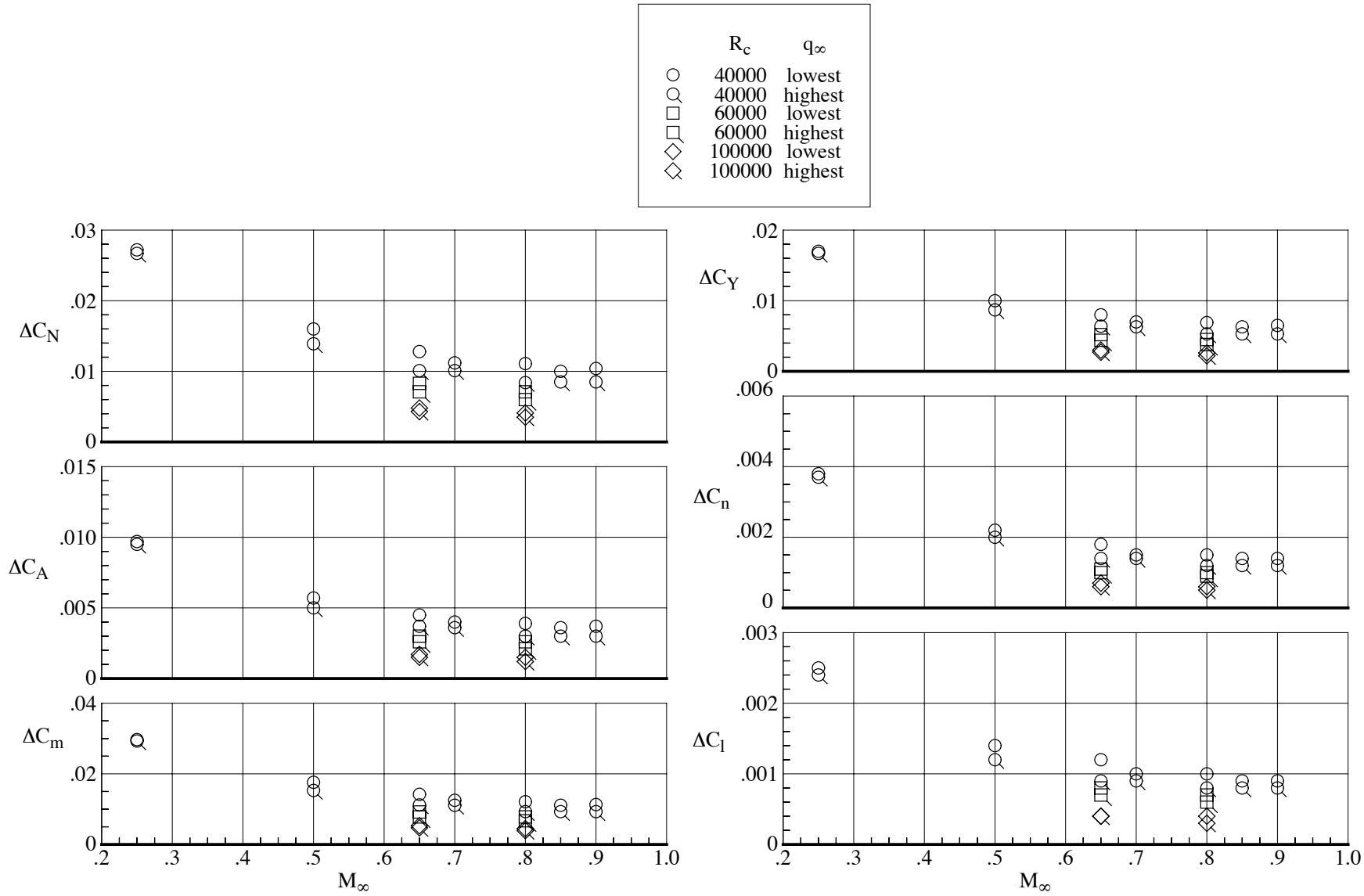

Figure 5. Aerodynamic coefficient accuracies (unswept wing reference constants) based on balance calibration accuracies for the range of freestream Reynolds number and (nominal) dynamic pressure conditions.

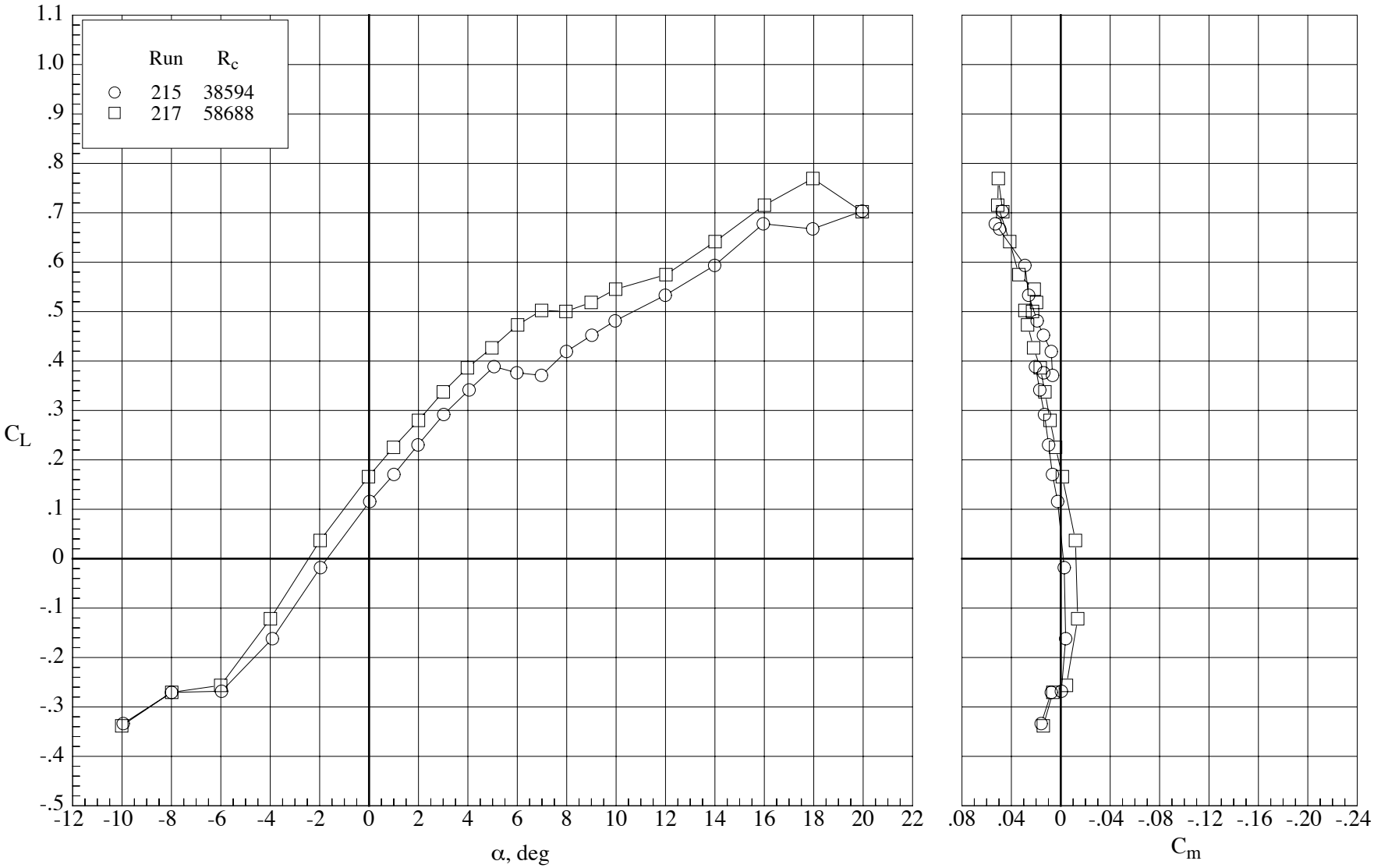

(a) Lift and pitching-moment coefficients.

Figure 6. Effect of Reynolds number on the longitudinal aerodynamic characteristics of the model with the Eppler 387 wing (bump off) at Mach number 0.65. $\delta_h = 0°$, $\delta_f = 0°$.

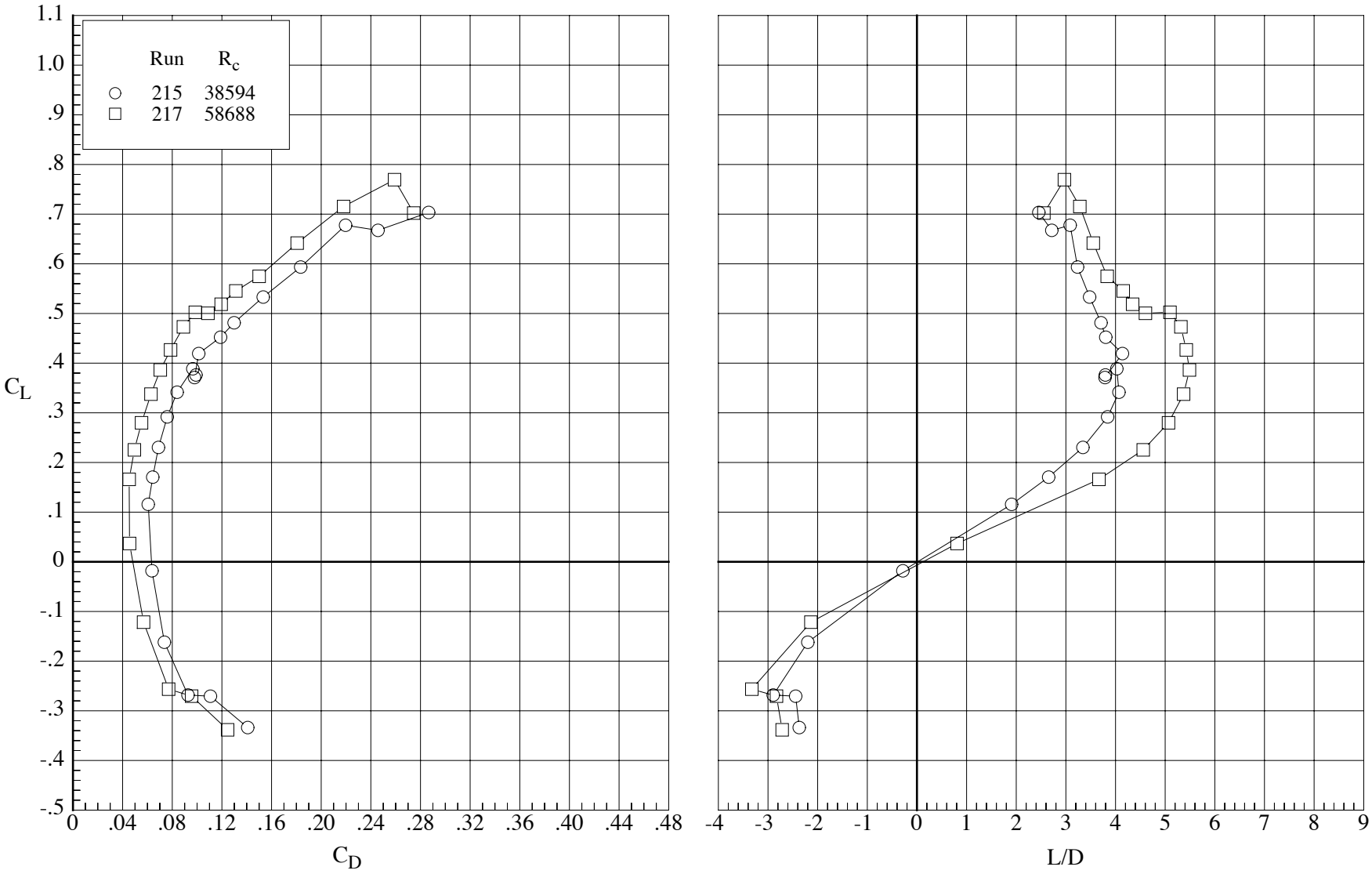

(b) Drag coefficient and lift-drag ratio.

Figure 6. Concluded.

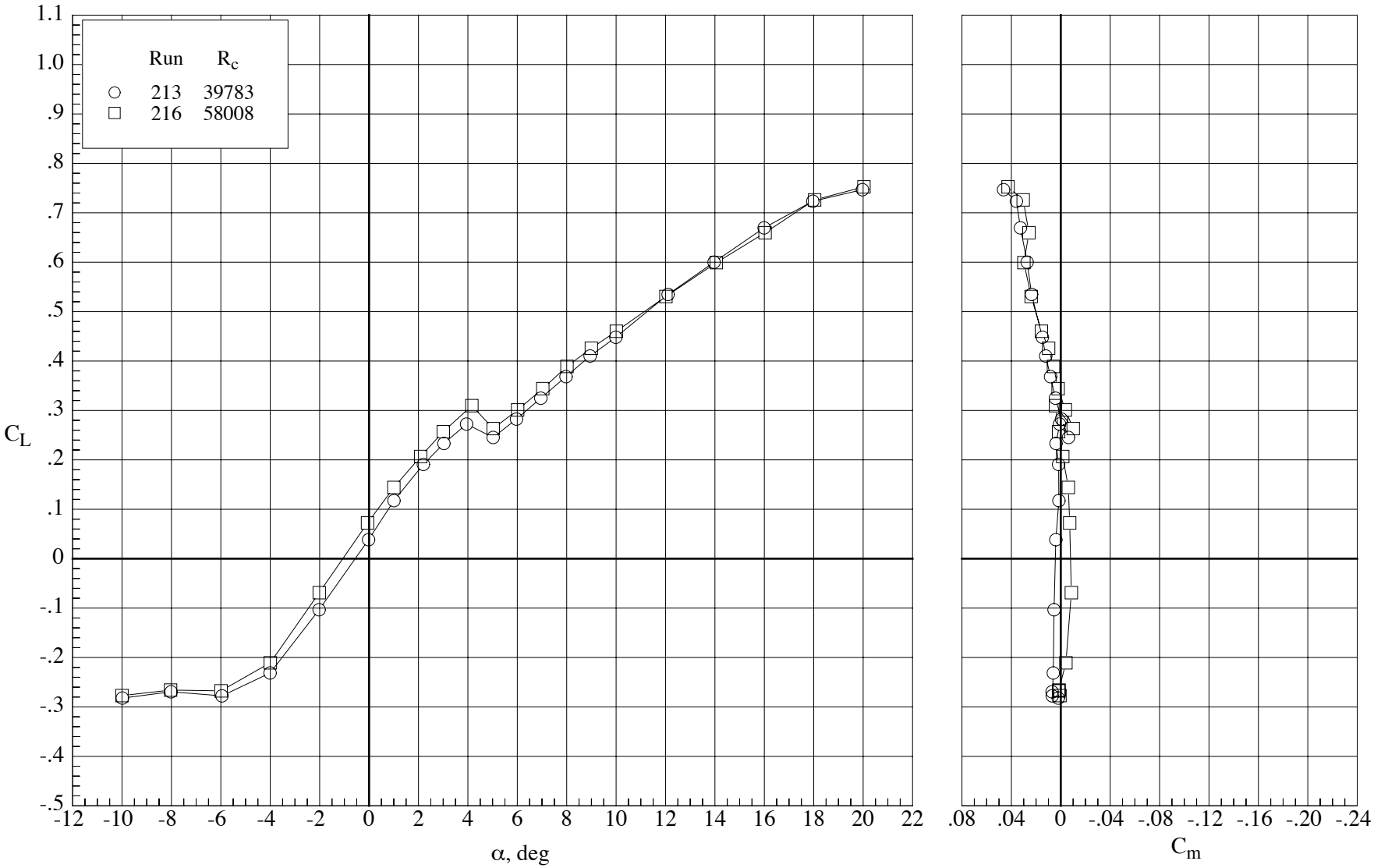

(a) Lift and pitching-moment coefficients.

Figure 7. Effect of Reynolds number on the longitudinal aerodynamic characteristics of the model with the Eppler 387 wing (bump off) at Mach number 0.80. $\delta_h = 0°$, $\delta_f = 0°$.

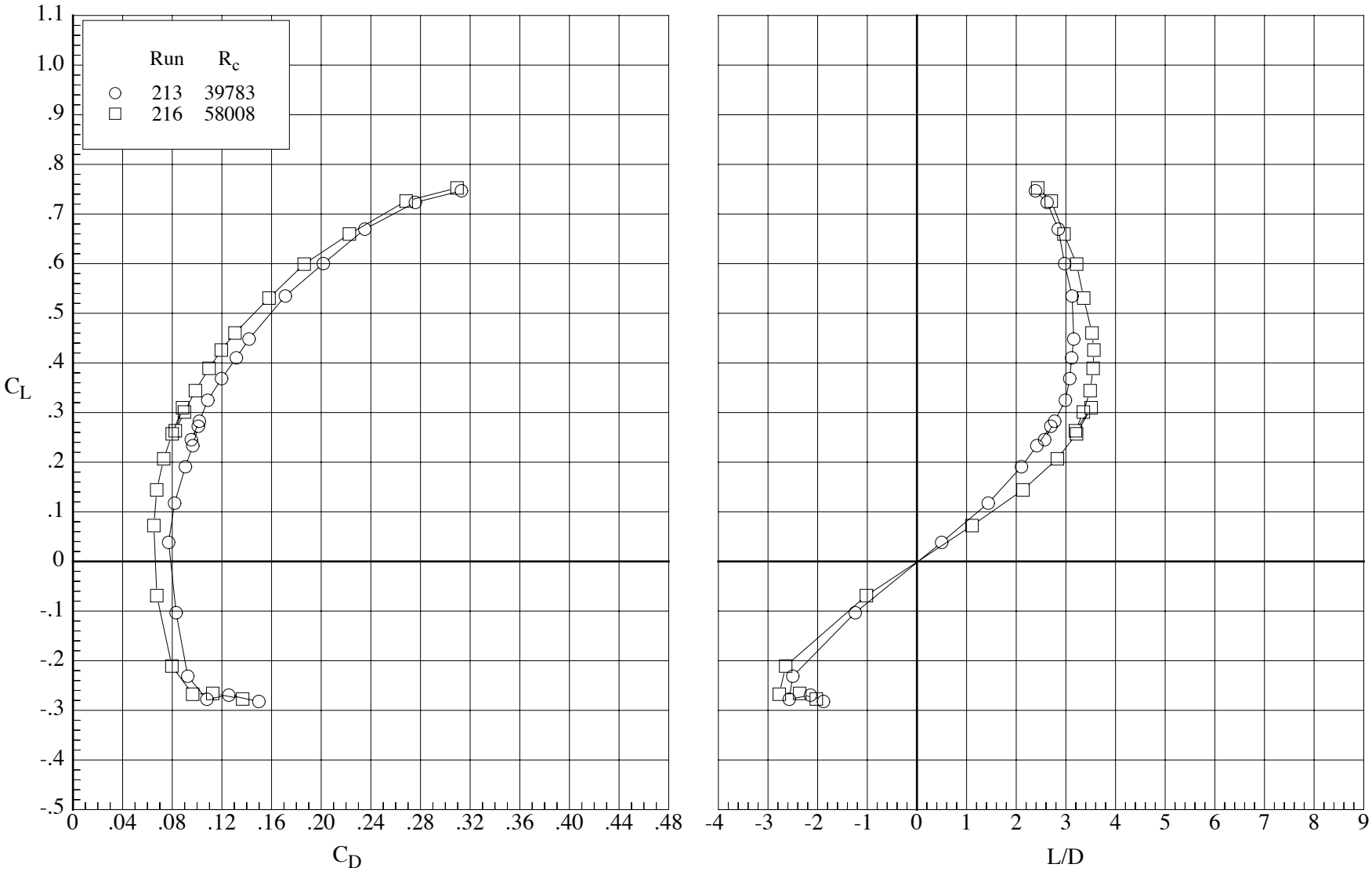

(b) Drag coefficient and lift-drag ratio.

Figure 7. Concluded.

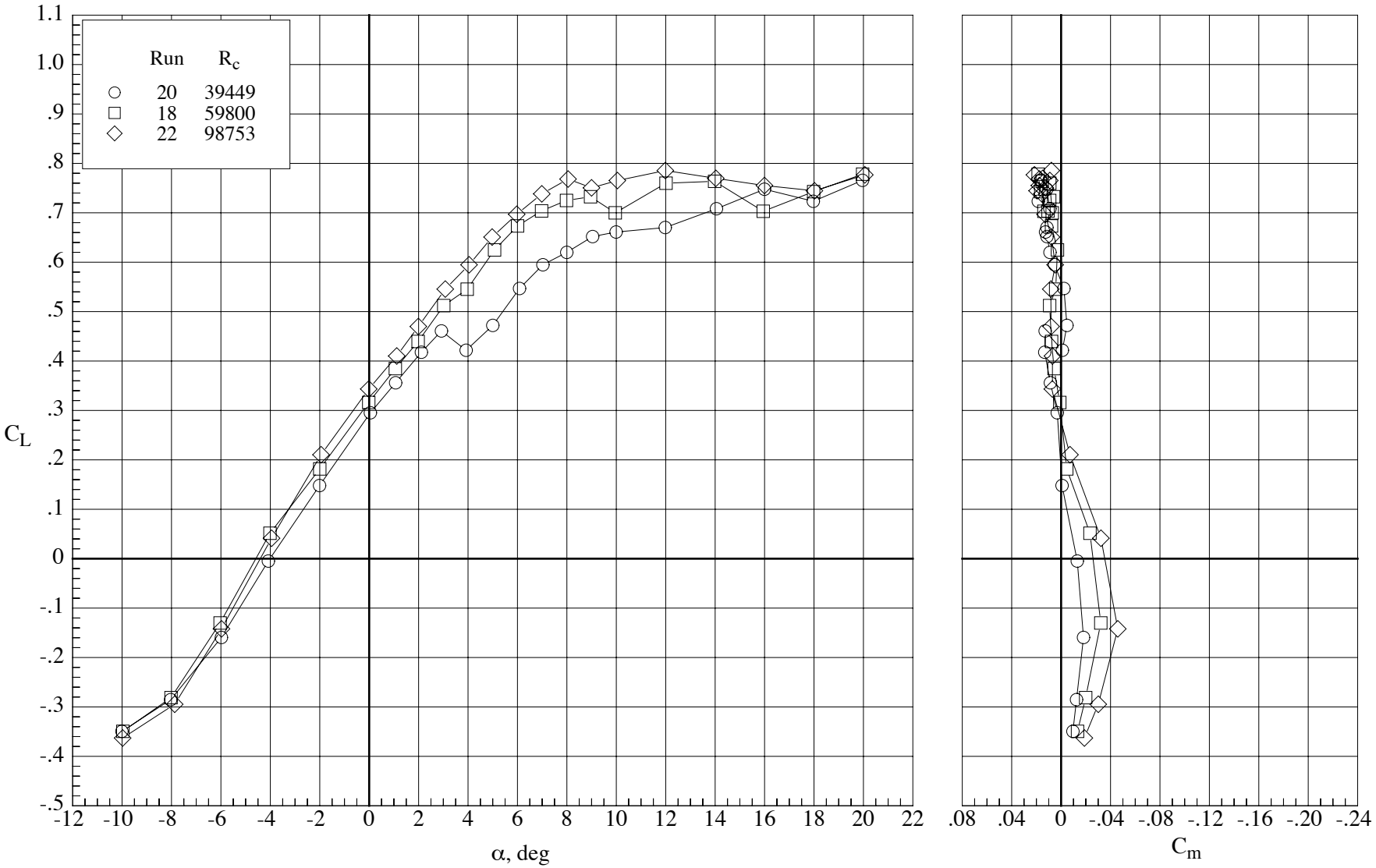

(a) Lift and pitching-moment coefficients.

Figure 8. Effect of Reynolds number on the longitudinal aerodynamic characteristics of the model with the MA-SC-1 wing (bump off) at Mach number 0.65. $\delta_h = 0°$, $\delta_f = 0°$.

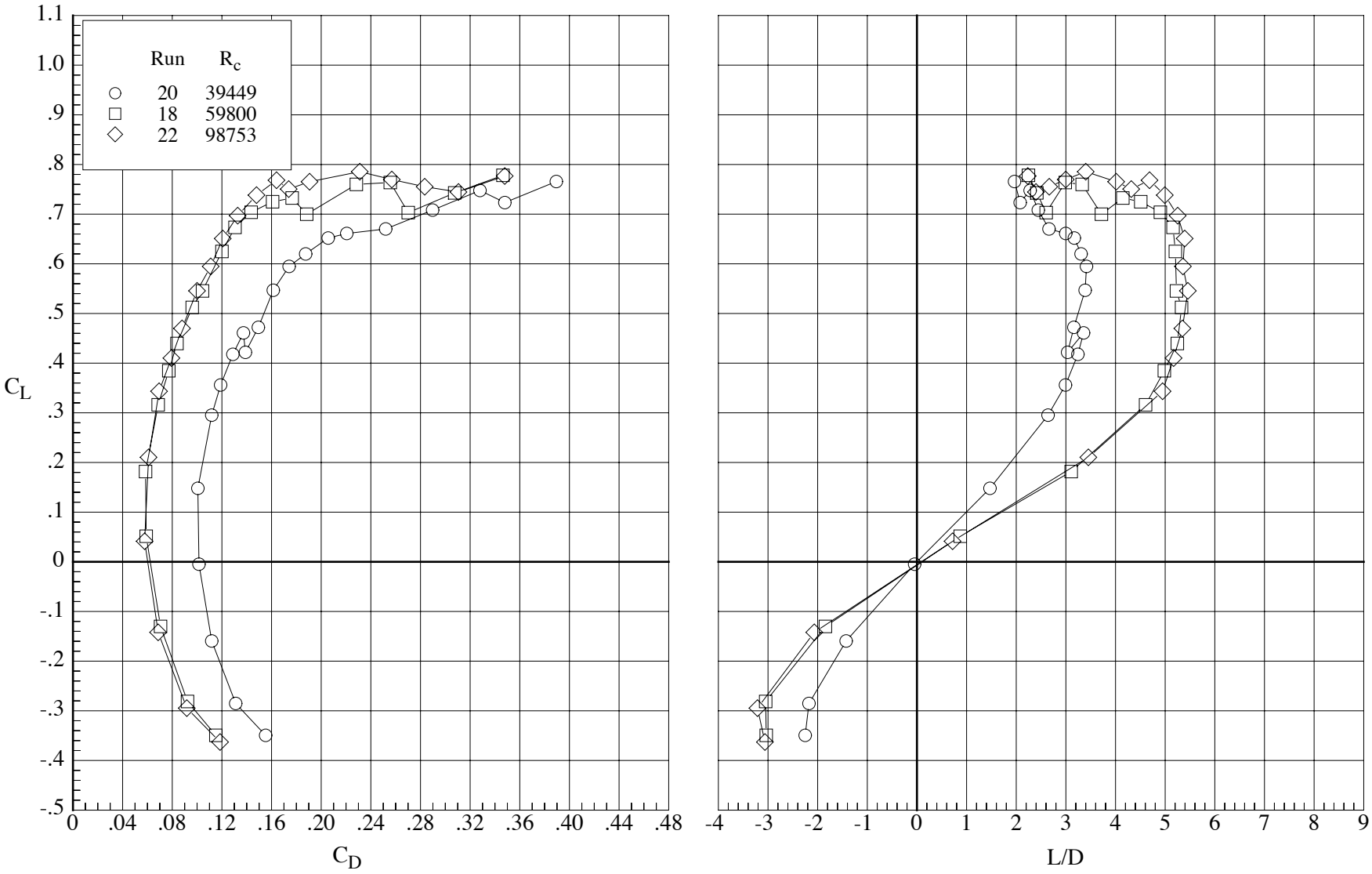

(b) Drag coefficient and lift-drag ratio.

Figure 8. Concluded.

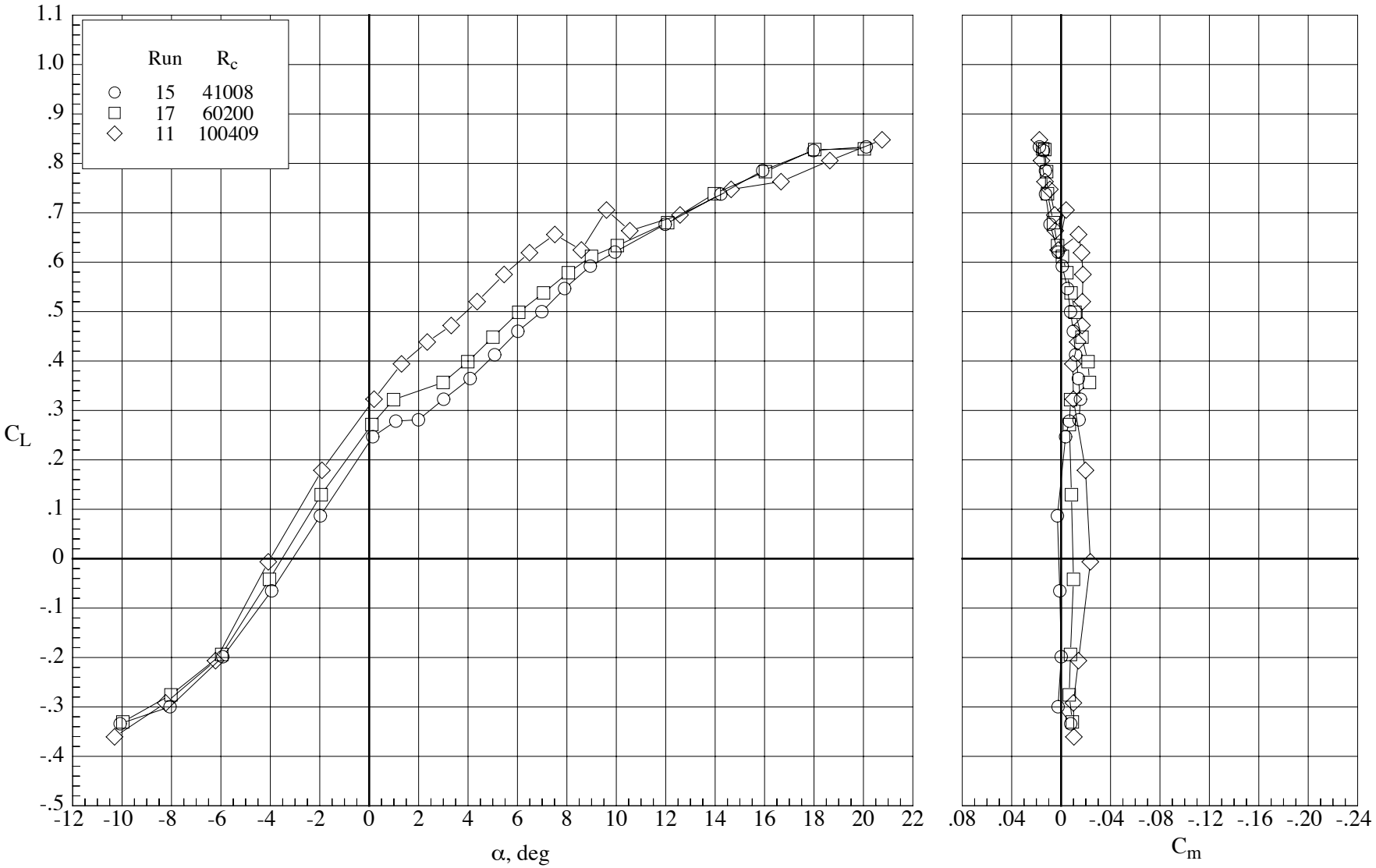

(a) Lift and pitching-moment coefficients.

Figure 9. Effect of Reynolds number on the longitudinal aerodynamic characteristics of the model with the MA-SC-1 wing (bump off) at Mach number 0.80. $\delta_h = 0°$, $\delta_f = 0°$.

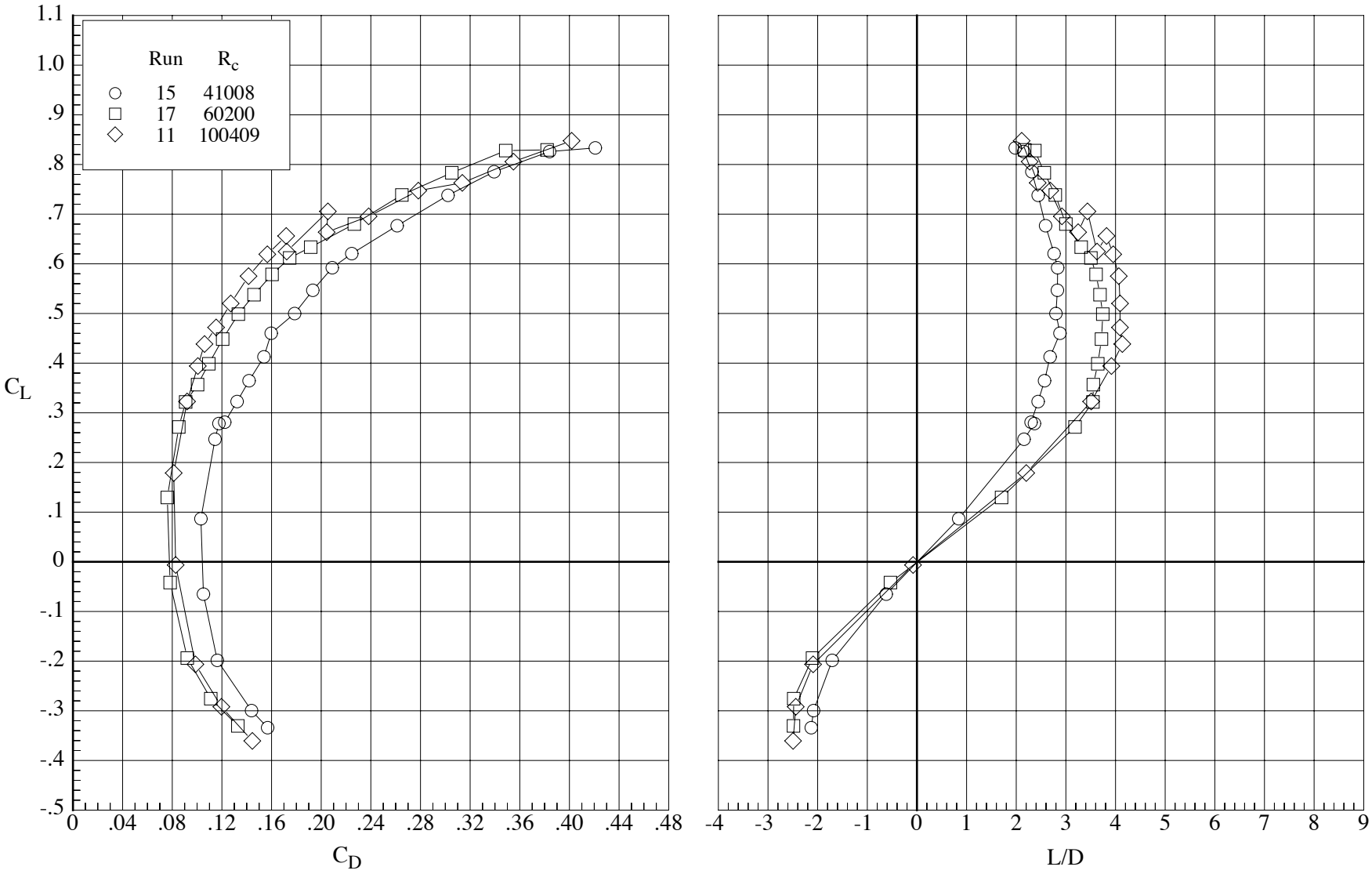

(b) Drag coefficient and lift-drag ratio.

Figure 9. Concluded.

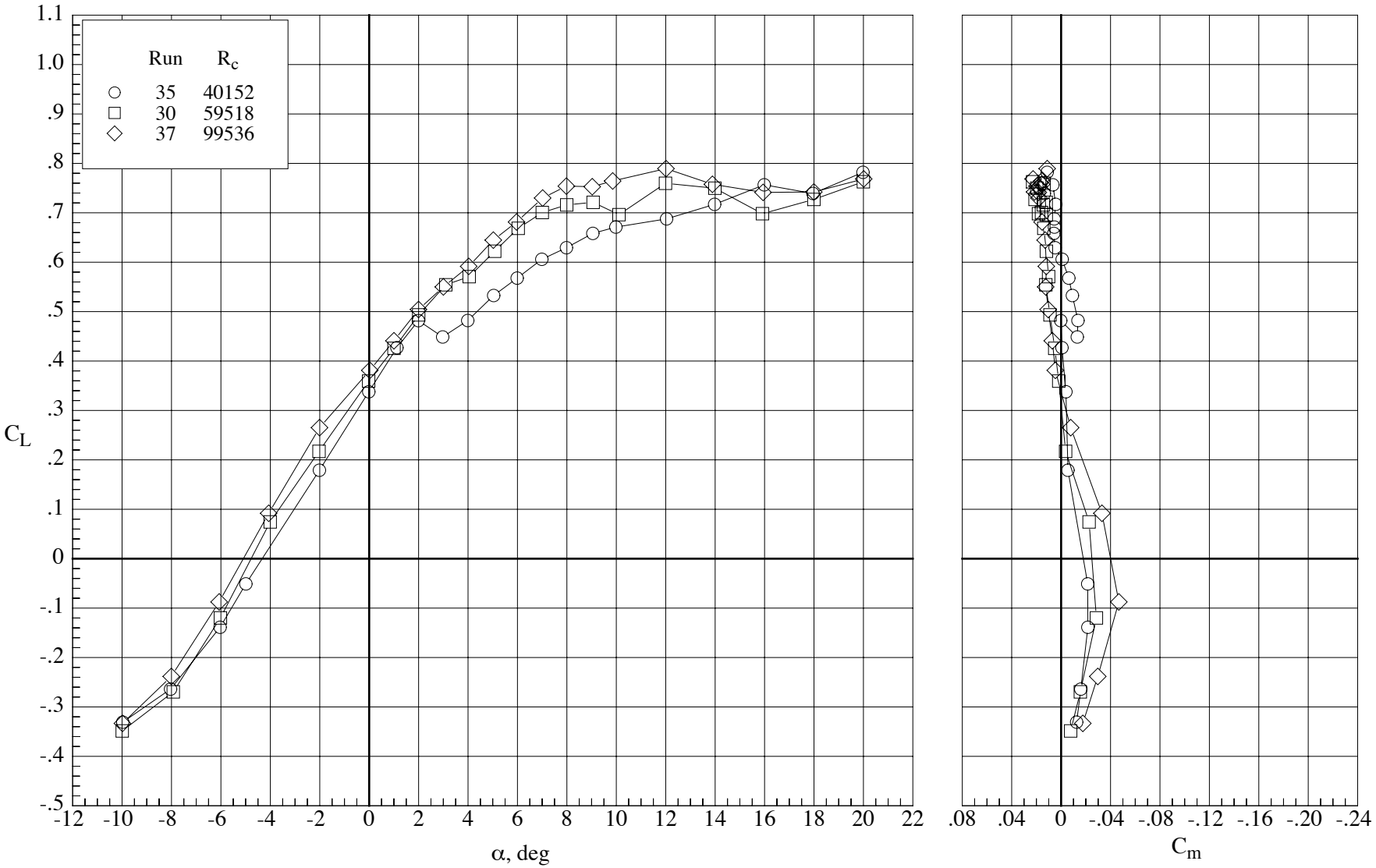

(a) Lift and pitching-moment coefficients.

Figure 10. Effect of Reynolds number on the longitudinal aerodynamic characteristics of the model with the MA-SC-1 wing (bump on) at Mach number 0.65. $\delta_h = 0°$, $\delta_f = 0°$.

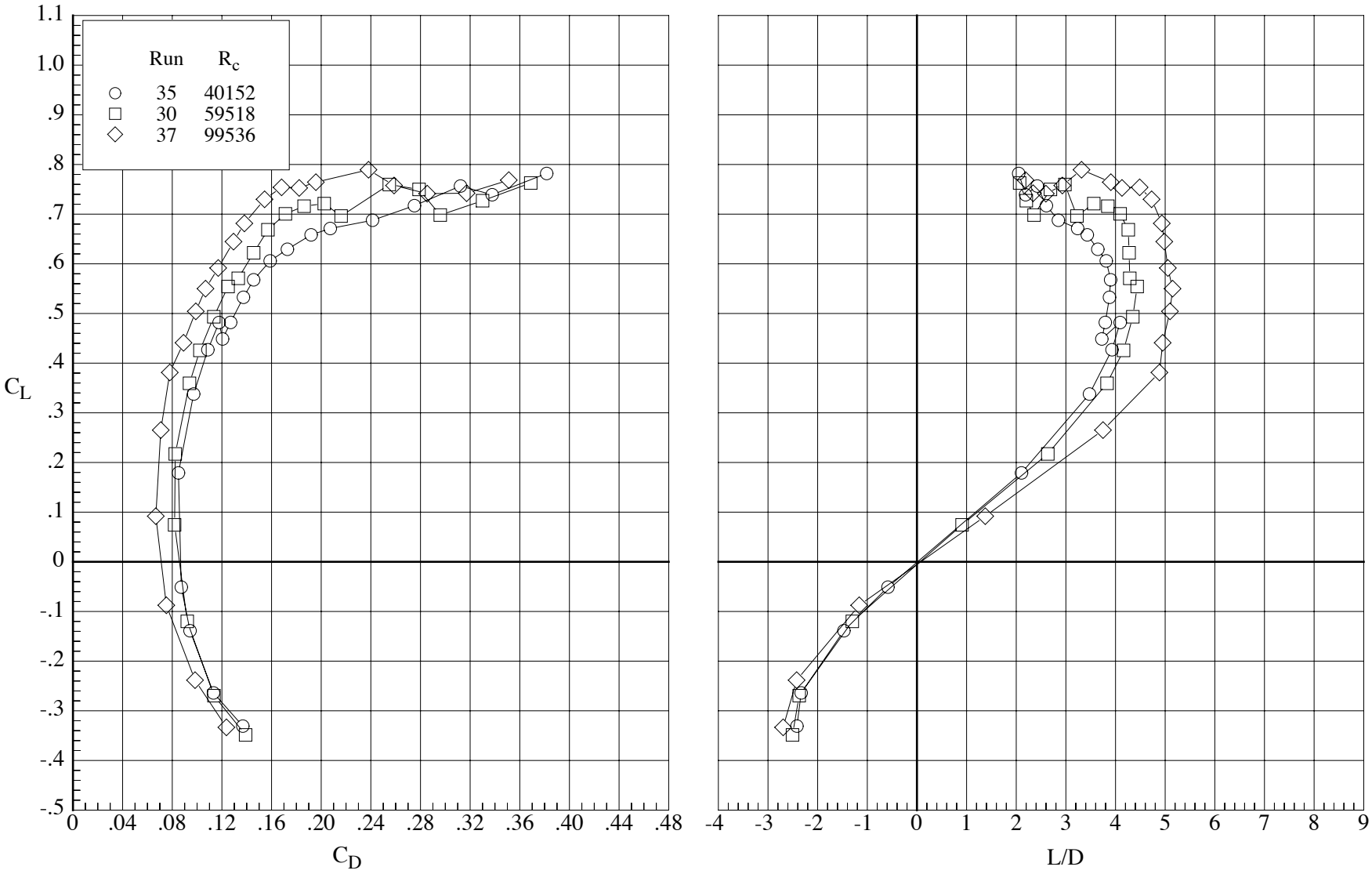

(b) Drag coefficient and lift-drag ratio.

Figure 10. Concluded.

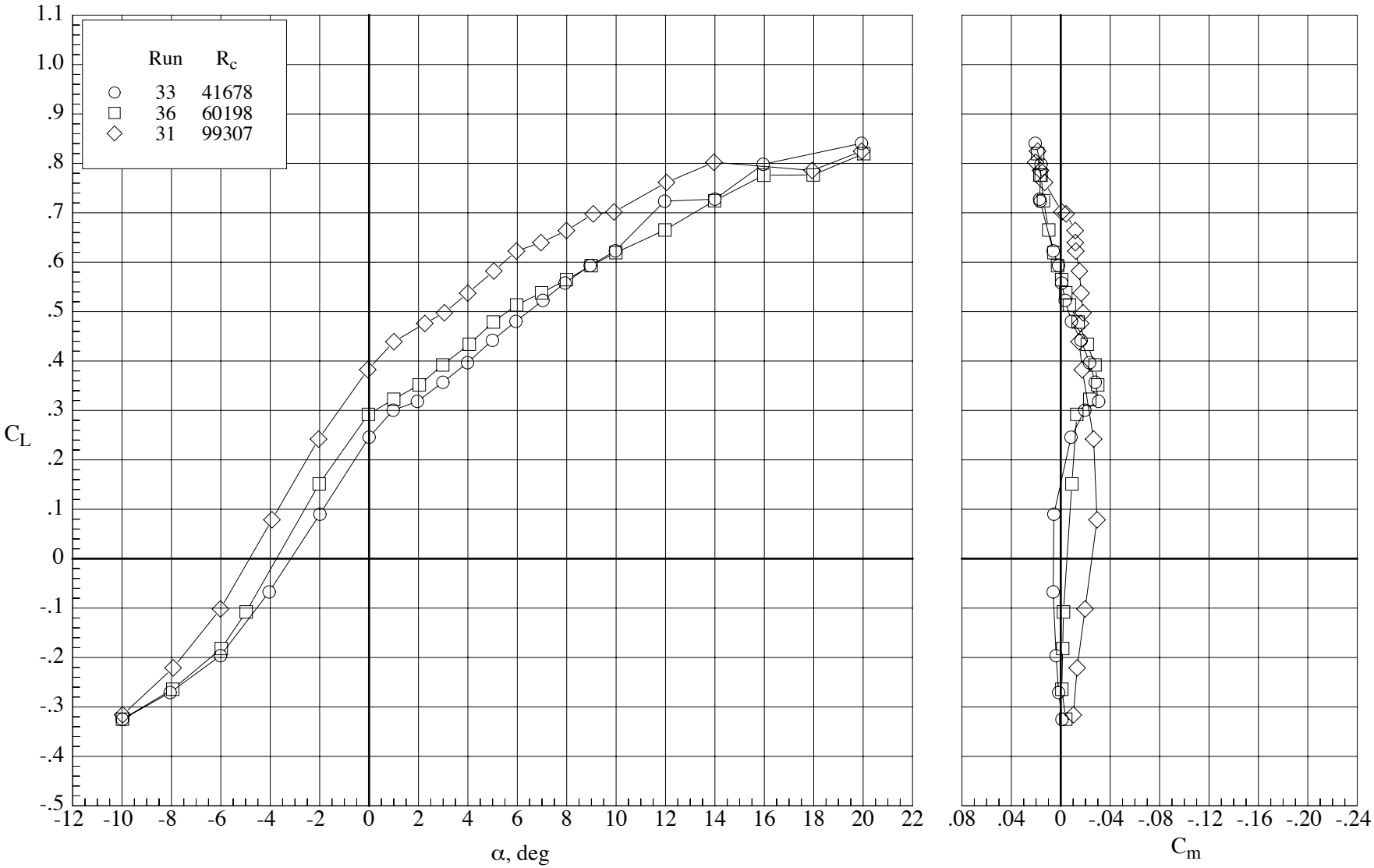

(a) Lift and pitching-moment coefficients.

Figure 11. Effect of Reynolds number on the longitudinal aerodynamic characteristics of the model with the MA-SC-1 wing (bump on) at Mach number 0.80. $\delta_h = 0°$, $\delta_f = 0°$.

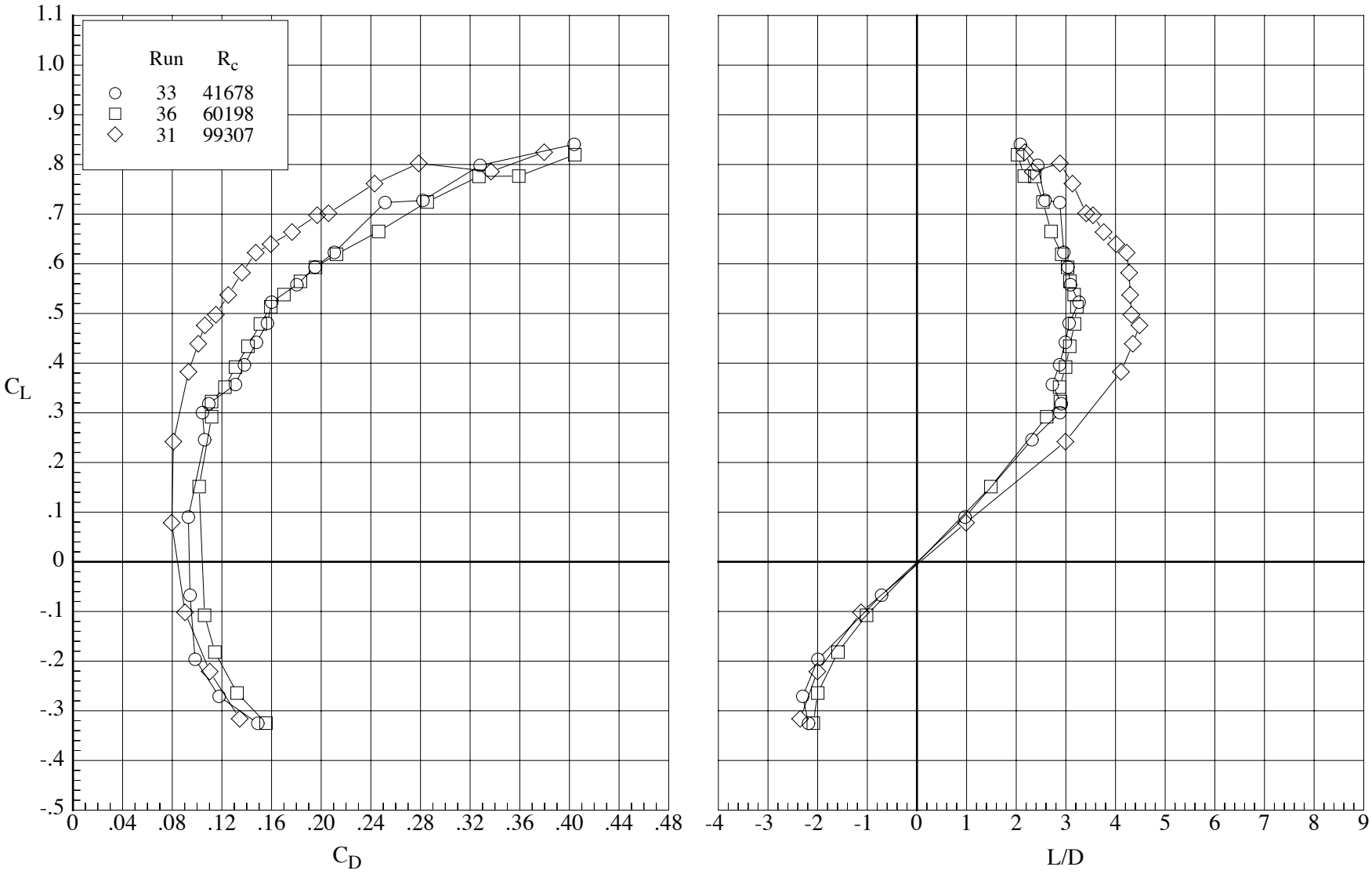

(b) Drag coefficient and lift-drag ratio.

Figure 11. Concluded.

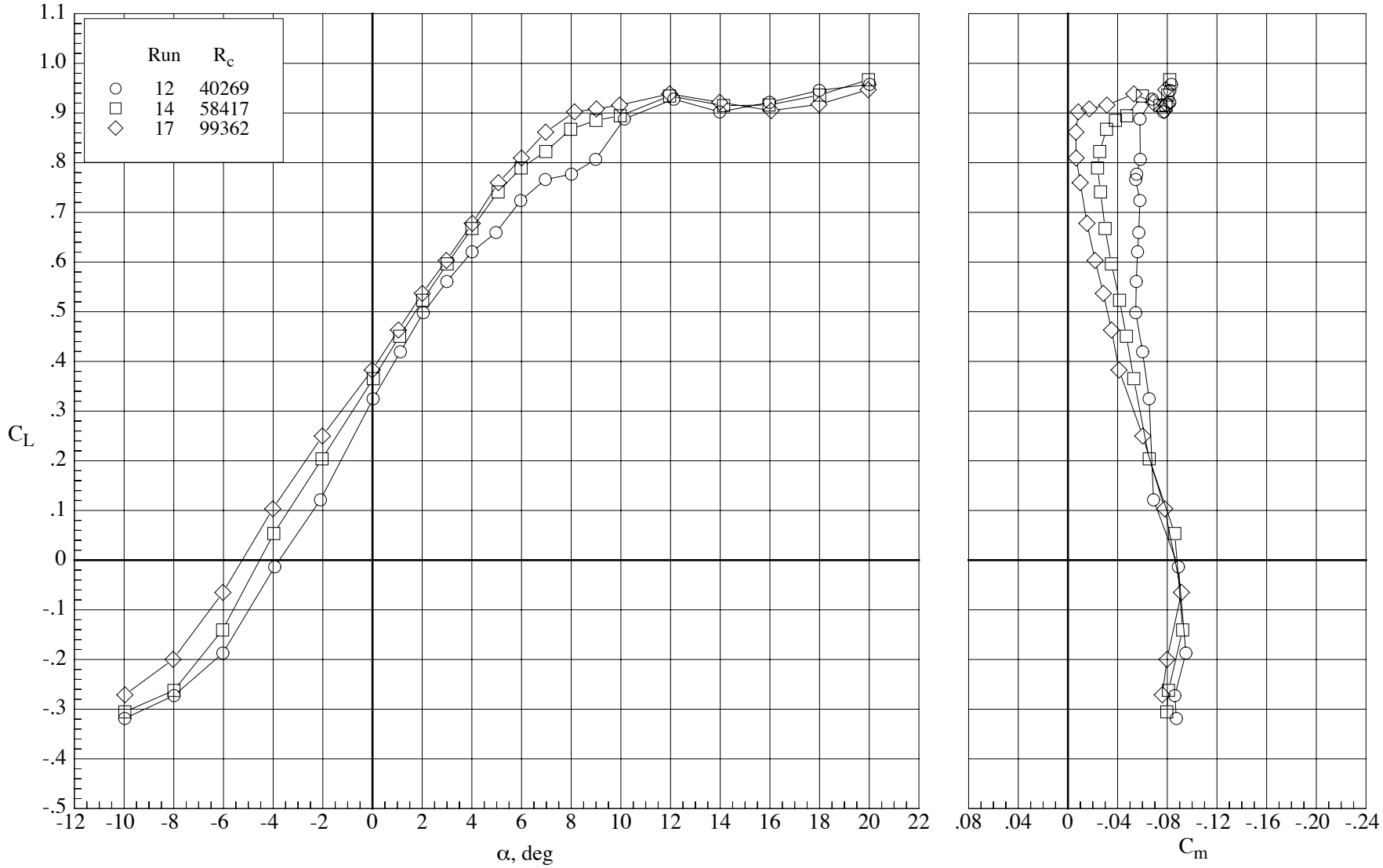

(a) Lift and pitching-moment coefficients.

Figure 12. Effect of Reynolds number on the longitudinal aerodynamic characteristics of the model with the MA-SC-1 wing (bump on) with the tails inverted and the lower fuselage removed at Mach number 0.65. $\delta_h = 0°$ and $\delta_f = 0°$.

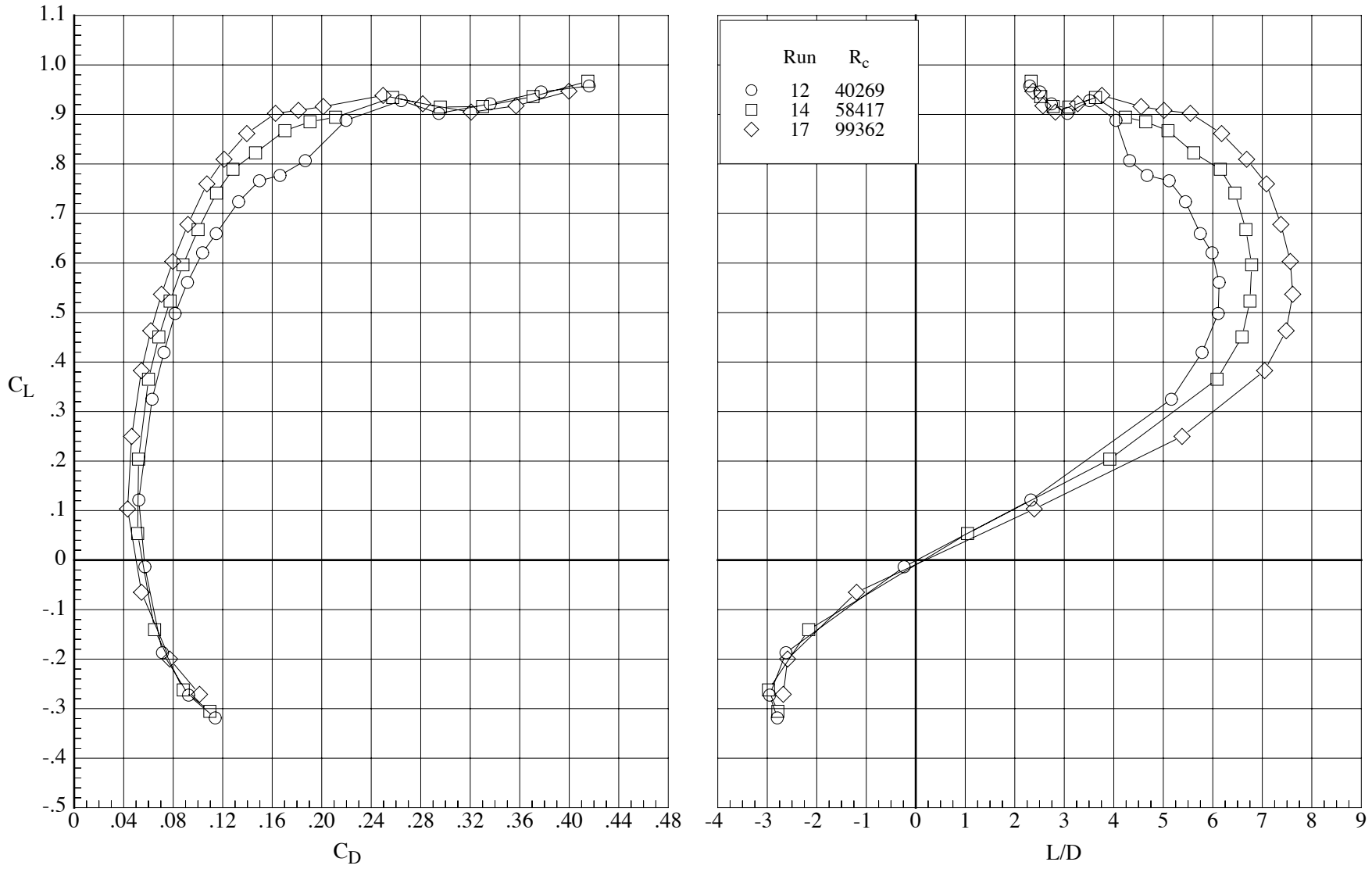

(b) Drag coefficient and lift-drag ratio.

Figure 12. Concluded.

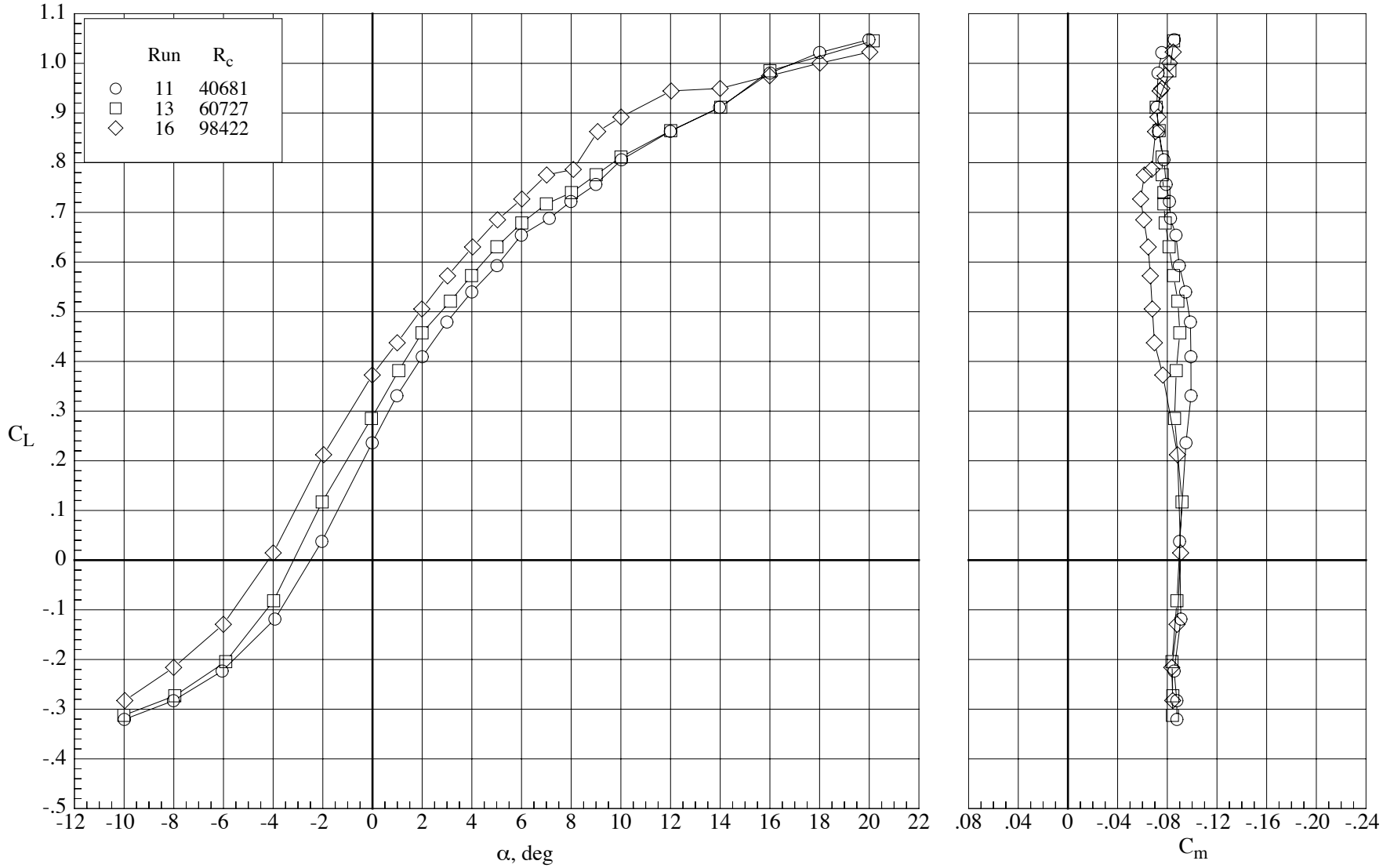

(a) Lift and pitching-moment coefficients.

Figure 13. Effect of Reynolds number on the longitudinal aerodynamic characteristics of the model with the MA-SC-1 wing (bump on) with the tails inverted and the lower fuselage removed at Mach number 0.80. $\delta_h = 0°$ and $\delta_f = 0°$.

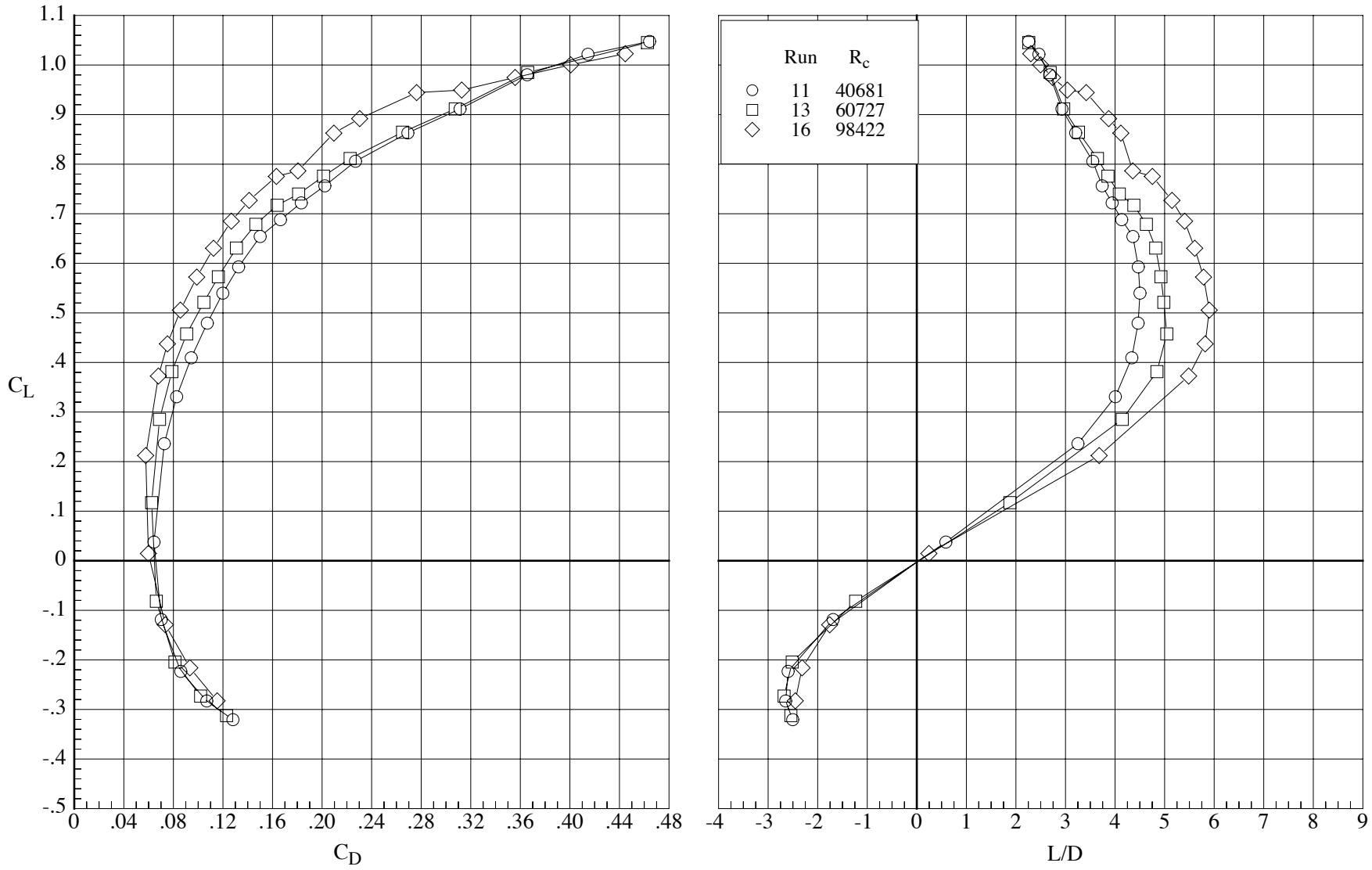

(b) Drag coefficient and lift-drag ratio.

Figure 13. Concluded.

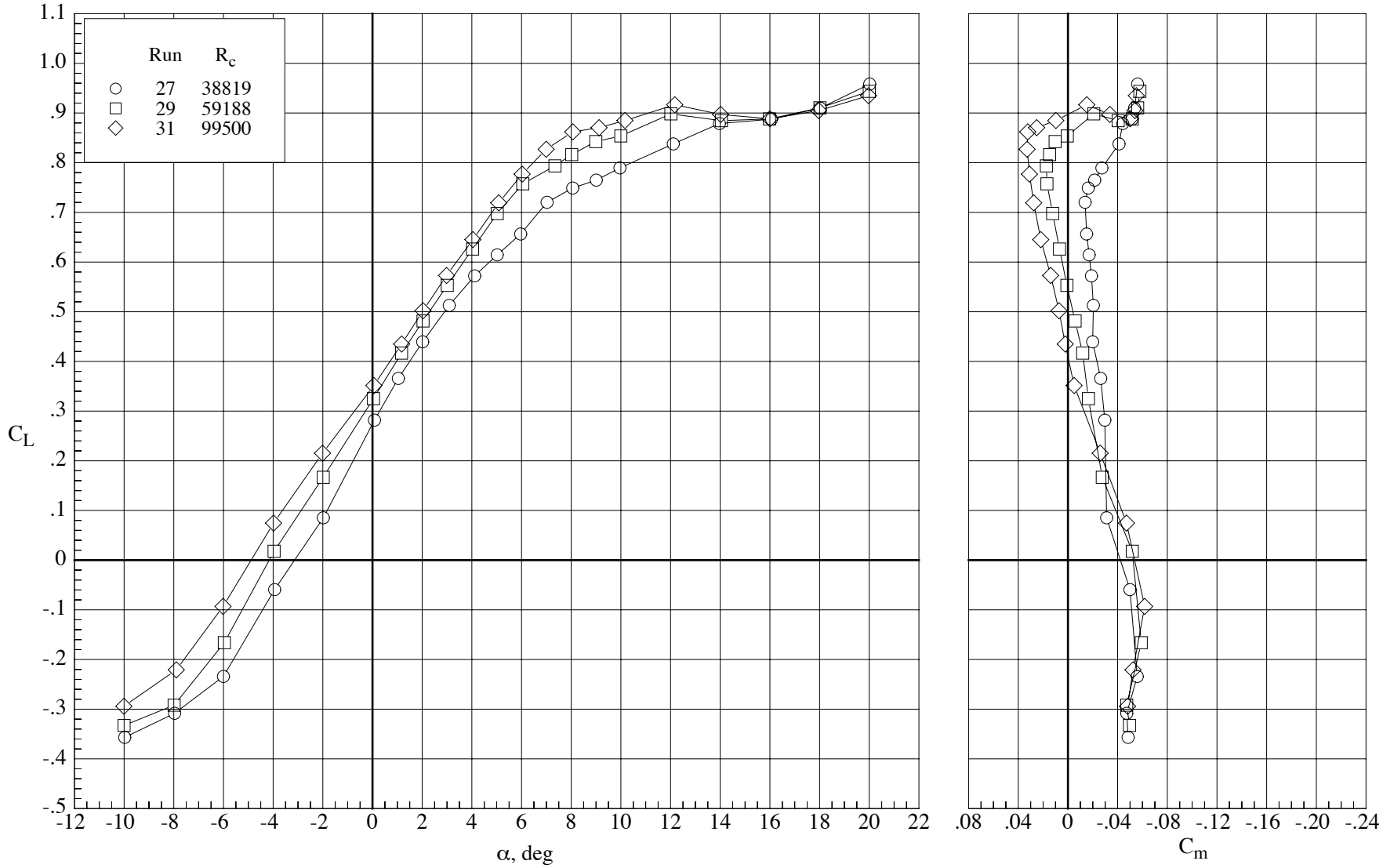

(a) Lift and pitching-moment coefficients.

Figure 14. Effect of Reynolds number on the longitudinal aerodynamic characteristics of the model with the MA-SC-1 wing (bump on) with the tails inverted and the lower fuselage removed at Mach number 0.65. $\delta_h = -5°$ and $\delta_f = 0°$.

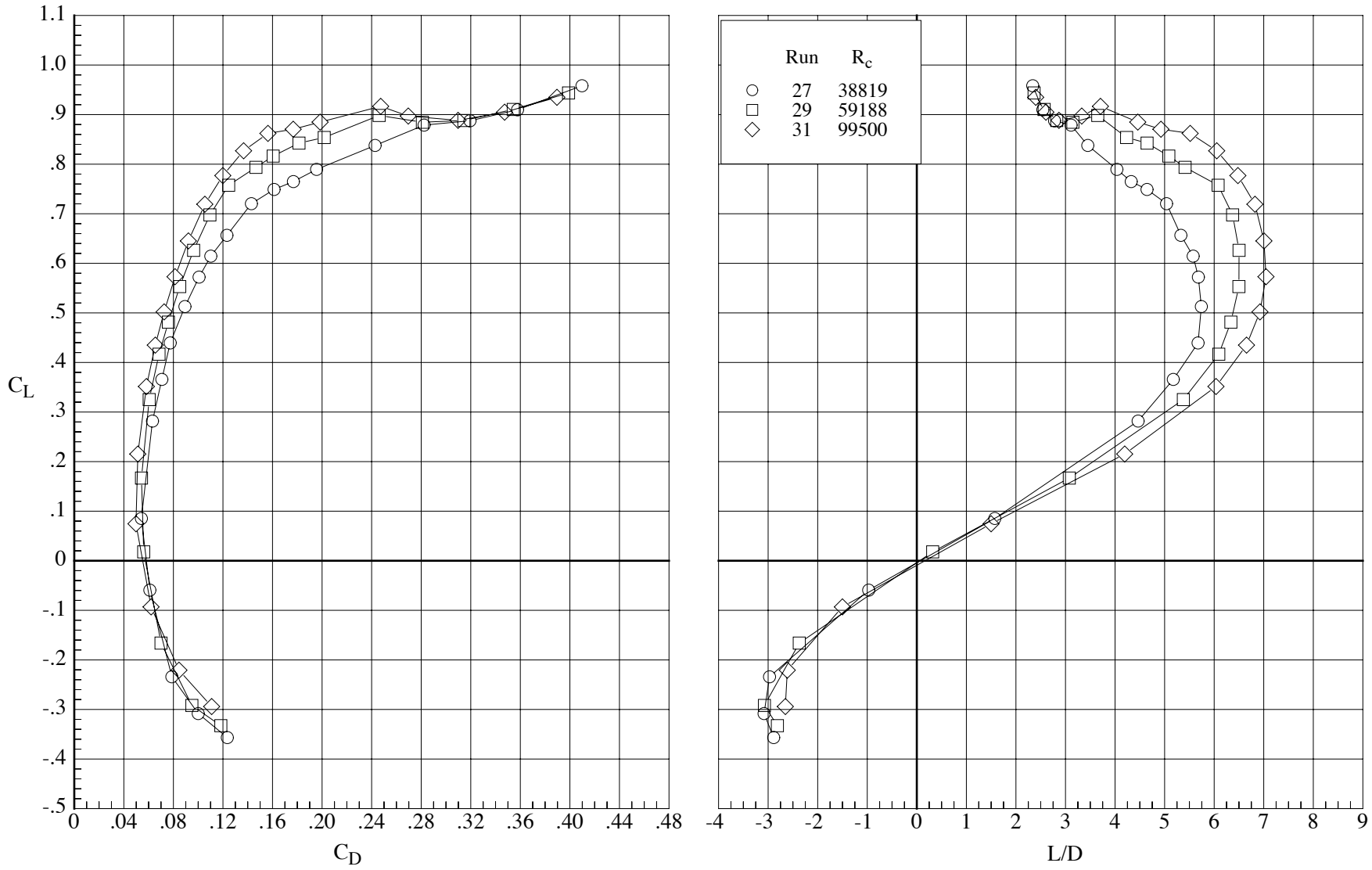

(b) Drag coefficient and lift-drag ratio.

Figure 14. Concluded.

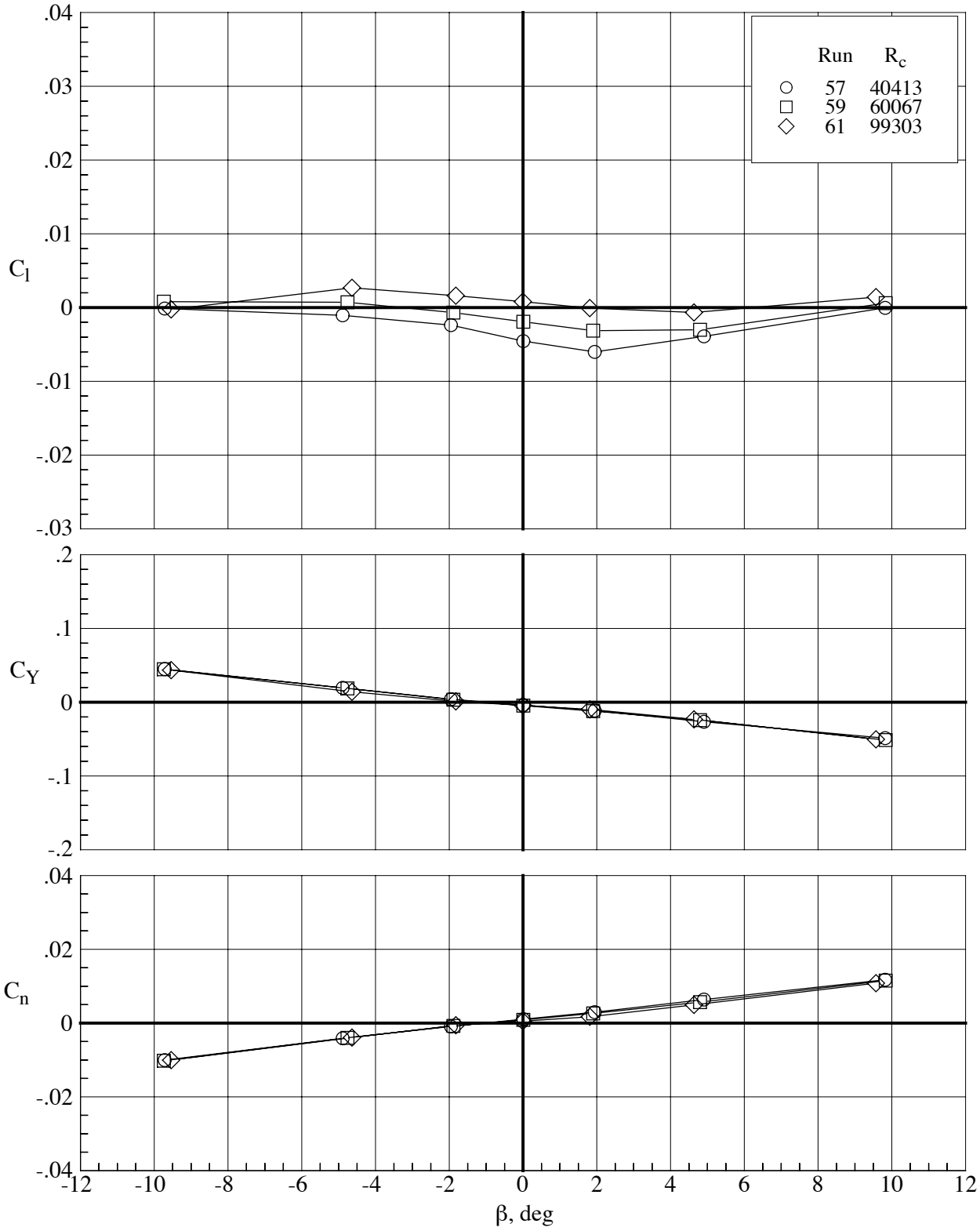

(a) Lateral-directional characteristics.

Figure 15. Aerodynamic characteristics of the model with the MA-SC-1 wing (bump on) with the tails inverted and a horizontal tail incidence of -5° at a Mach number of 0.65 at three different Reynolds numbers and an angle of attack of 4°.

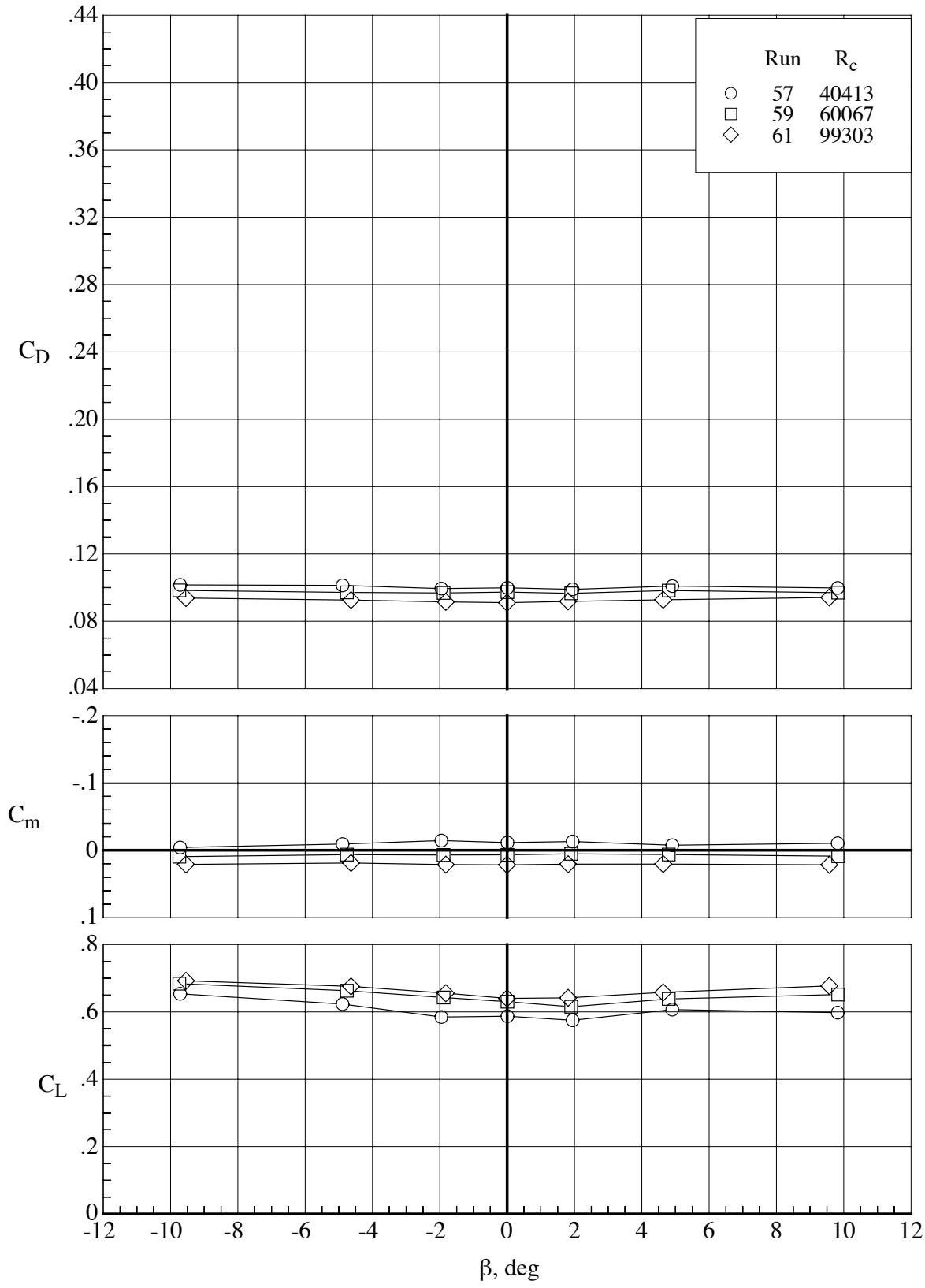

(b) Lift, drag, and pitching-moment coefficients.

Figure 15. Concluded.

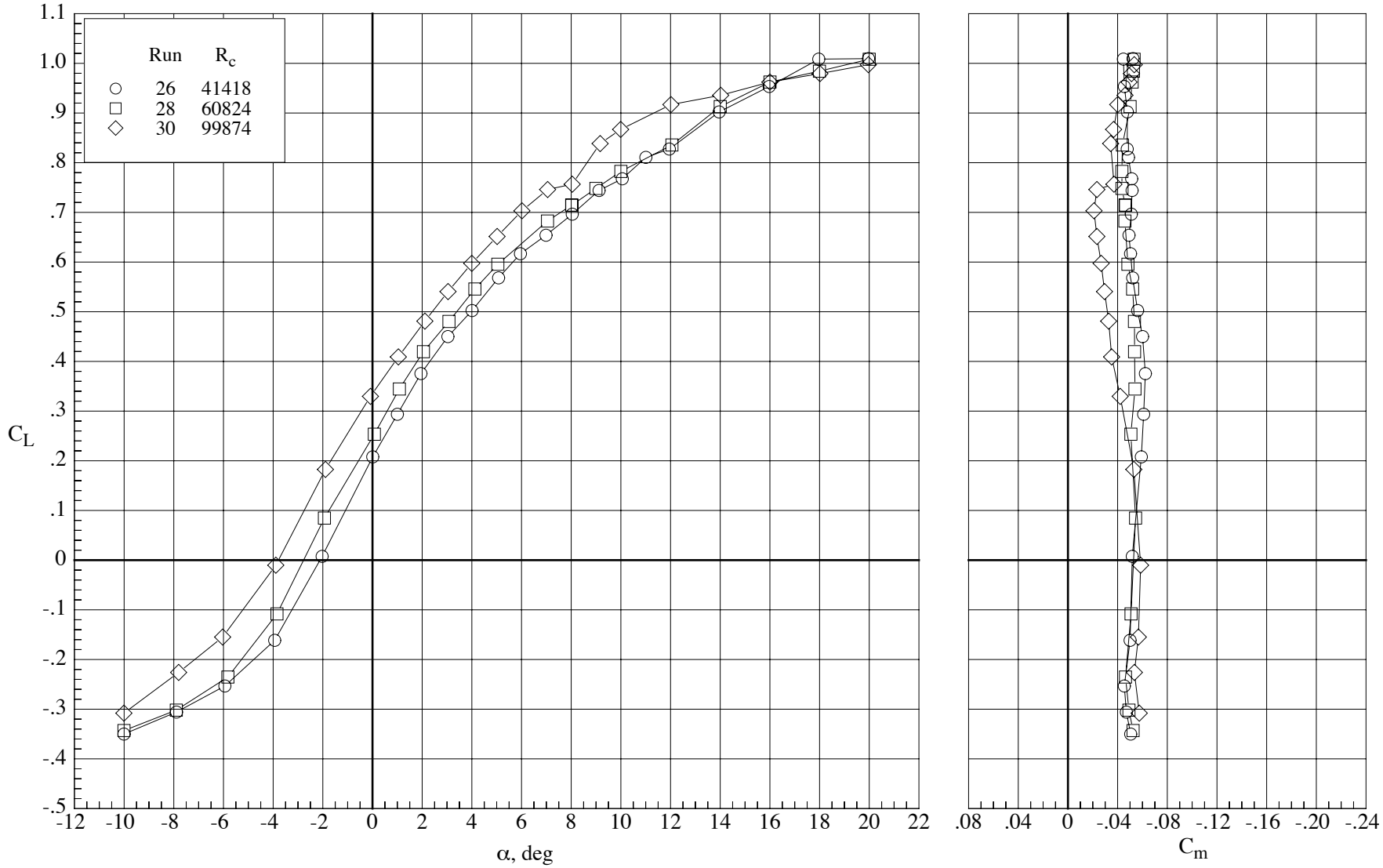

(a) Lift and pitching-moment coefficients.

Figure 16. Effect of Reynolds number on the longitudinal aerodynamic characteristics of the model with the MA-SC-1 wing (bump on) with the tails inverted and the lower fuselage removed at Mach number 0.80. $\delta_h = -5°$ and $\delta_f = 0°$.

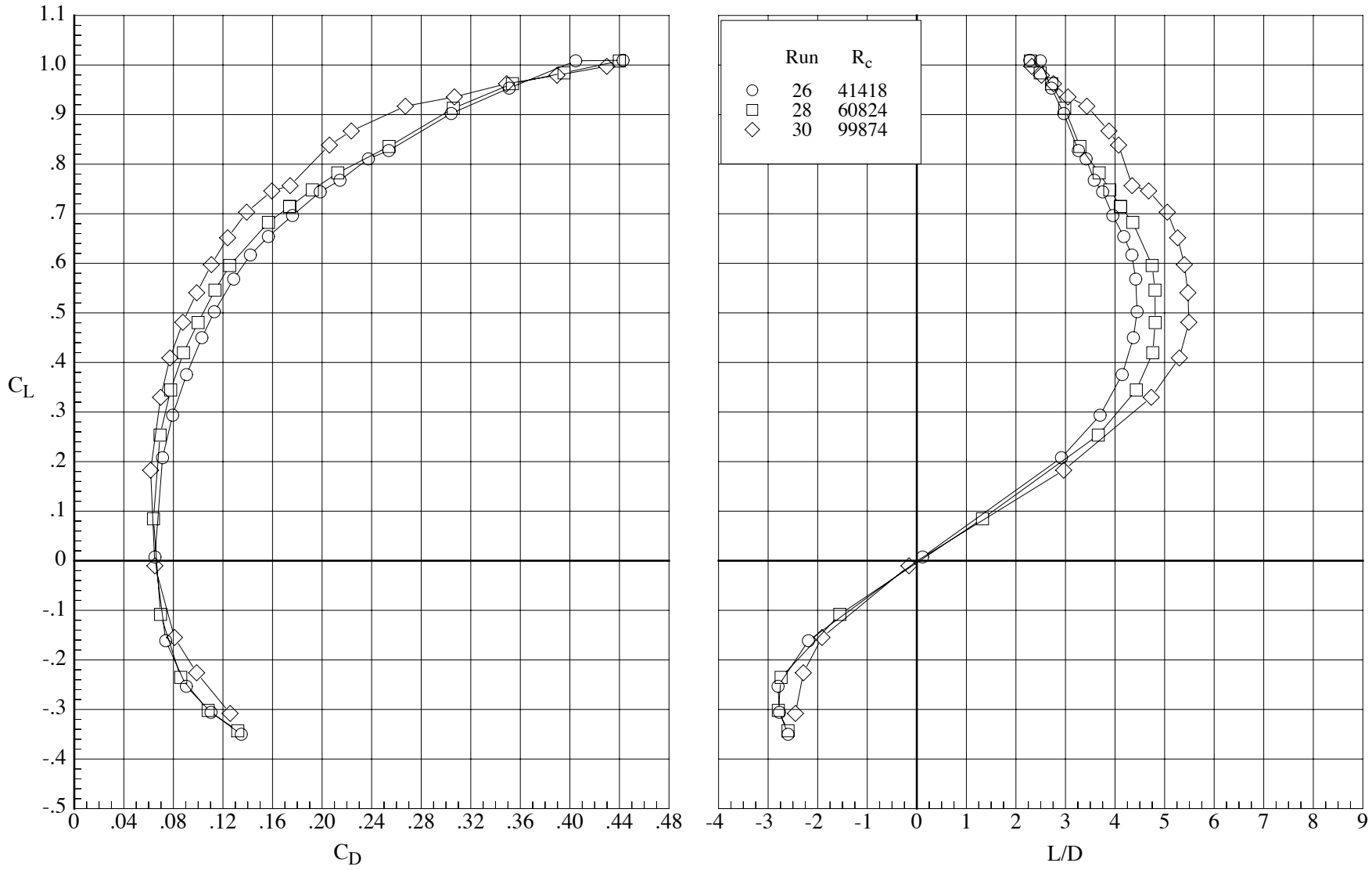

(b) Drag coefficient and lift-drag ratio.

Figure 16. Concluded.

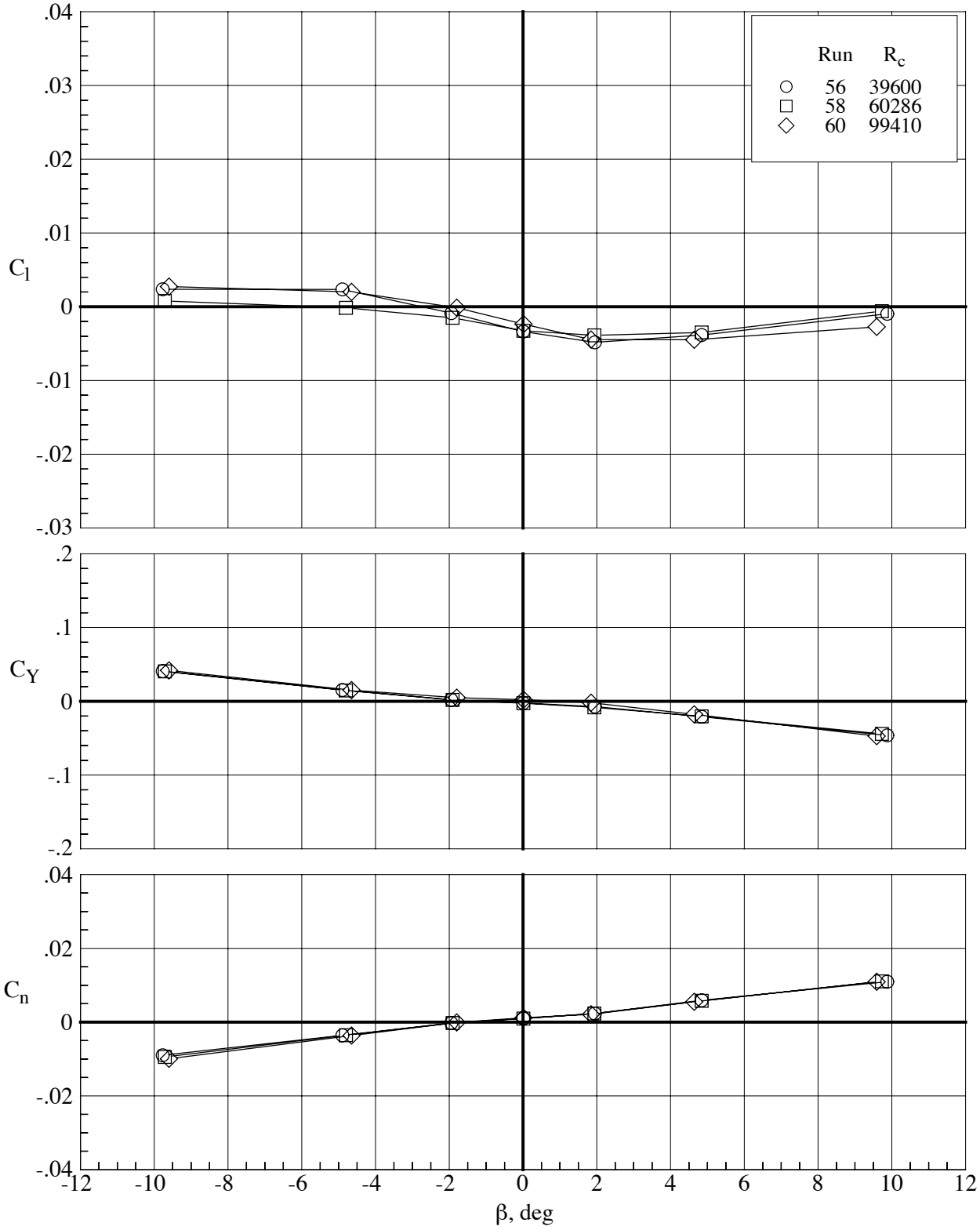

(a) Lateral-directional characteristics.

Figure 17. Aerodynamic characteristics of the model with the MA-SC-1 wing (bump on) with the tails inverted and a horizontal tail incidence of -5° at a Mach number of 0.80 at three different Reynolds numbers and an angle of attack of 4°.

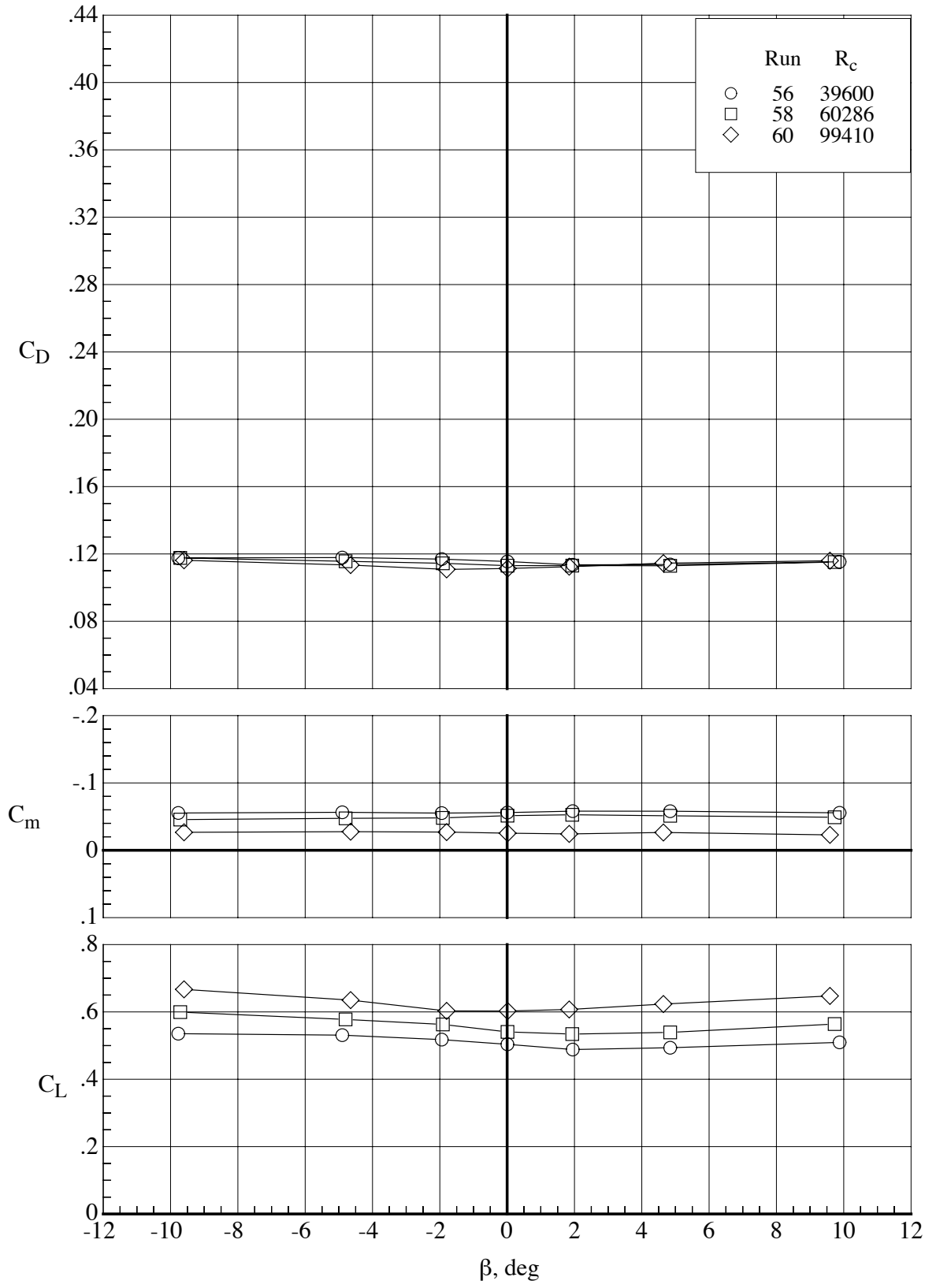

(b) Lift, drag, and pitching-moment coefficients.

Figure 17. Concluded.

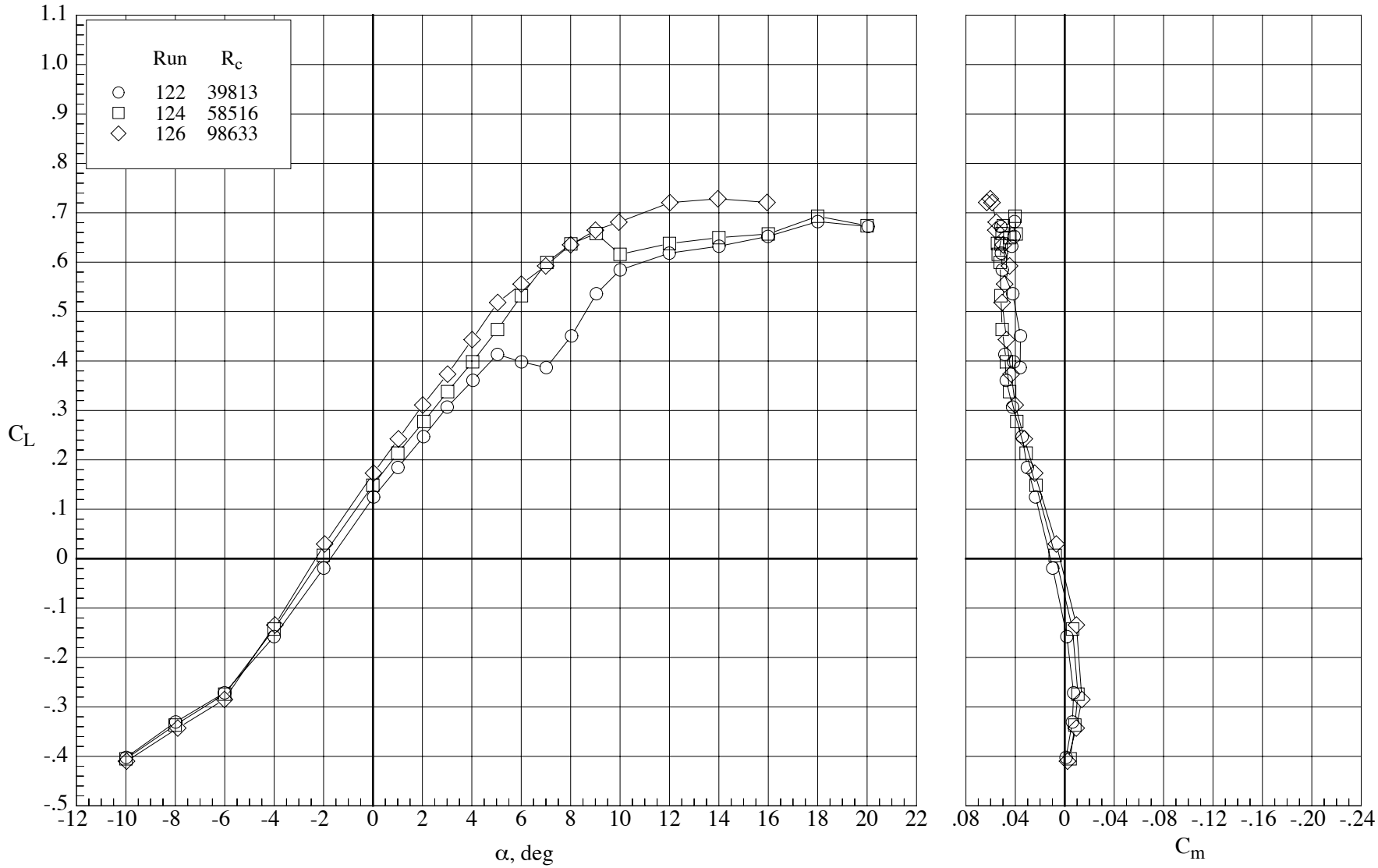

(a) Lift and pitching-moment coefficients.

Figure 18. Effect of Reynolds number on the longitudinal aerodynamic characteristics of the model with the MA-SF-1 wing (bump off) at Mach number 0.65. $\delta_h = 0°$, $\delta_f = 0°$.

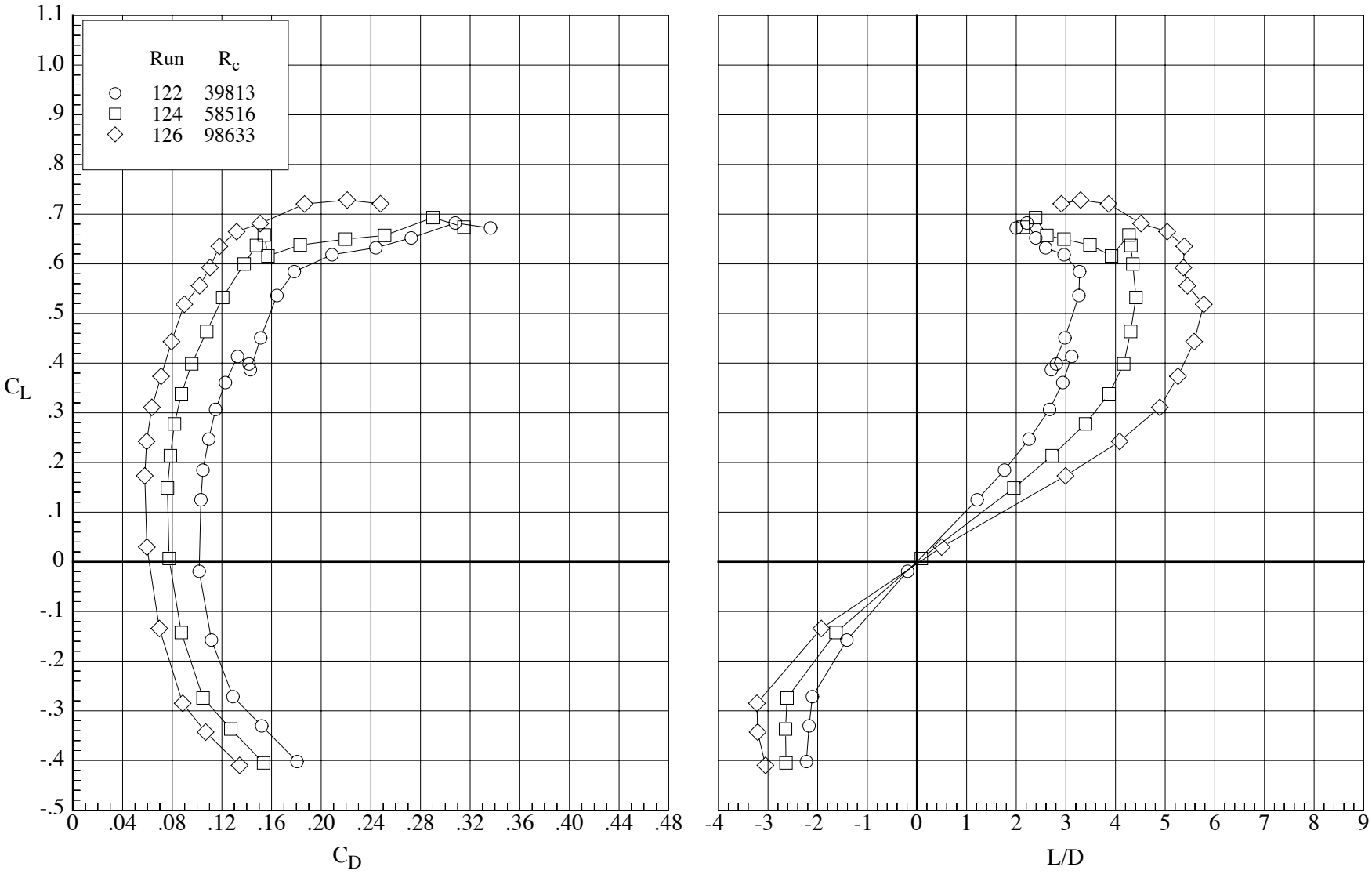

(b) Drag coefficient and lift-drag ratio.

Figure 18. Concluded.

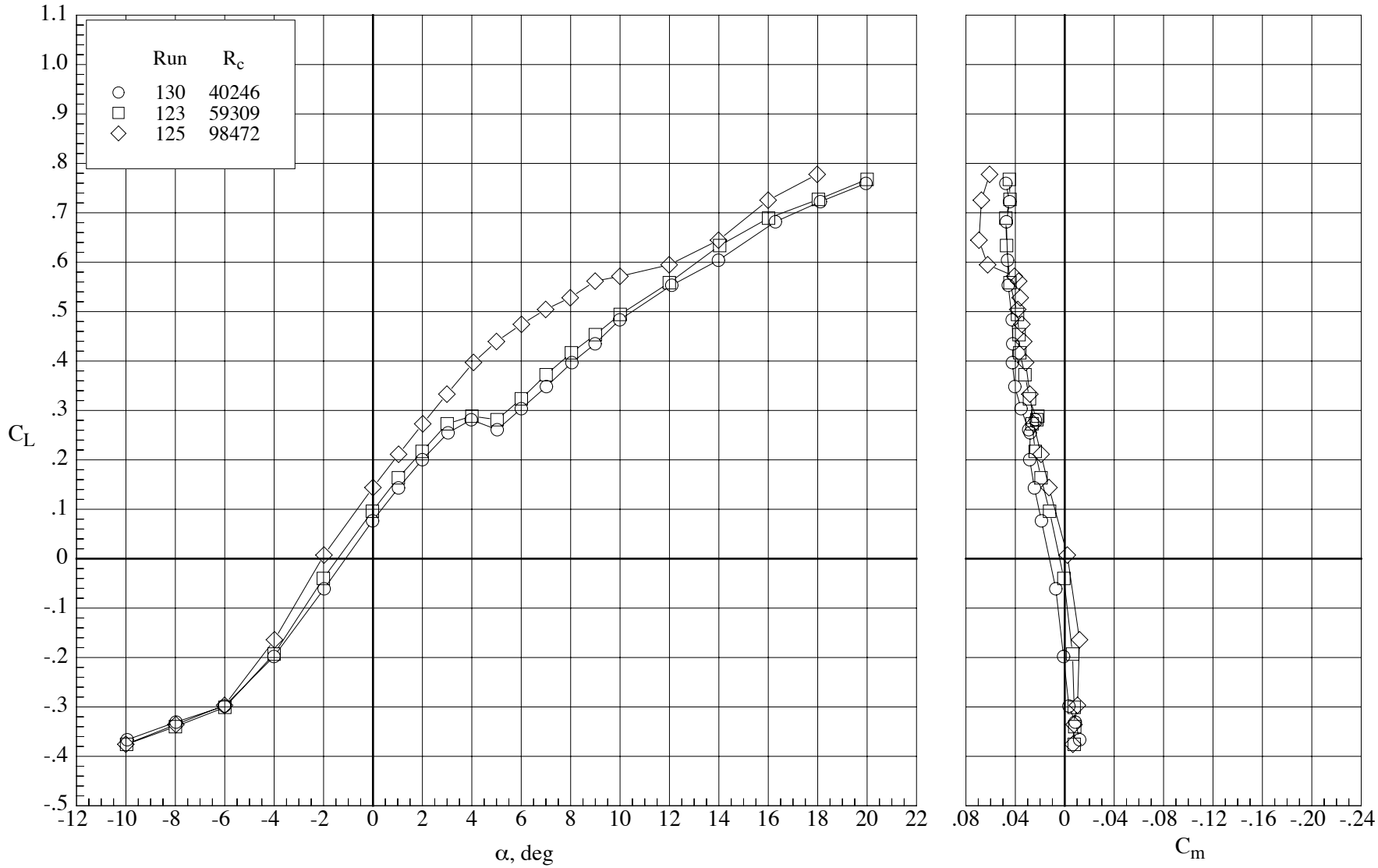

(a) Lift and pitching-moment coefficients.

Figure 19. Effect of Reynolds number on the longitudinal aerodynamic characteristics of the model with the MA-SF-1 wing (bump off) at Mach number 0.80. $\delta_h = 0°$, $\delta_f = 0°$.

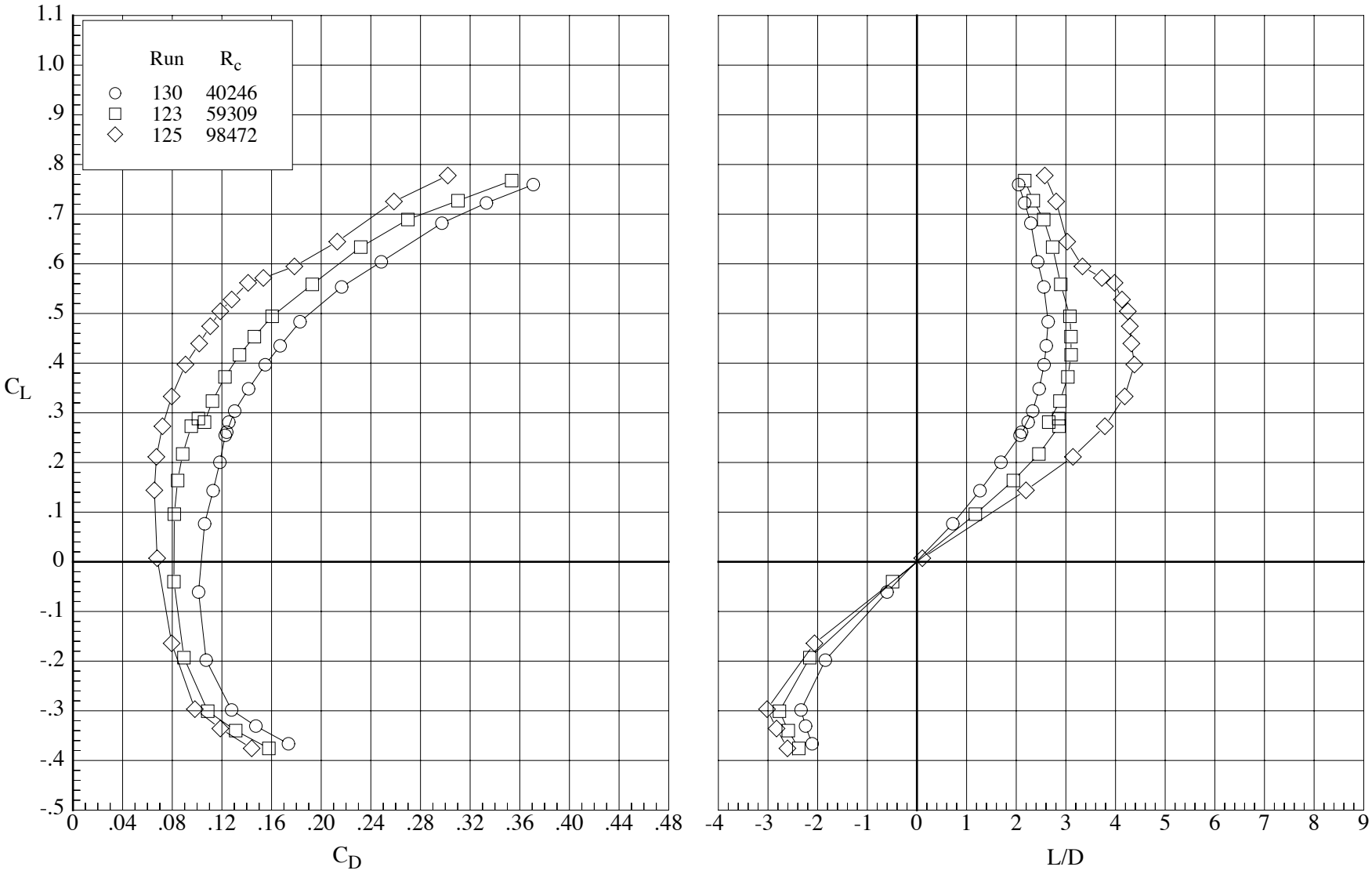

(b) Drag coefficient and lift-drag ratio.

Figure 19. Concluded.

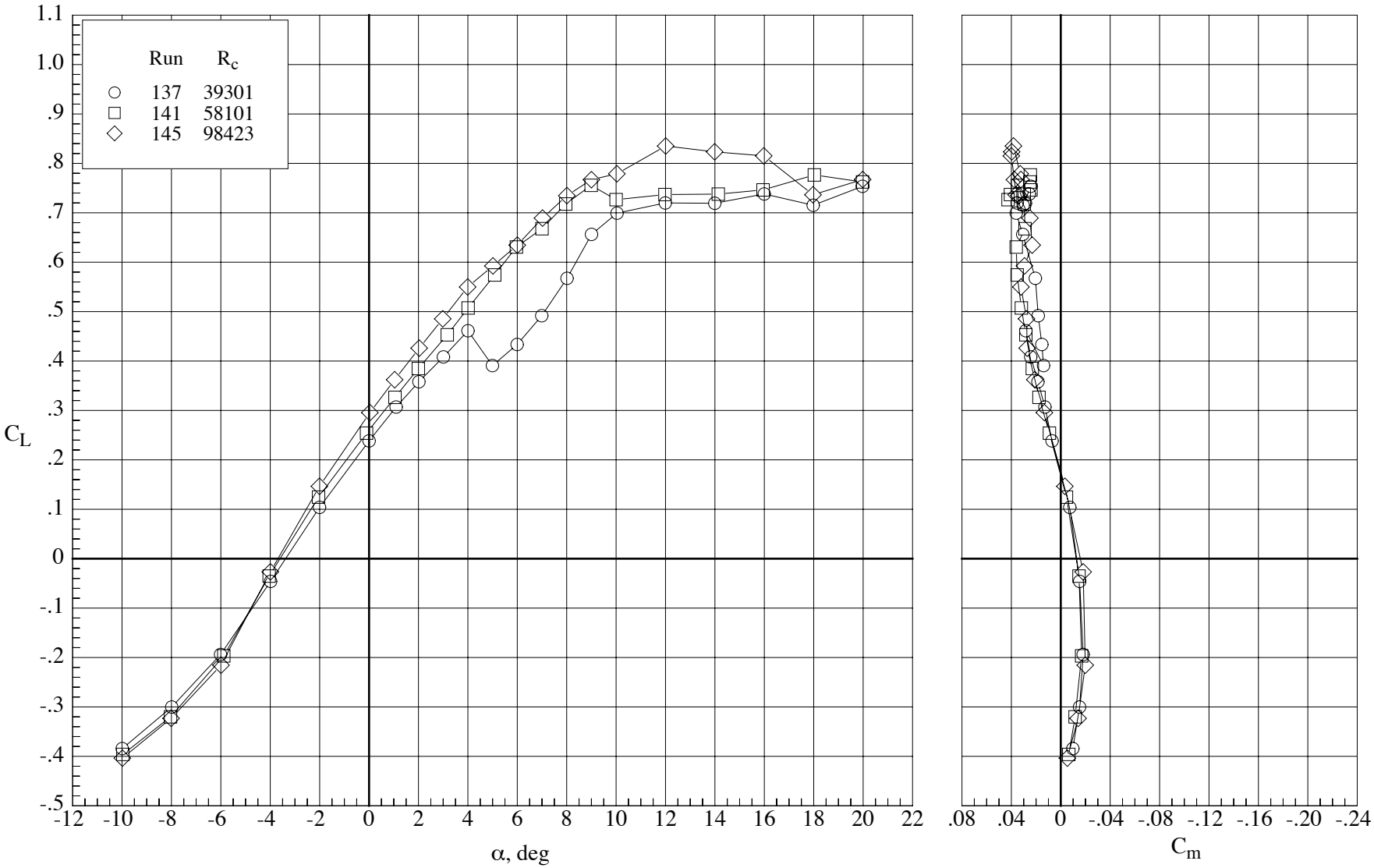

(a) Lift and pitching-moment coefficients.

Figure 20. Effect of Reynolds number on the longitudinal aerodynamic characteristics of the model with the MA-SF-1 wing (bump off) at Mach number 0.65. $\delta_h = 0°$, $\delta_f = 10°$.

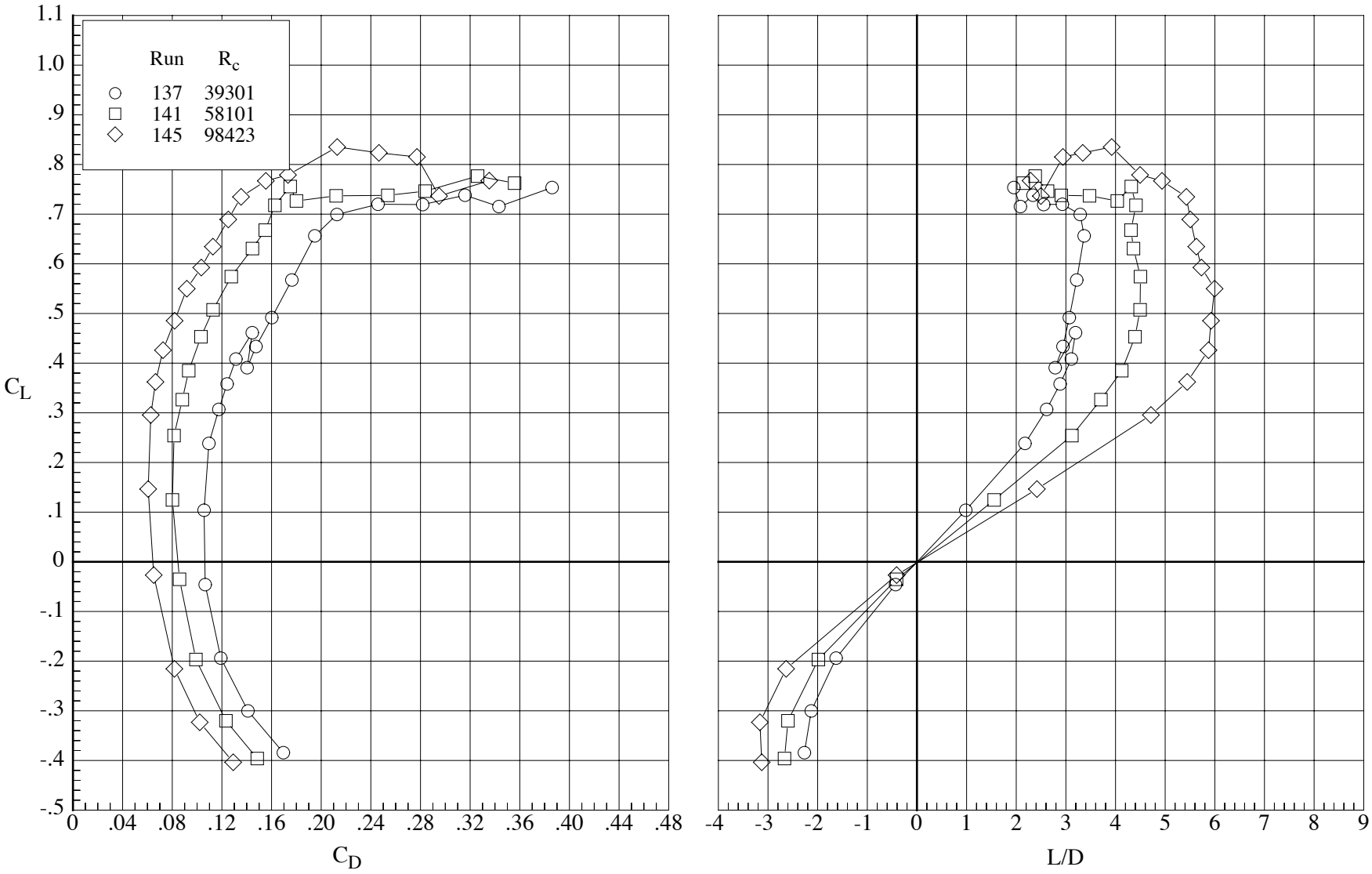

(b) Drag coefficient and lift-drag ratio.

Figure 20. Concluded.

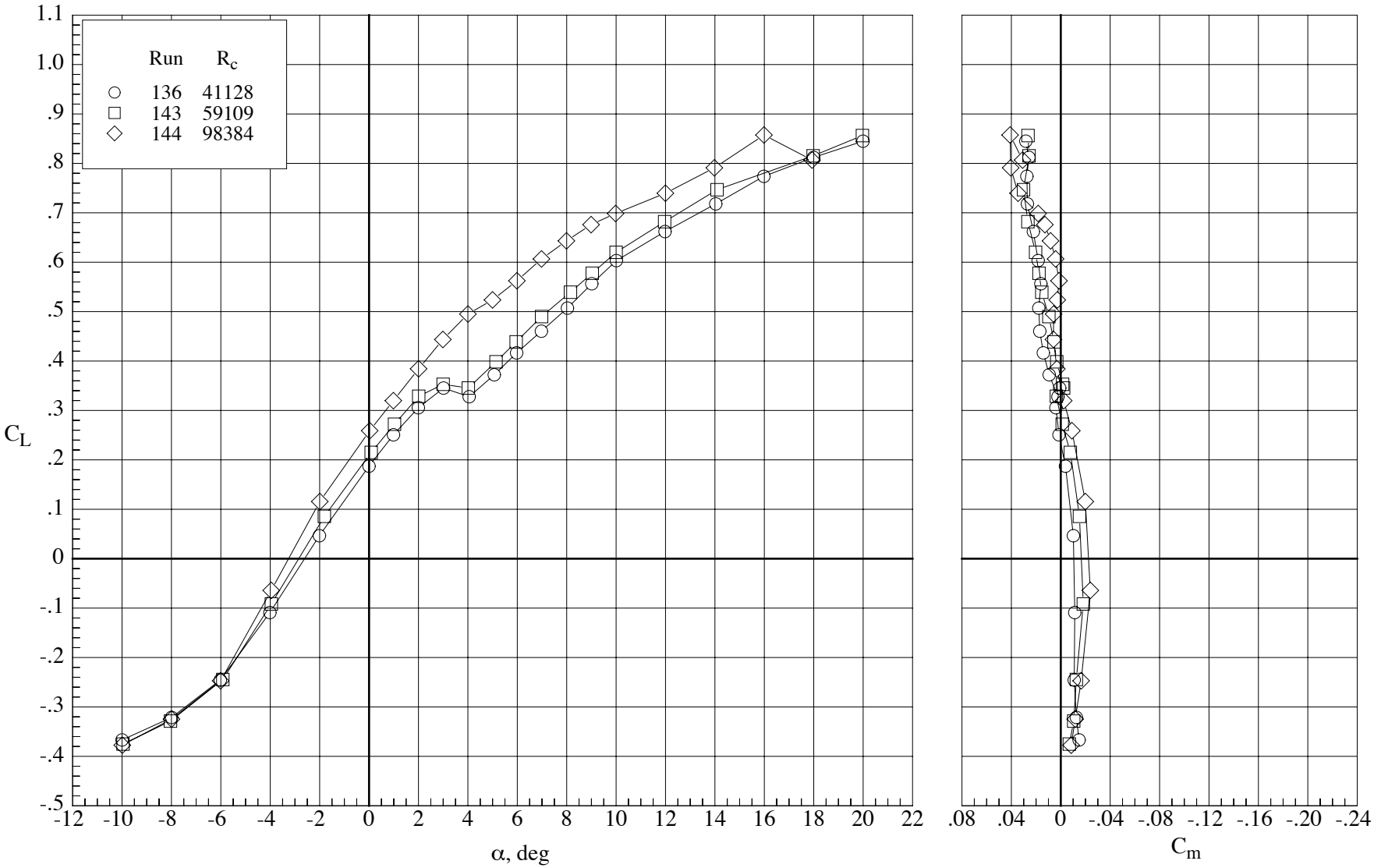

(a) Lift and pitching-moment coefficients.

Figure 21. Effect of Reynolds number on the longitudinal aerodynamic characteristics of the model with the MA-SF-1 wing (bump off) at Mach number 0.80. $\delta_h = 0°$, $\delta_f = 10°$.

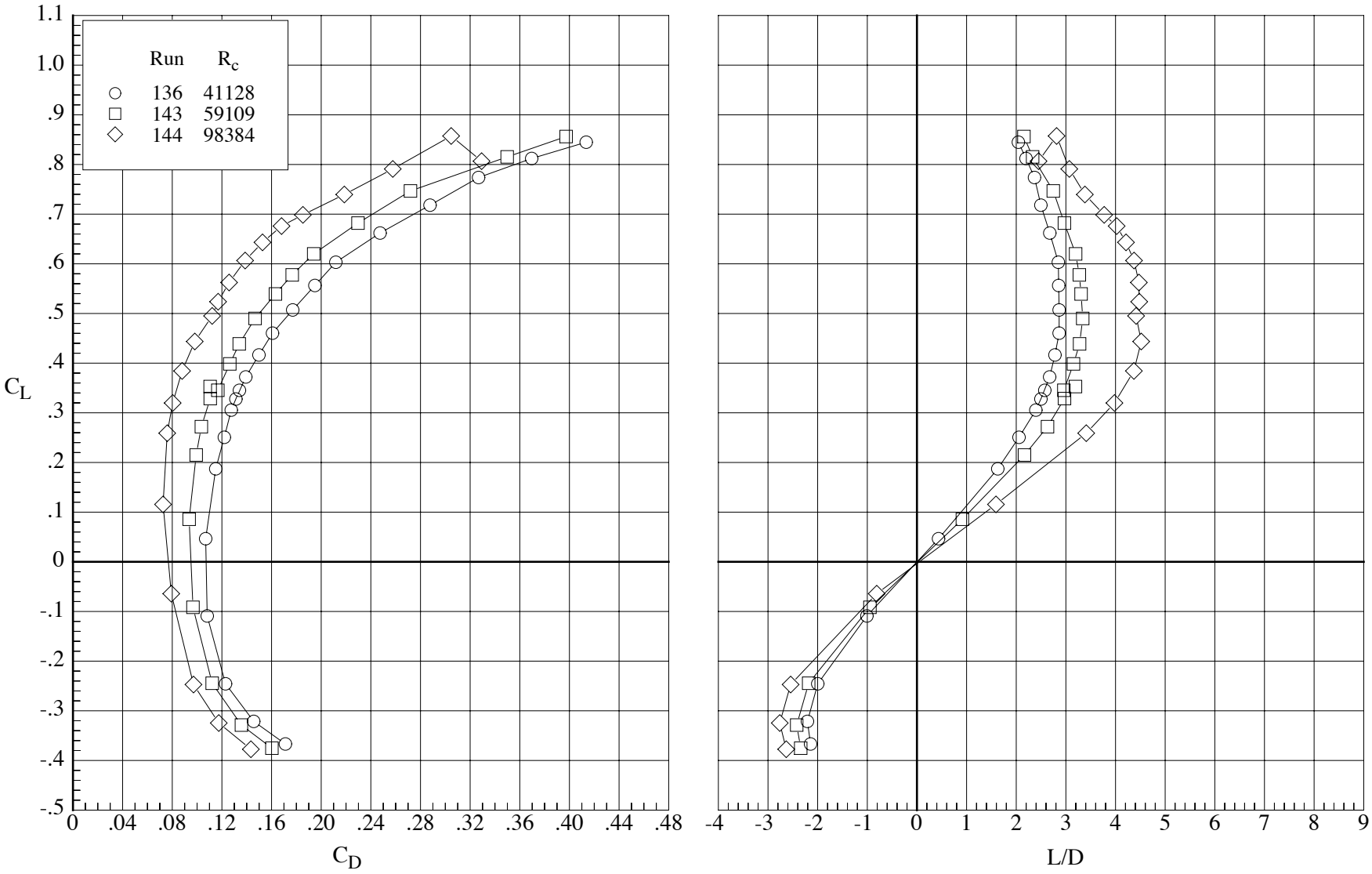

(b) Drag coefficient and lift-drag ratio.

Figure 21. Concluded.

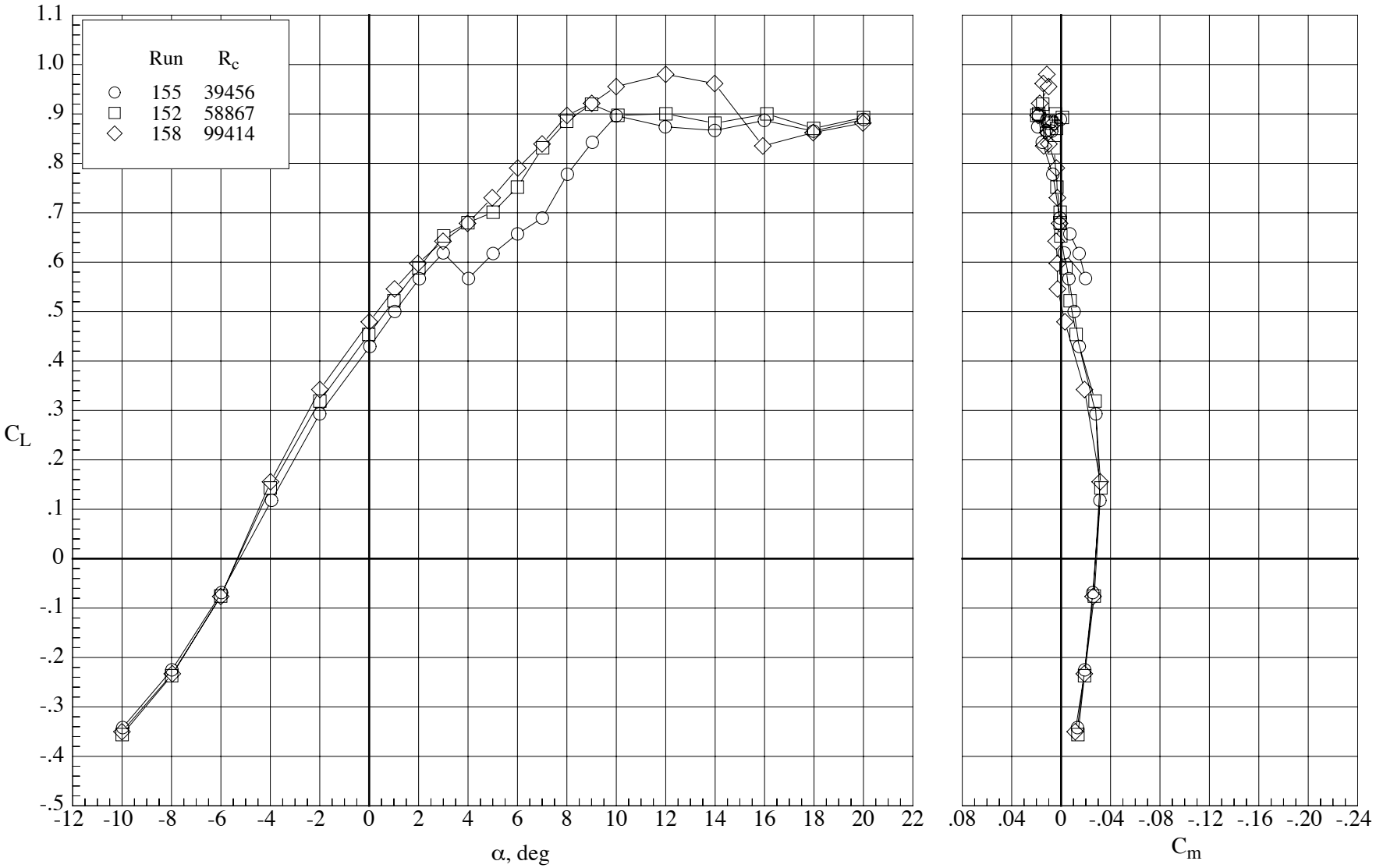

(a) Lift and pitching-moment coefficients.

Figure 22. Effect of Reynolds number on the longitudinal aerodynamic characteristics of the model with the MA-SF-1 wing (bump off) at Mach number 0.65. $\delta_h = 0°$, $\delta_f = 30°$.

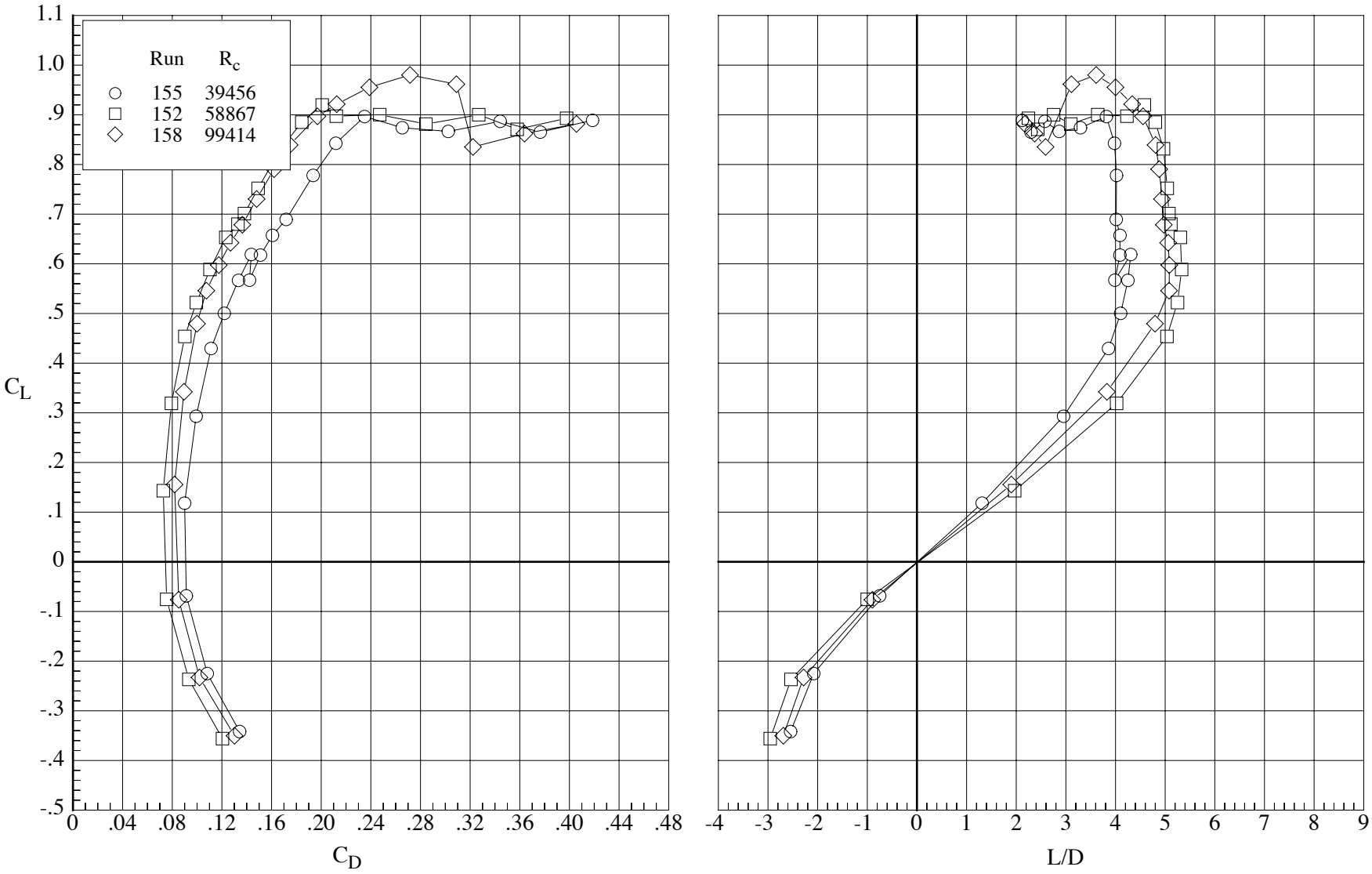

(b) Drag coefficient and lift-drag ratio.

Figure 22. Concluded.

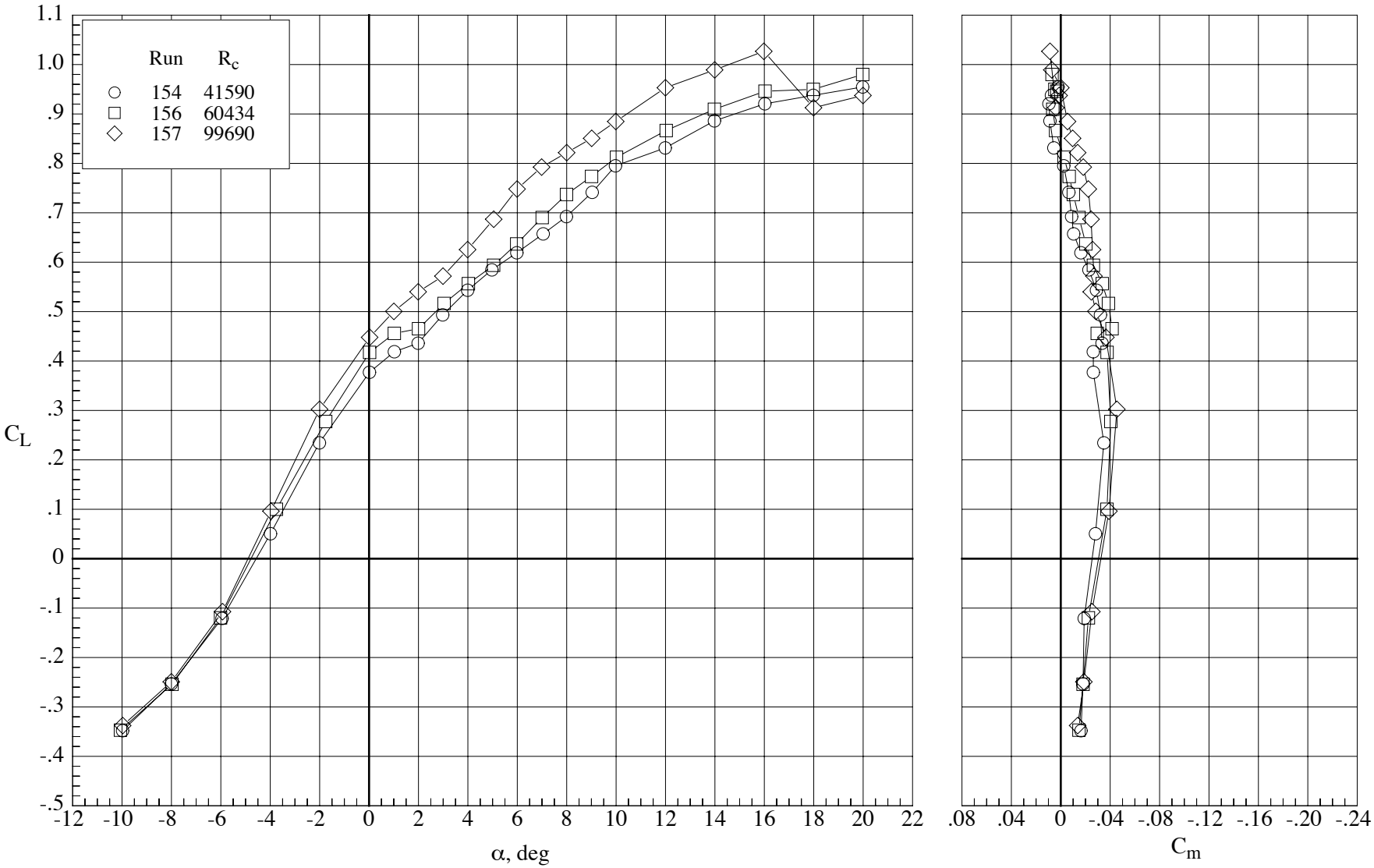

(a) Lift and pitching-moment coefficients.

Figure 23. Effect of Reynolds number on the longitudinal aerodynamic characteristics of the model with the MA-SF-1 wing (bump off) at Mach number 0.80. $\delta_h = 0°$, $\delta_f = 30°$.

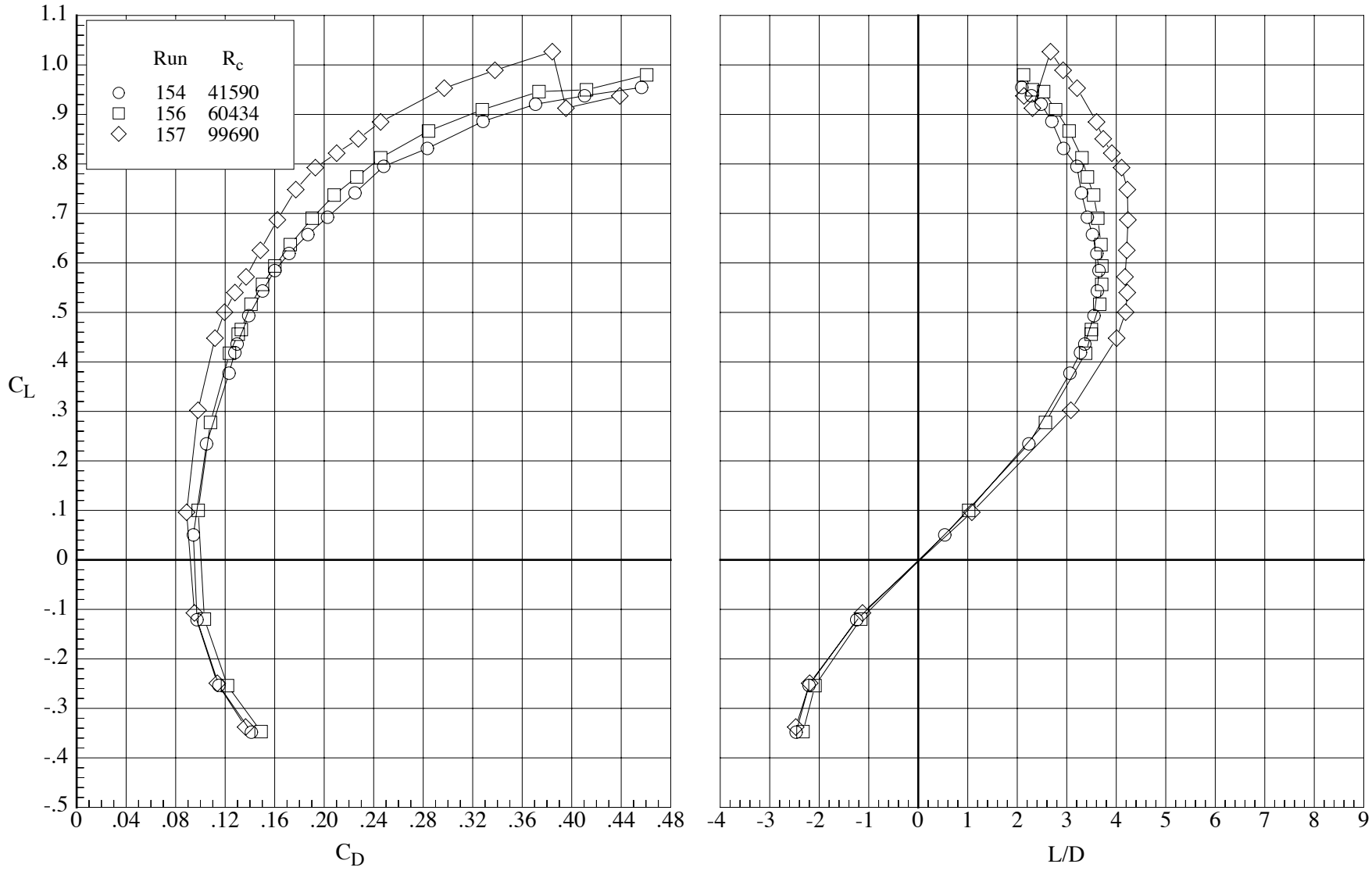

(b) Drag coefficient and lift-drag ratio.

Figure 23. Concluded.

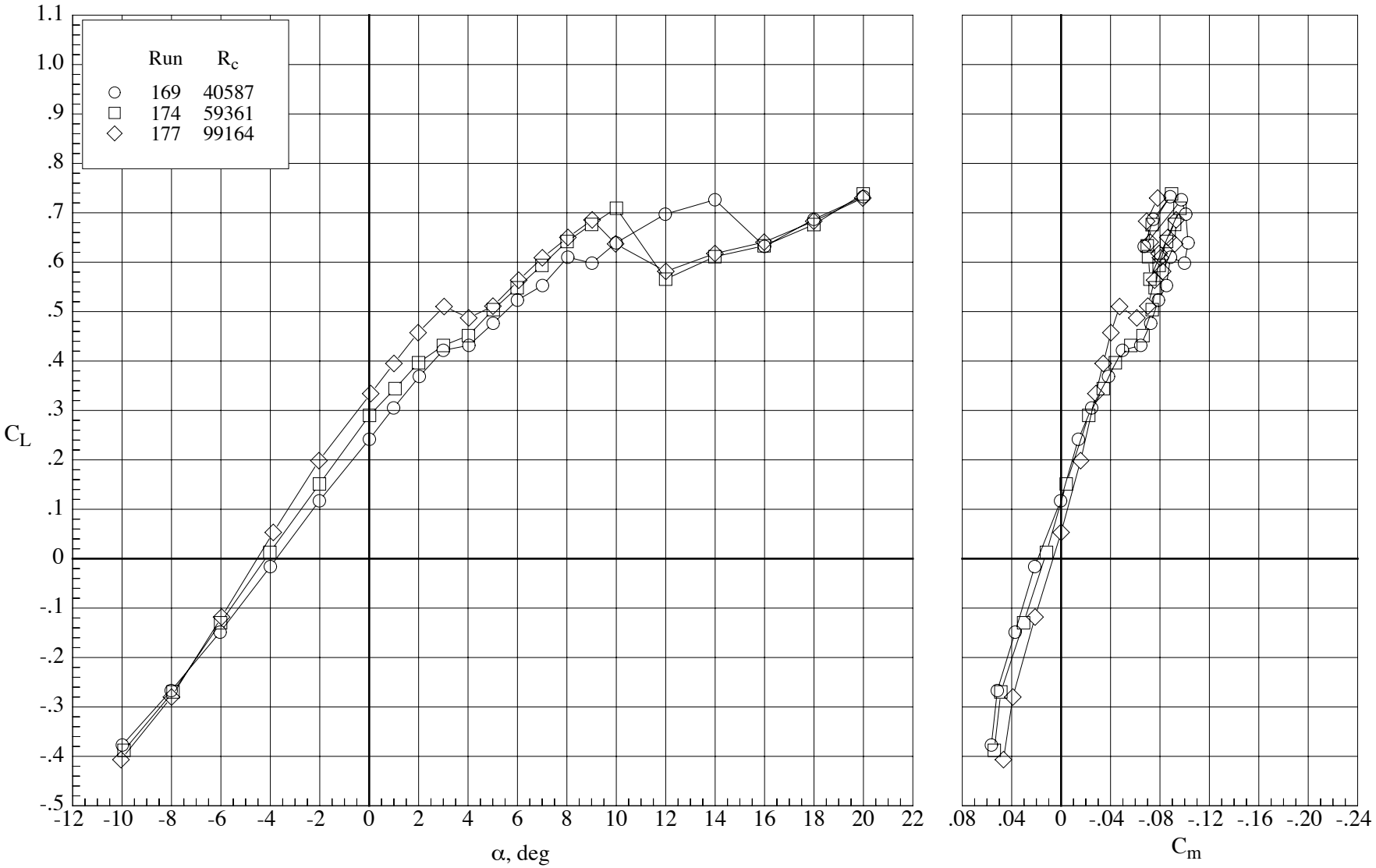

(a) Lift and pitching-moment coefficients.

Figure 24. Effect of Reynolds number on the longitudinal aerodynamic characteristics of the model with the MA-SC-1t wing (bump on) at Mach number 0.65. $\delta_h = 0°$, $\delta_f = 0°$.

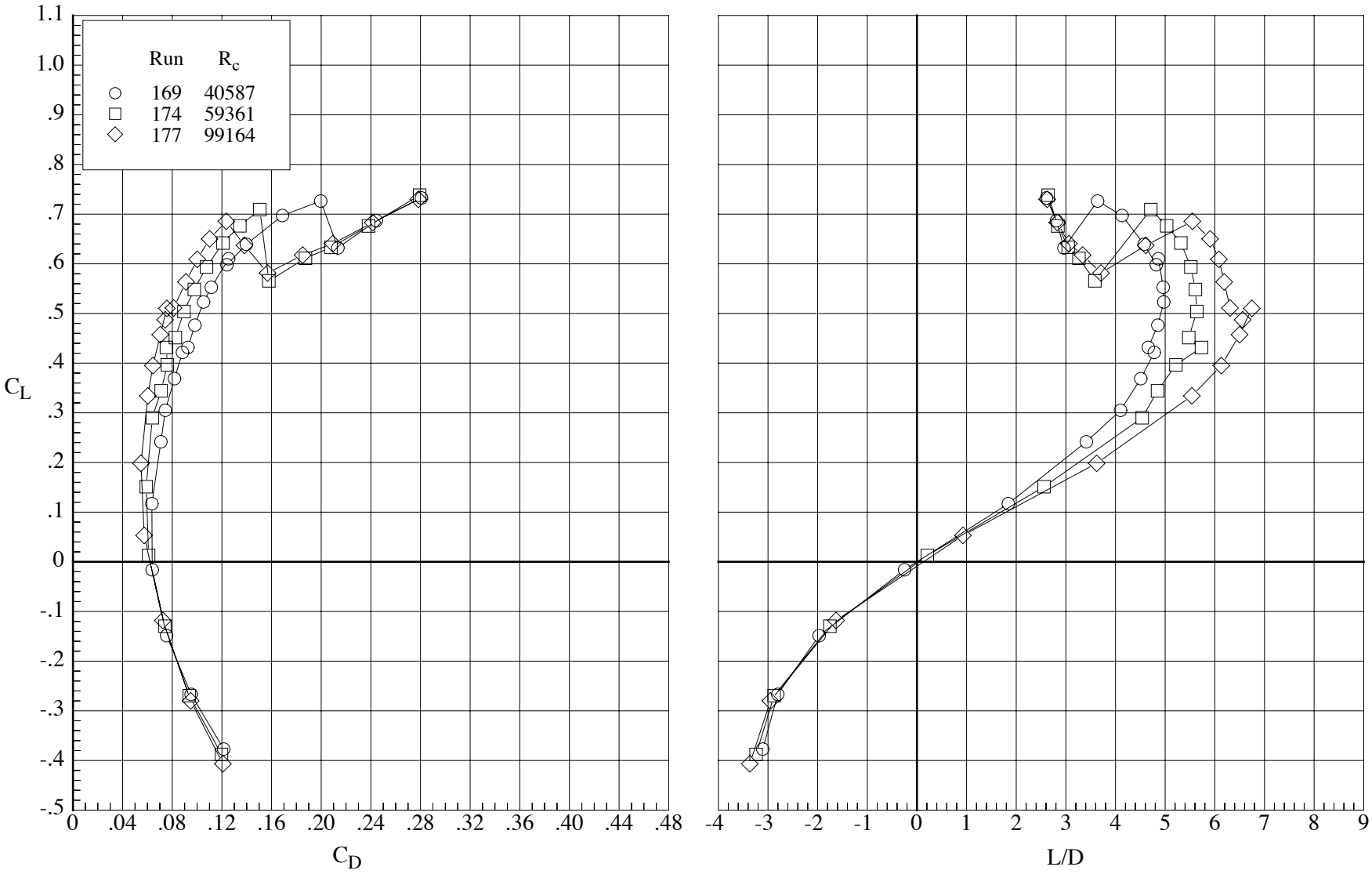

(b) Drag coefficient and lift-drag ratio.

Figure 24. Concluded.

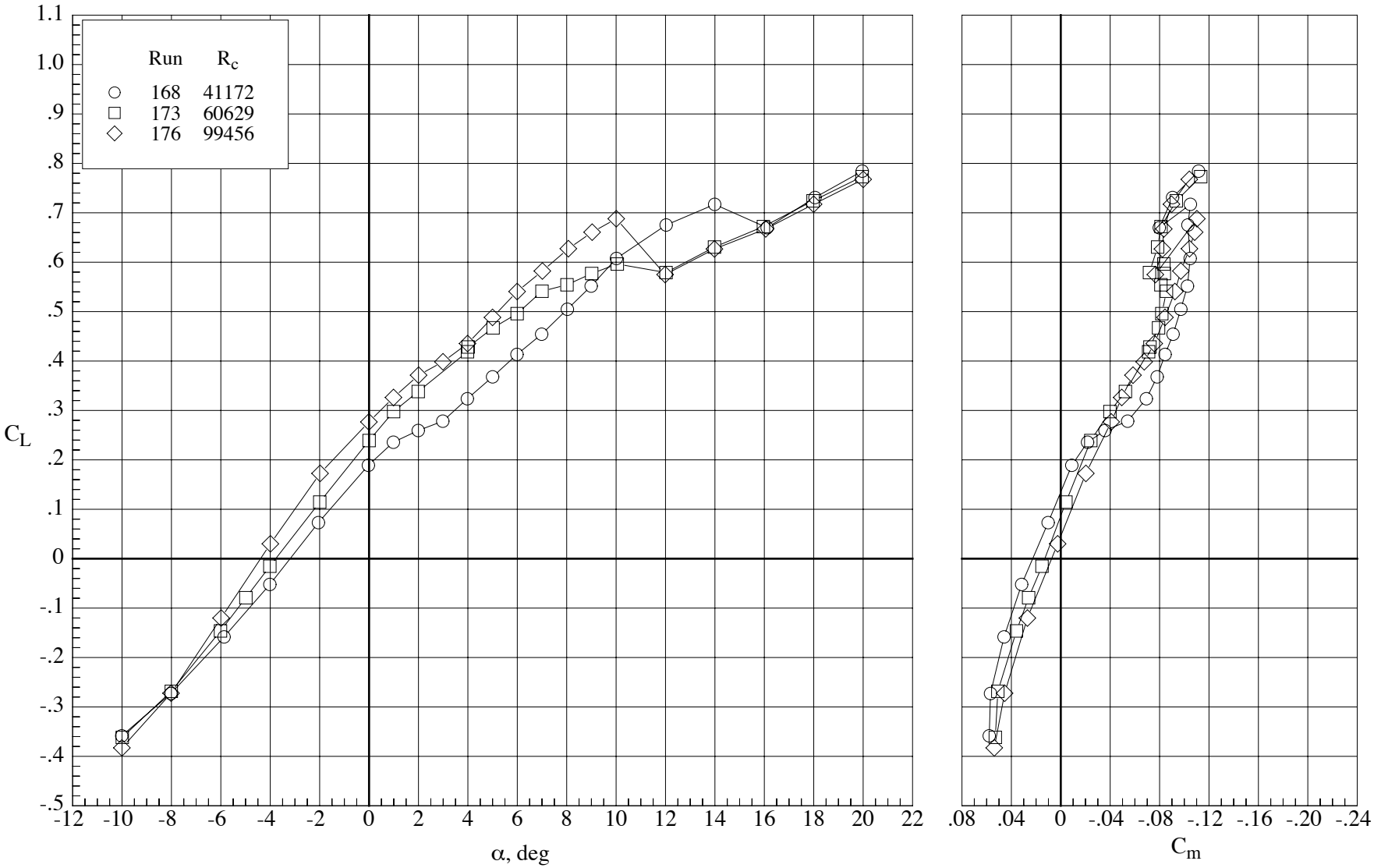

(a) Lift and pitching-moment coefficients.

Figure 25. Effect of Reynolds number on the longitudinal aerodynamic characteristics of the model with the MA-SC-1t wing (bump on) at Mach number 0.80. $\delta_h = 0°$, $\delta_f = 0°$.

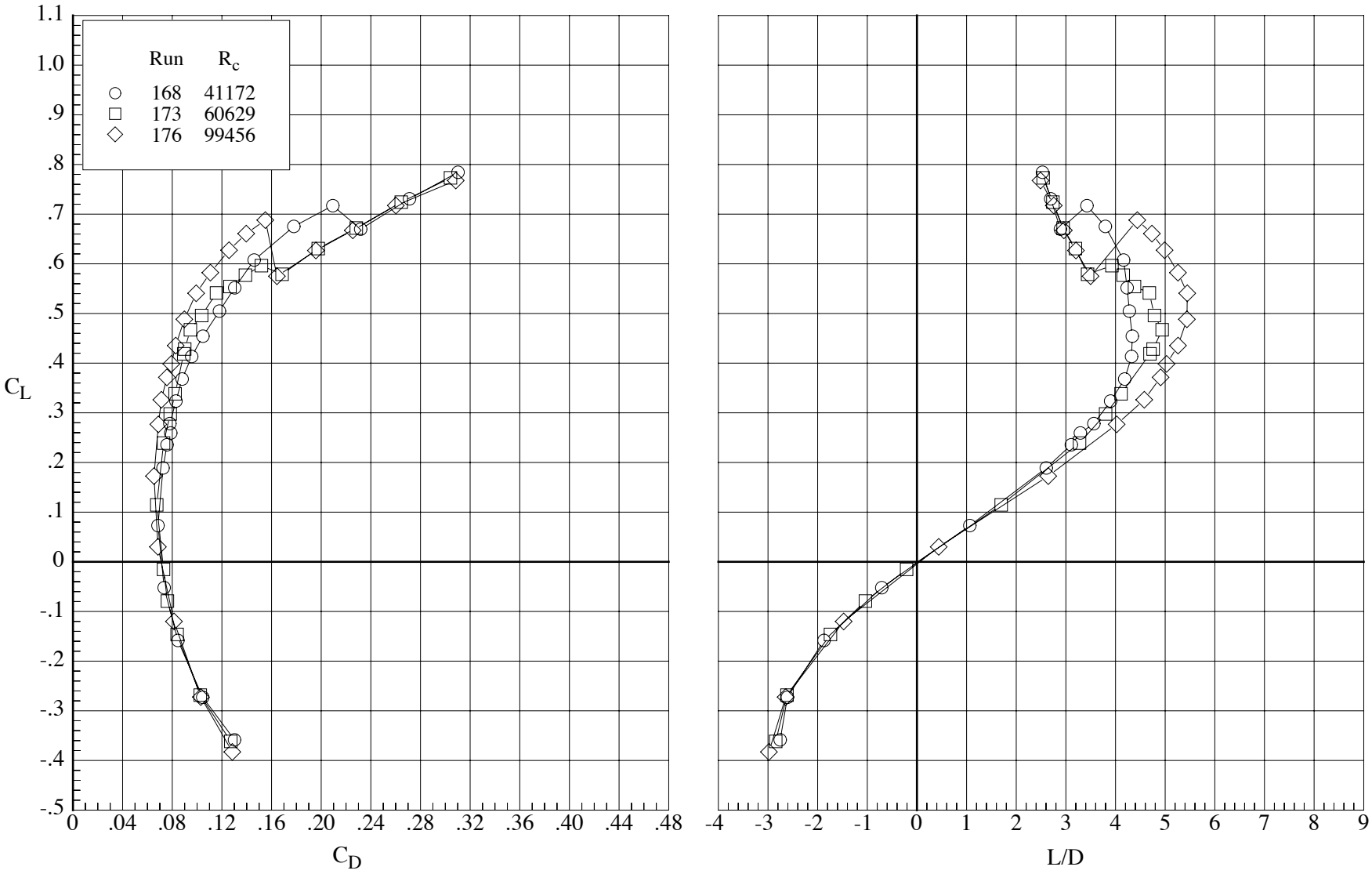

(b) Drag coefficient and lift-drag ratio.

Figure 25. Concluded.

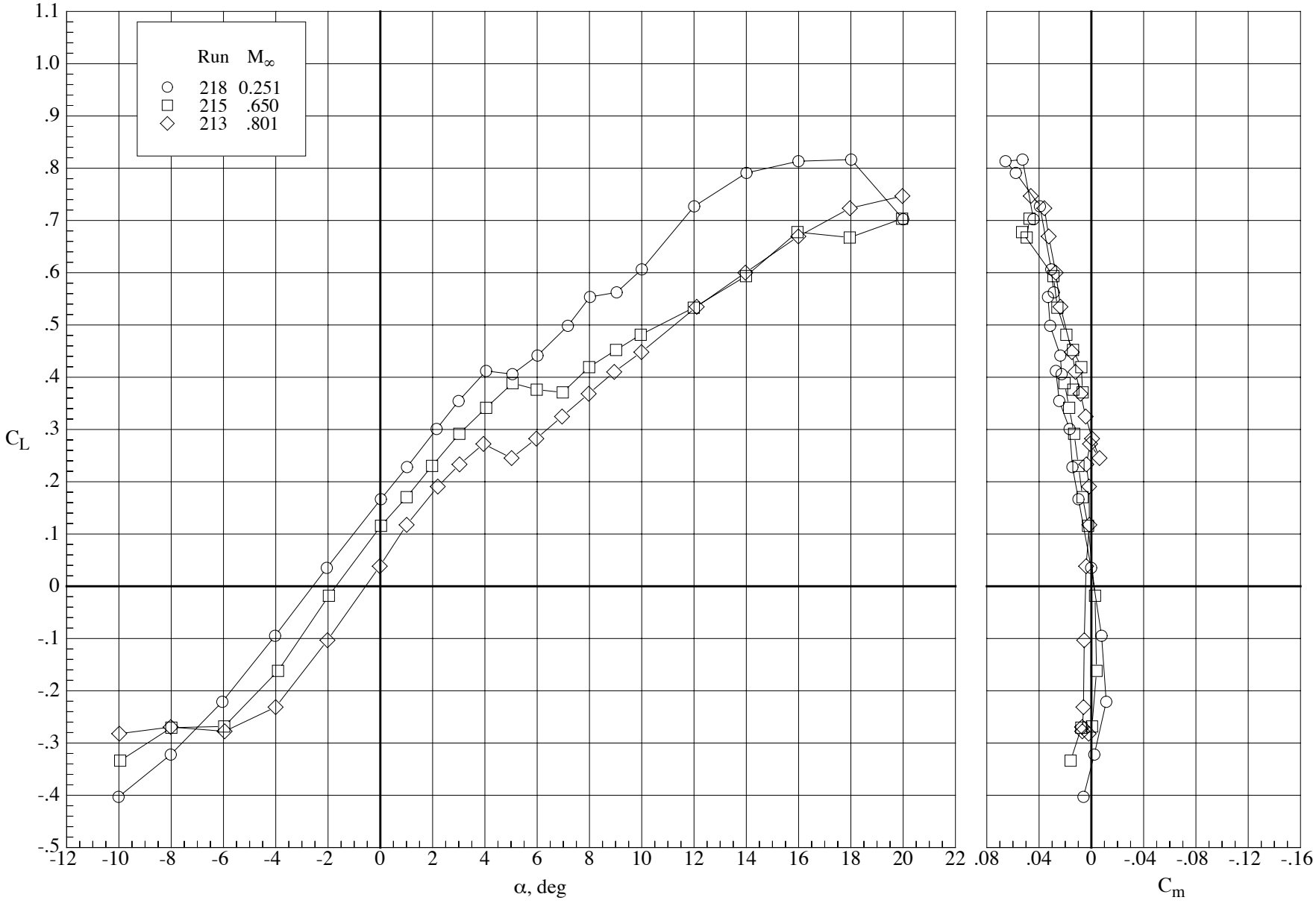

(a) Lift and pitching-moment coefficients.

Figure 26. Effect of Mach number on the longitudinal aerodynamic characteristics of the model with the Eppler 387 wing at a Reynolds number of 40,000. $\delta_h = 0°$ and $\delta_f = 0°$.

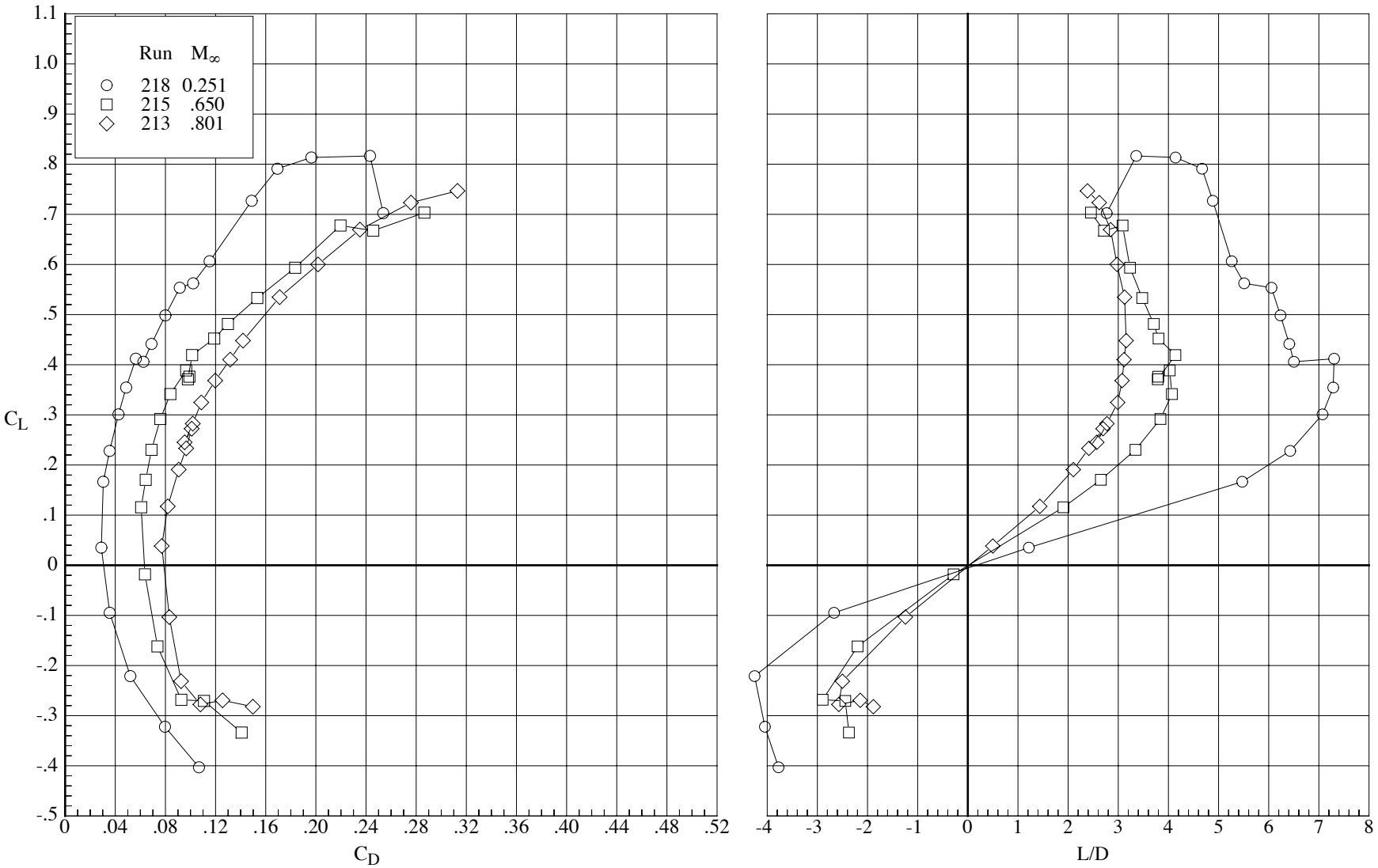

(b) Drag coefficient and lift-drag ratio.

Figure 26. Concluded.

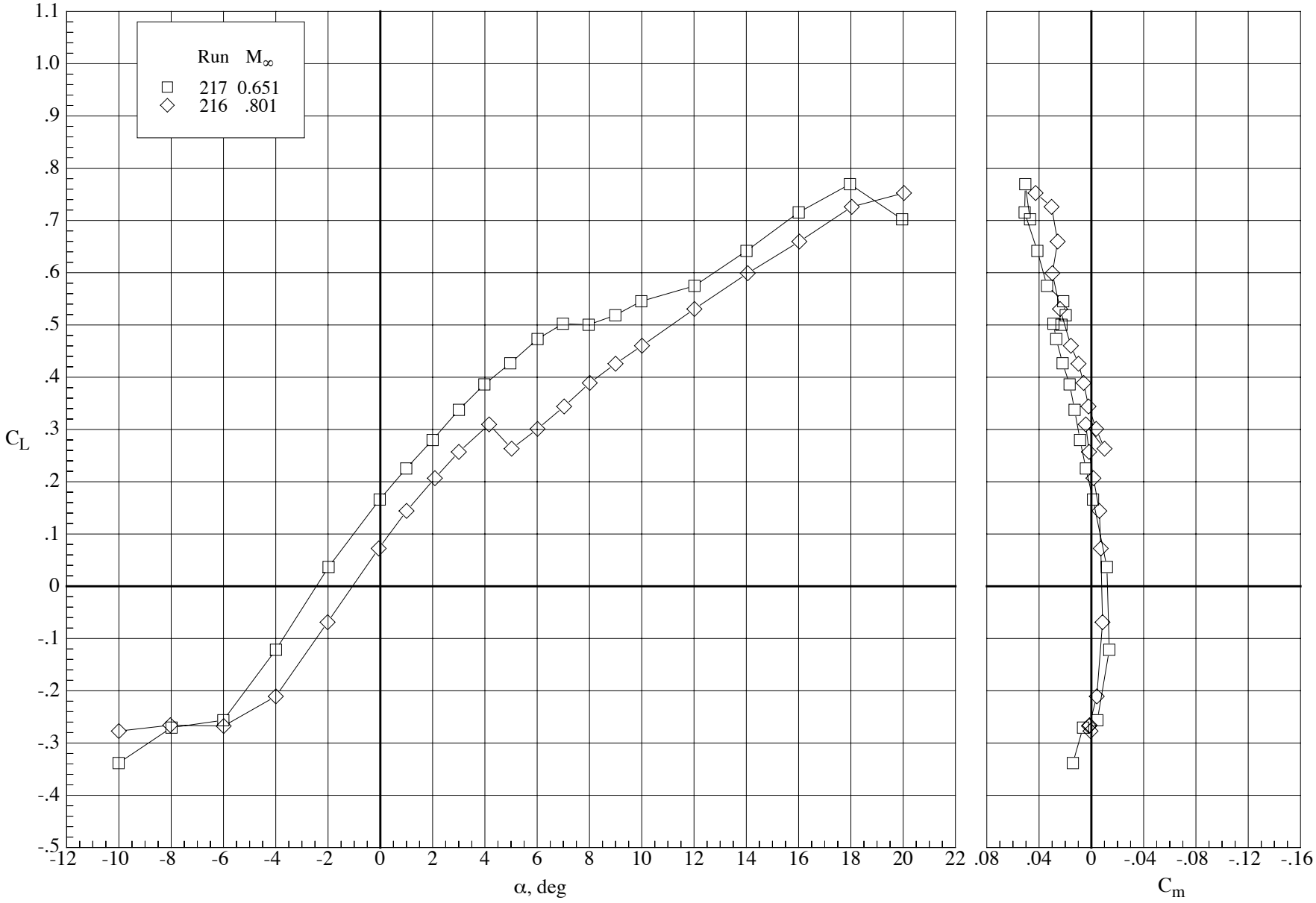

(a) Lift and pitching-moment coefficients.

Figure 27. Effect of Mach number on the longitudinal aerodynamic characteristics of the model with the Eppler 387 wing at a Reynolds number of 60,000. $\delta_h = 0°$ and $\delta_f = 0°$.

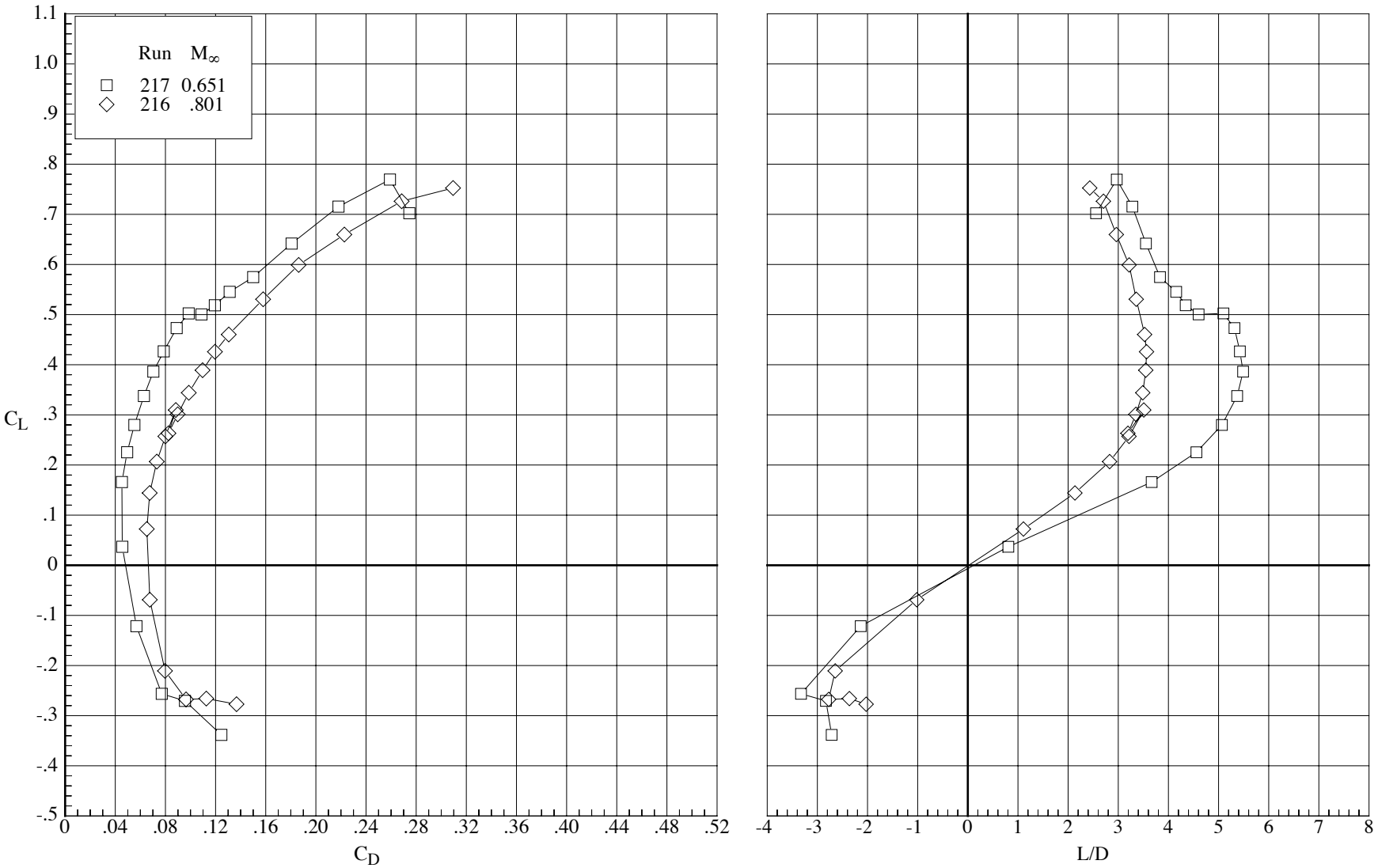

(b) Drag coefficient and lift-drag ratio.

Figure 27. Concluded.

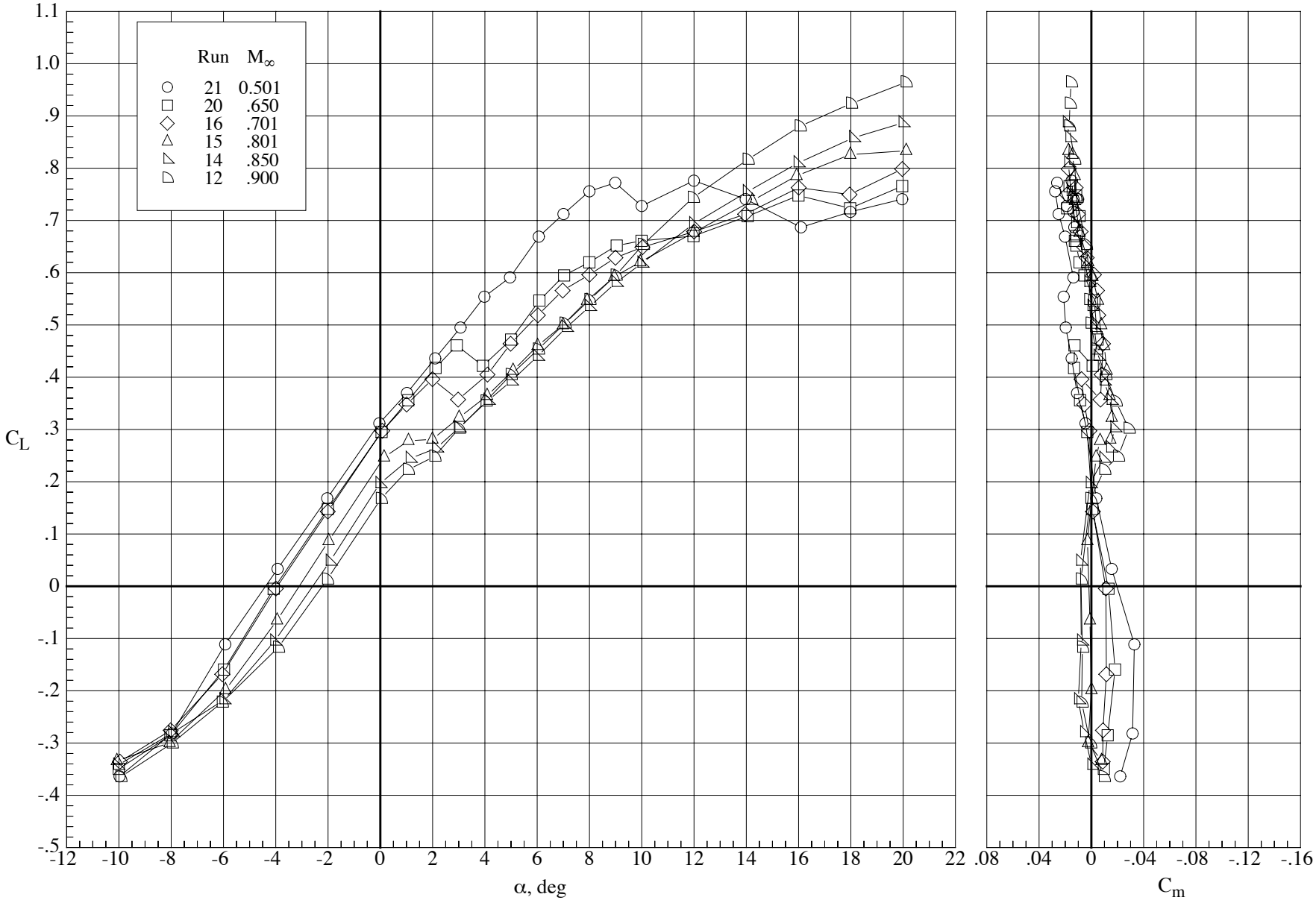

(a) Lift and pitching-moment coefficients.

Figure 28. Effect of Mach number on the longitudinal aerodynamic characteristics of the model with the MA-SC-1 wing (bump off) at a Reynolds number of 40,000. $\delta_h = 0°$ and $\delta_f = 0°$.

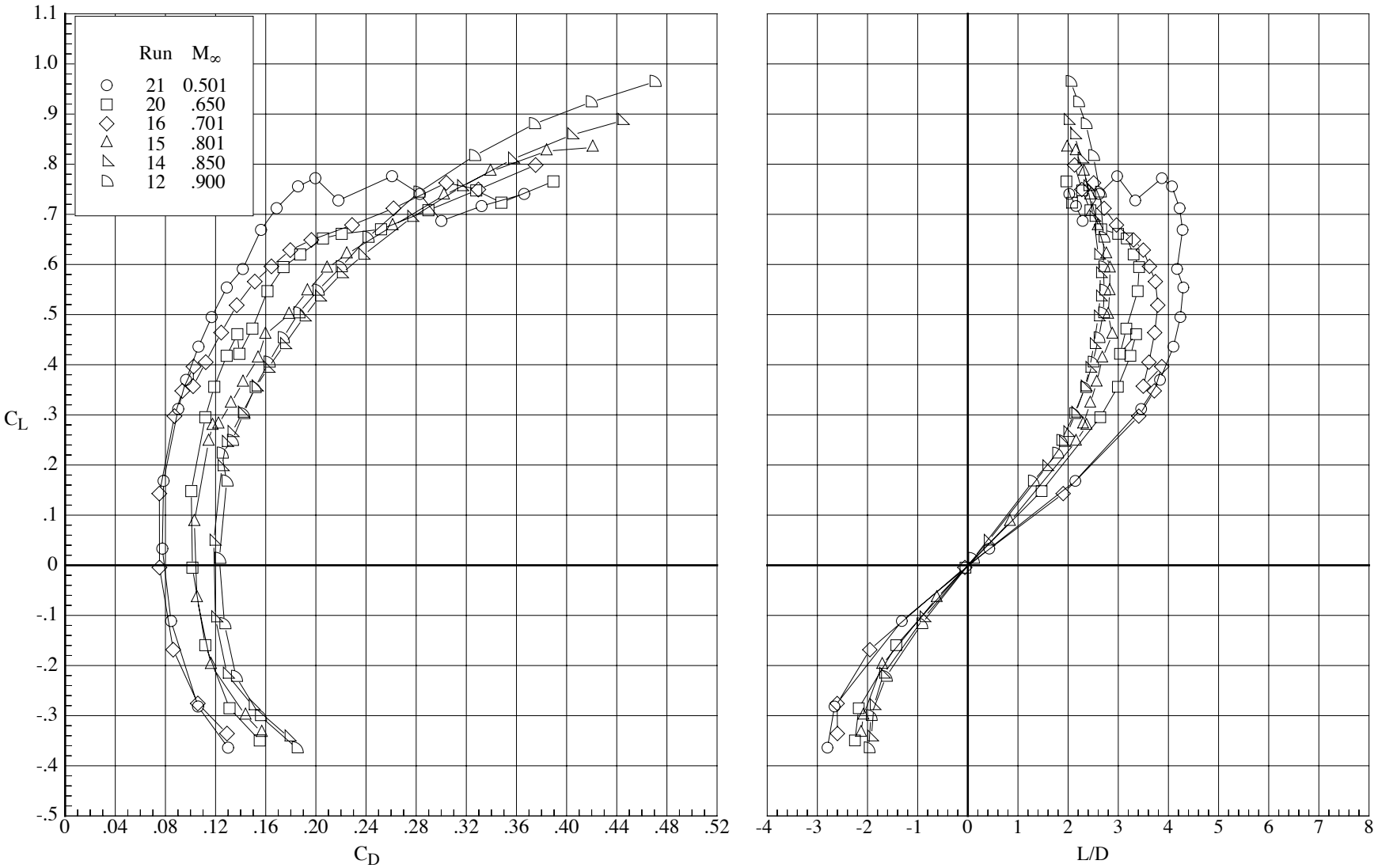

(b) Drag coefficient and lift-drag ratio.

Figure 28. Concluded.

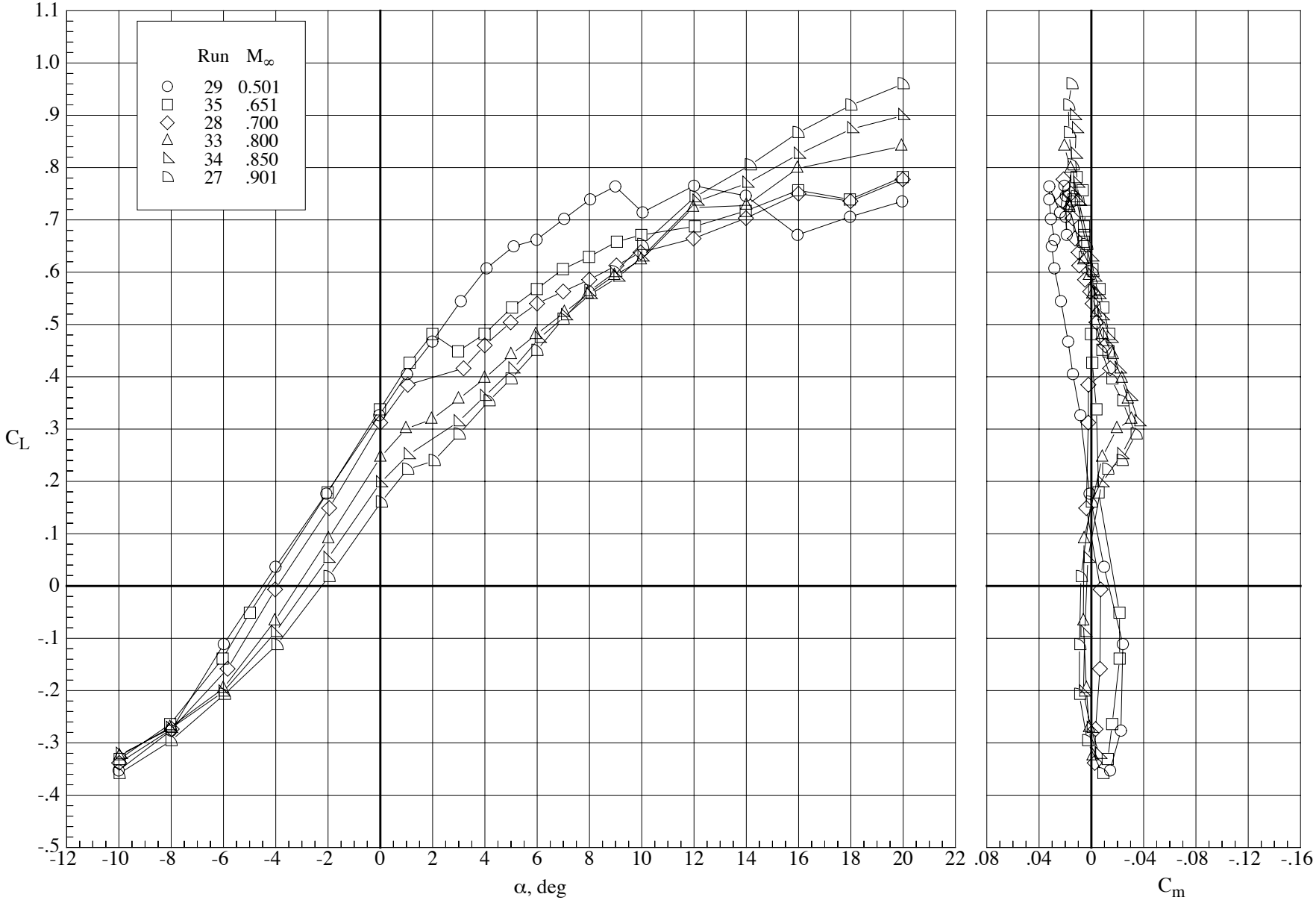

(a) Lift and pitching-moment coefficients.

Figure 29. Effect of Mach number on the longitudinal aerodynamic characteristics of the model with the MA-SC-1 wing (bump on) at a Reynolds number of 40,000. $\delta_h = 0°$ and $\delta_f = 0°$.

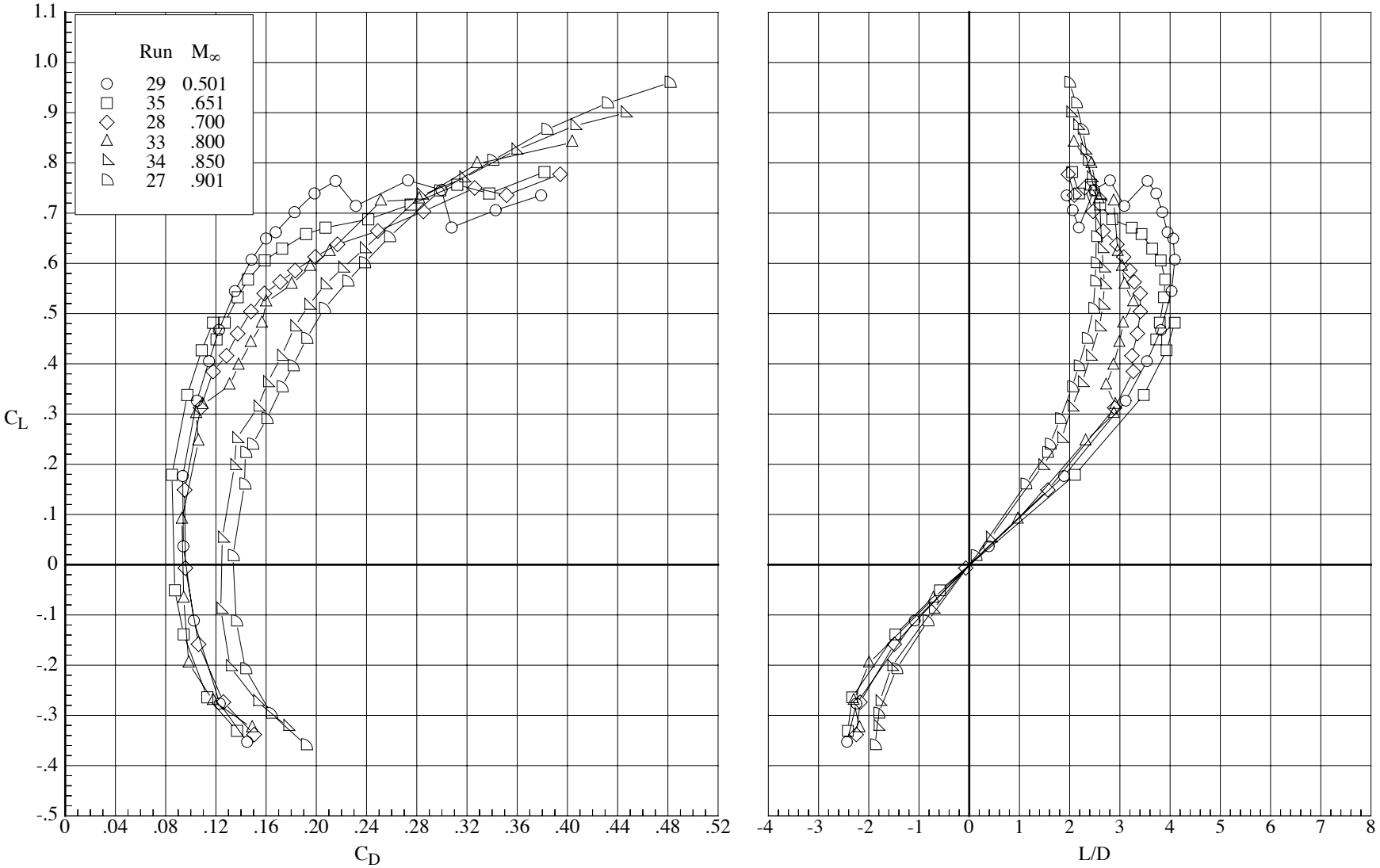

(b) Drag coefficient and lift-drag ratio.

Figure 29. Concluded.

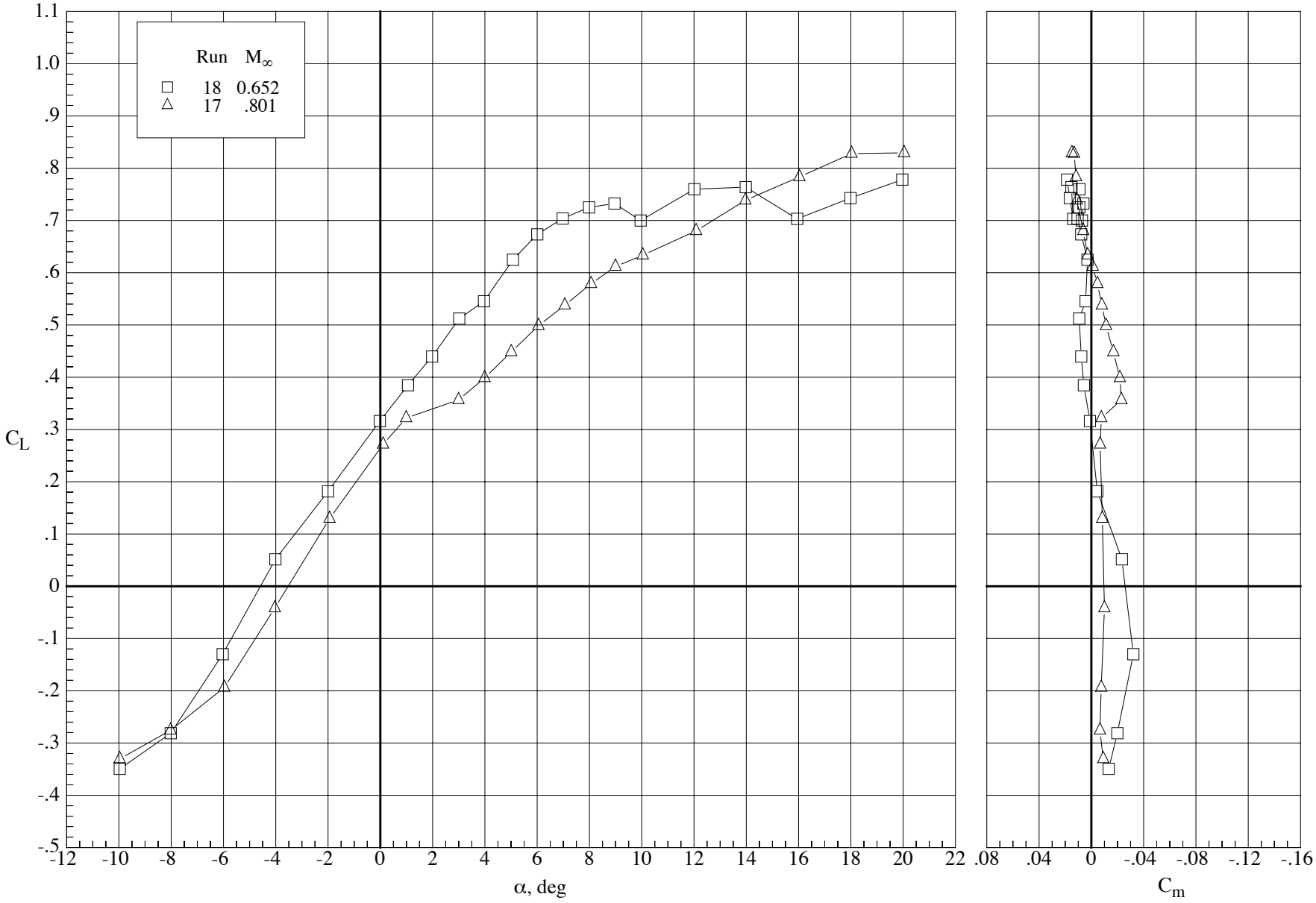

(a) Lift and pitching-moment coefficients.

Figure 30. Effect of Mach number on the longitudinal aerodynamic characteristics of the model with the MA-SC-1 wing (bump off) at a Reynolds number of 60,000. $\delta_h = 0°$ and $\delta_f = 0°$.

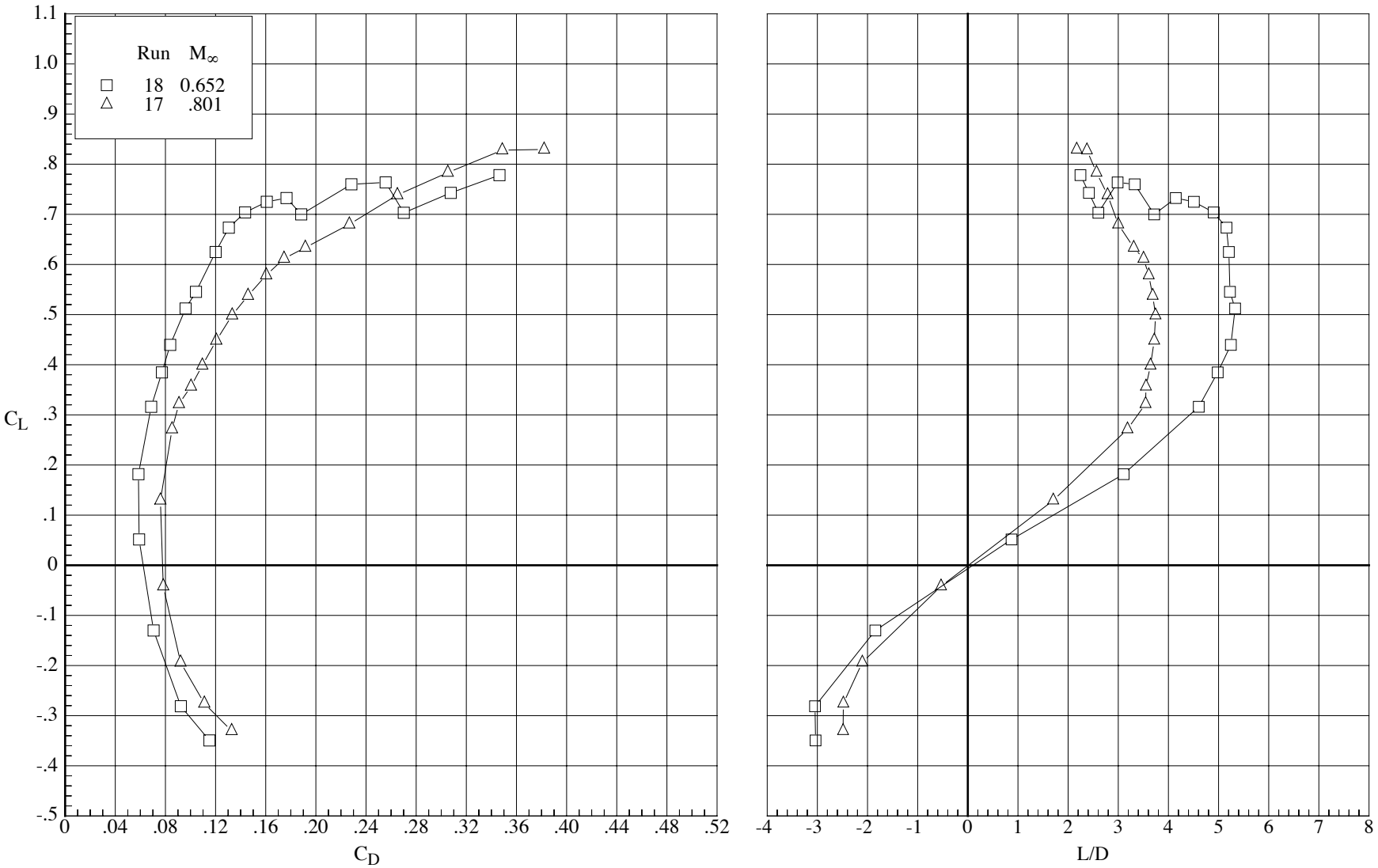

(b) Drag coefficient and lift-drag ratio.

Figure 30. Concluded.

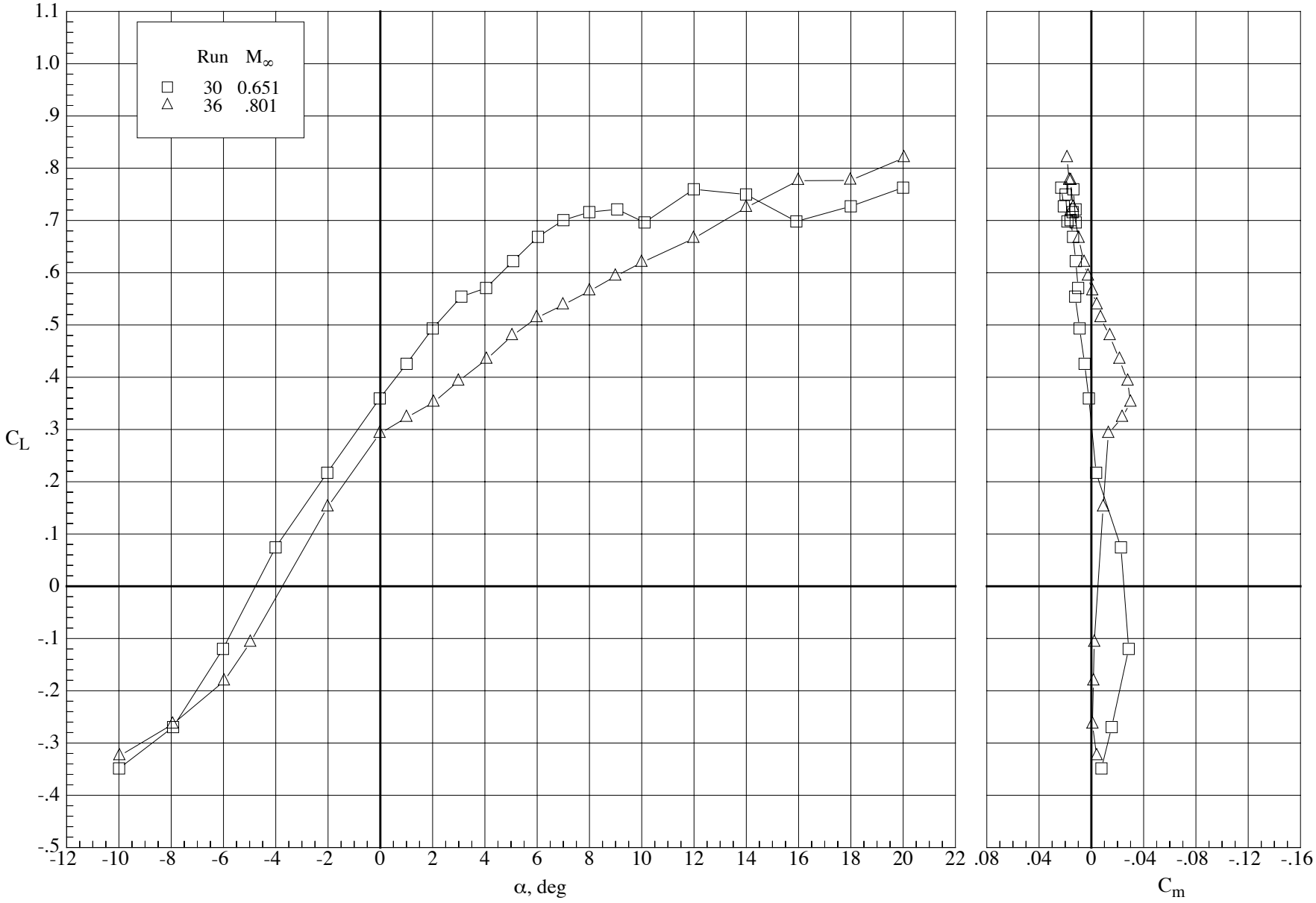

(a) Lift and pitching-moment coefficients.

Figure 31. Effect of Mach number on the longitudinal aerodynamic characteristics of the model with the MA-SC-1 wing (bump on) at a Reynolds number of 60,000. $\delta_h = 0°$ and $\delta_f = 0°$.

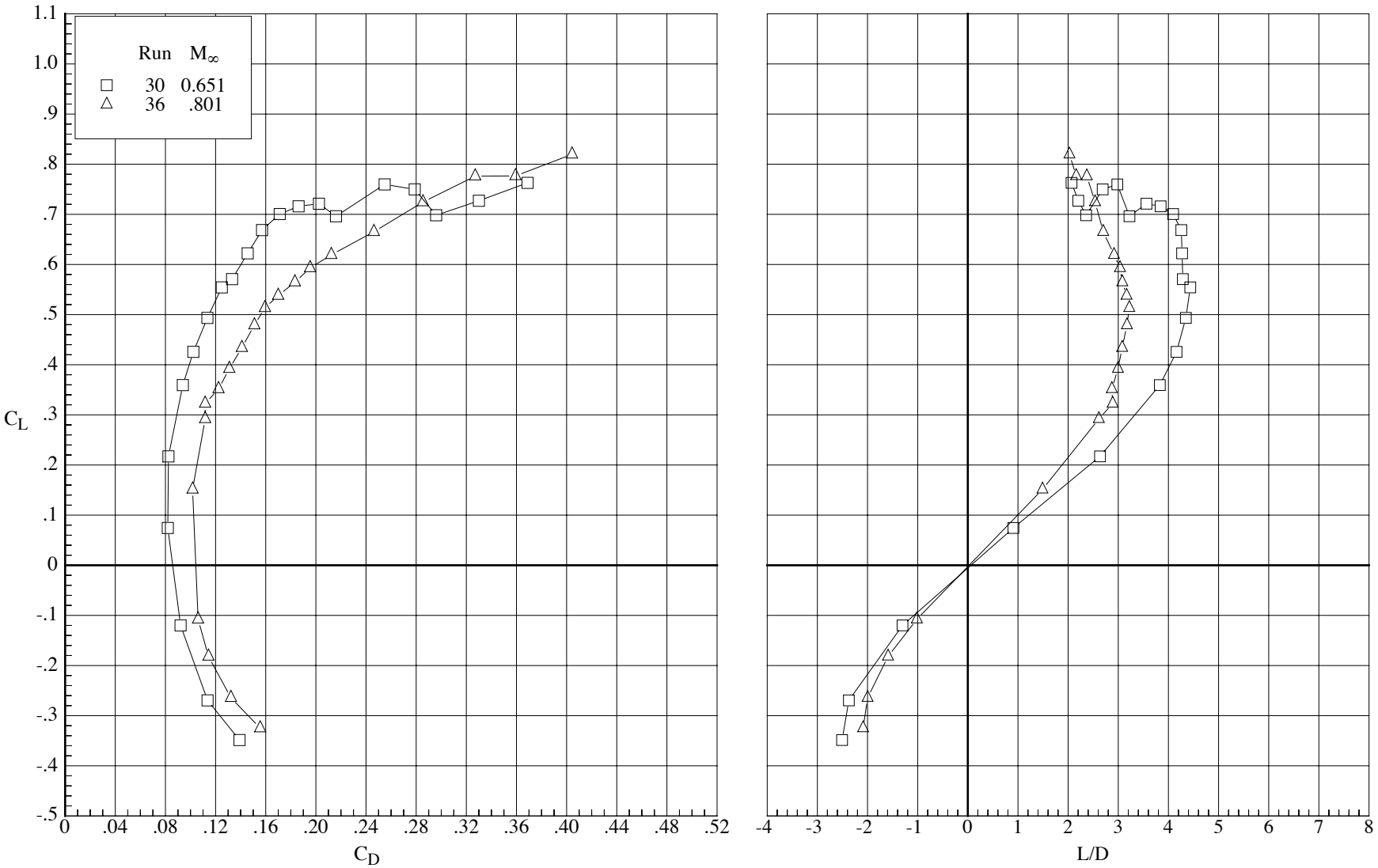

(b) Drag coefficient and lift-drag ratio.

Figure 31. Concluded.

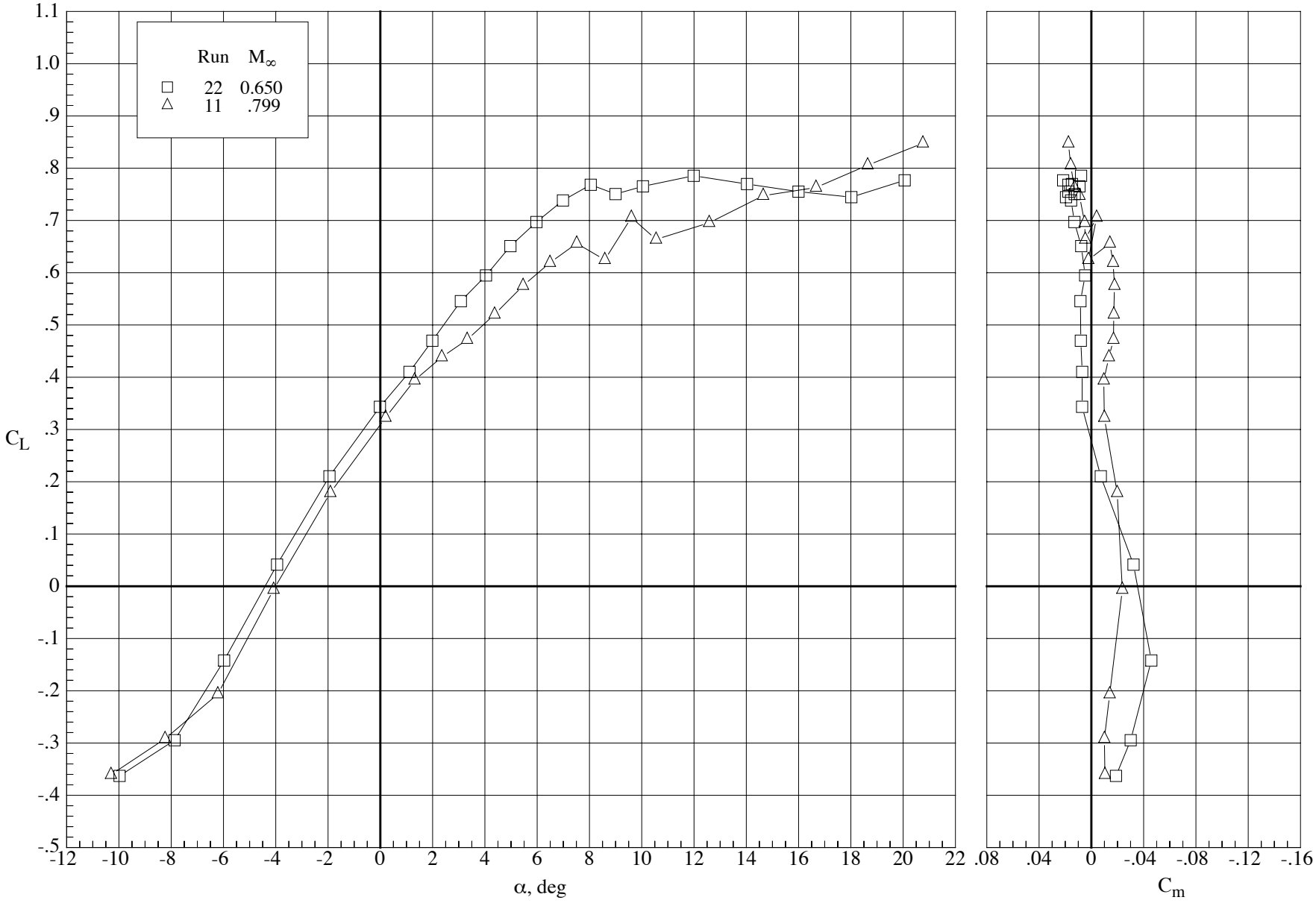

(a) Lift and pitching-moment coefficients.

Figure 32. Effect of Mach number on the longitudinal aerodynamic characteristics of the model with the MA-SC-1 wing (bump off) at a Reynolds number of 100,000. $\delta_h = 0°$ and $\delta_f = 0°$.

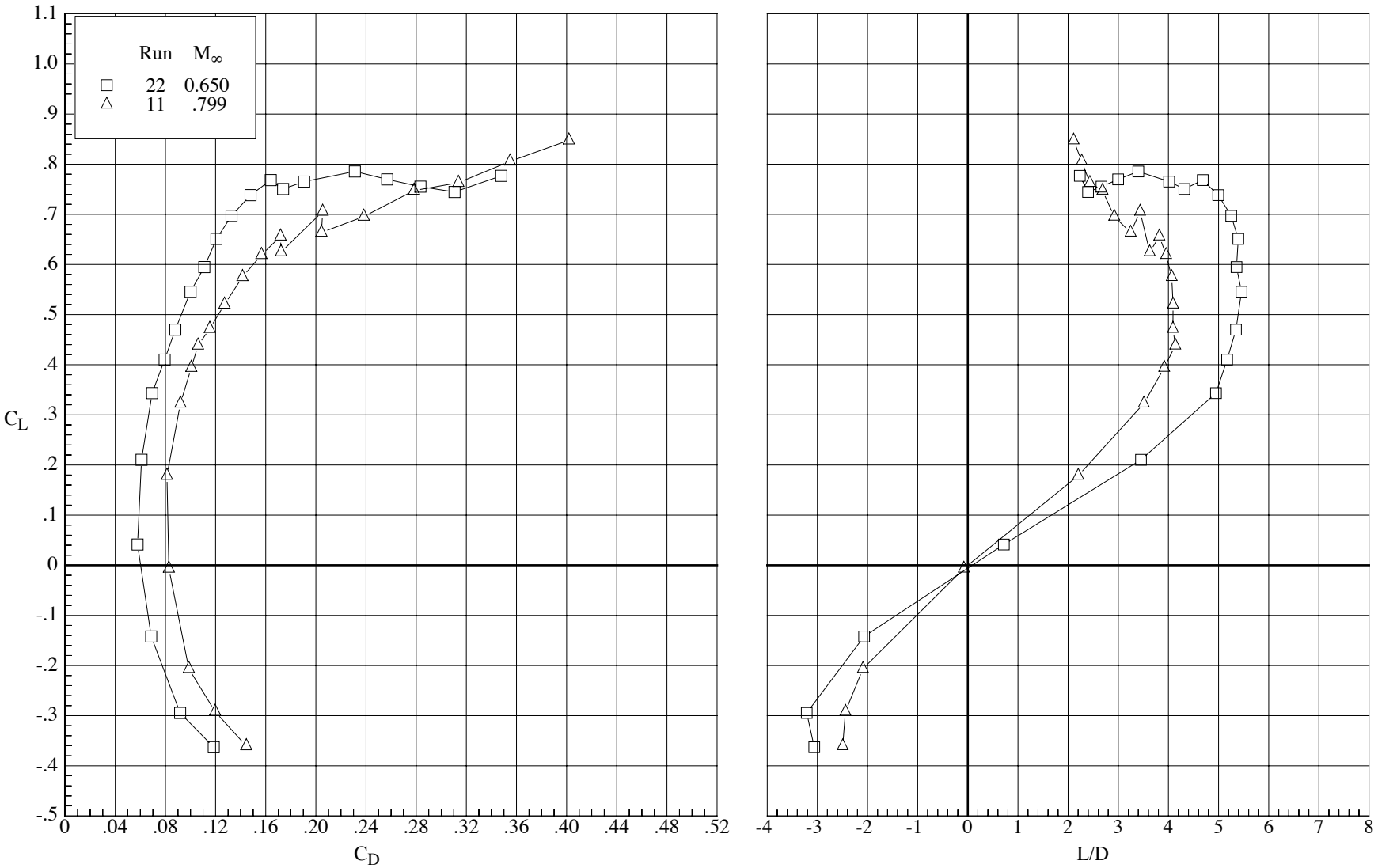

(b) Drag coefficient and lift-drag ratio.

Figure 32. Concluded.

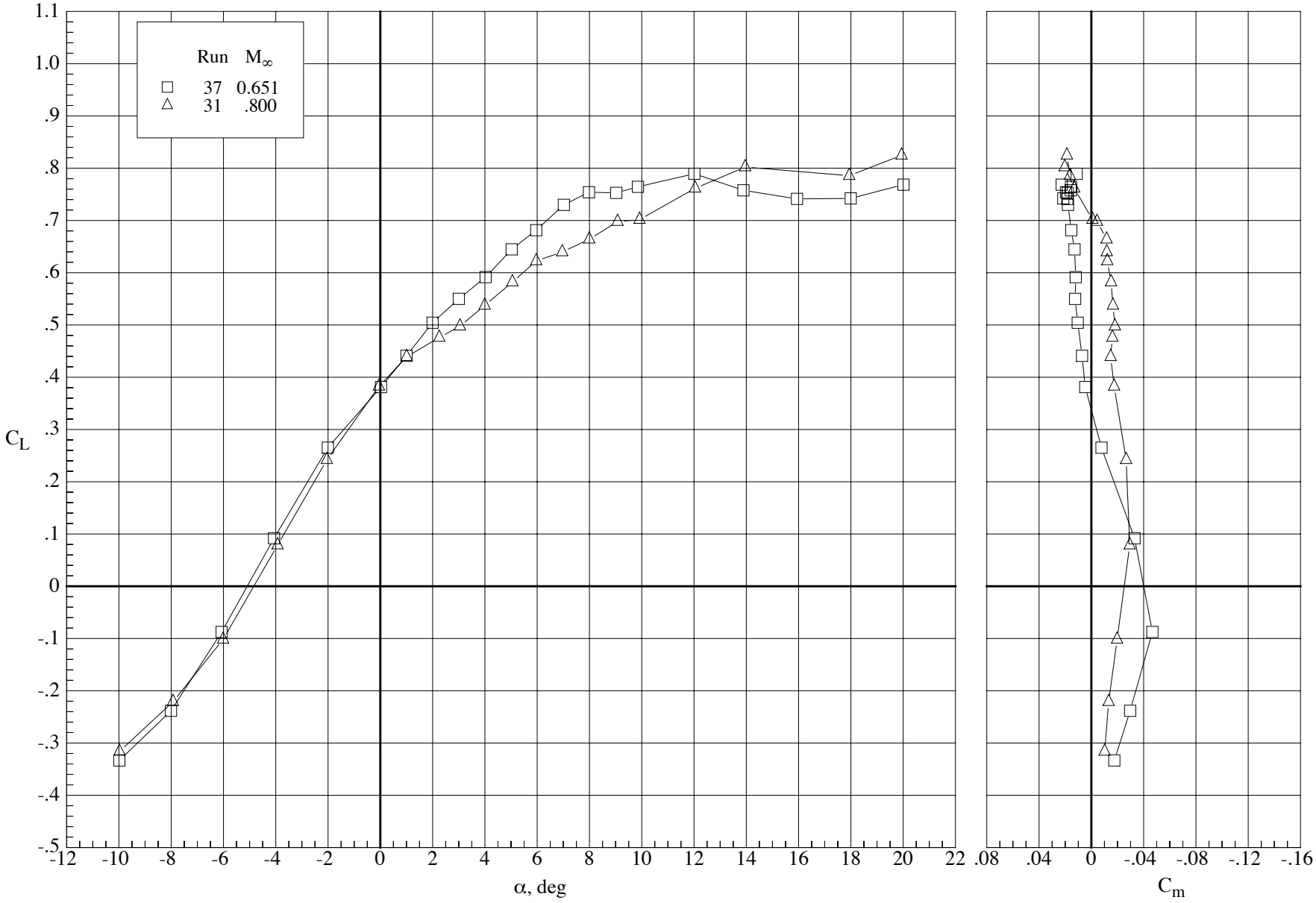

(a) Lift and pitching-moment coefficients.

Figure 33. Effect of Mach number on the longitudinal aerodynamic characteristics of the model with the MA-SC-1 wing (bump on) at a Reynolds number of 100,000. $\delta_h = 0°$ and $\delta_f = 0°$.

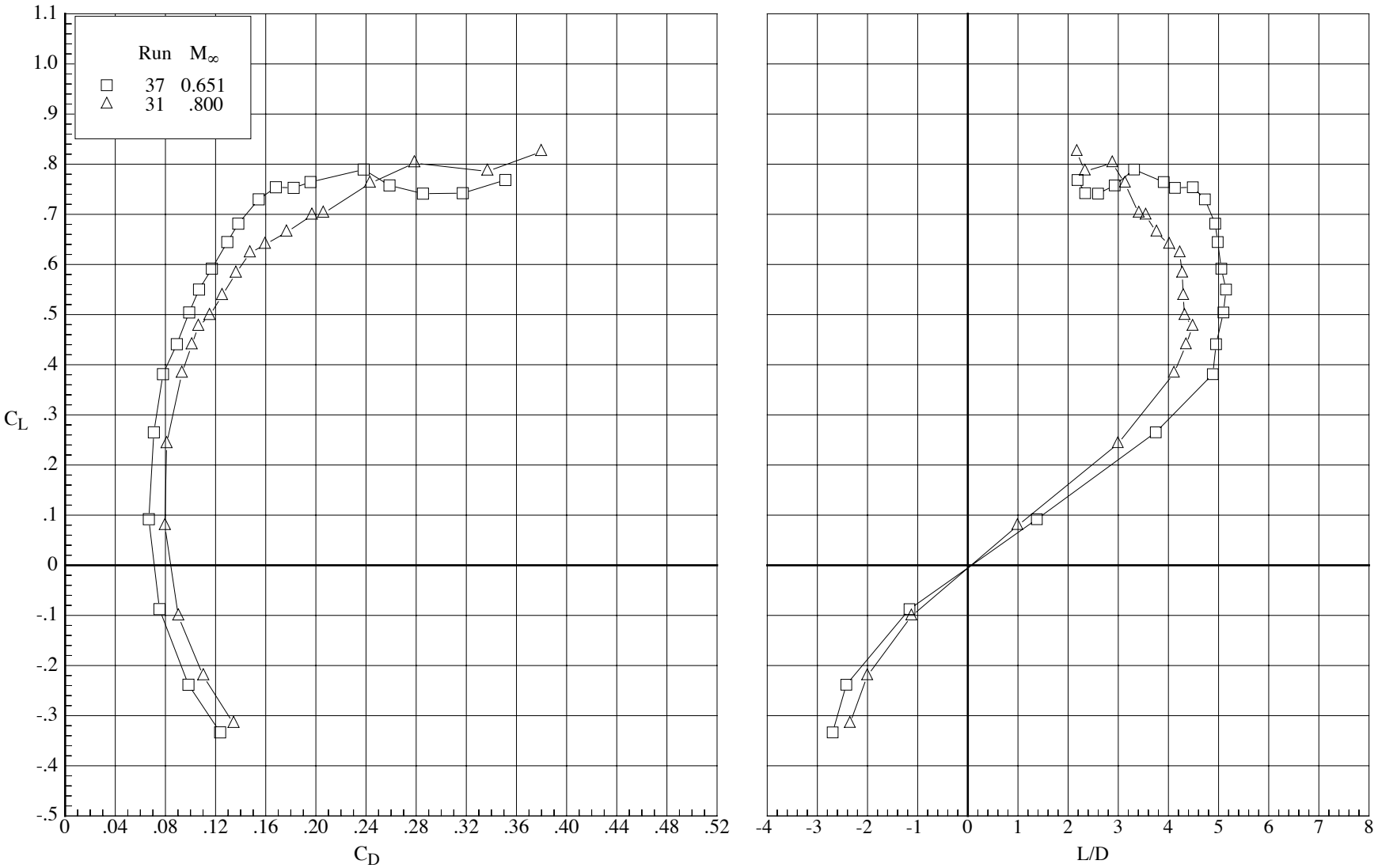

(b) Drag coefficient and lift-drag ratio.

Figure 33. Concluded.

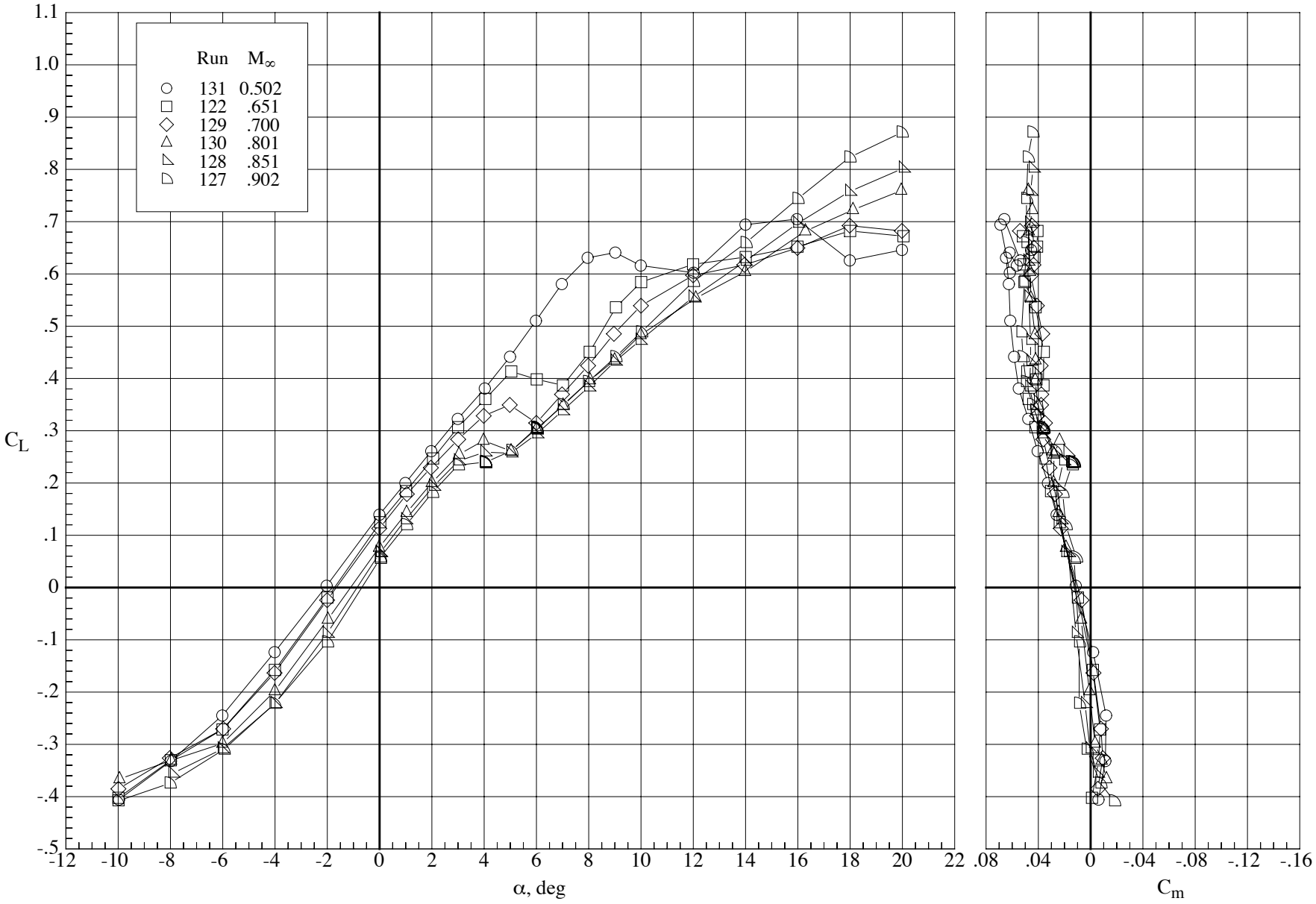

(a) Lift and pitching-moment coefficients.

Figure 34. Effect of Mach number on the longitudinal aerodynamic characteristics of the model with the MA-SF-1 wing (bump off) at a Reynolds number of 40,000. $\delta_h = 0°$ and $\delta_f = 0°$.

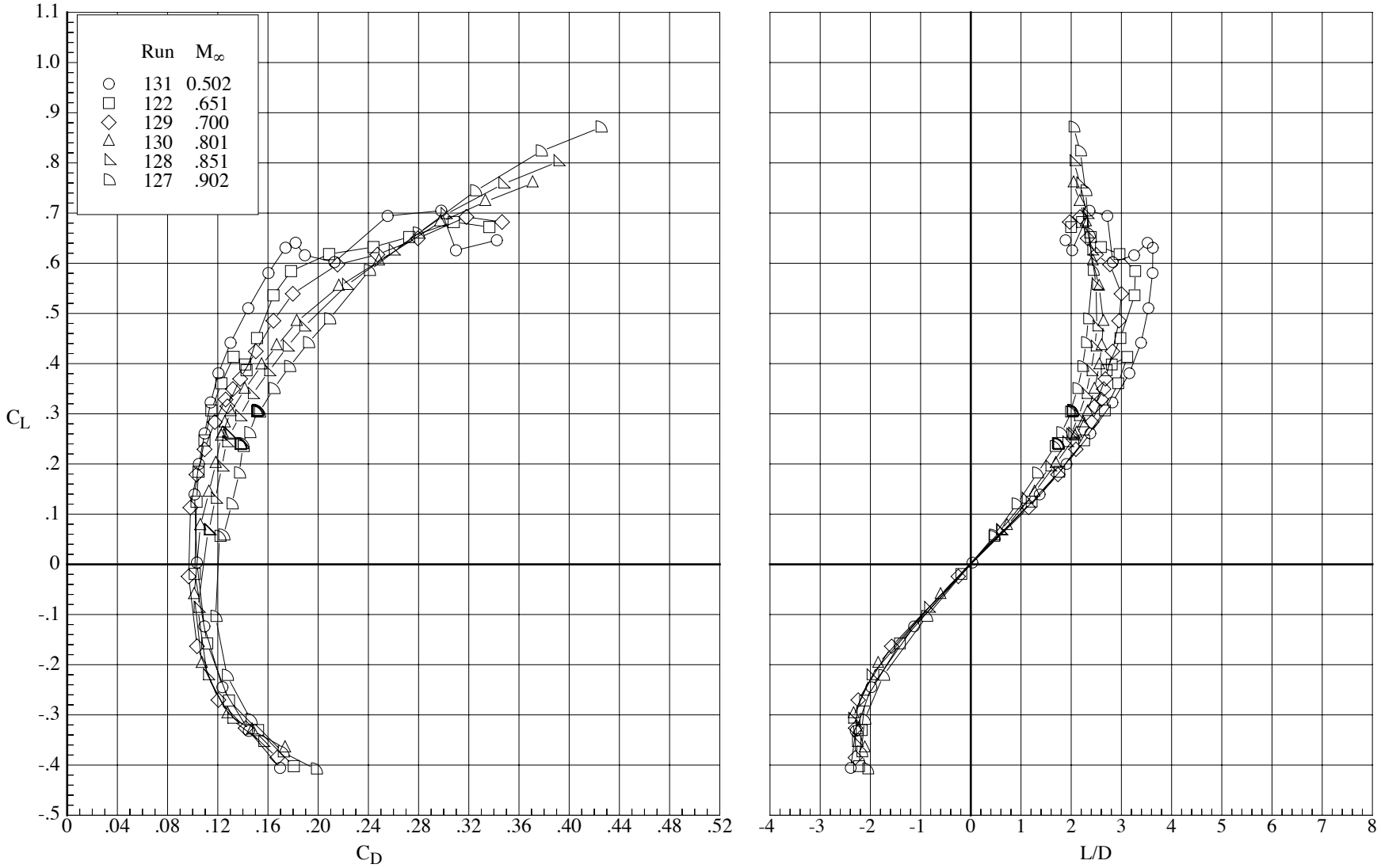

(b) Drag coefficient and lift-drag ratio.

Figure 34. Concluded.

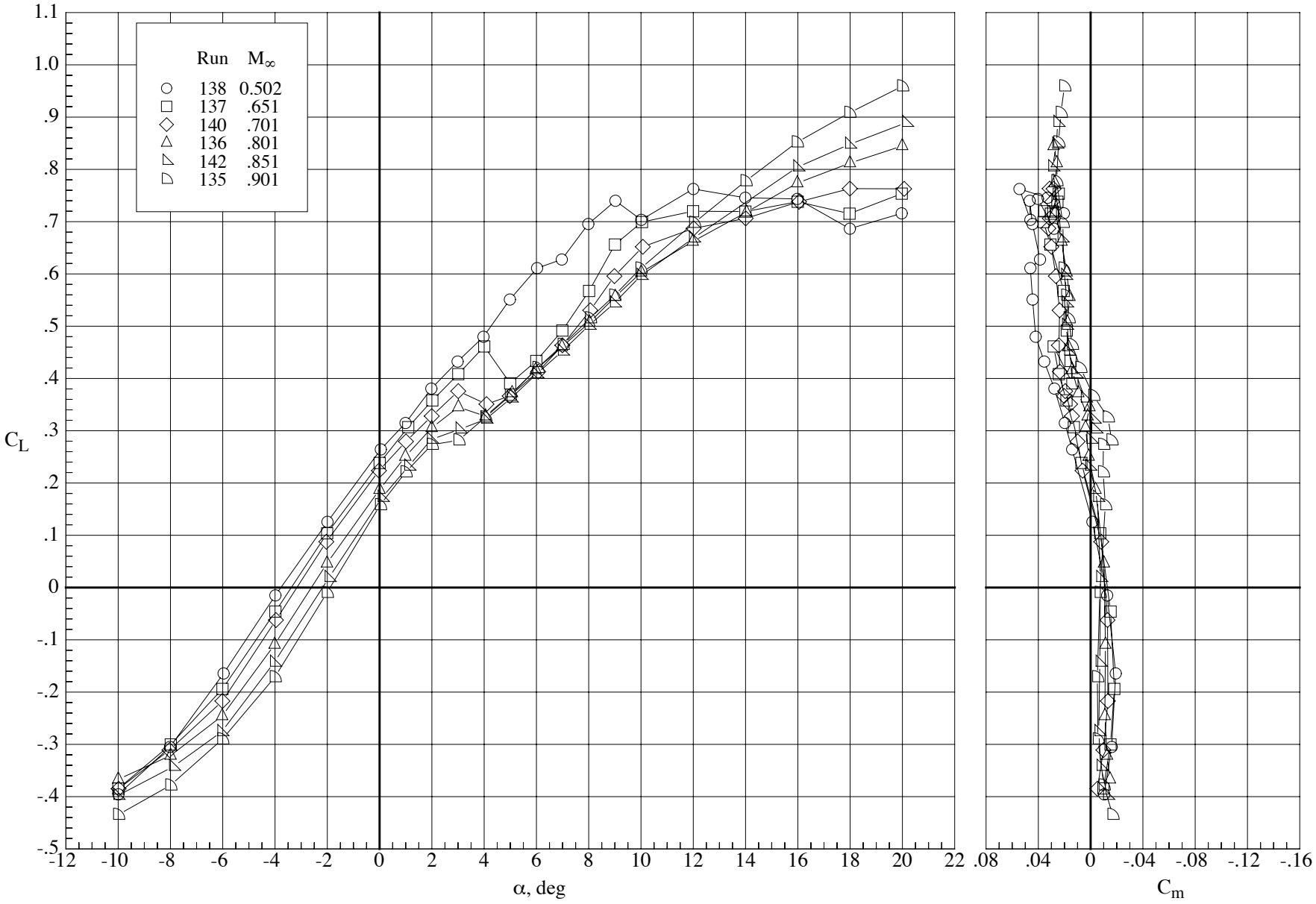

(a) Lift and pitching-moment coefficients.

Figure 35. Effect of Mach number on the longitudinal aerodynamic characteristics of the model with the MA-SF-1 wing (bump off) at a Reynolds number of 40,000. $\delta_h = 0°$ and $\delta_f = 10°$.

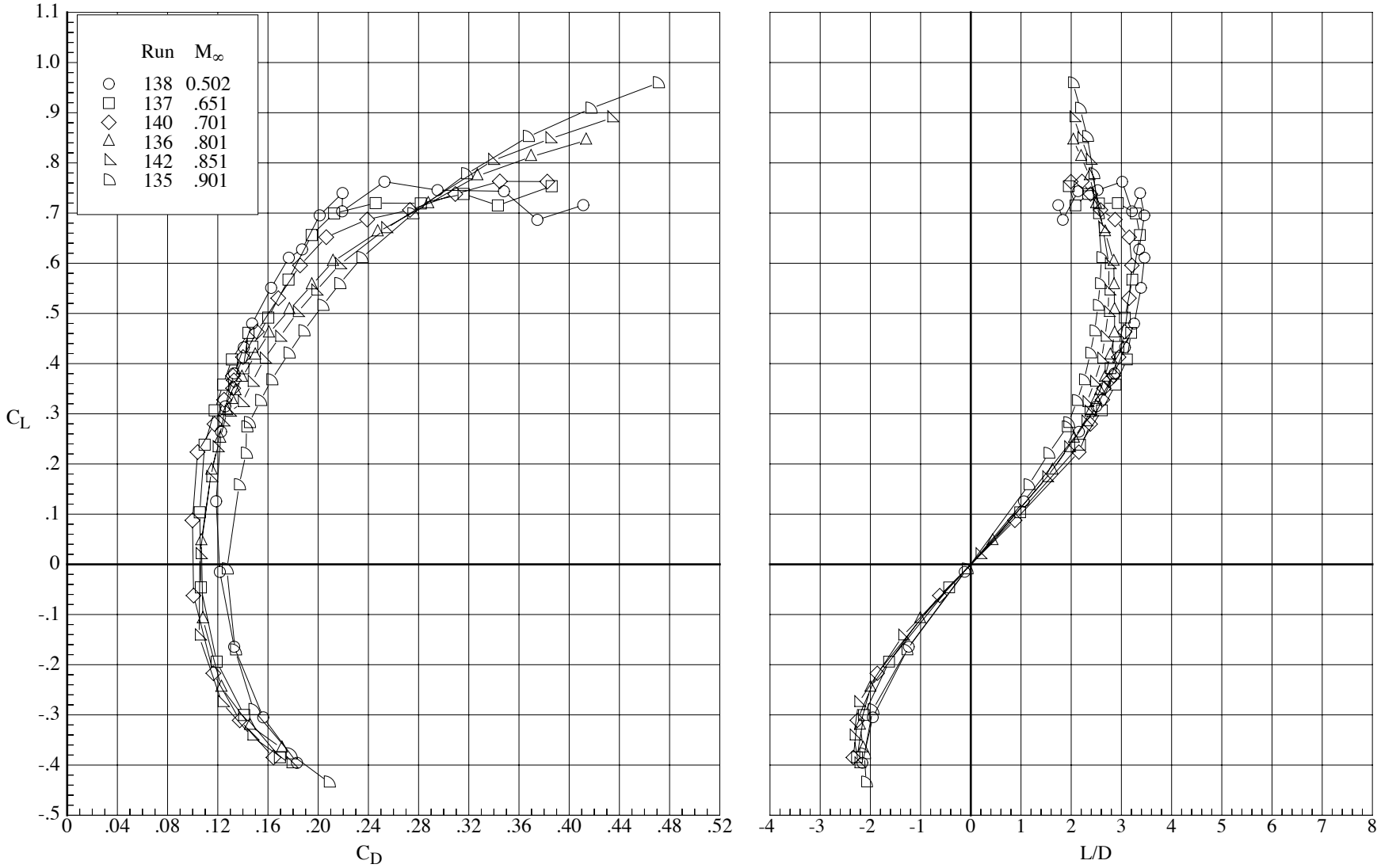

(b) Drag coefficient and lift-drag ratio.

Figure 35. Concluded.

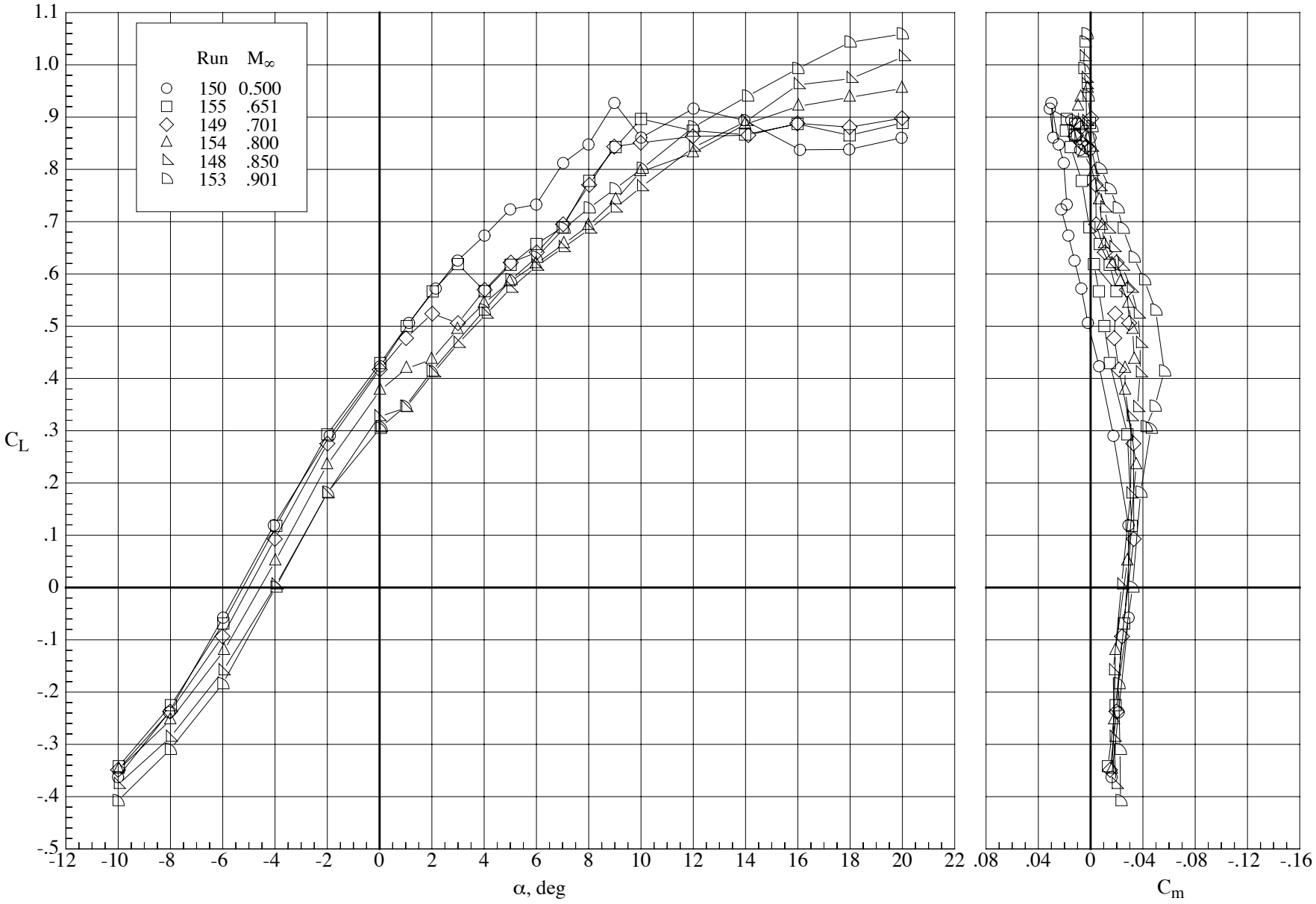

(a) Lift and pitching-moment coefficients.

Figure 36. Effect of Mach number on the longitudinal aerodynamic characteristics of the model with the MA-SF-1 wing (bump off) at a Reynolds number of 40,000. $\delta_h = 0°$ and $\delta_f = 30°$.

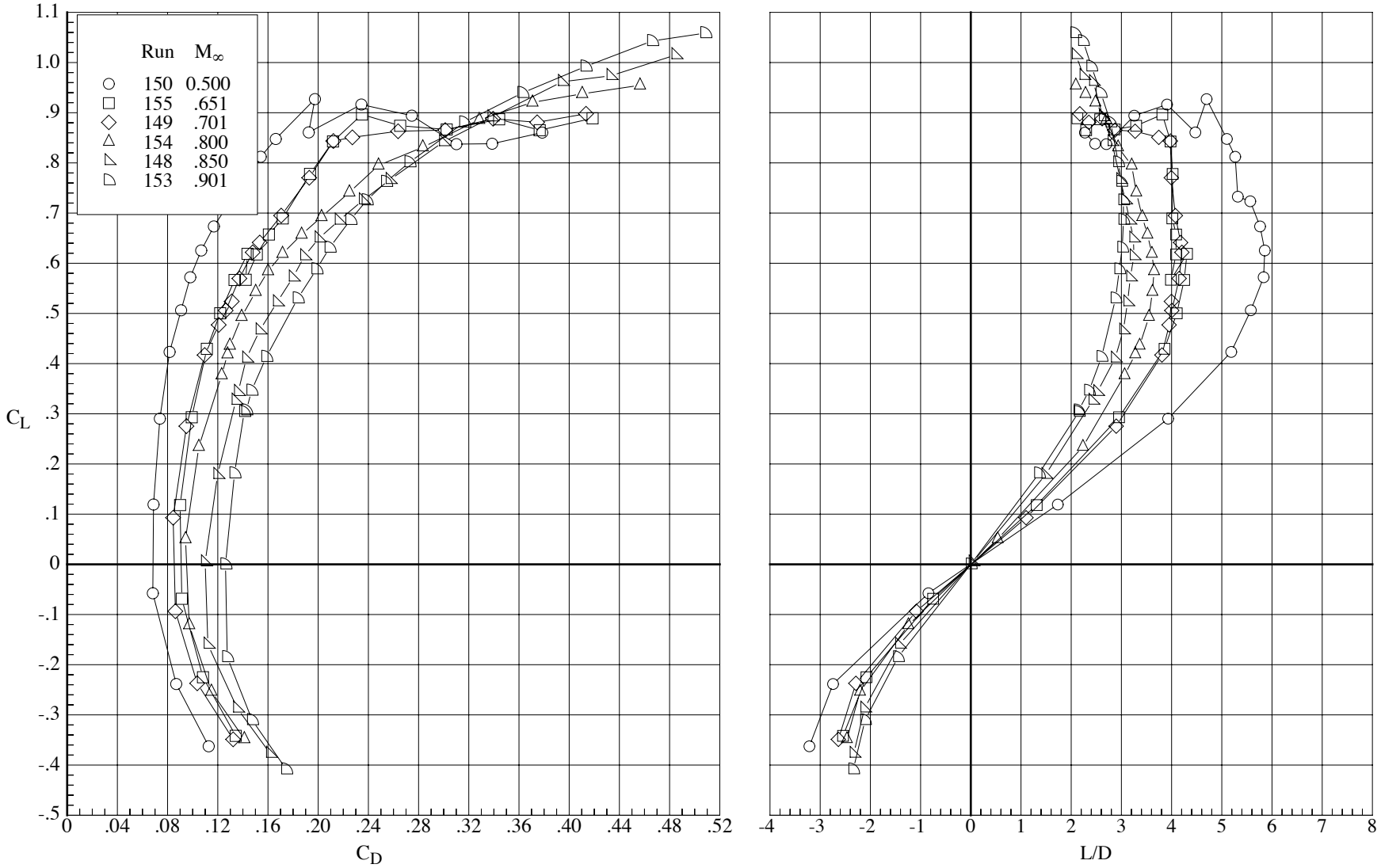

(b) Drag coefficient and lift-drag ratio.

Figure 36. Concluded.

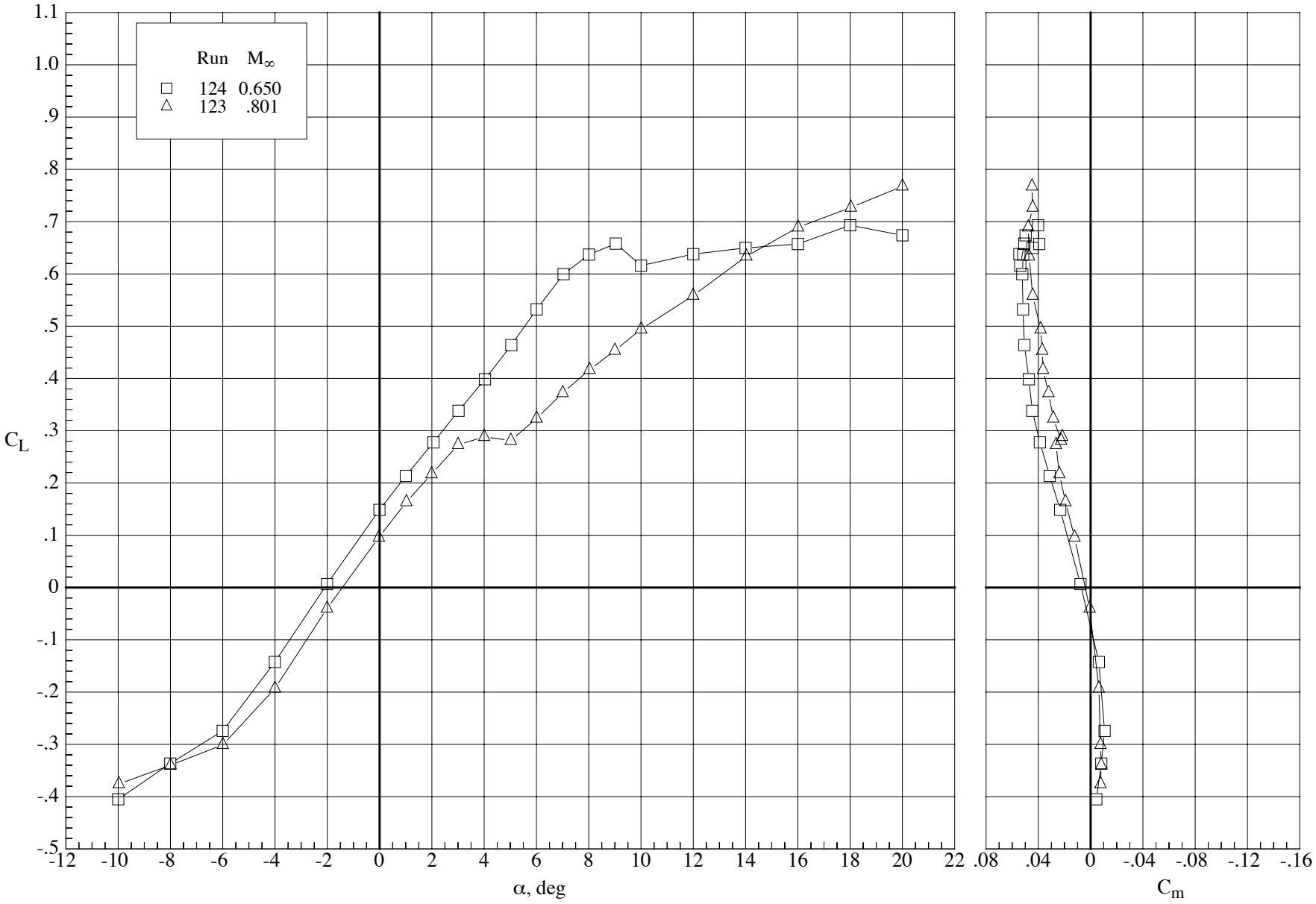

(a) Lift and pitching-moment coefficients.

Figure 37. Effect of Mach number on the longitudinal aerodynamic characteristics of the model with the MA-SF-1 wing (bump off) at a Reynolds number of 60,000. $\delta_h = 0°$ and $\delta_f = 0°$.

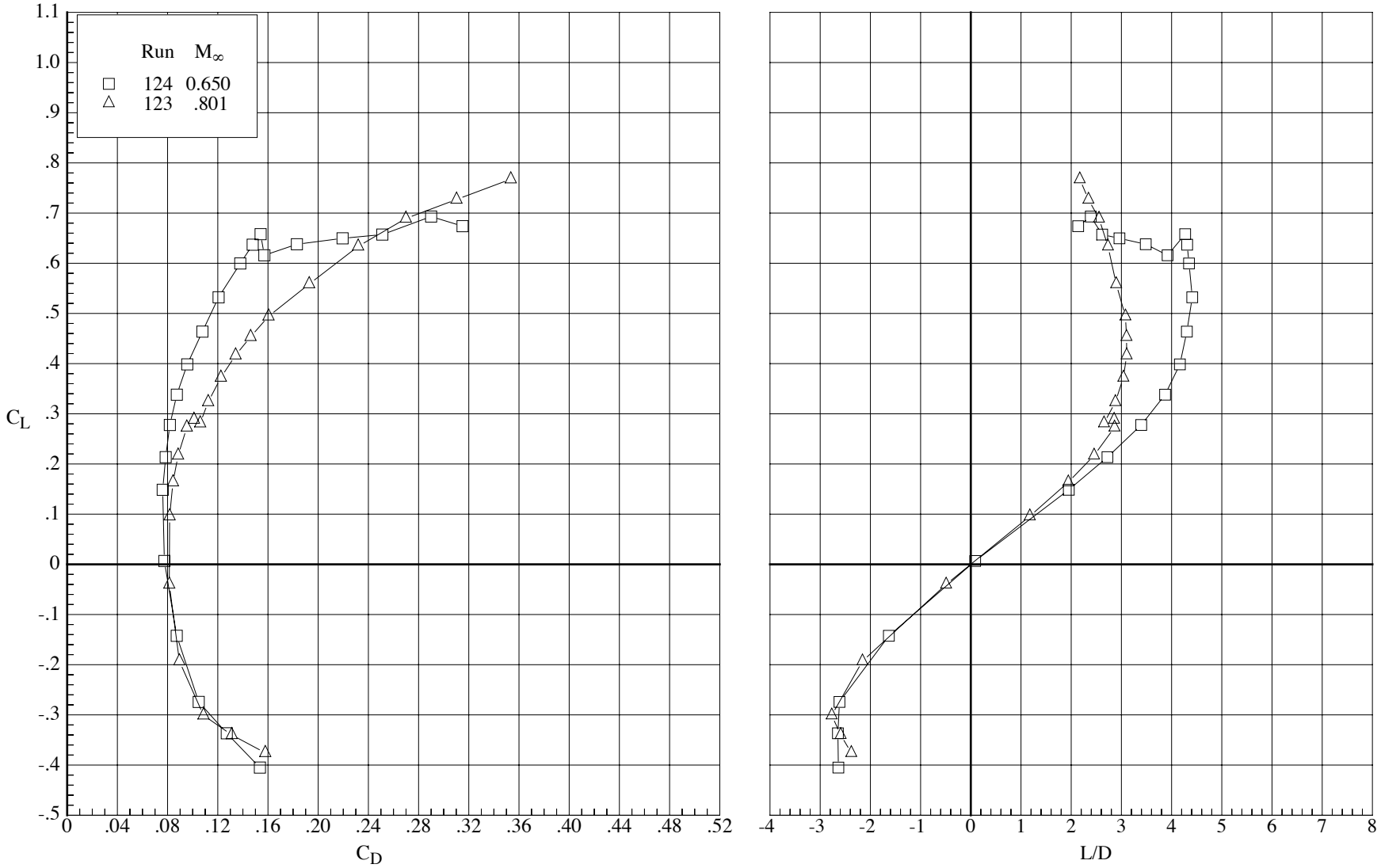

(b) Drag coefficient and lift-drag ratio.

Figure 37. Concluded.

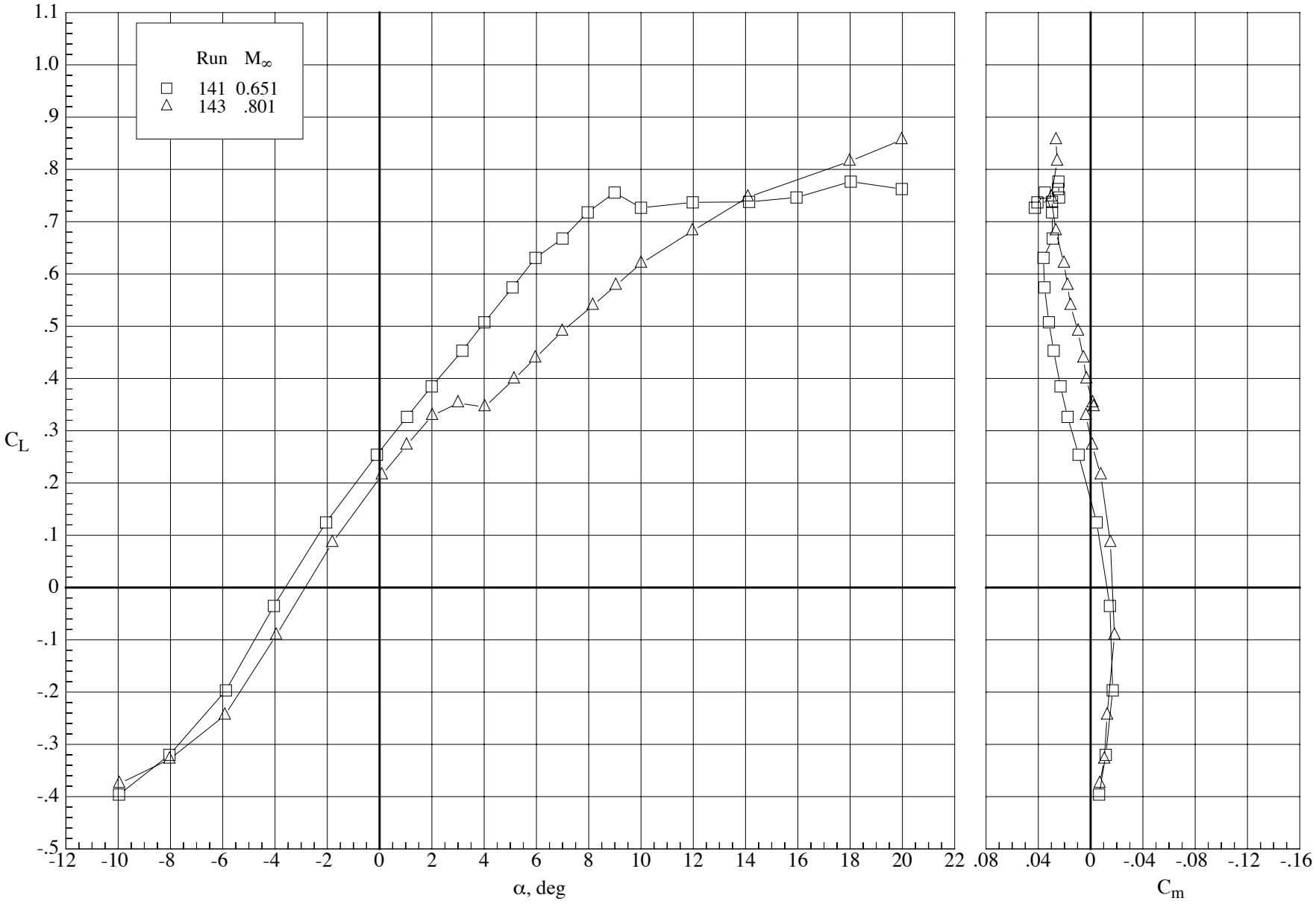

(a) Lift and pitching-moment coefficients.

Figure 38. Effect of Mach number on the longitudinal aerodynamic characteristics of the model with the MA-SF-1 wing (bump off) at a Reynolds number of 60,000. $\delta_h = 0°$ and $\delta_f = 10°$.

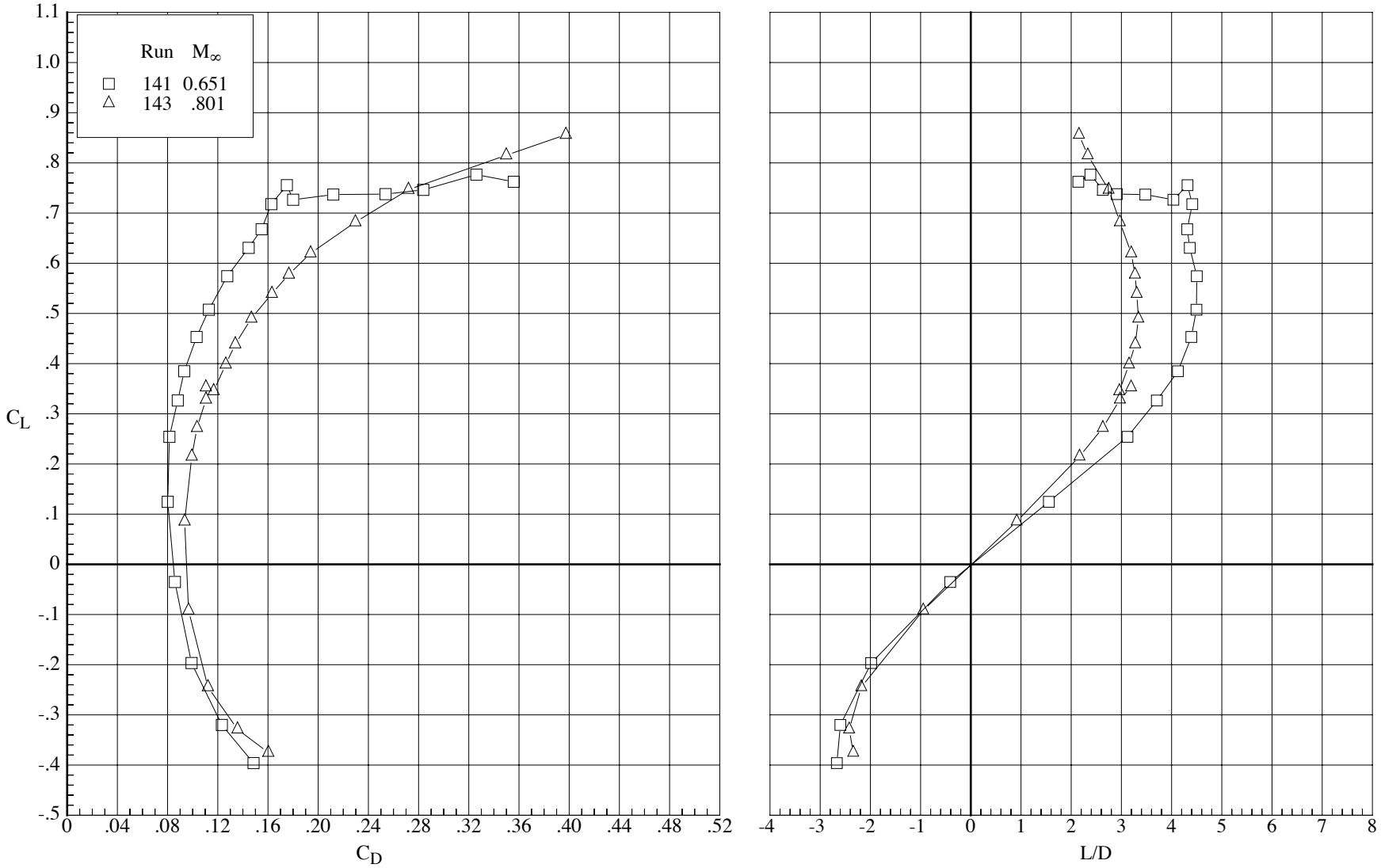

(b) Drag coefficient and lift-drag ratio.

Figure 38. Concluded.

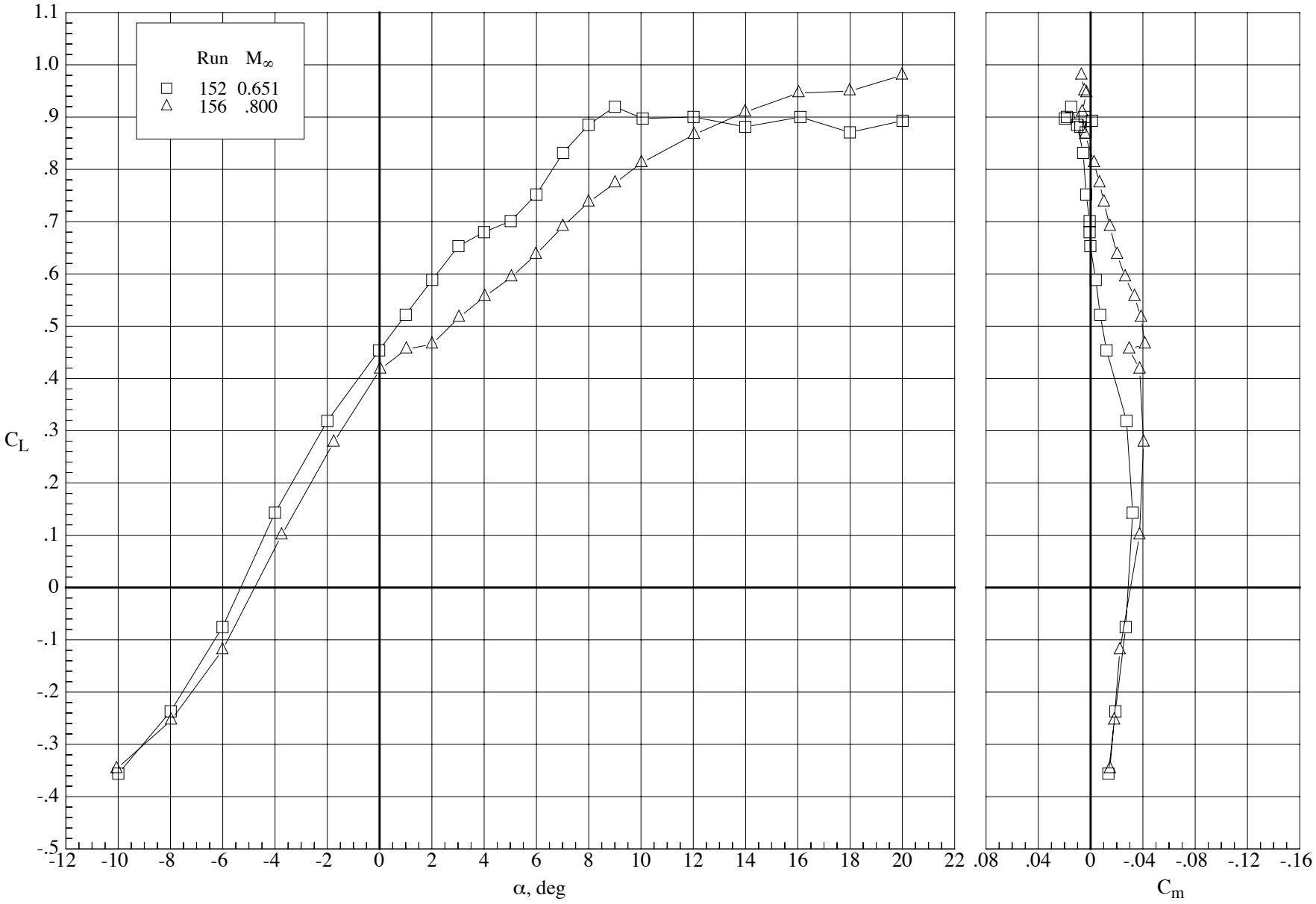

(a) Lift and pitching-moment coefficients.

Figure 39. Effect of Mach number on the longitudinal aerodynamic characteristics of the model with the MA-SF-1 wing (bump off) at a Reynolds number of 60,000. $\delta_h = 0°$ and $\delta_f = 30°$.

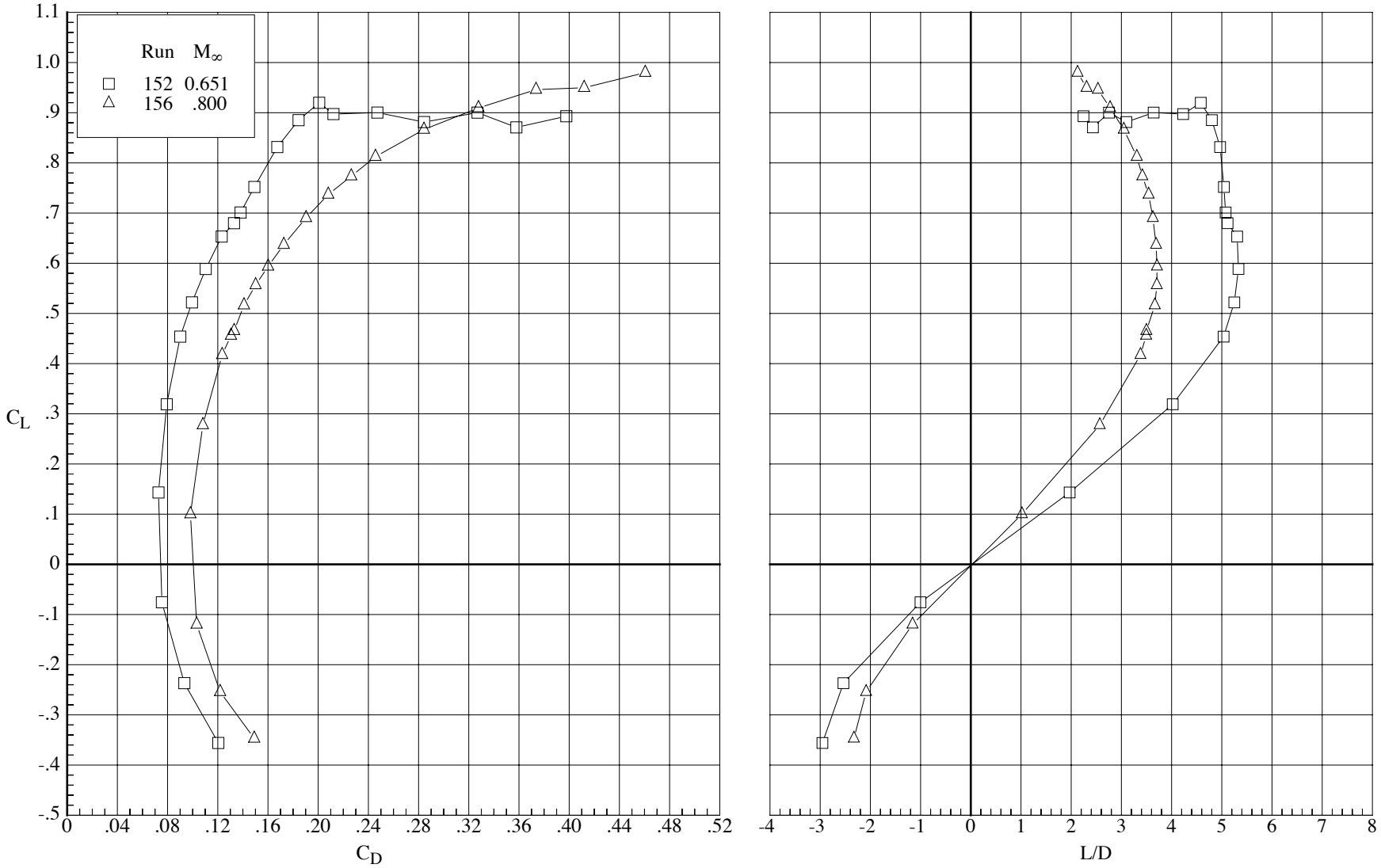

(b) Drag coefficient and lift-drag ratio.

Figure 39. Concluded.

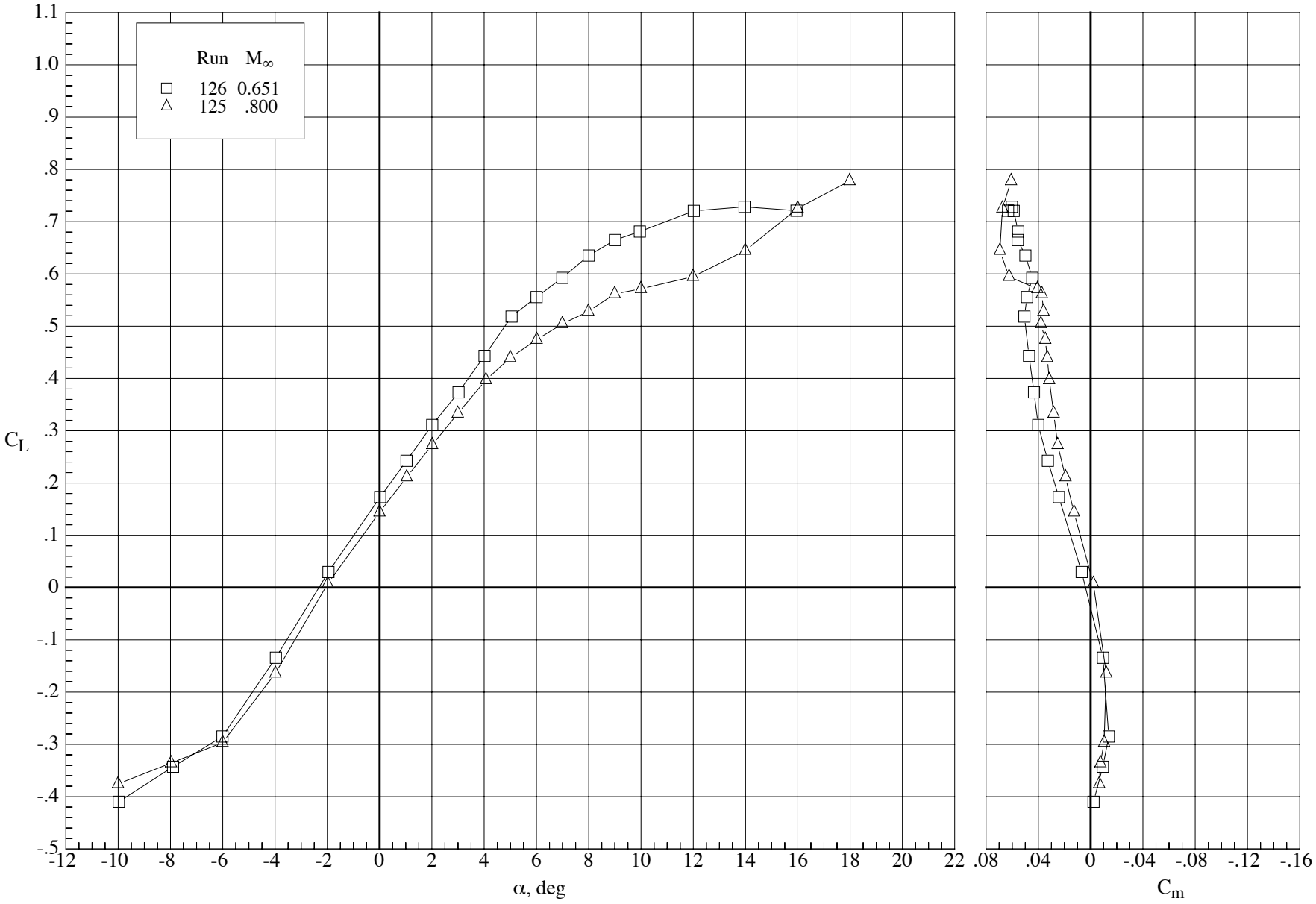

(a) Lift and pitching-moment coefficients.

Figure 40. Effect of Mach number on the longitudinal aerodynamic characteristics of the model with the MA-SF-1 wing (bump off) at a Reynolds number of 100,000. $\delta_h = 0°$ and $\delta_f = 0°$.

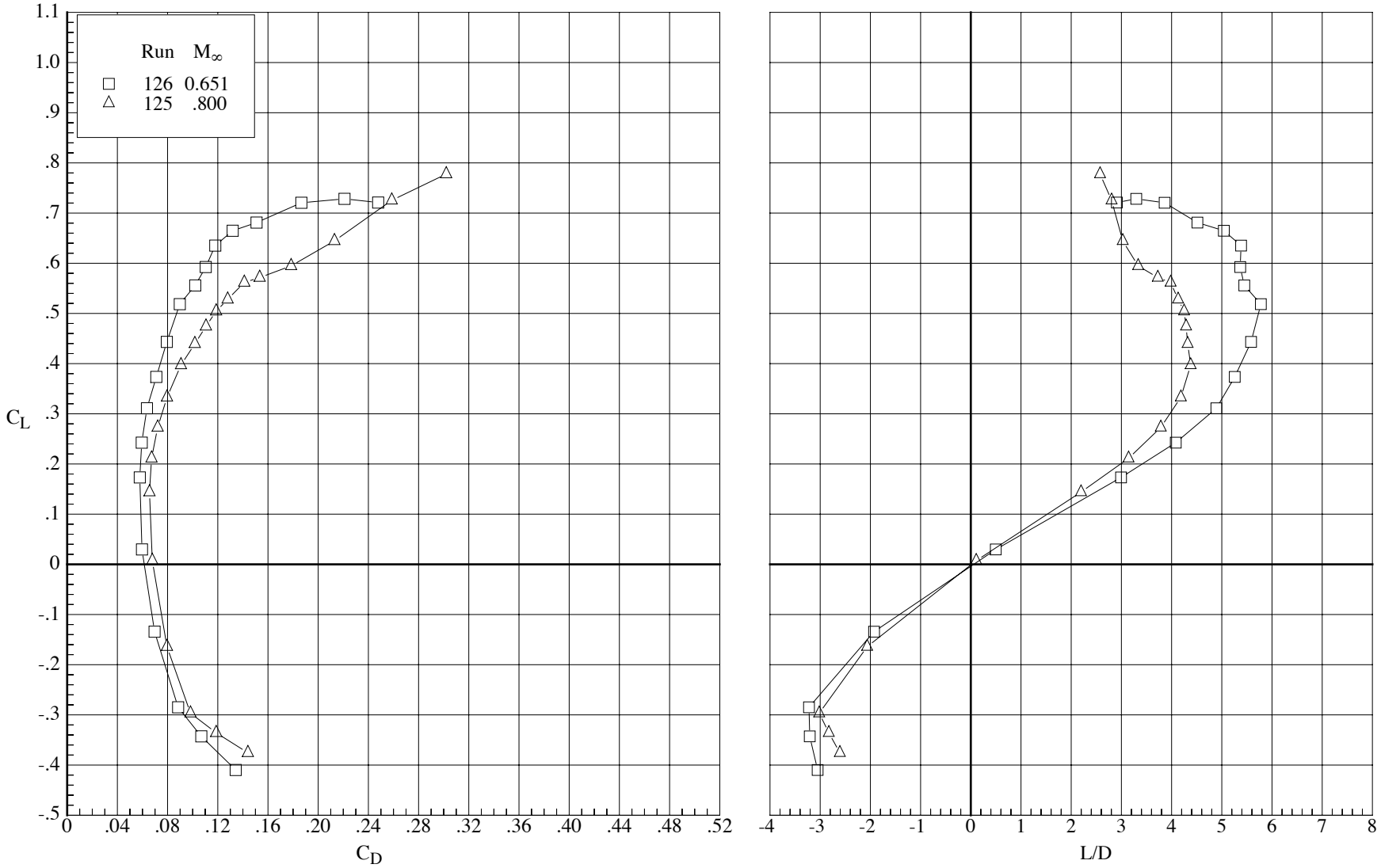

(b) Drag coefficient and lift-drag ratio.

Figure 40. Concluded.

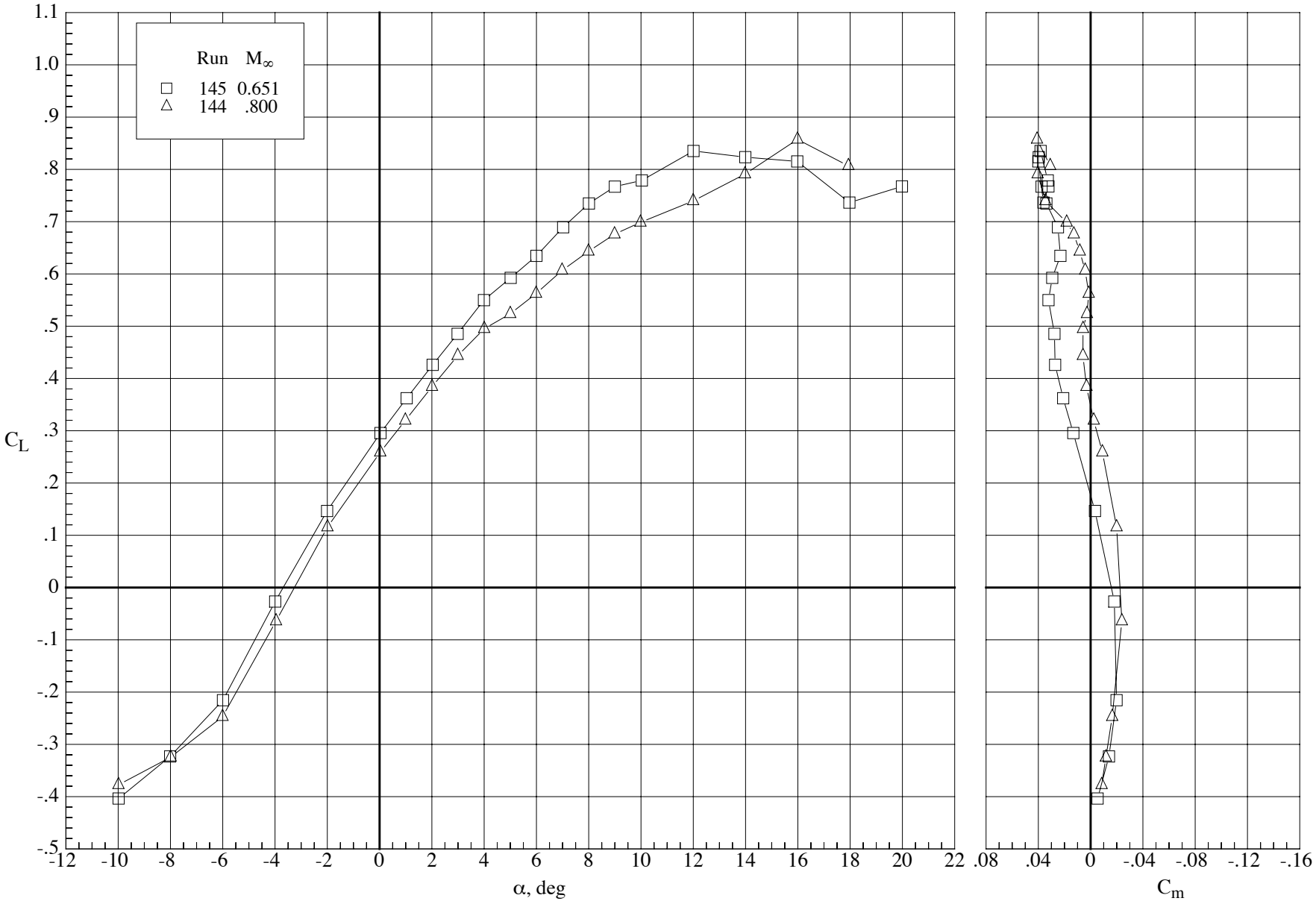

(a) Lift and pitching-moment coefficients.

Figure 41. Effect of Mach number on the longitudinal aerodynamic characteristics of the model with the MA-SF-1 wing (bump off) at a Reynolds number of 100,000. $\delta_h = 0°$ and $\delta_f = 10°$.

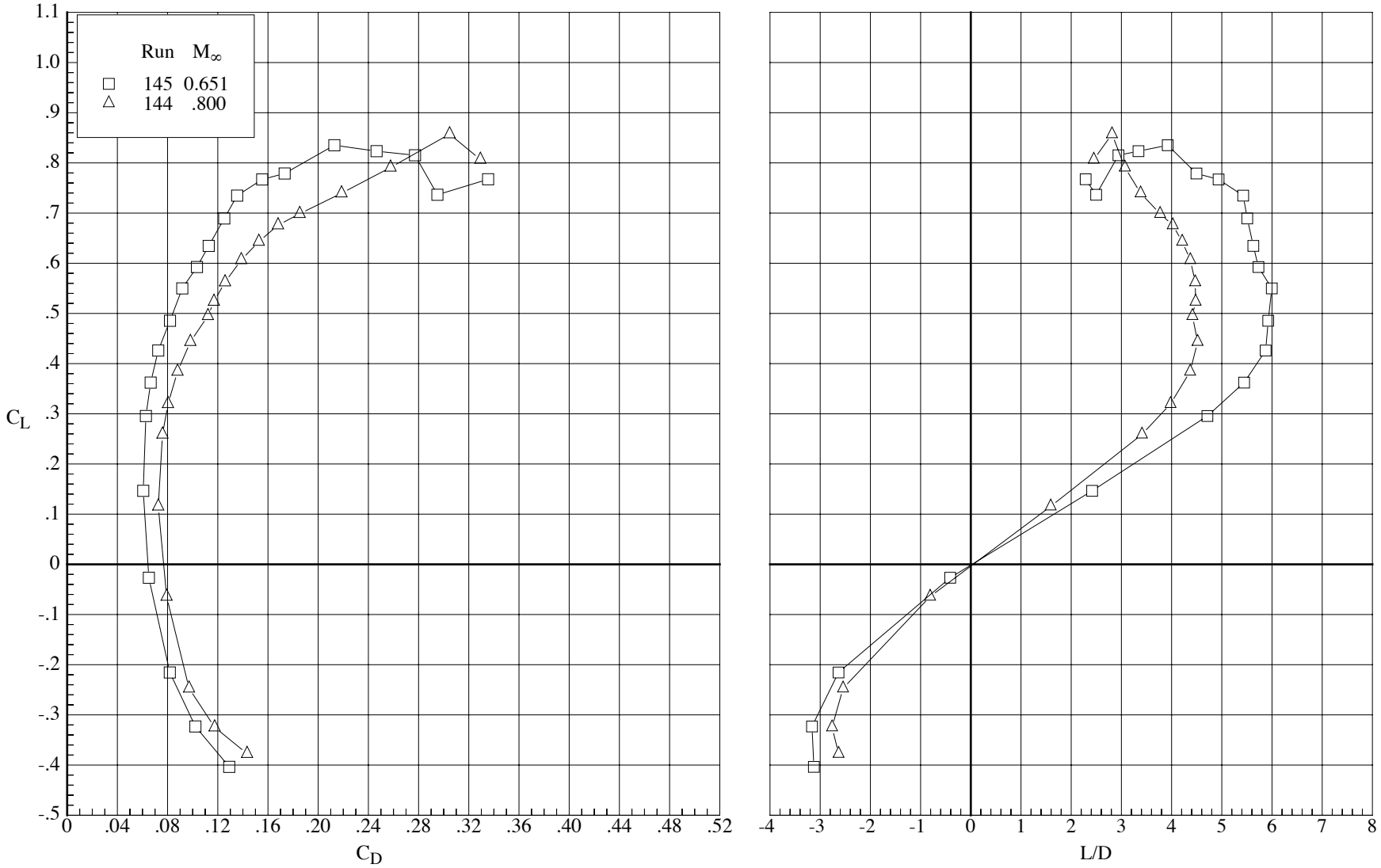

(b) Drag coefficient and lift-drag ratio.

Figure 41. Concluded.

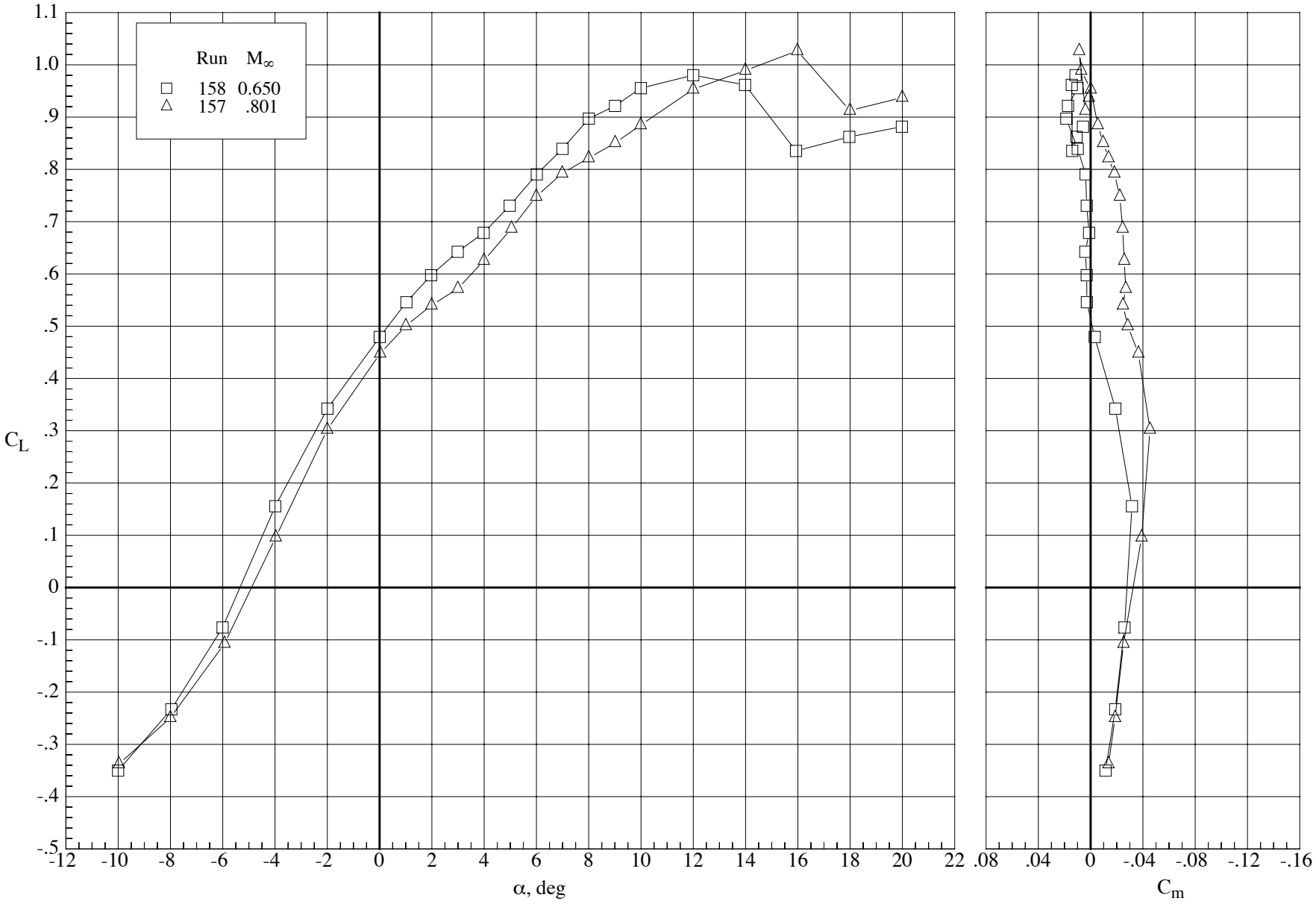

(a) Lift and pitching-moment coefficients.

Figure 42. Effect of Mach number on the longitudinal aerodynamic characteristics of the model with the MA-SF-1 wing (bump off) at a Reynolds number of 100,000. $\delta_h = 0°$ and $\delta_f = 30°$.

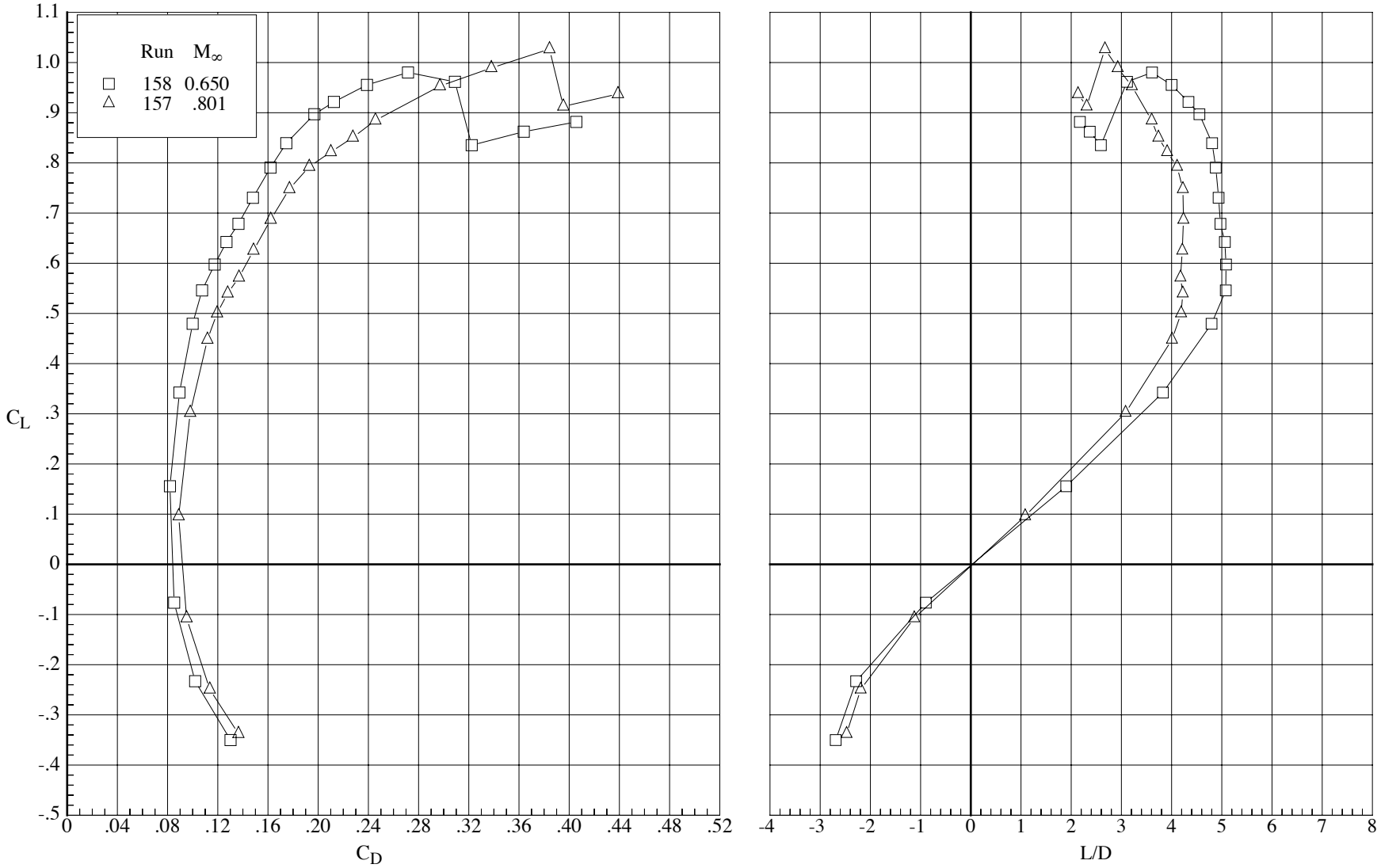

(b) Drag coefficient and lift-drag ratio.

Figure 42. Concluded.

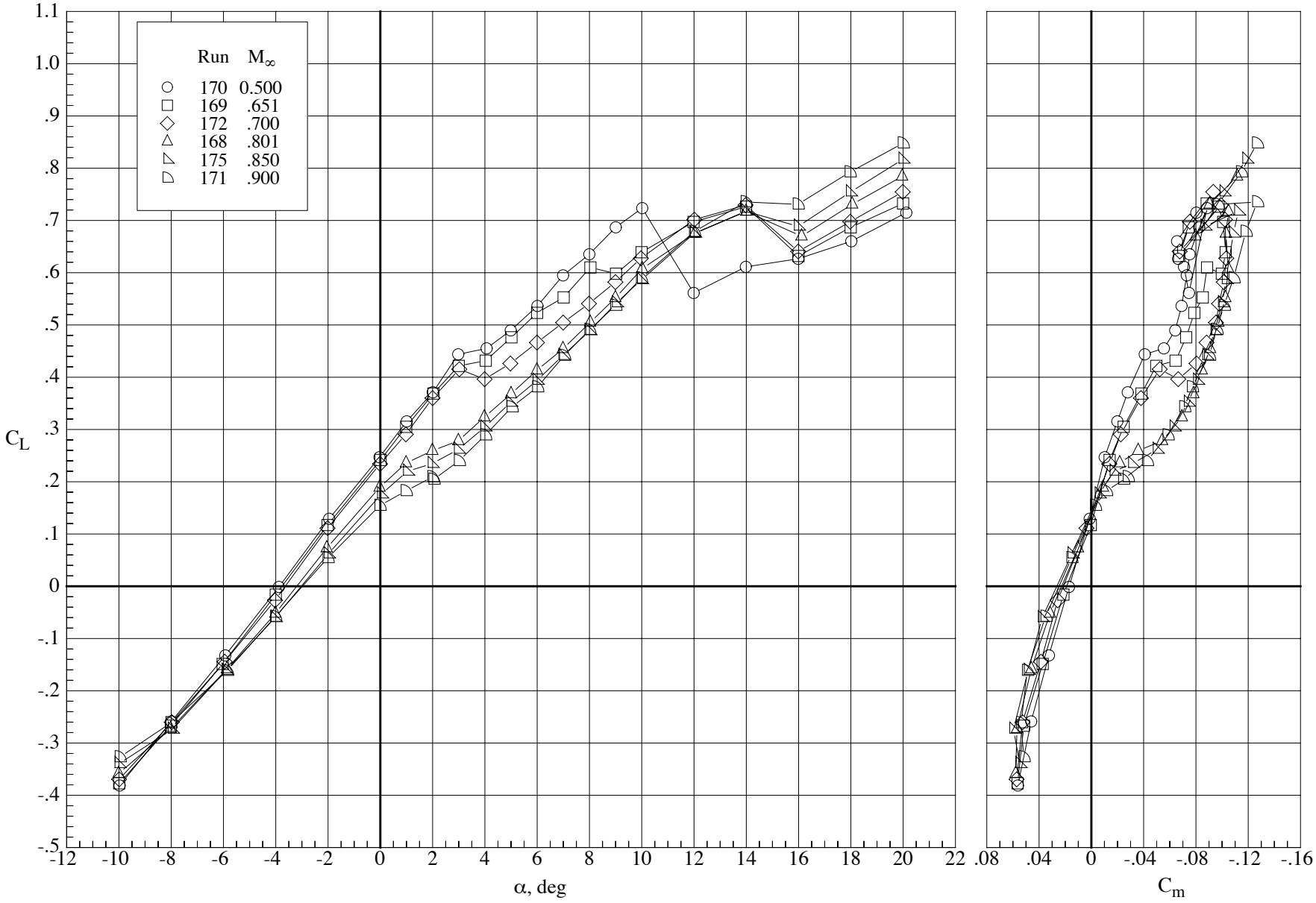

(a) Lift and pitching-moment coefficients.

Figure 43. Effect of Mach number on the longitudinal aerodynamic characteristics of the model with the MA-SC-1t wing at a Reynolds number of 40,000. $\delta_h = 0°$ and $\delta_f = 0°$.

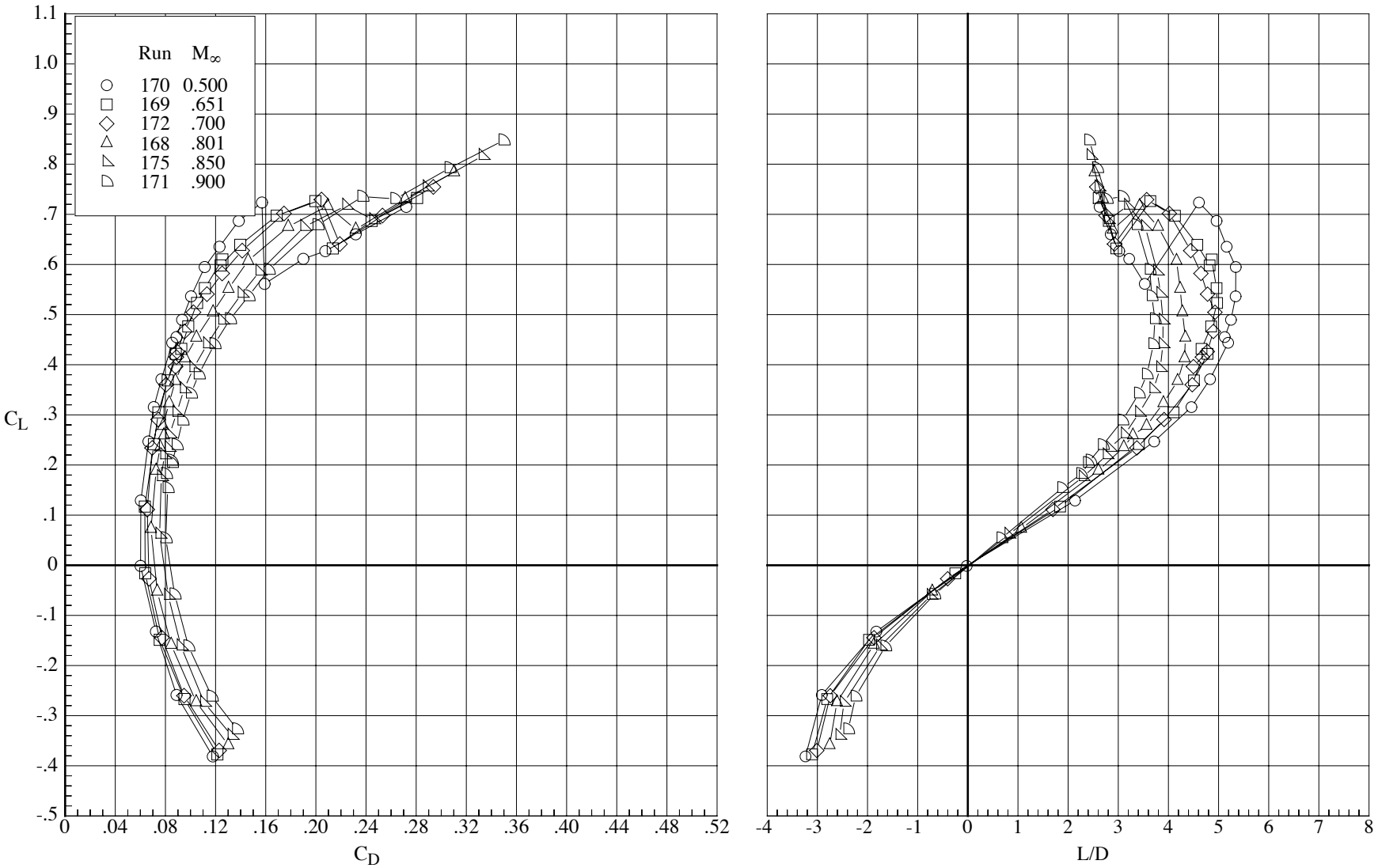

(b) Drag coefficient and lift-drag ratio.

Figure 43. Concluded.

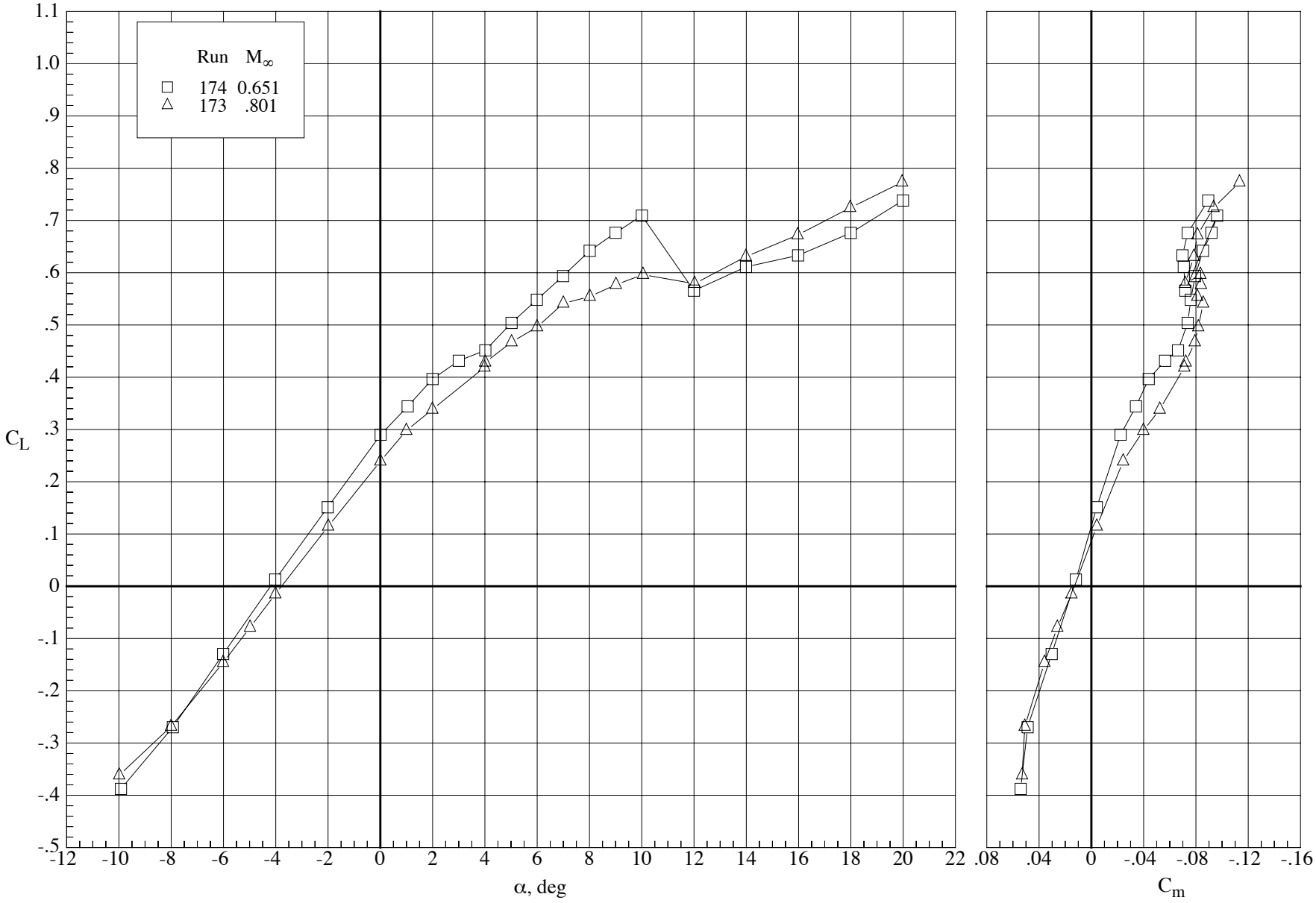

(a) Lift and pitching-moment coefficients.

Figure 44. Effect of Mach number on the longitudinal aerodynamic characteristics of the model with the MA-SC-1t wing at a Reynolds number of 60,000. $\delta_h = 0°$ and $\delta_f = 0°$.

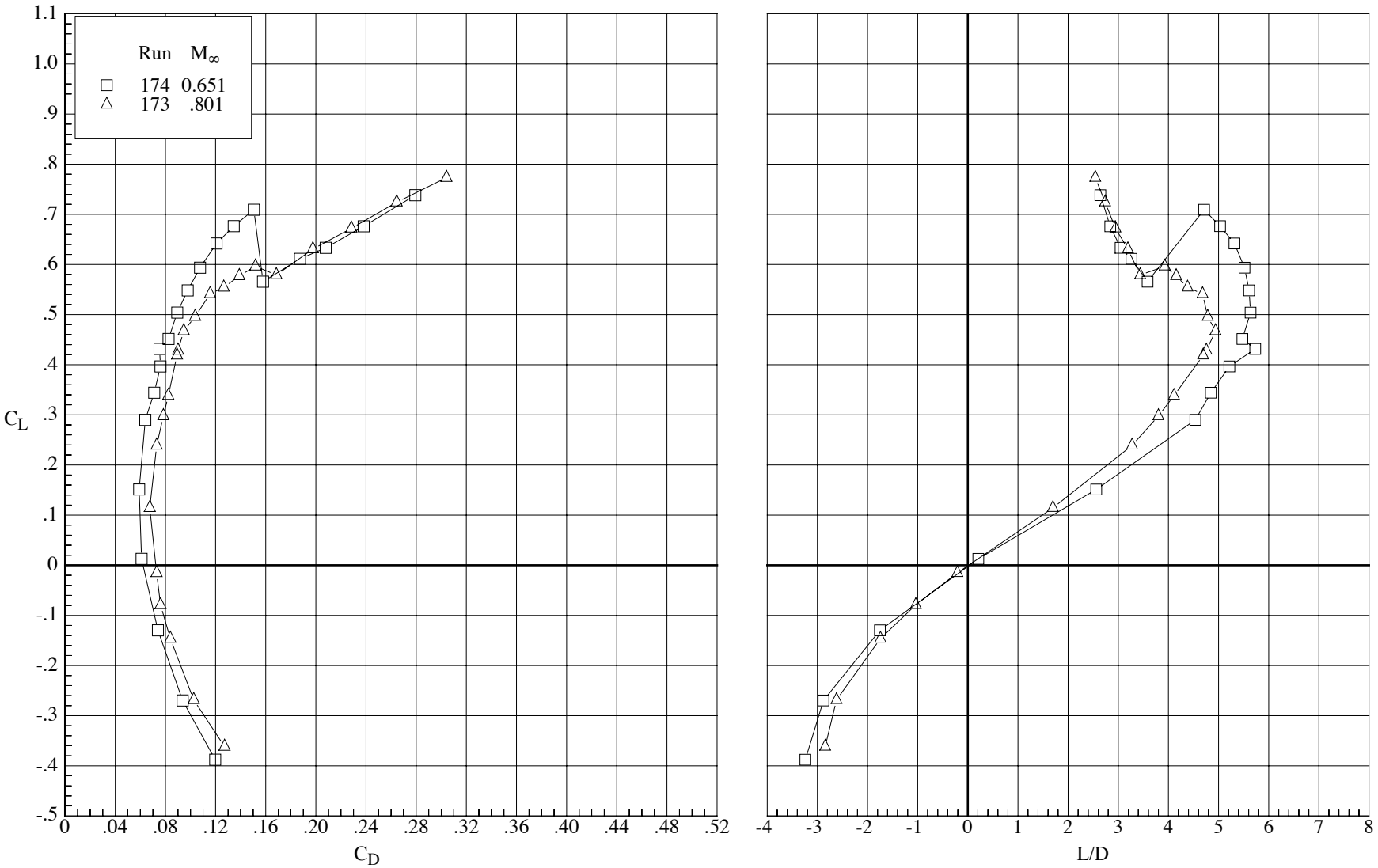

(b) Drag coefficient and lift-drag ratio.

Figure 44. Concluded.

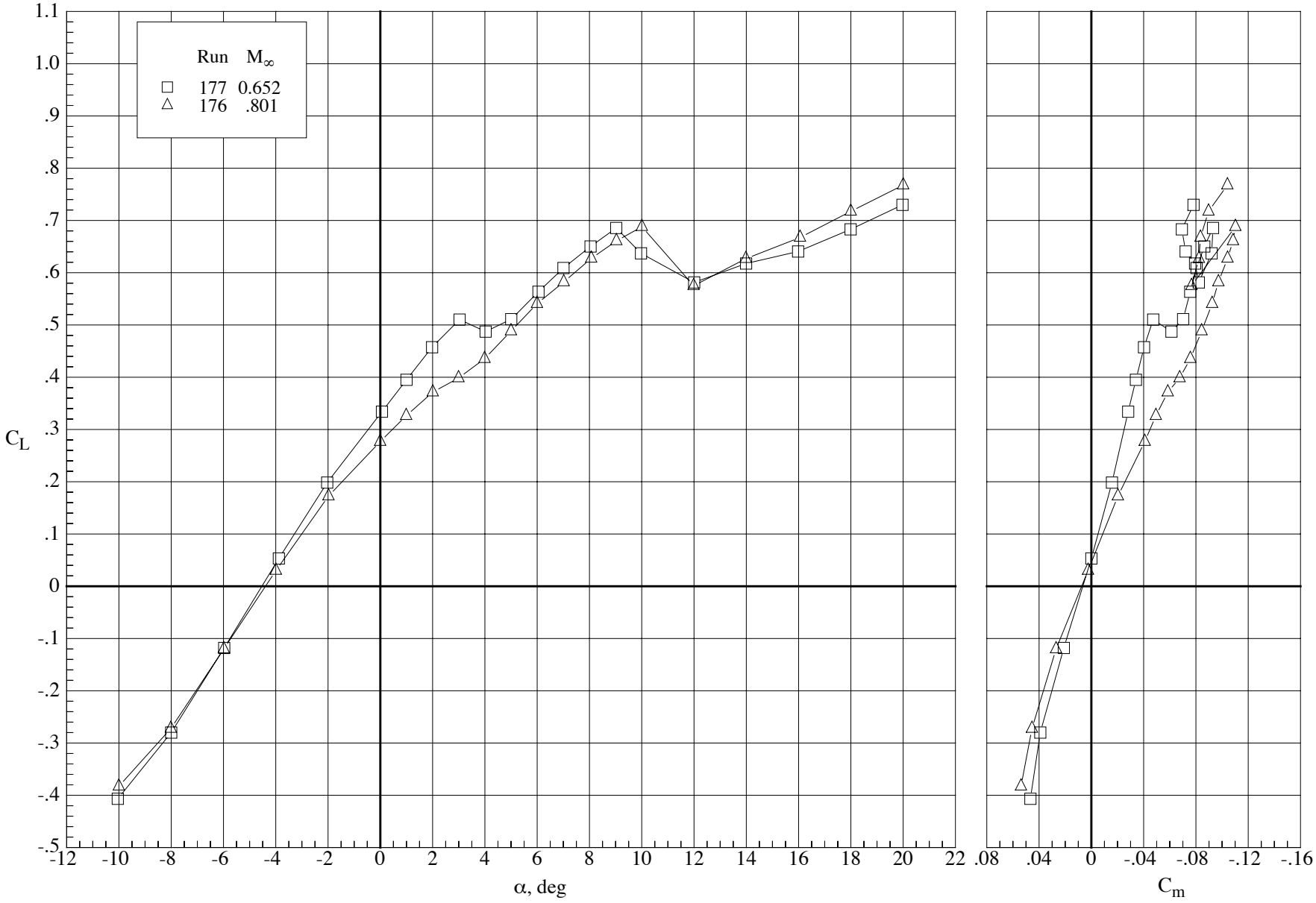

(a) Lift and pitching-moment coefficients.

Figure 45. Effect of Mach number on the longitudinal aerodynamic characteristics of the model with the MA-SC-1t wing at a Reynolds number of 100,000. $\delta_h = 0°$ and $\delta_f = 0°$.

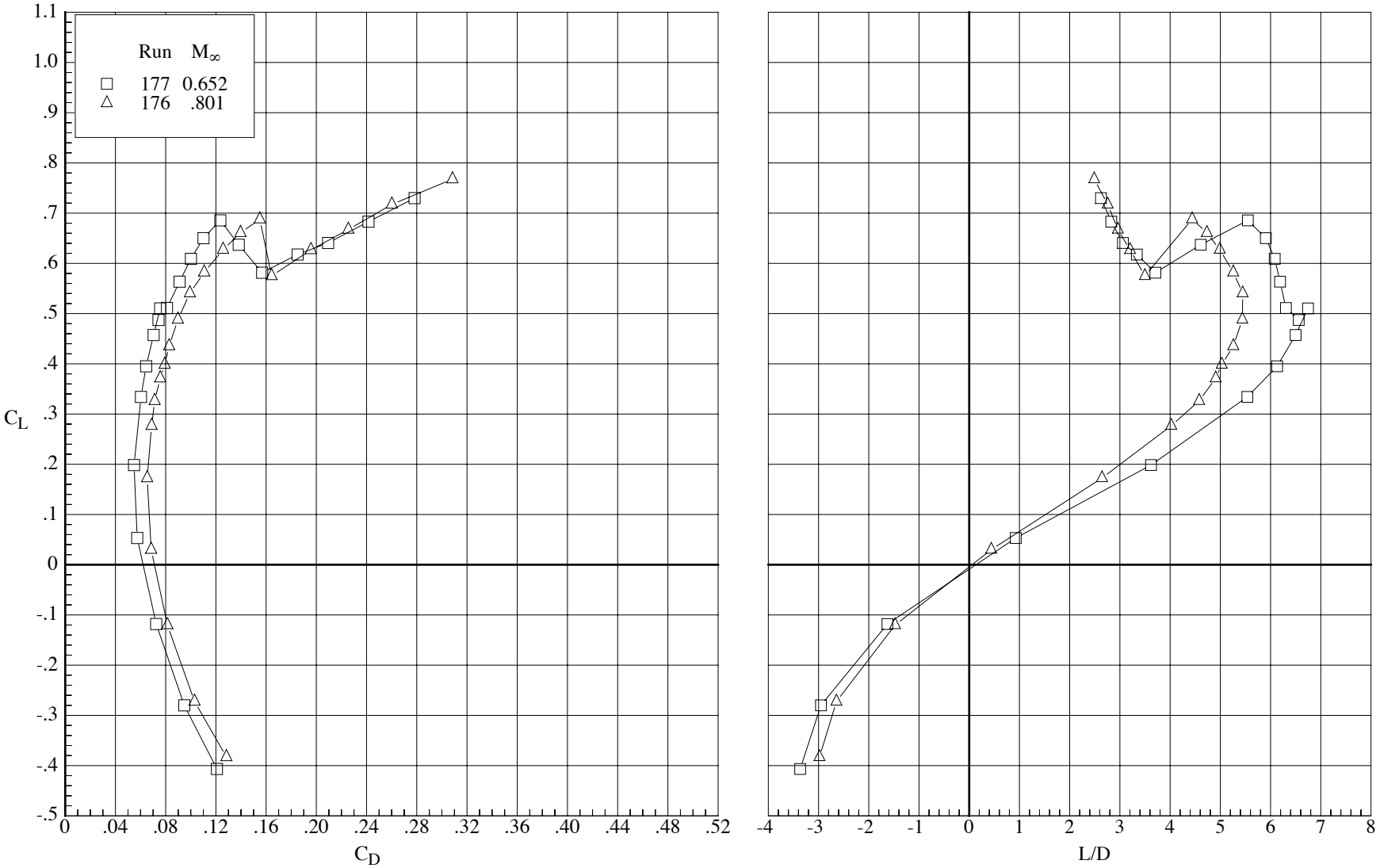

(b) Drag coefficient and lift-drag ratio.

Figure 45. Concluded.

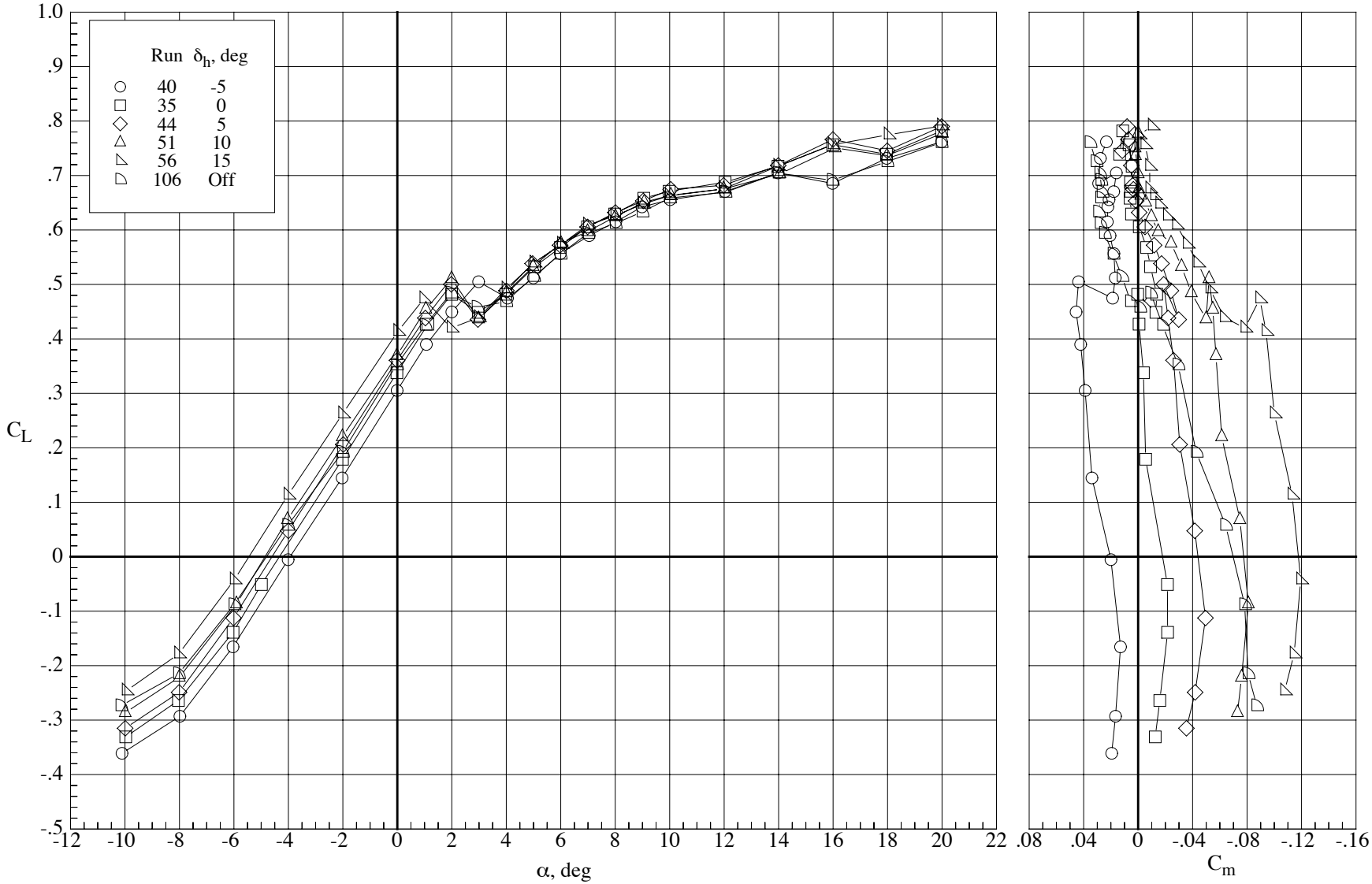

(a) Lift and pitching-moment coefficients.

Figure 46. Effect of tails and horizontal tail incidence on the longitudinal aerodynamic characteristics of the model with the MA-SC-1 wing (bump on) at a Reynolds number of 40,000 and a Mach number of 0.65.

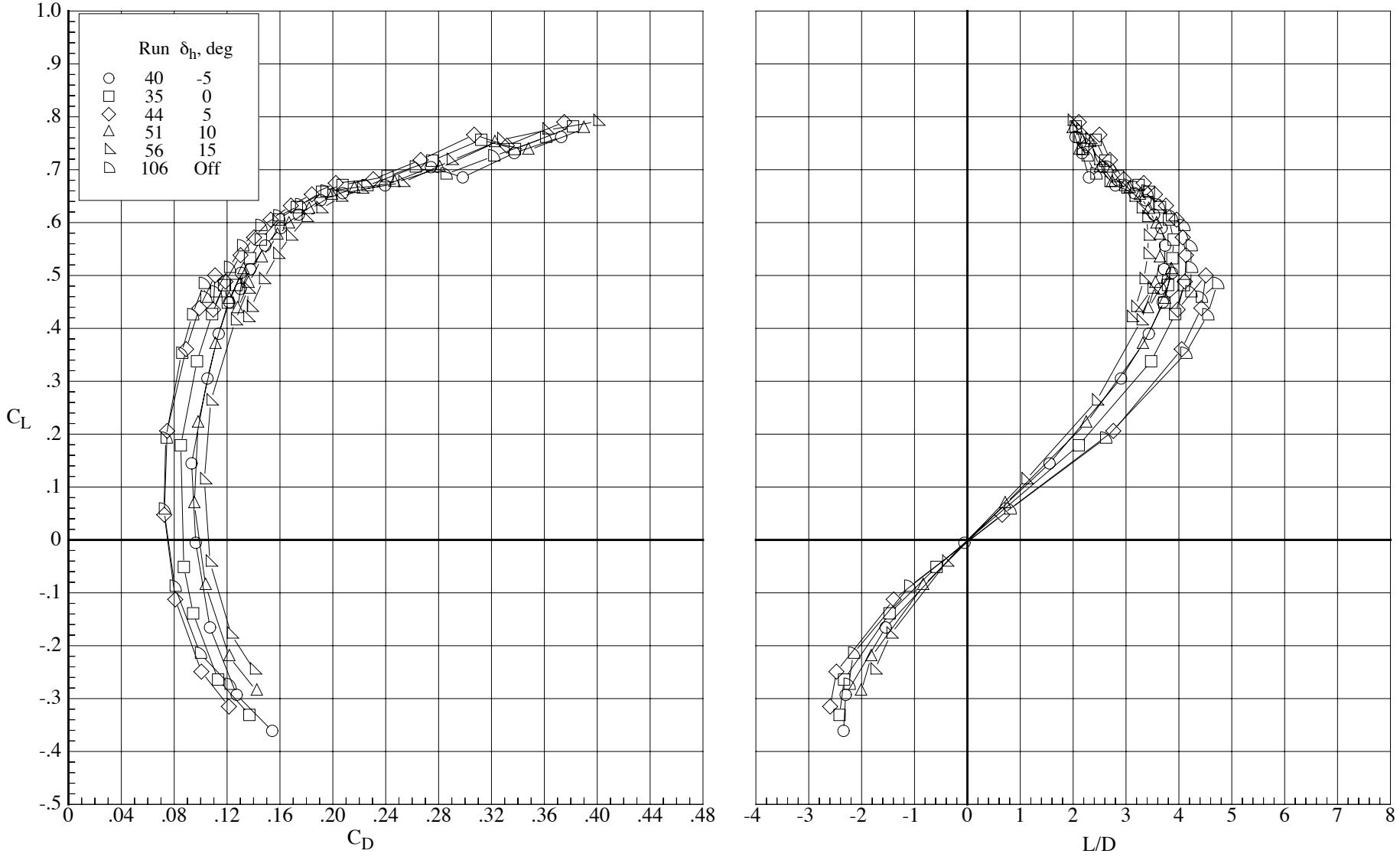

(b) Drag coefficient and lift-drag ratio.

Figure 46. Concluded.

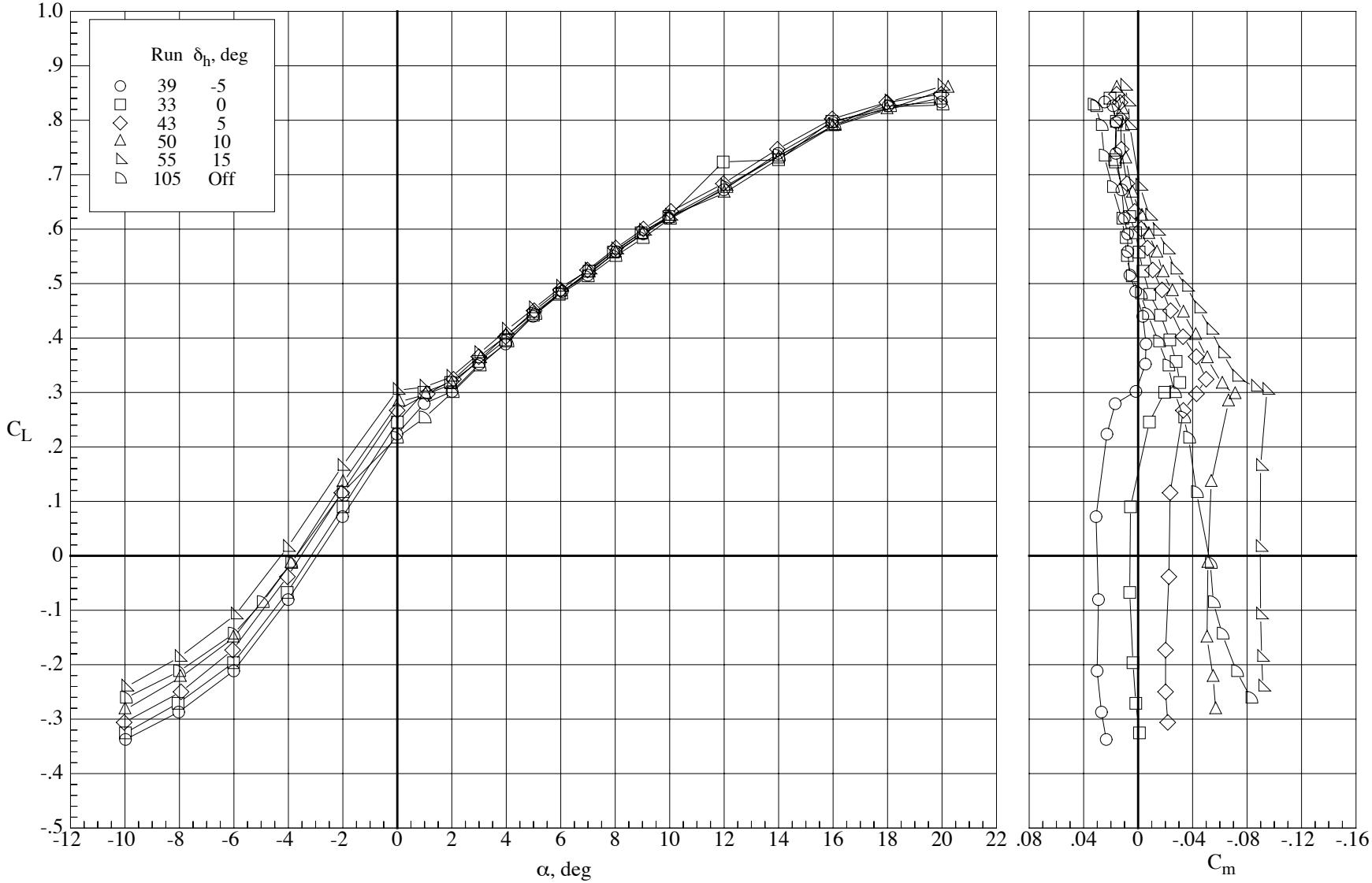

(a) Lift and pitching-moment coefficients.

Figure 47. Effect of tails and horizontal tail incidence on the longitudinal aerodynamic characteristics of the model with the MA-SC-1 wing (bump on) at a Reynolds number of 40,000 and a Mach number of 0.80.

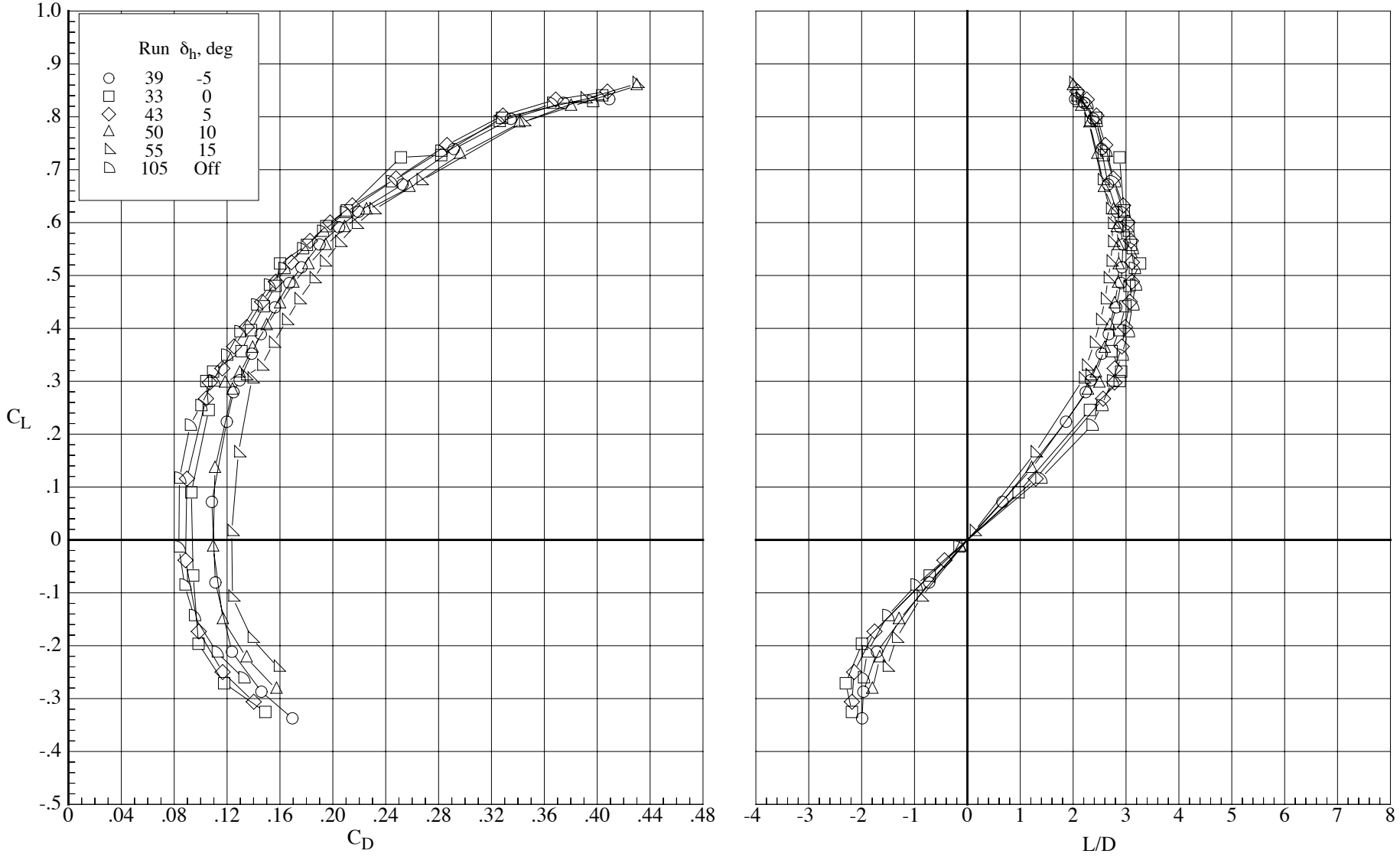

(b) Drag coefficient and lift-drag ratio.

Figure 47. Concluded.

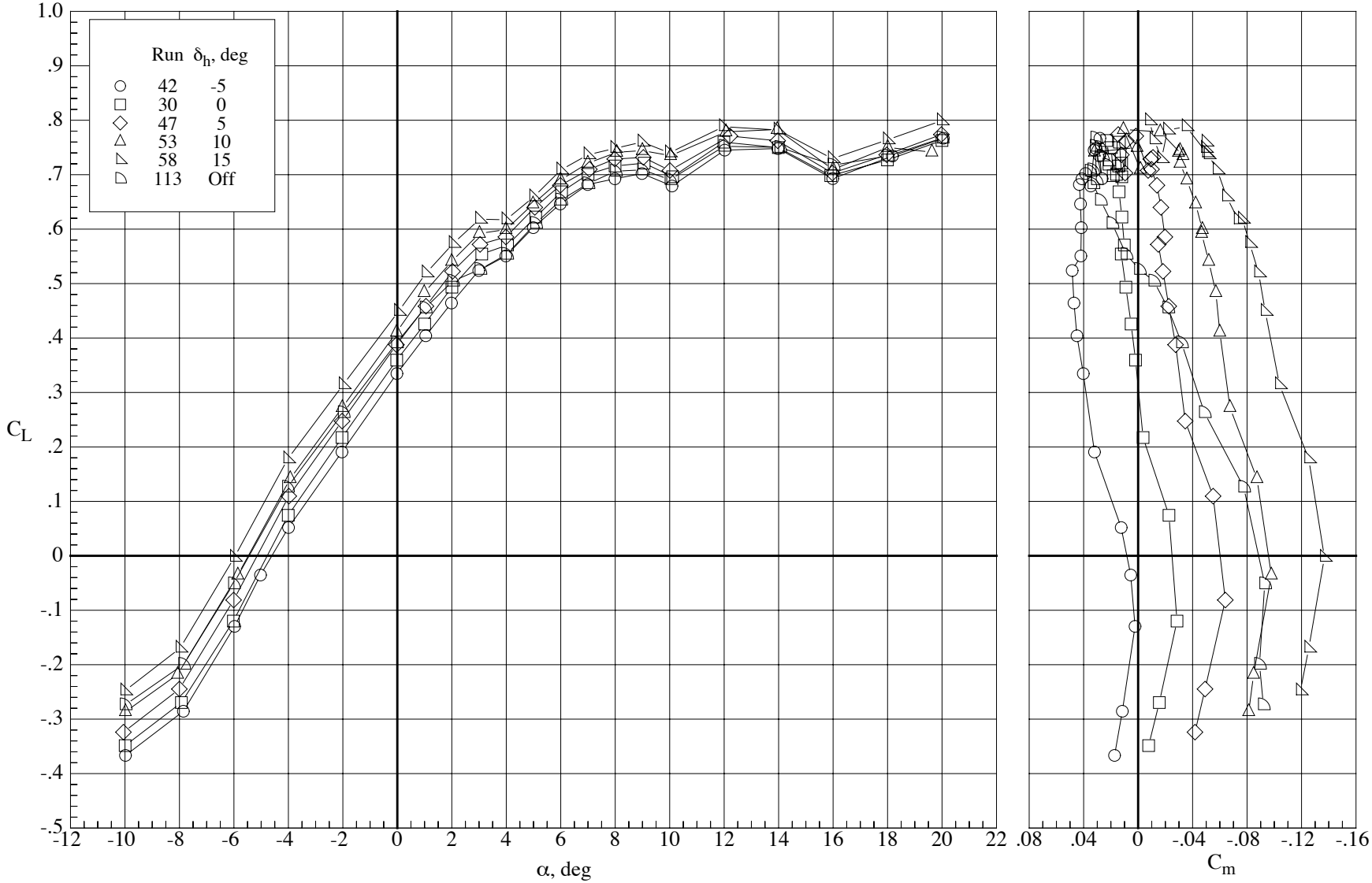

(a) Lift and pitching-moment coefficients.

Figure 48. Effect of tails and horizontal tail incidence on the longitudinal aerodynamic characteristics of the model with the MA-SC-1 wing (bump on) at a Reynolds number of 60,000 and a Mach number of 0.65.

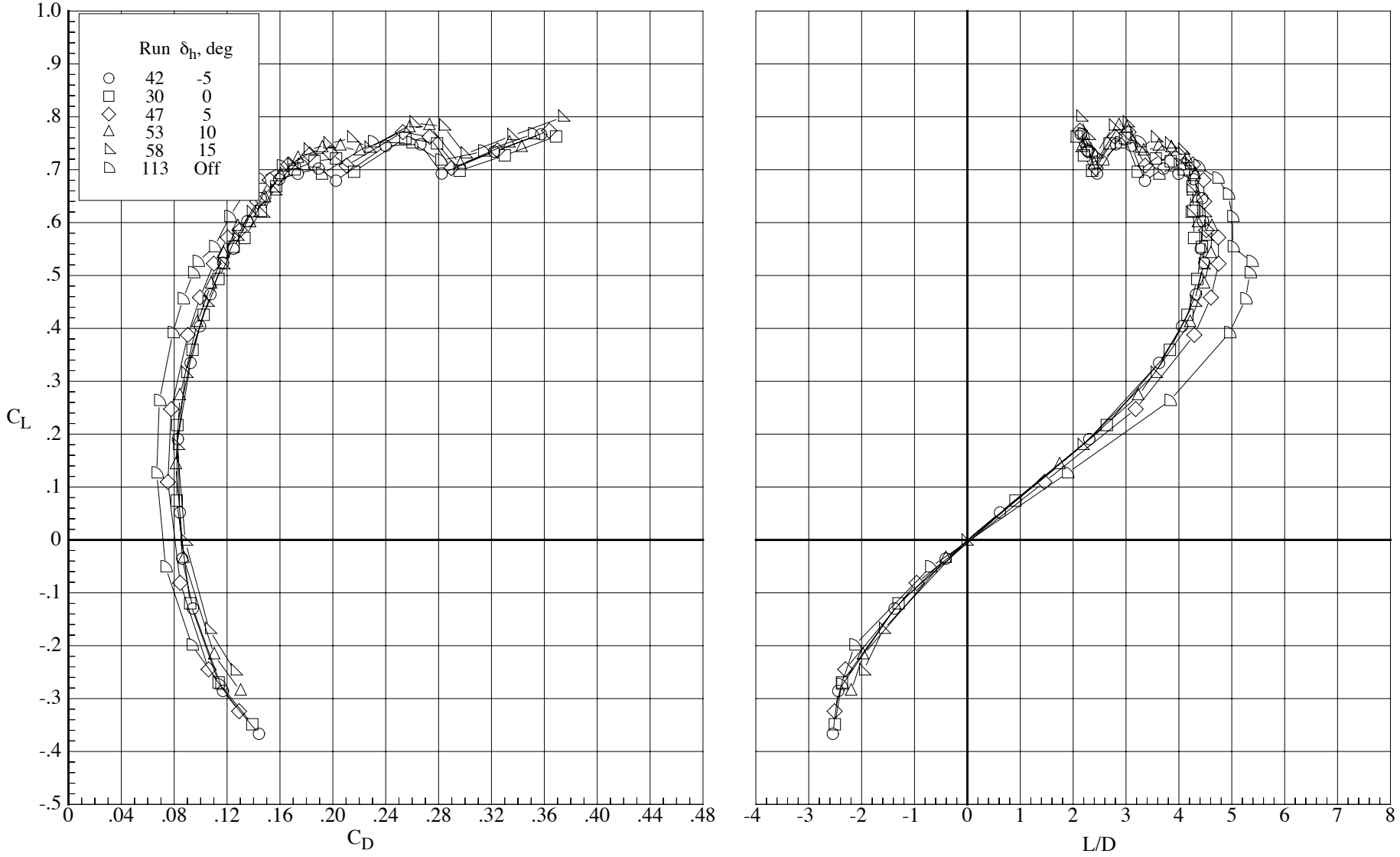

(b) Drag coefficient and lift-drag ratio.

Figure 48. Concluded.

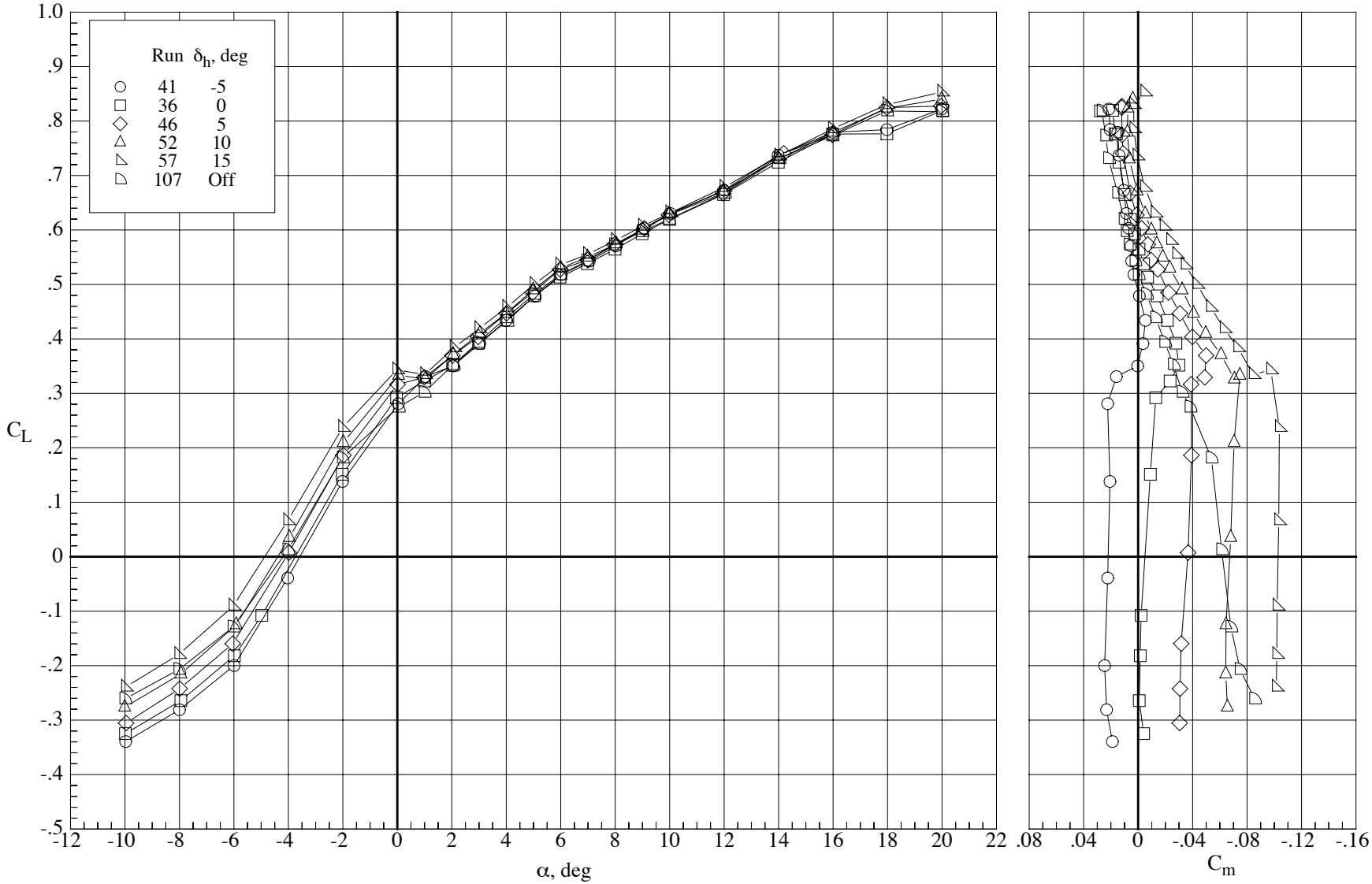

(a) Lift and pitching-moment coefficients.

Figure 49. Effect of tails and horizontal tail incidence on the longitudinal aerodynamic characteristics of the model with the MA-SC-1 wing (bump on) at a Reynolds number of 60,000 and a Mach number of 0.80.

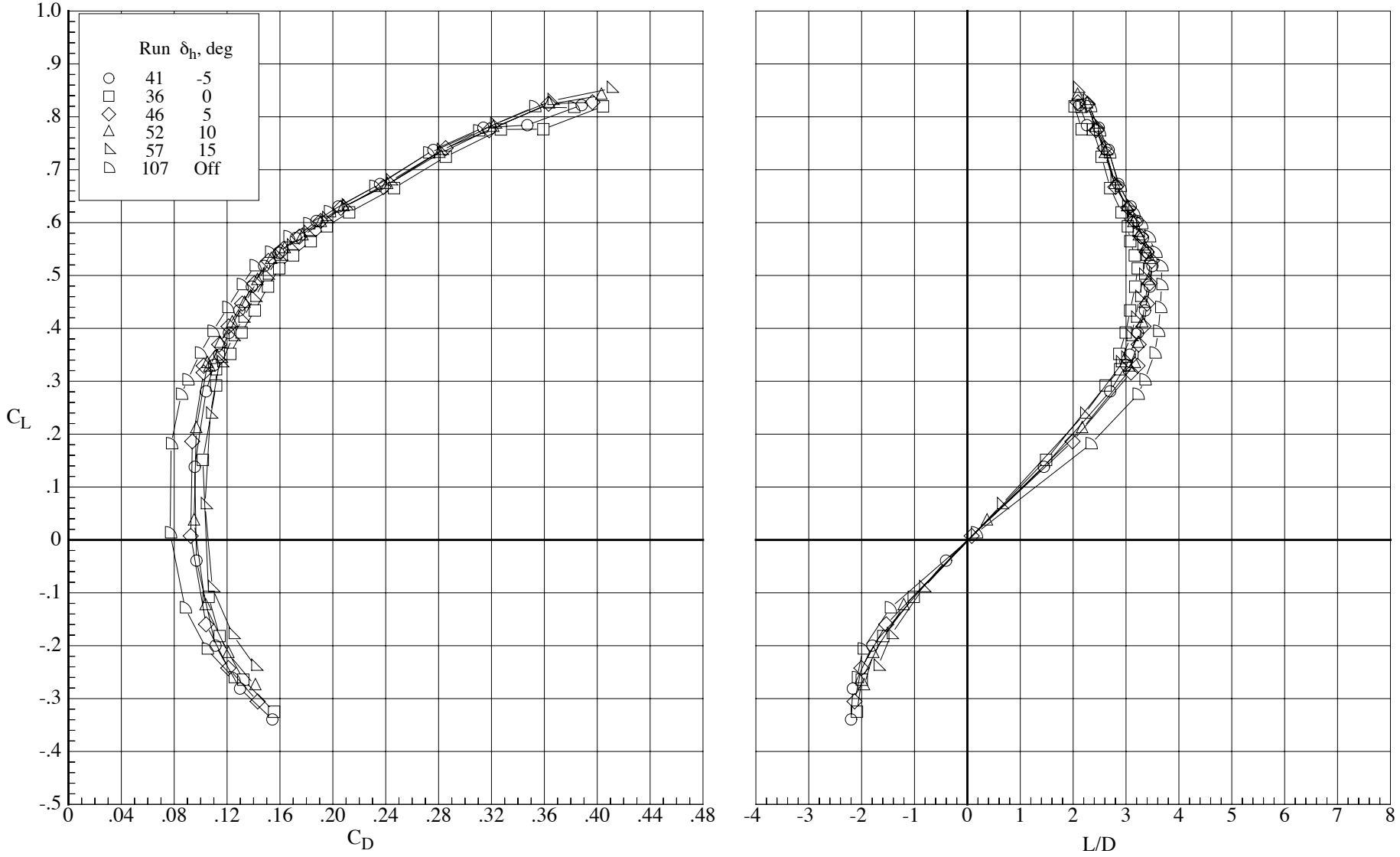

(b) Drag coefficient and lift-drag ratio.

Figure 49. Concluded.

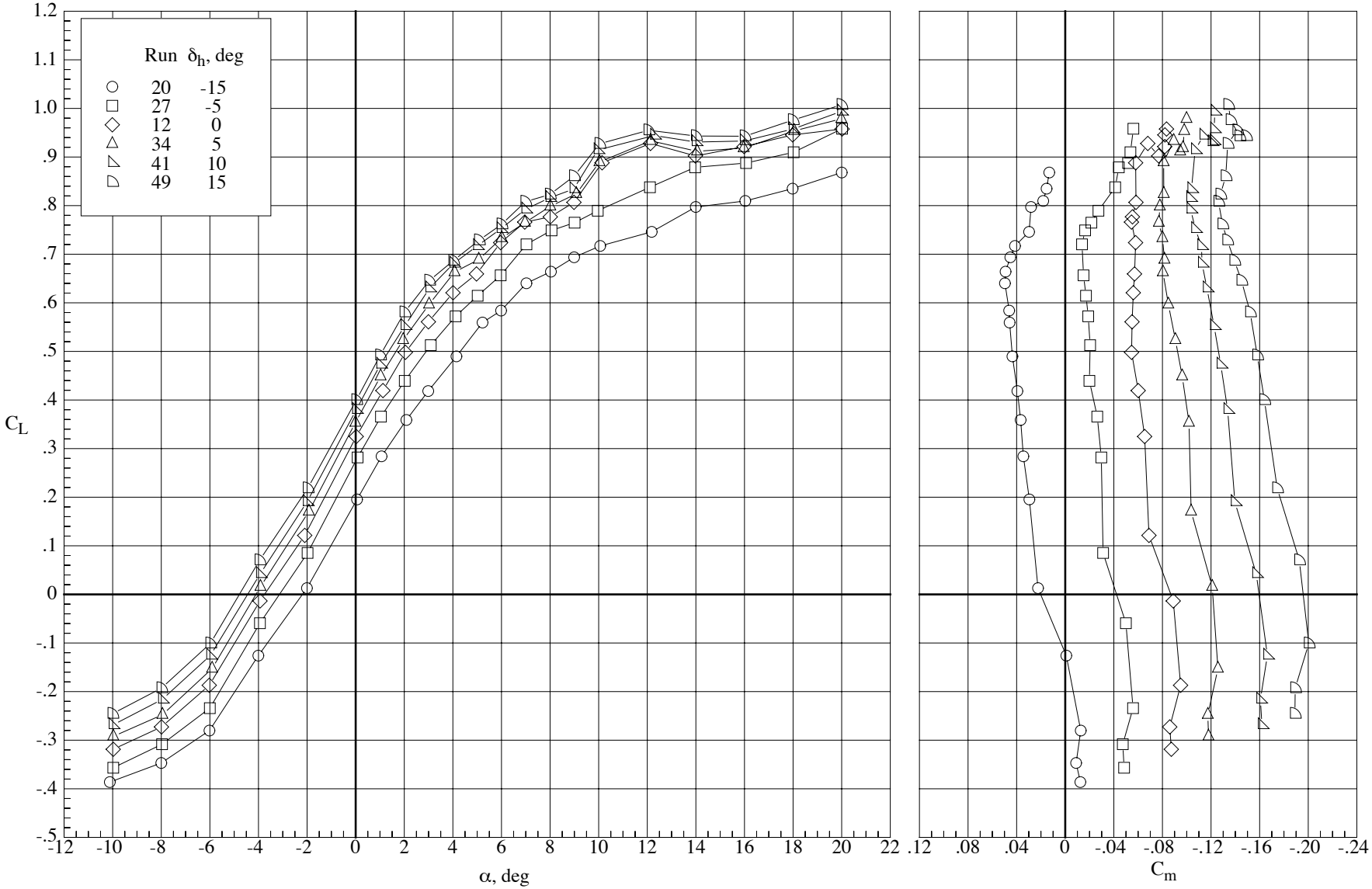

(a) Lift and pitching-moment coefficients.

Figure 50. Effect of horizontal tail incidence on the longitudinal aerodynamic characteristics of the model with the MA-SC-1 wing (bump on) with the tails inverted and the lower fuselage fairing removed at a Reynolds number of 40,000 and a Mach number of 0.65.

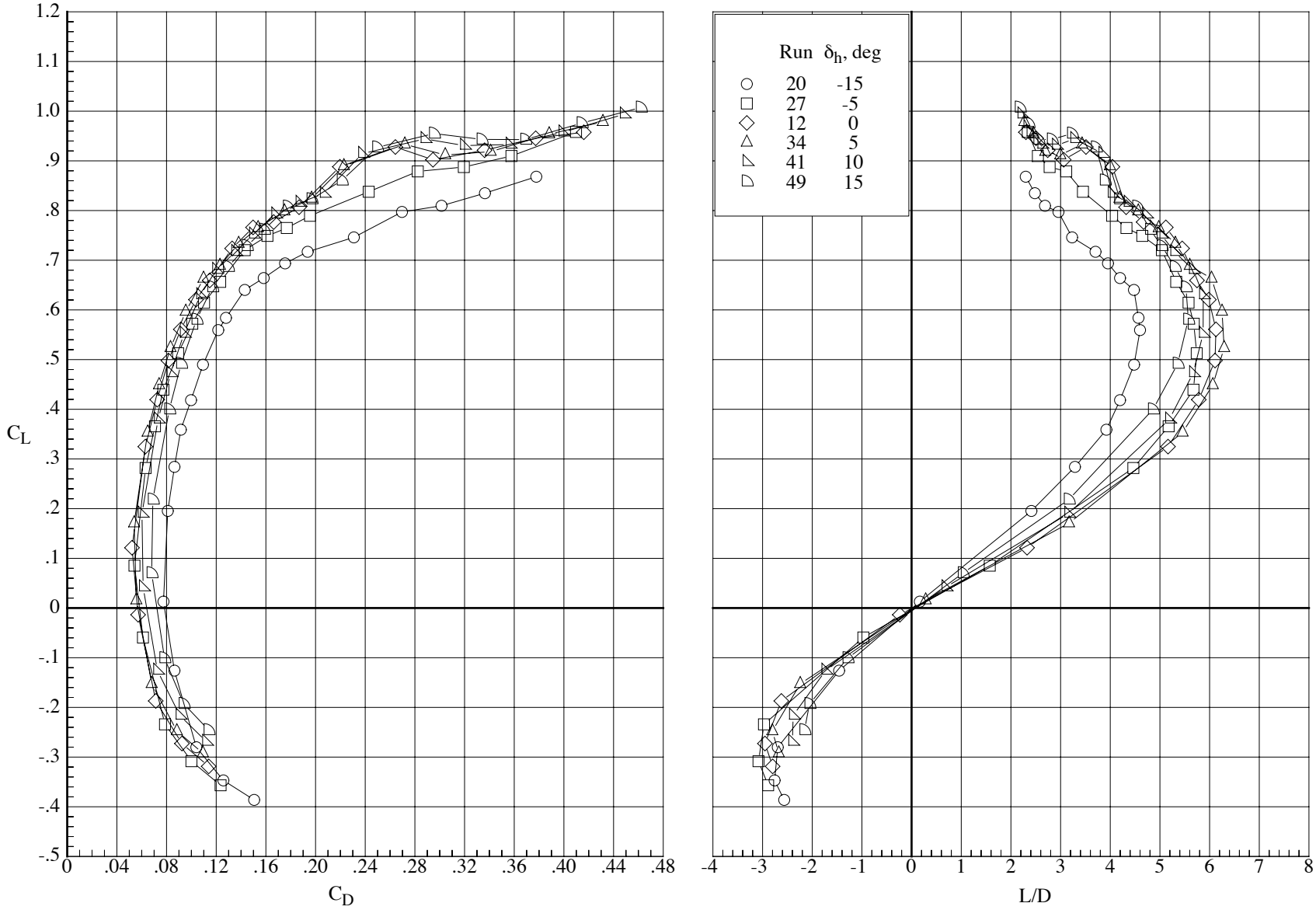

(b) Drag coefficient and lift-drag ratio.

Figure 50. Concluded.

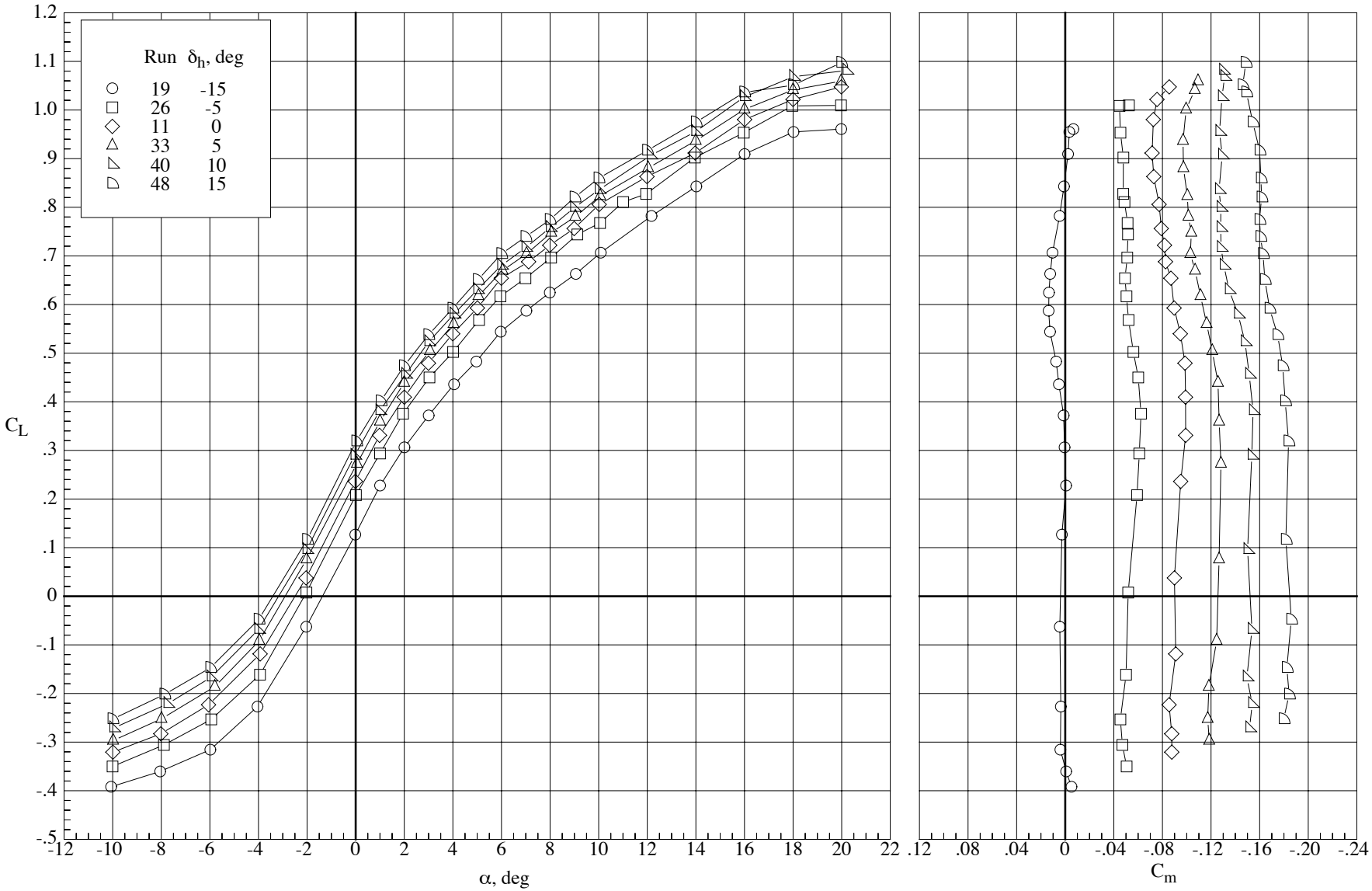

(a) Lift and pitching-moment coefficients.

Figure 51. Effect of horizontal tail incidence on the longitudinal aerodynamic characteristics of the model with the MA-SC-1 wing (bump on) with the tails inverted and the lower fuselage fairing removed at a Reynolds number of 40,000 and a Mach number of 0.80.

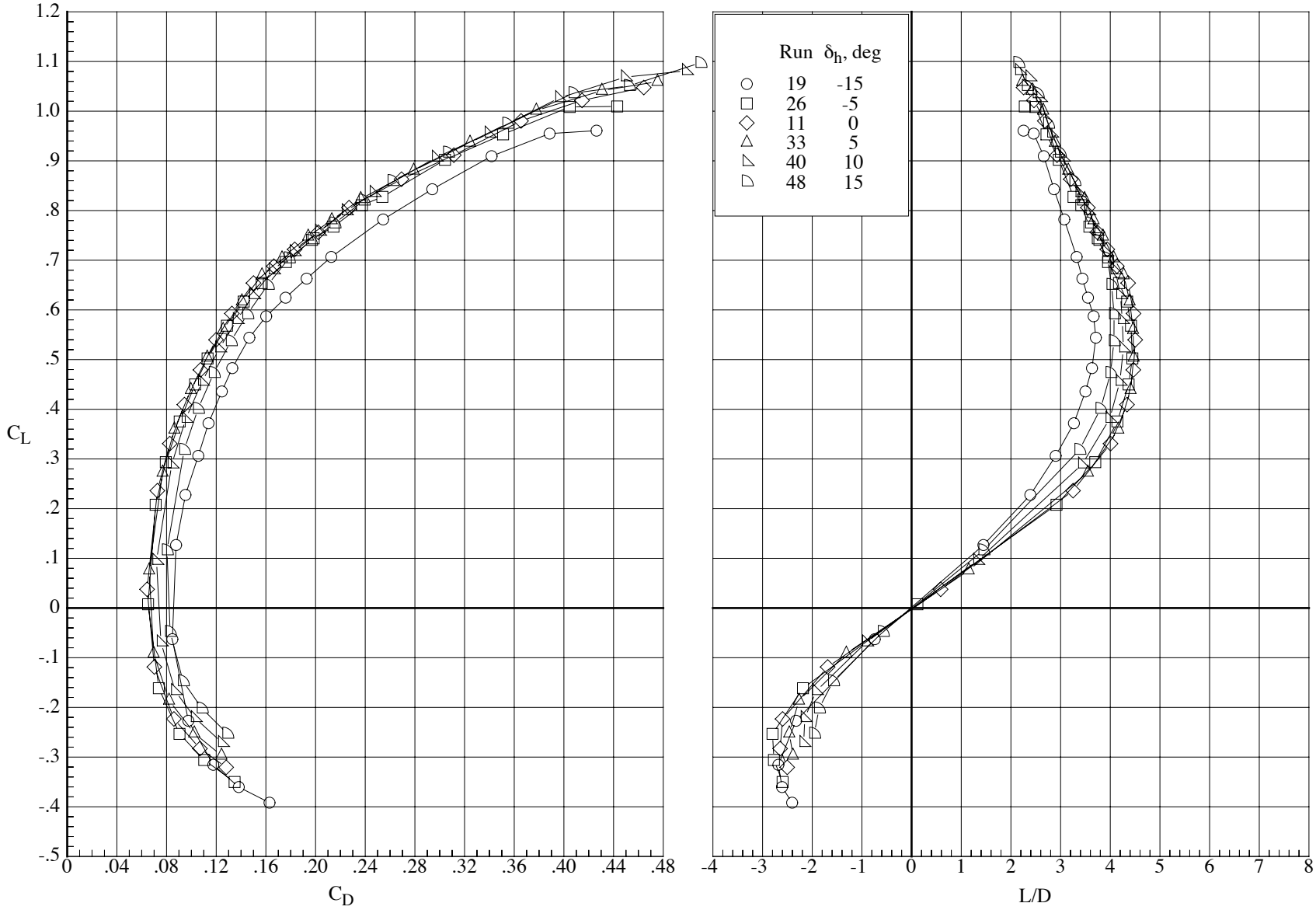

(b) Drag coefficient and lift-drag ratio.

Figure 51. Concluded.

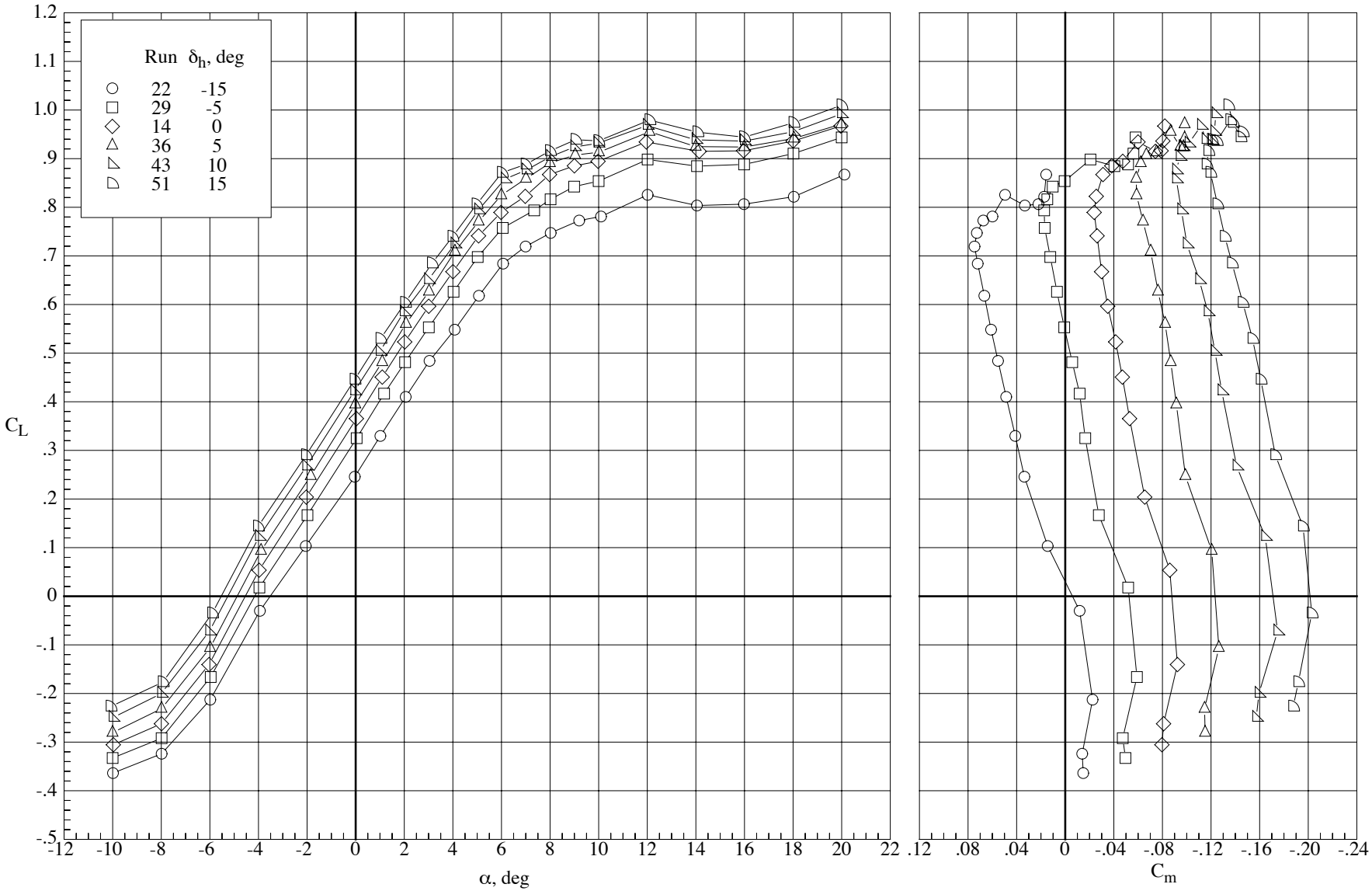

(a) Lift and pitching-moment coefficients.

Figure 52. Effect of horizontal tail incidence on the longitudinal aerodynamic characteristics of the model with the MA-SC-1 wing (bump on) with the tails inverted and the lower fuselage fairing removed at a Reynolds number of 60,000 and a Mach number of 0.65.

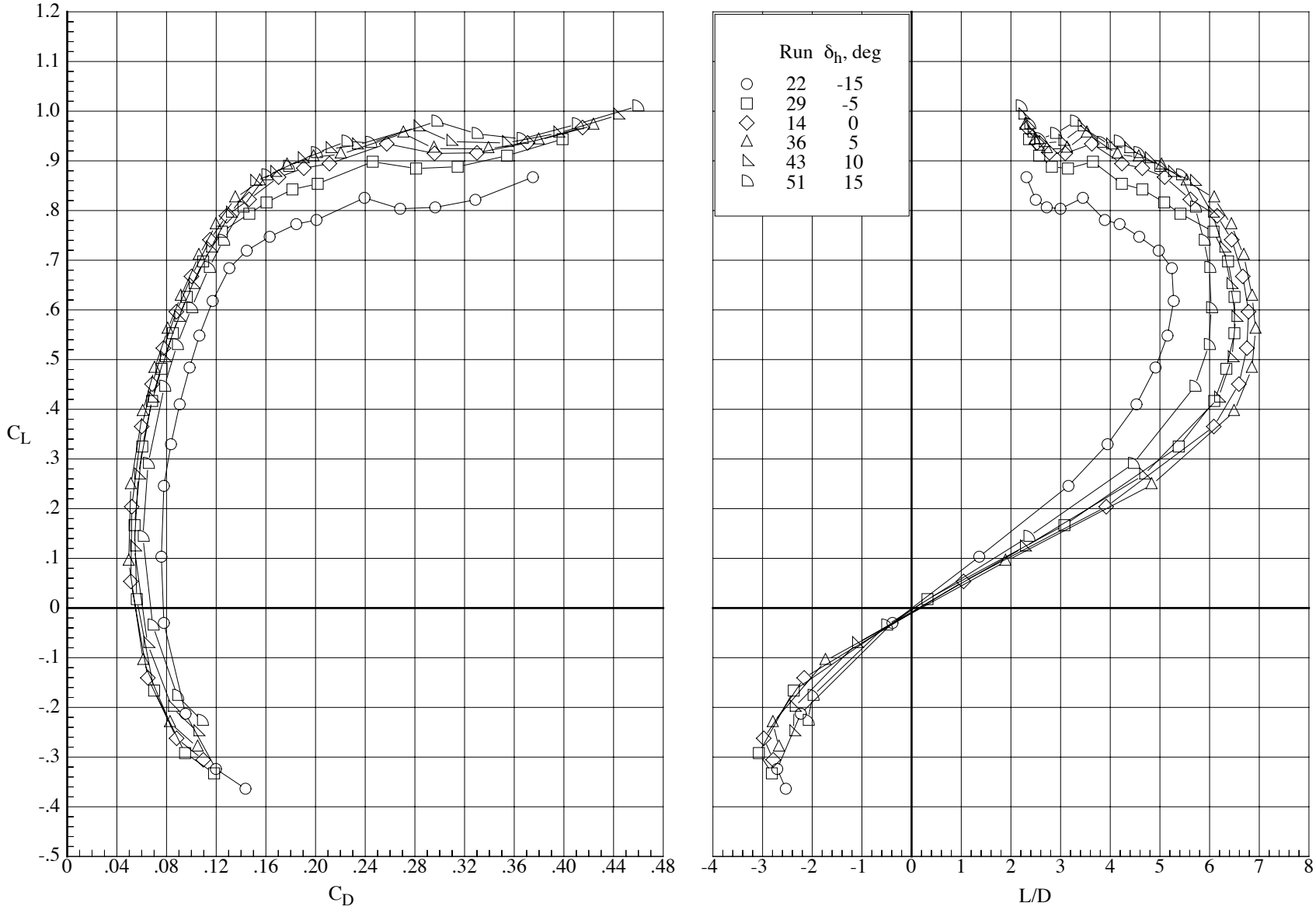

(b) Drag coefficient and lift-drag ratio.

Figure 52. Concluded.

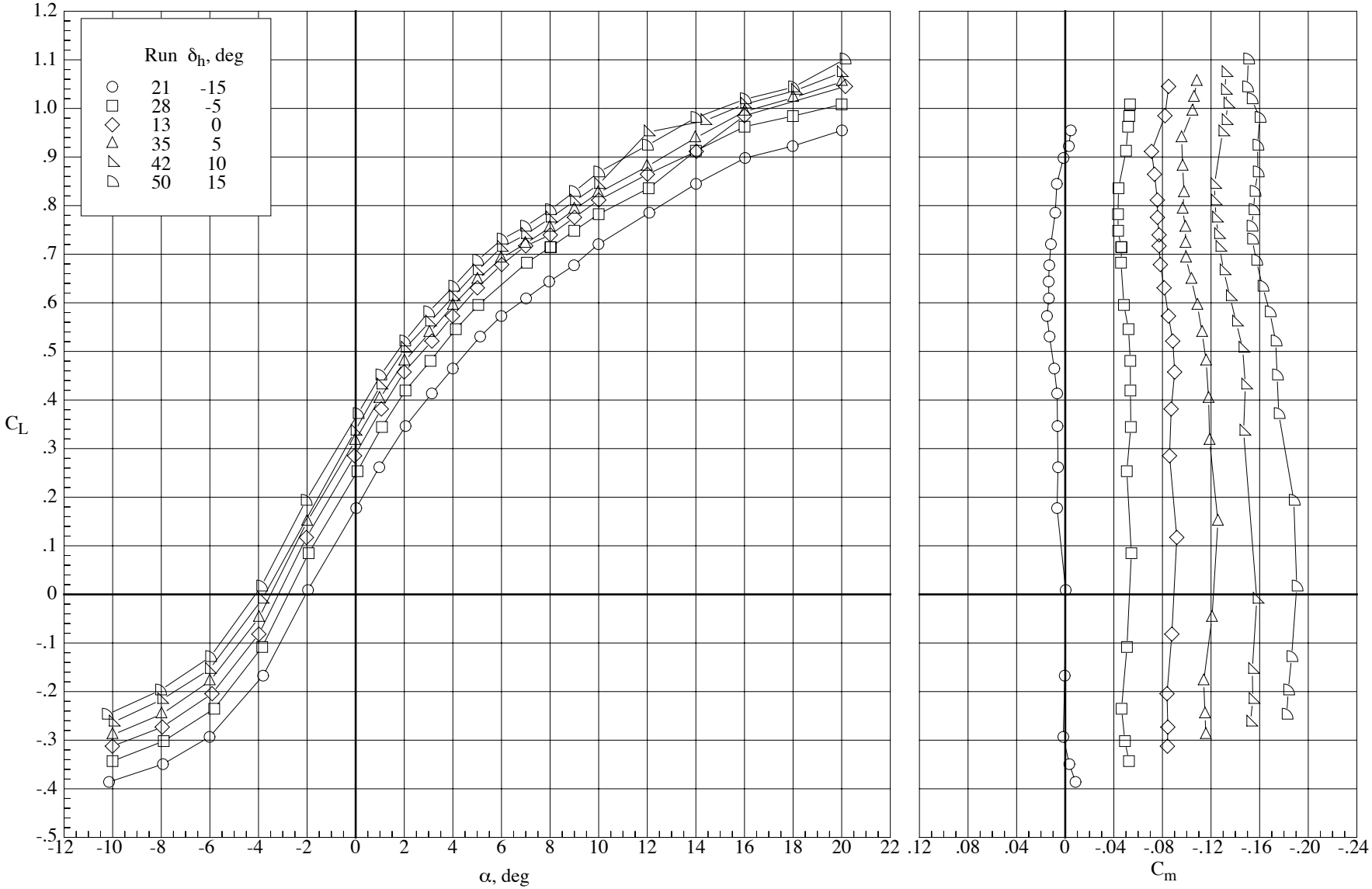

(a) Lift and pitching-moment coefficients.

Figure 53. Effect of horizontal tail incidence on the longitudinal aerodynamic characteristics of the model with the MA-SC-1 wing (bump on) with the tails inverted and the lower fuselage fairing removed at a Reynolds number of 60,000 and a Mach number of 0.80.

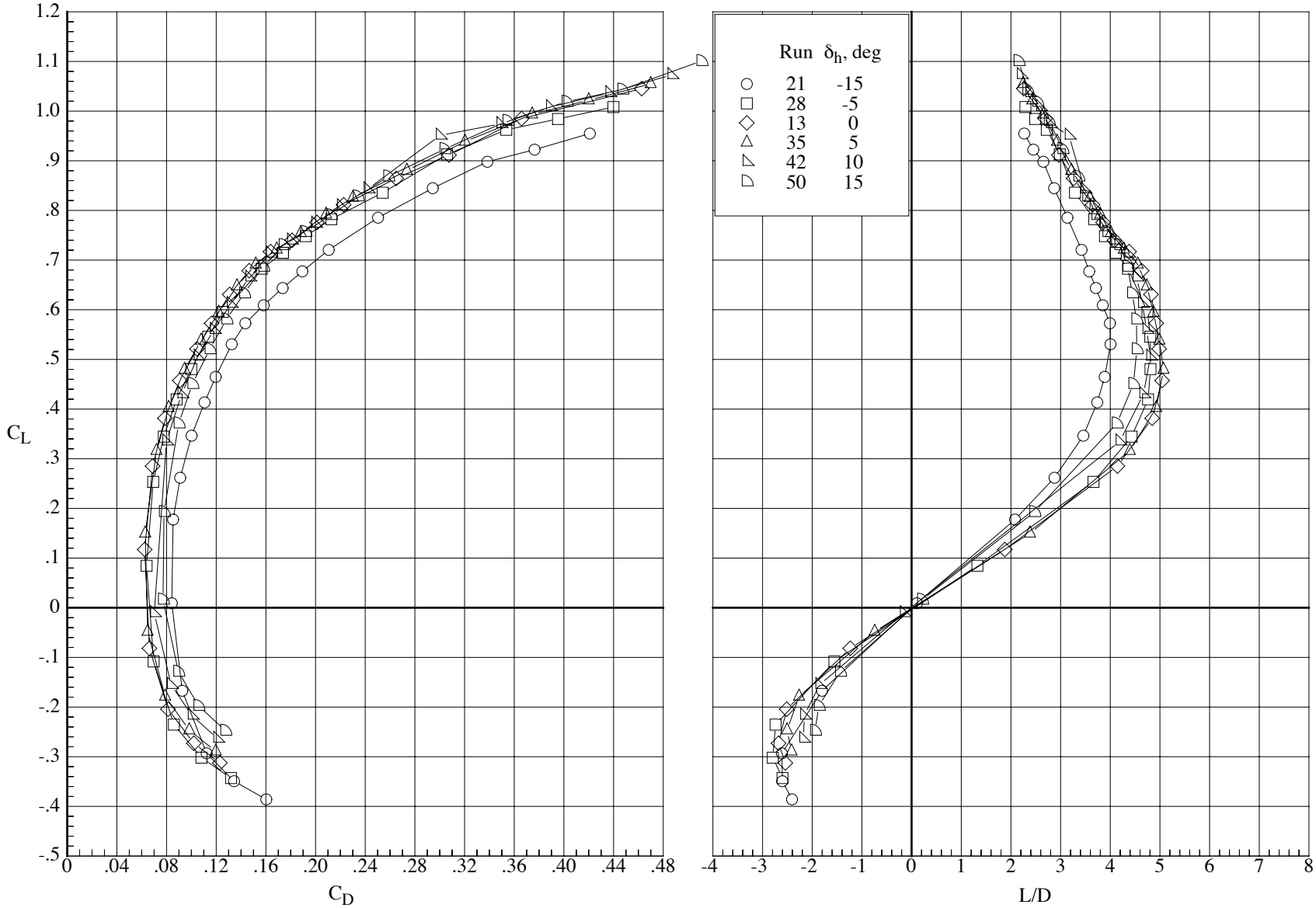

(b) Drag coefficient and lift-drag ratio.

Figure 53. Concluded.

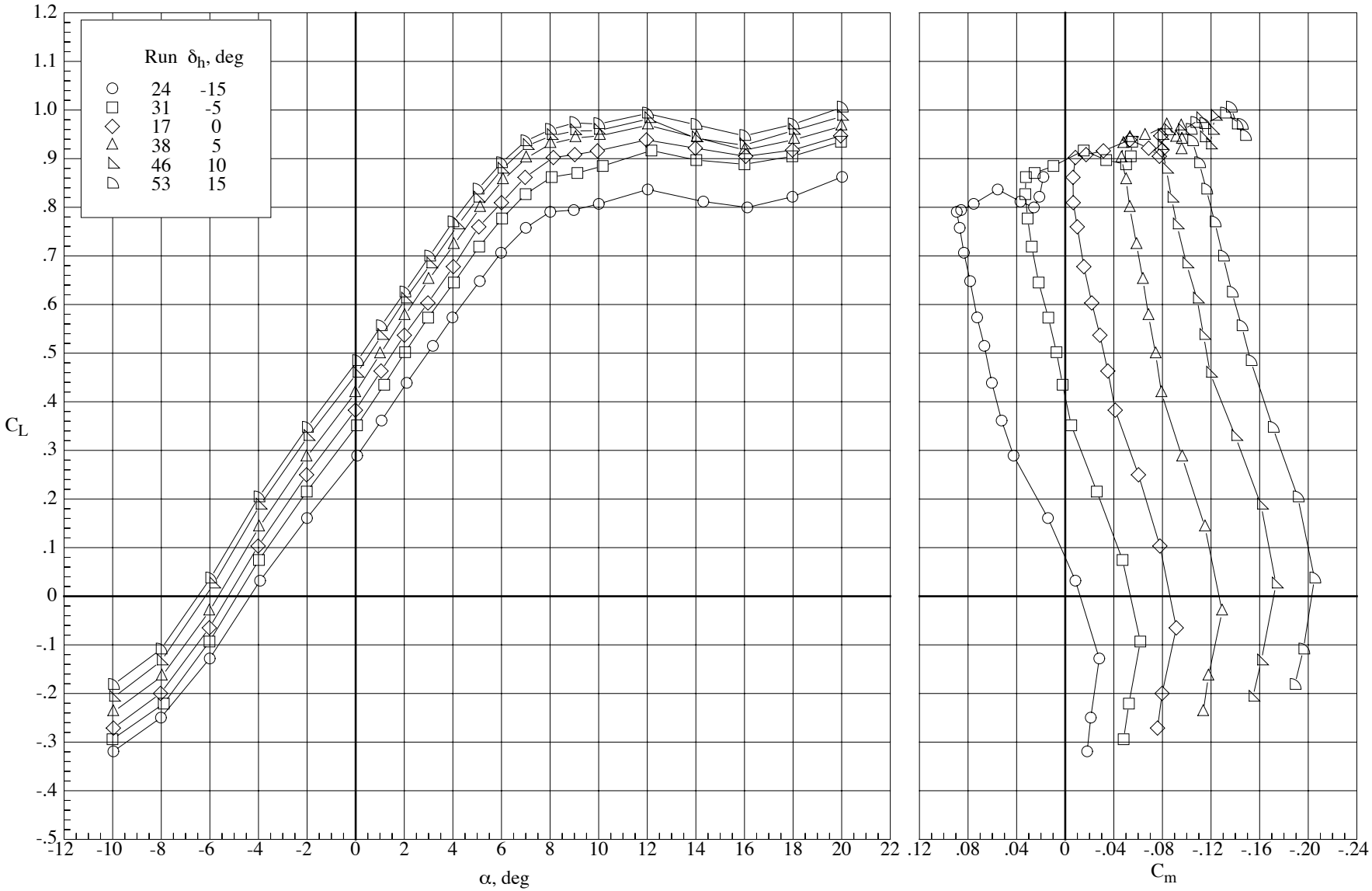

(a) Lift and pitching-moment coefficients.

Figure 54. Effect of horizontal tail incidence on the longitudinal aerodynamic characteristics of the model with the MA-SC-1 wing (bump on) with the tails inverted and the lower fuselage fairing removed at a Reynolds number of 100,000 and a Mach number of 0.65.

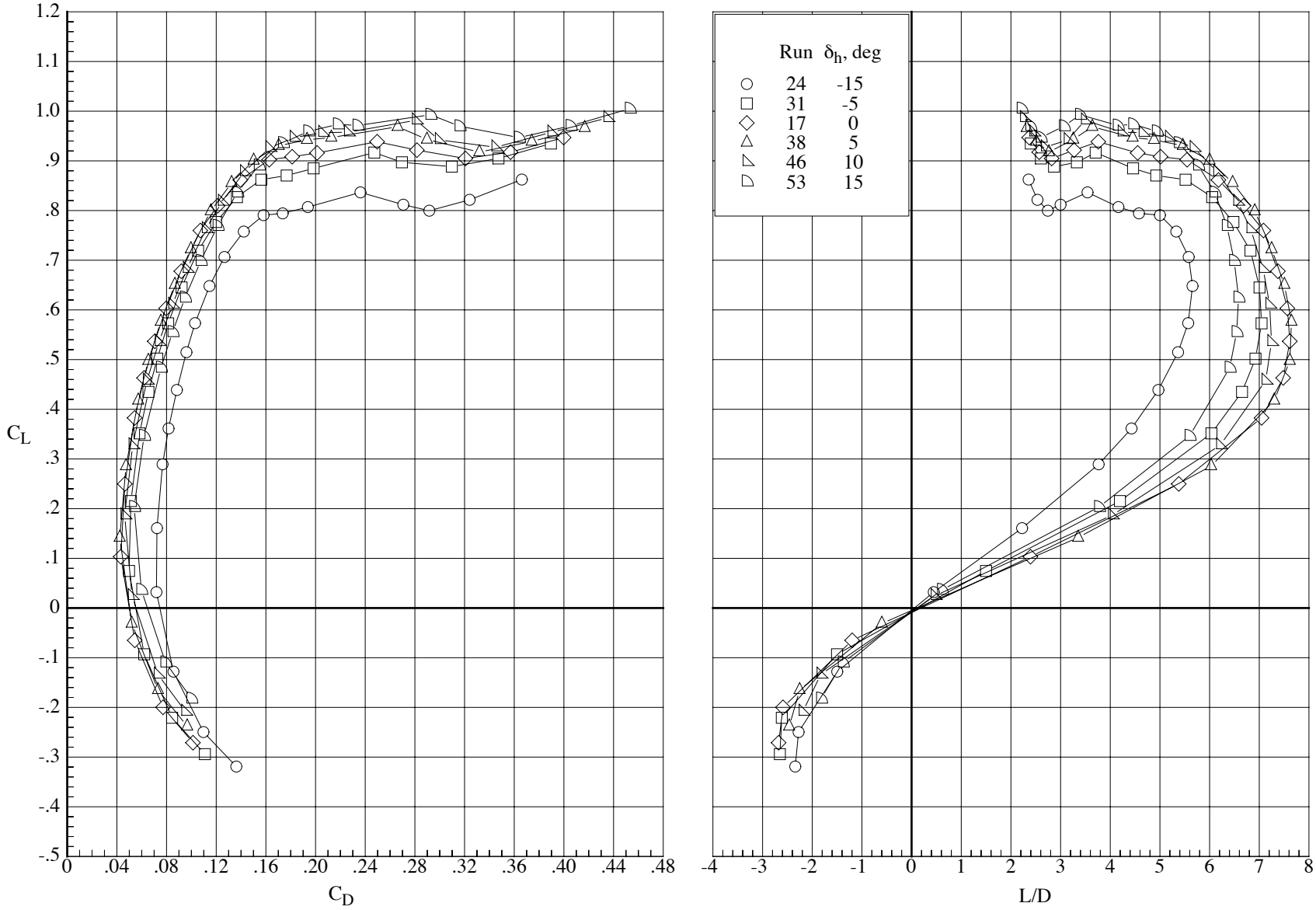

(b) Drag coefficient and lift-drag ratio.

Figure 54. Concluded.

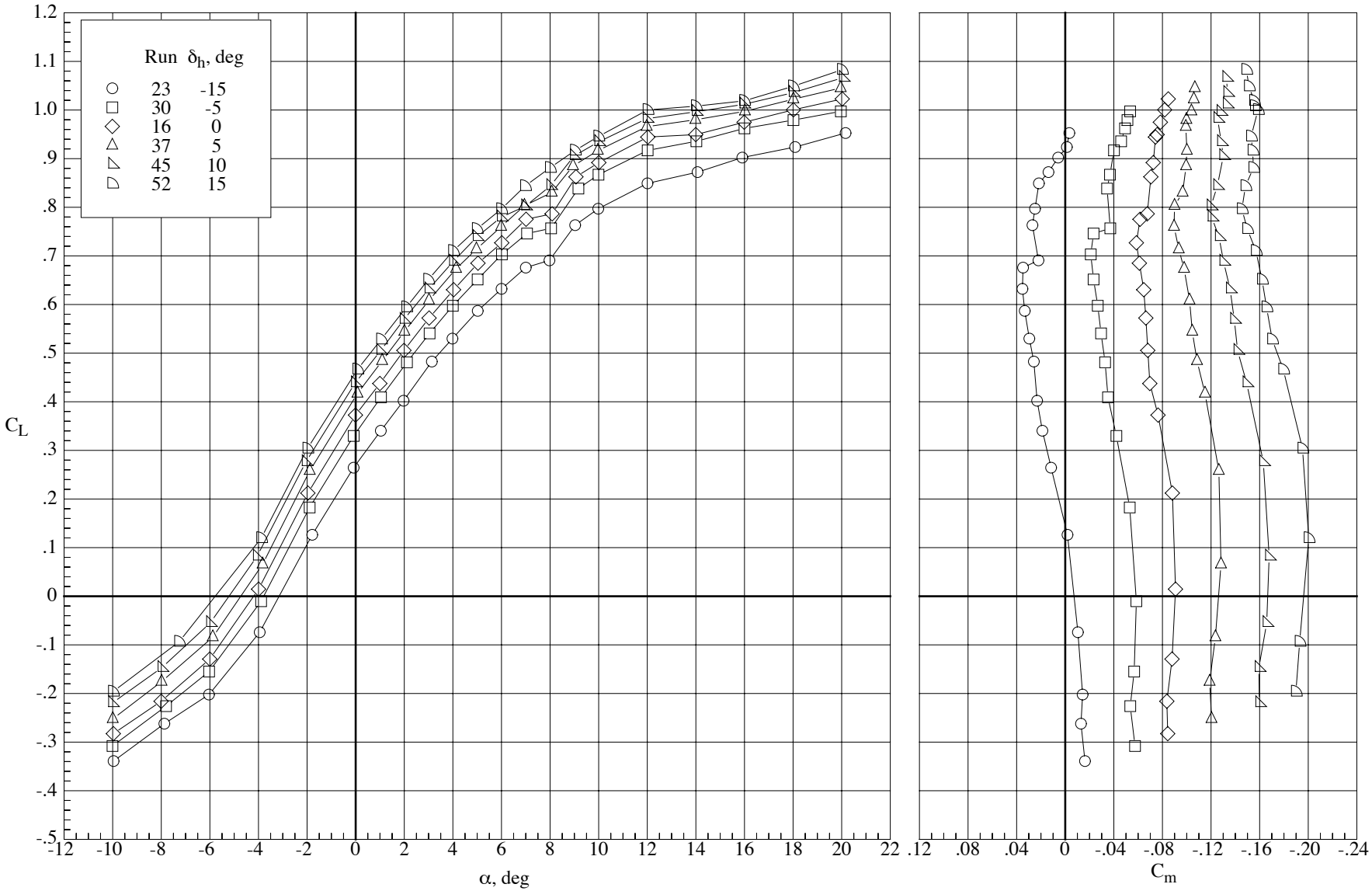

(a) Lift and pitching-moment coefficients.

Figure 55. Effect of horizontal tail incidence on the longitudinal aerodynamic characteristics of the model with the MA-SC-1 wing (bump on) with the tails inverted and the lower fuselage fairing removed at a Reynolds number of 100,000 and a Mach number of 0.80.

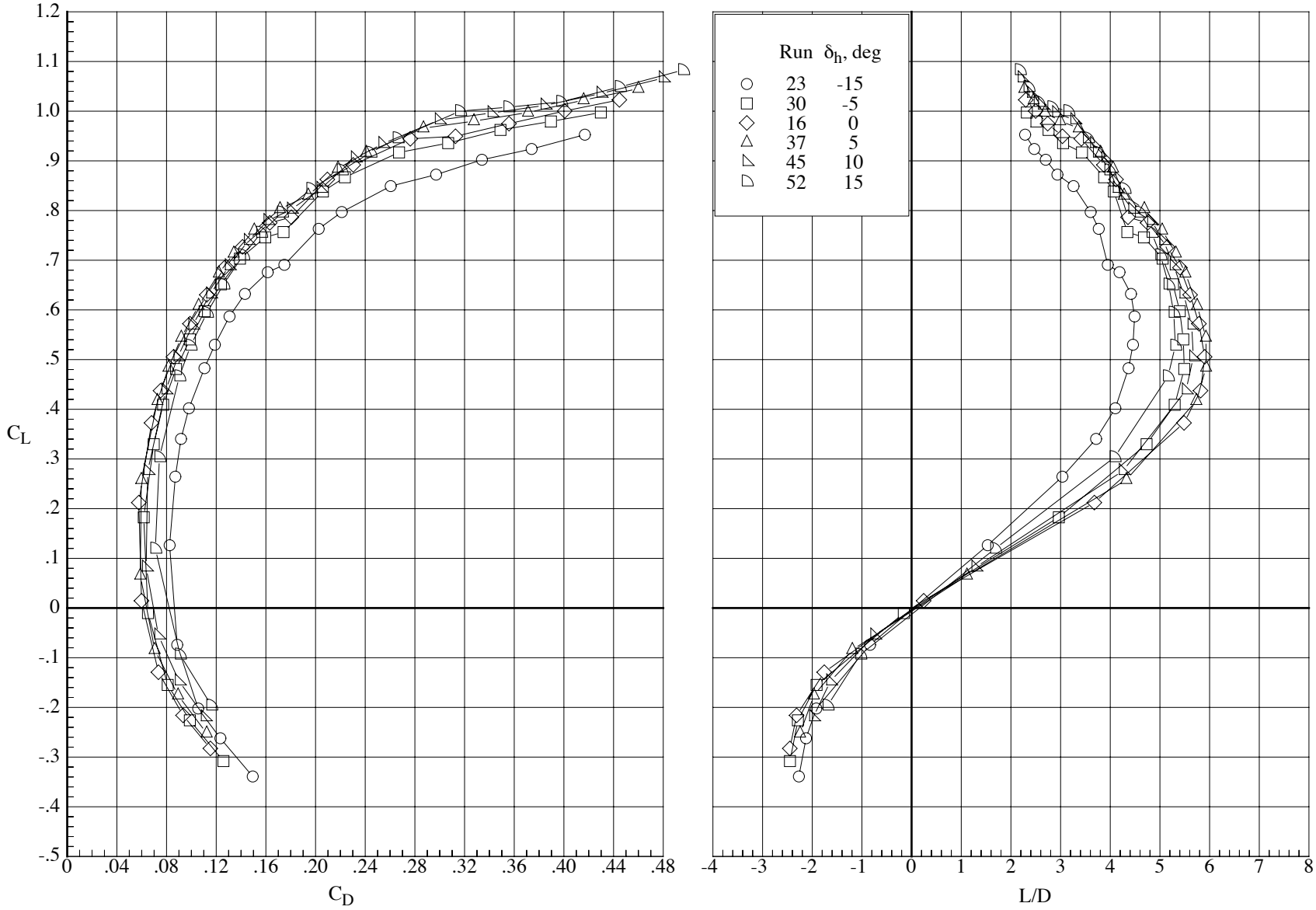

(b) Drag coefficient and lift-drag ratio.

Figure 55. Concluded.

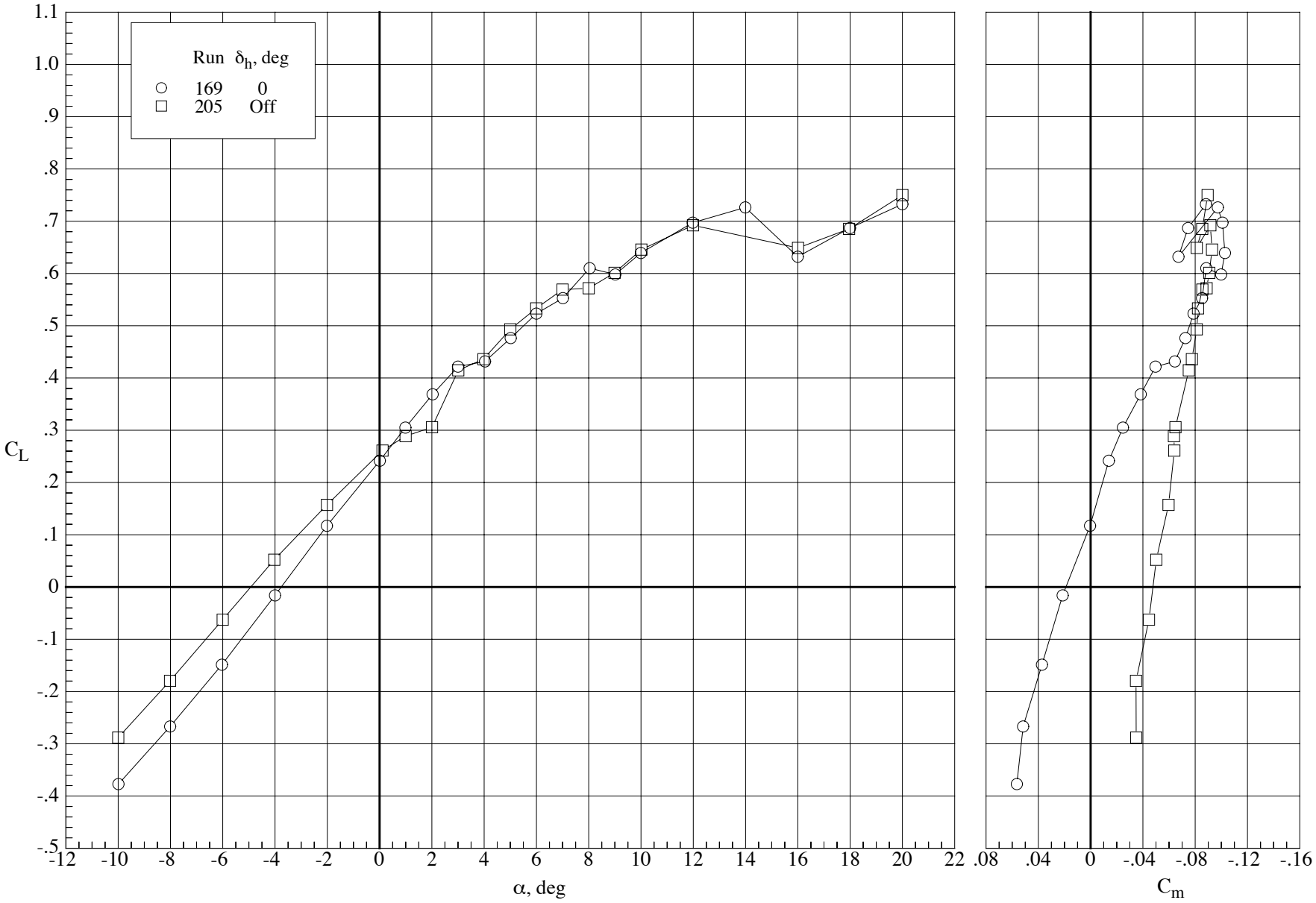

(a) Lift and pitching-moment coefficients.

Figure 56. Effect of tails on the longitudinal aerodynamic characteristics of the model with the MA-SC-1t wing (bump on) at a Reynolds number of 40,000 and a Mach number of 0.65.

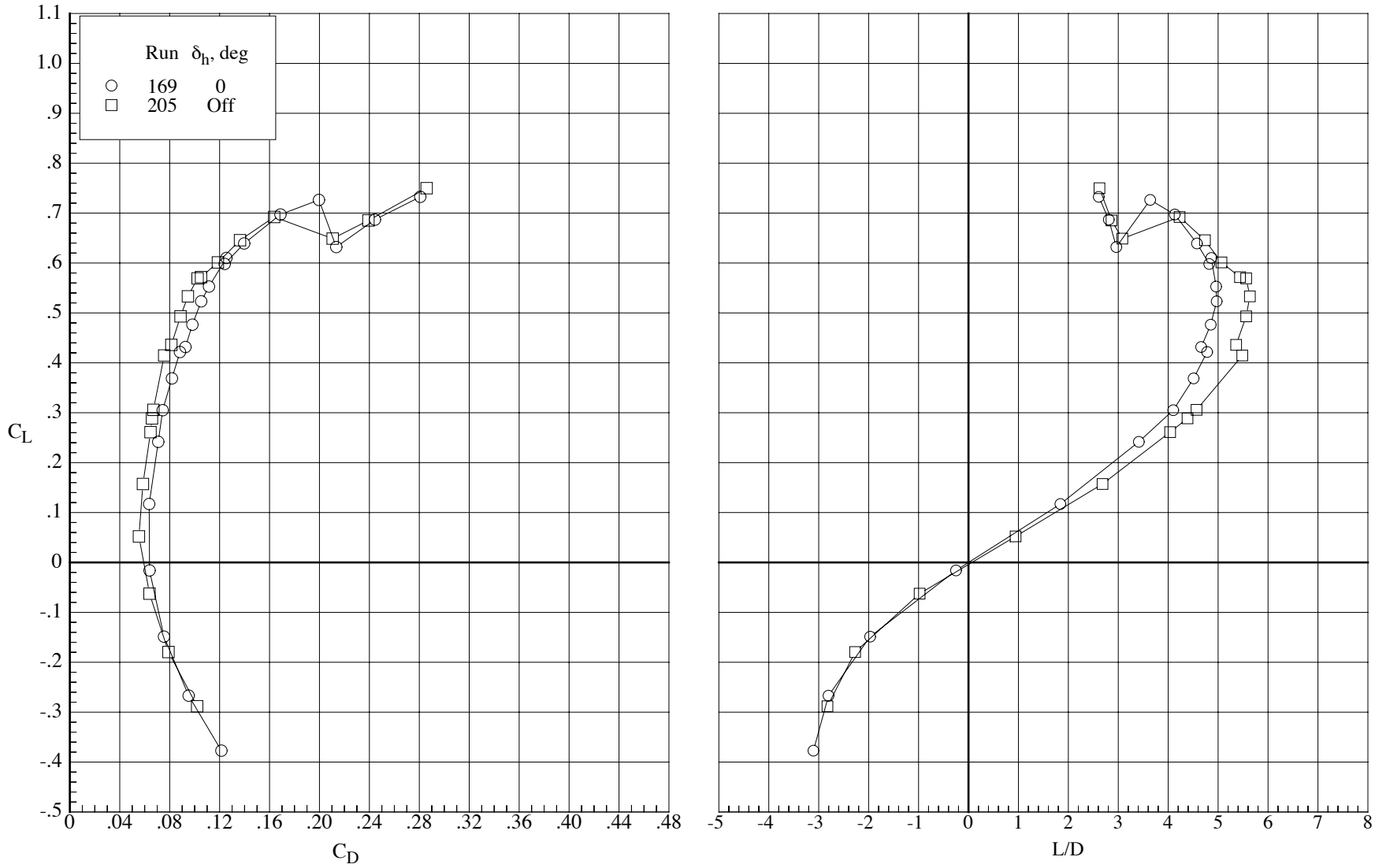

(b) Drag coefficient and lift-drag ratio.

Figure 56. Concluded.

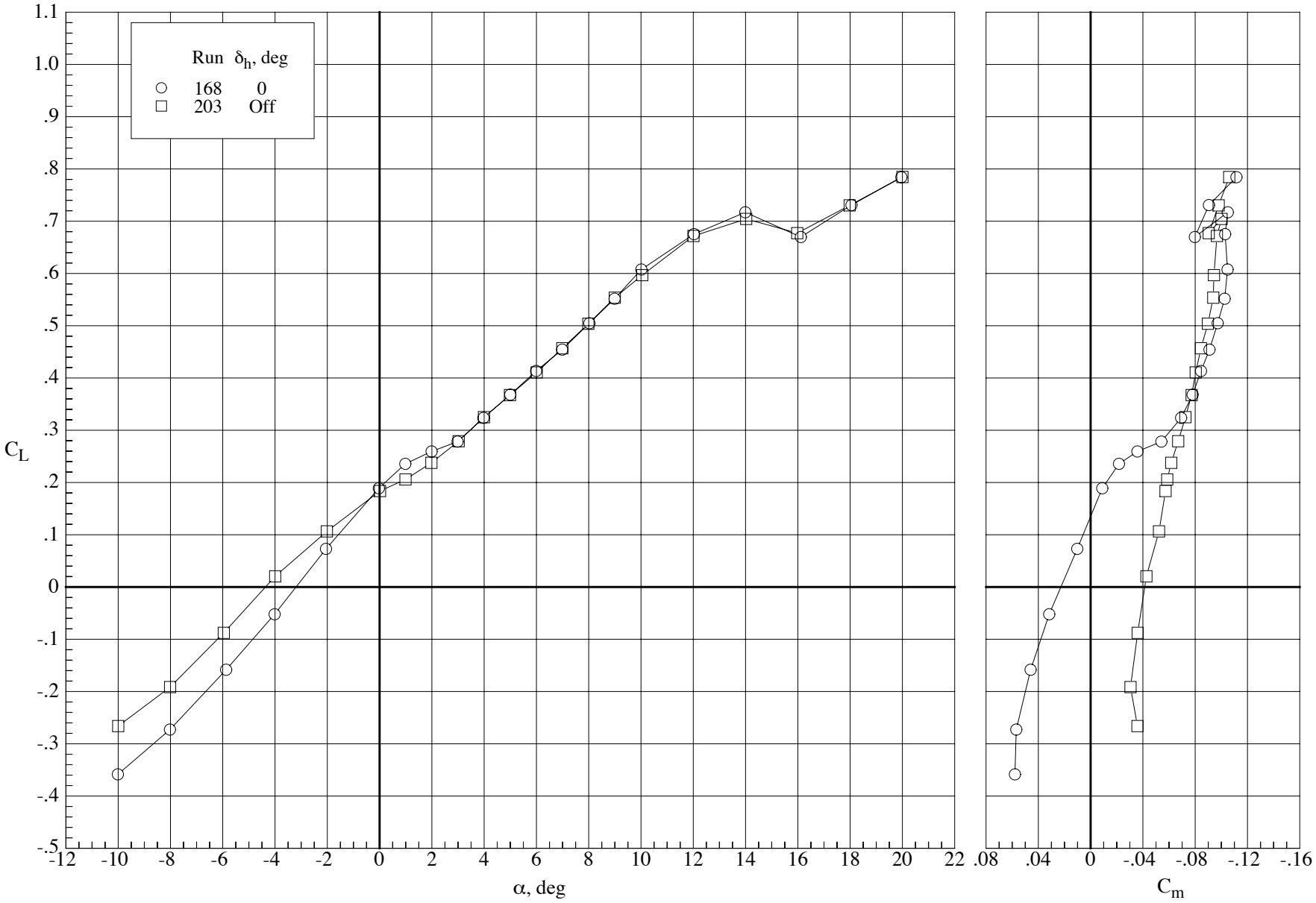

(a) Lift and pitching-moment coefficients.

Figure 57. Effect of tails on the longitudinal aerodynamic characteristics of the model with the MA-SC-1t wing (bump on) at a Reynolds number of 40,000 and a Mach number of 0.80.

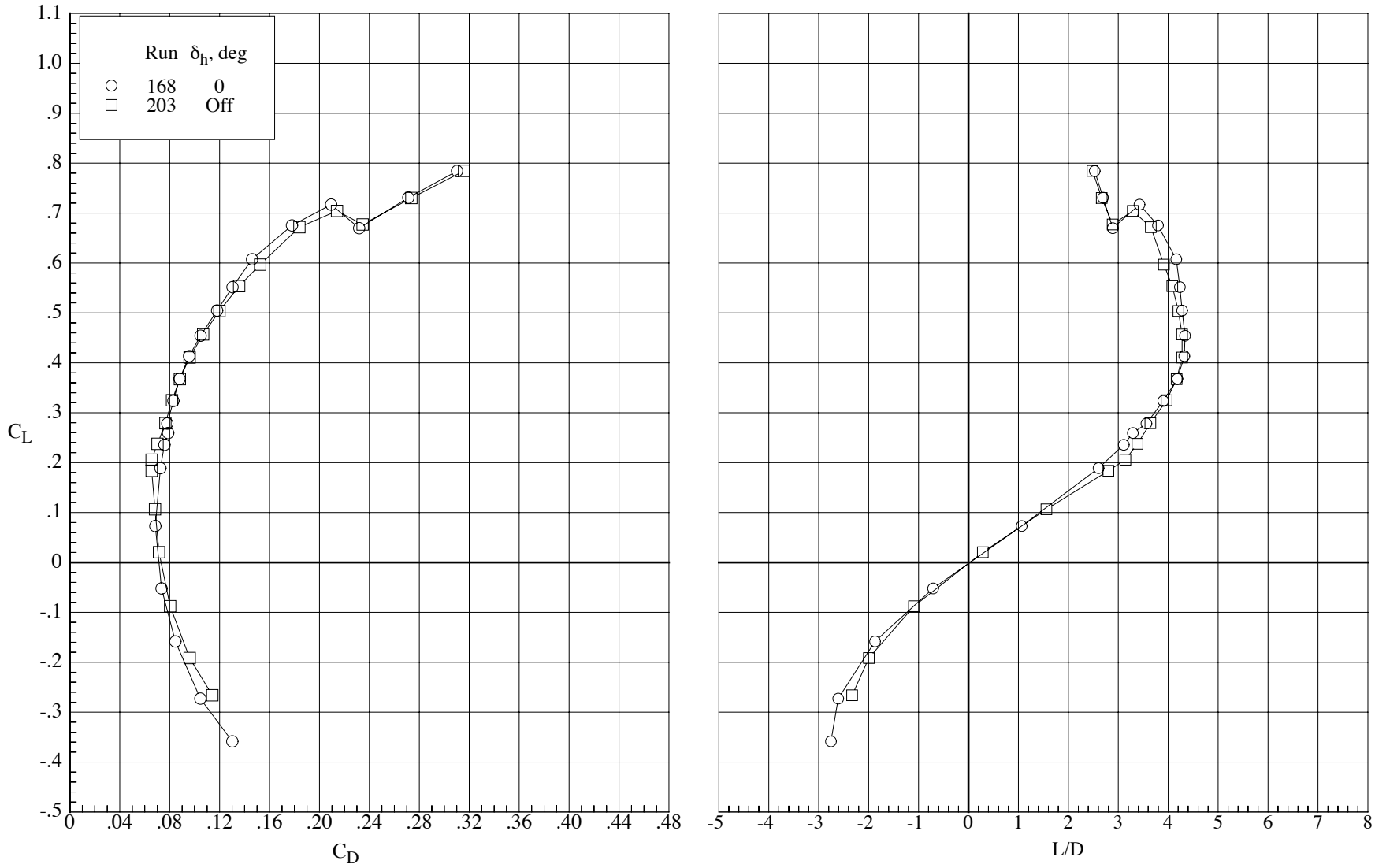

(b) Drag coefficient and lift-drag ratio.

Figure 57. Concluded.

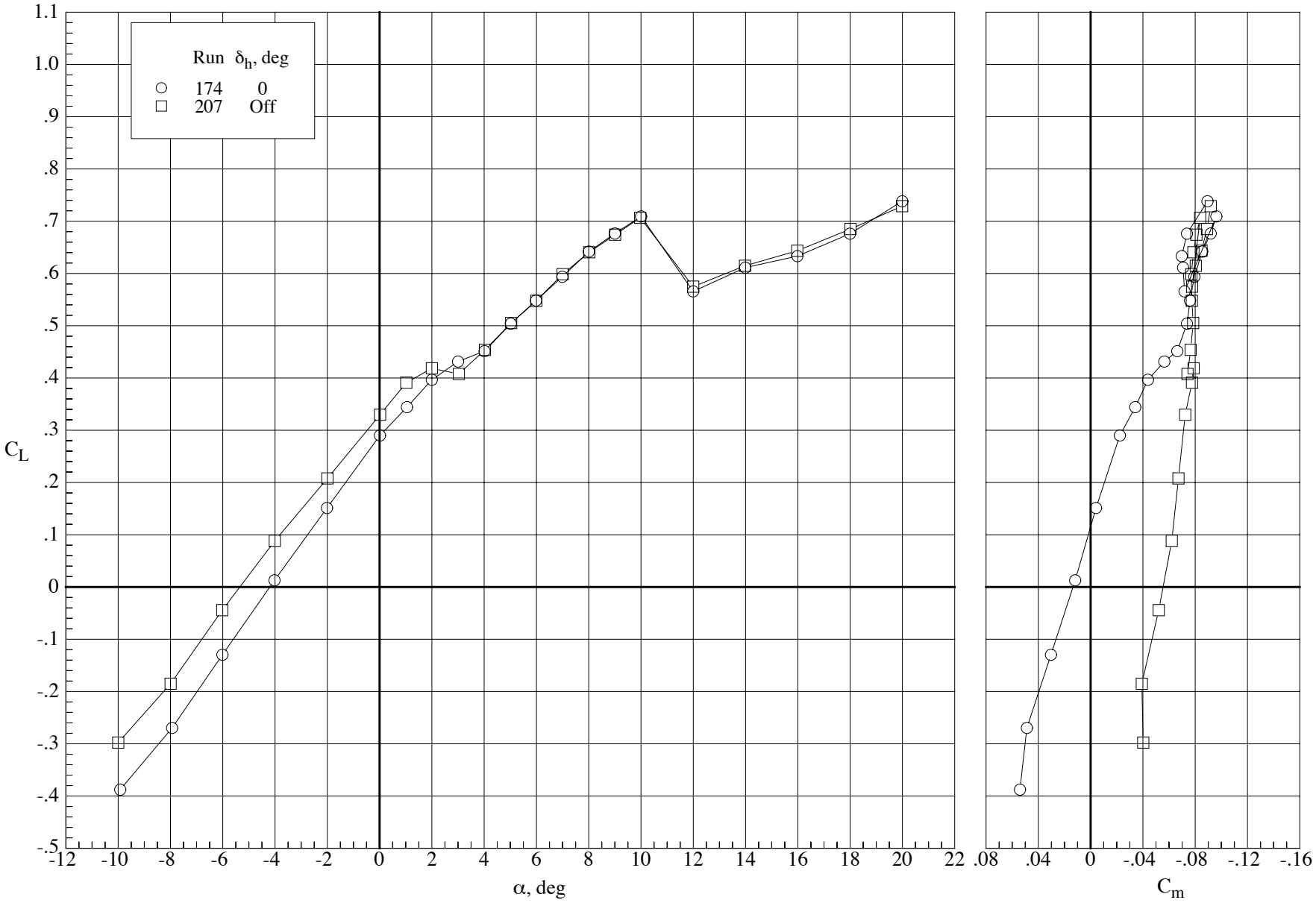

(a) Lift and pitching-moment coefficients.

Figure 58. Effect of tails on the longitudinal aerodynamic characteristics of the model with the MA-SC-1t wing (bump on) at a Reynolds number of 60,000 and a Mach number of 0.65.

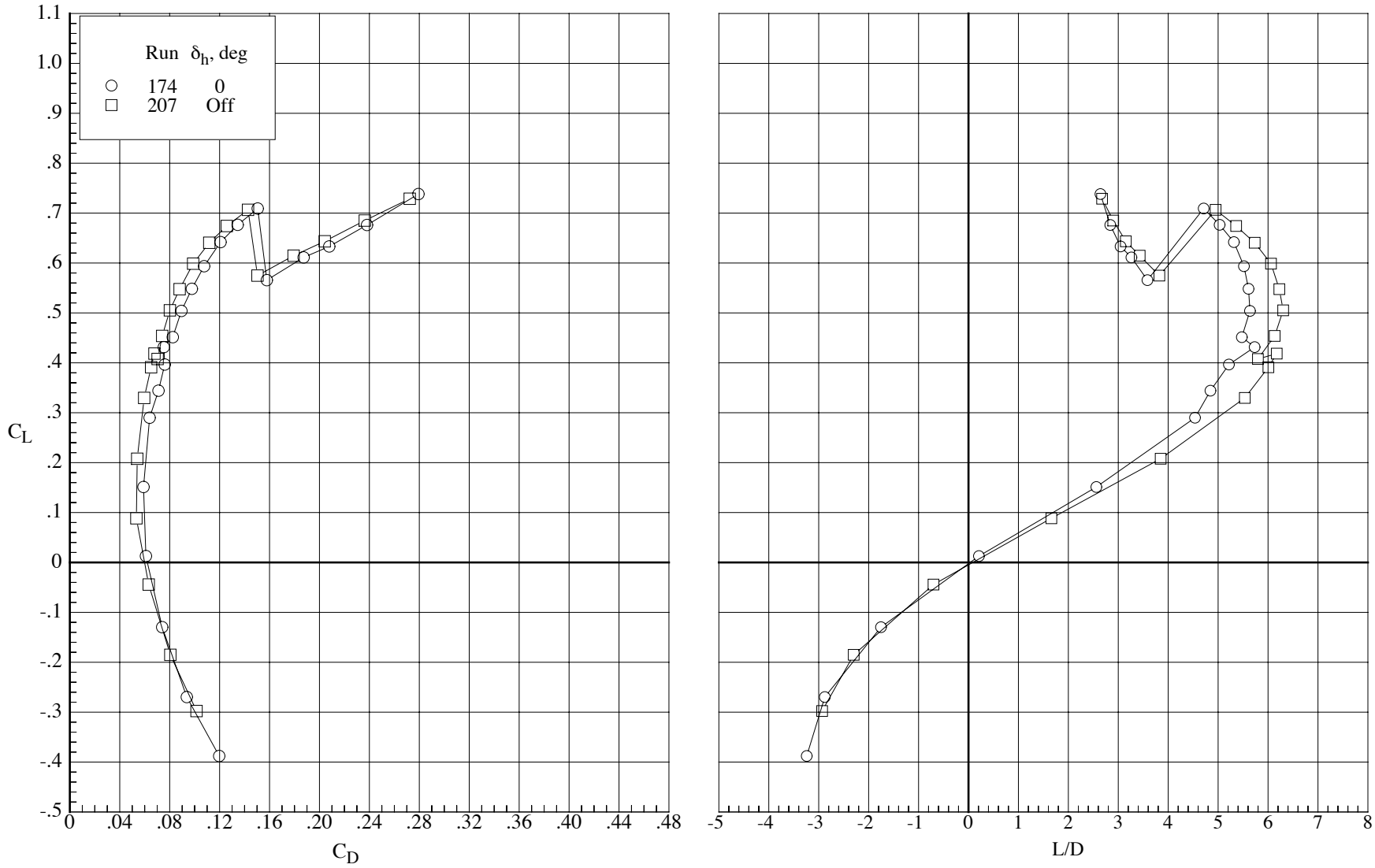

(b) Drag coefficient and lift-drag ratio.

Figure 58. Concluded.

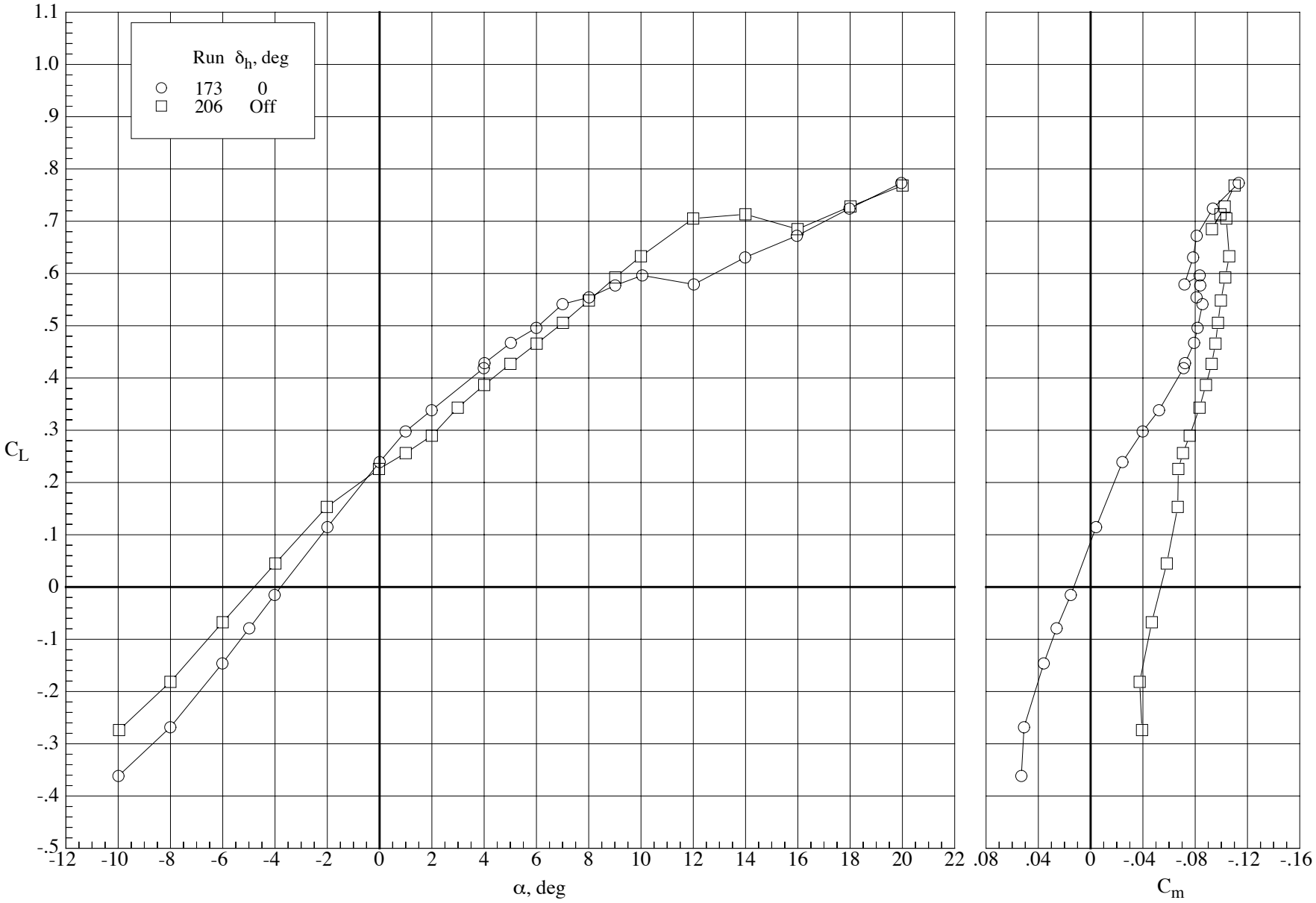

(a) Lift and pitching-moment coefficients.

Figure 59. Effect of tails on the longitudinal aerodynamic characteristics of the model with the MA-SC-1t wing (bump on) at a Reynolds number of 60,000 and a Mach number of 0.80.

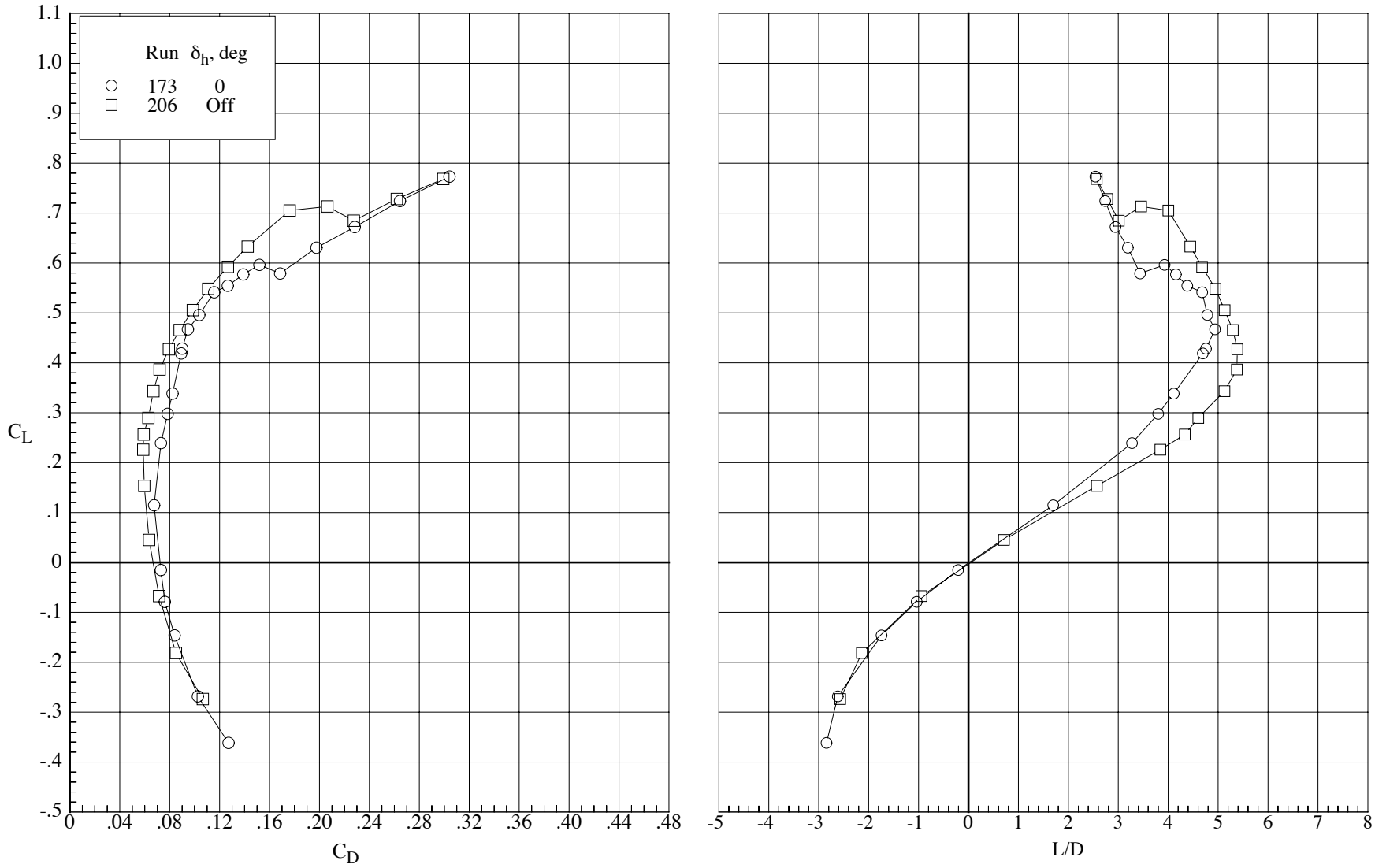

(b) Drag coefficient and lift-drag ratio.

Figure 59. Concluded.

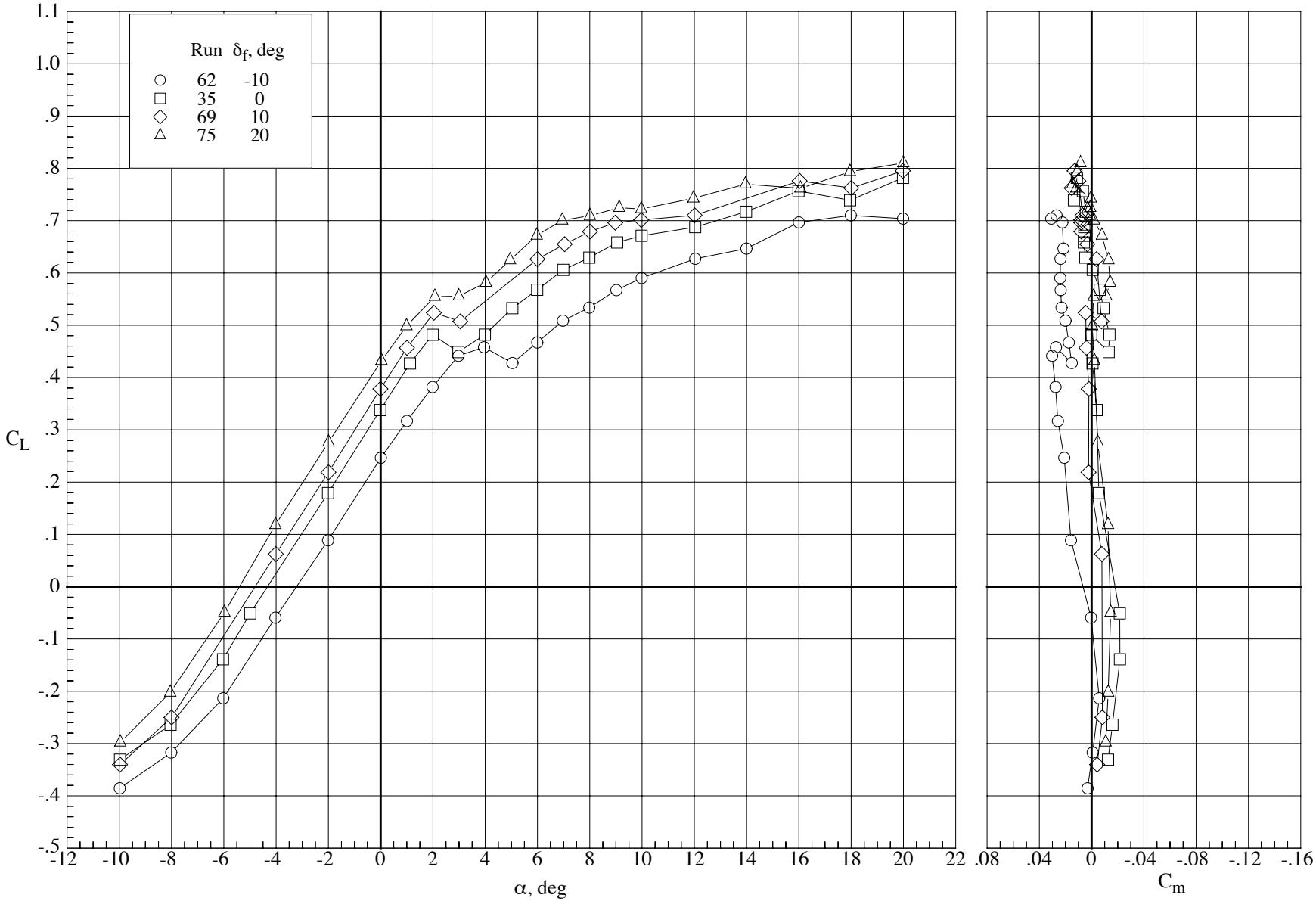

(a) Lift and pitching-moment coefficients.

Figure 60. Effect of right wing trailing edge flap deflection on the aerodynamic characteristics of the model with the MA-SC-1 wing (bump on) at a Reynolds number of 40,000 and a Mach number of 0.65. $\delta_h = 0°$.

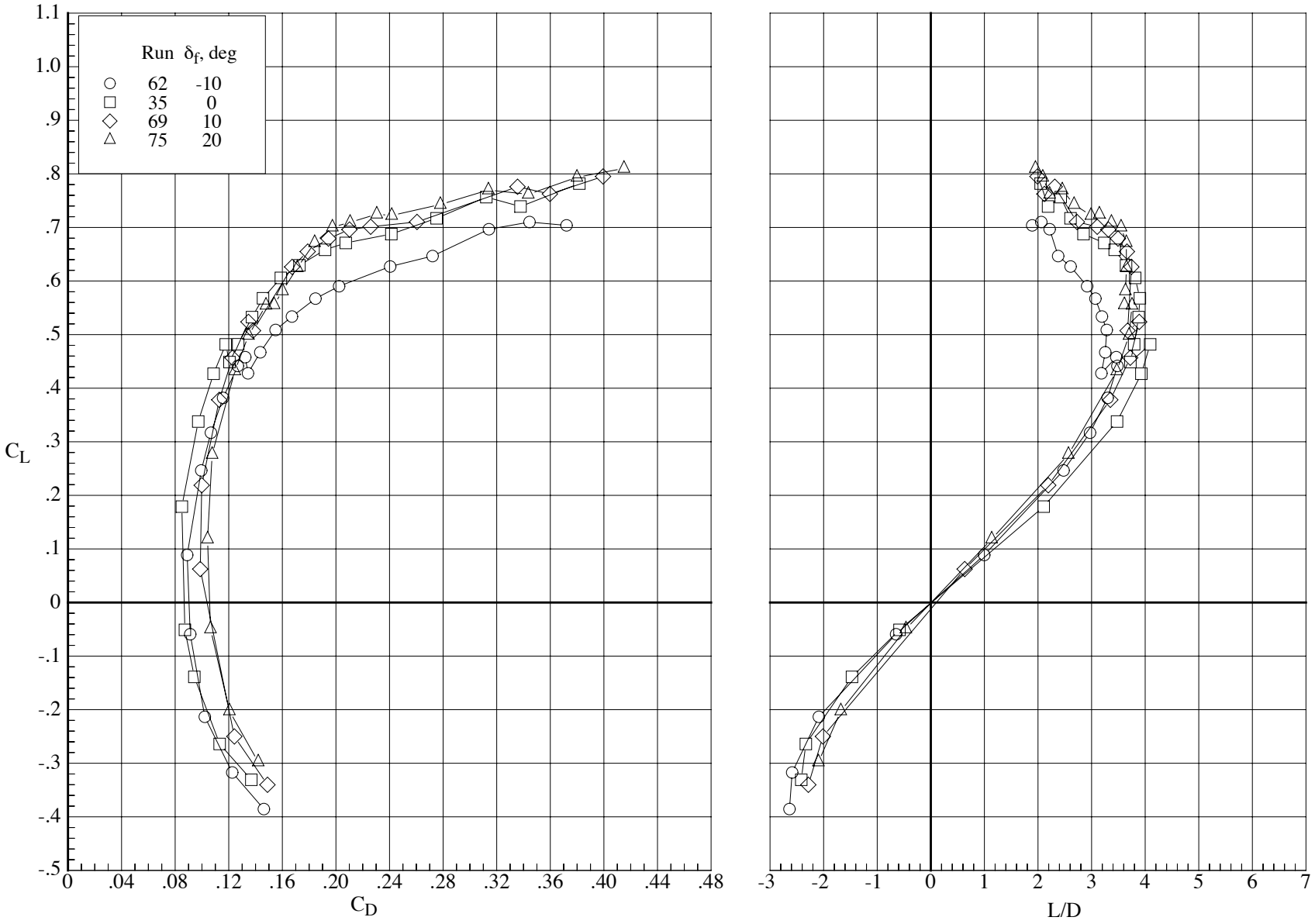

(b) Drag coefficient and lift-drag ratio.

Figure 60. Continued.

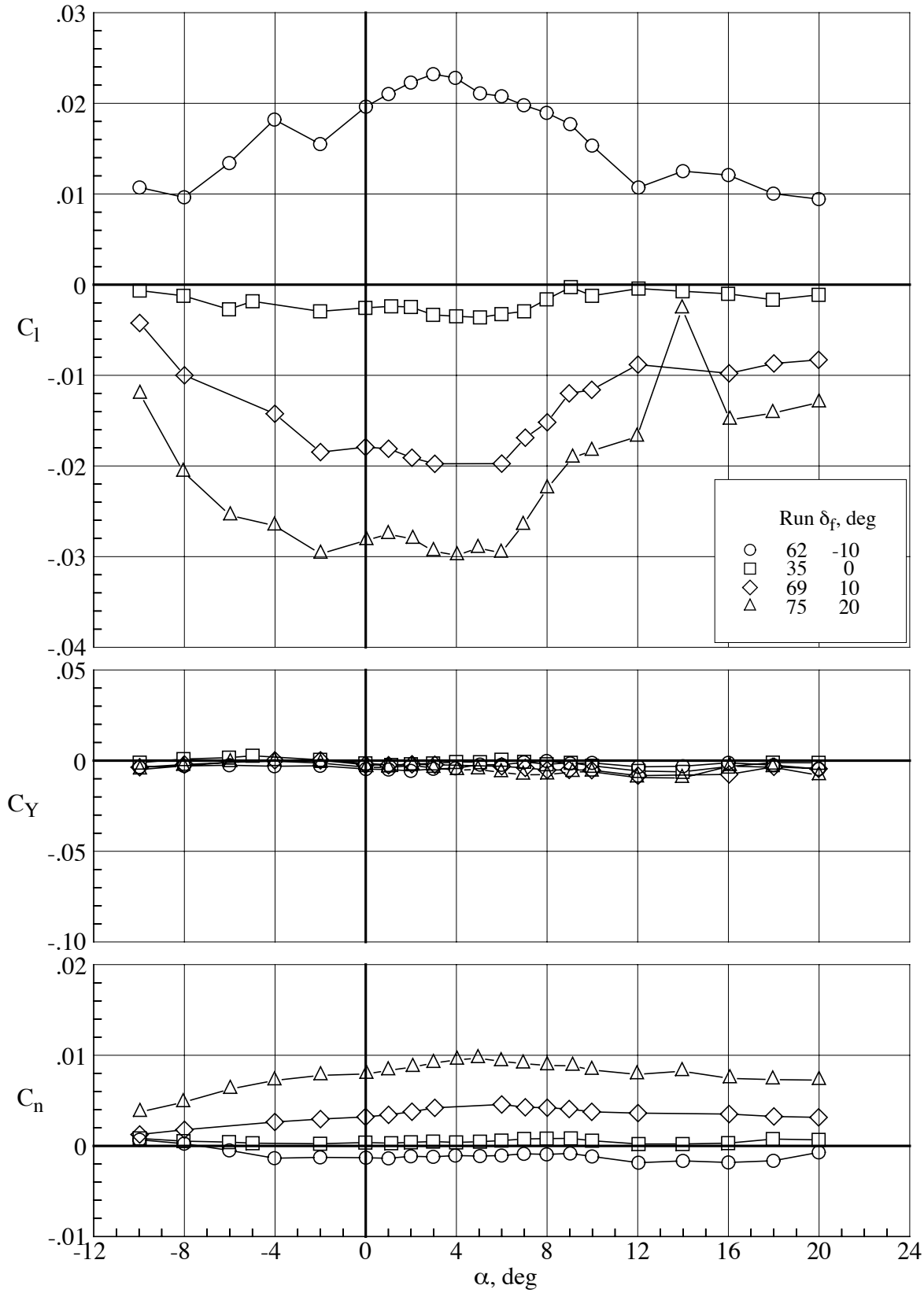

(c) Lateral-directional coefficients.

Figure 60. Concluded.

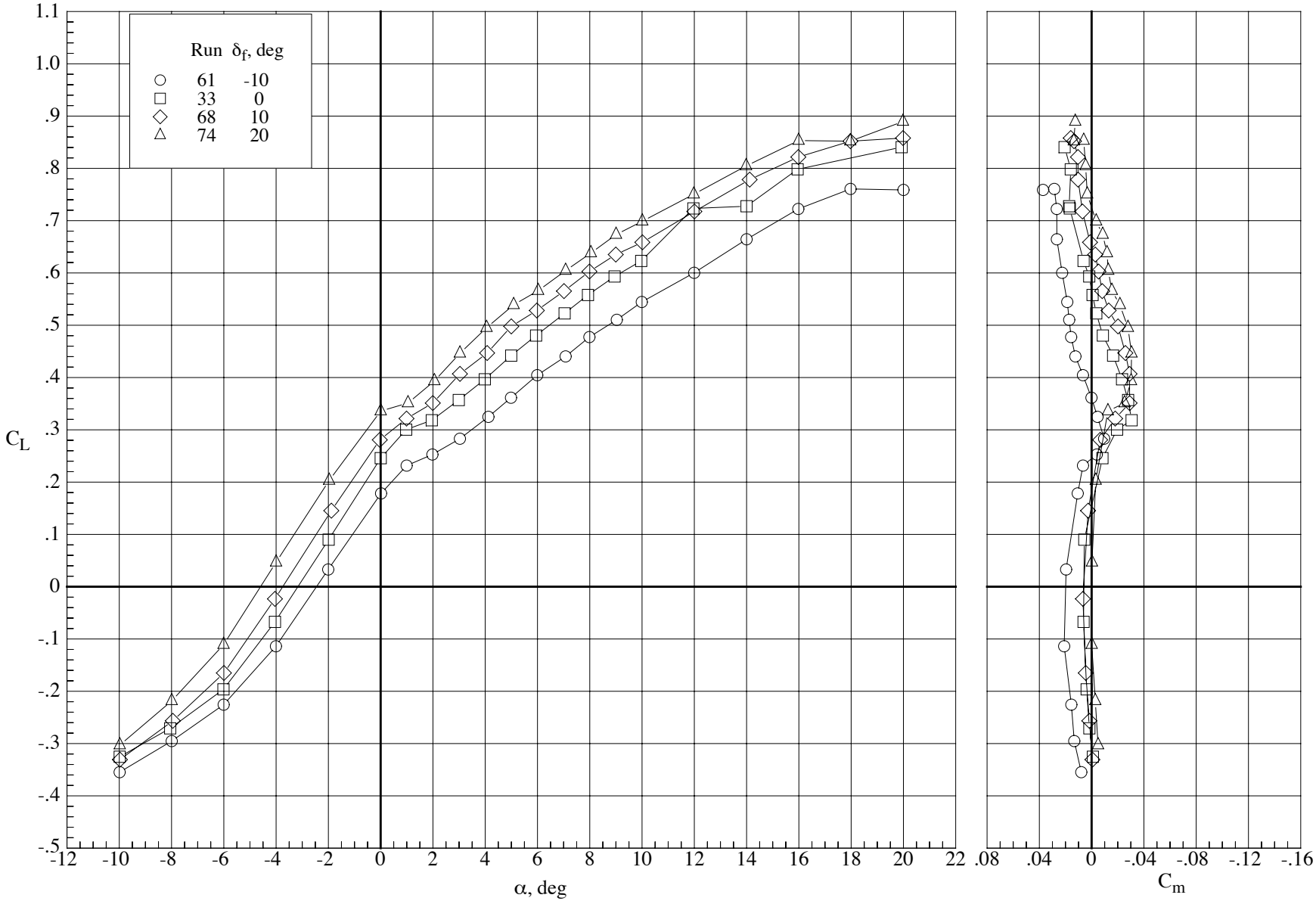

(a) Lift and pitching-moment coefficients.

Figure 61. Effect of right wing trailing edge flap deflection on the aerodynamic characteristics of the model with the MA-SC-1 wing (bump on) at a Reynolds number of 40,000 and a Mach number of 0.80. $\delta_h = 0°$.

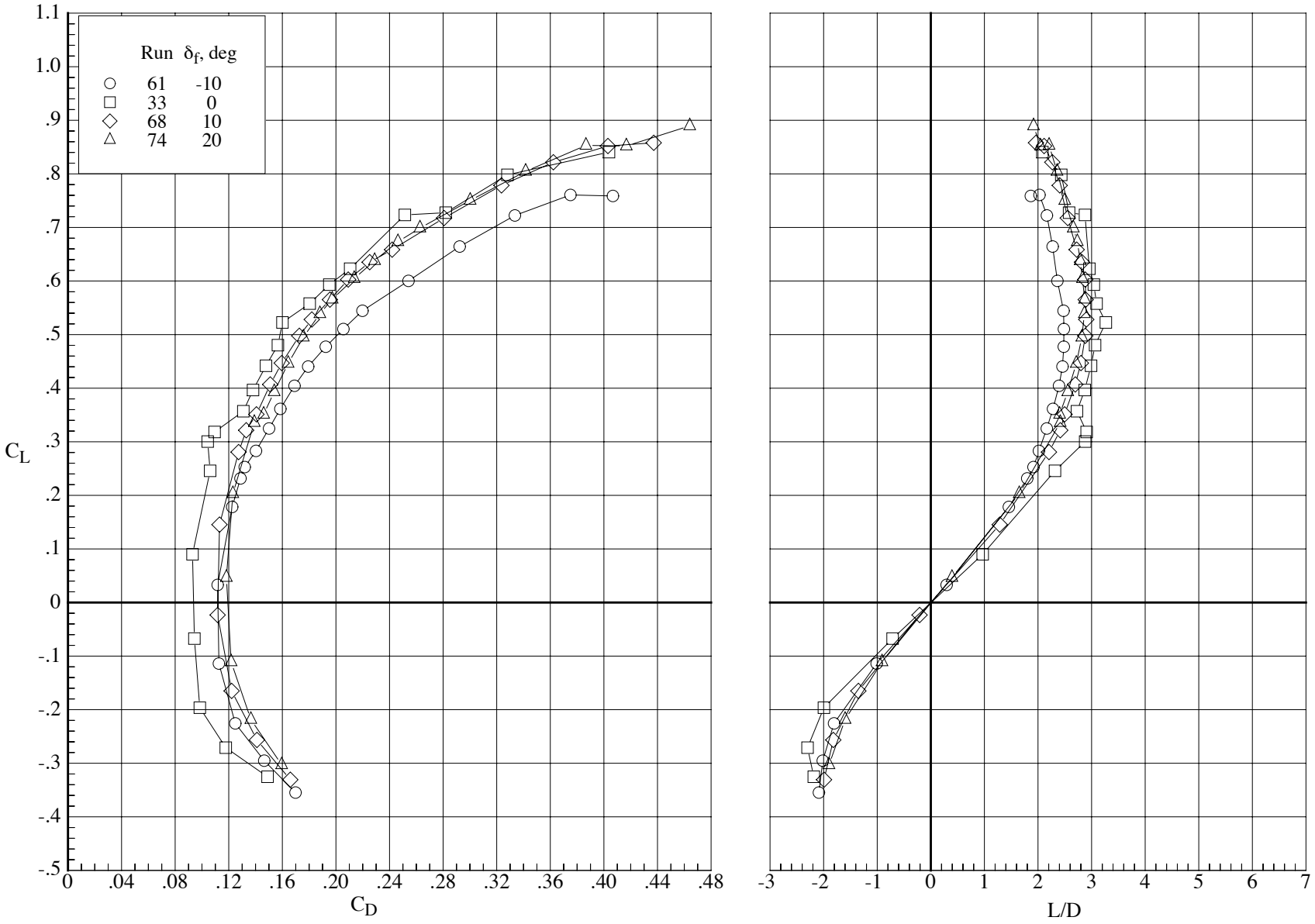

(b) Drag coefficient and lift-drag ratio.

Figure 61. Continued.

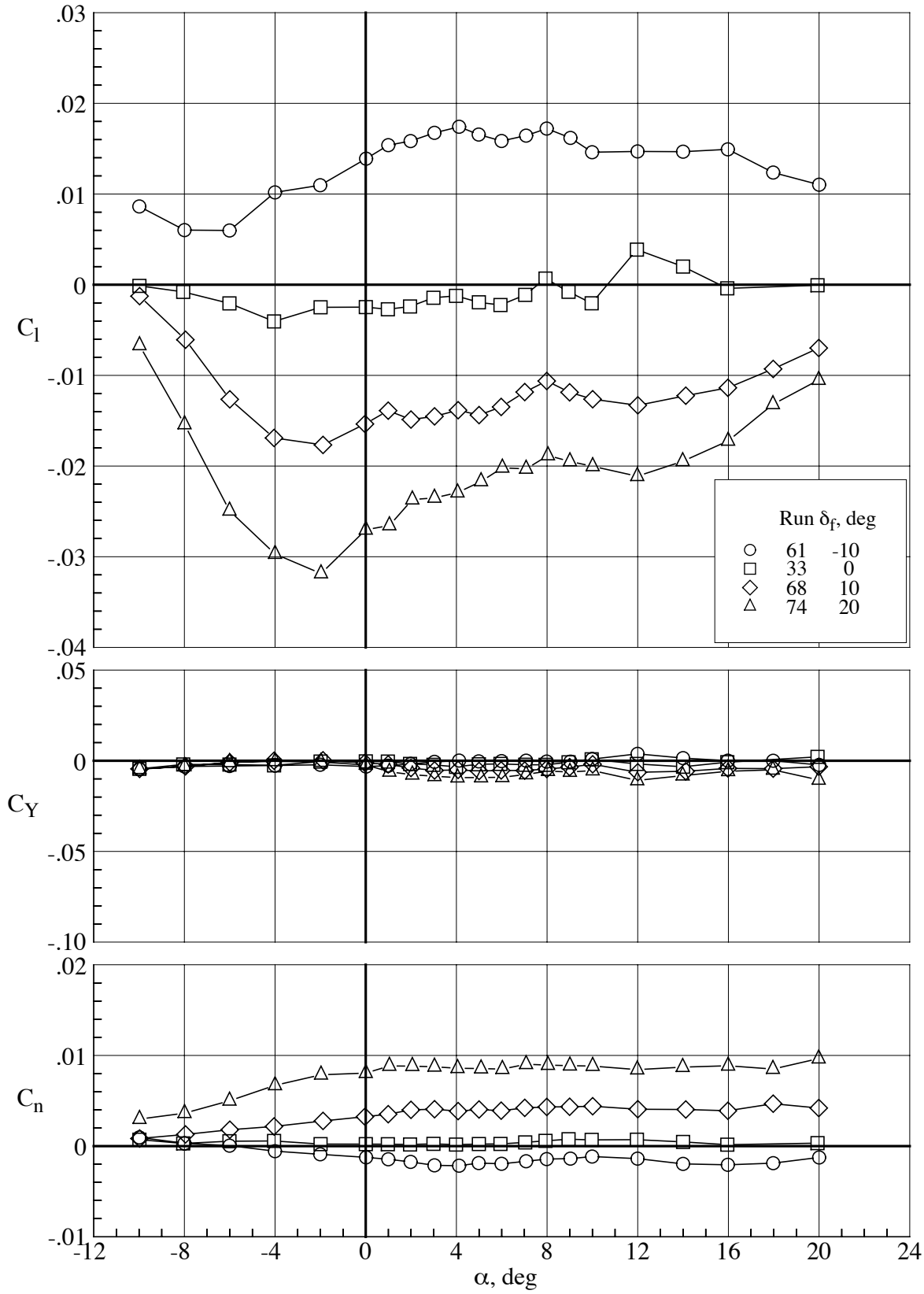

(c) Lateral-directional coefficients.

Figure 61. Concluded.

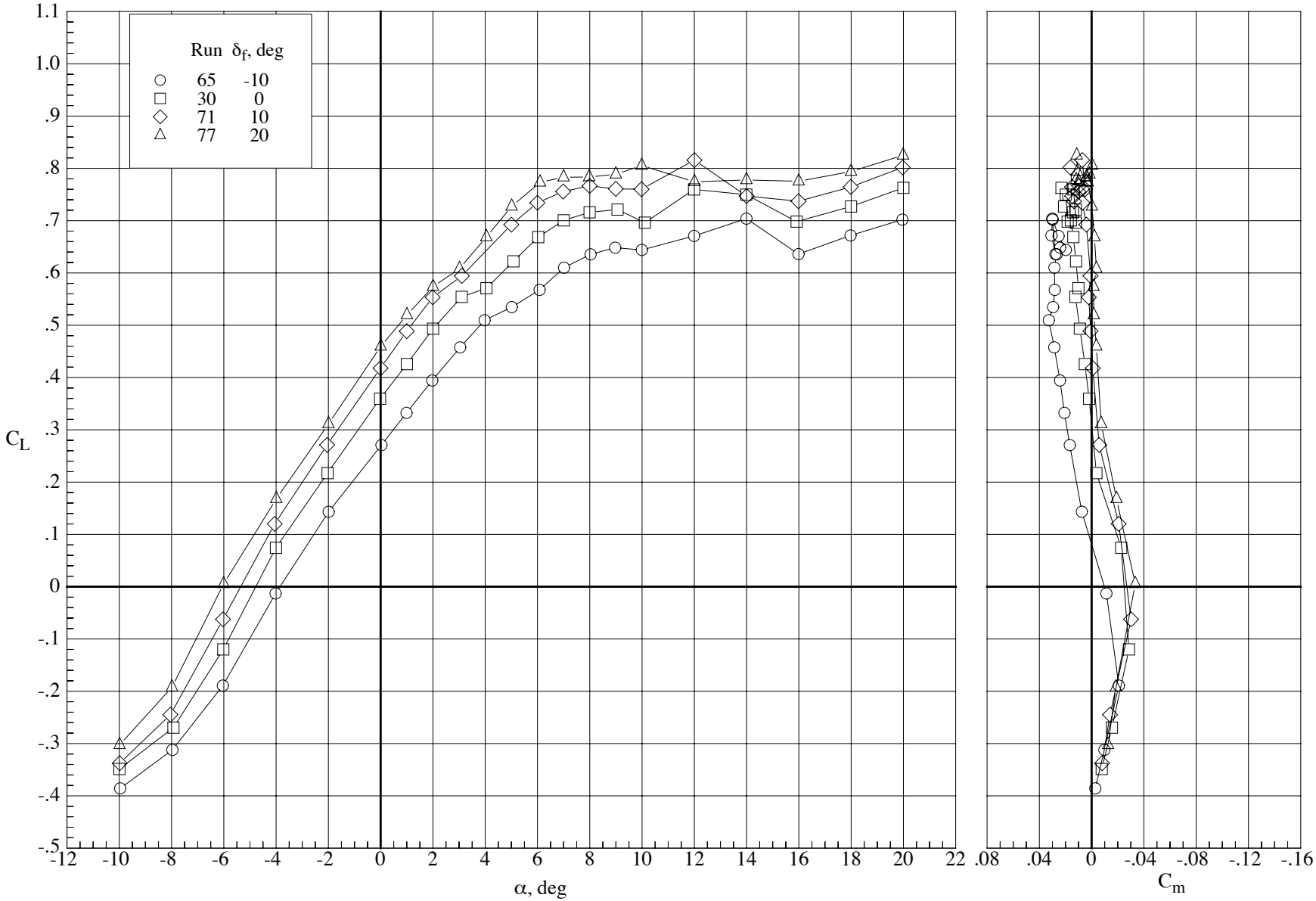

(a) Lift and pitching-moment coefficients.

Figure 62. Effect of right wing trailing edge flap deflection on the aerodynamic characteristics of the model with the MA-SC-1 wing (bump on) at a Reynolds number of 60,000 and a Mach number of 0.65. $\delta_h = 0°$.

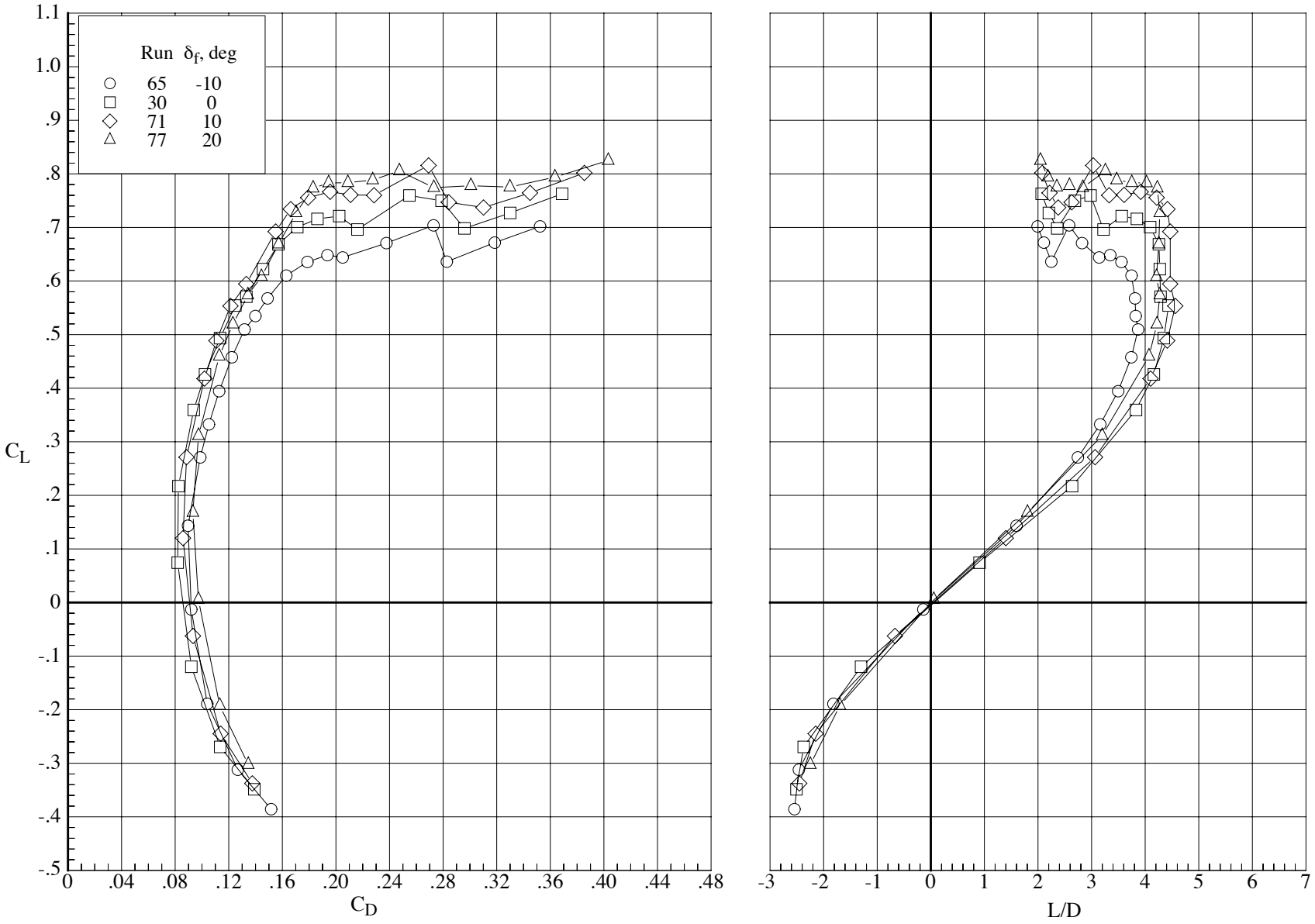

(b) Drag coefficient and lift-drag ratio.

Figure 62. Continued.

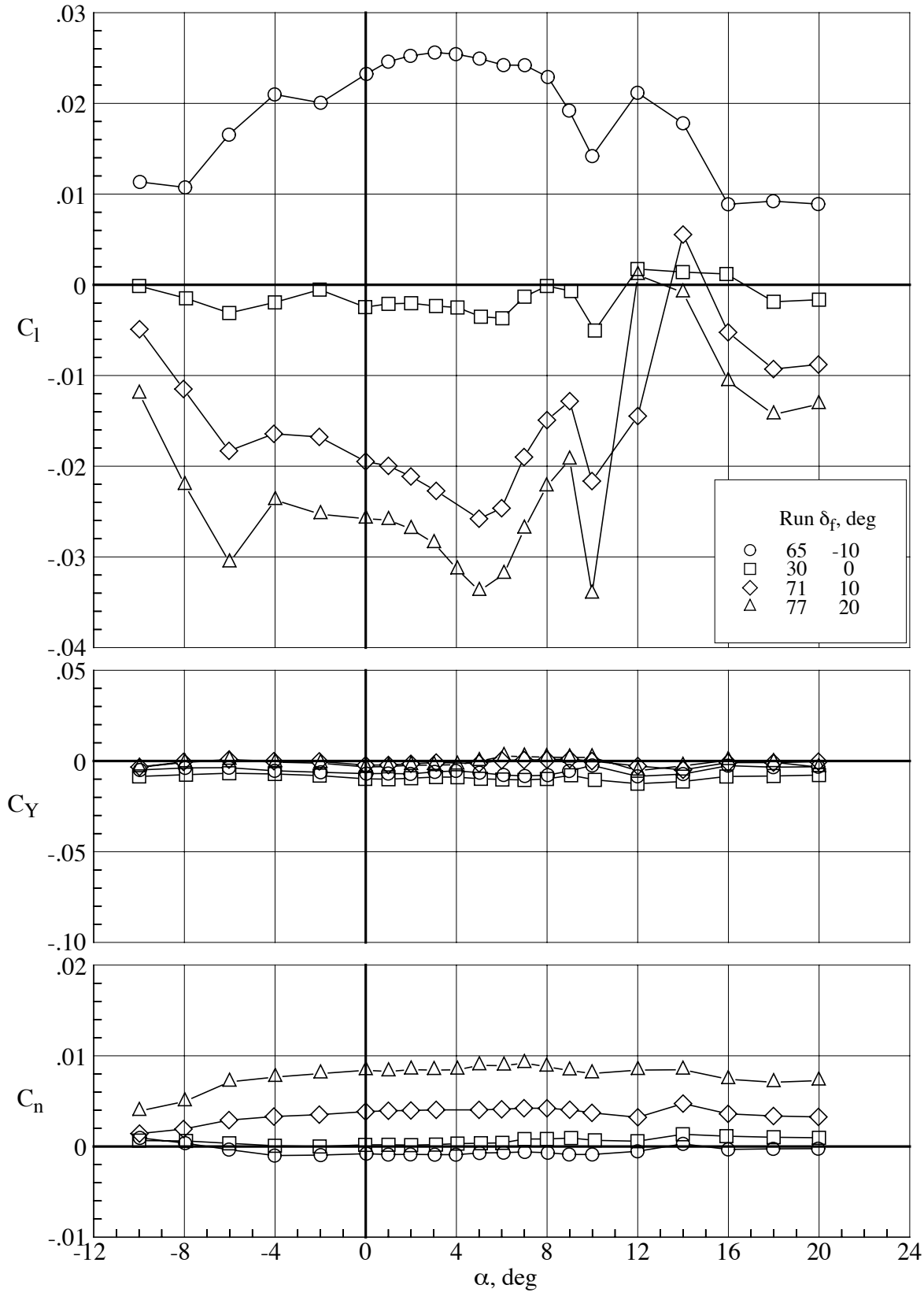

(c) Lateral-directional coefficients.

Figure 62. Concluded.

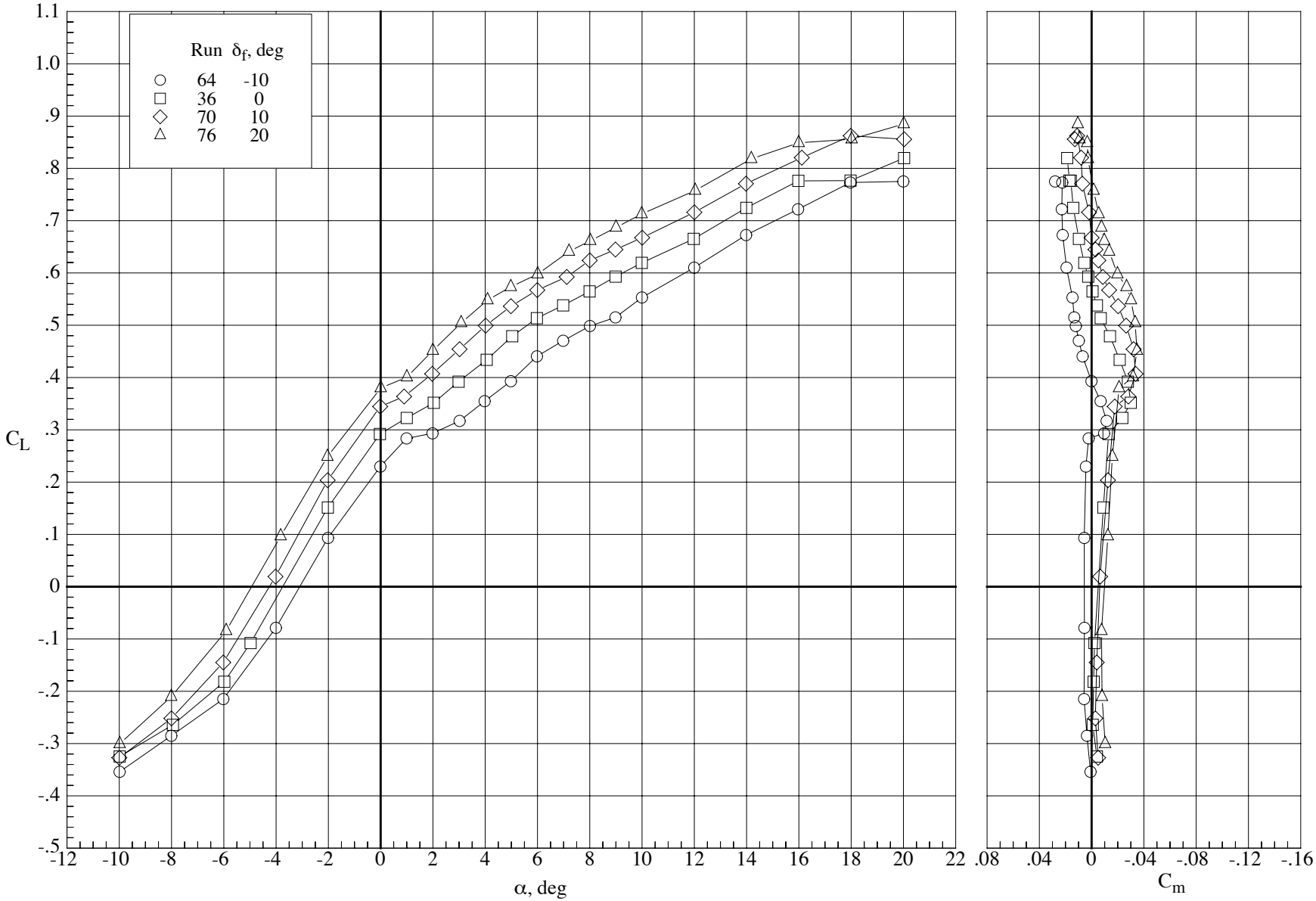

(a) Lift and pitching-moment coefficients.

Figure 63. Effect of right wing trailing edge flap deflection on the aerodynamic characteristics of the model with the MA-SC-1 wing (bump on) at a Reynolds number of 60,000 and a Mach number of 0.80. $\delta_h = 0°$.

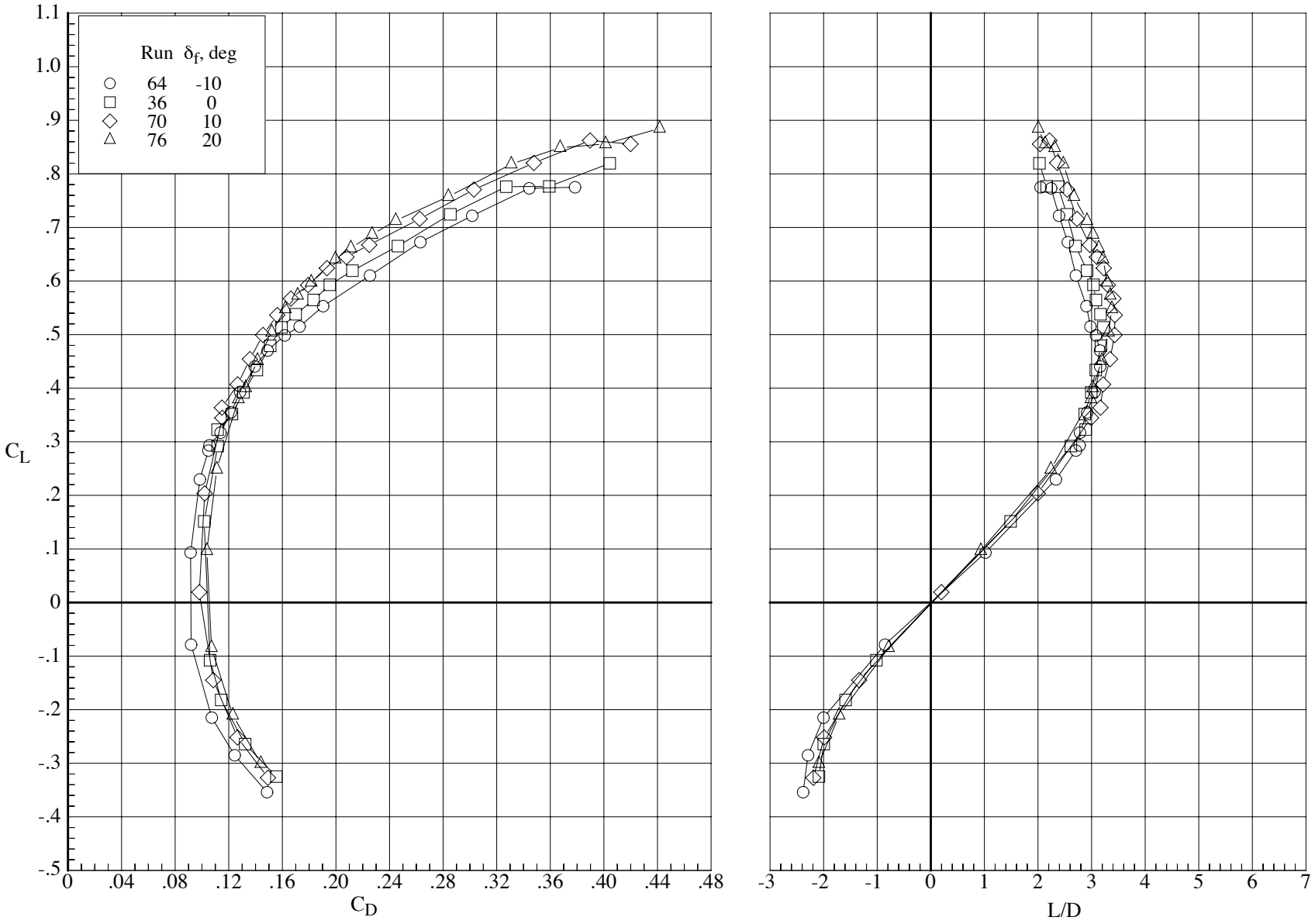

(b) Drag coefficient and lift-drag ratio.

Figure 63. Continued.

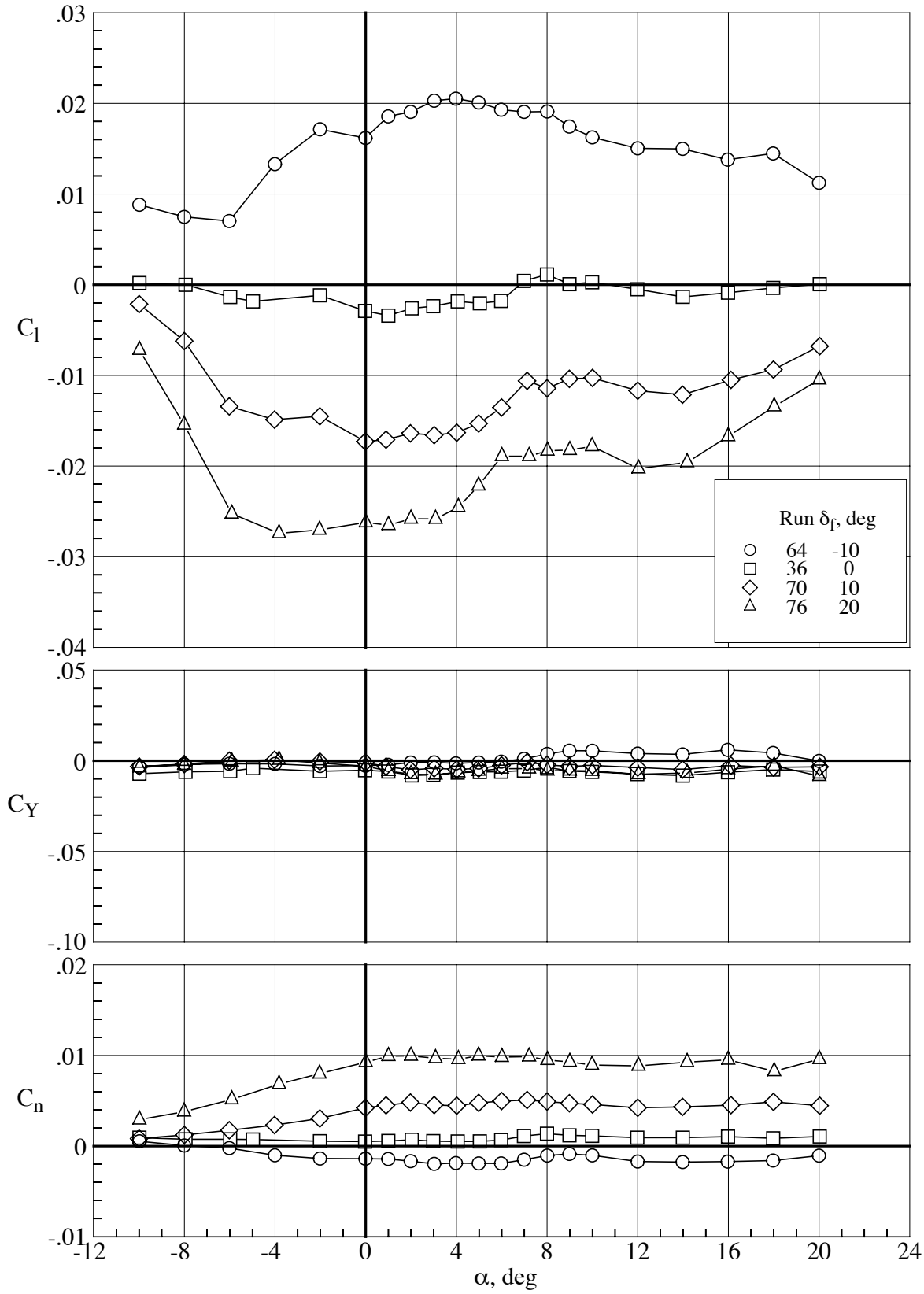

(c) Lateral-directional coefficients.

Figure 63. Concluded.

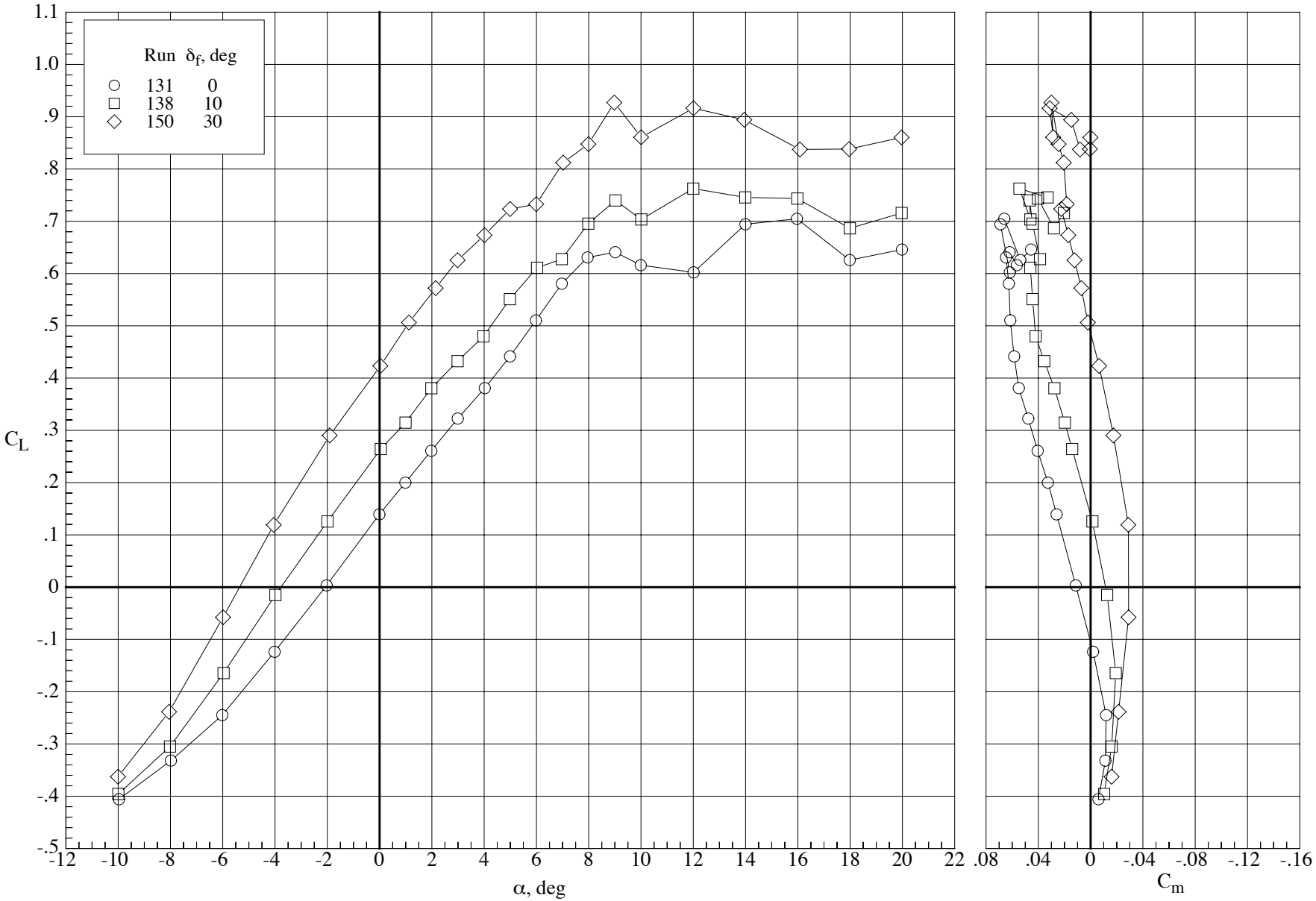

(a) Lift and pitching-moment coefficients.

Figure 64. Effect of wing trailing edge flap deflection on the longitudinal aerodynamic characteristics of the model with the MA-SF-1 wing at a Reynolds number of 40,000 and a Mach number of 0.50. $\delta_h = 0°$.

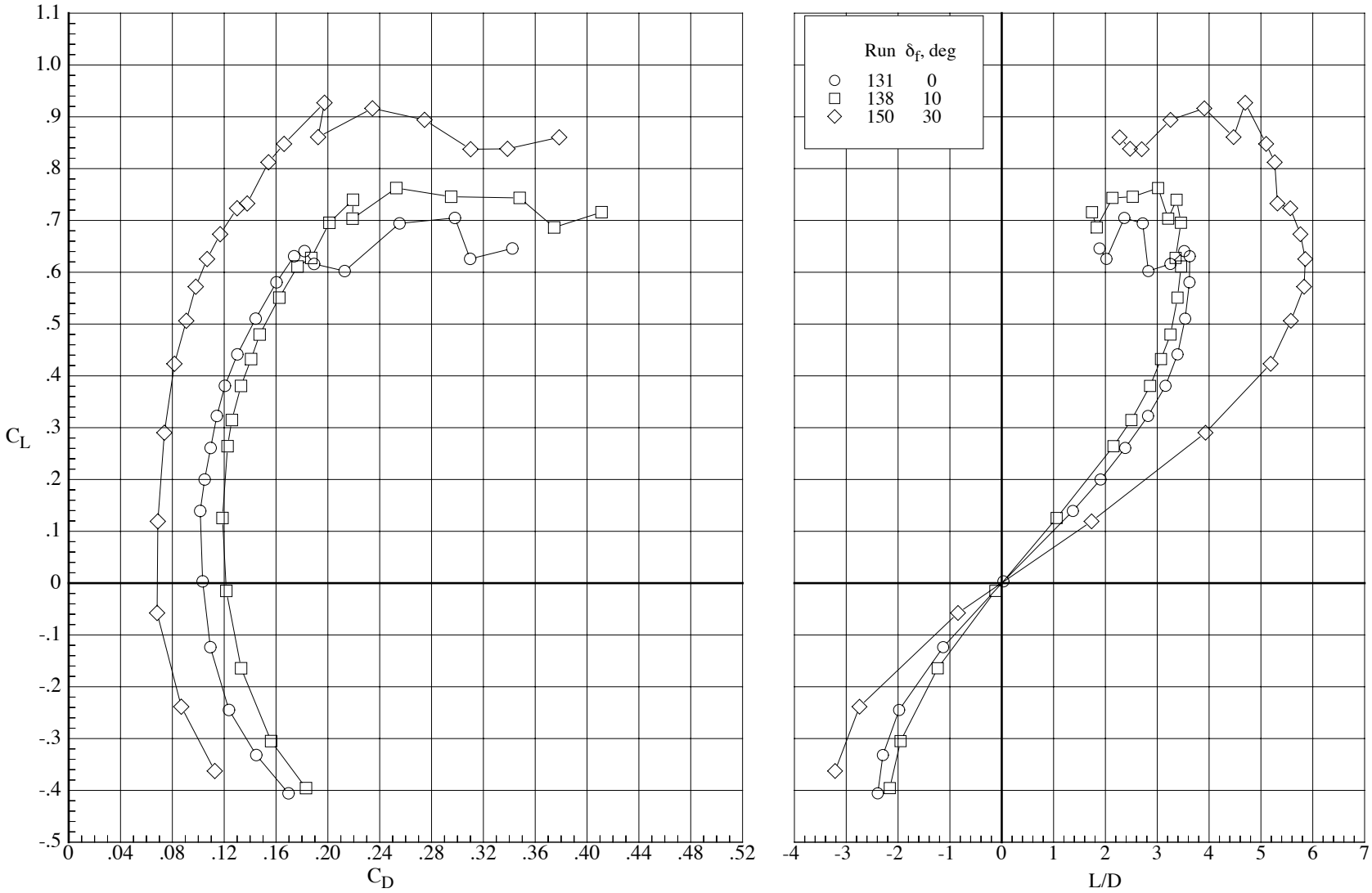

(b) Drag coefficient and lift-drag ratio.

Figure 64. Concluded.

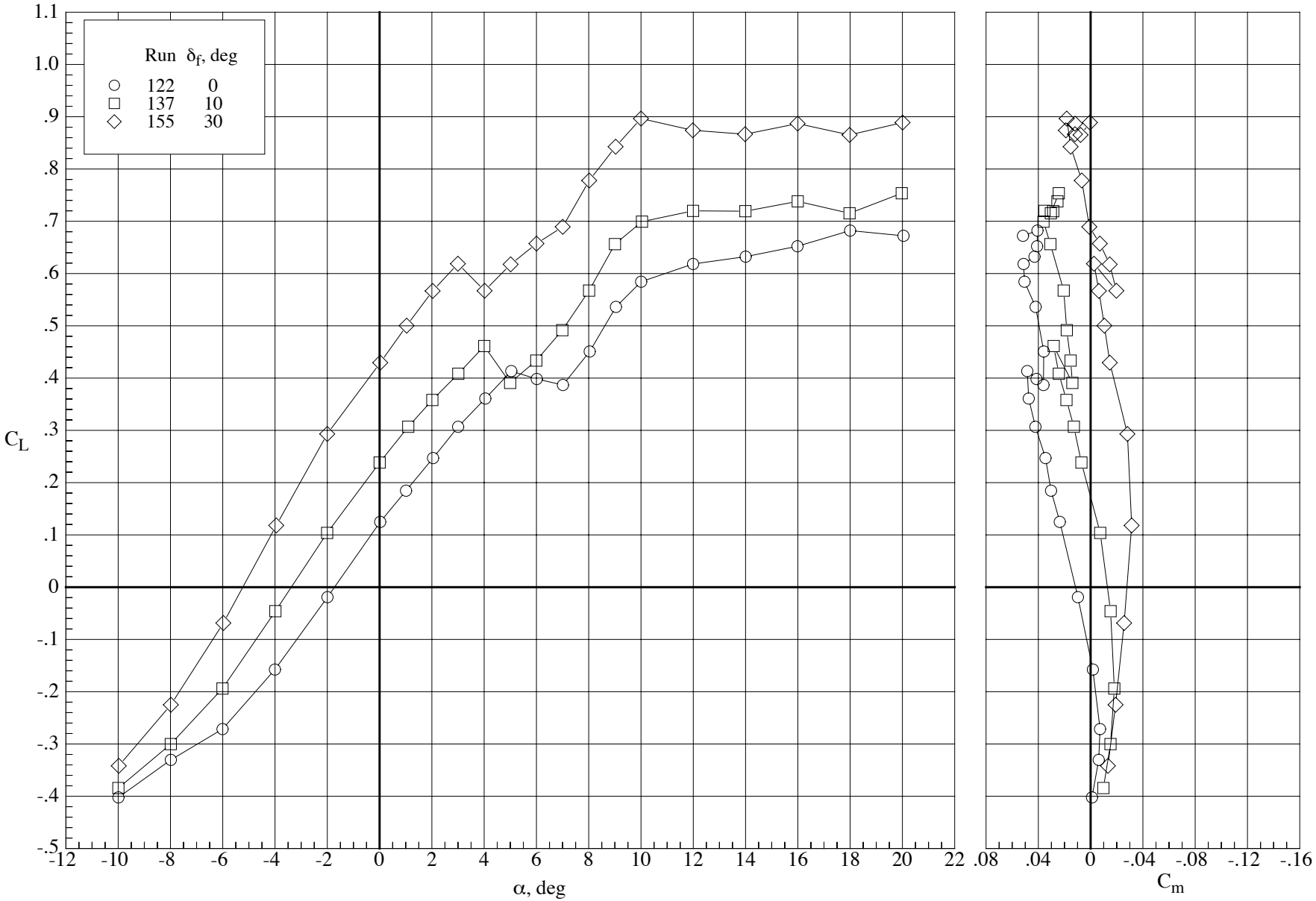

(a) Lift and pitching-moment coefficients.

Figure 65. Effect of wing trailing edge flap deflection on the longitudinal aerodynamic characteristics of the model with the MA-SF-1 wing at a Reynolds number of 40,000 and a Mach number of 0.65. $\delta_h = 0°$.

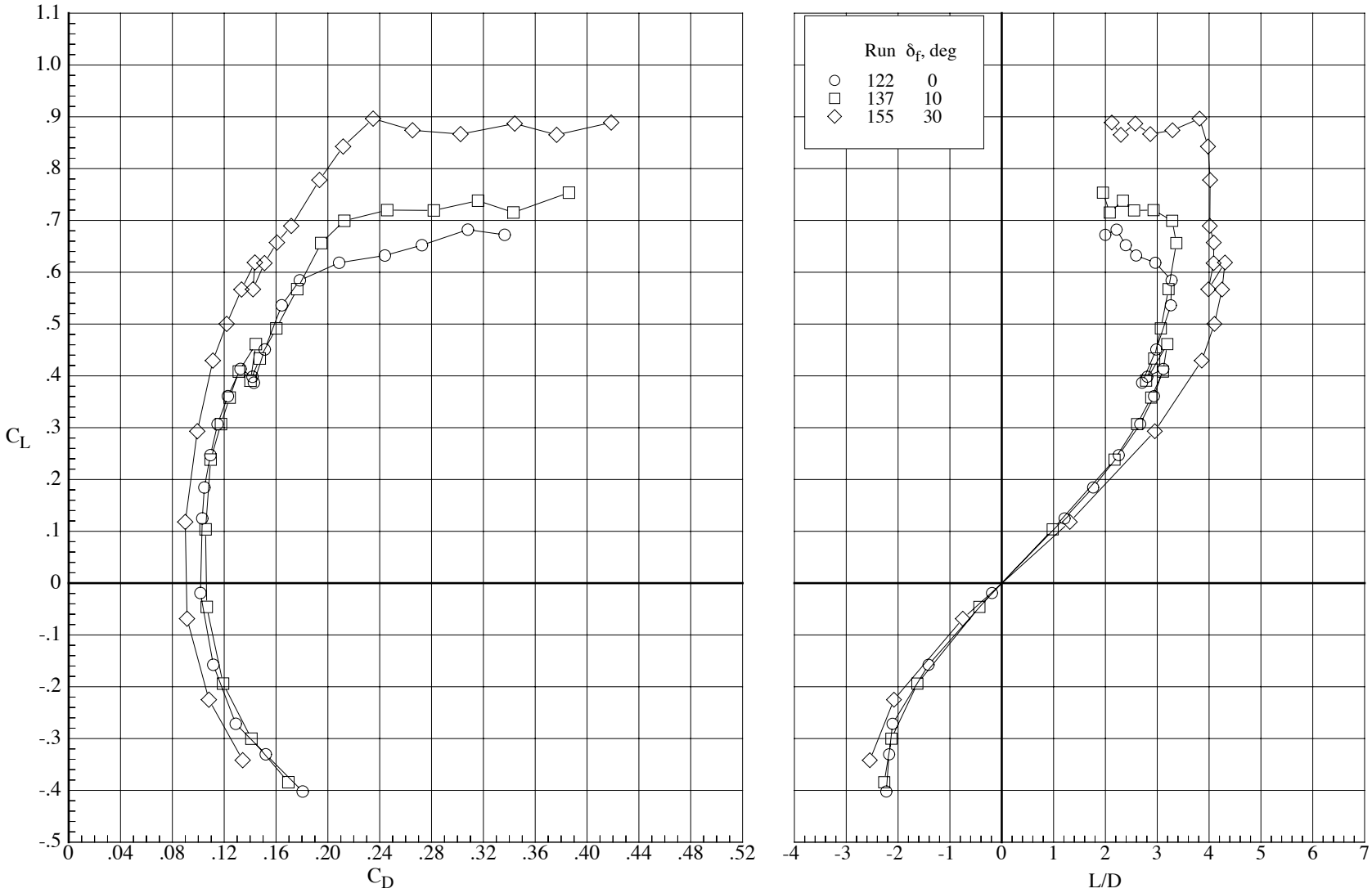

(b) Drag coefficient and lift-drag ratio.

Figure 65. Concluded.

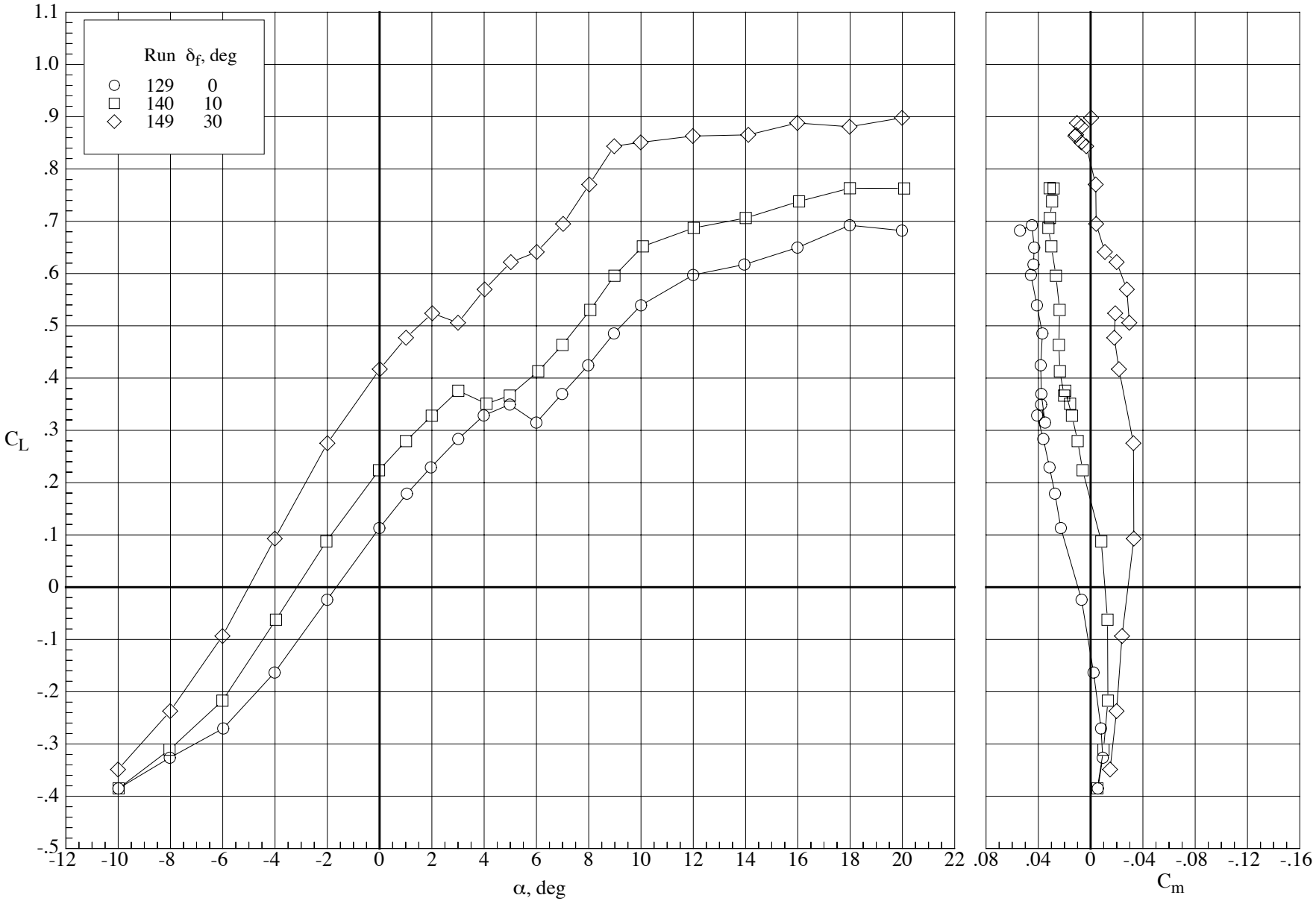

(a) Lift and pitching-moment coefficients.

Figure 66. Effect of wing trailing edge flap deflection on the longitudinal aerodynamic characteristics of the model with the MA-SF-1 wing at a Reynolds number of 40,000 and a Mach number of 0.70. $\delta_h = 0°$.

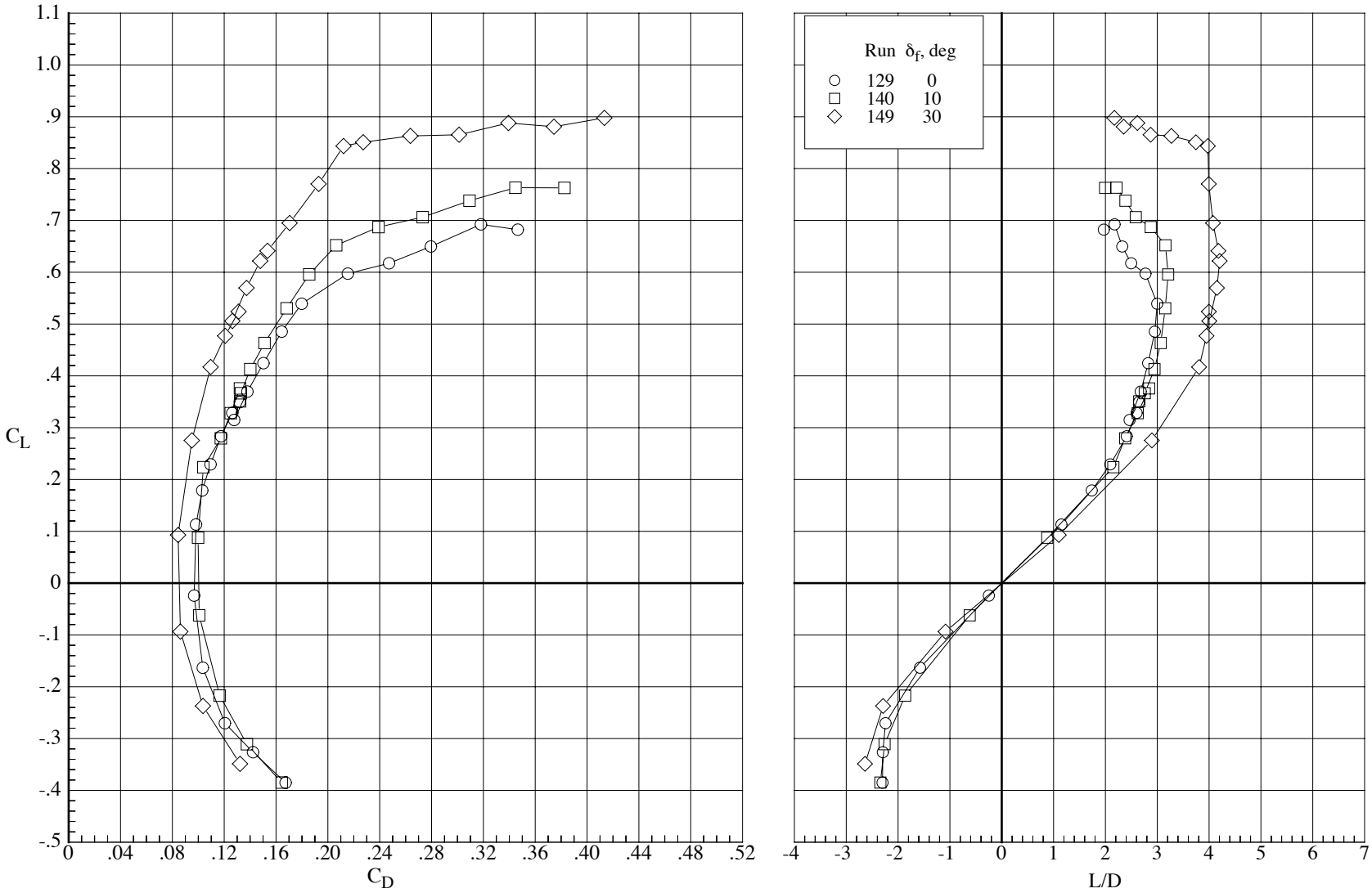

(b) Drag coefficient and lift-drag ratio.

Figure 66. Concluded.

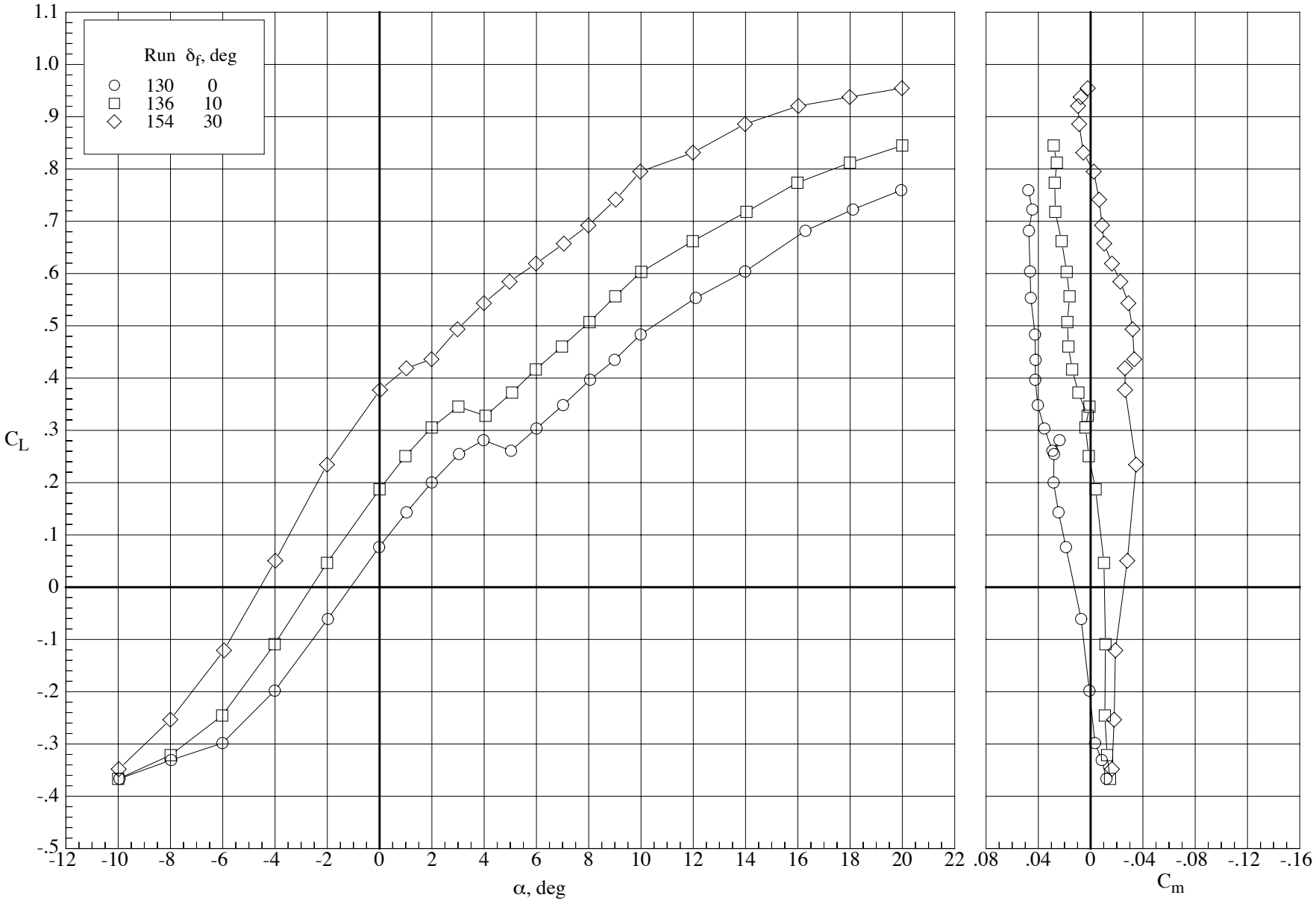

(a) Lift and pitching-moment coefficients.

Figure 67. Effect of wing trailing edge flap deflection on the longitudinal aerodynamic characteristics of the model with the MA-SF-1 wing at a Reynolds number of 40,000 and a Mach number of 0.80. $\delta_h = 0°$.

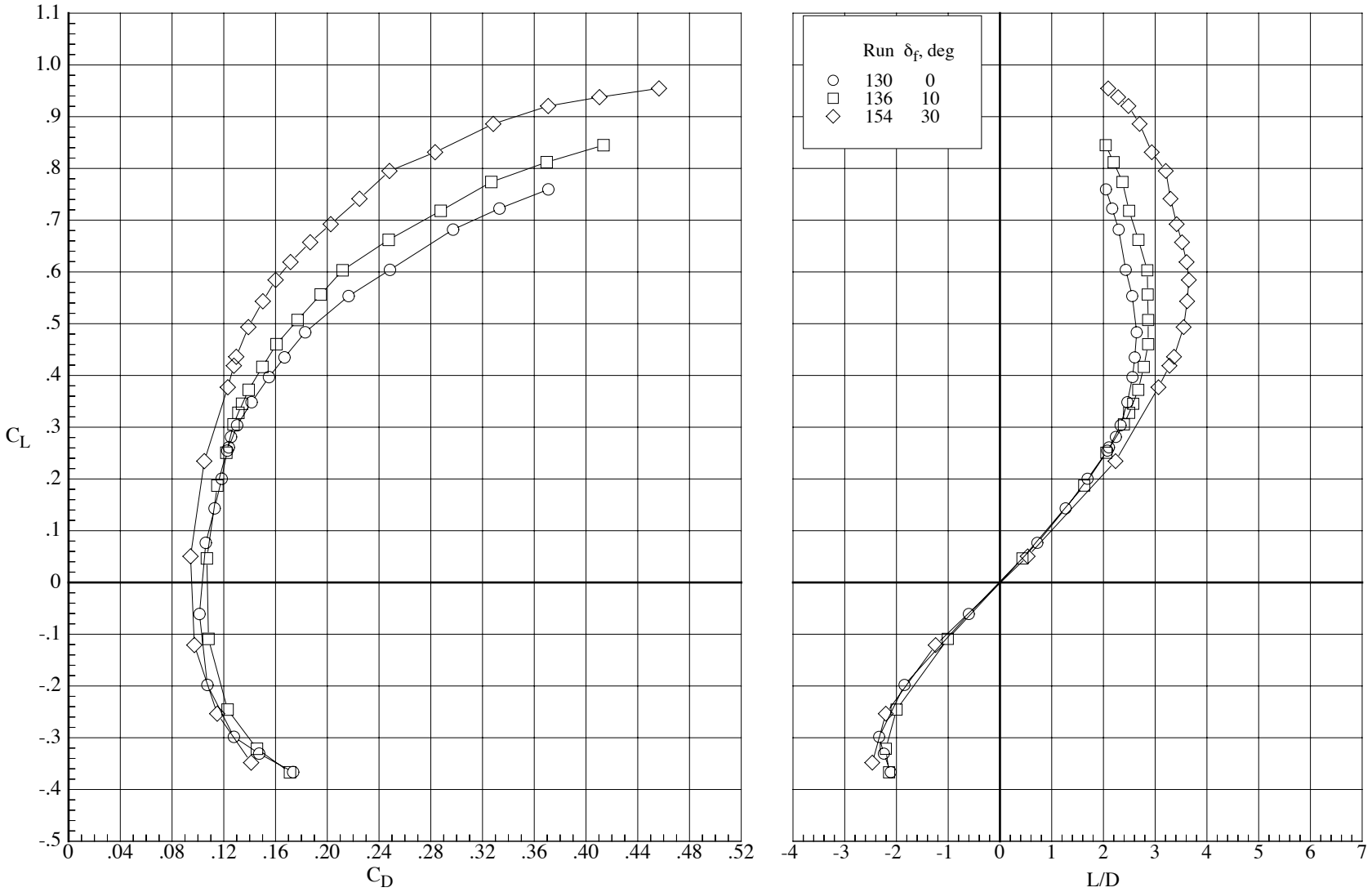

(b) Drag coefficient and lift-drag ratio.

Figure 67. Concluded.

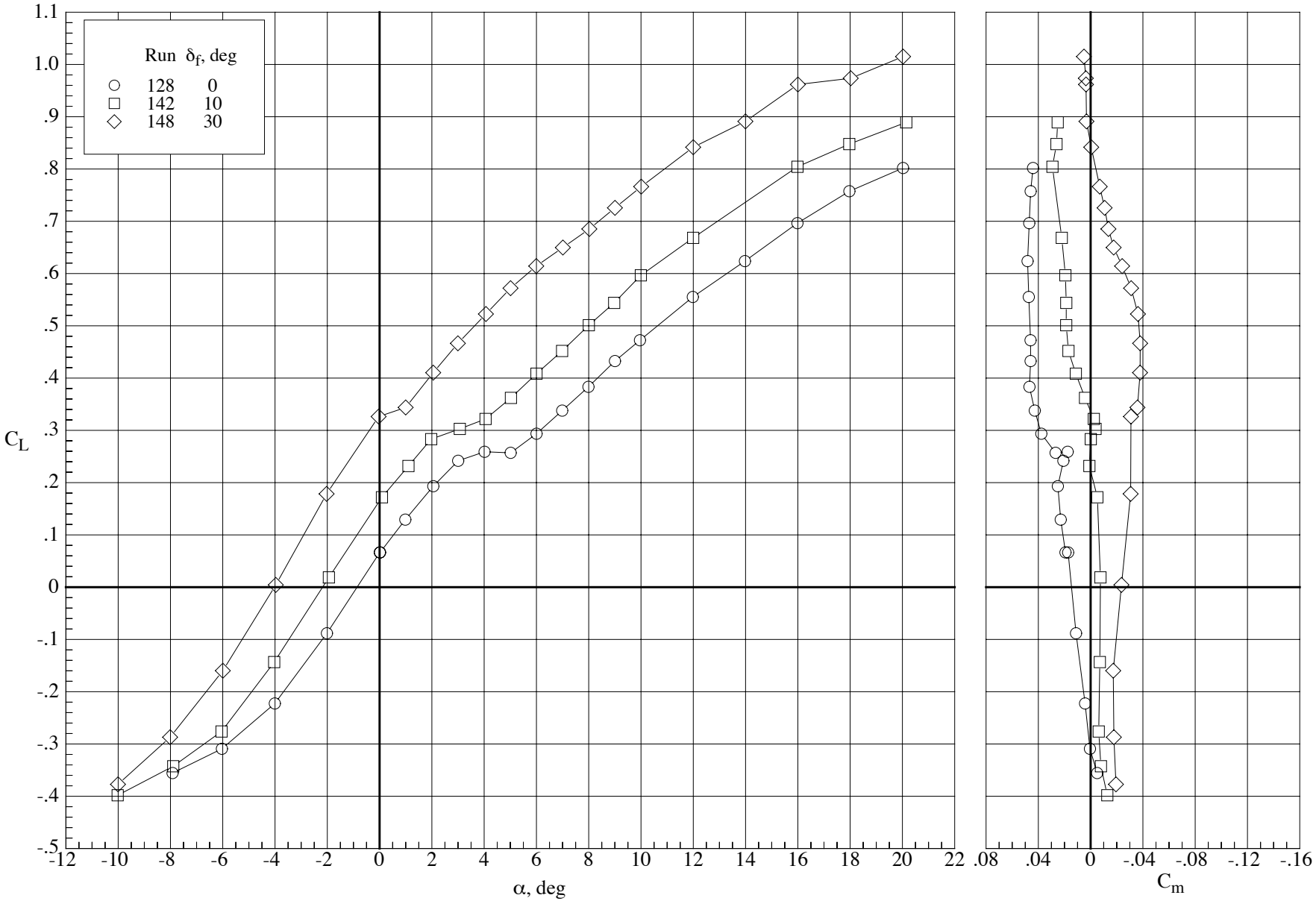

(a) Lift and pitching-moment coefficients.

Figure 68. Effect of wing trailing edge flap deflection on the longitudinal aerodynamic characteristics of the model with the MA-SF-1 wing at a Reynolds number of 40,000 and a Mach number of 0.85. $\delta_h = 0°$.

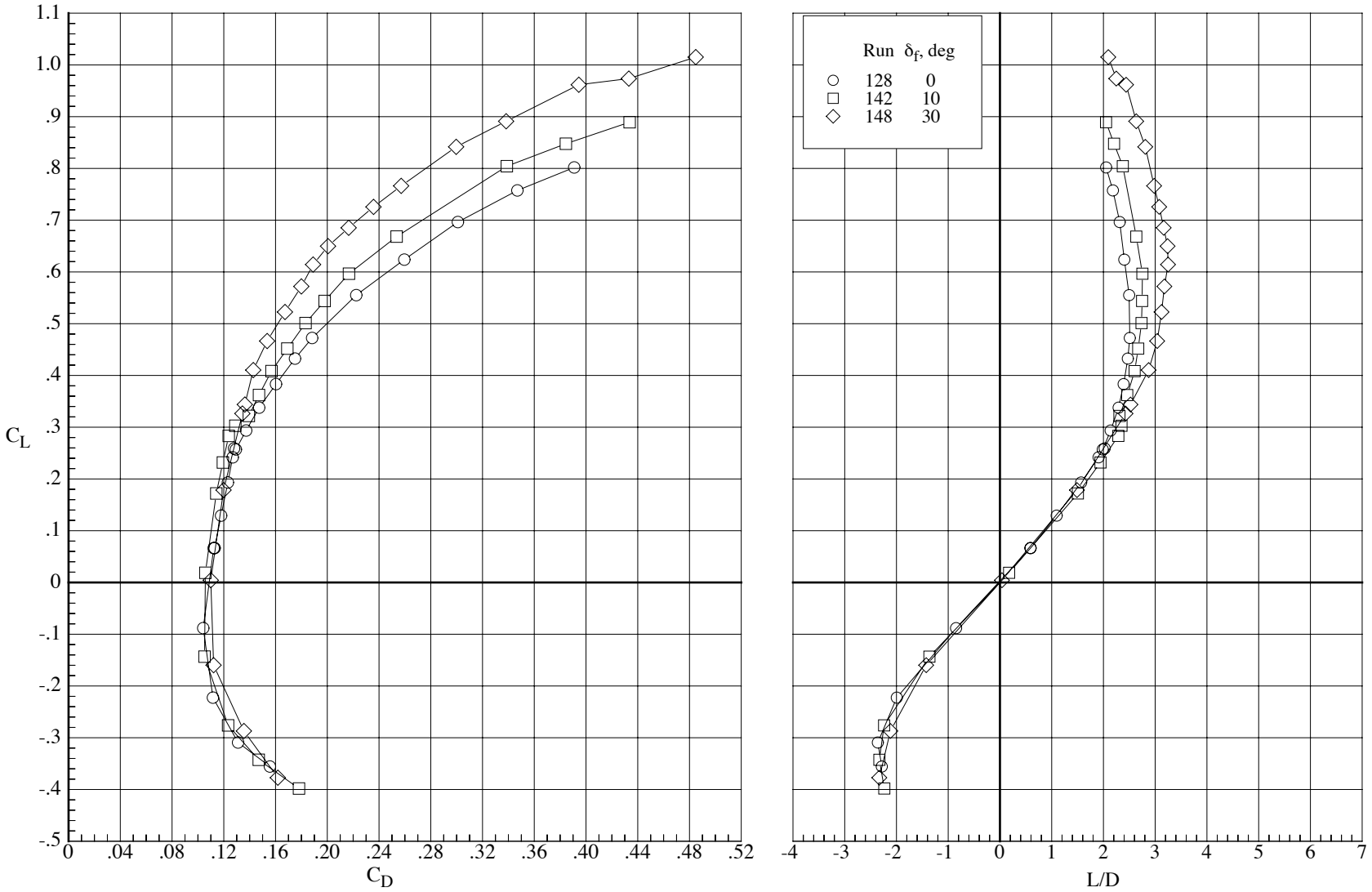

(b) Drag coefficient and lift-drag ratio.

Figure 68. Concluded.

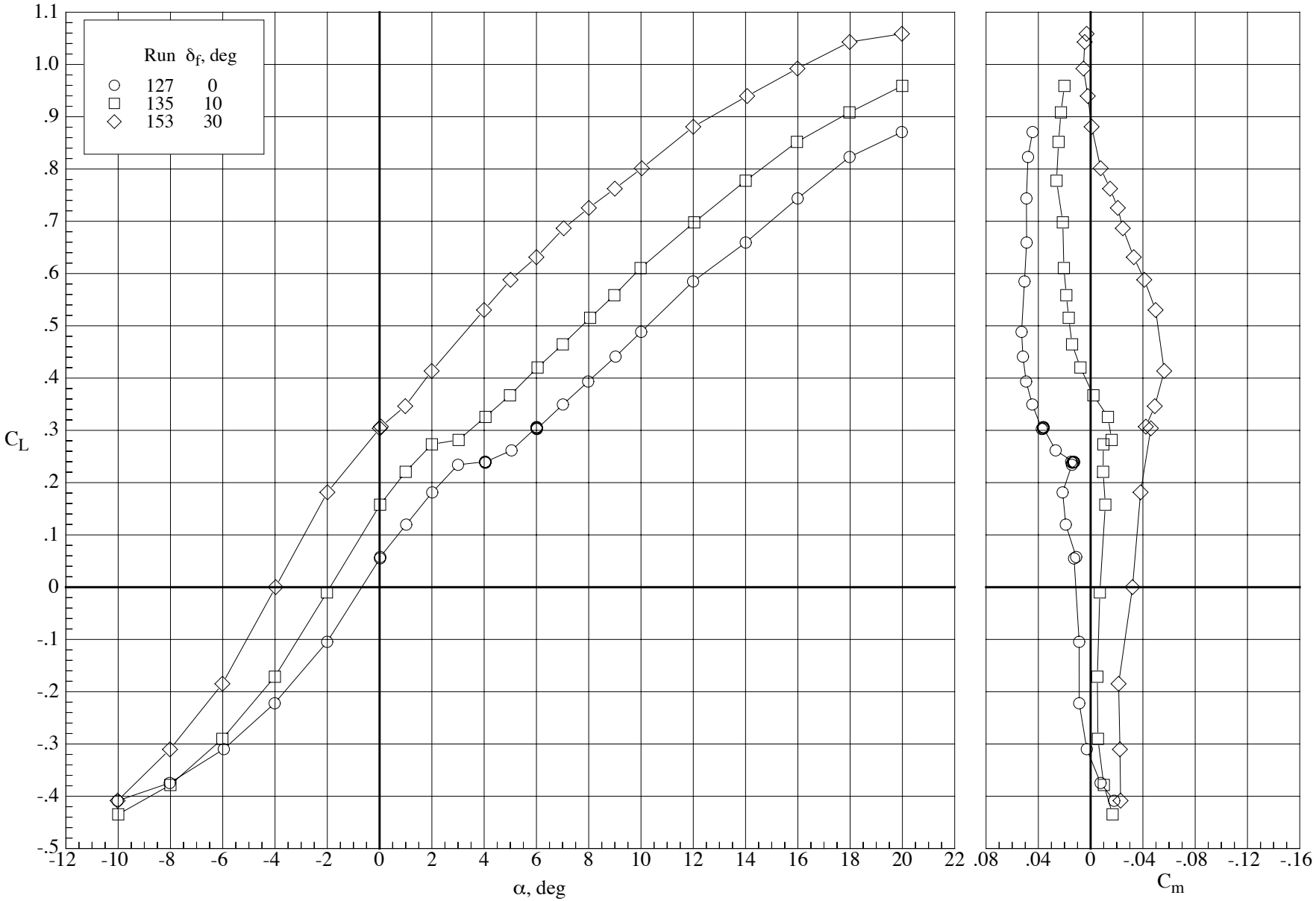

(a) Lift and pitching-moment coefficients.

Figure 69. Effect of wing trailing edge flap deflection on the longitudinal aerodynamic characteristics of the model with the MA-SF-1 wing at a Reynolds number of 40,000 and a Mach number of 0.90. $\delta_h = 0°$.

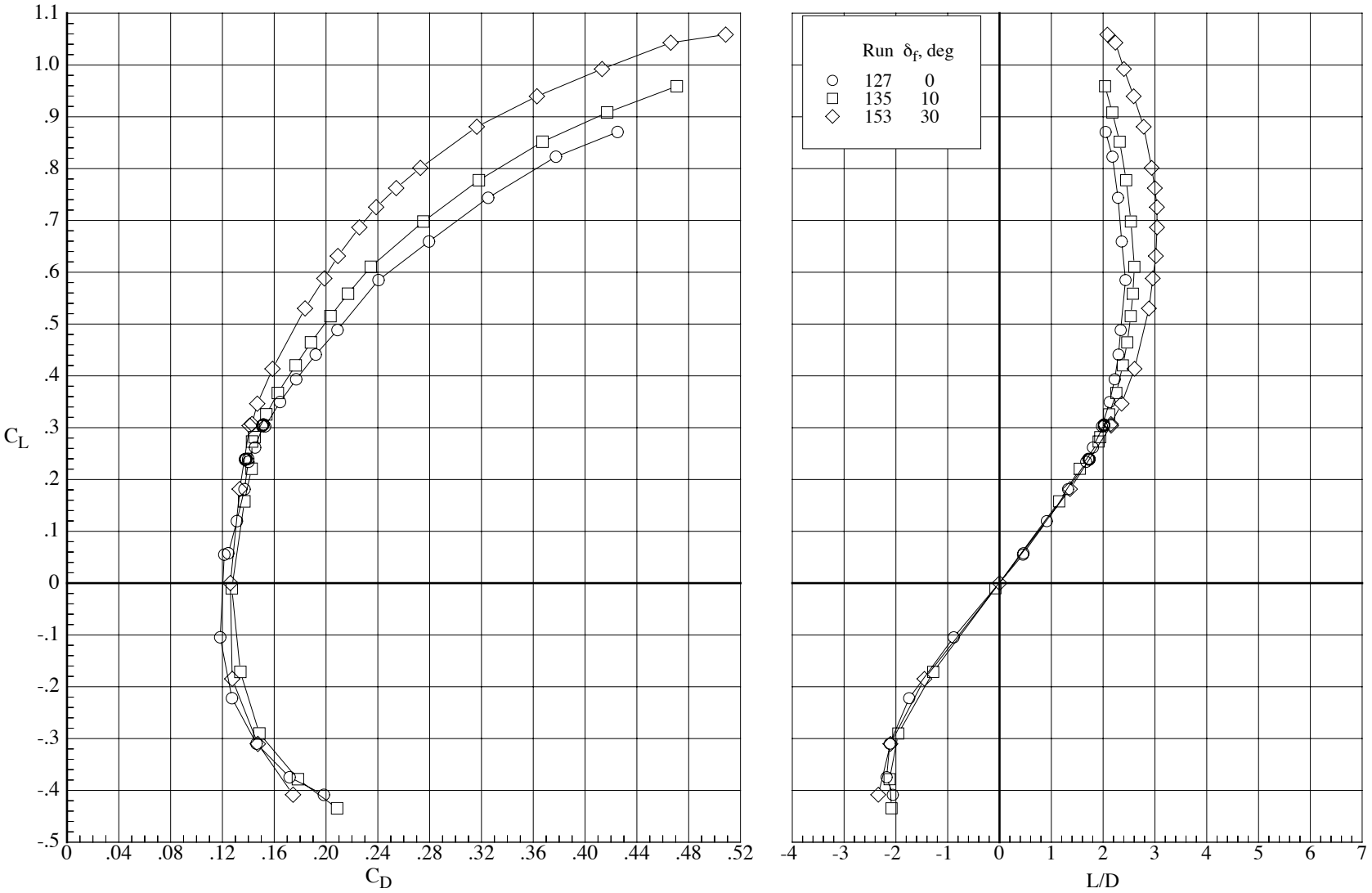

(b) Drag coefficient and lift-drag ratio.

Figure 69. Concluded.

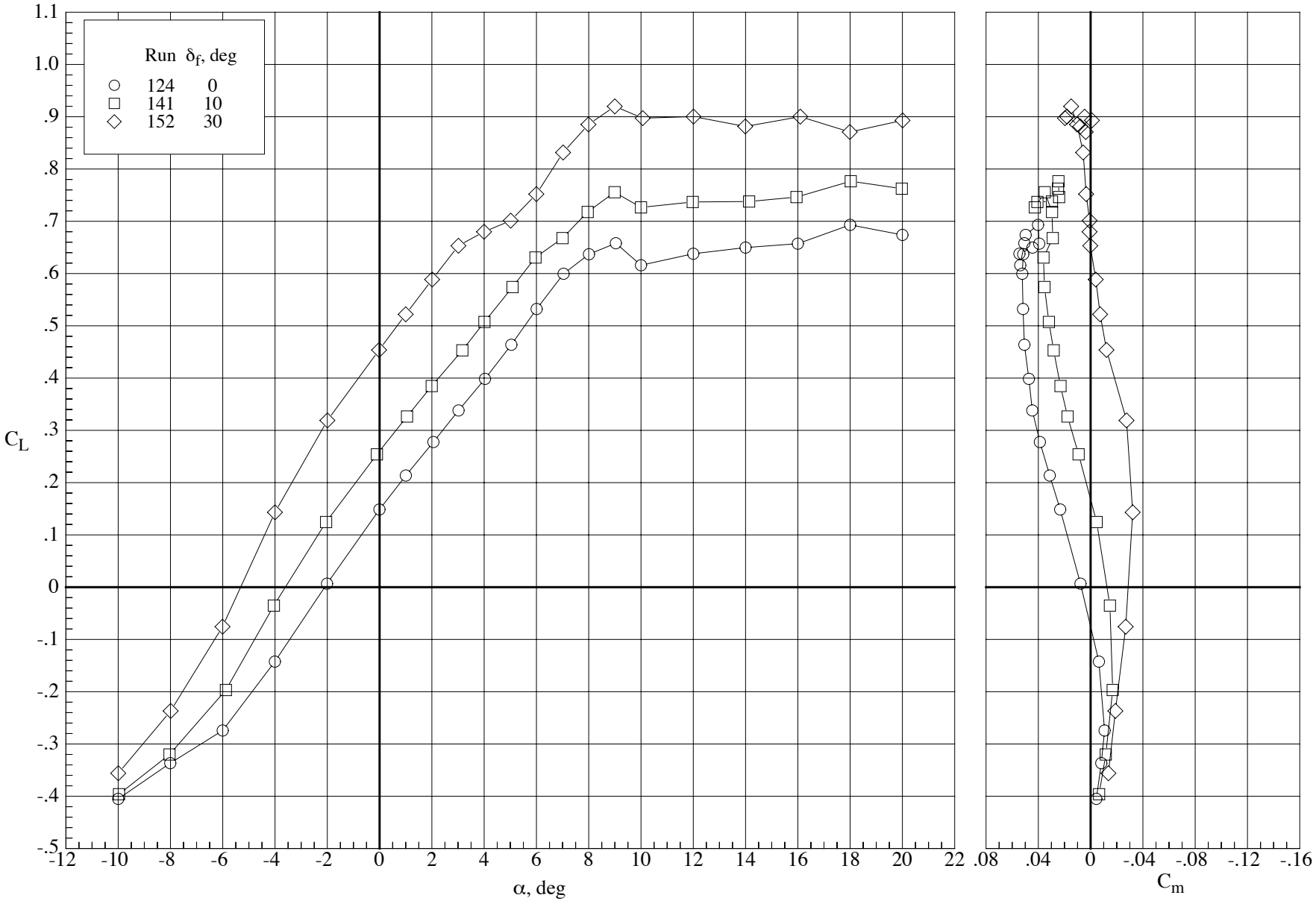

(a) Lift and pitching-moment coefficients.

Figure 70. Effect of wing trailing edge flap deflection on the longitudinal aerodynamic characteristics of the model with the MA-SF-1 wing at a Reynolds number of 60,000 and a Mach number of 0.65. $\delta_h = 0°$.

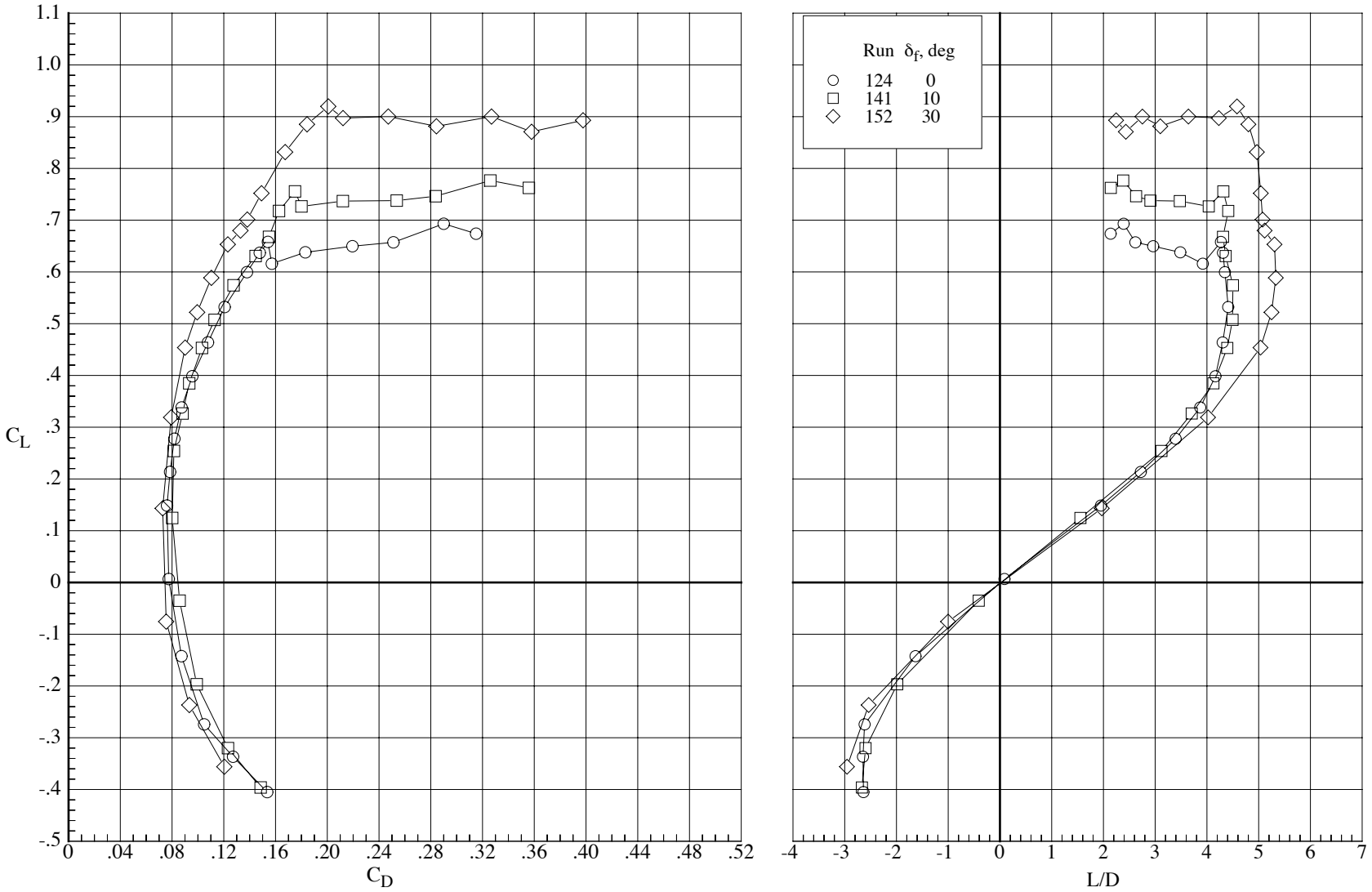

(b) Drag coefficient and lift-drag ratio.

Figure 70. Concluded.

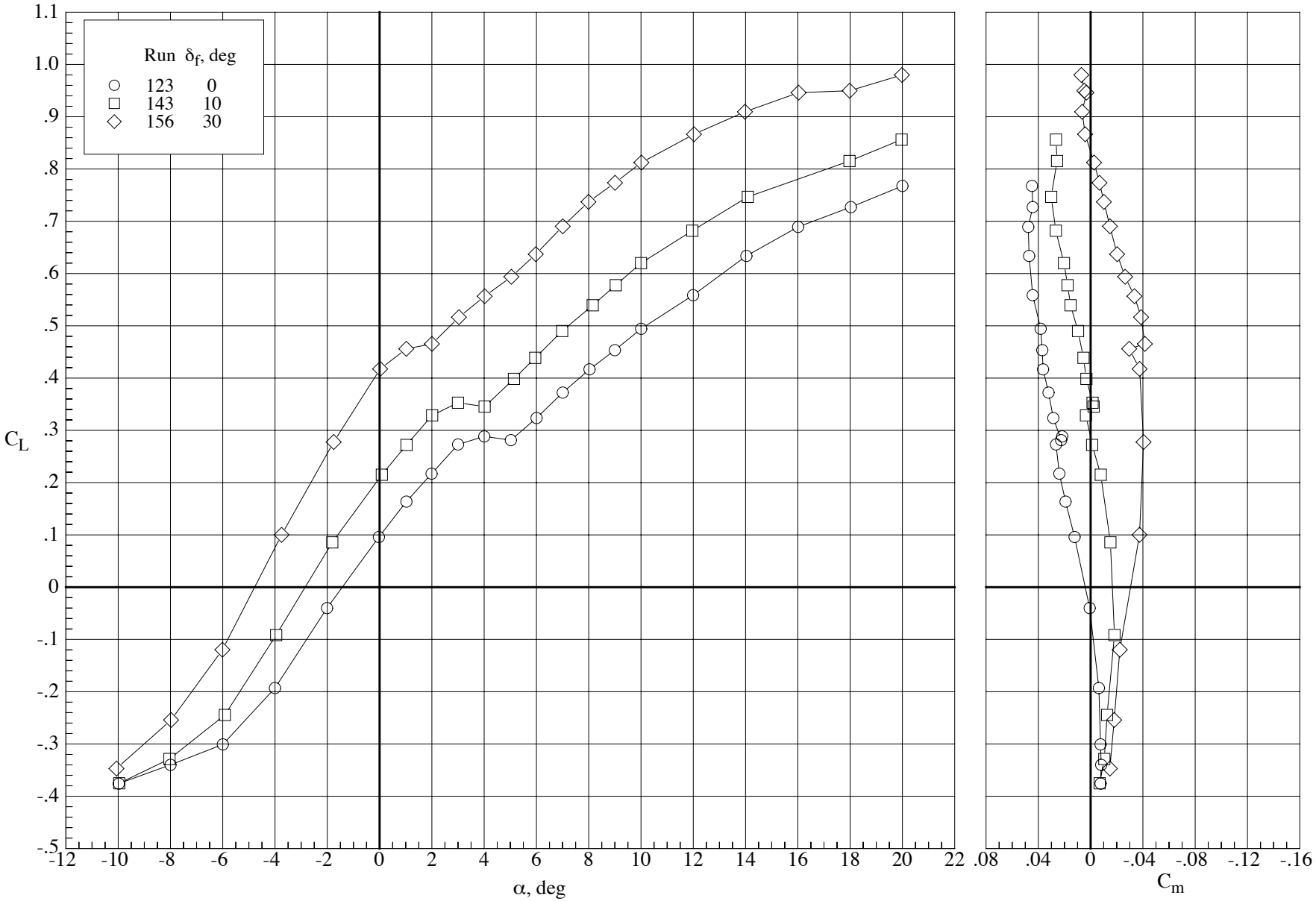

(a) Lift and pitching-moment coefficients.

Figure 71. Effect of wing trailing edge flap deflection on the longitudinal aerodynamic characteristics of the model with the MA-SF-1 wing at a Reynolds number of 60,000 and a Mach number of 0.80. $\delta_h = 0°$.

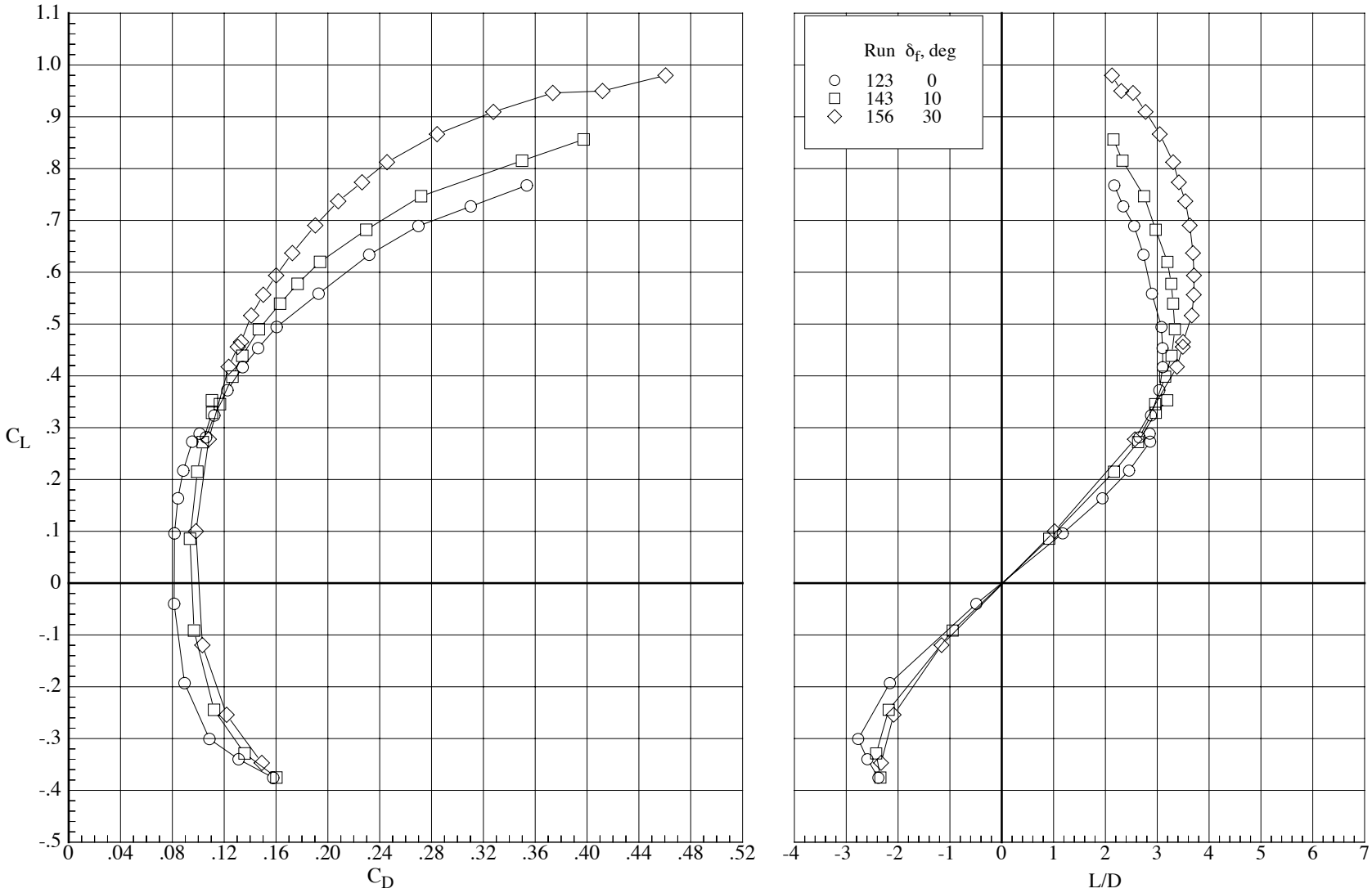

(b) Drag coefficient and lift-drag ratio.

Figure 71. Concluded.

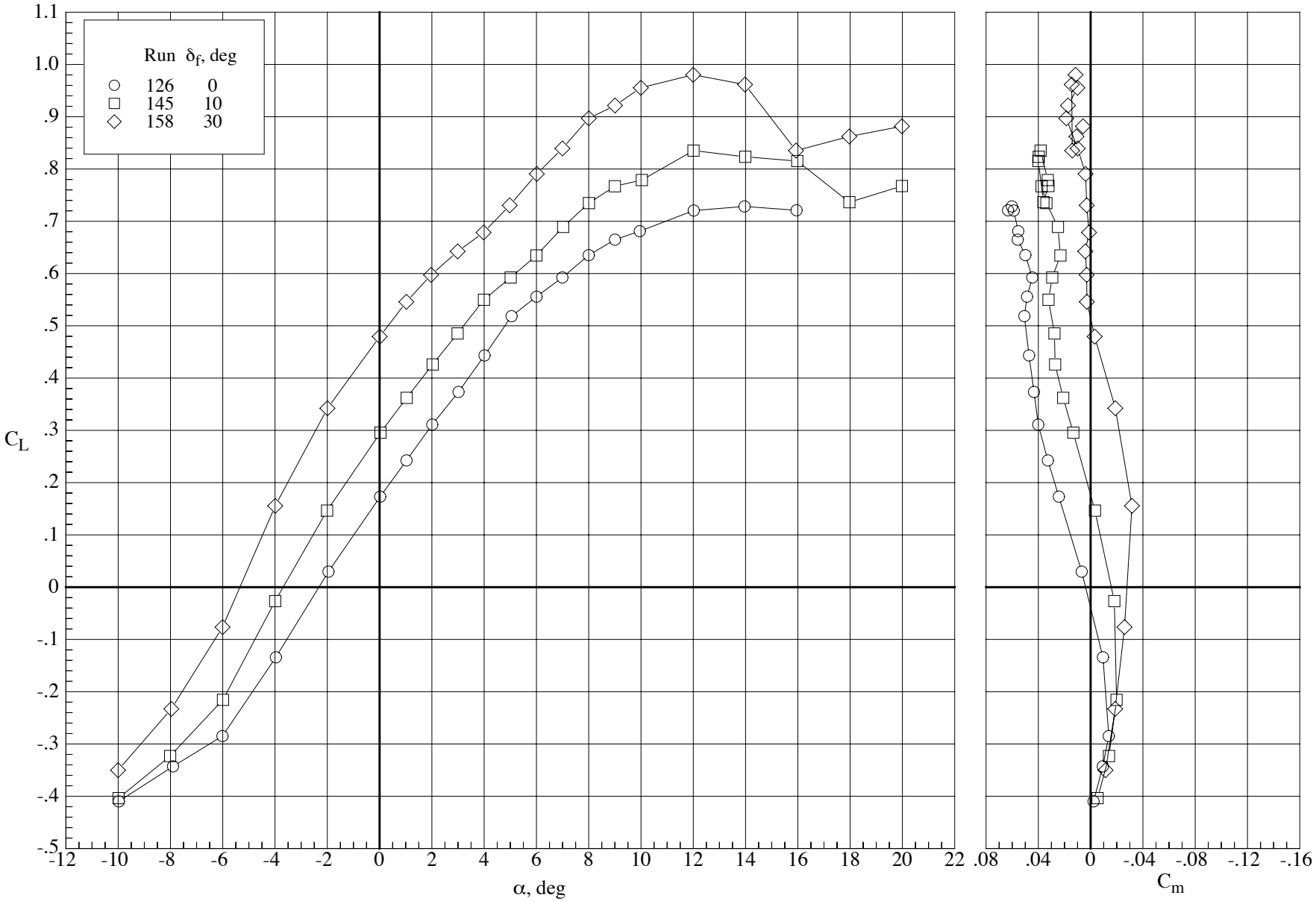

(a) Lift and pitching-moment coefficients.

Figure 72. Effect of wing trailing edge flap deflection on the longitudinal aerodynamic characteristics of the model with the MA-SF-1 wing at a Reynolds number of 100,000 and a Mach number of 0.65. $\delta_h = 0°$.

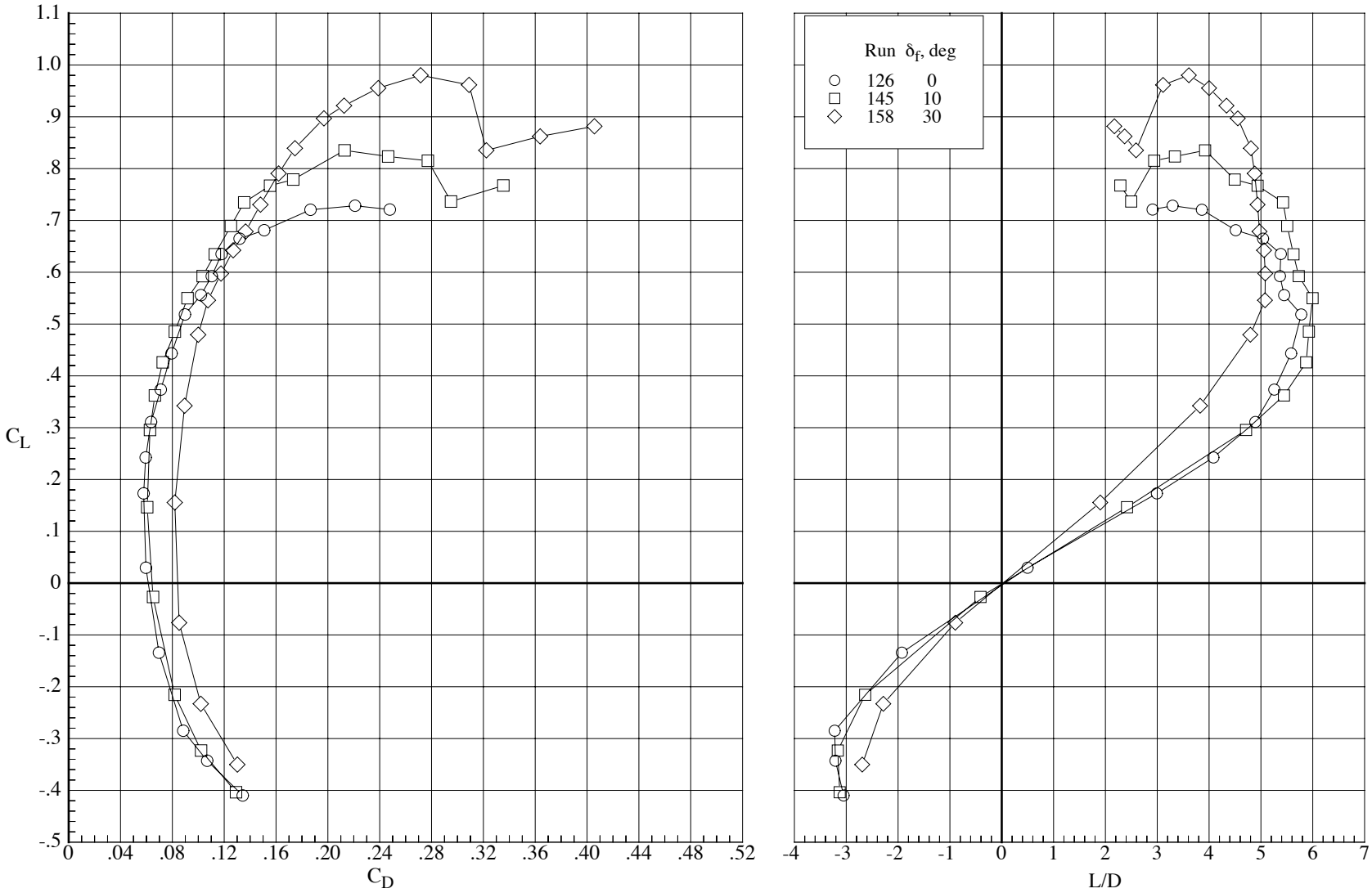

(b) Drag coefficient and lift-drag ratio.

Figure 72. Concluded.

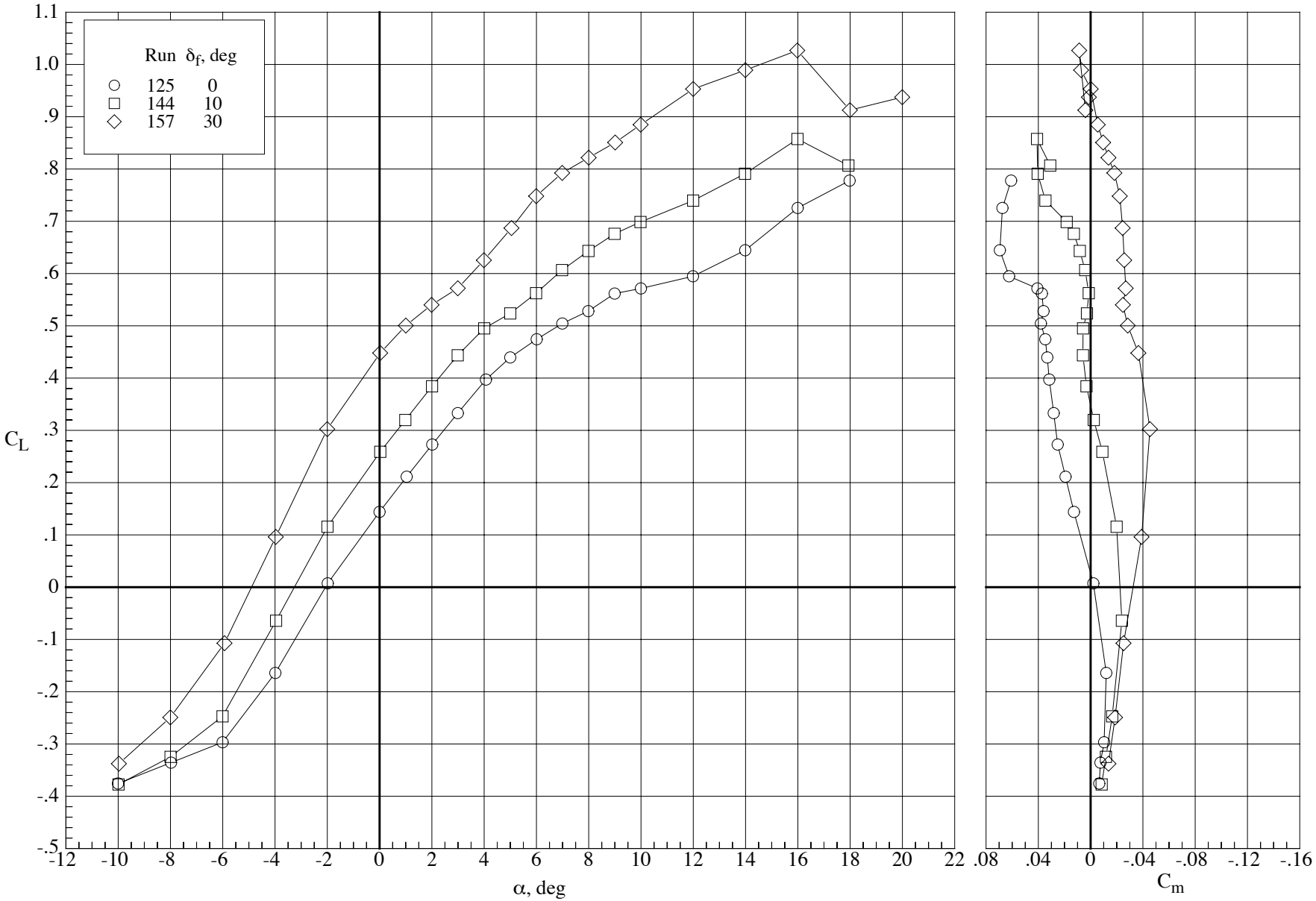

(a) Lift and pitching-moment coefficients.

Figure 73. Effect of wing trailing edge flap deflection on the longitudinal aerodynamic characteristics of the model with the MA-SF-1 wing at a Reynolds number of 100,000 and a Mach number of 0.80. $\delta_h = 0°$.

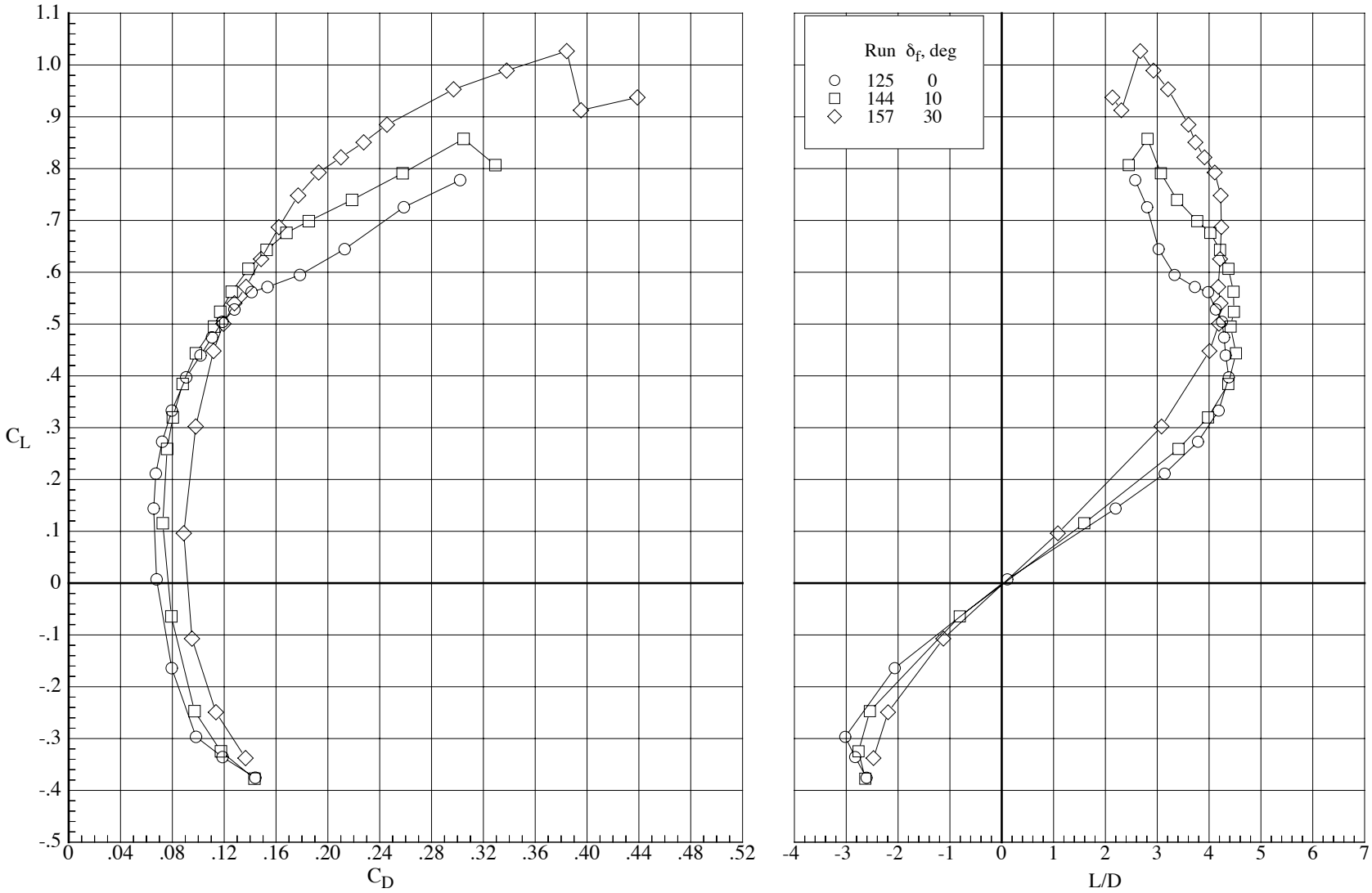

(b) Drag coefficient and lift-drag ratio.

Figure 73. Concluded.

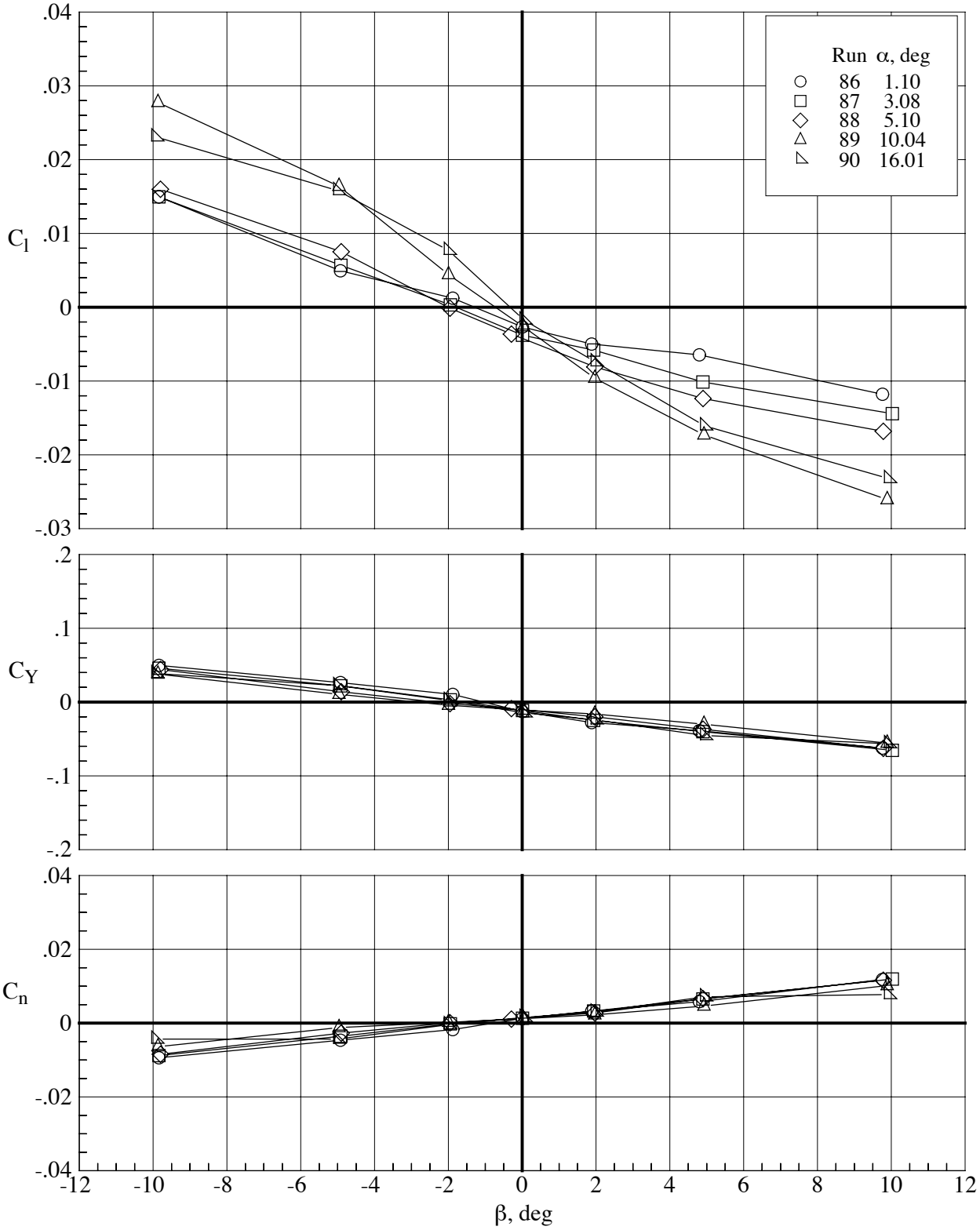

(a) Lateral-directional characteristics.

Figure 74. Aerodynamic characteristics of the model with the MA-SC-1 wing (bump on) at a Mach number of 0.65 and a Reynolds number of 40,000 at five angles of attack. $\delta_h = 0°$ and $\delta_f = 0°$.

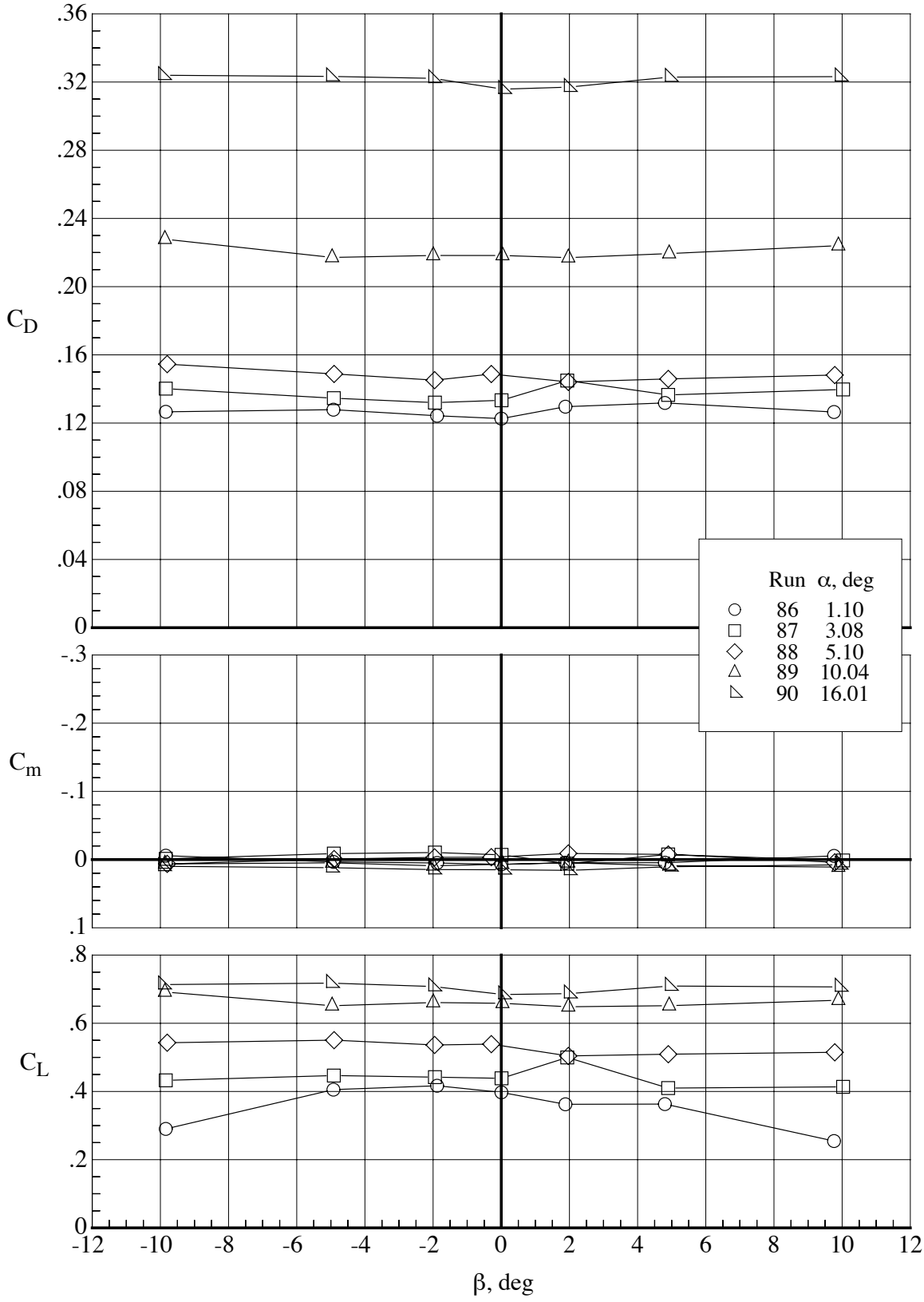

(b) Lift, drag, and pitching-moment coefficients.

Figure 74. Concluded.

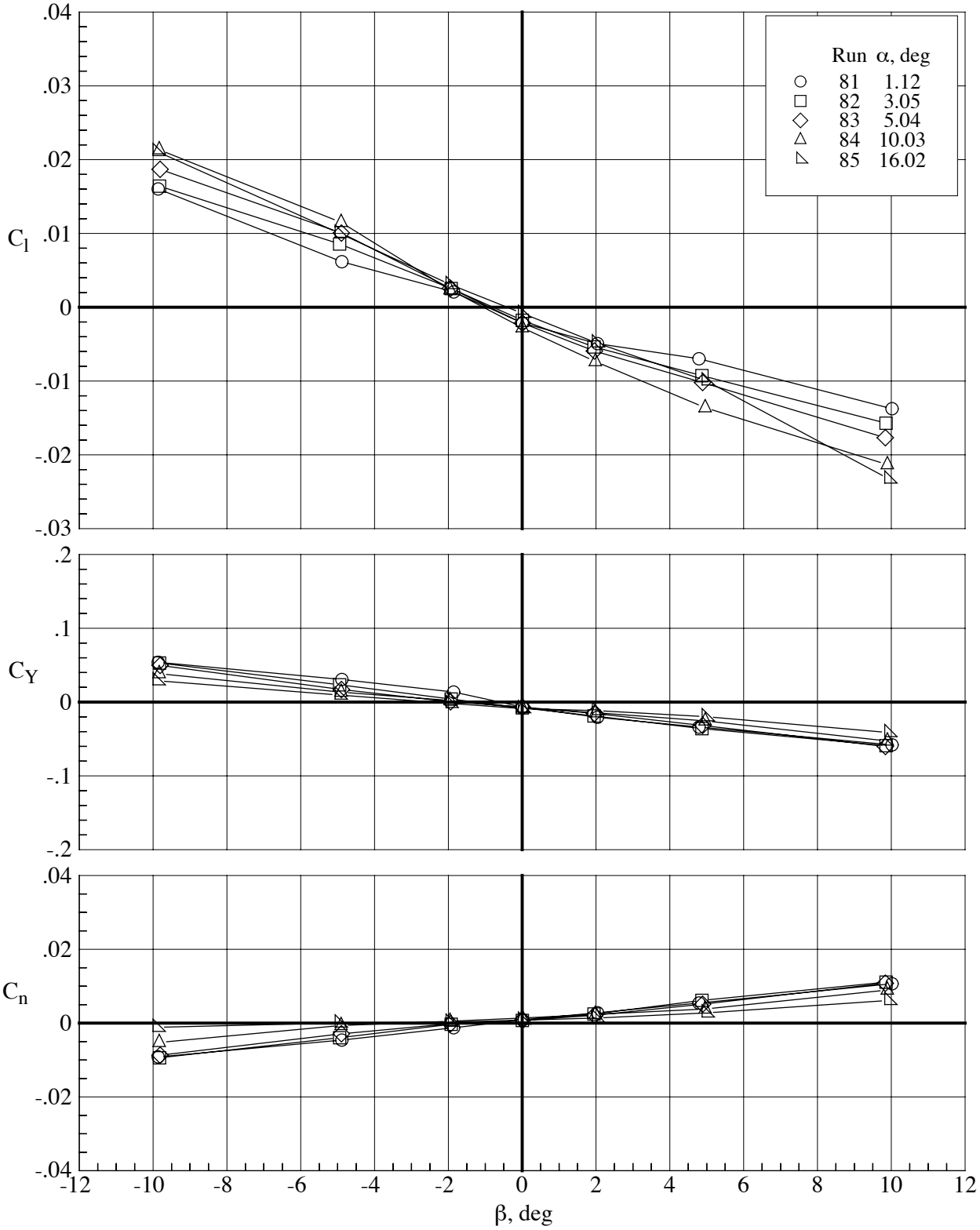

(a) Lateral-directional characteristics.

Figure 75. Aerodynamic characteristics of the model with the MA-SC-1 wing (bump on) at a Mach number of 0.80 and a Reynolds number of 40,000 at five angles of attack. $\delta_h = 0°$ and $\delta_f = 0°$.

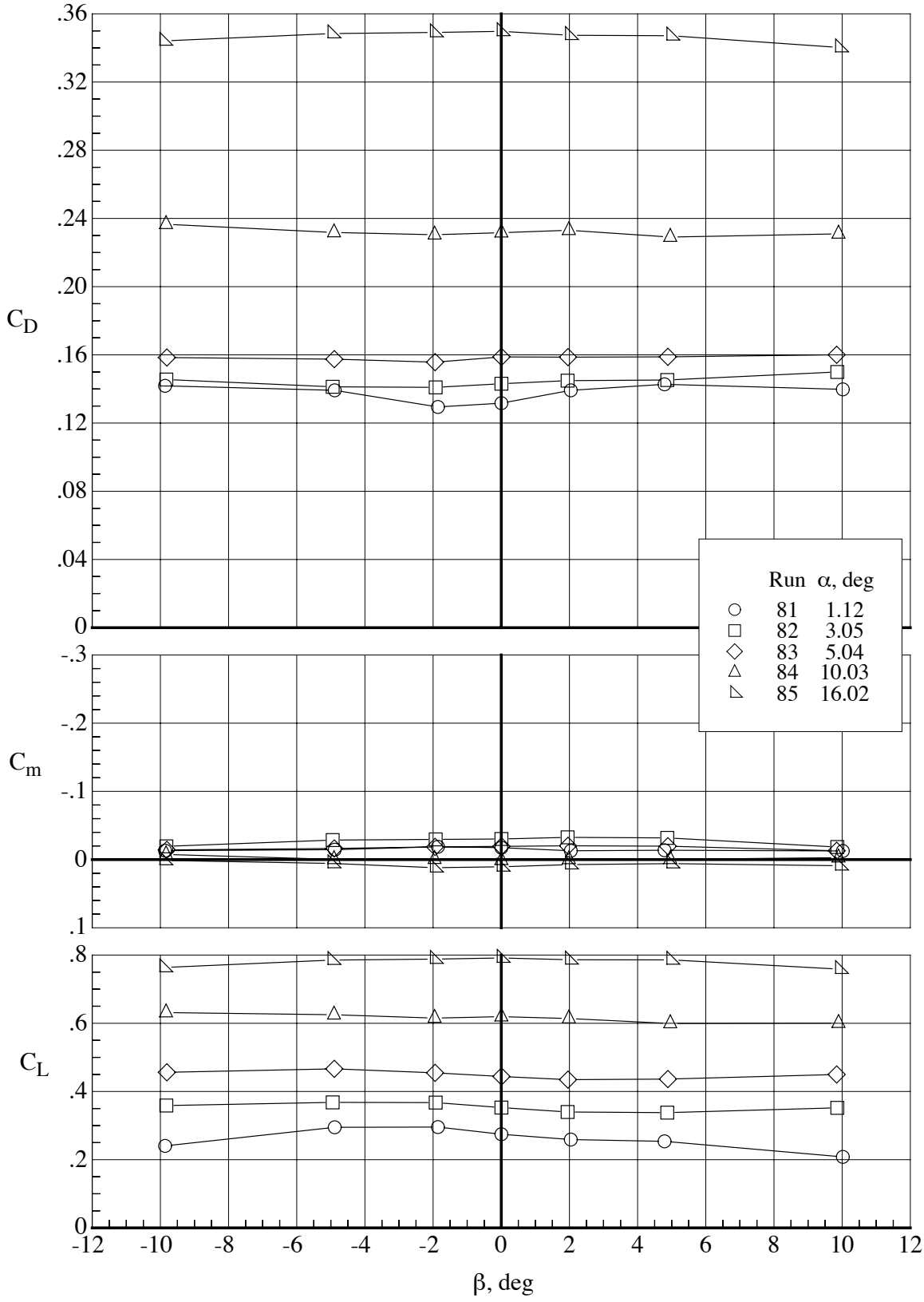

(b) Lift, drag, and pitching-moment coefficients.

Figure 75. Concluded.

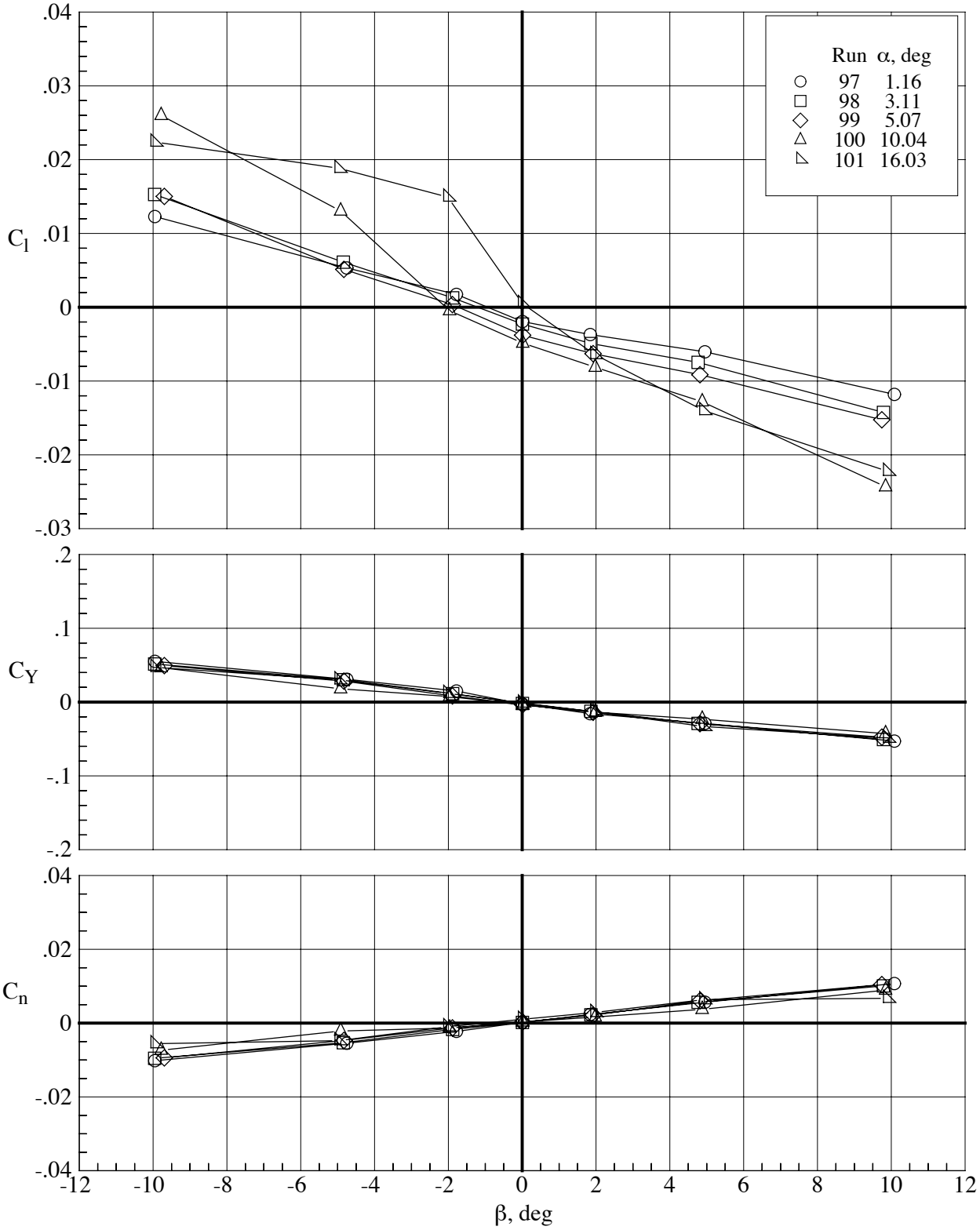

(a) Lateral-directional characteristics.

Figure 76. Aerodynamic characteristics of the model with the MA-SC-1 wing (bump on) at a Mach number of 0.65 and a Reynolds number of 60,000 at five angles of attack. $\delta_h = °$ and $\delta_f = 0°$.

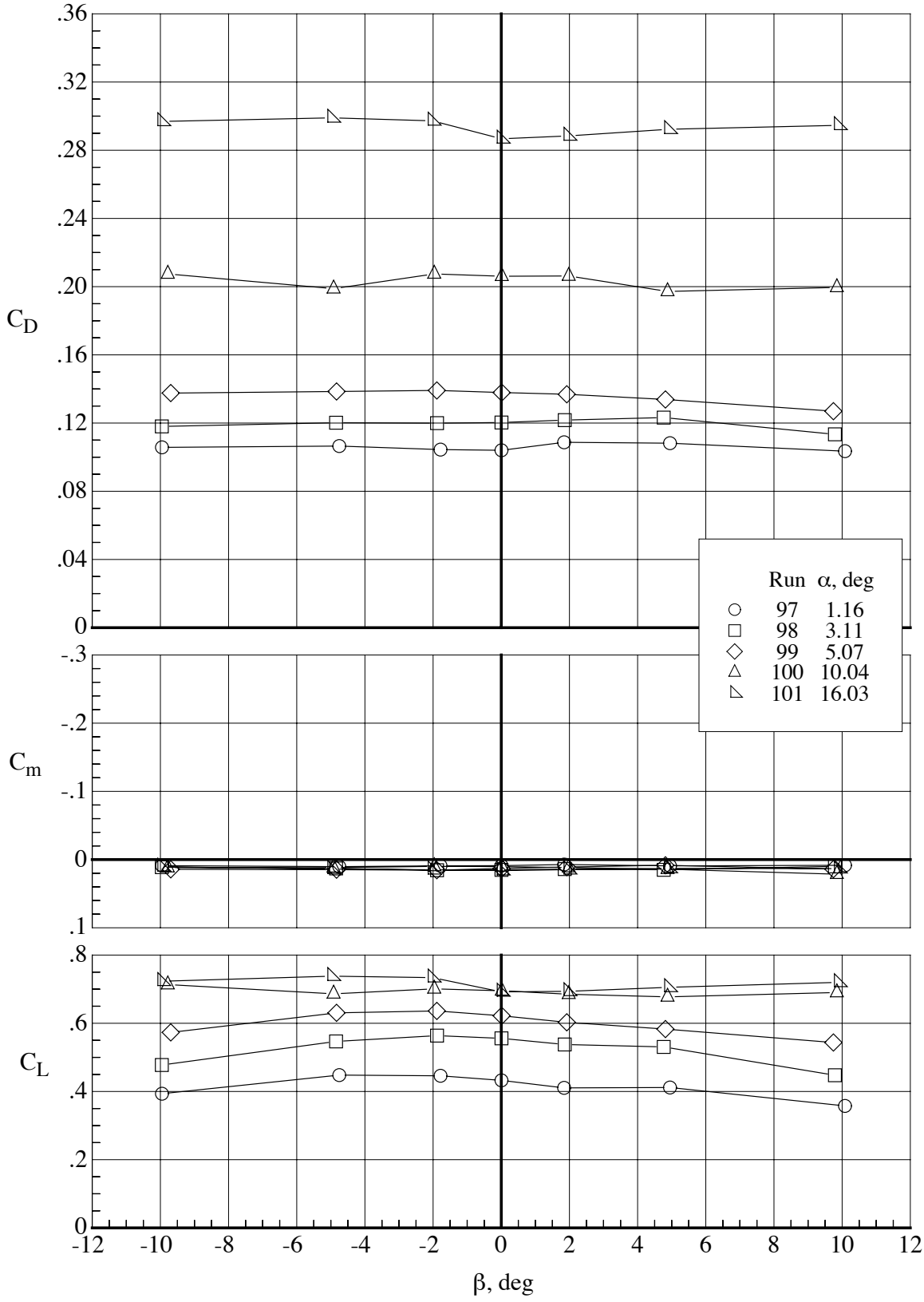

(b) Lift, drag, and pitching-moment coefficients.

Figure 76. Concluded.

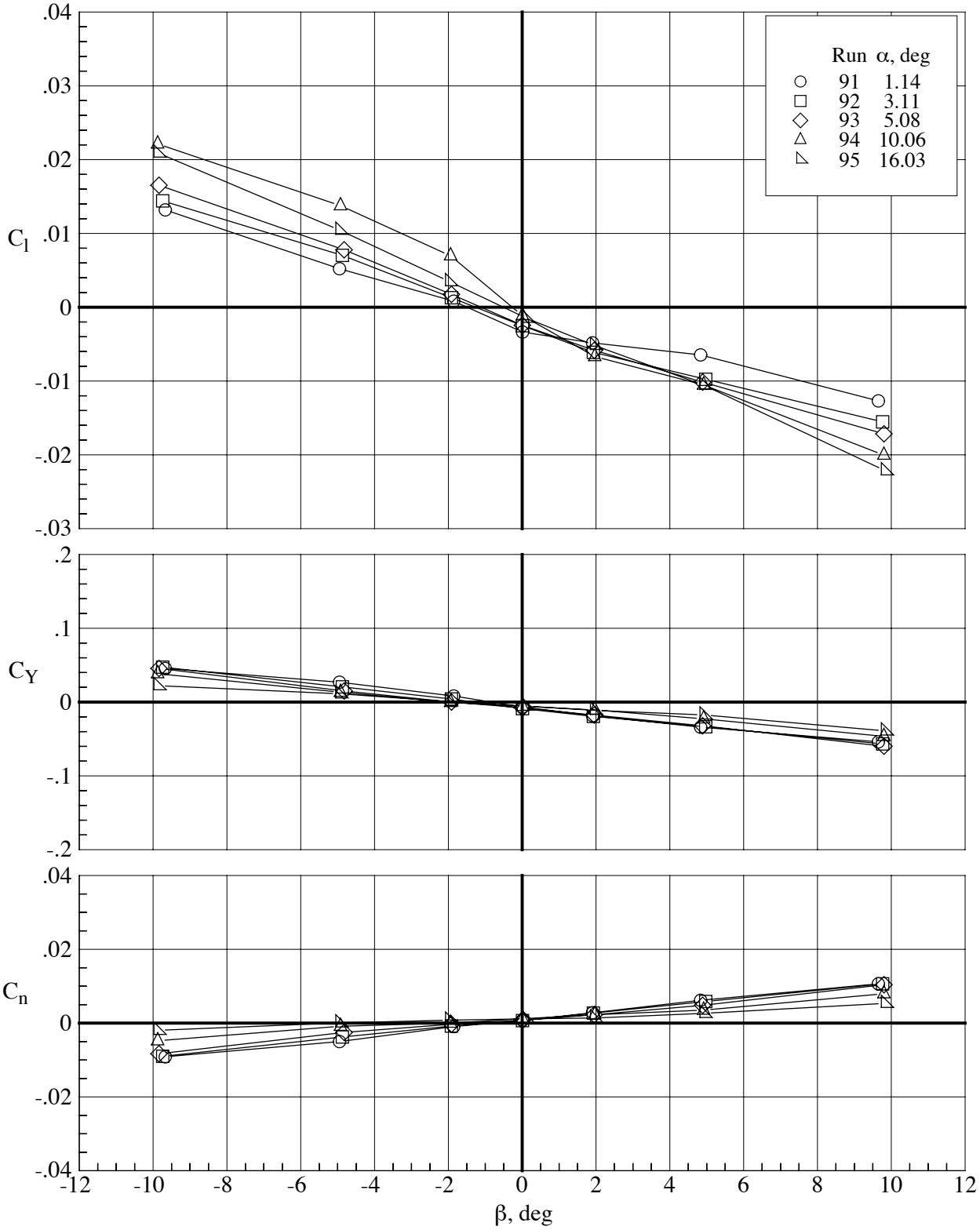

(a) Lateral-directional characteristics.

Figure 77. Aerodynamic characteristics of the model with the MA-SC-1 wing (bump on) at a Mach number of 0.80 and a Reynolds number of 60,000 at five angles of attack. $\delta_h = 0°$ and $\delta_f = 0°$.

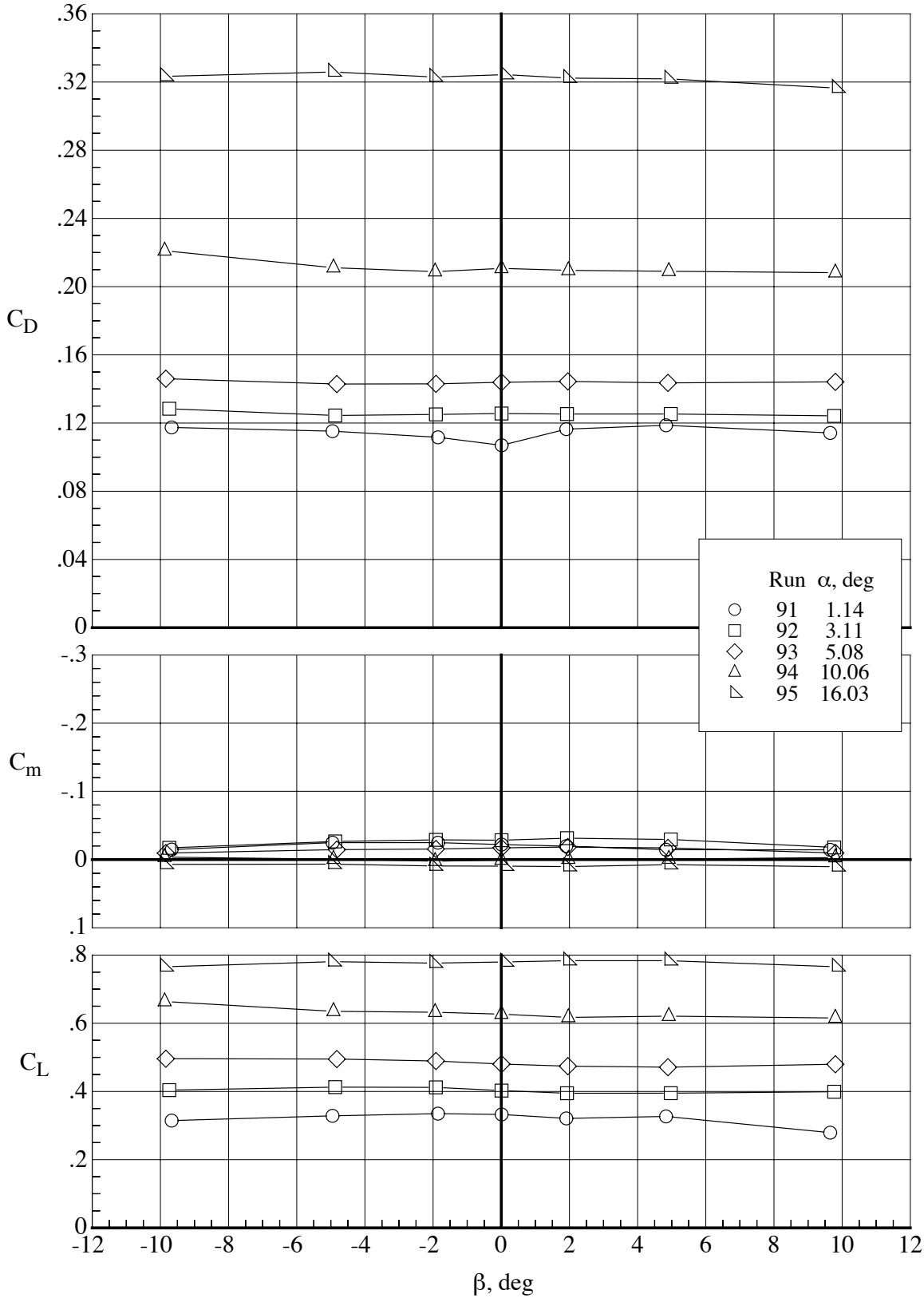

(b) Lift, drag, and pitching-moment coefficients.

Figure 77. Concluded.

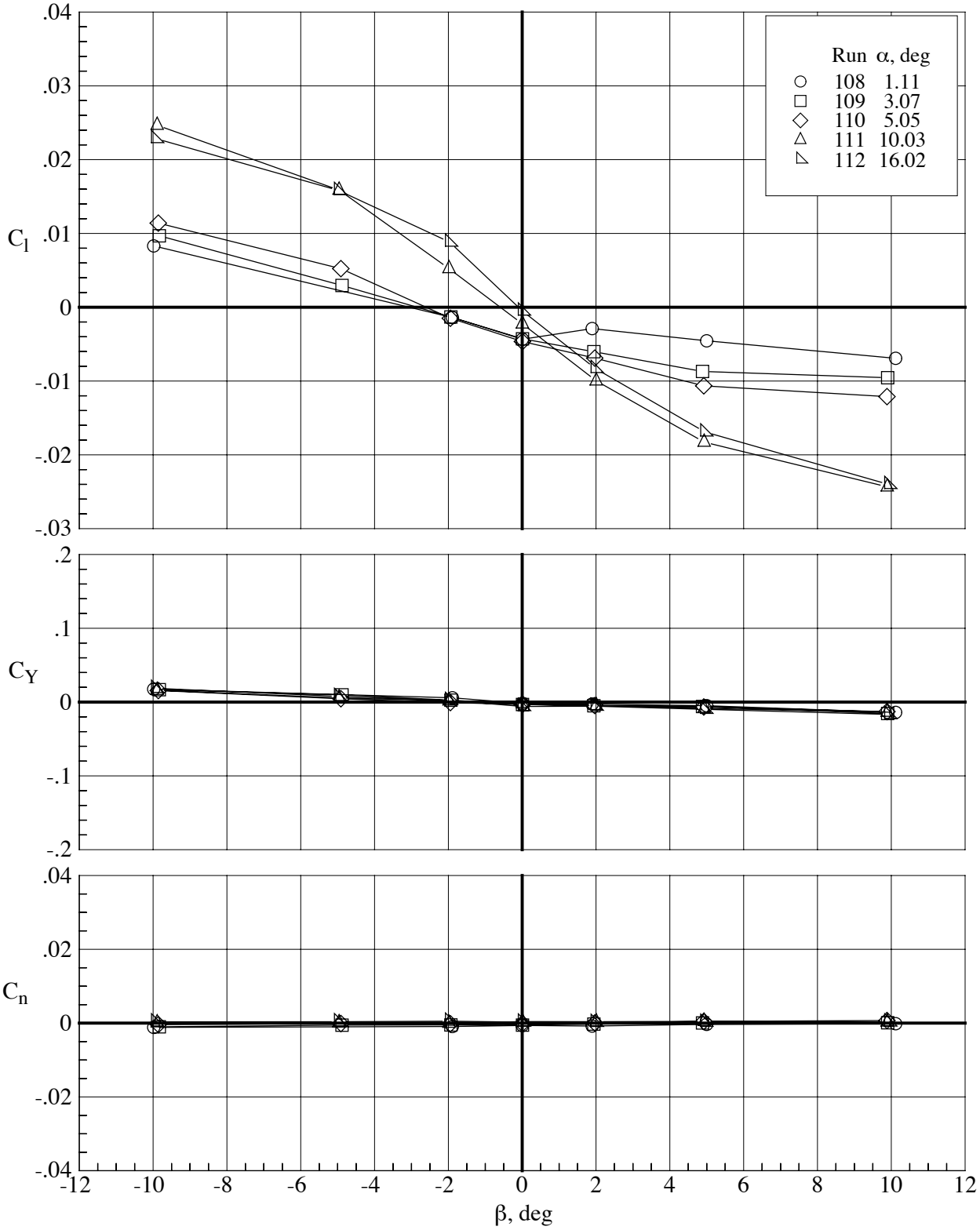

(a) Lateral-directional characteristics.

Figure 78. Aerodynamic characteristics of the model with the MA-SC-1 wing (bump on) at a Mach number of 0.65 and a Reynolds number of 40,000 at five angles of attack. Tails off and $\delta_f = 0°$.

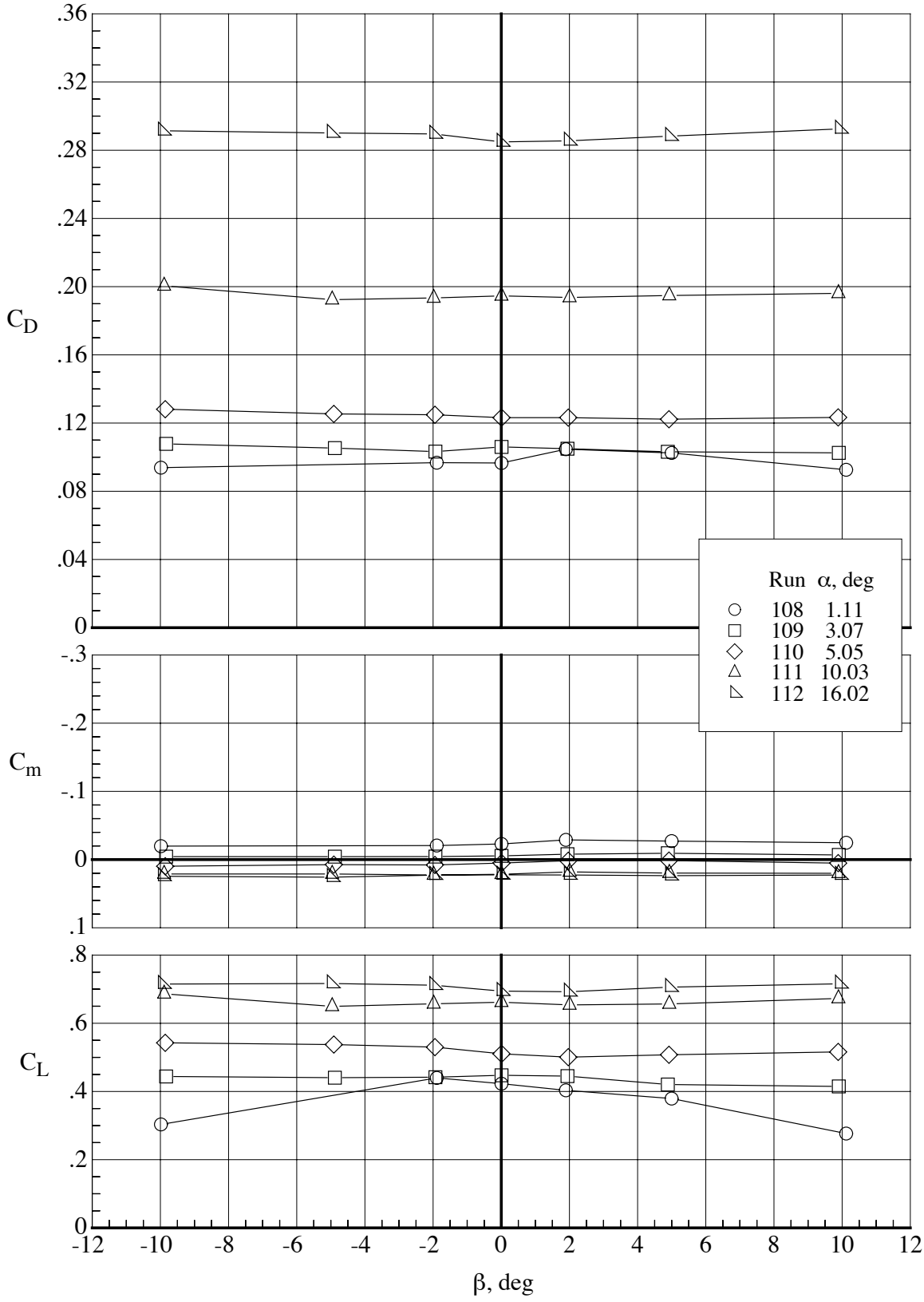

(b) Lift, drag, and pitching-moment coefficients.

Figure 78. Concluded.

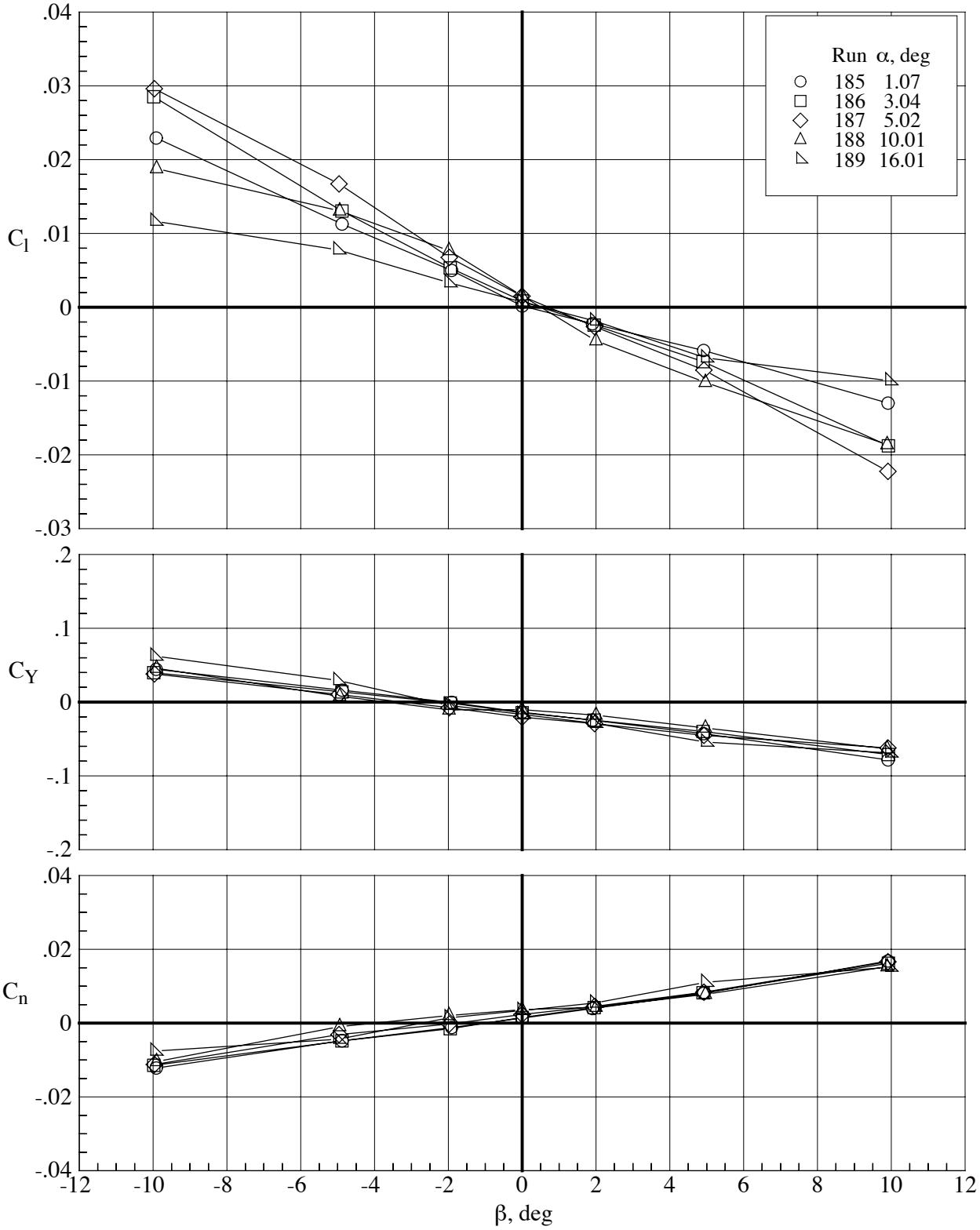

(a) Lateral-directional characteristics.

Figure 79. Aerodynamic characteristics of the model with the MA-SC-1t wing (bump on) at a Mach number of 0.65 and a Reynolds number of 40,000 at five angles of attack. $\delta_h = 0°$ and $\delta_f = 0°$.

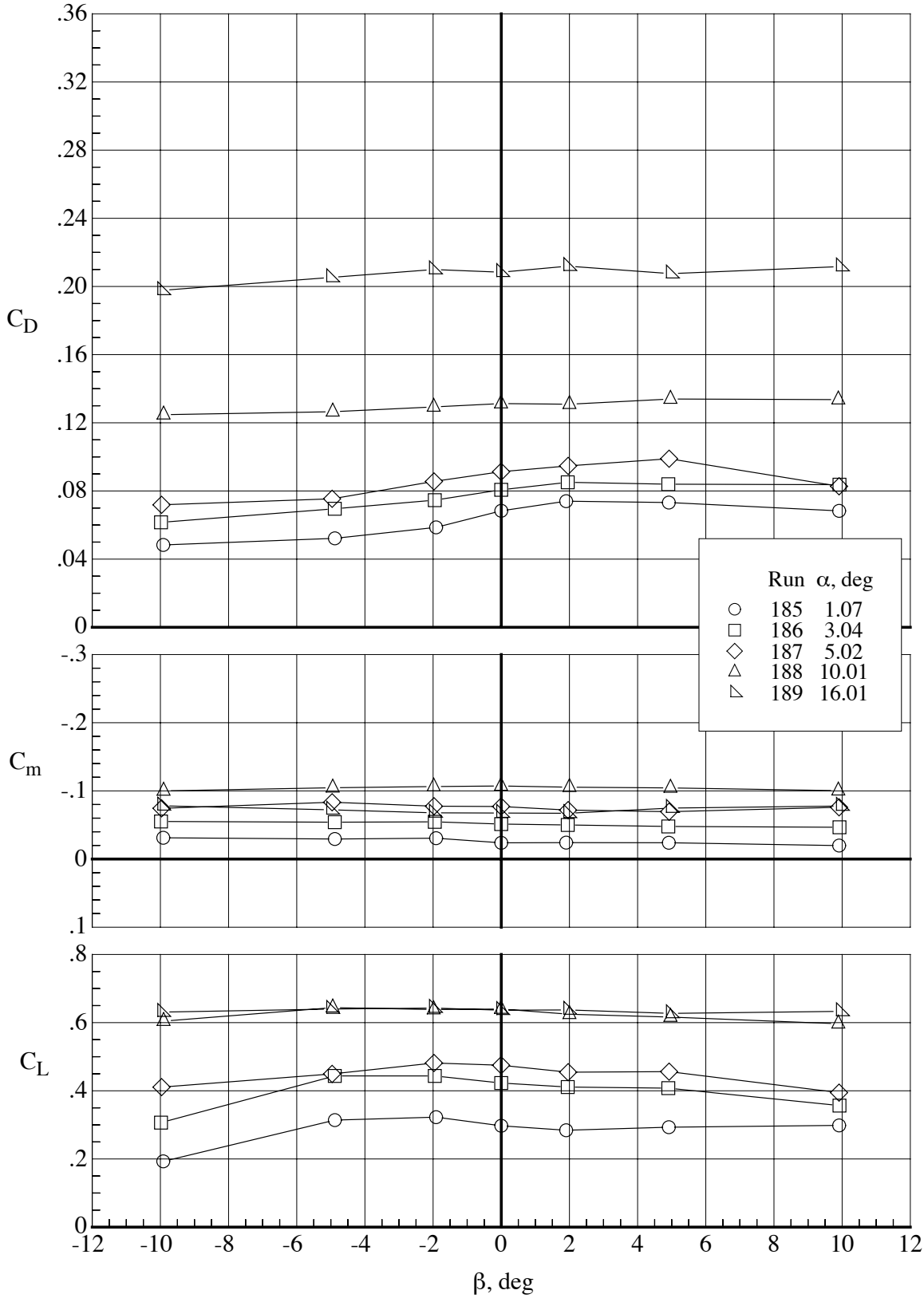

(b) Lift, drag, and pitching-moment coefficients.

Figure 79. Concluded.

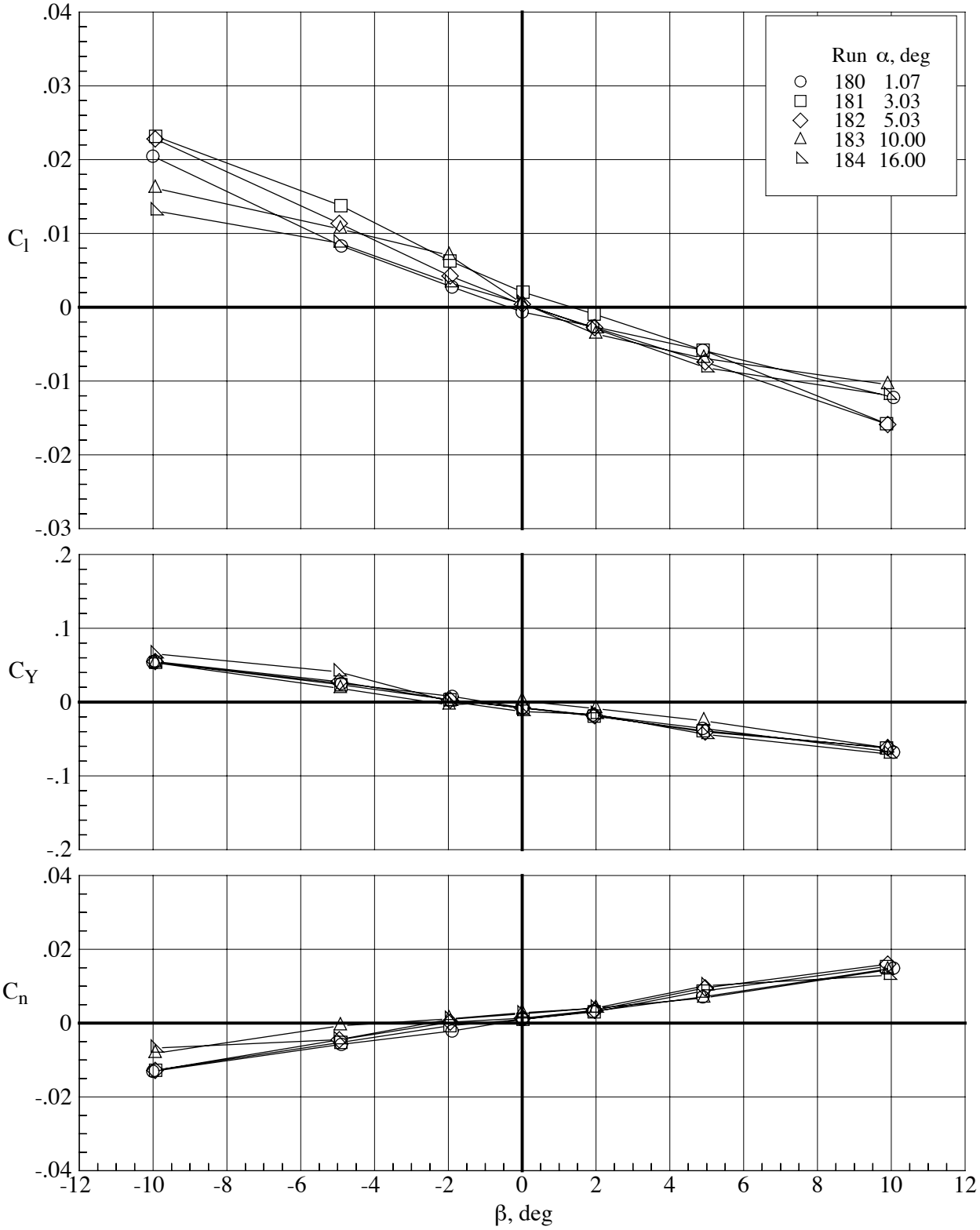

(a) Lateral-directional characteristics.

Figure 80. Aerodynamic characteristics of the model with the MA-SC-1t wing (bump on) at a Mach number of 0.80 and a Reynolds number of 40,000 at five angles of attack. $\delta_h = 0°$ and $\delta_f = 0°$.

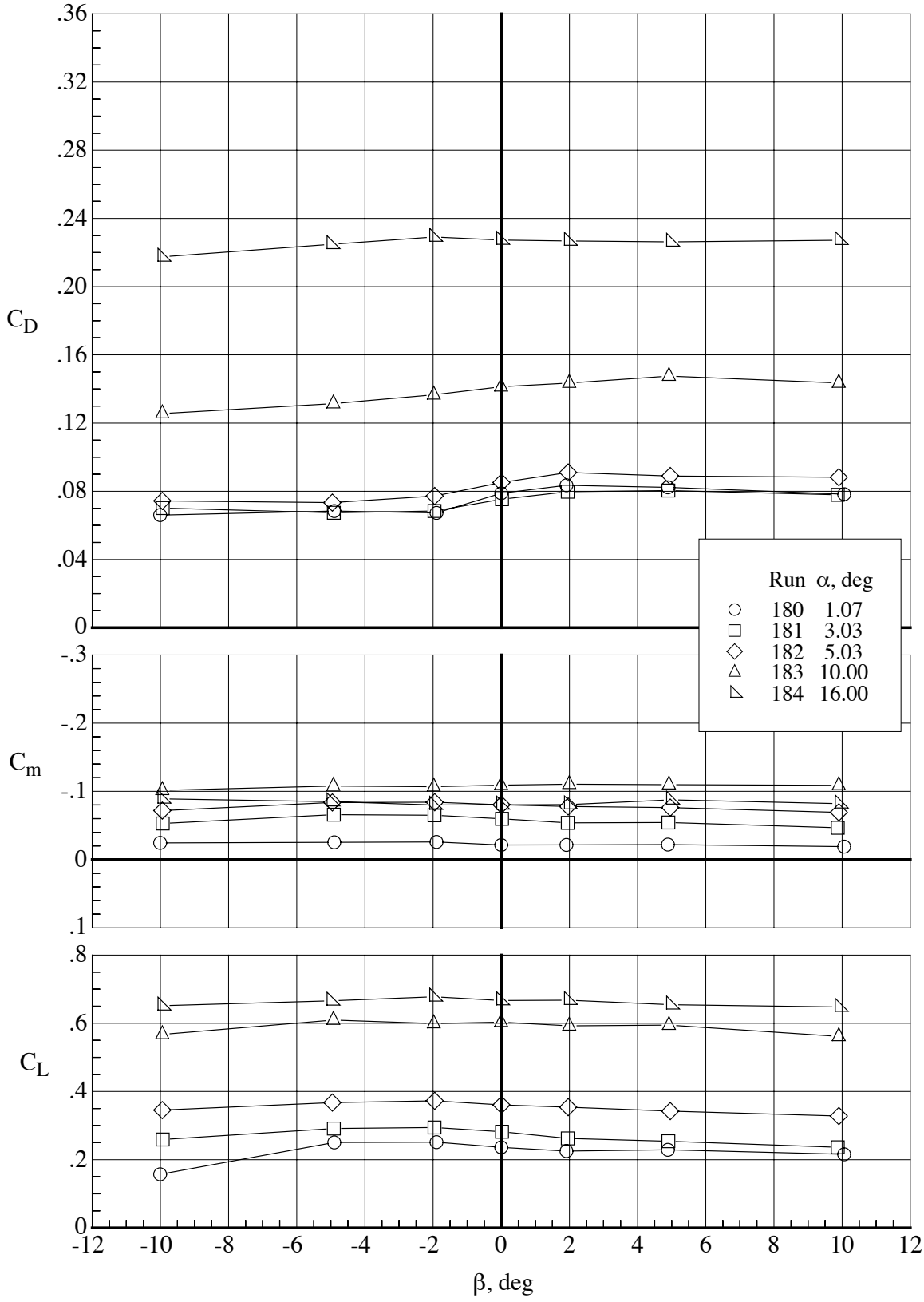

(b) Lift, drag, and pitching-moment coefficients.

Figure 80. Concluded.

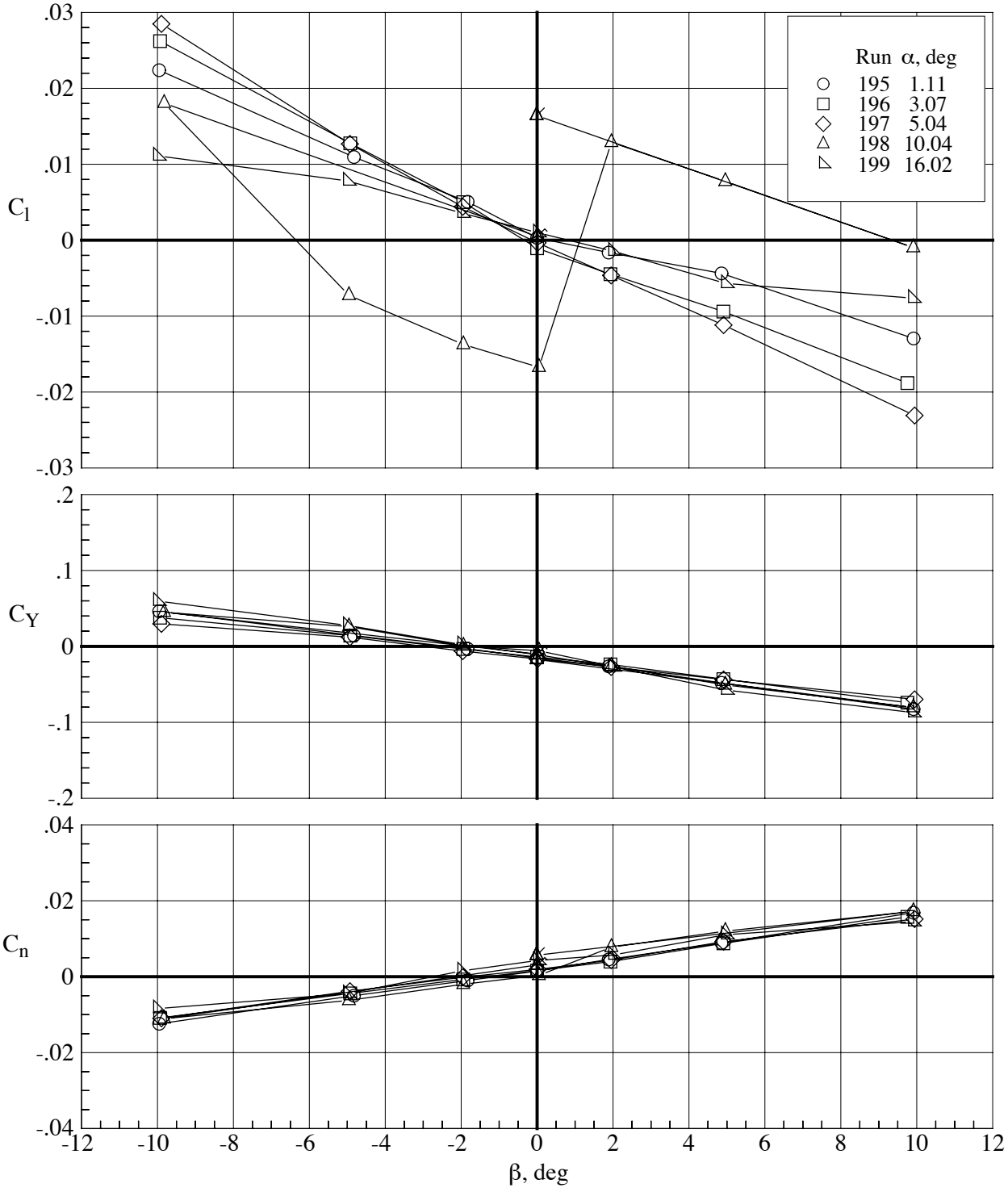

(a) Lateral-directional characteristics.

Figure 81. Aerodynamic characteristics of the model with the MA-SC-1t wing (bump on) at a Mach number of 0.65 and a Reynolds number of 60,000 at five angles of attack. $\delta_h = 0°$ and $\delta_f = 0°$. The equilateral triangle symbols with the bent flags indicate data taken at $\beta = 0°$ before the start of the angle of sideslip sweep from -10° while the equilateral triangle symbols with the straight flags indicate data taken upon return to $\beta = 0°$ after completion of the sidesip angle sweep.

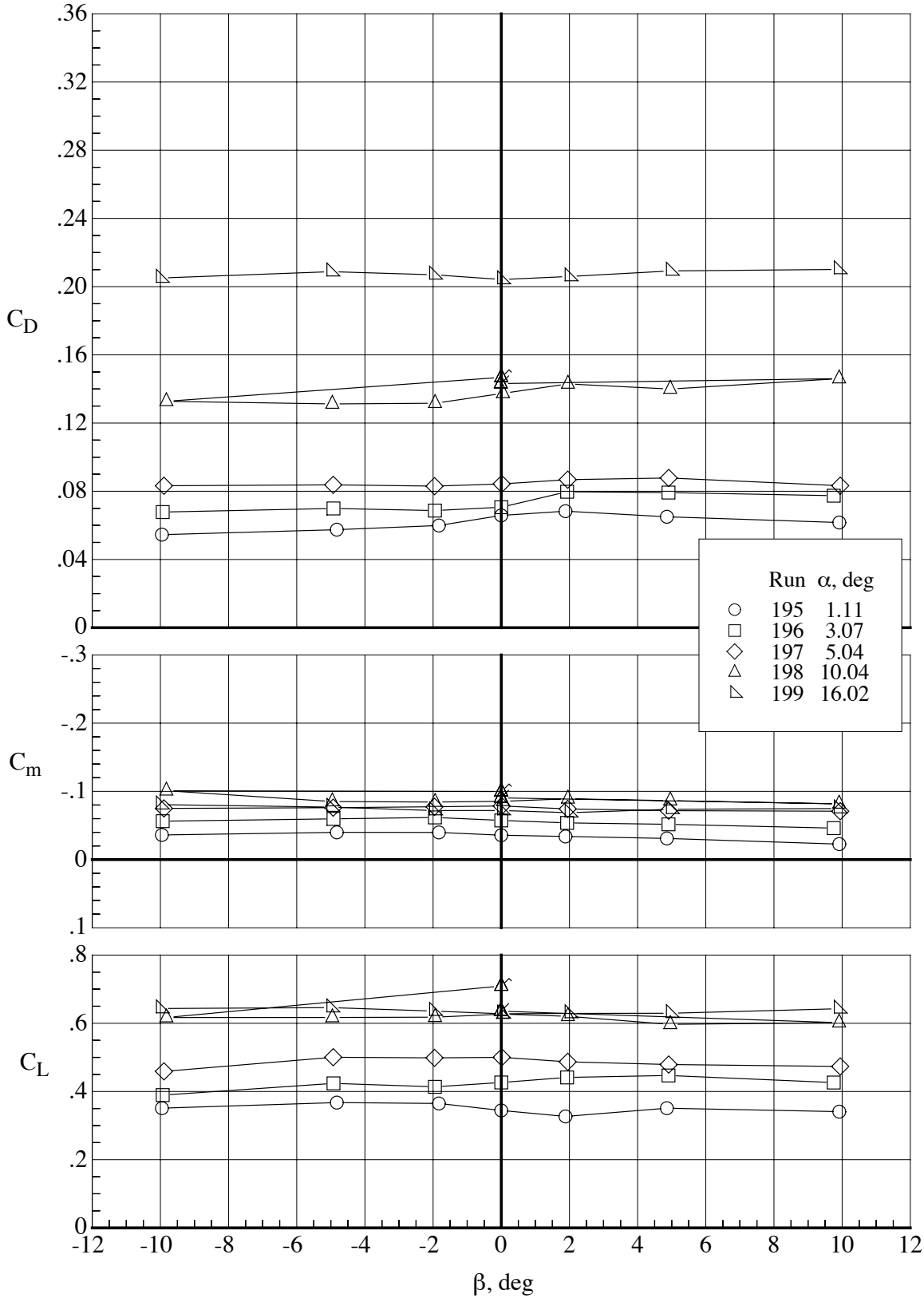

(b) Lift, drag, and pitching-moment coefficients.

Figure 81. Concluded.

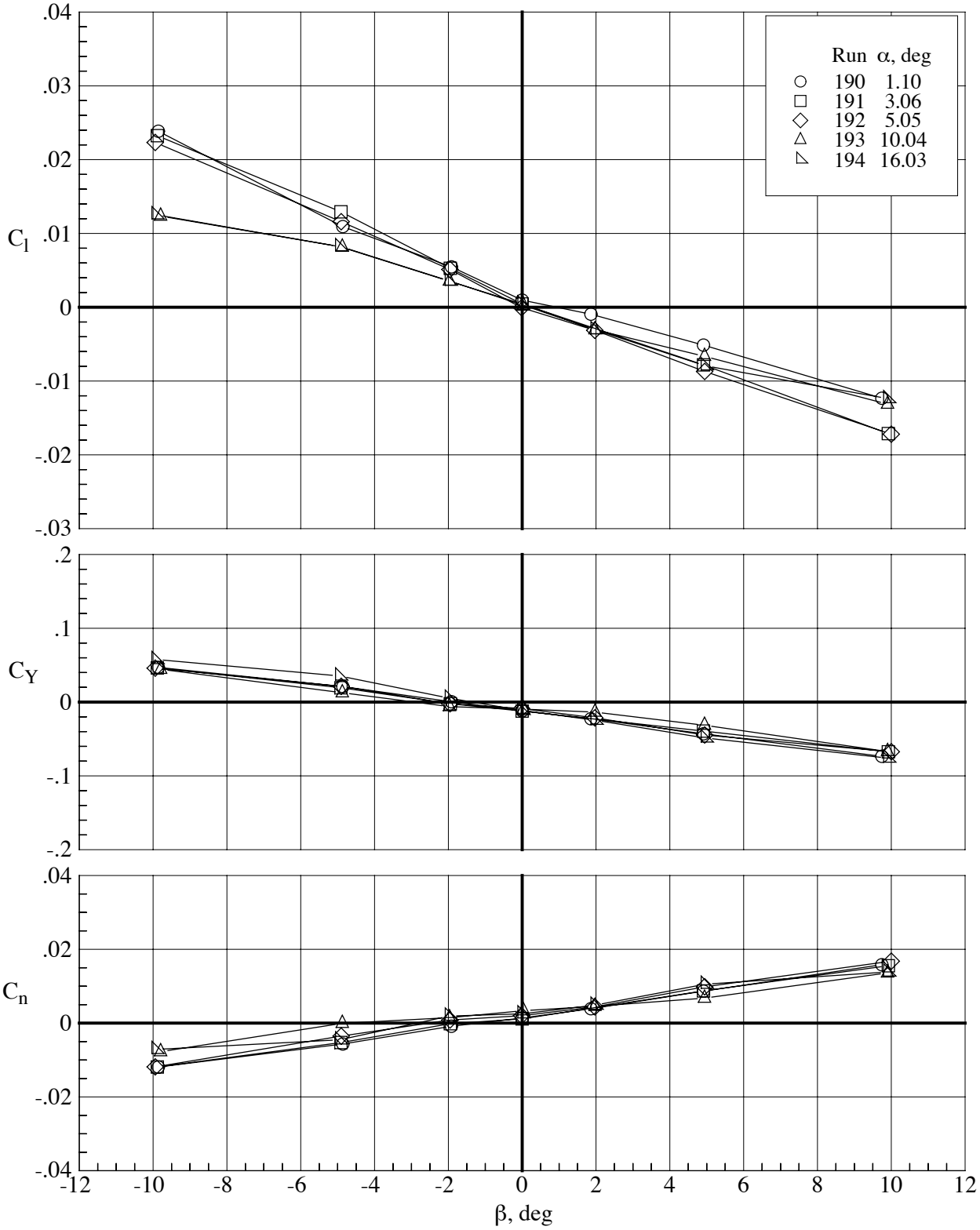

(a) Lateral-directional characteristics.

Figure 82. Aerodynamic characteristics of the model with the MA-SC-1t wing (bump on) at a Mach number of 0.80 and a Reynolds number of 60,000 at five angles of attack. $\delta_h = 0°$ and $\delta_f = 0°$.

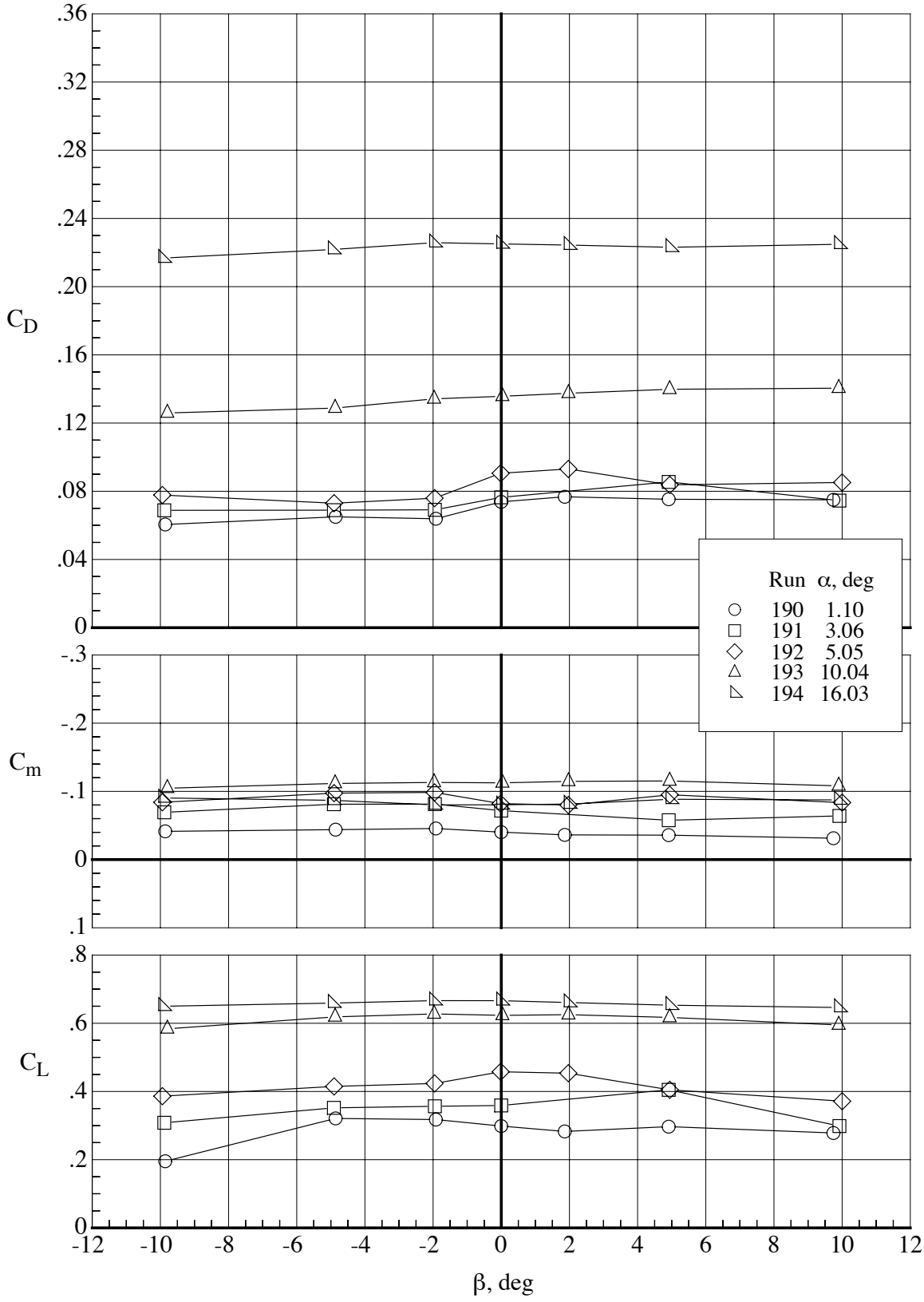

(b) Lift, drag, and pitching-moment coefficients.

Figure 82. Concluded.

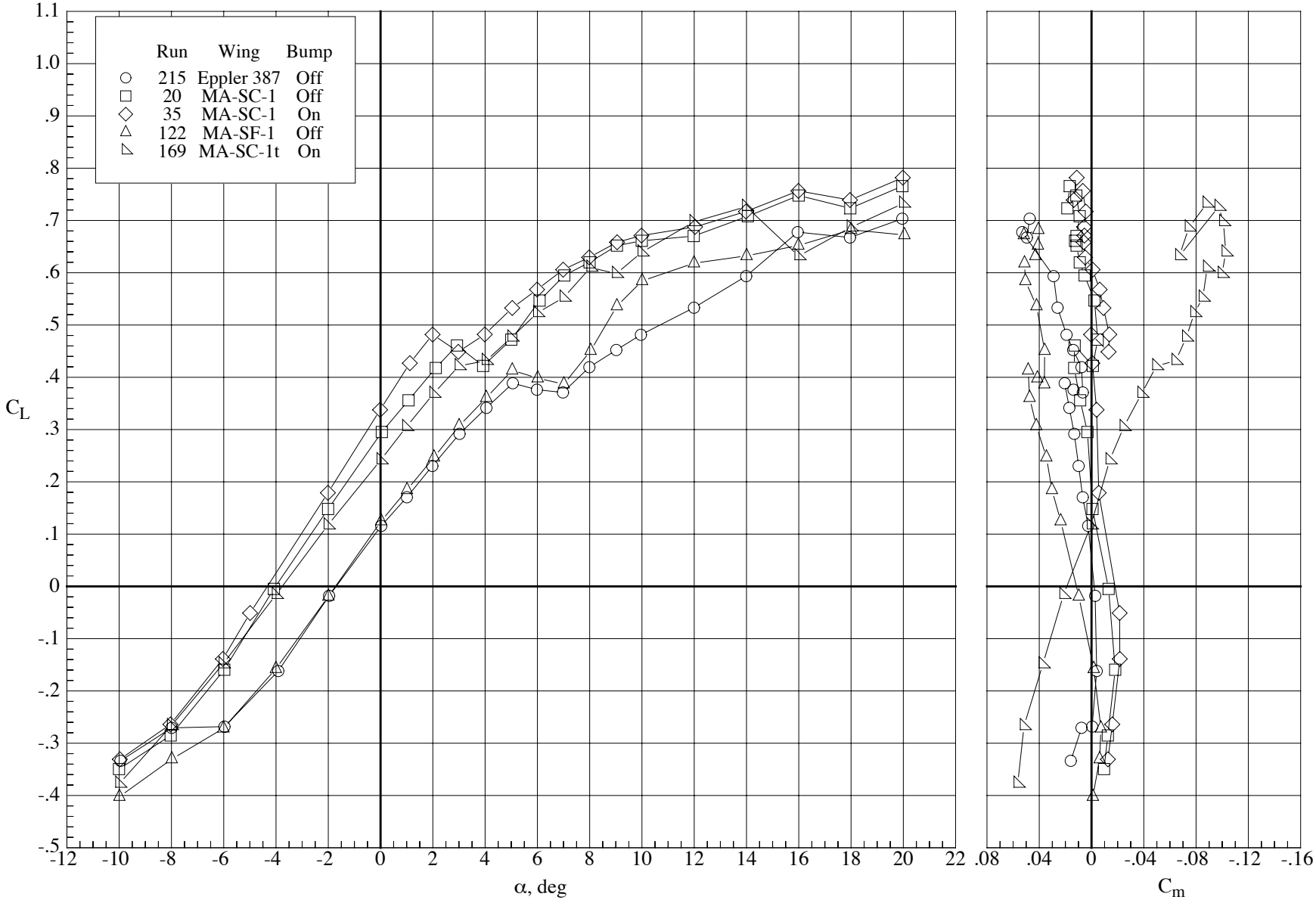

(a) Lift and pitching-moment coefficients.

Figure 83. Effect of wing configuration and bump on the longitudinal aerodynamic characteristics of the model at a Mach number of 0.65 and a Reynolds number of 40,000. $\delta_h = 0°$ and $\delta_f = 0°$.

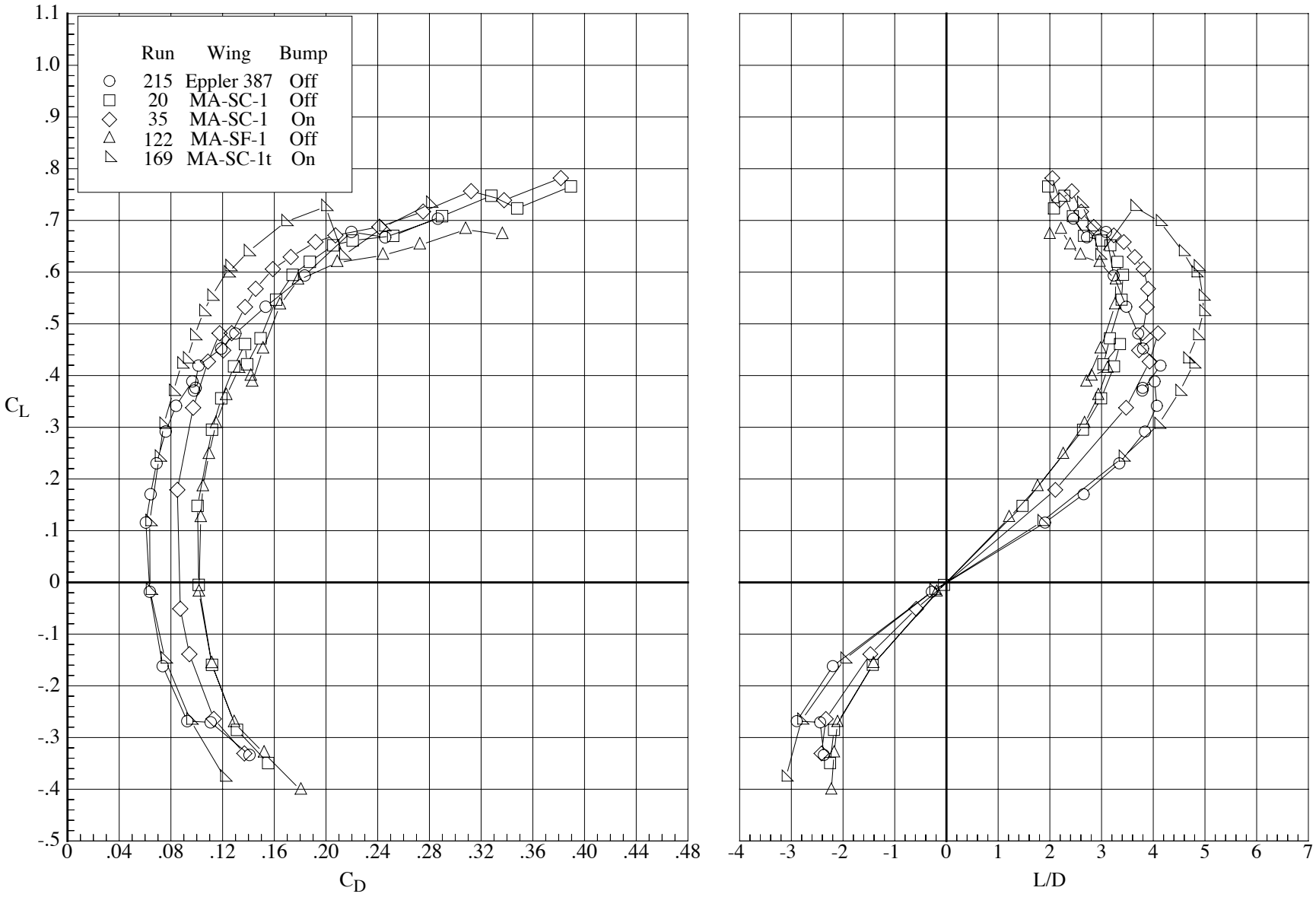

(b) Drag coefficient and lift-drag ratio.

Figure 83. Concluded.

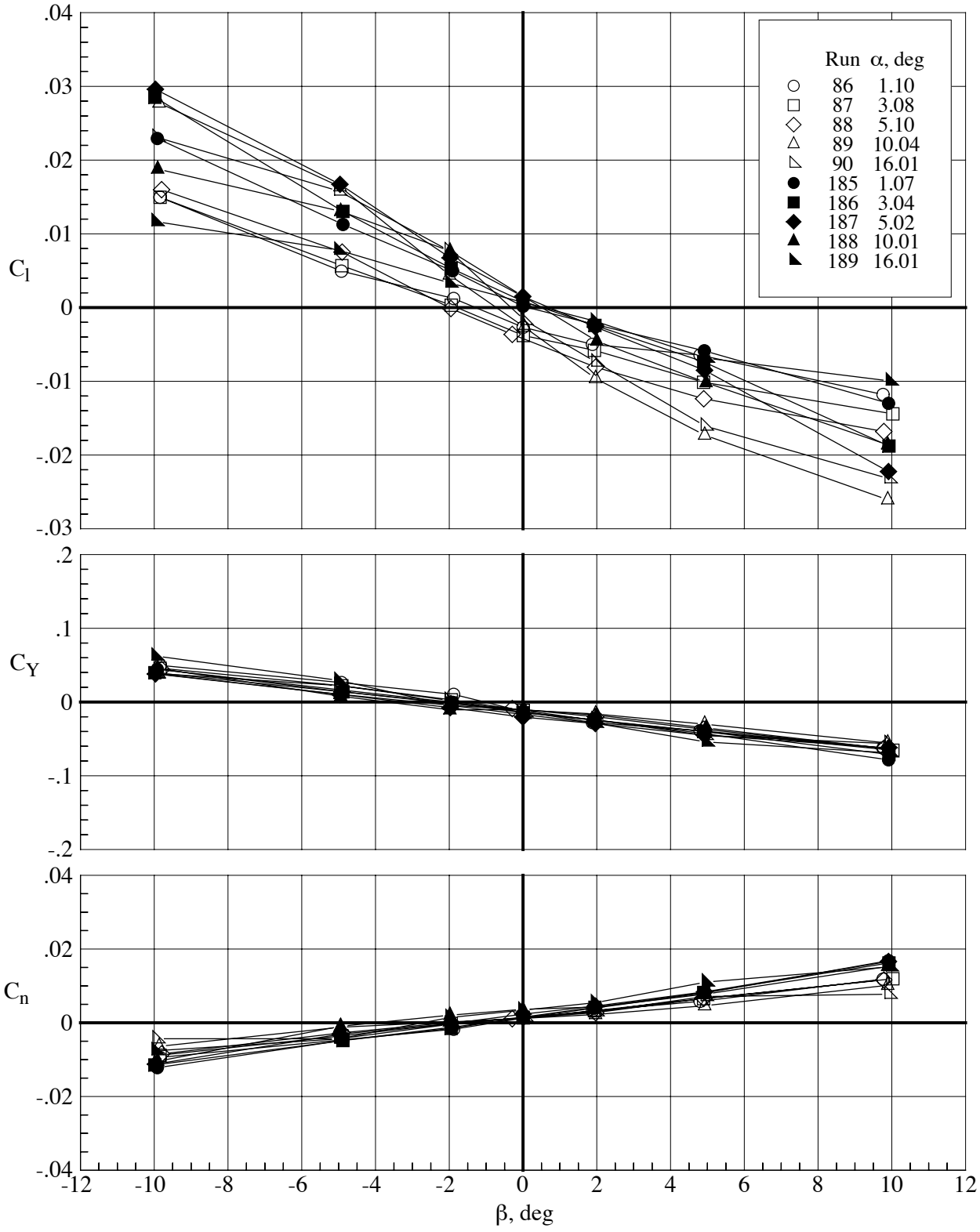

(a) Lateral-directional characteristics.

Figure 84. Effect of wing configuration (bump on) on the aerodynamic characteristics of the model at a Mach number of 0.65 and a Reynolds number of 40,000 at five angles of attack. $\delta_h = 0°$ and $\delta_f = 0°$. The open symbols indicate the MA-SC-1 wing configuration and the solid symbols indicate the MA-SC-1t wing configuration.

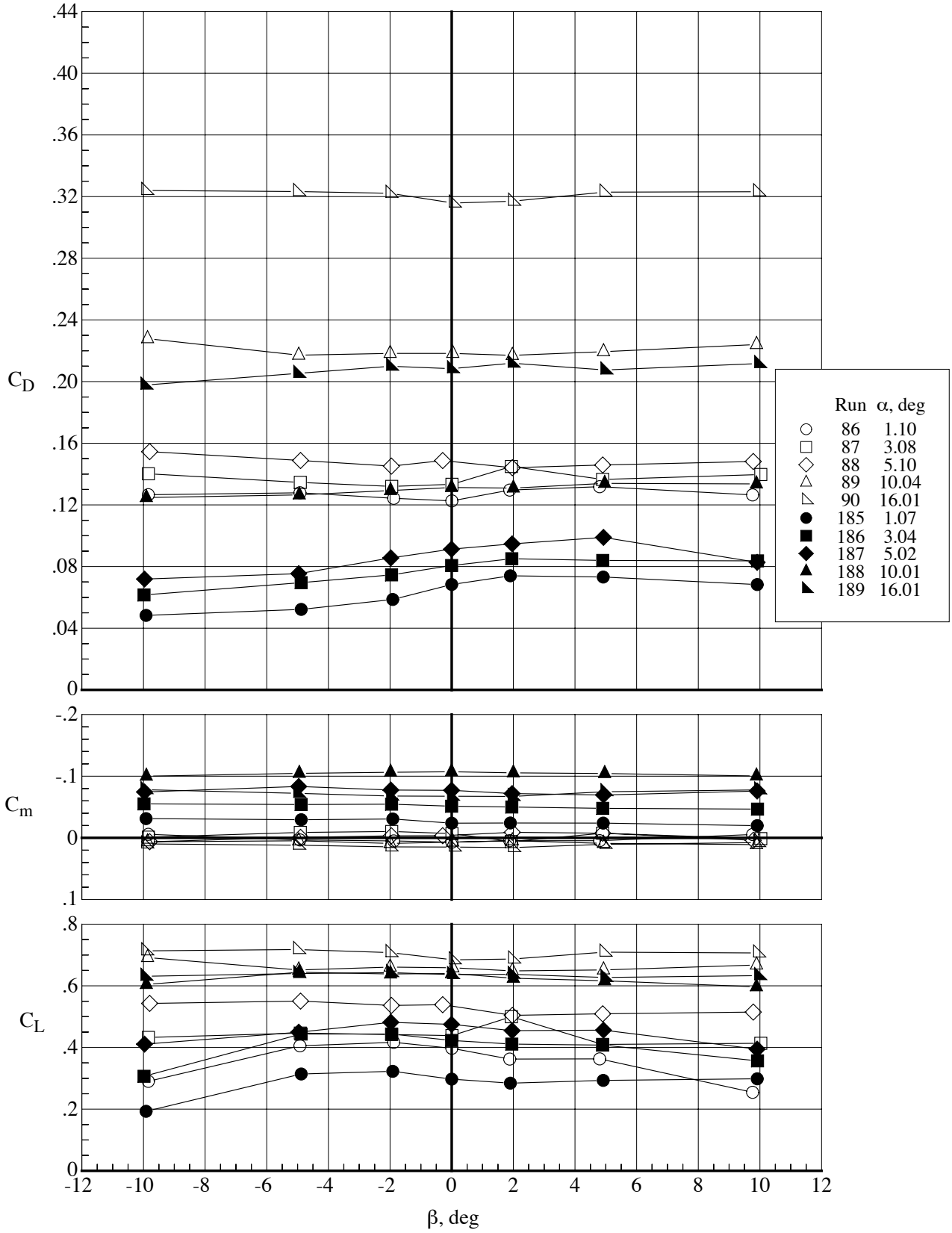

(b) Lift, drag, and pitching-moment coefficients.

Figure 84. Concluded.

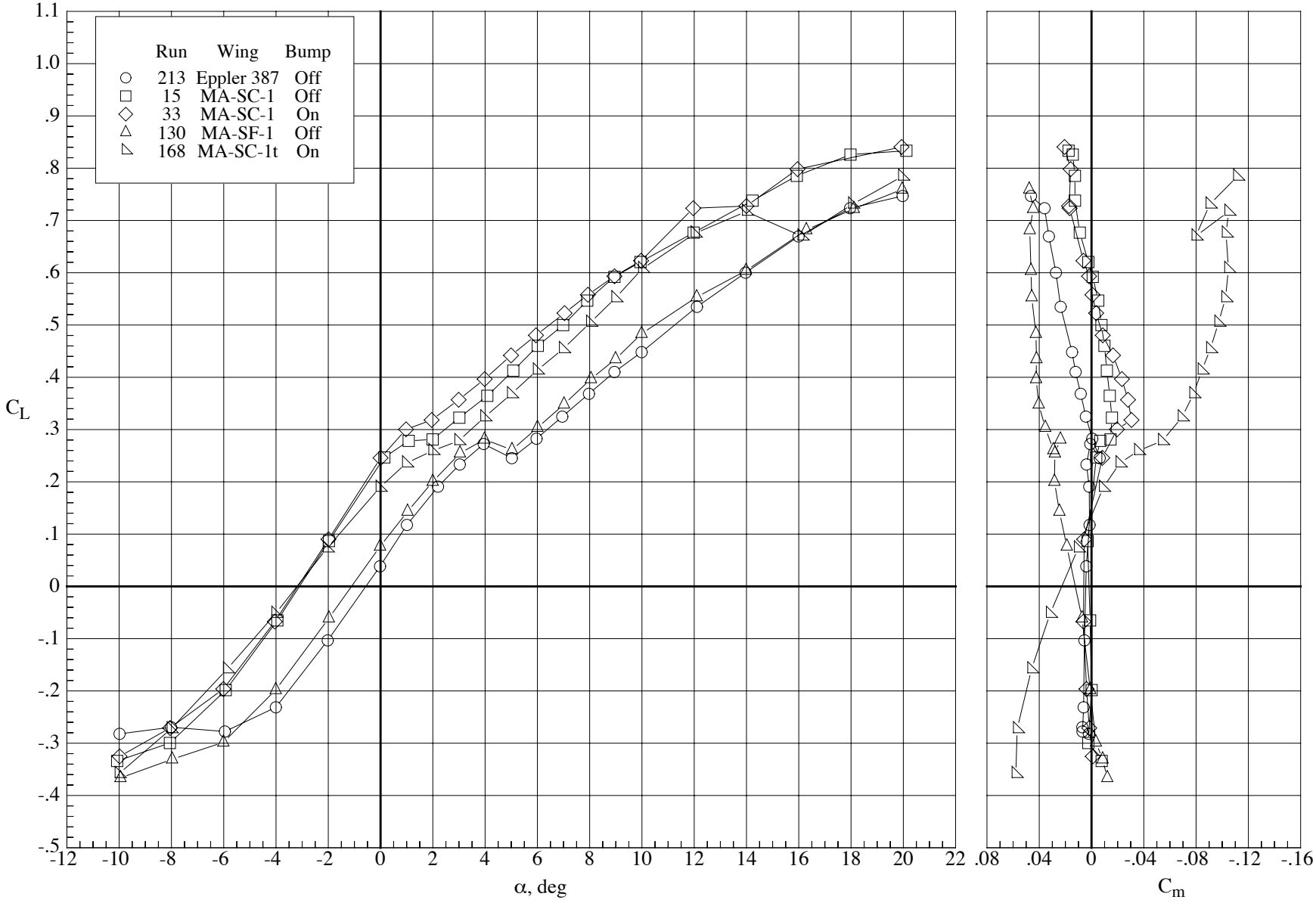

(a) Lift and pitching-moment coefficients.

Figure 85. Effect of wing configuration and bump on the longitudinal aerodynamic characteristics of the model at a Mach number of 0.80 and a Reynolds number of 40,000. $\delta_h = 0°$ and $\delta_f = 0°$.

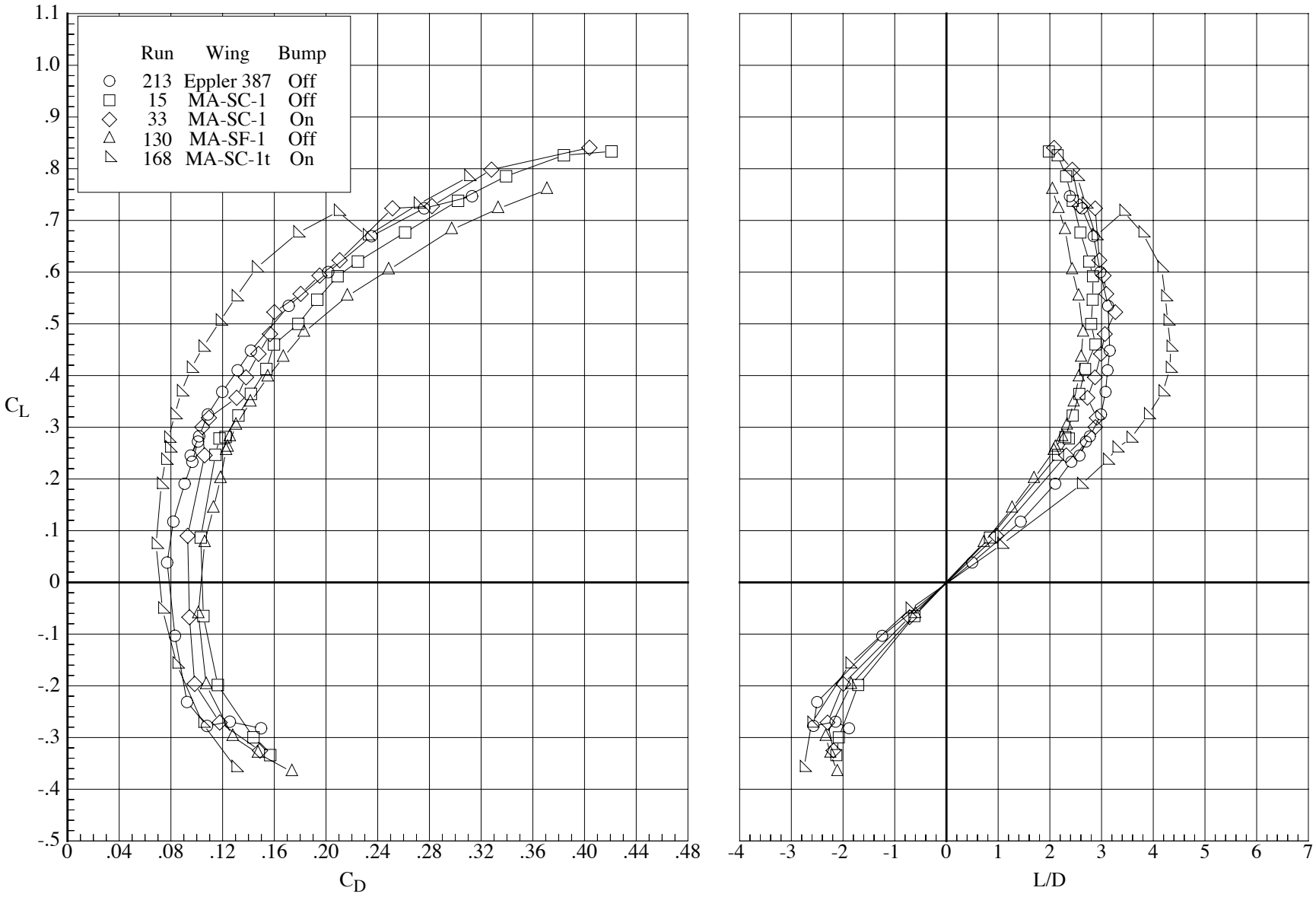

(b) Drag coefficient and lift-drag ratio.

Figure 85. Concluded.

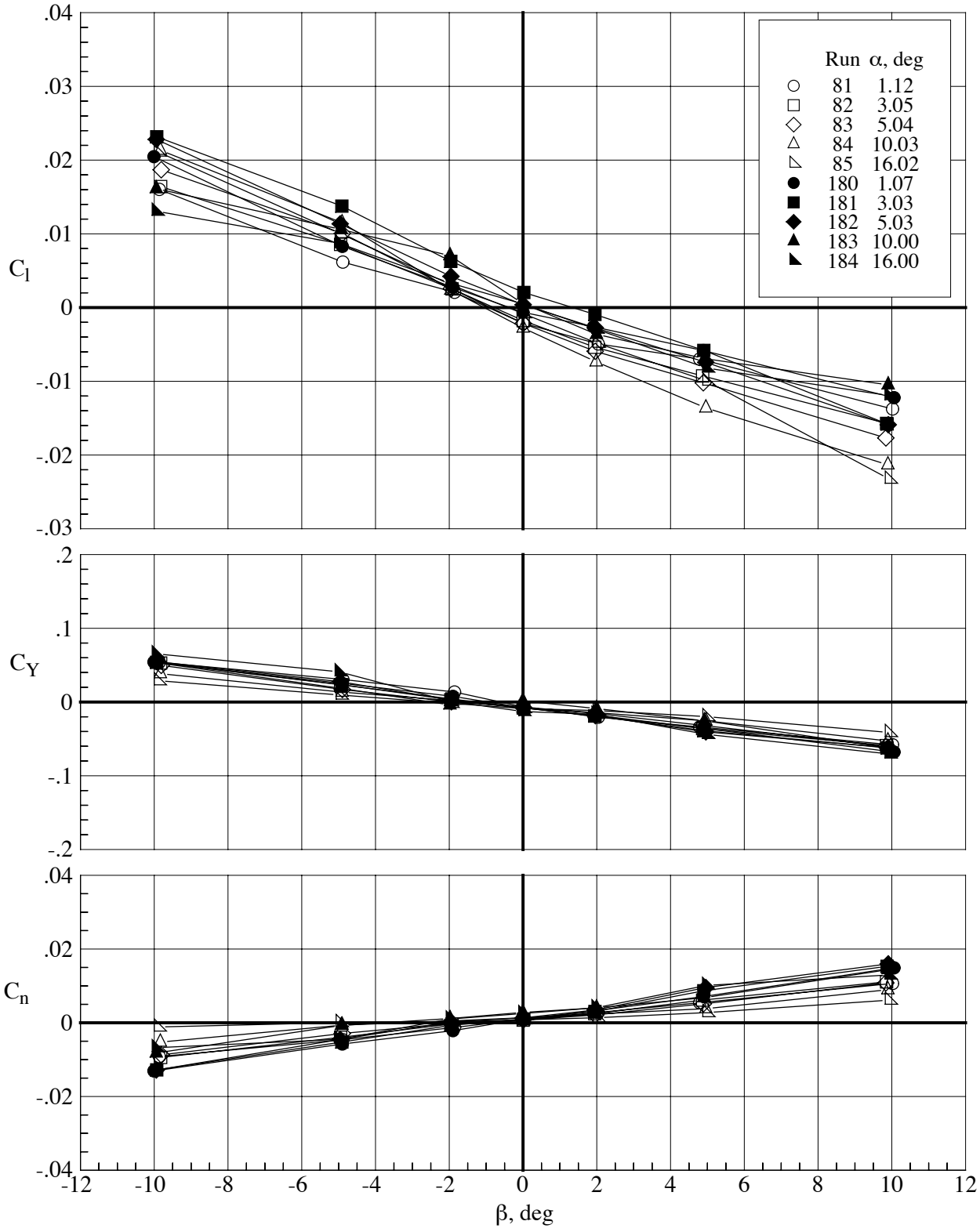

(a) Lateral-directional characteristics.

Figure 86. Effect of wing configuration (bump on) on the aerodynamic characteristics of the model at a Mach number of 0.80 and a Reynolds number of 40,000 at five angles of attack. $\delta_h = 0°$ and $\delta_f = 0°$. The open symbols indicate the MA-SC-1 wing configuration and the solid symbols indicate the MA-SC-1t wing configuration.

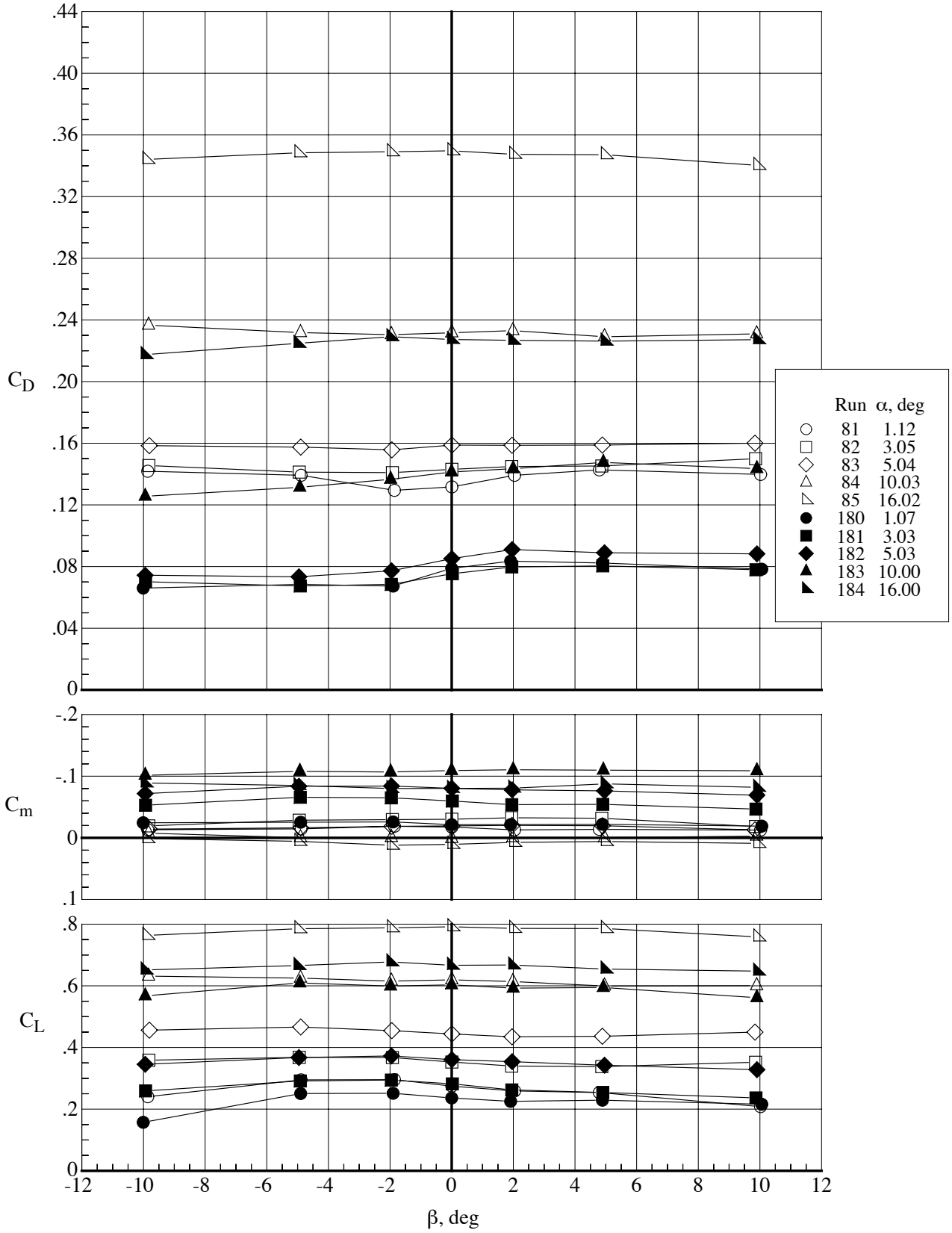

(b) Lift, drag, and pitching-moment coefficients.

Figure 86. Concluded.

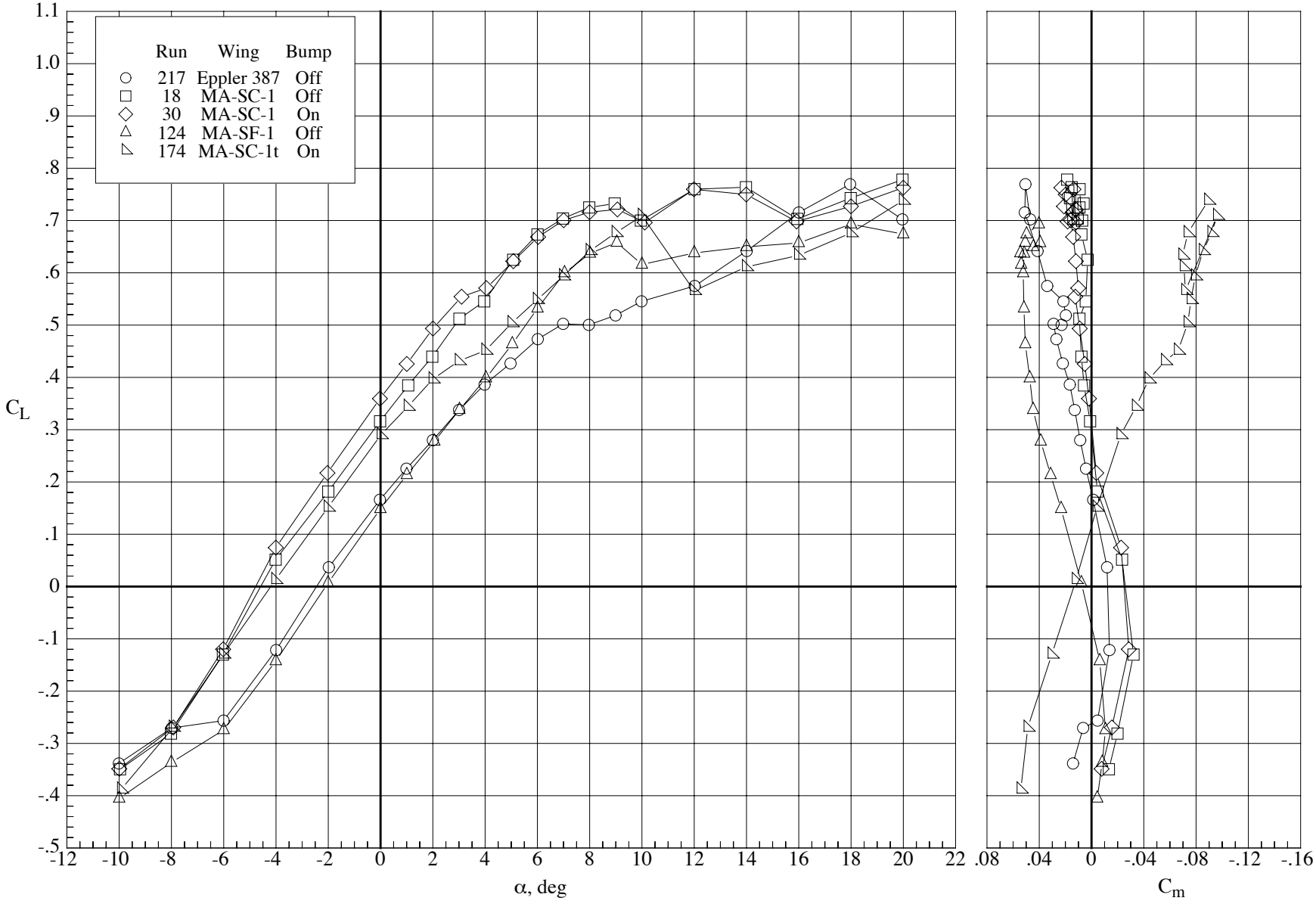

(a) Lift and pitching-moment coefficients.

Figure 87. Effect of wing configuration and bump on the longitudinal aerodynamic characteristics of the model at a Mach number of 0.65 and a Reynolds number of 60,000. $\delta_h = 0°$ and $\delta_f = 0°$.

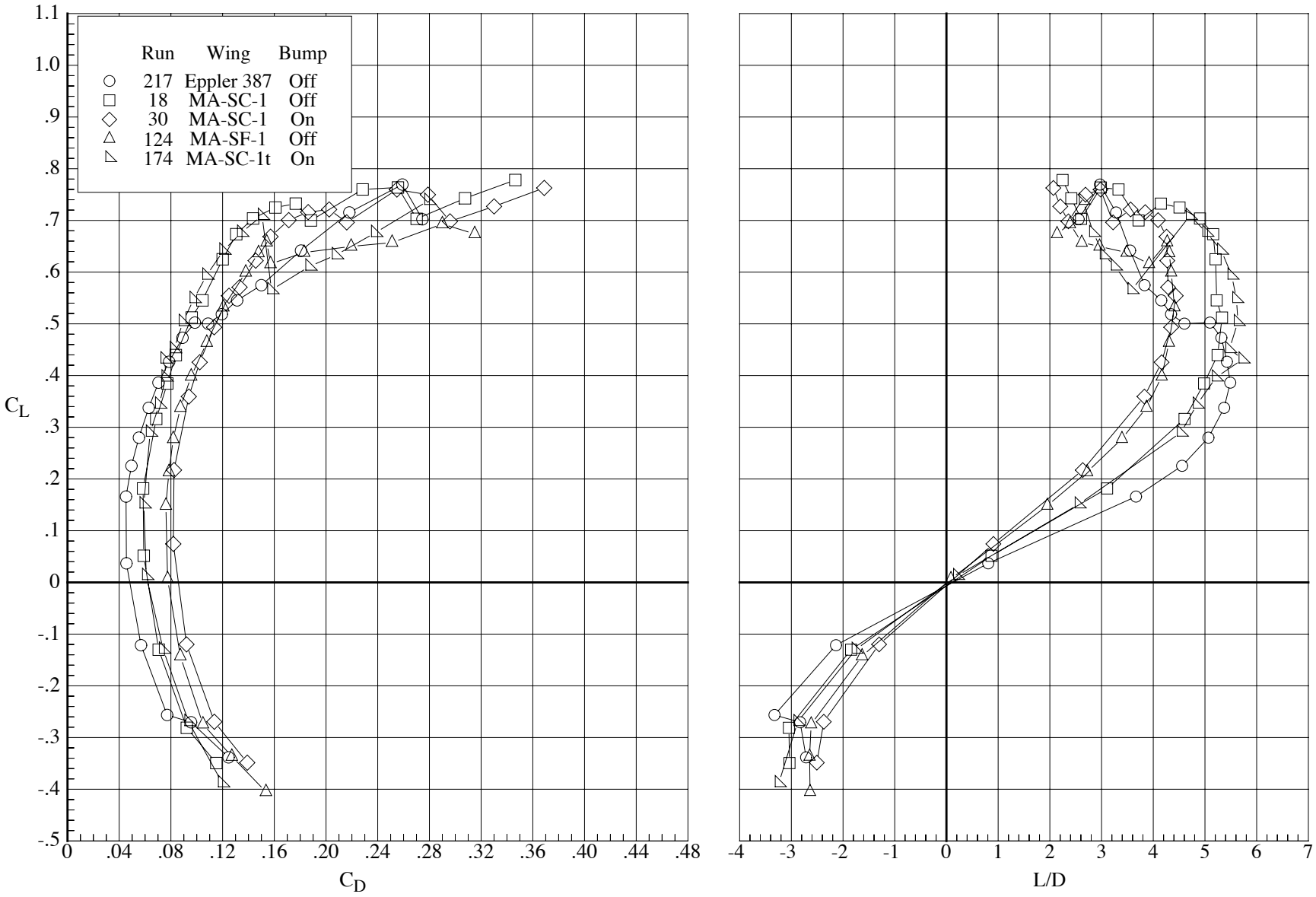

(b) Drag coefficient and lift-drag ratio.

Figure 87. Concluded.

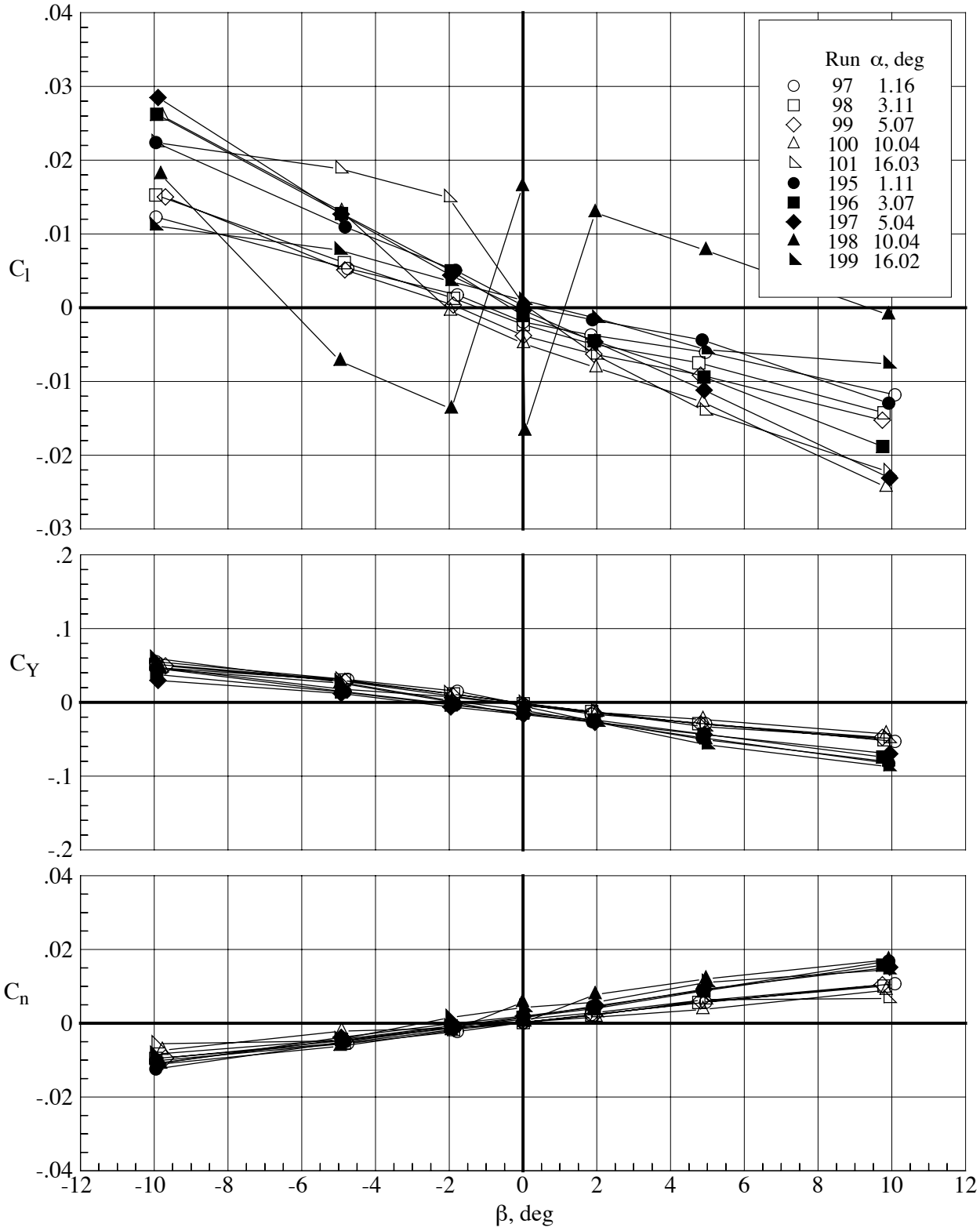

(a) Lateral-directional characteristics.

Figure 88. Effect of wing configuration (bump on) on the aerodynamic characteristics of the model at a Mach number of 0.65 and a Reynolds number of 60,000 at five angles of attack. $\delta_h = 0°$ and $\delta_f = 0°$. The open symbols indicate the MA-SC-1 wing configuration and the solid symbols indicate the MA-SC-1t wing configuration.

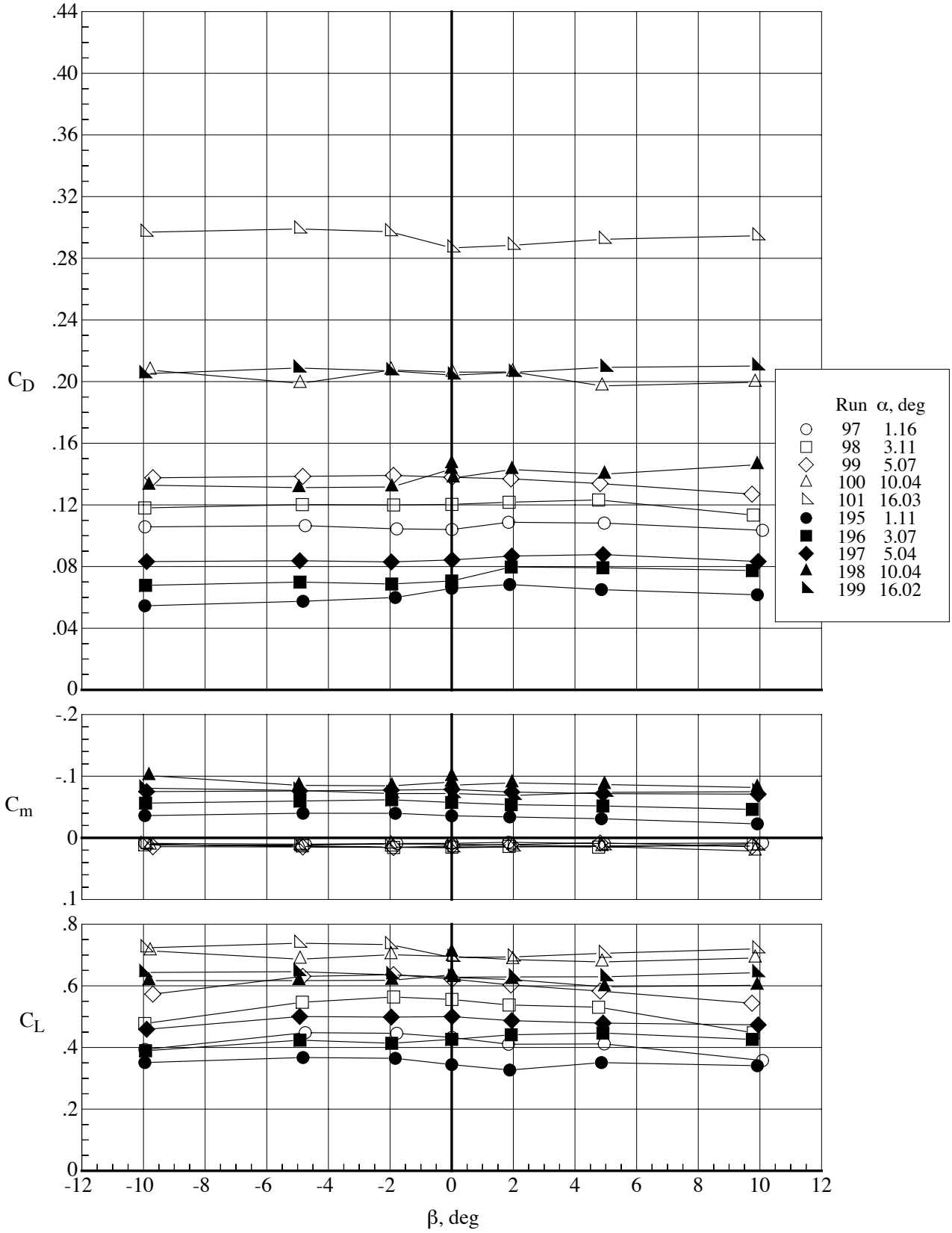

(b) Lift, drag, and pitching-moment coefficients.

Figure 88. Concluded.

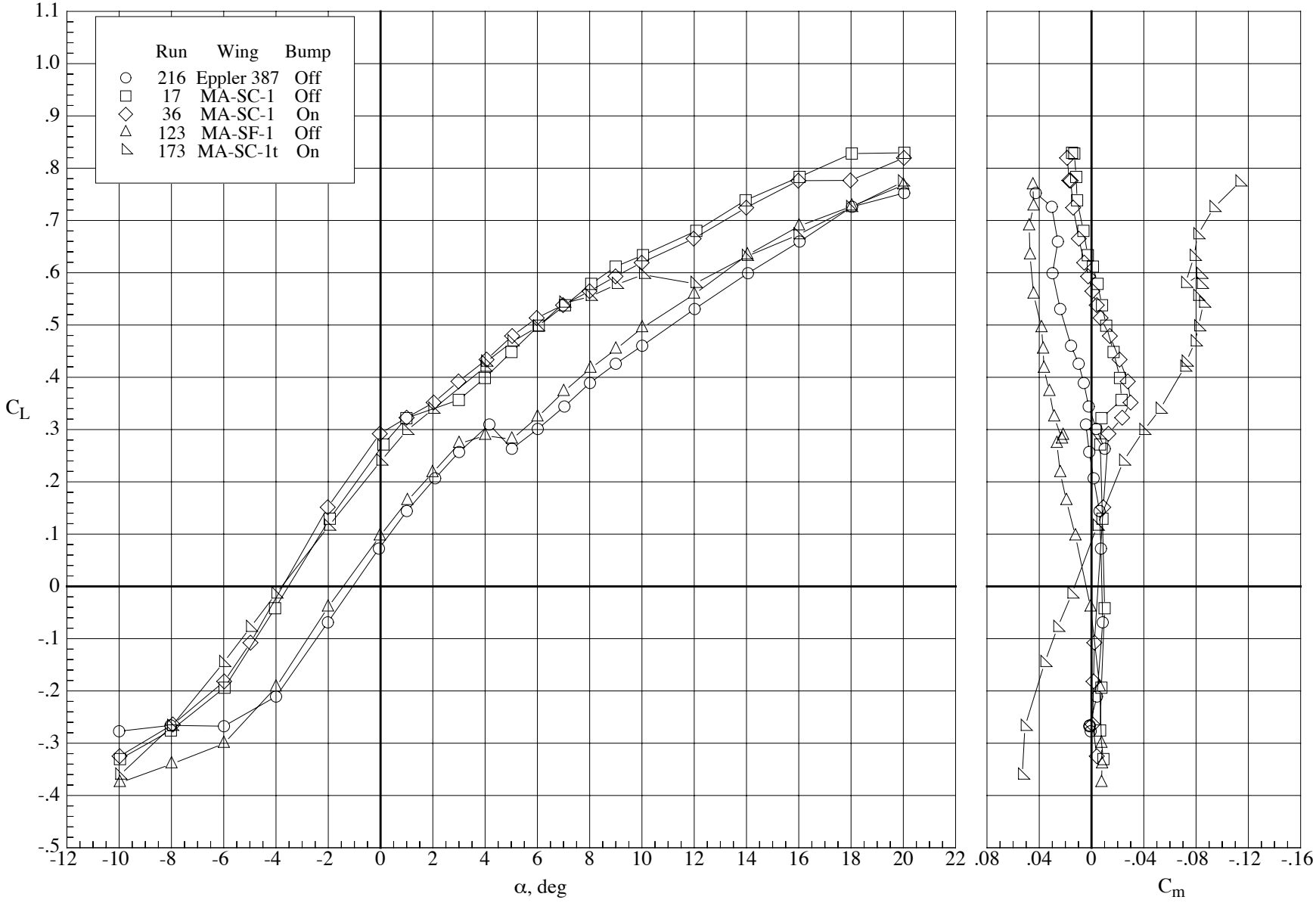

(a) Lift and pitching-moment coefficients.

Figure 89. Effect of wing configuration and bump on the longitudinal aerodynamic characteristics of the model at a Mach number of 0.80 and a Reynolds number of 60,000. $\delta_h = 0°$ and $\delta_f = 0°$.

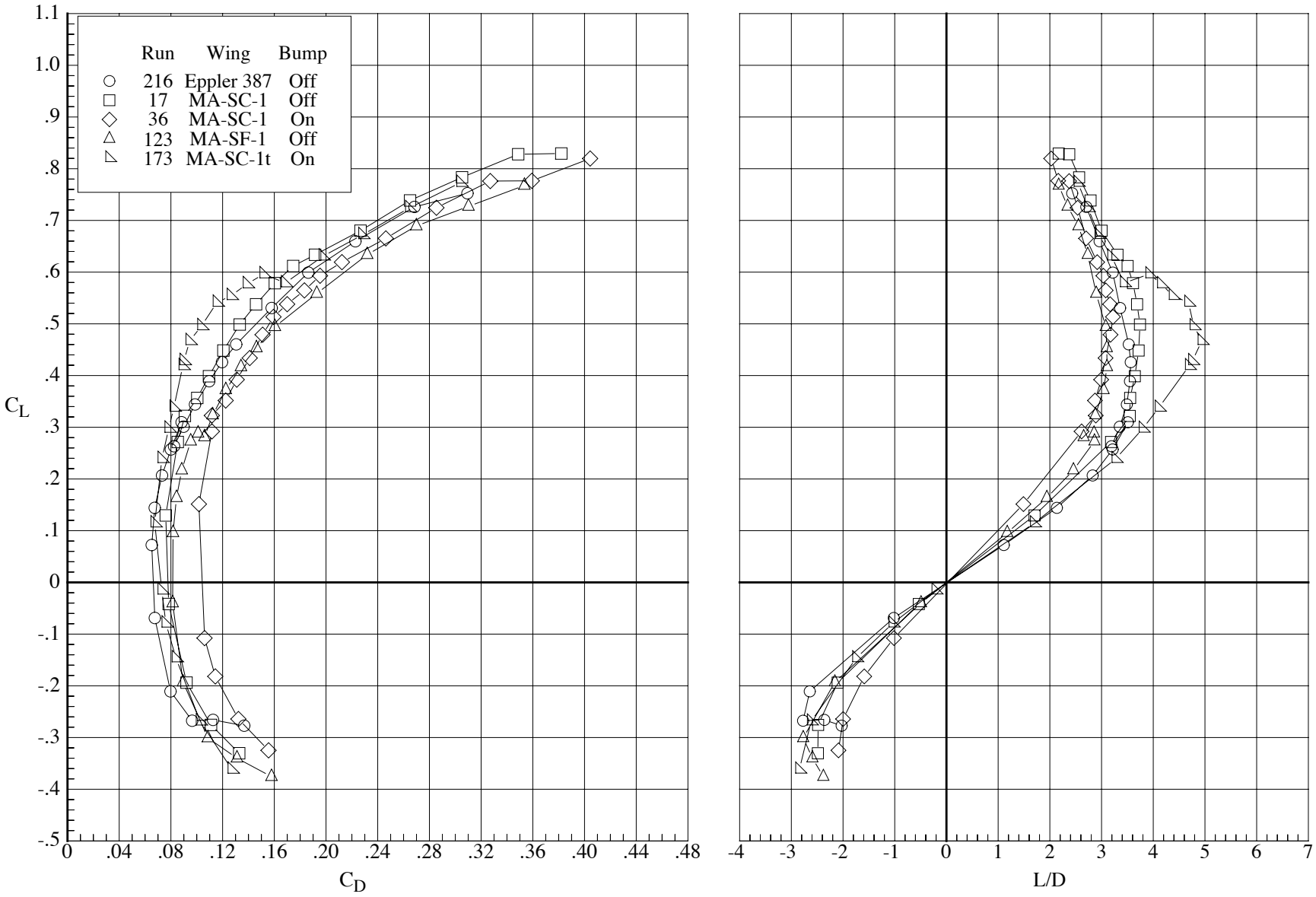

(b) Drag coefficient and lift-drag ratio.

Figure 89. Concluded.

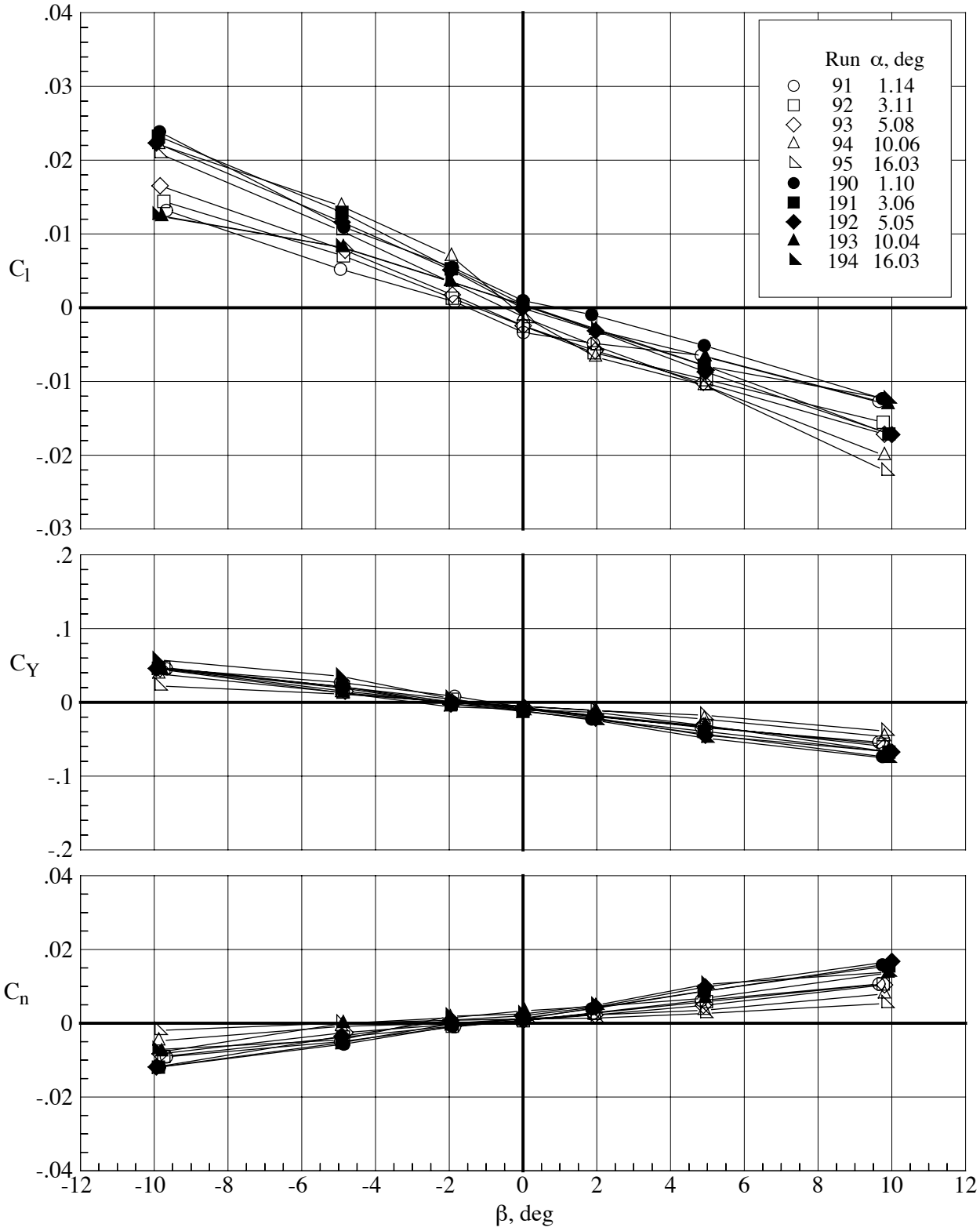

(a) Lateral-directional characteristics.

Figure 90. Effect of wing configuration (bump on) on the aerodynamic characteristics of the model at a Mach number of 0.80 and a Reynolds number of 60,000 at five angles of attack. $\delta_h = 0°$ and $\delta_f = 0°$. The open symbols indicate the MA-SC-1 wing configuration and the solid symbols indicate the MA-SC-1t wing configuration.

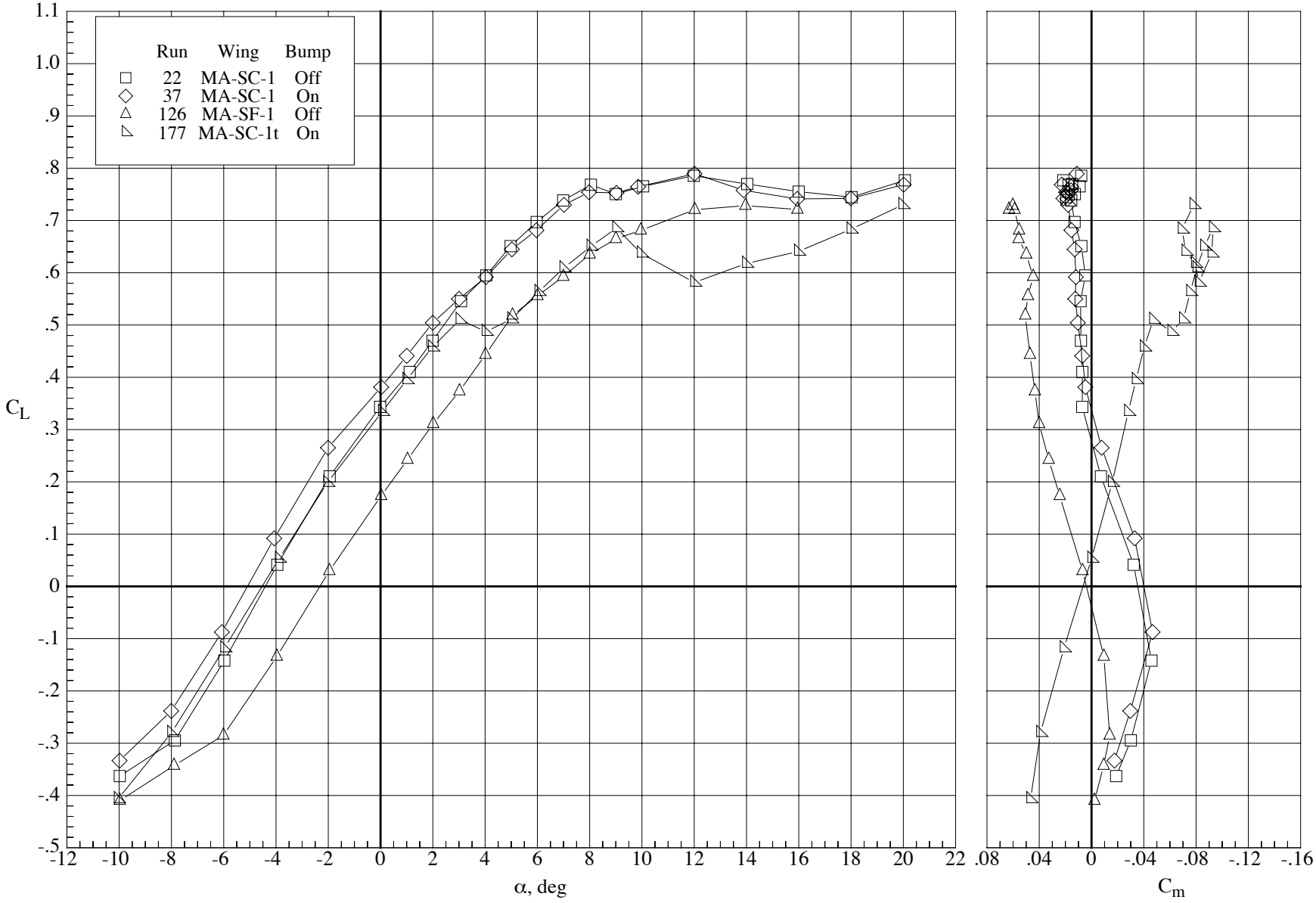

(a) Lift and pitching-moment coefficients.

Figure 91. Effect of wing configuration and bump on the longitudinal aerodynamic characteristics of the model at a Mach number of 0.65 and a Reynolds number of 100,000. $\delta_h = 0°$ and $\delta_f = 0°$.

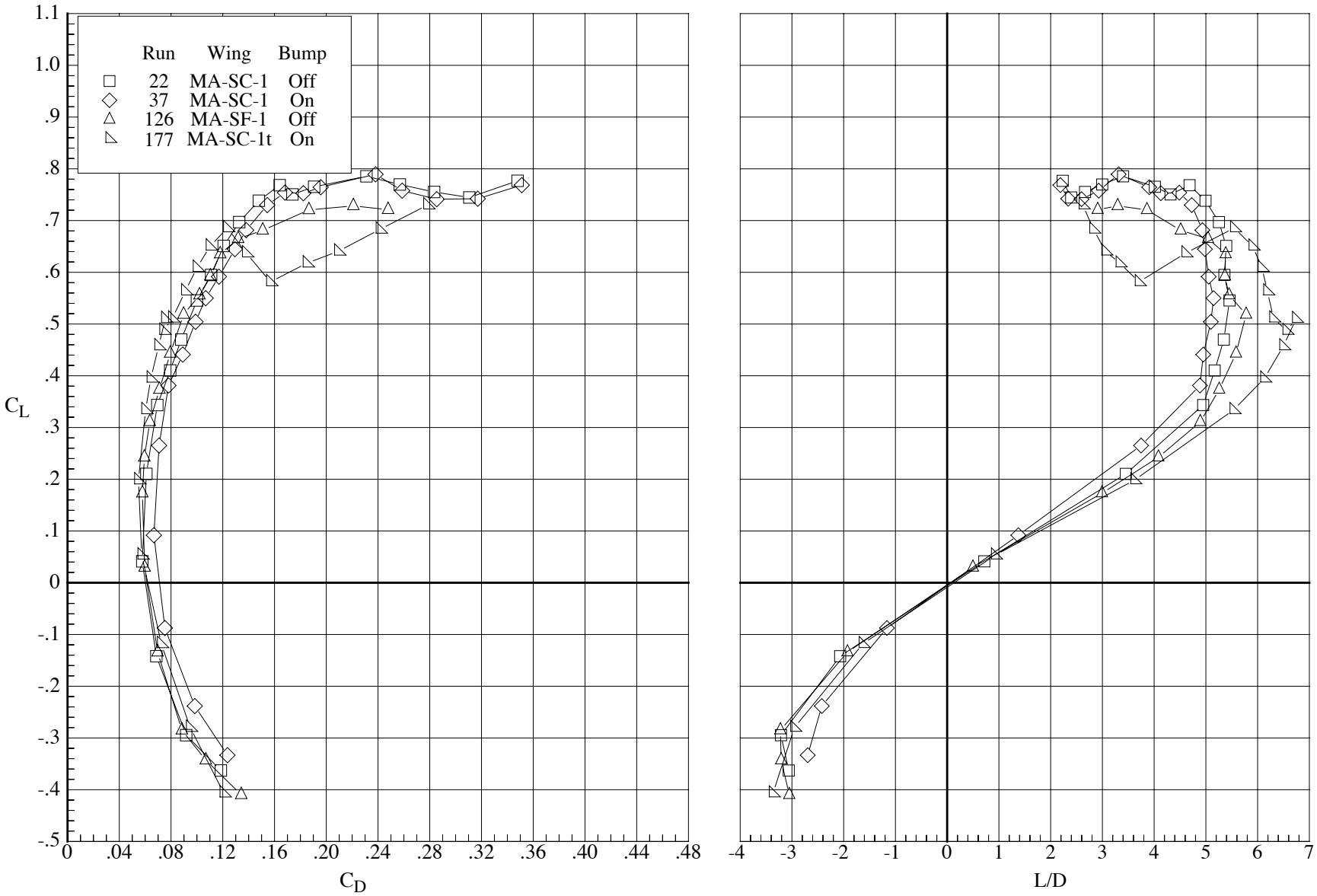

(b) Drag coefficient and lift-drag ratio.

Figure 91. Concluded.

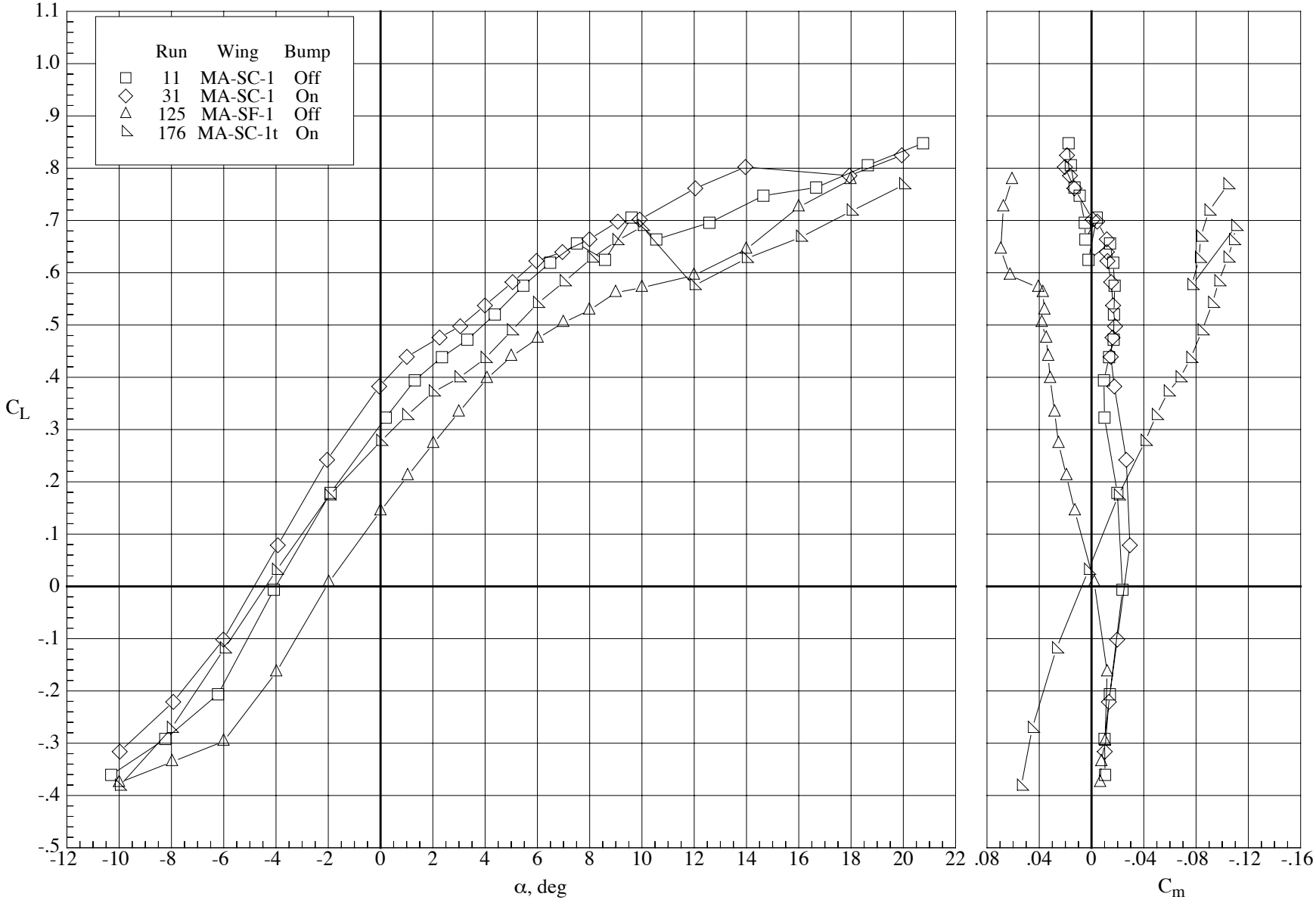

(a) Lift and pitching-moment coefficients.

Figure 92. Effect of wing configuration and bump on the longitudinal aerodynamic characteristics of the model at a Mach number of 0.80 and a Reynolds number of 100,000. $\delta_h = 0°$ and $\delta_f = 0°$.

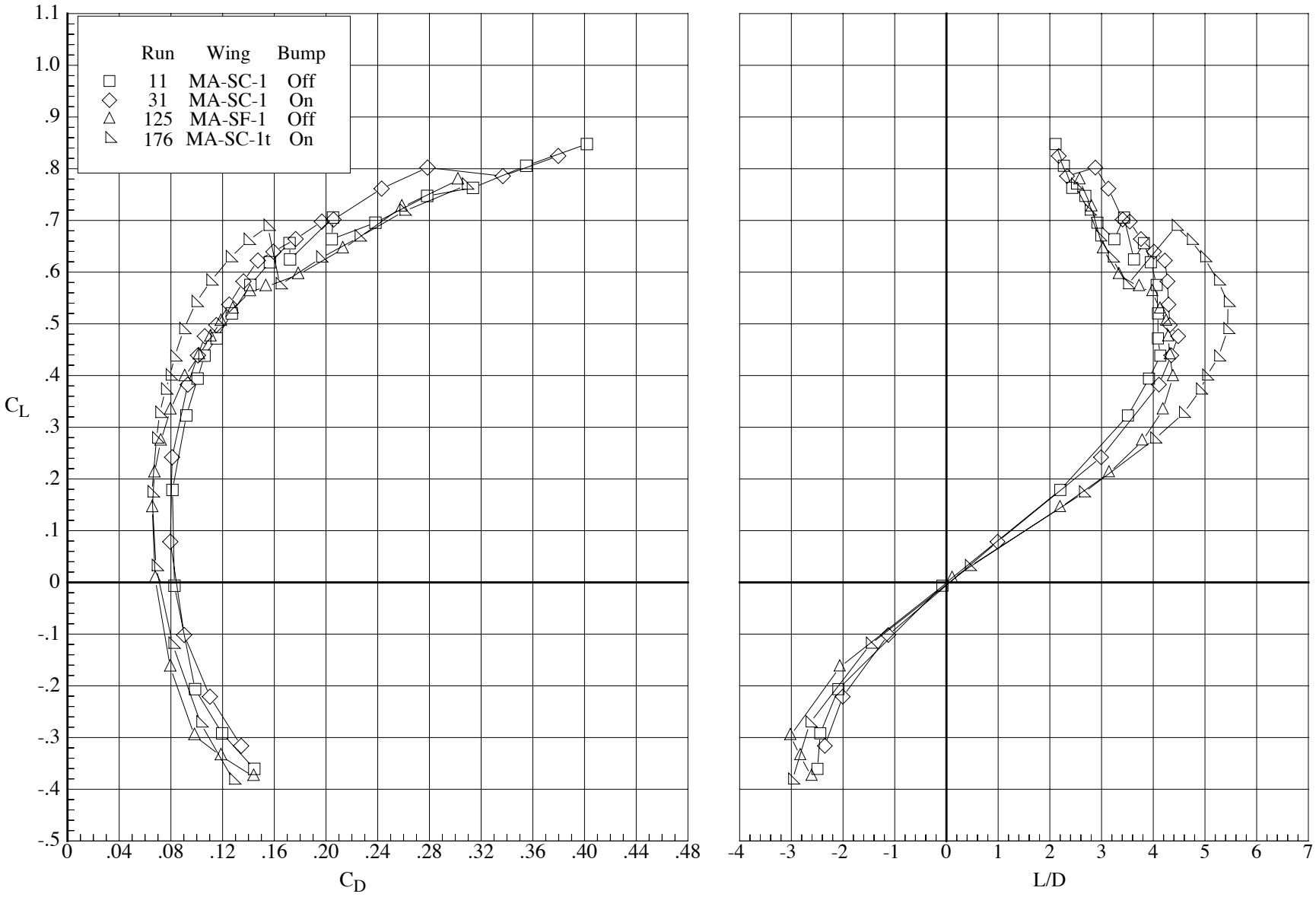

(b) Drag coefficient and lift-drag ratio.

Figure 92. Concluded.

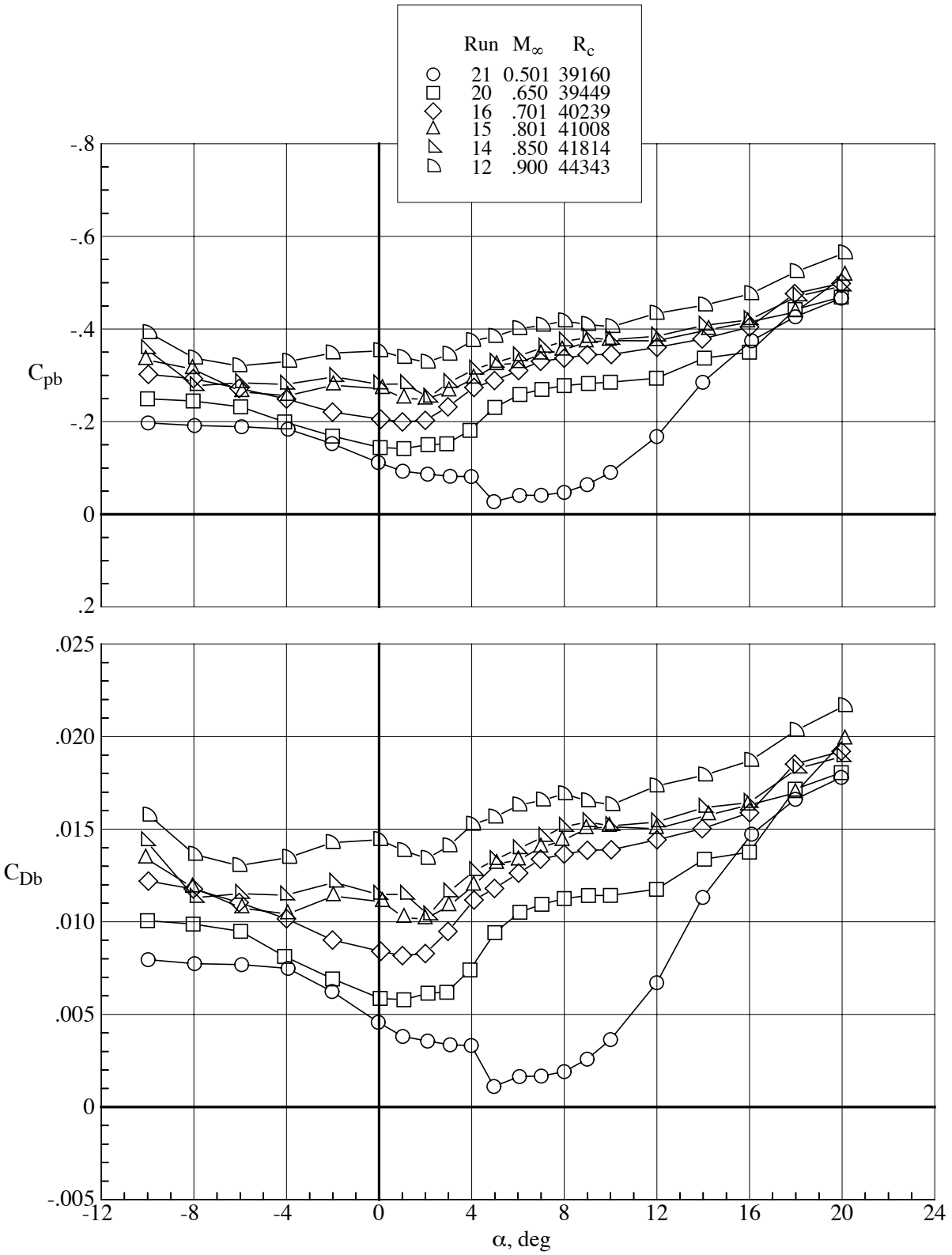

(a) Variation of base drag and pressure coefficients with angle of attack.

Figure 93. Typical magnitudes and variations of base drag and pressure coefficients with angles of attack and sideslip at a Reynolds number of 40,000. Test 540.

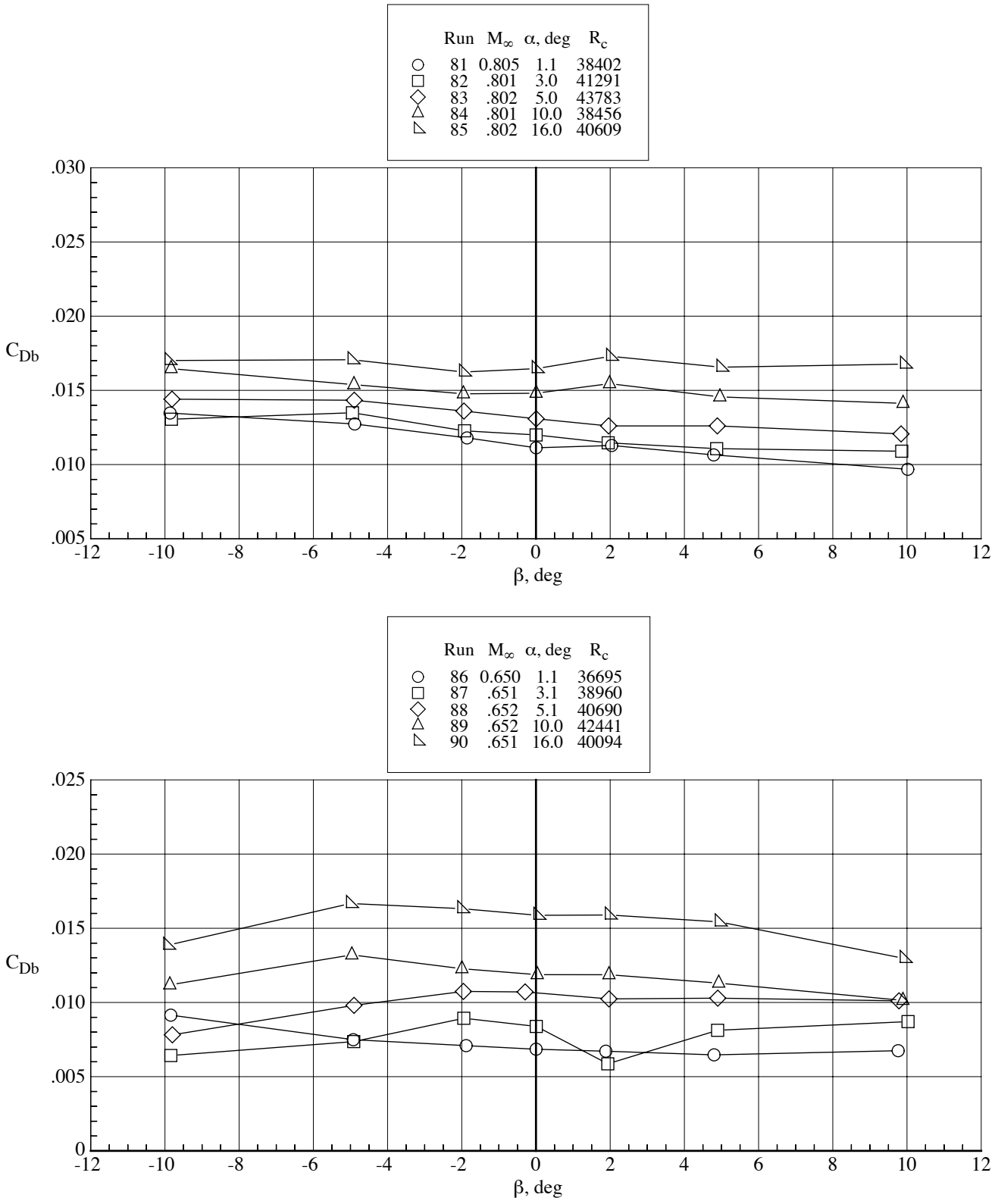

(b) Variation of base drag coefficient with angle of sideslip.

Figure 93. Concluded.

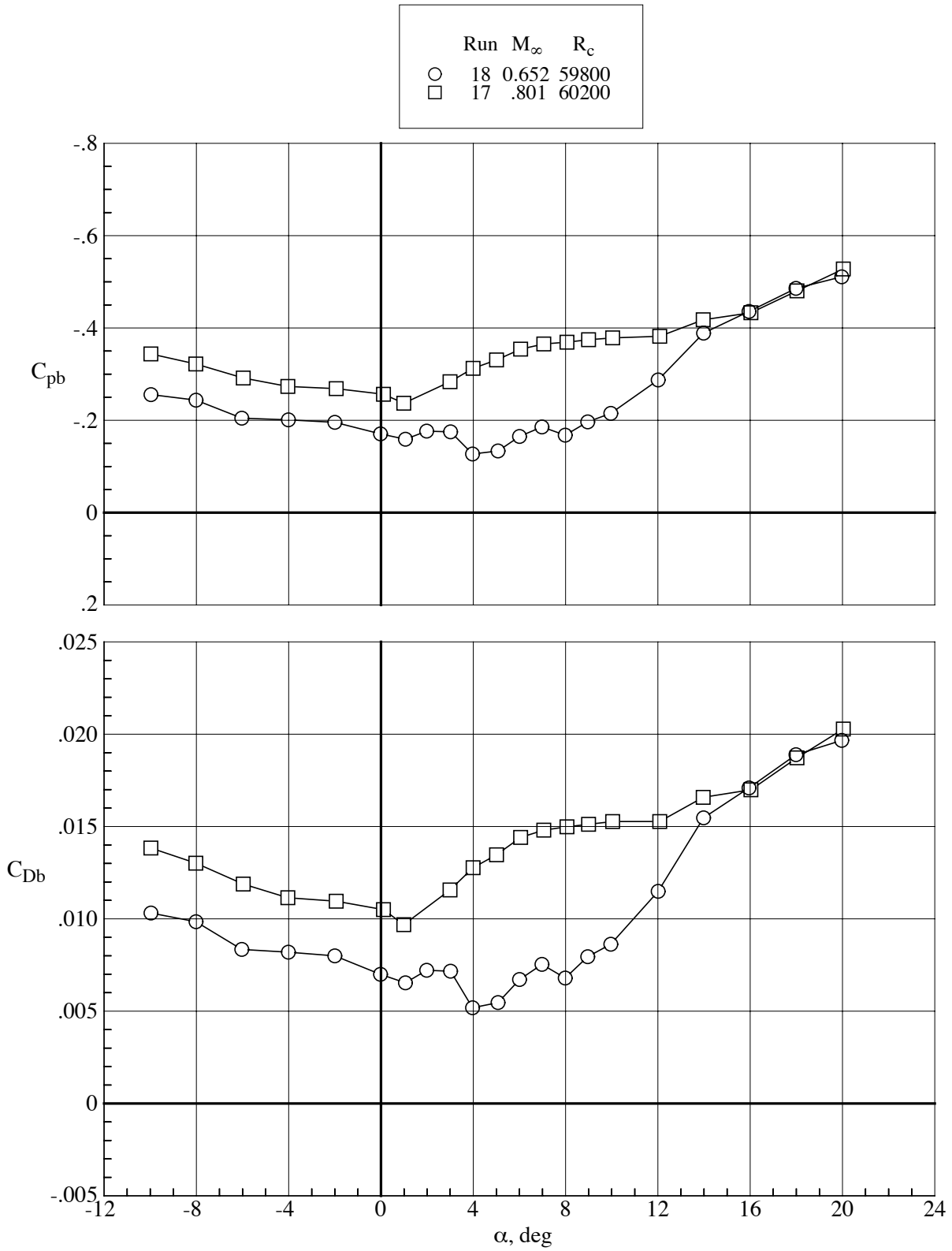

(a) Variation of base drag and pressure coefficients with angle of attack.

Figure 94. Typical magnitudes and variations of base drag and pressure coefficients with angles of attack and sideslip at a Reynolds number of 60,000. Test 540.

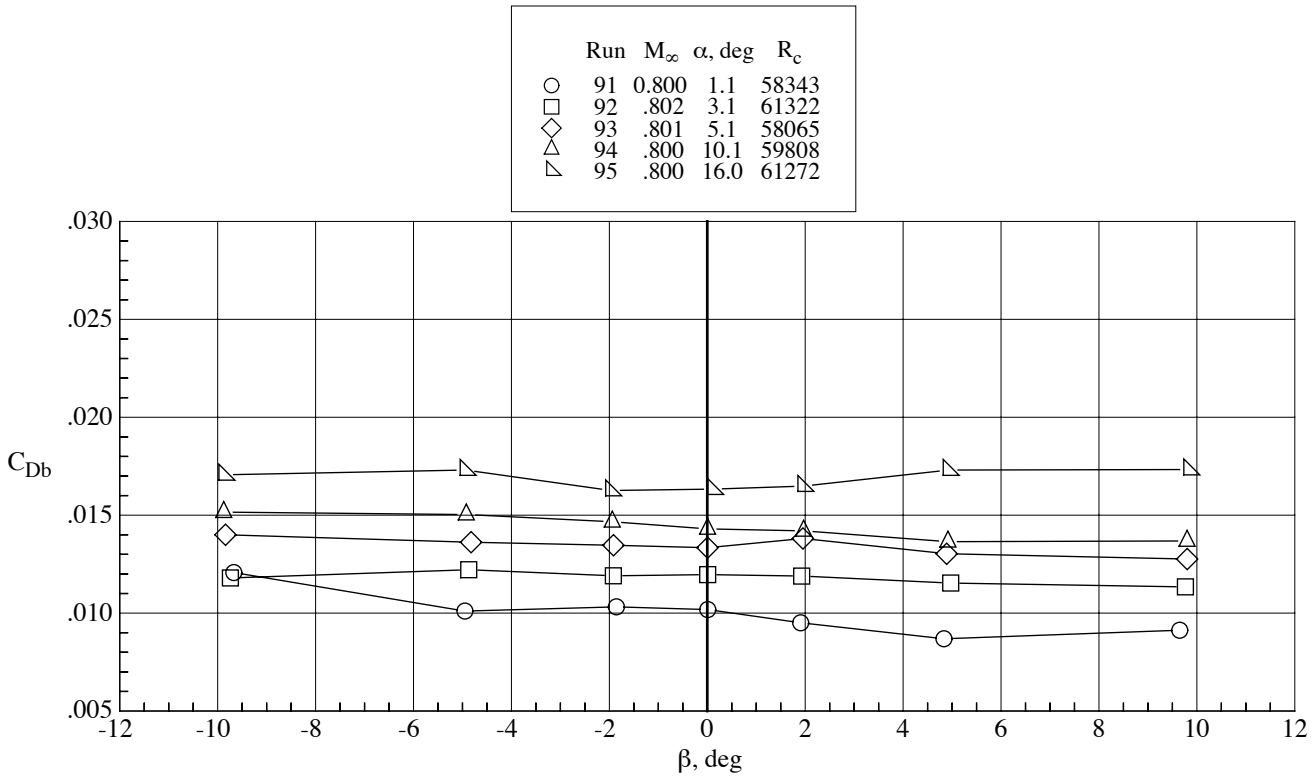

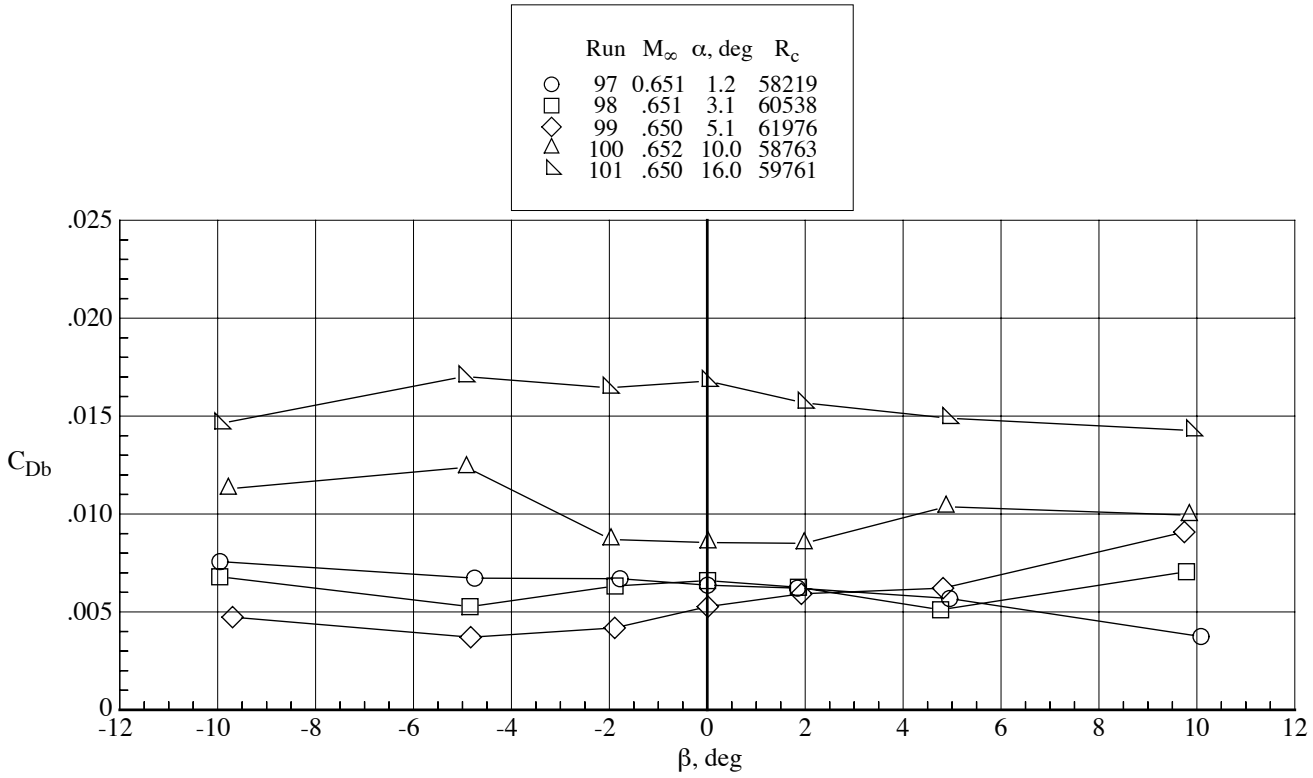

(b) Variation of base drag coefficient with angle of sideslip.

Figure 94. Concluded.

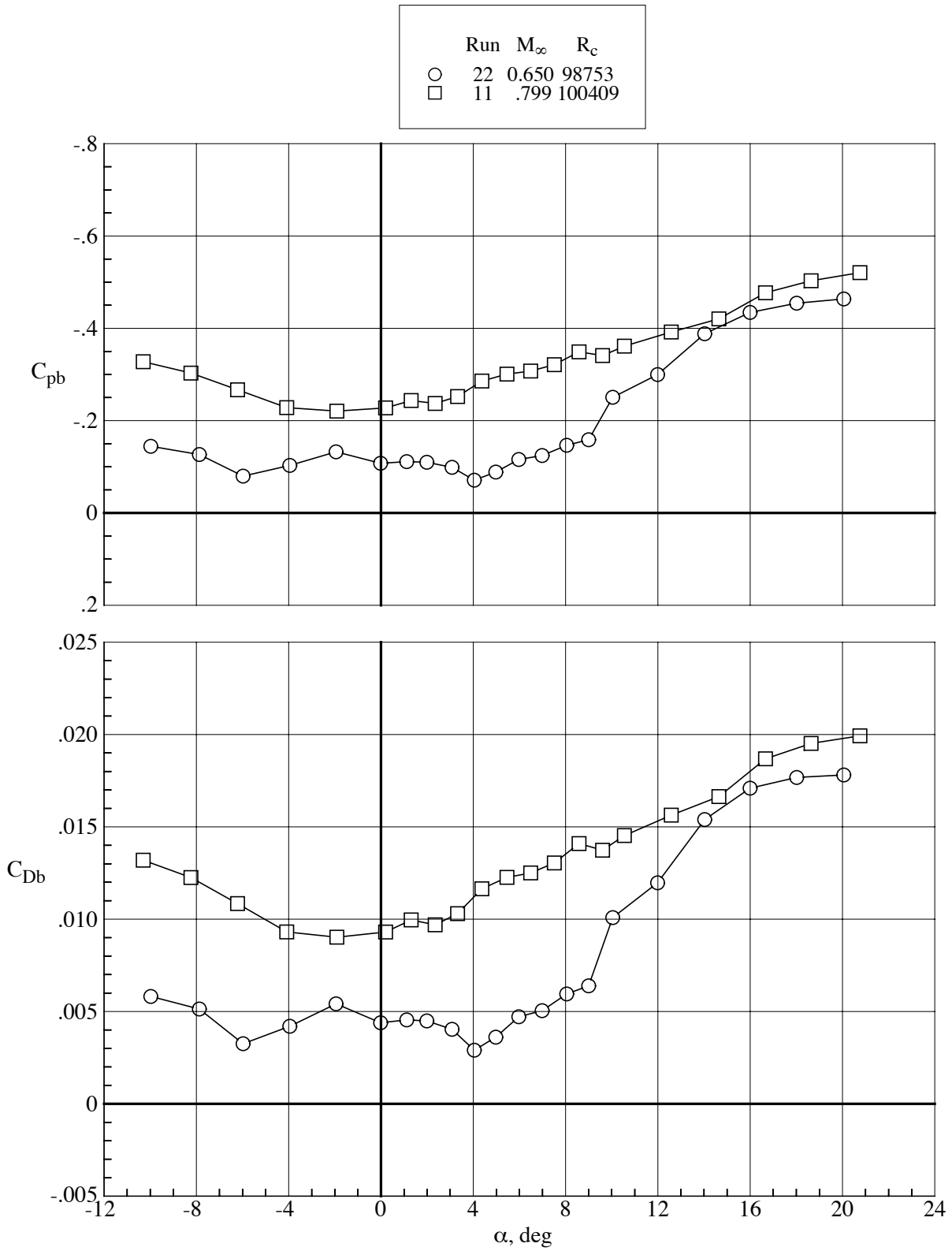

Figure 95. Typical magnitudes and variations of base drag and pressure coefficients with angle of attack at a Reynolds number of 100,000. Test 540.

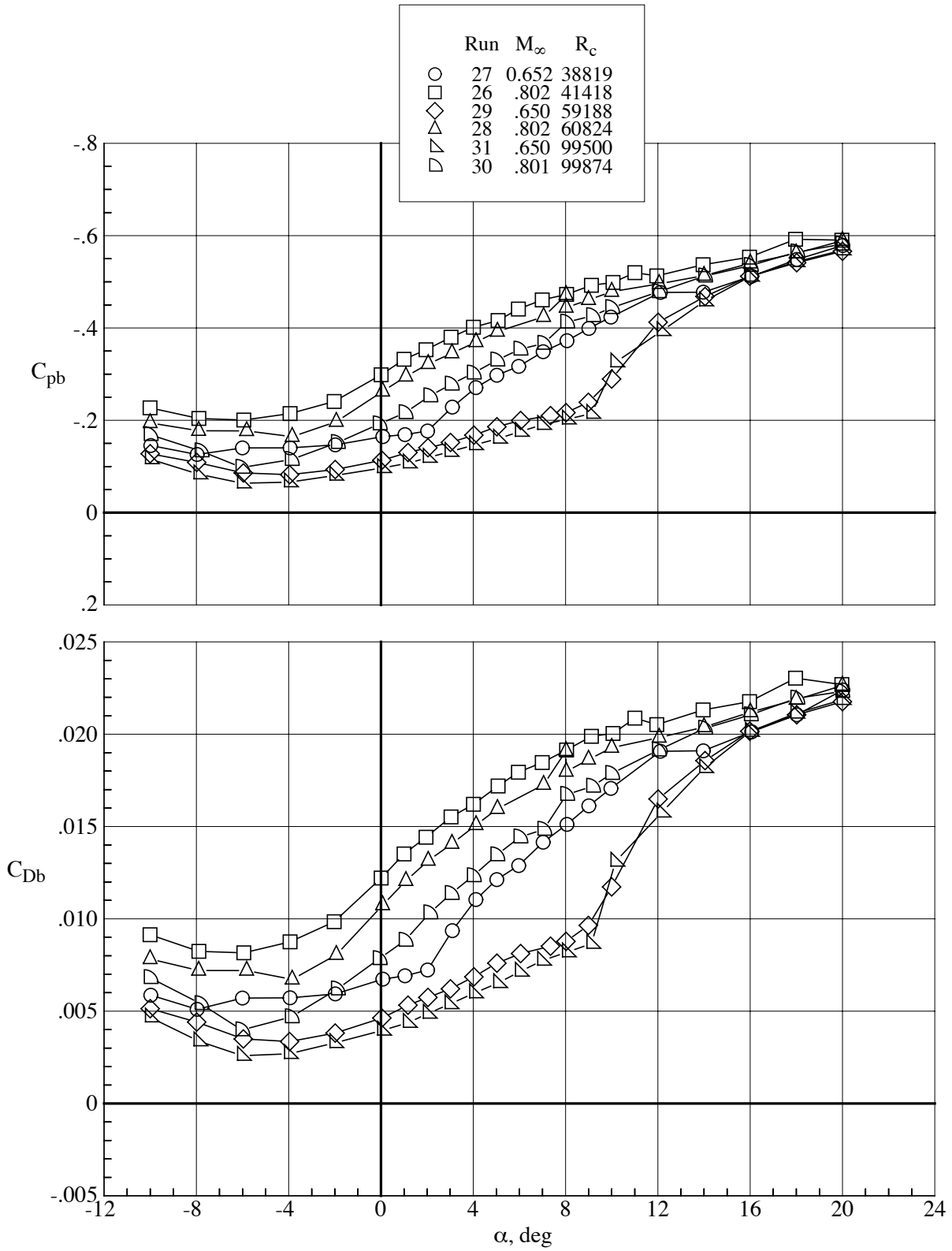

(a) Variation of base drag and pressure coefficients with angle of attack.

Figure 96. Typical magnitudes and variations of base drag and pressure coefficients with angles of attack and sideslip at three Reynolds numbers for the model with the lower fuselage removed and the tails inverted. Test 541.

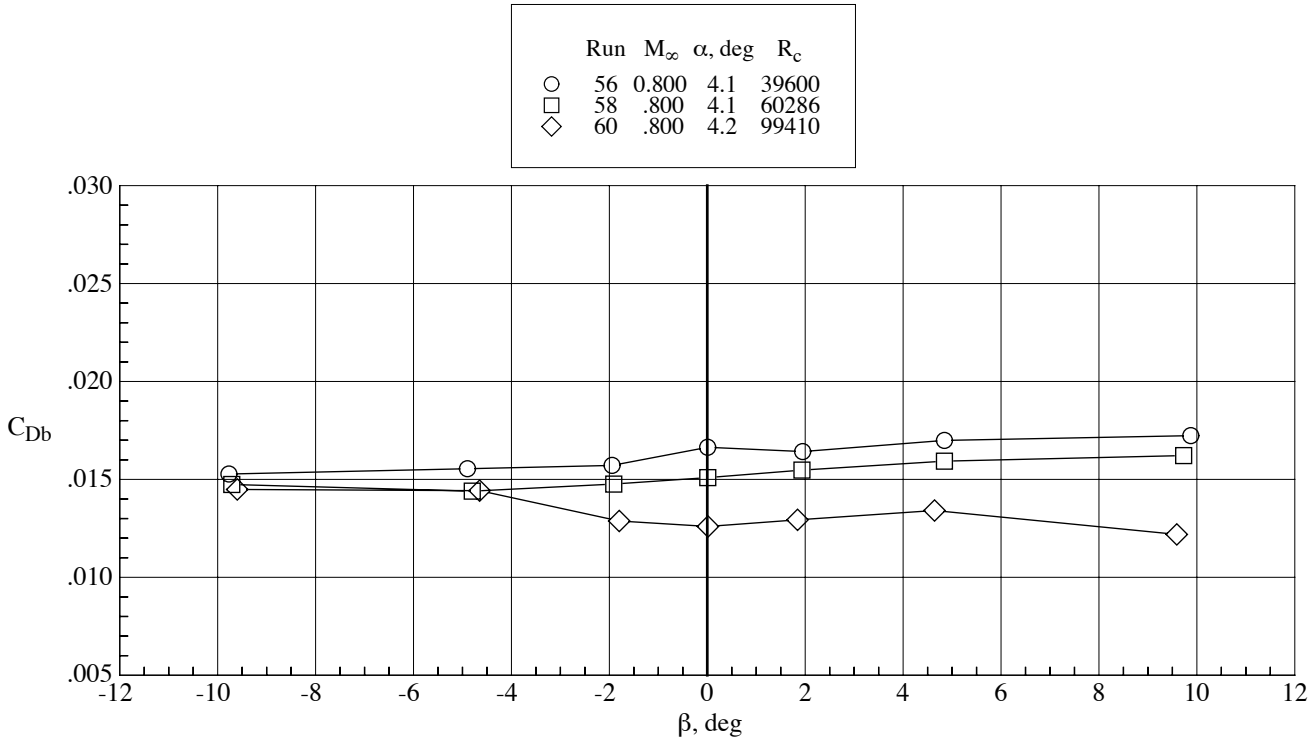

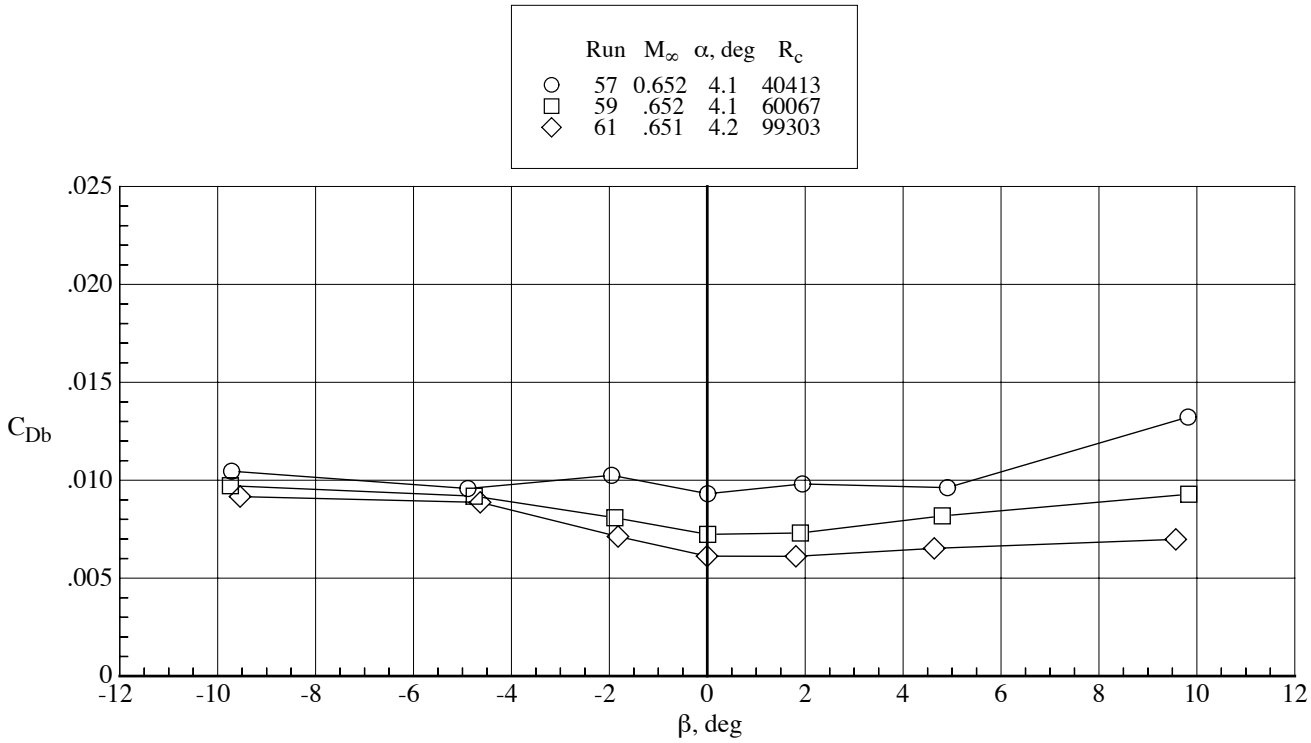

(b) Variation of base drag coefficient with angle of sideslip.

Figure 96. Concluded.

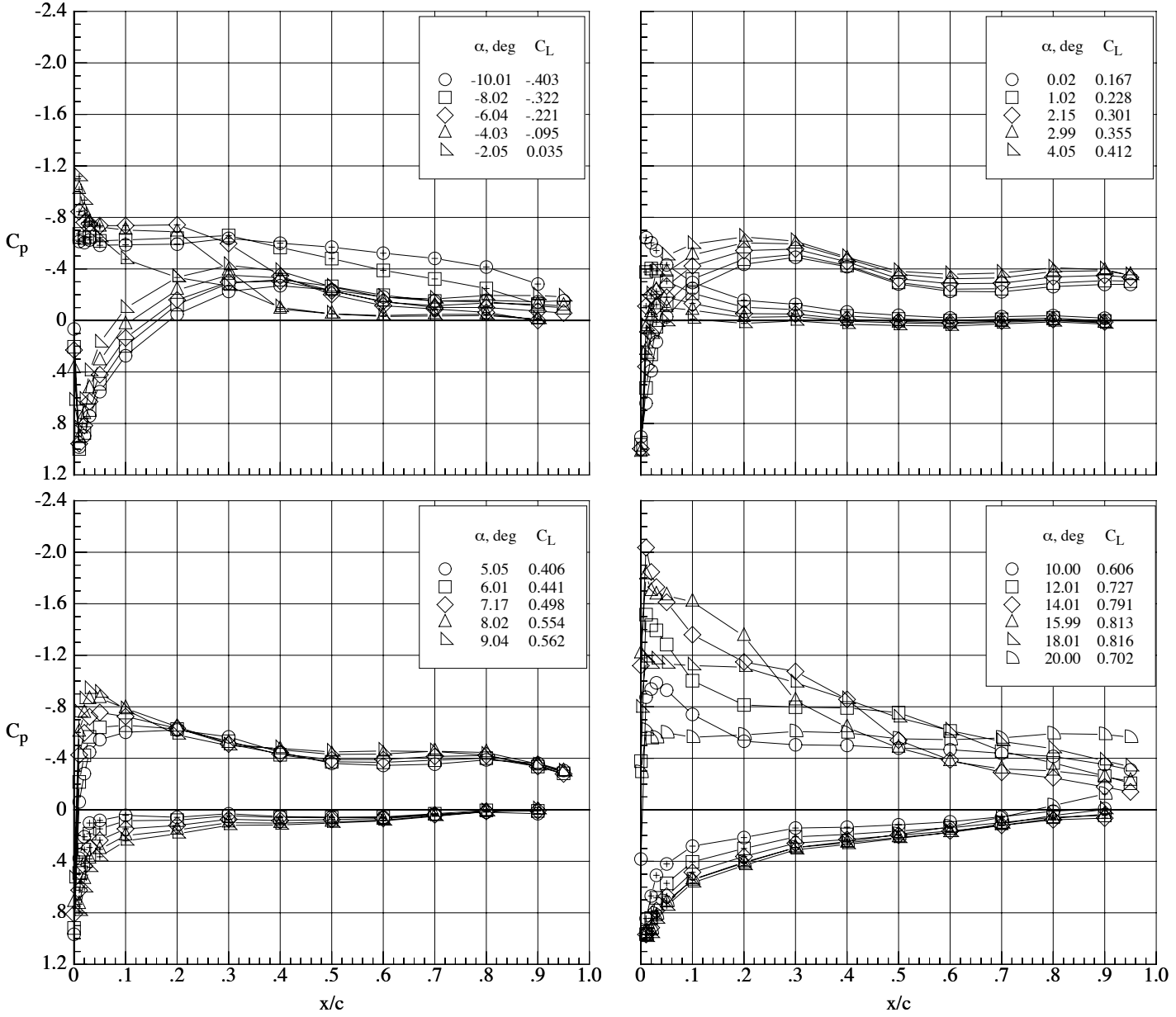

(a) Mach number 0.25.

Figure 97. Chordwise pressure coefficient distributions on the Eppler 387 wing (bump off) at a Reynolds number of 40,000. $\delta_h = 0°$ and $\delta_f = 0°$.

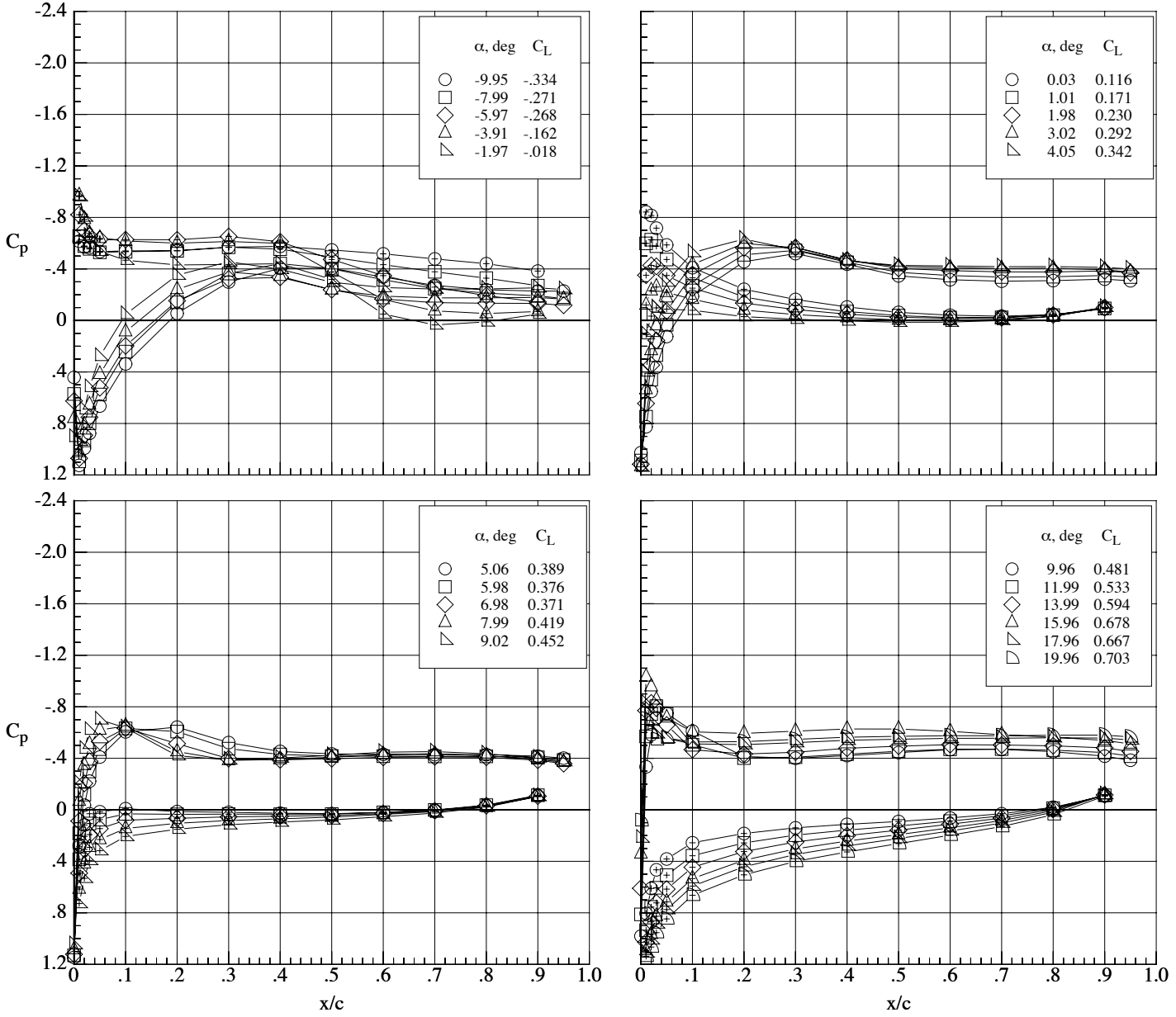

(b) Mach number 0.65.

Figure 97. Continued.

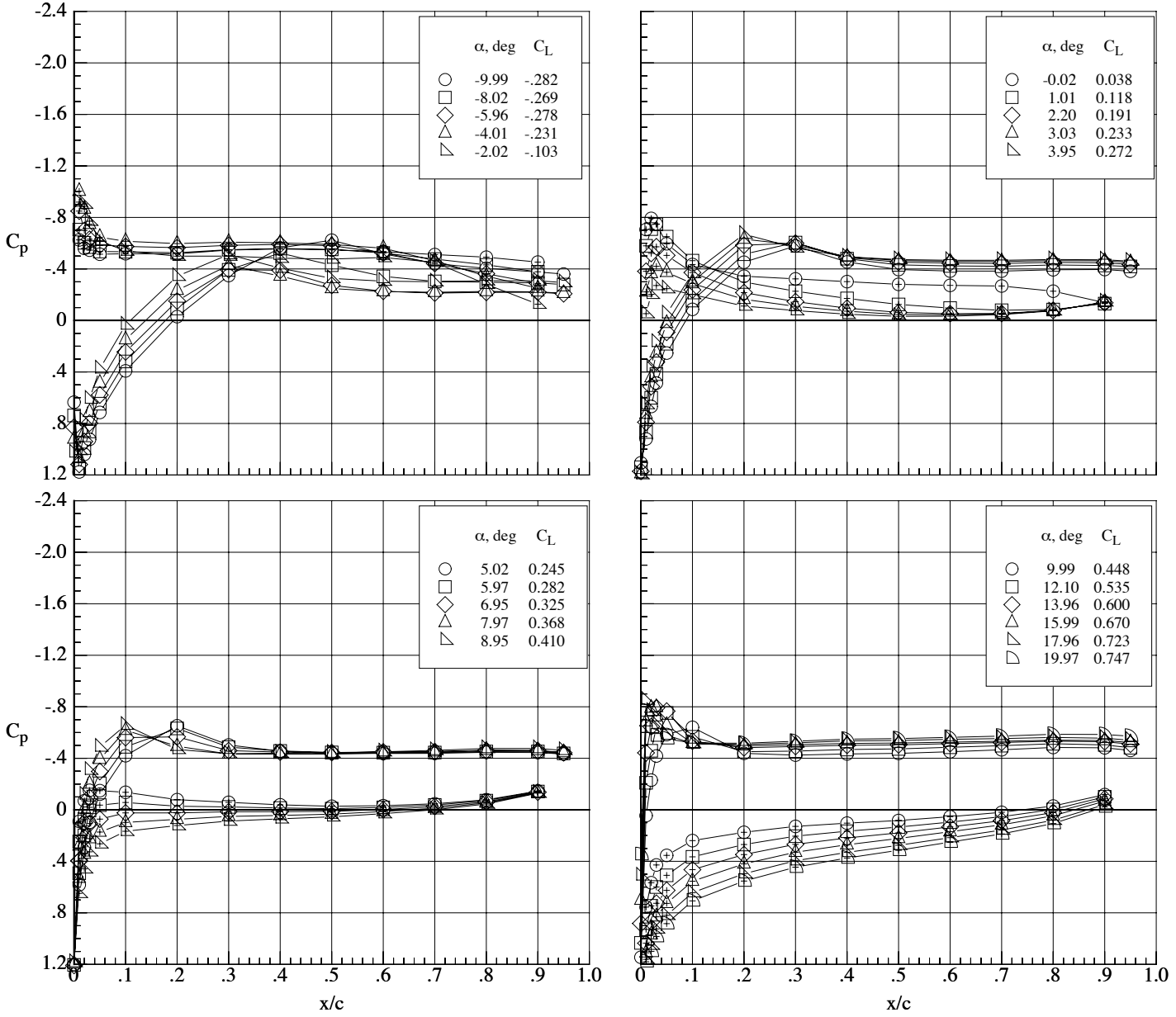

(c) Mach number 0.80.

Figure 97. Concluded.

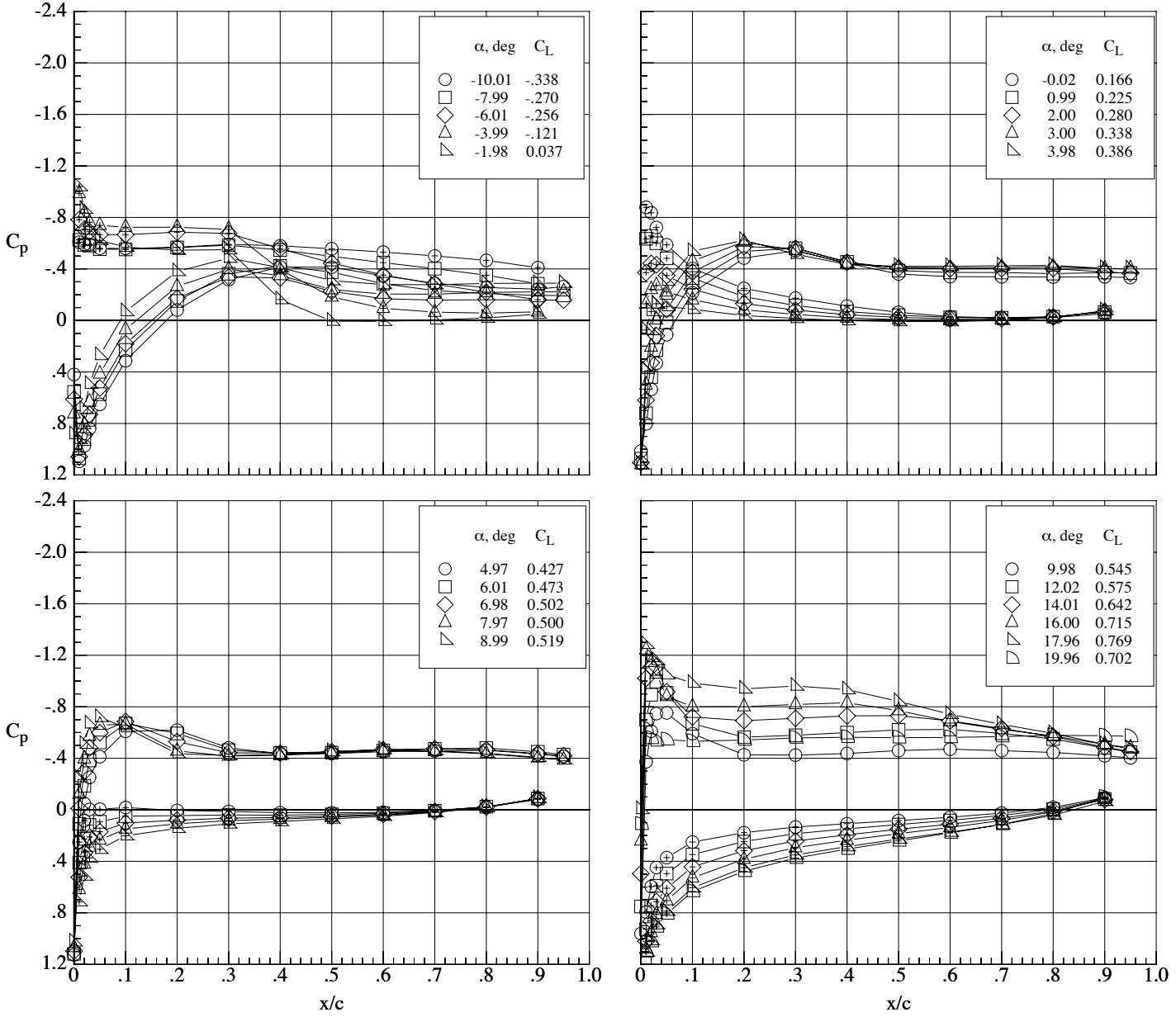

(a) Mach number 0.65.

Figure 98. Chordwise pressure coefficient distributions on the Eppler 387 wing (bump off) at a Reynolds number of 60,000. $\delta_h = 0°$ and $\delta_f = 0°$.

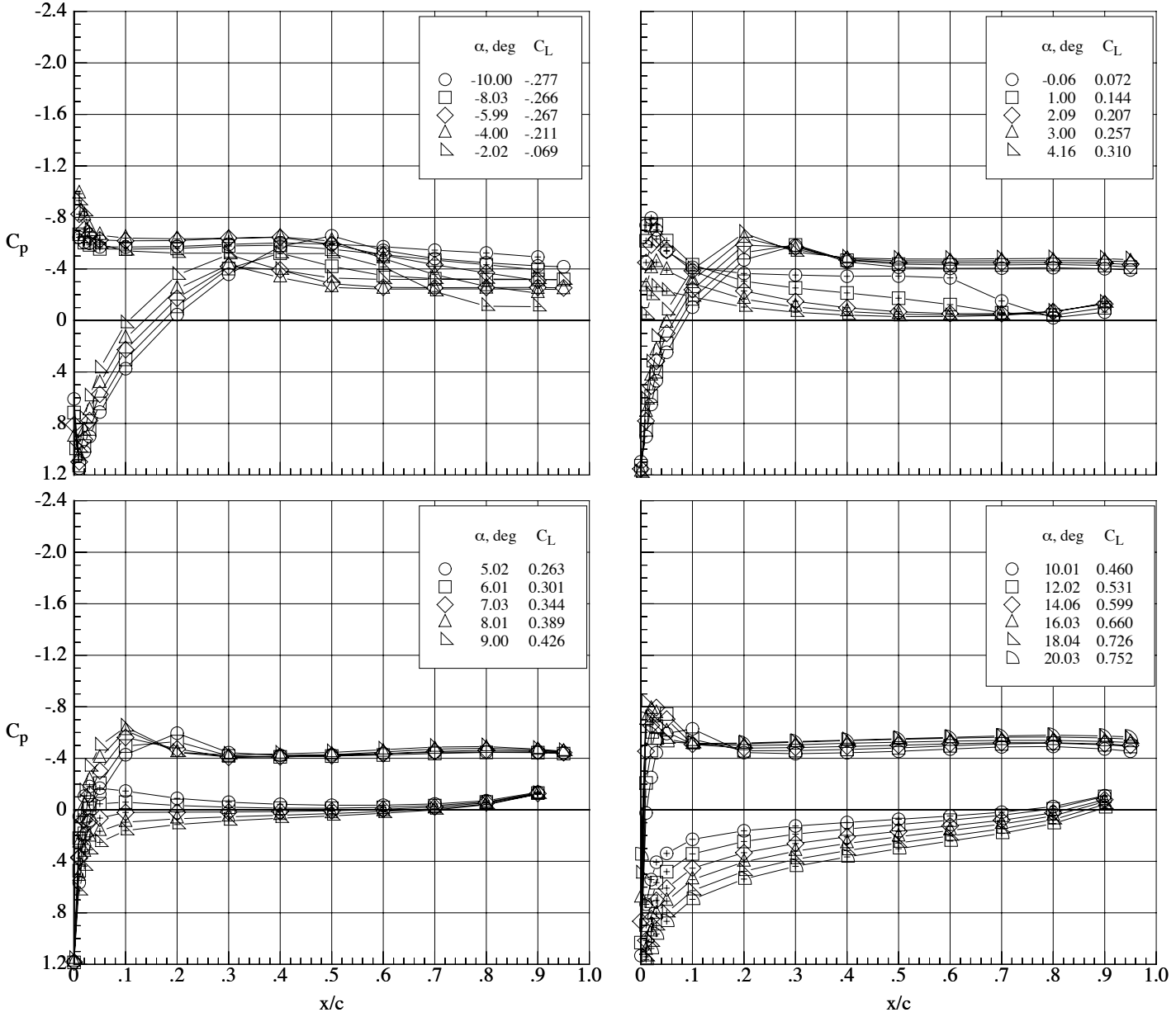

(b) Mach number 0.80.

Figure 98. Concluded.

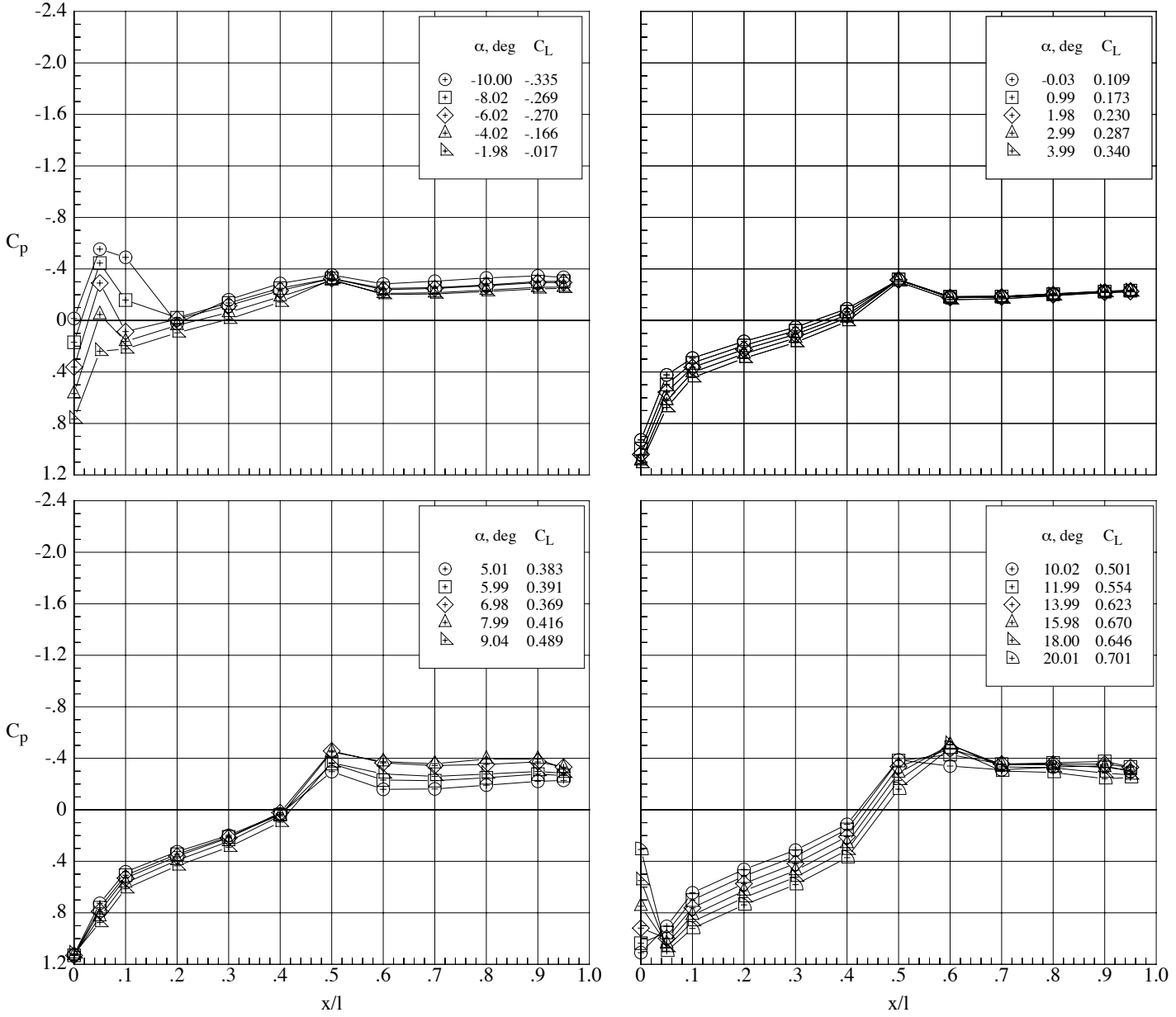

(a) Mach number 0.65.

Figure 99. Model centerline pressure coefficient distributions on the lower fuselage fairing and wing at a Reynolds number of 40,000. Wing with Eppler 387 airfoil and $\delta_h = 0°$ and $\delta_f = 0°$.

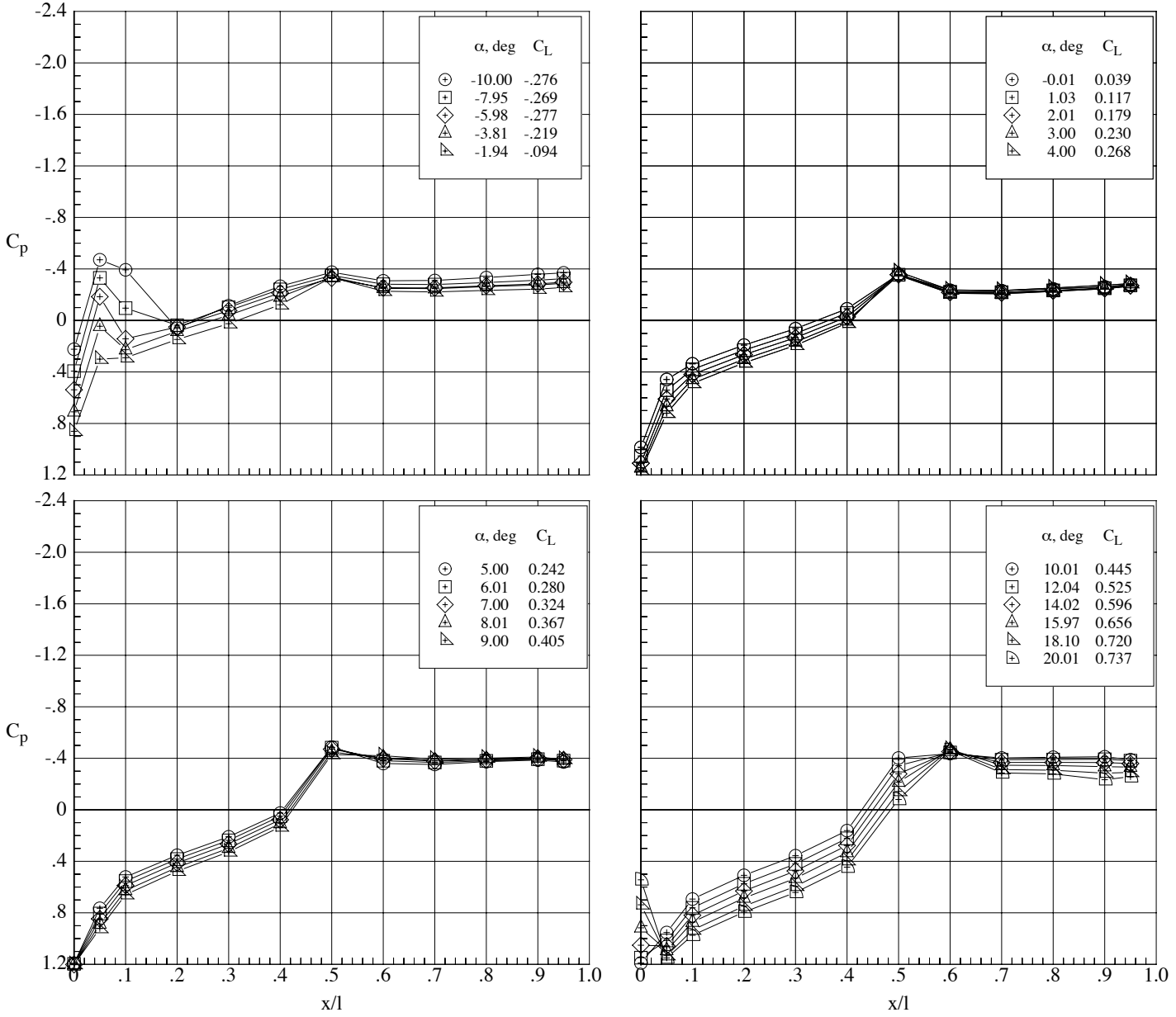

(b) Mach number 0.80.

Figure 99. Concluded.

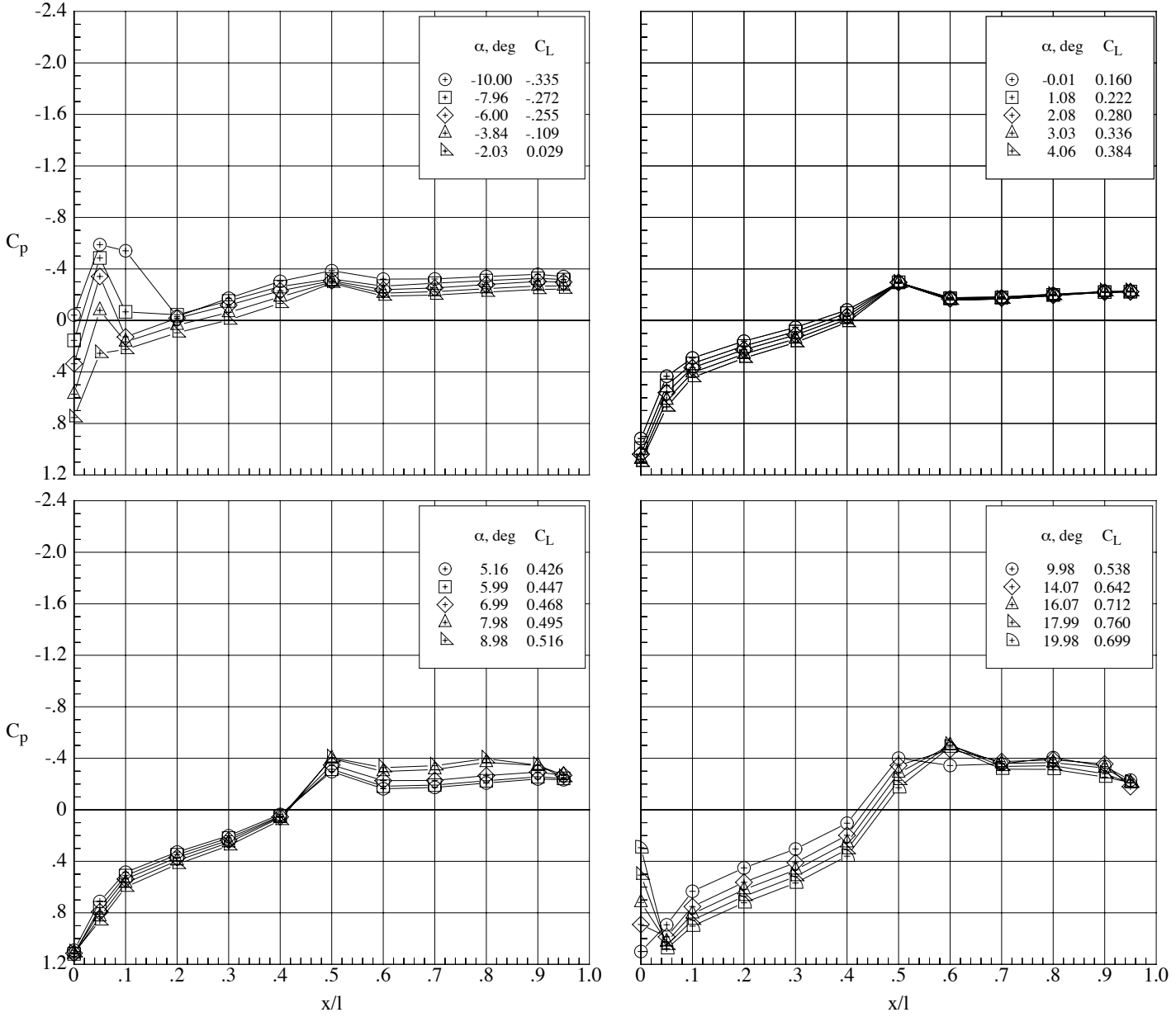

(a) Mach number 0.65.

Figure 100. Model centerline pressure coefficient distributions on the lower fuselage fairing and wing at a Reynolds number of 60,000. Wing with Eppler 387 airfoil and $\delta_h = 0°$ and $\delta_f = 0°$.

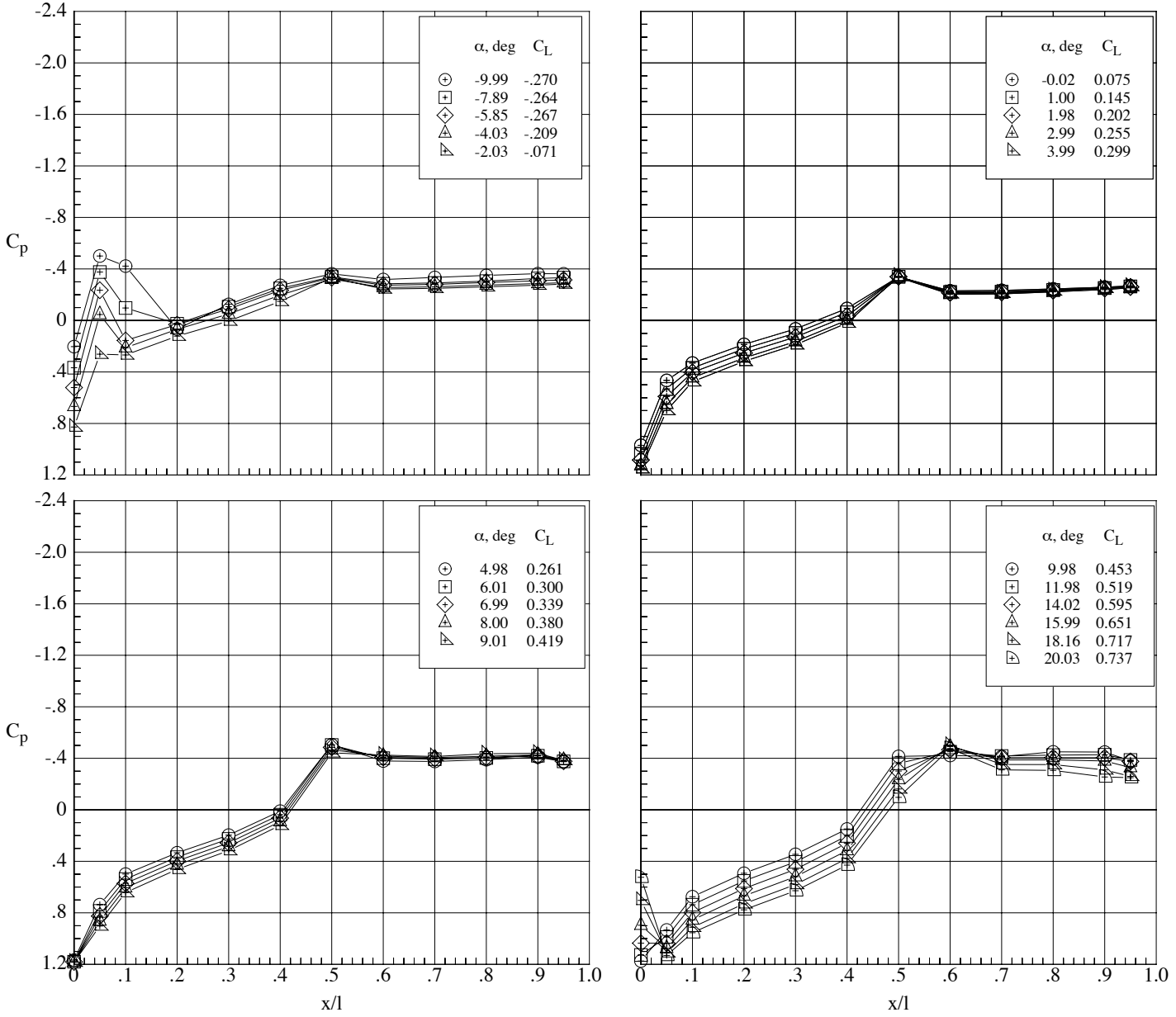

(b) Mach number 0.80.

Figure 100. Concluded.

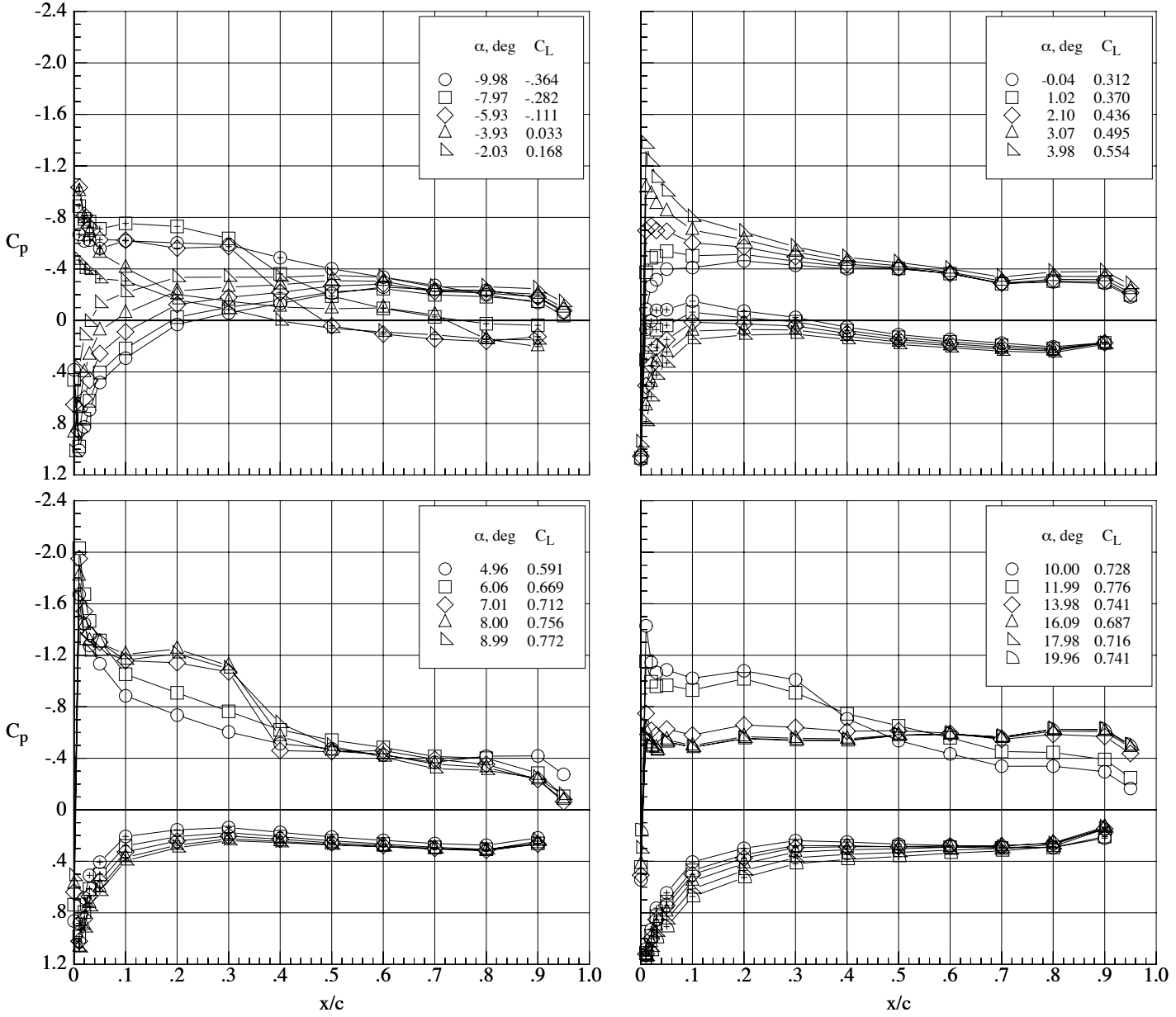

(a) Mach number 0.50.

Figure 101. Chordwise pressure coefficient distributions on the MA-SC-1 wing (bump off) at a Reynolds number of 40,000. $\delta_h = 0°$ and $\delta_f = 0°$.

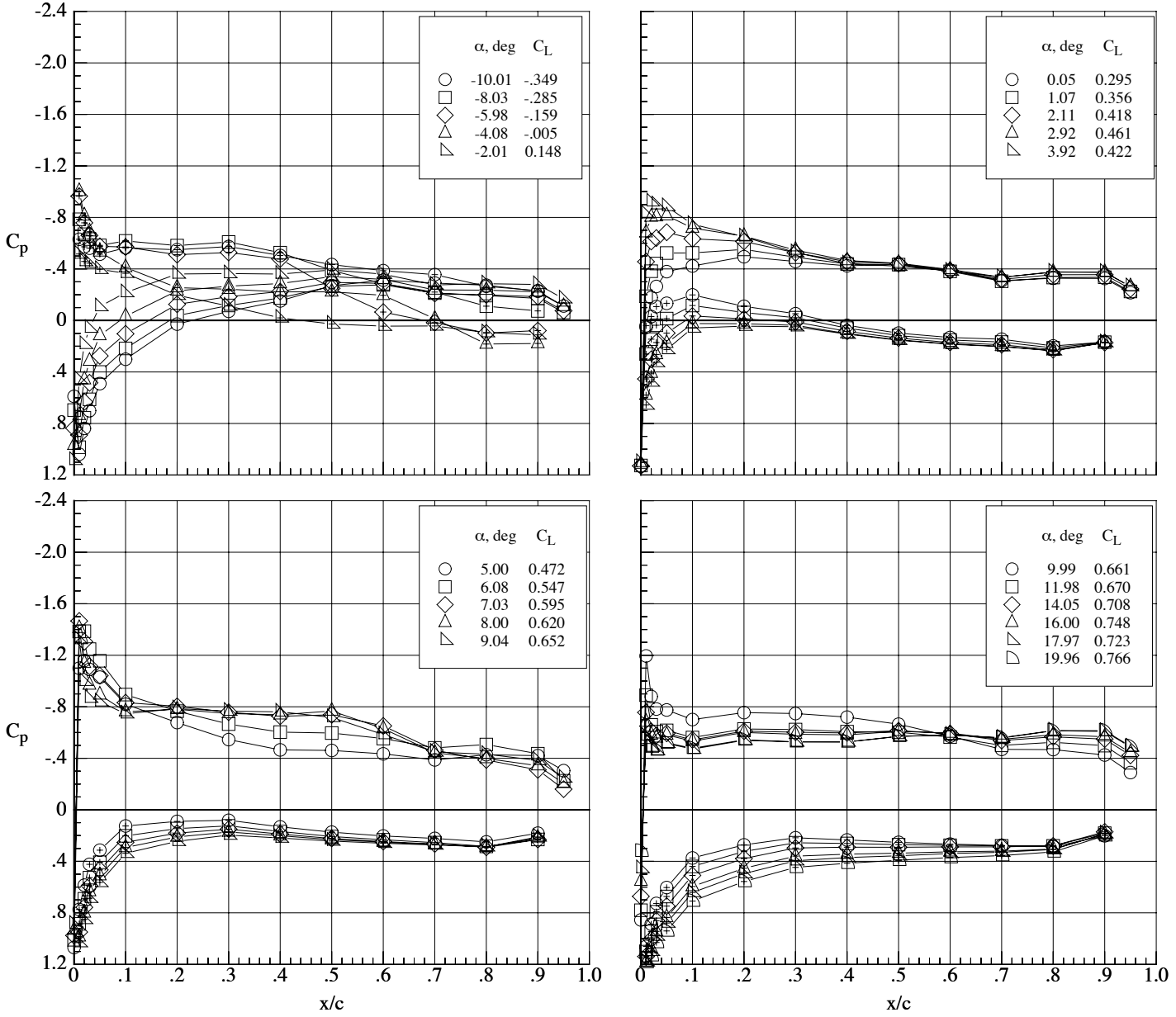

(b) Mach number 0.65.

Figure 101. Continued.

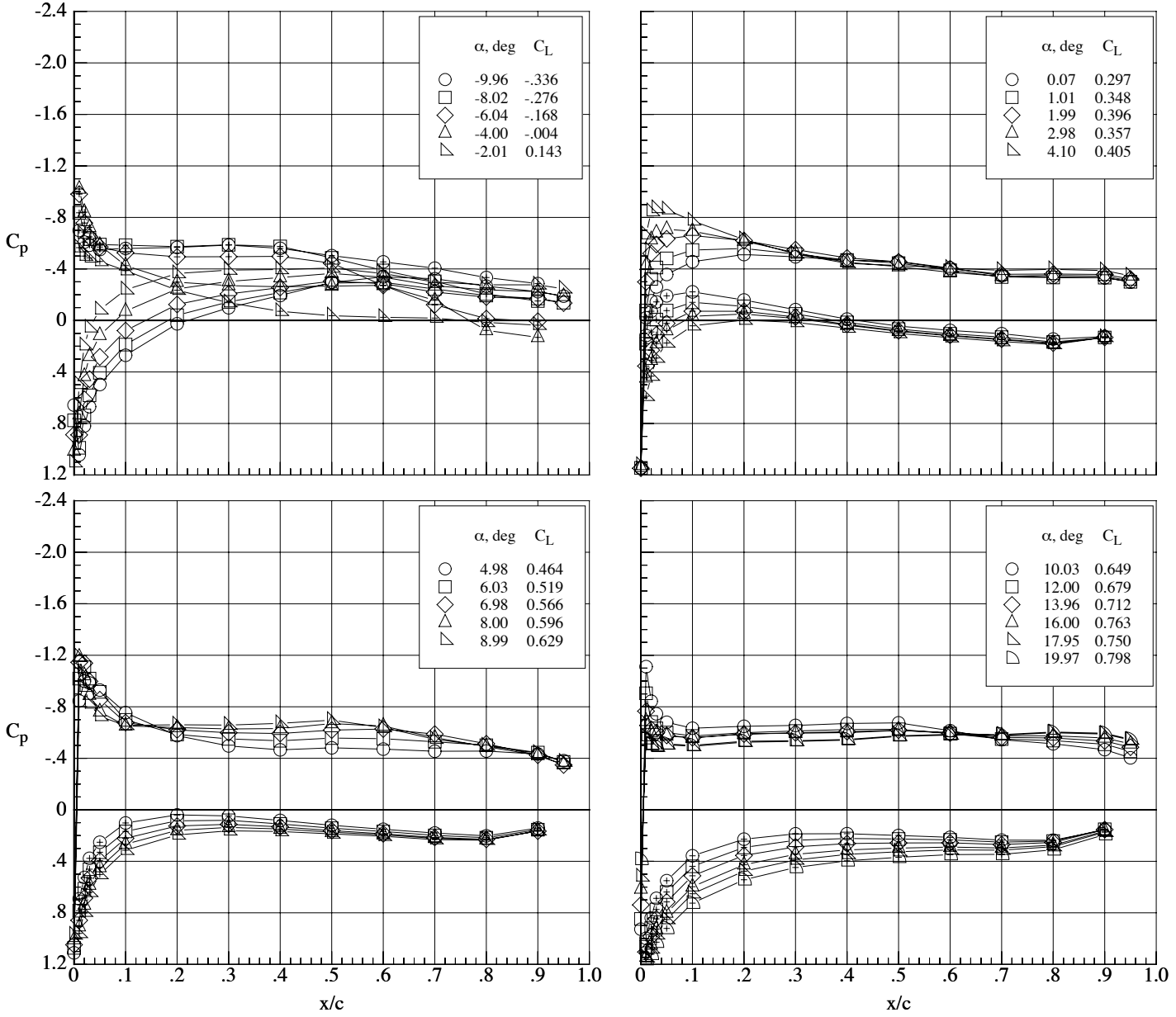

(c) Mach number 0.70.

Figure 101. Continued.

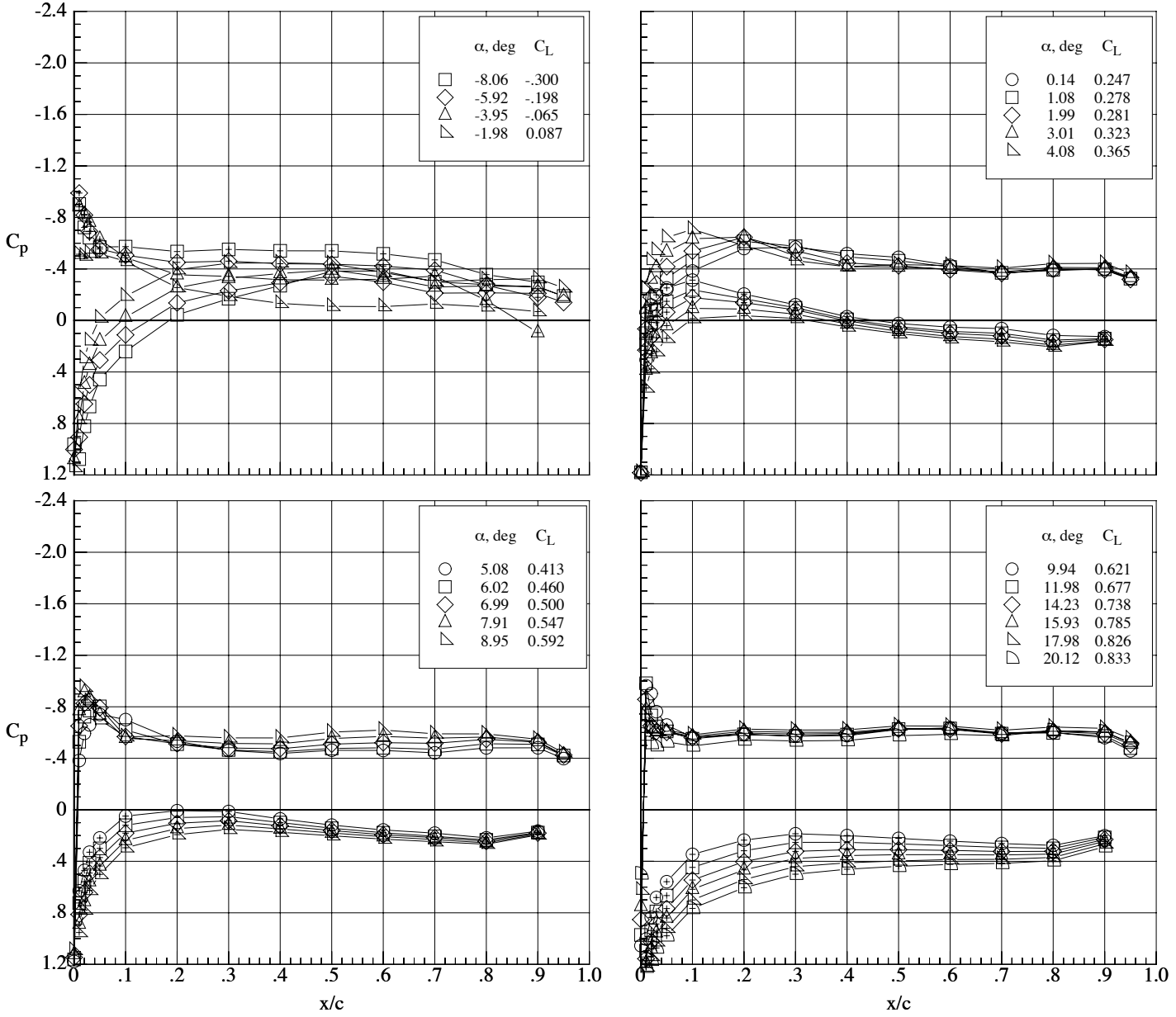

(d) Mach number 0.80.

Figure 101. Continued.

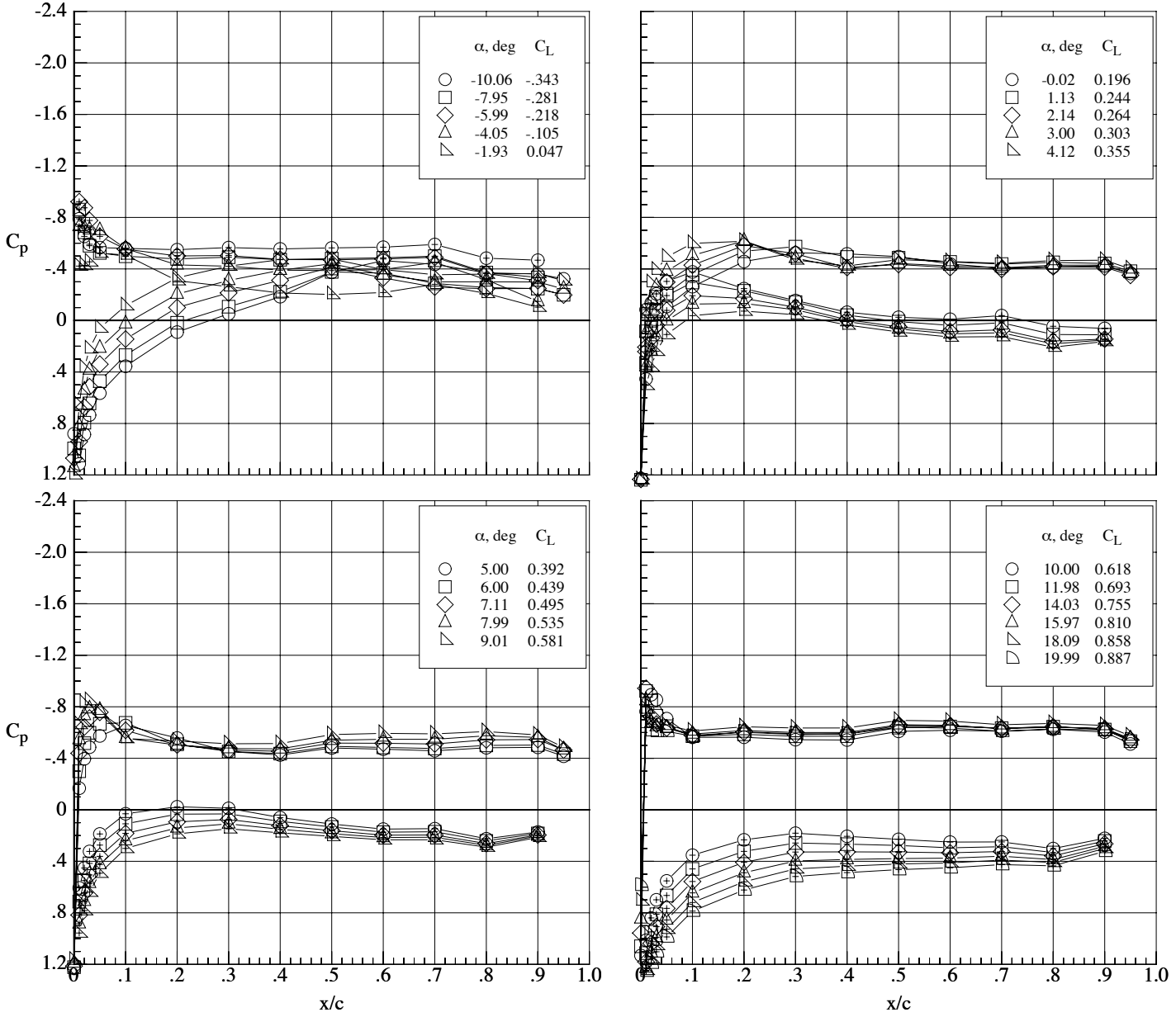

(e) Mach number 0.85.

Figure 101. Continued.

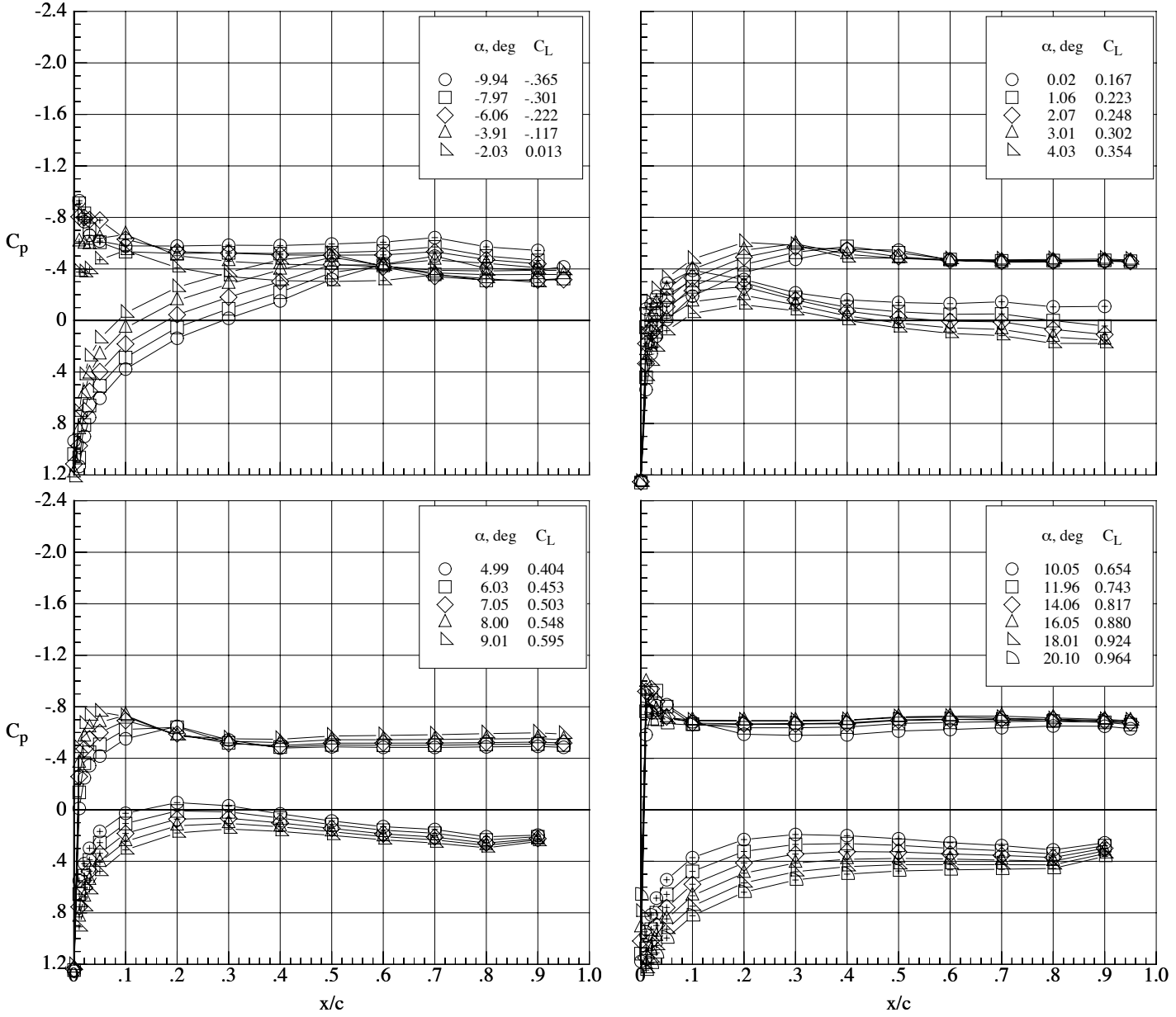

(f) Mach number 0.90.

Figure 101. Concluded.

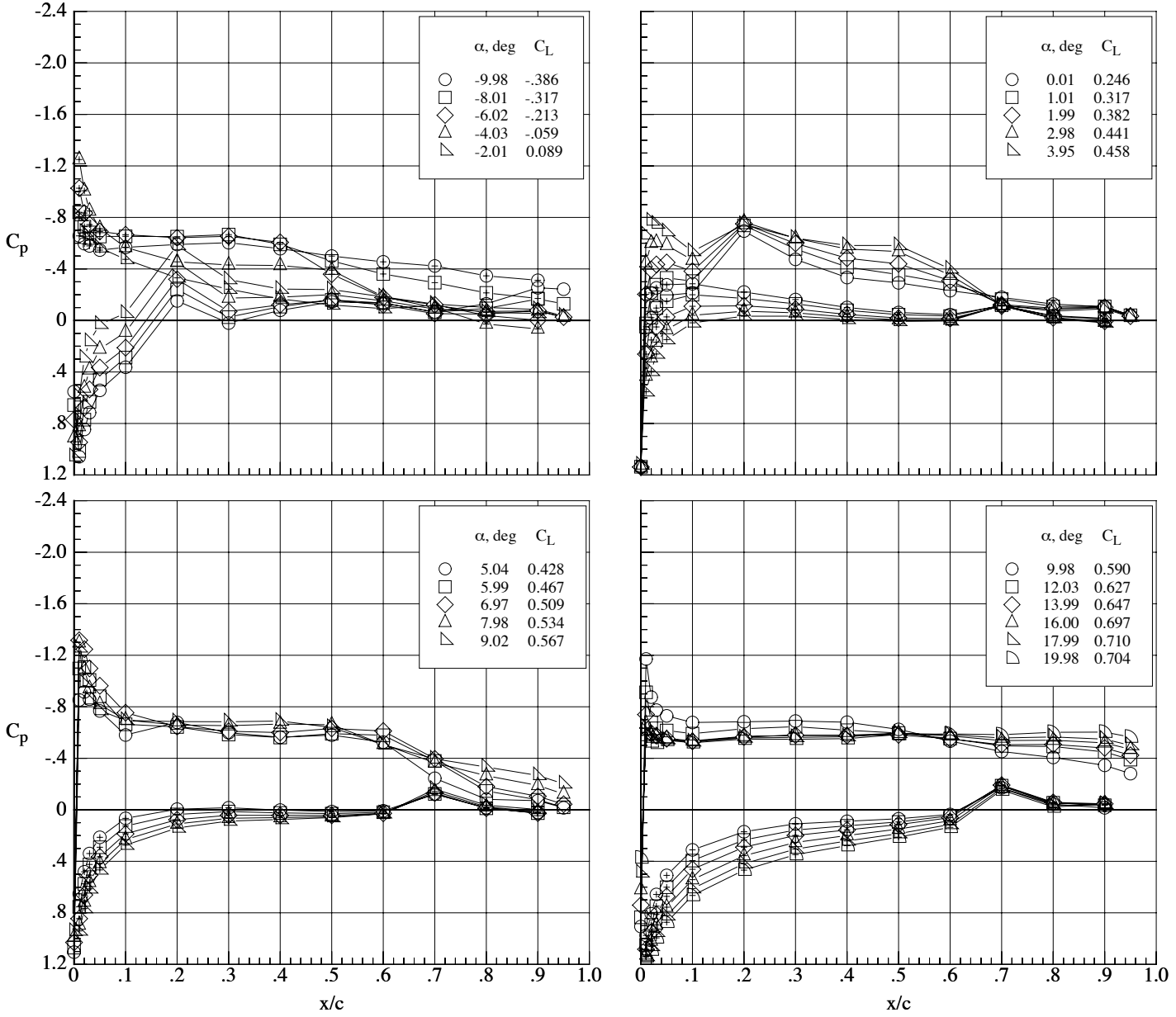

(a) Mach number 0.65.

Figure 102. Chordwise pressure coefficient distributions on the MA-SC-1 wing (bump on) at a Reynolds number of 40,000. $\delta_h = 0°$ and $\delta_f = -10°$.

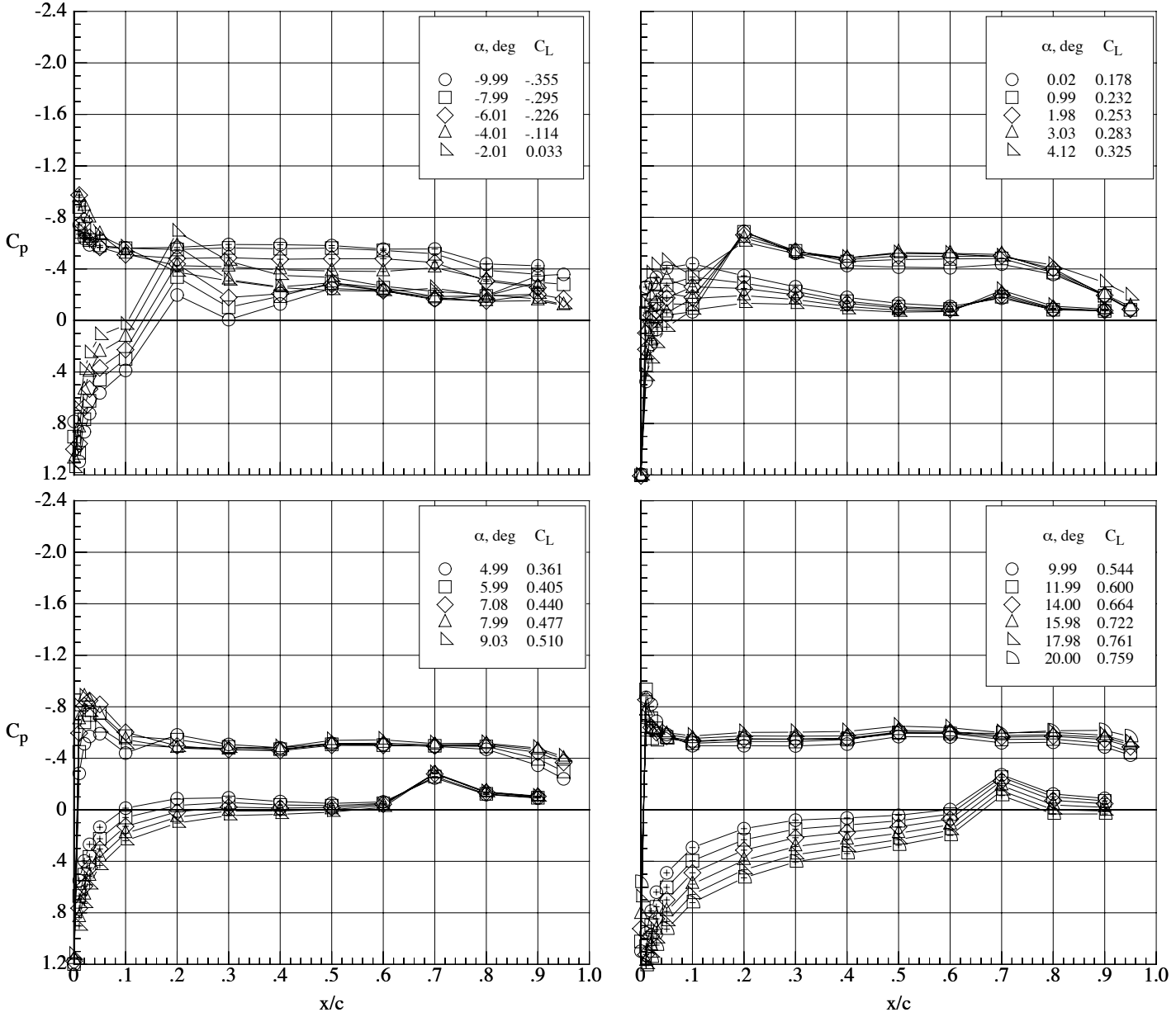

(b) Mach number 0.80.

Figure 102. Concluded.

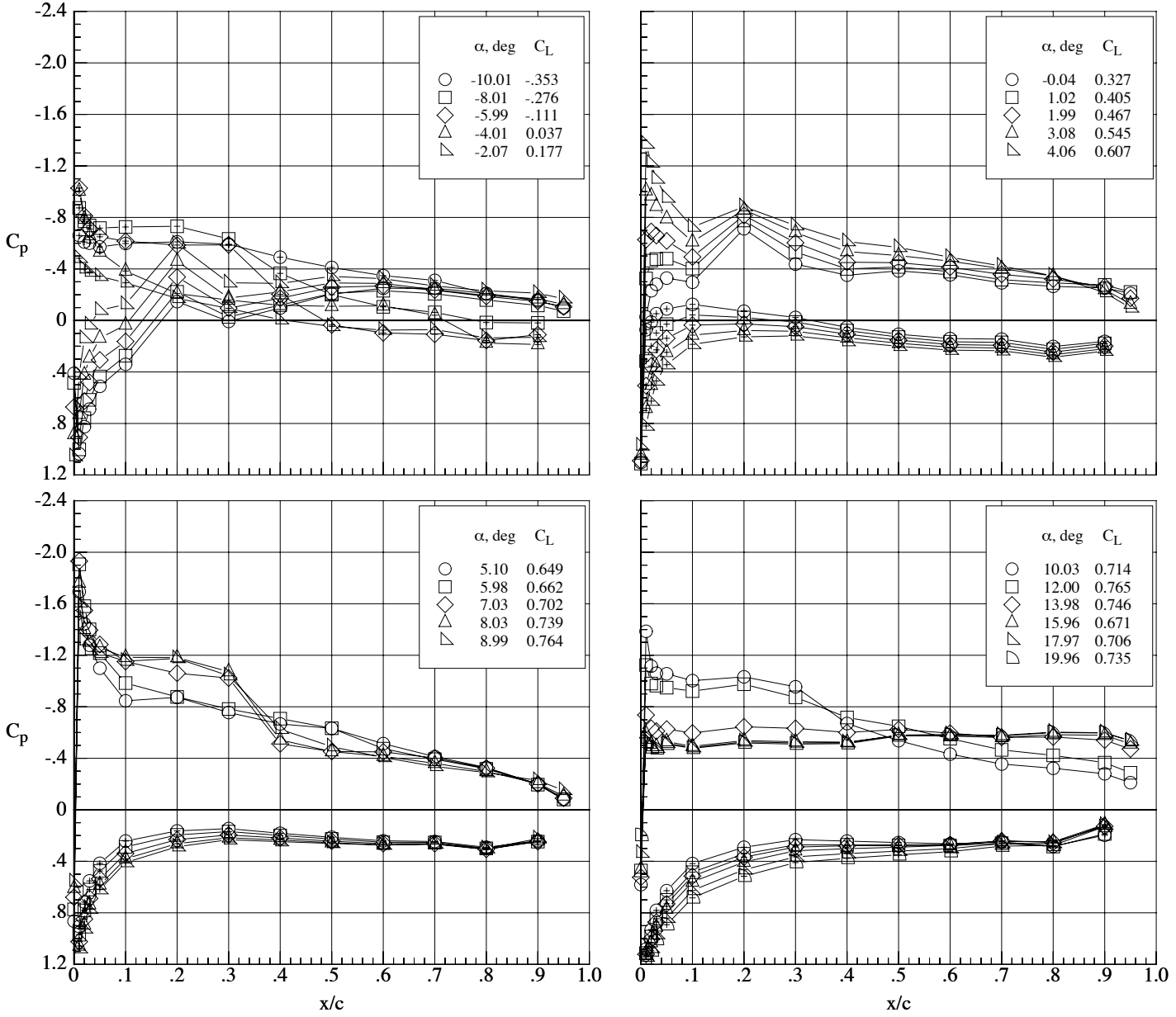

(a) Mach number 0.50.

Figure 103. Chordwise pressure coefficient distributions on the MA-SC-1 wing (bump on) at a Reynolds number of 40,000. $\delta_h = 0°$ and $\delta_f = 0°$.

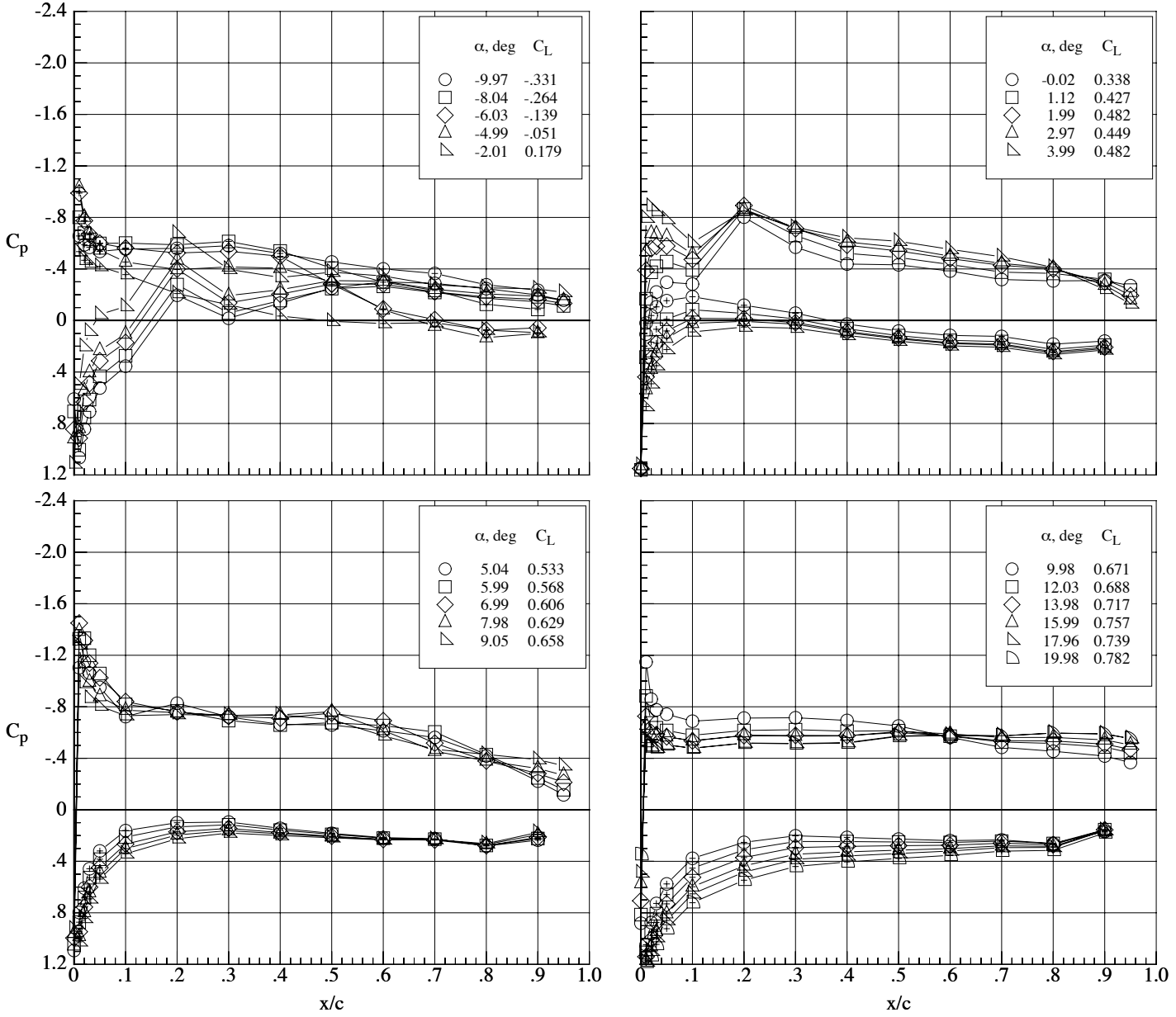

(b) Mach number 0.65.

Figure 103. Continued.

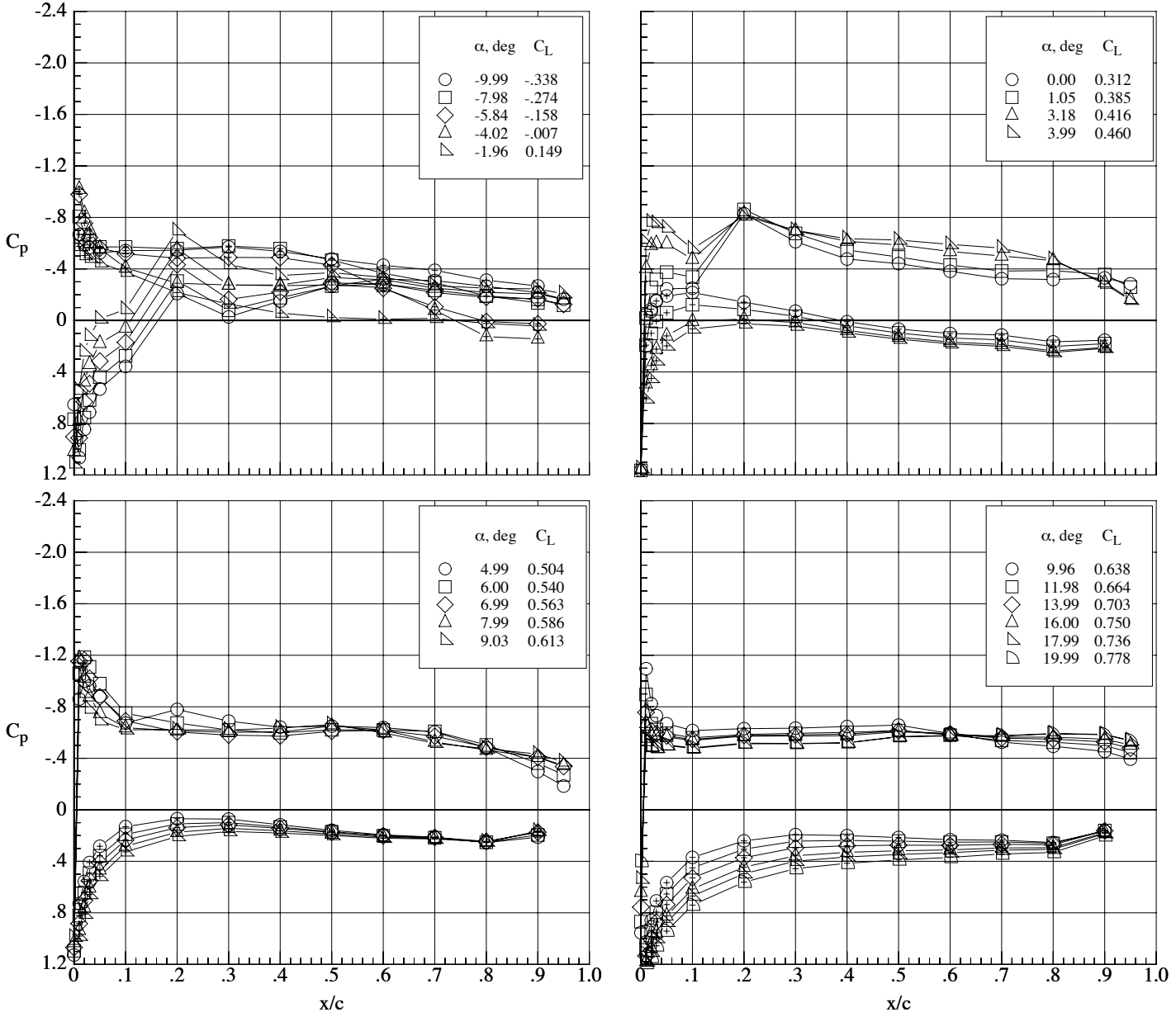

(c) Mach number 0.70.

Figure 103. Continued.

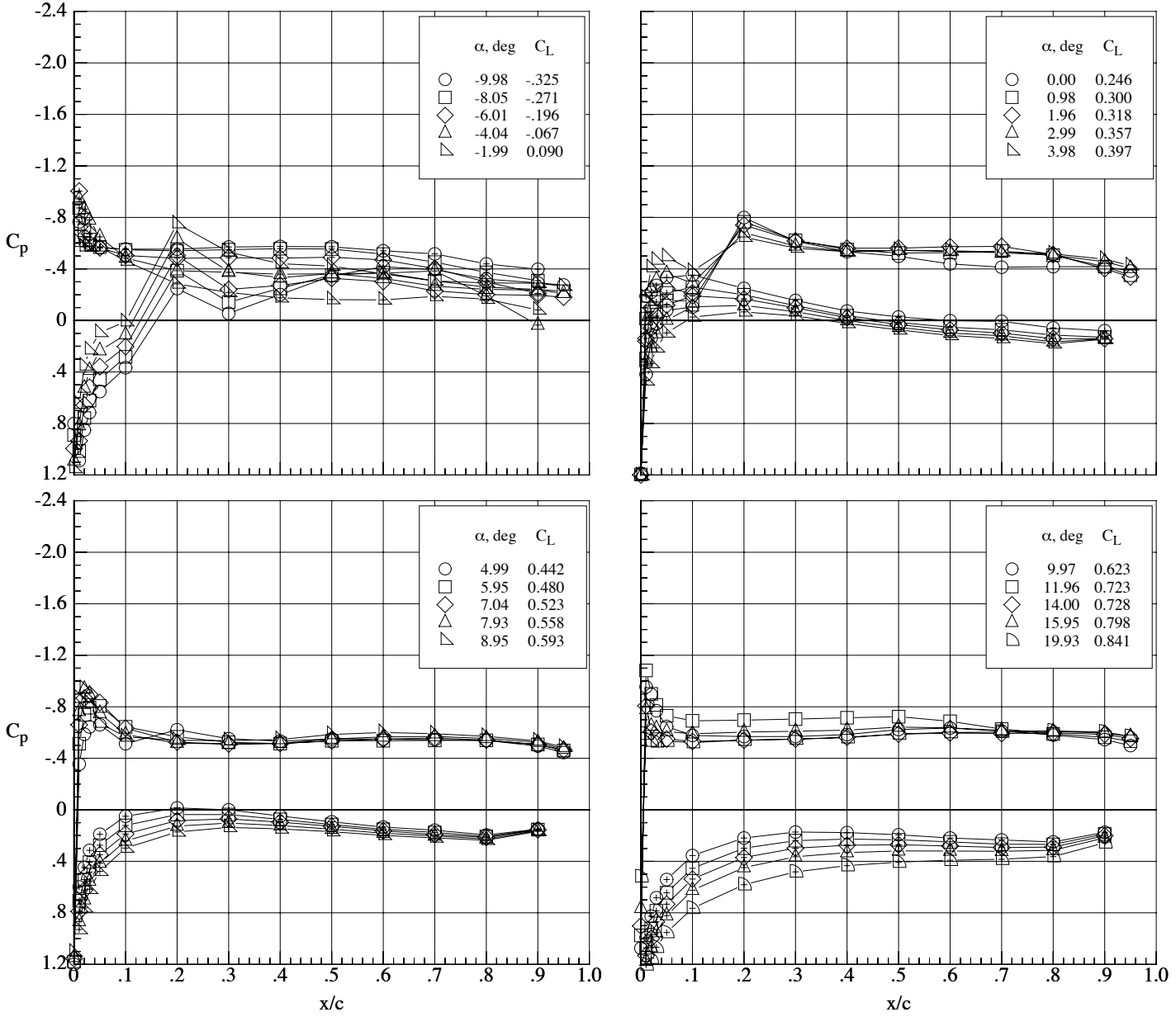

(d) Mach number 0.80.

Figure 103. Continued.

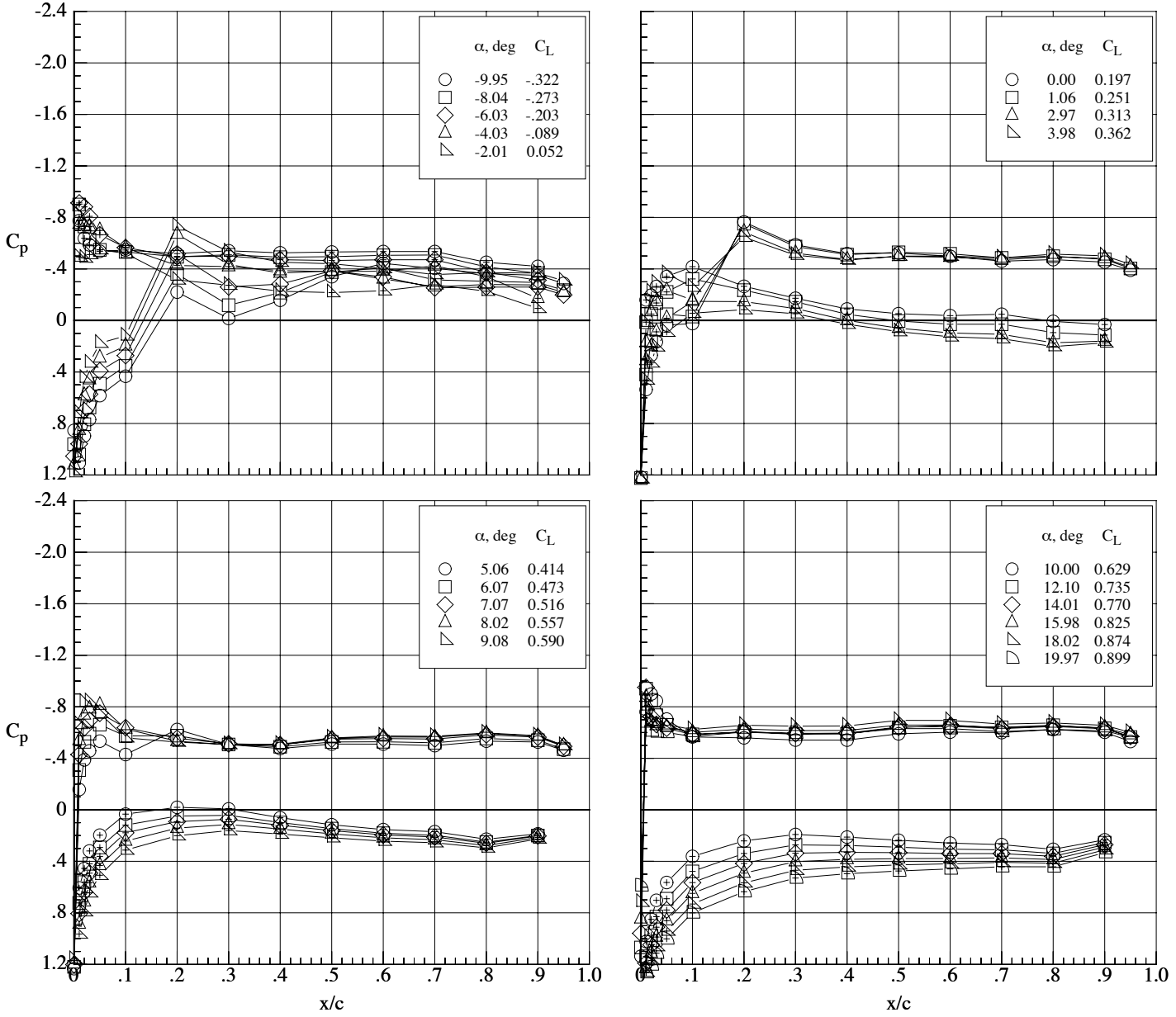

(e) Mach number 0.85.

Figure 103. Continued.

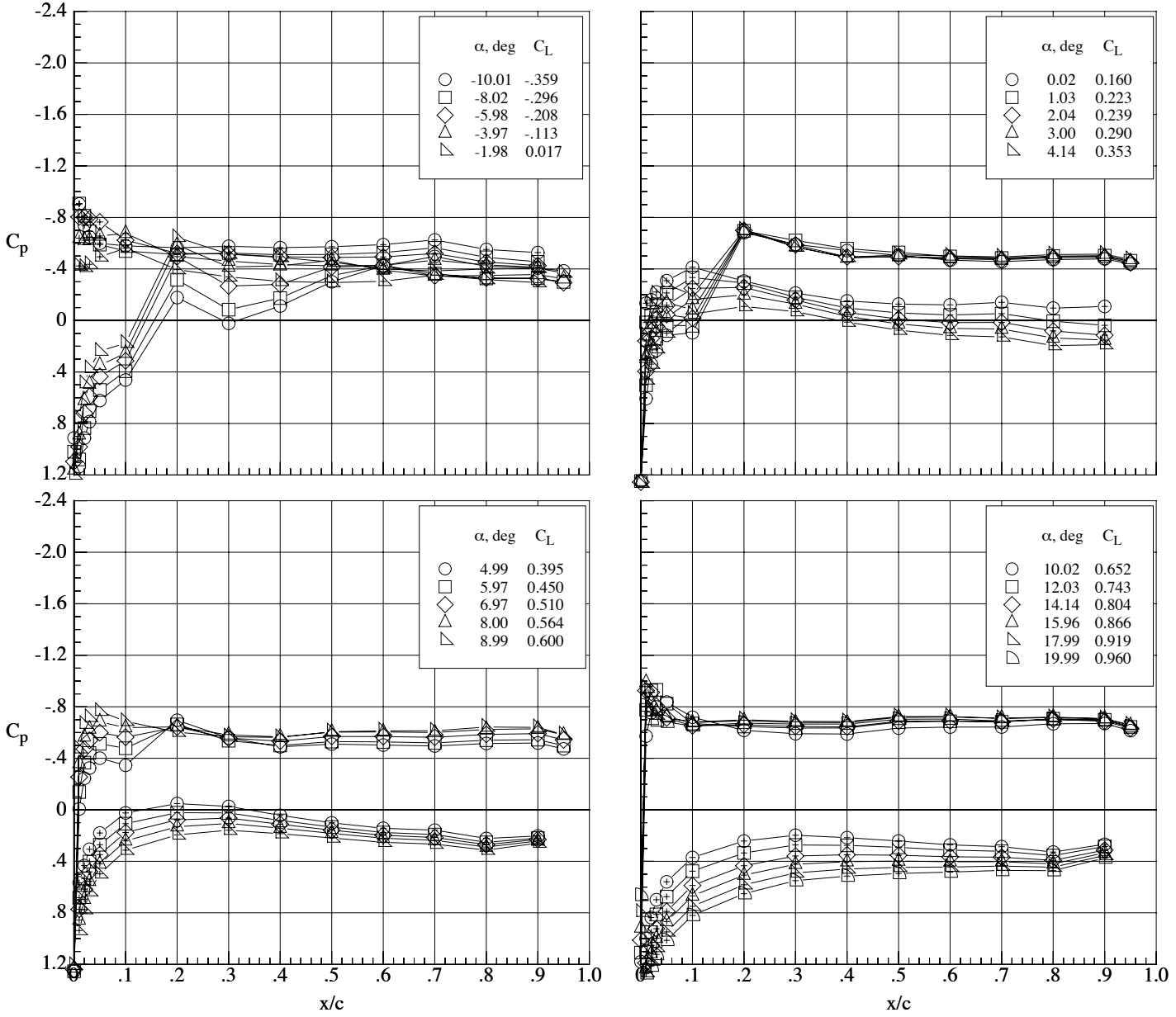

(f) Mach number 0.90.

Figure 103. Concluded.

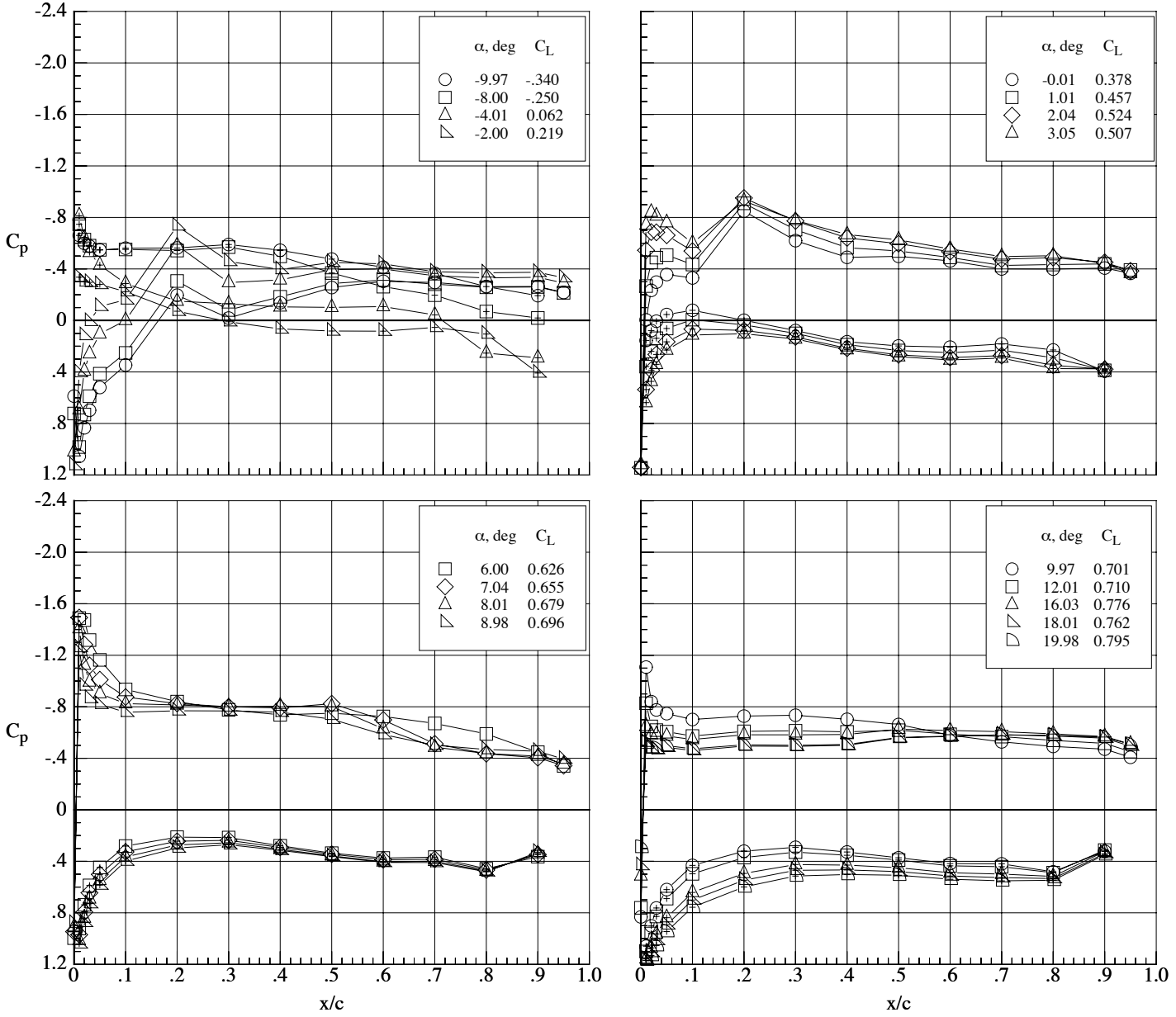

(a) Mach number 0.65.

Figure 104. Chordwise pressure coefficient distributions on the MA-SC-1 wing (bump on) at a Reynolds number of 40,000. $\delta_h = 0°$ and $\delta_f = 10°$.

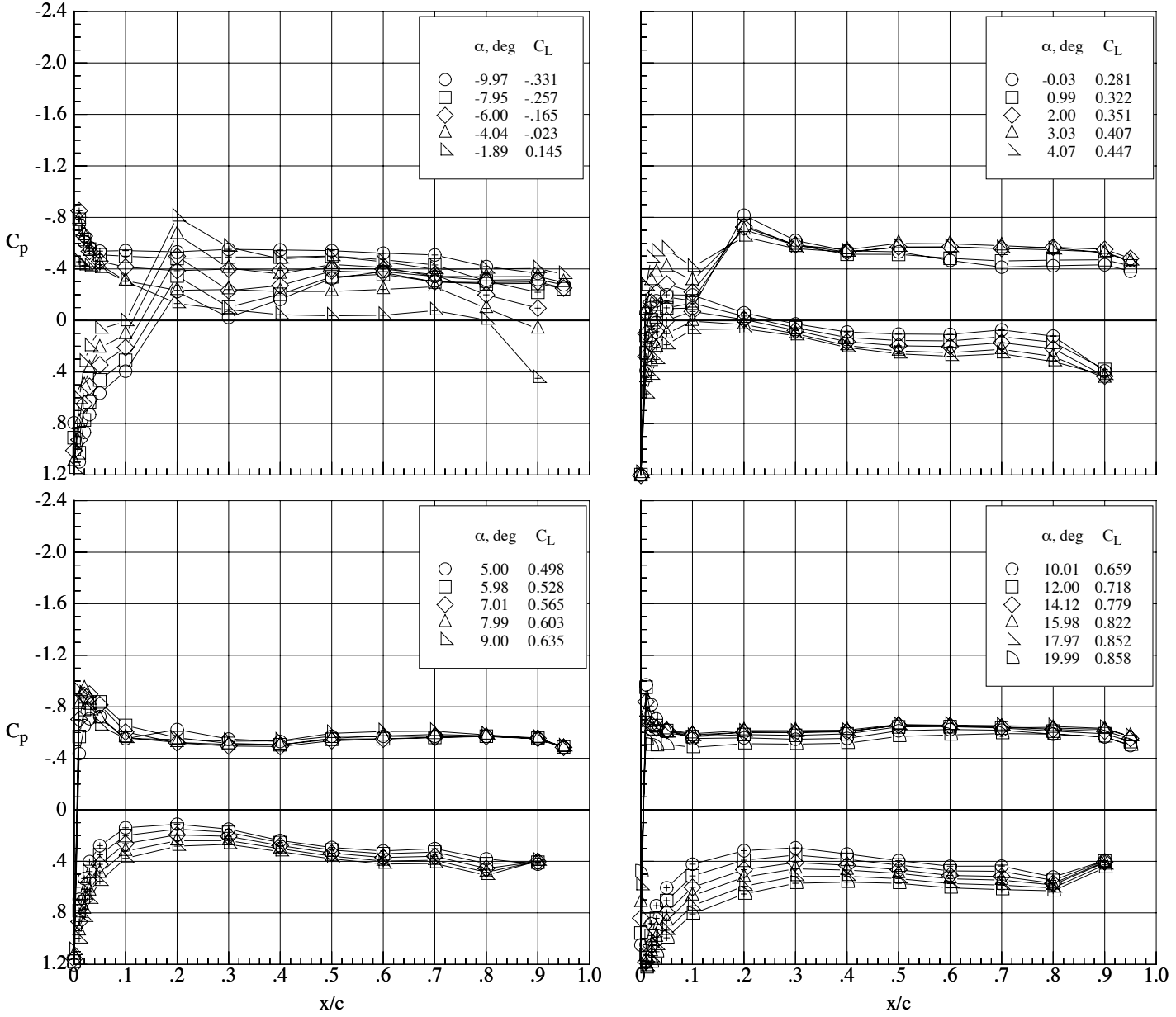

(b) Mach number 0.80.

Figure 104. Concluded.

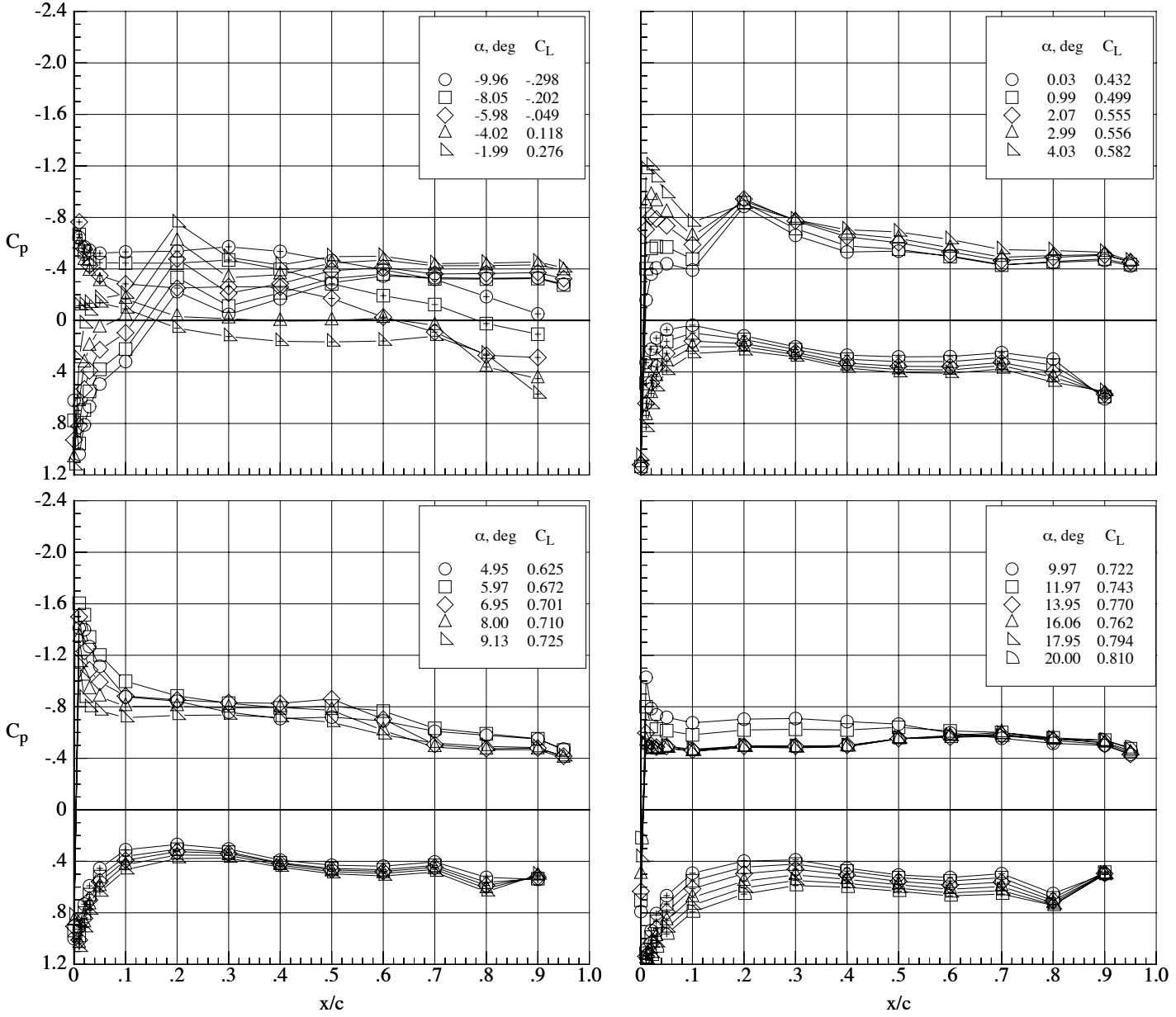

(a) Mach number 0.65.

Figure 105. Chordwise pressure coefficient distributions on the MA-SC-1 wing (bump on) at a Reynolds number of 40,000. $\delta_h = 0°$ and $\delta_f = 20°$.

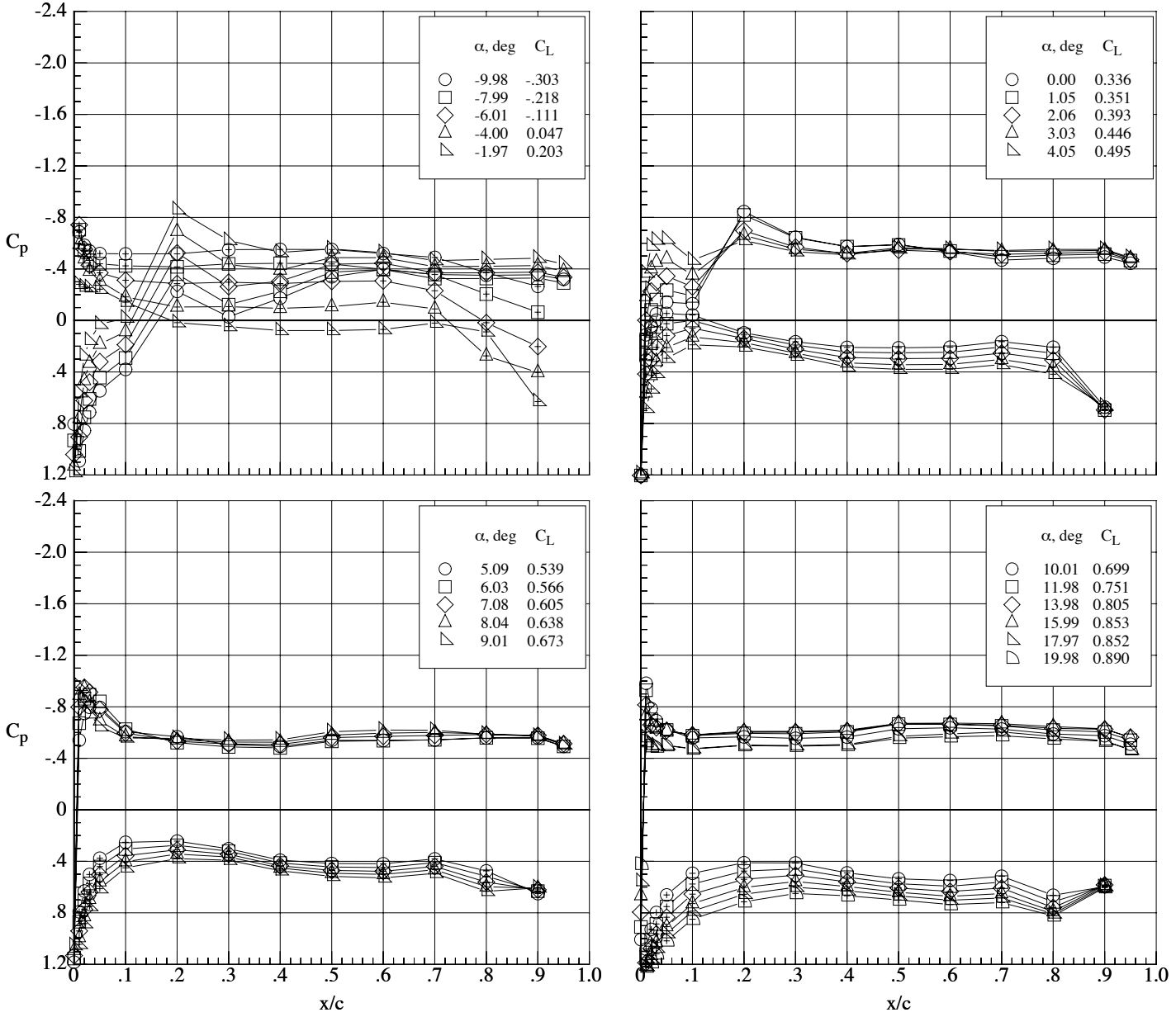

(b) Mach number 0.80.

Figure 105. Concluded.

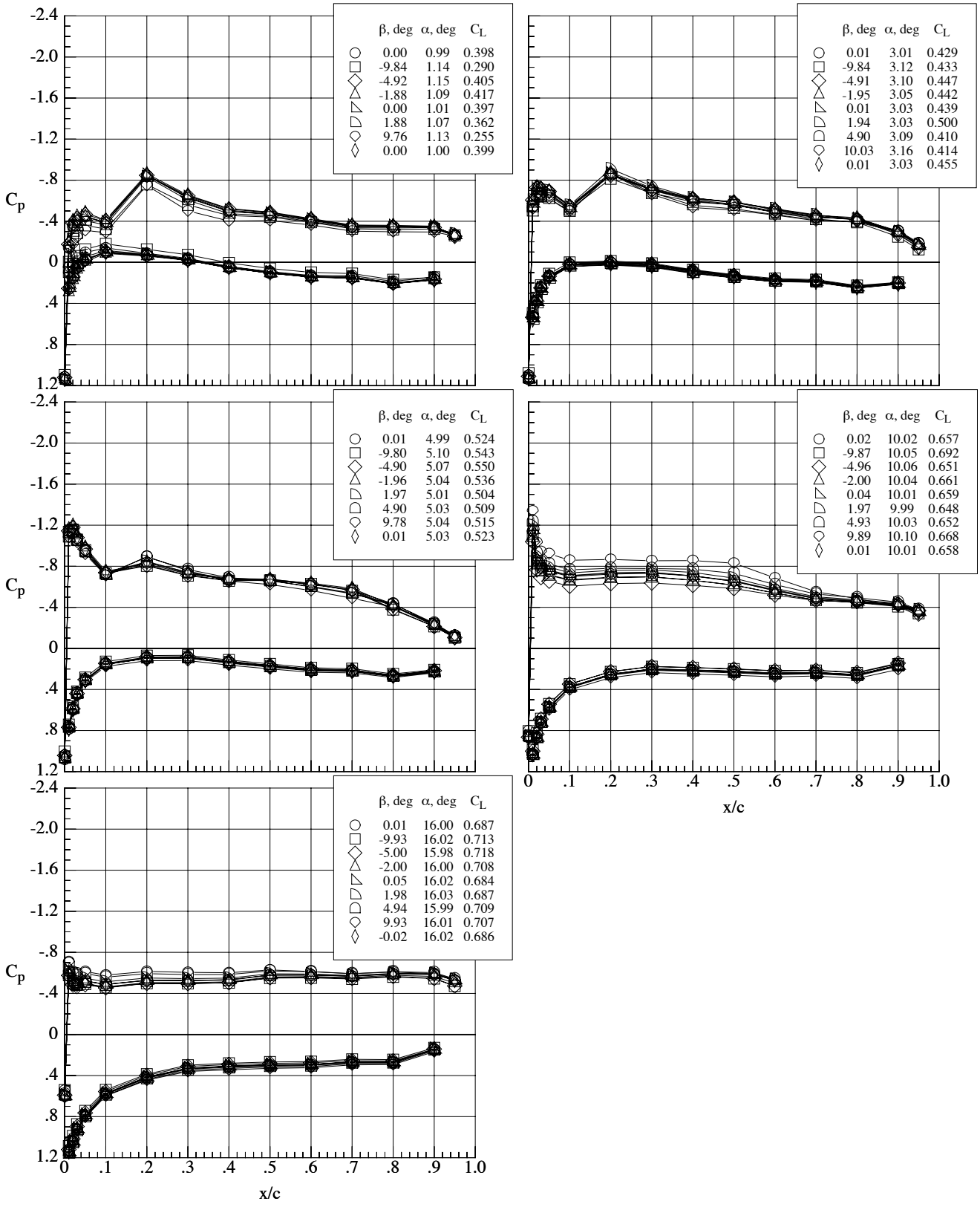

(a) Mach number 0.65.

Figure 106. Chordwise pressure coefficient distributions on the MA-SC-1 wing (bump on) at a Reynolds number of 40,000 over a range of sideslip angles. $\delta_h = 0°$ and $\delta_f = 0°$.

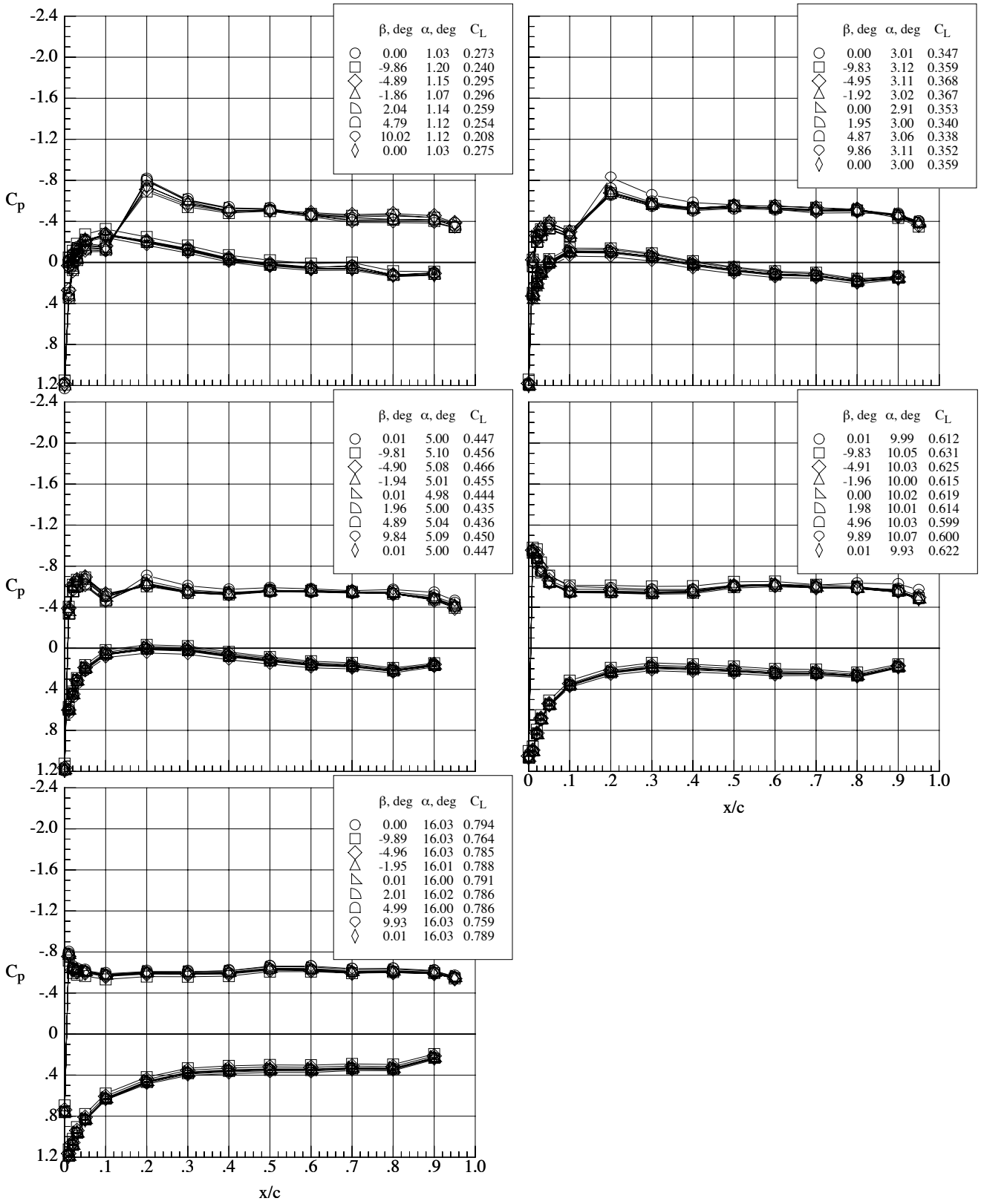

(b) Mach number 0.80.

Figure 106. Concluded.

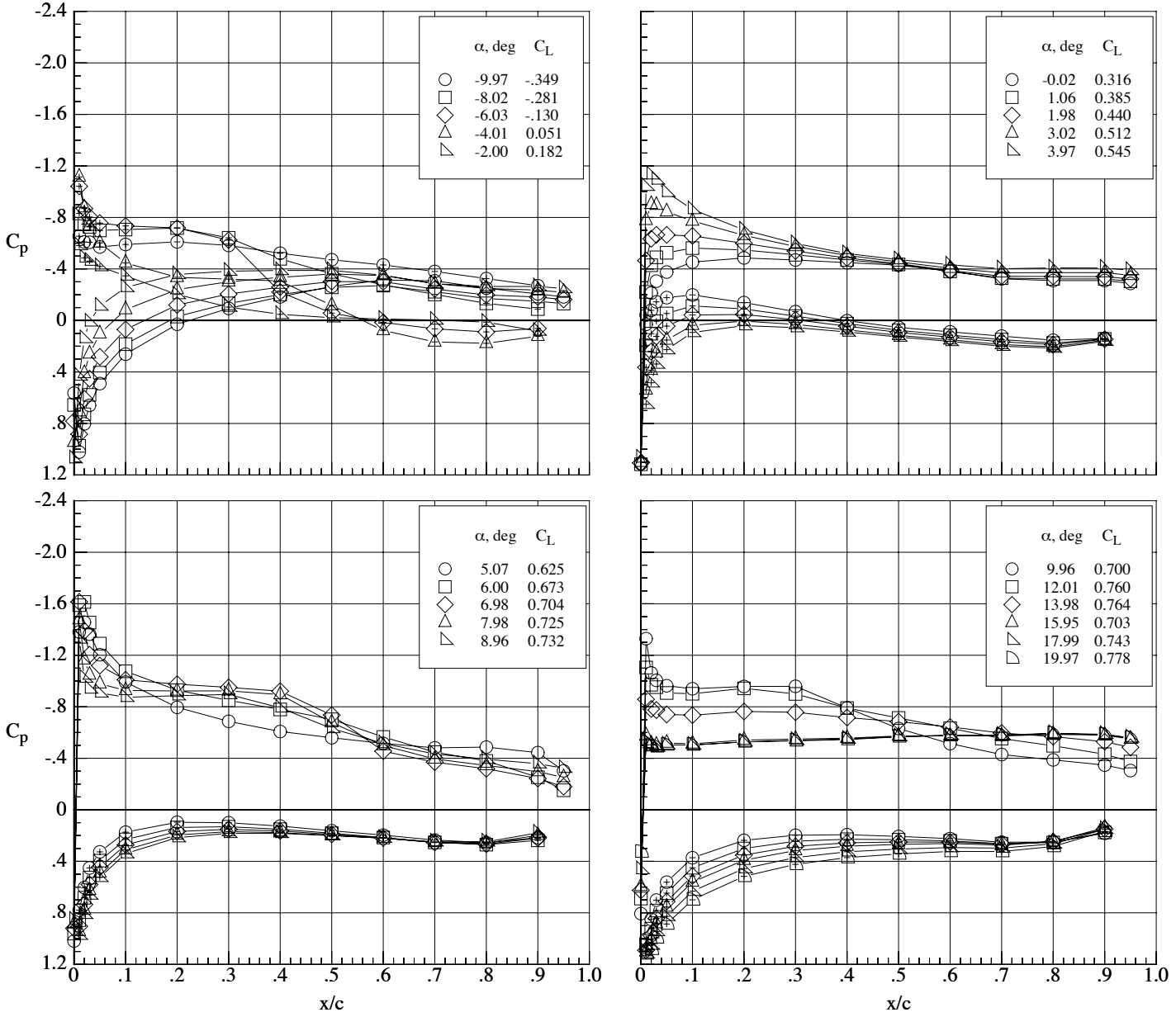

(a) Mach number 0.65.

Figure 107. Chordwise pressure coefficient distributions on the MA-SC-1 wing (bump off) at a Reynolds number of 60,000. $\delta_h = 0°$ and $\delta_f = 0°$.

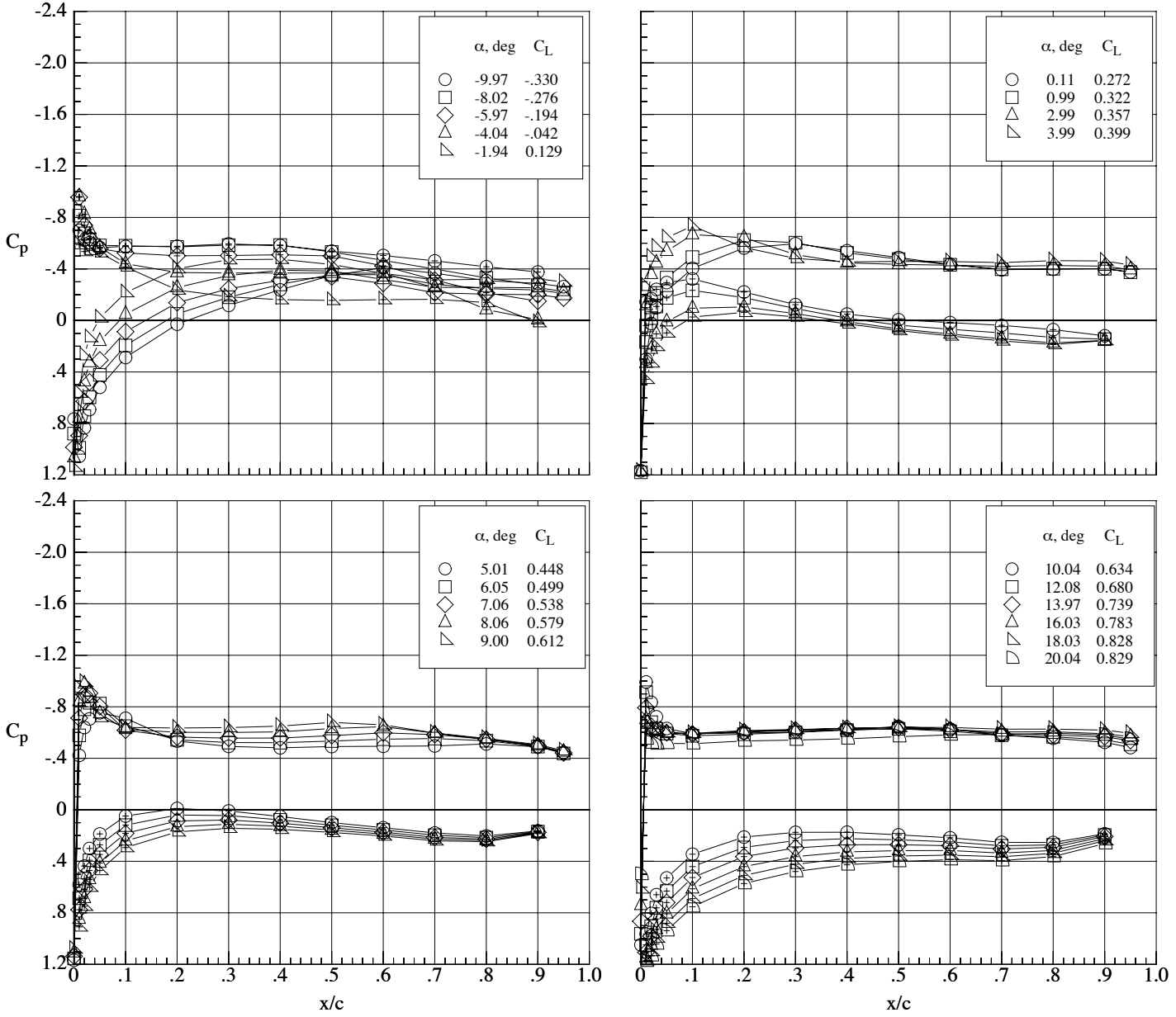

(b) Mach number 0.80.

Figure 107. Concluded.

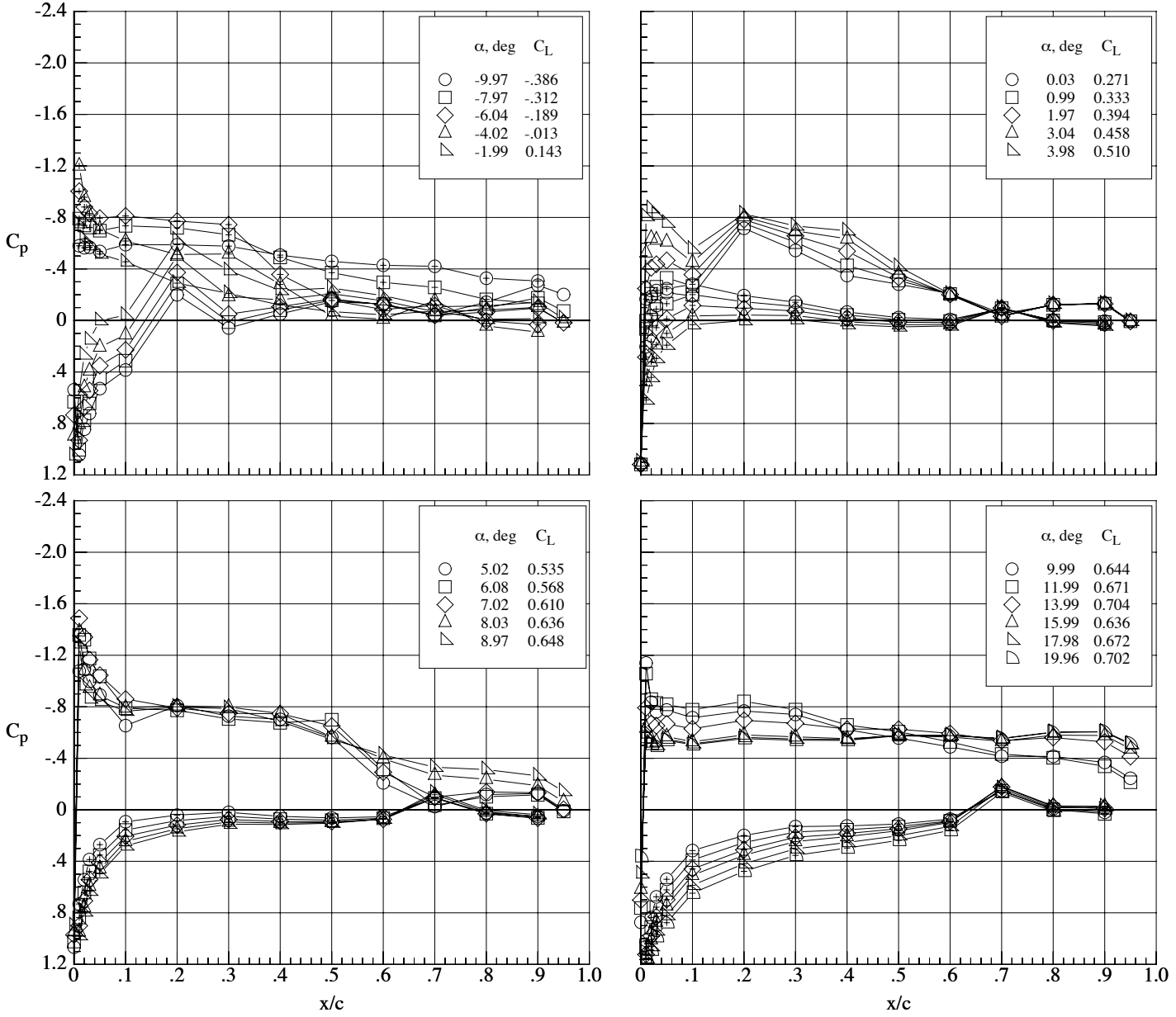

(a) Mach number 0.65.

Figure 108. Chordwise pressure coefficient distributions on the MA-SC-1 wing (bump on) at a Reynolds number of 60,000. $\delta_h = 0°$ and $\delta_f = -10°$.

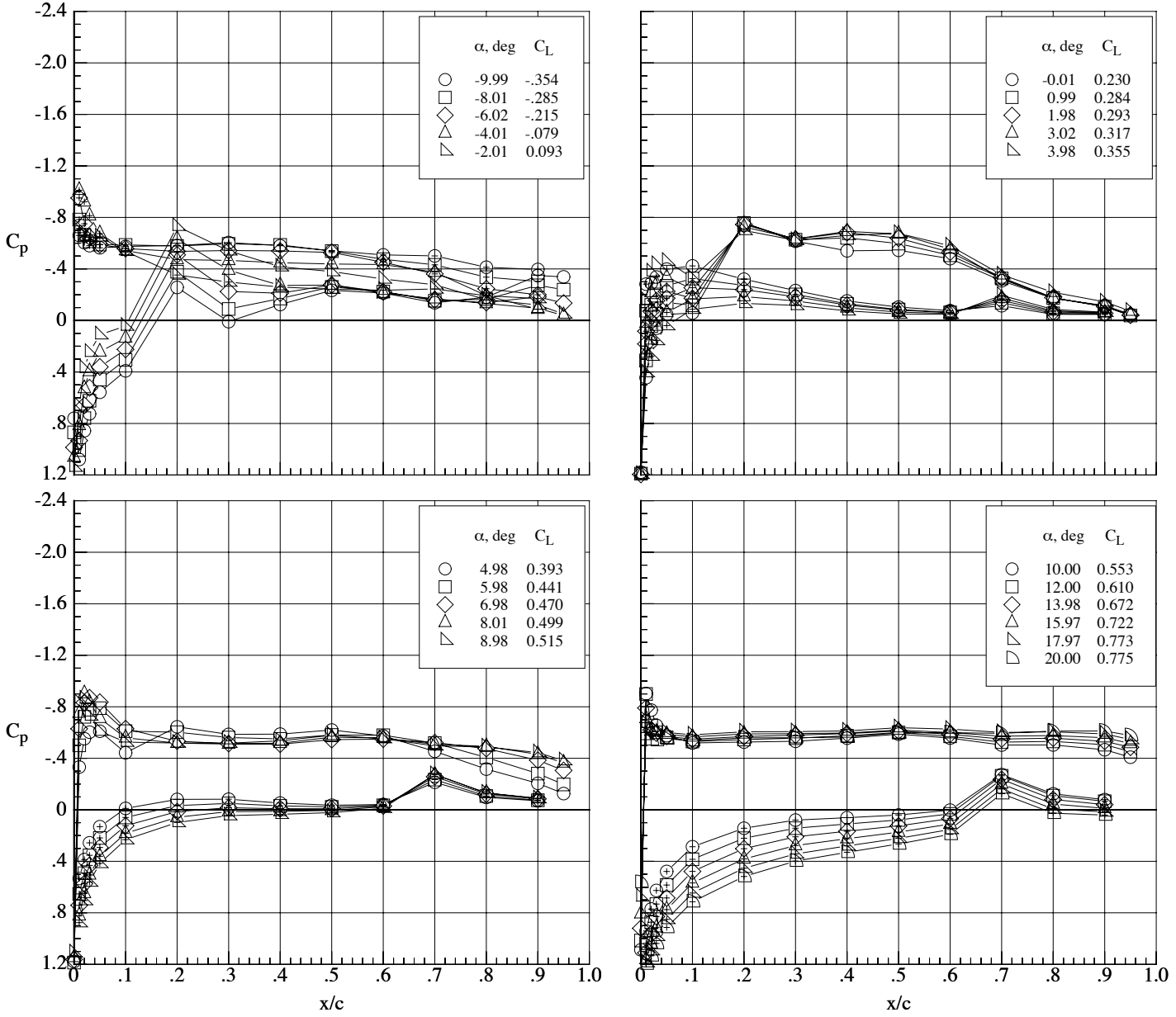

(b) Mach number 0.80.

Figure 108. Concluded.

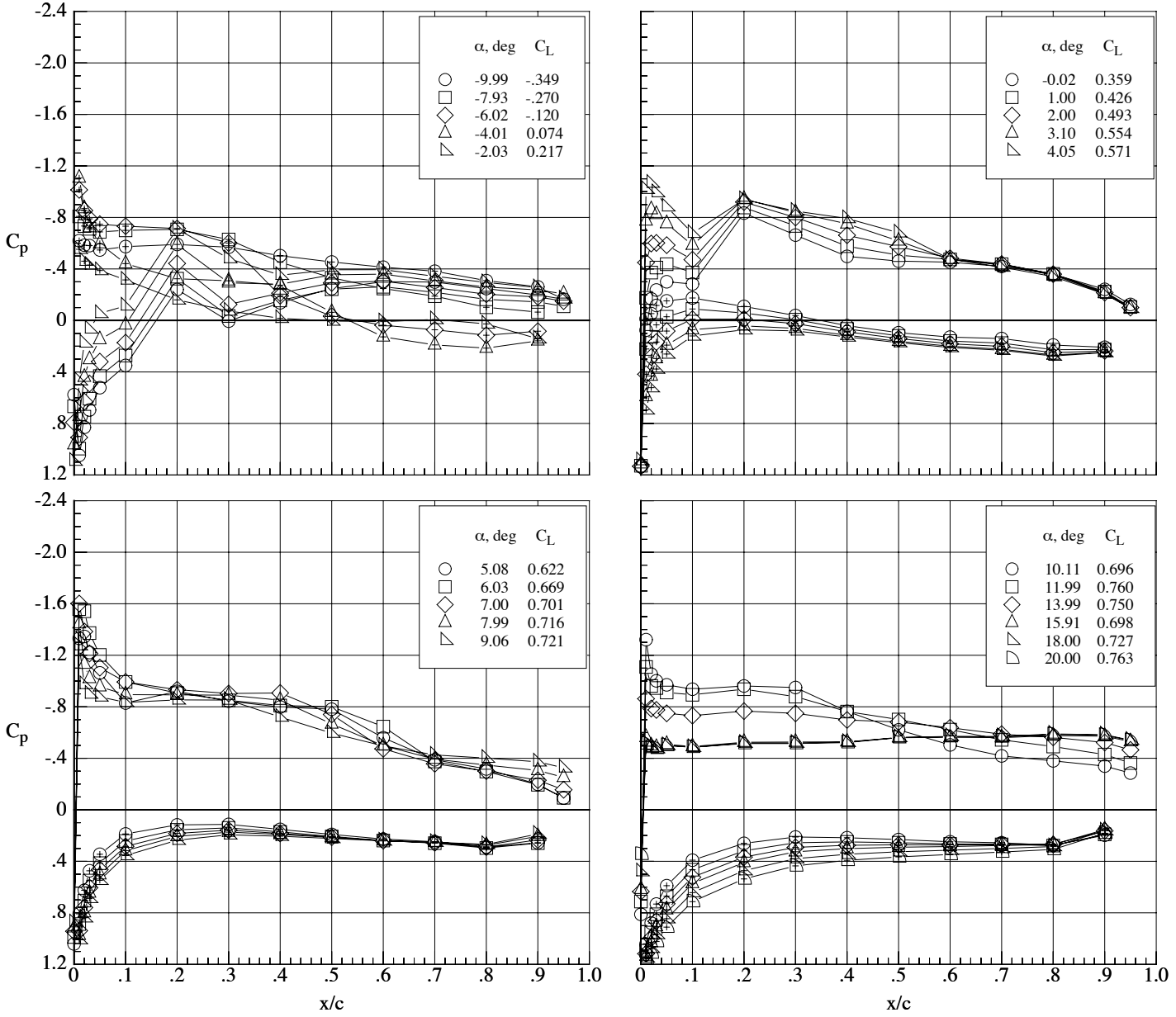

(a) Mach number 0.65.

Figure 109. Chordwise pressure coefficient distributions on the MA-SC-1 wing (bump on) at a Reynolds number of 60,000. $\delta_h = 0°$ and $\delta_f = 0°$.

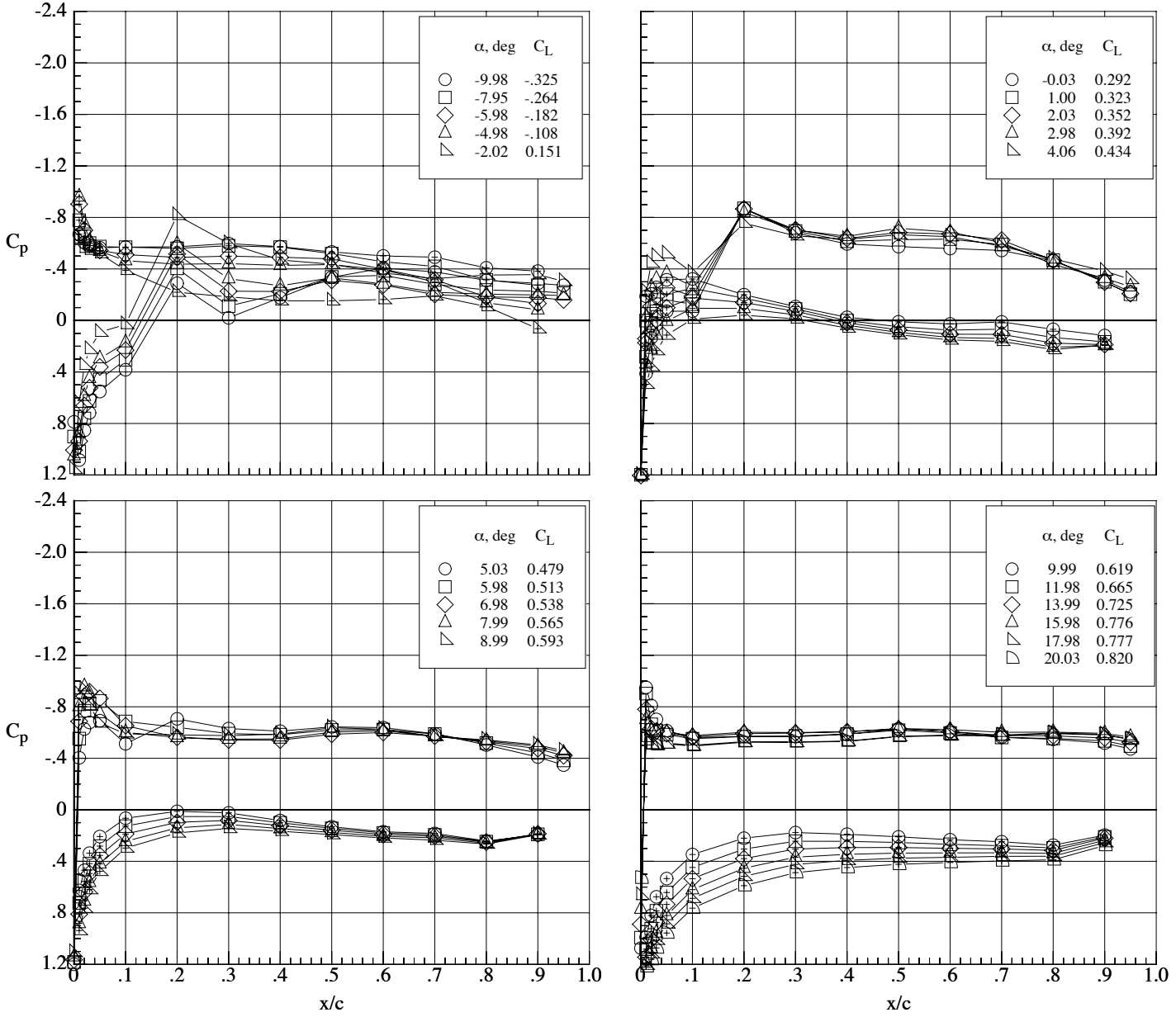

(b) Mach number 0.80.

Figure 109. Concluded.

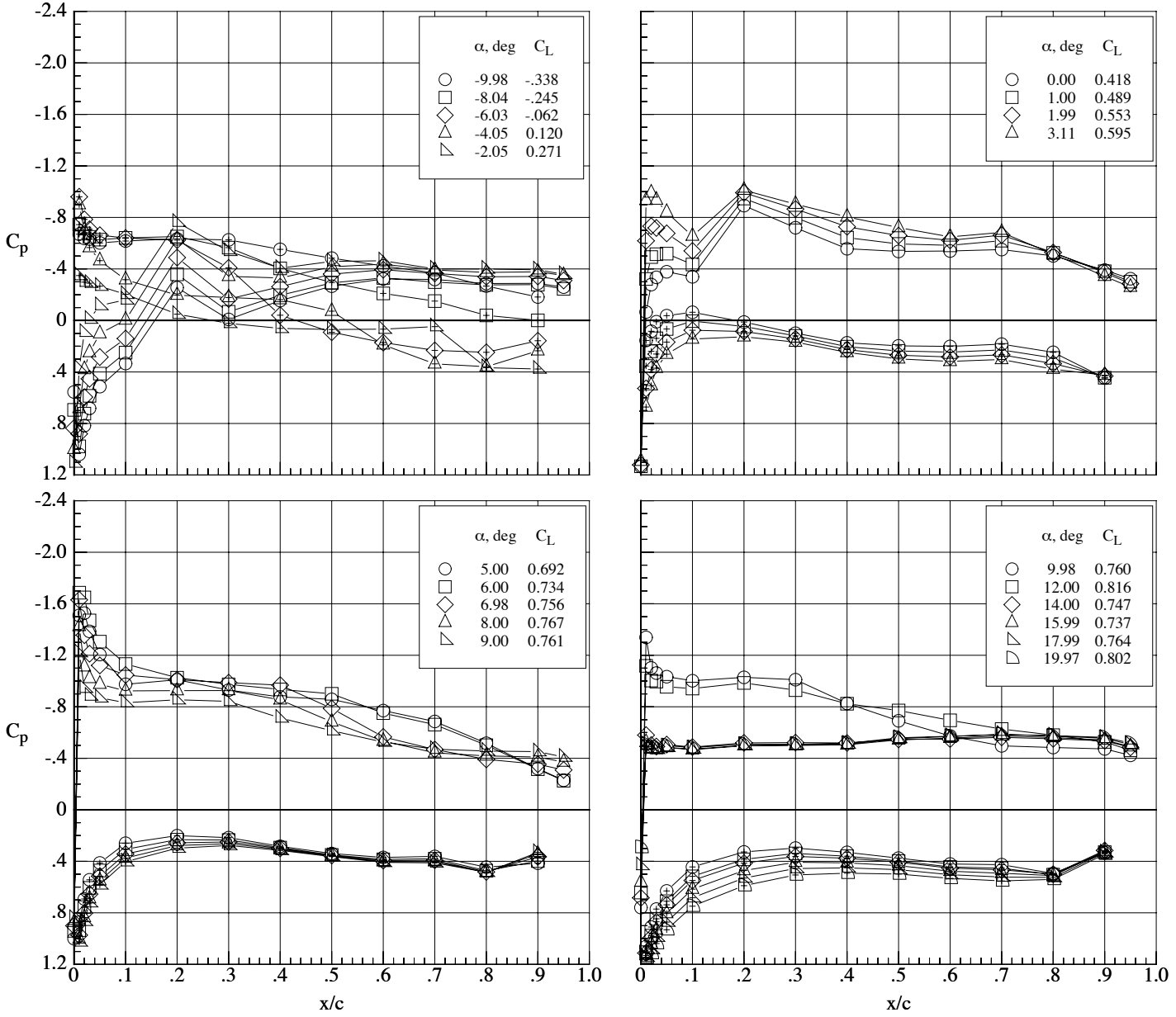

(a) Mach number 0.65.

Figure 110. Chordwise pressure coefficient distributions on the MA-SC-1 wing (bump on) at a Reynolds number of 60,000. $\delta_h = 0°$ and $\delta_f = 10°$.

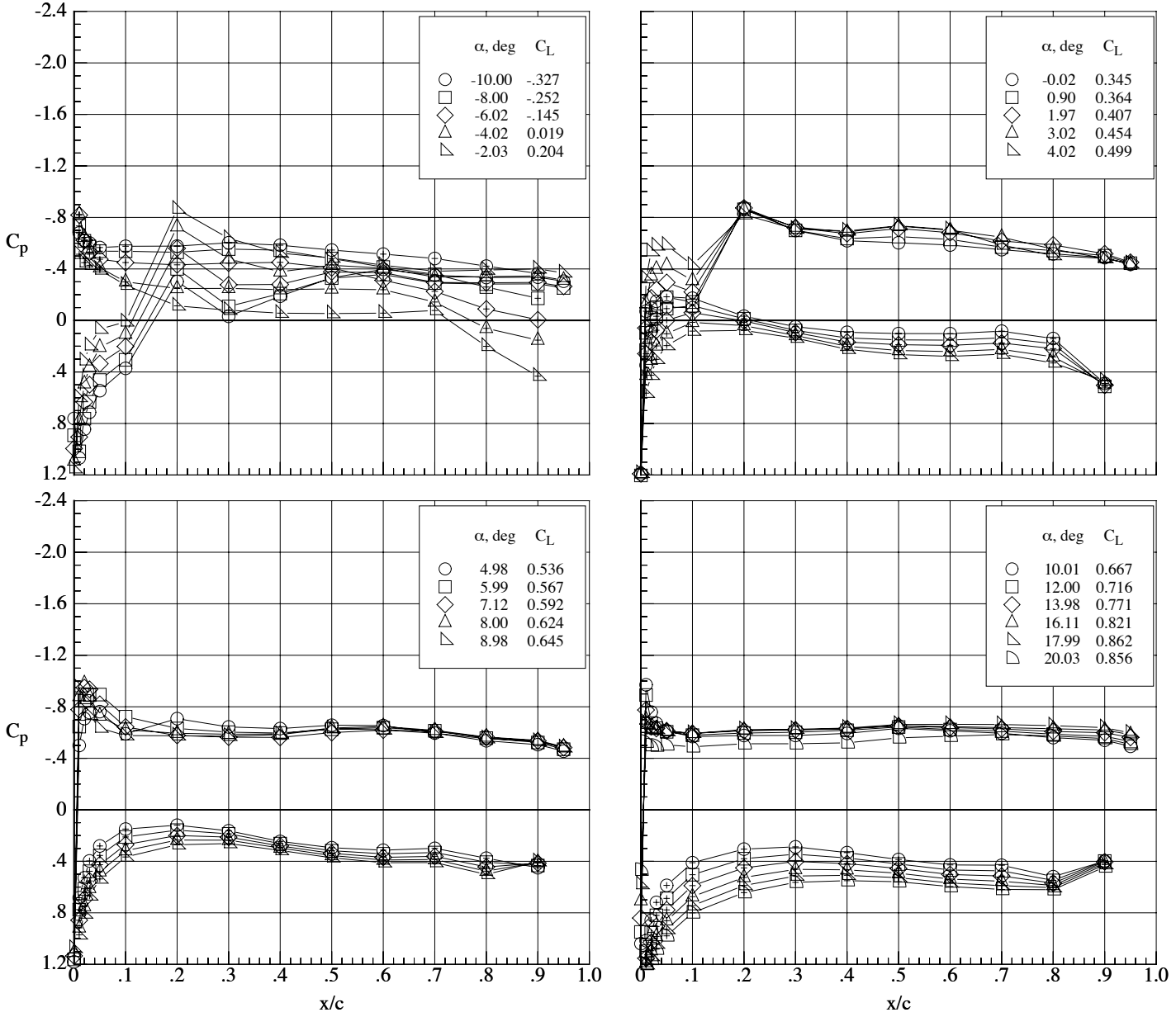

(b) Mach number 0.80.

Figure 110. Concluded.

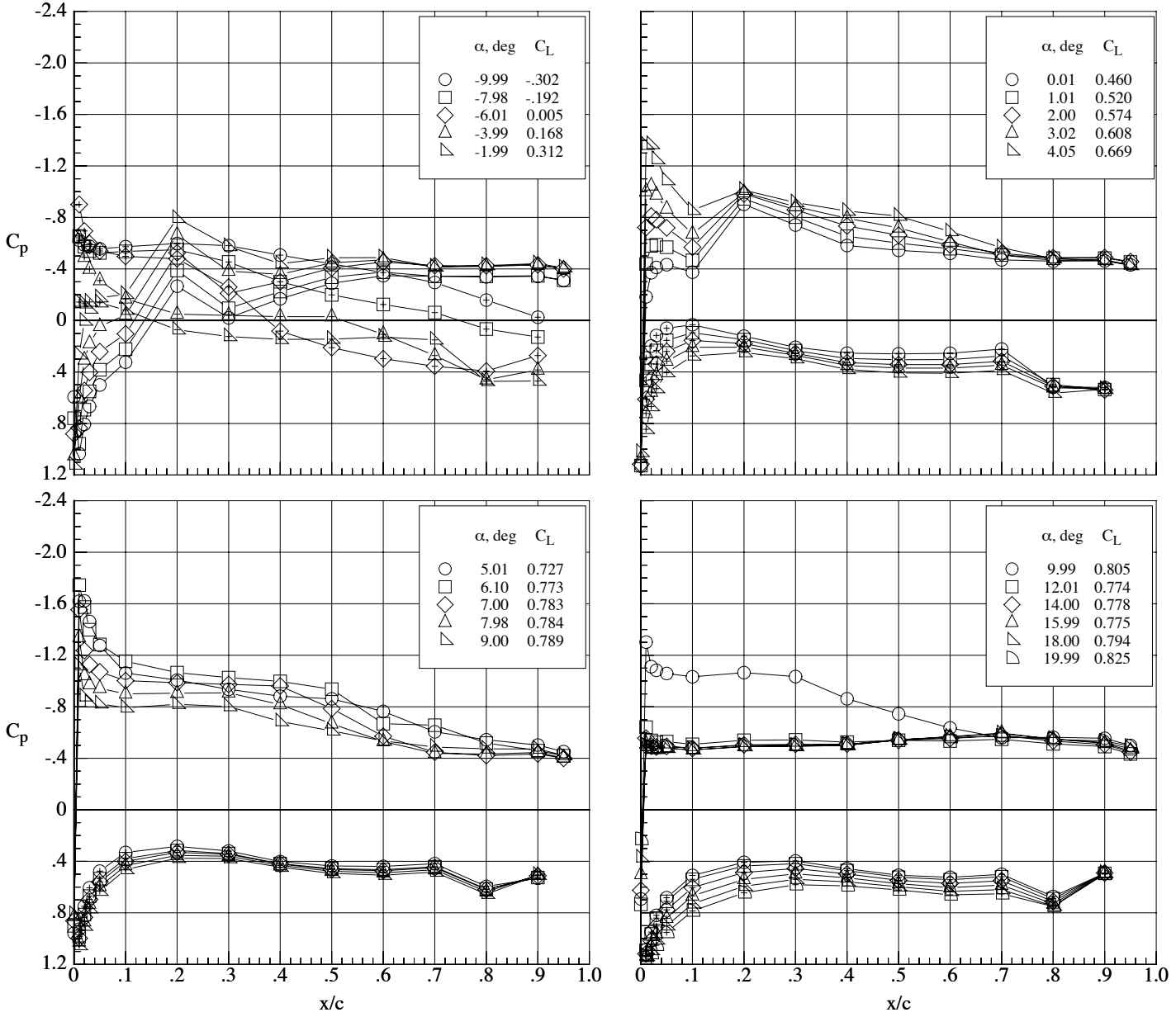

(a) Mach number 0.65.

Figure 111. Chordwise pressure coefficient distributions on the MA-SC-1 wing (bump on) at a Reynolds number of 60,000. $\delta_h = 0°$ and $\delta_f = 20°$.

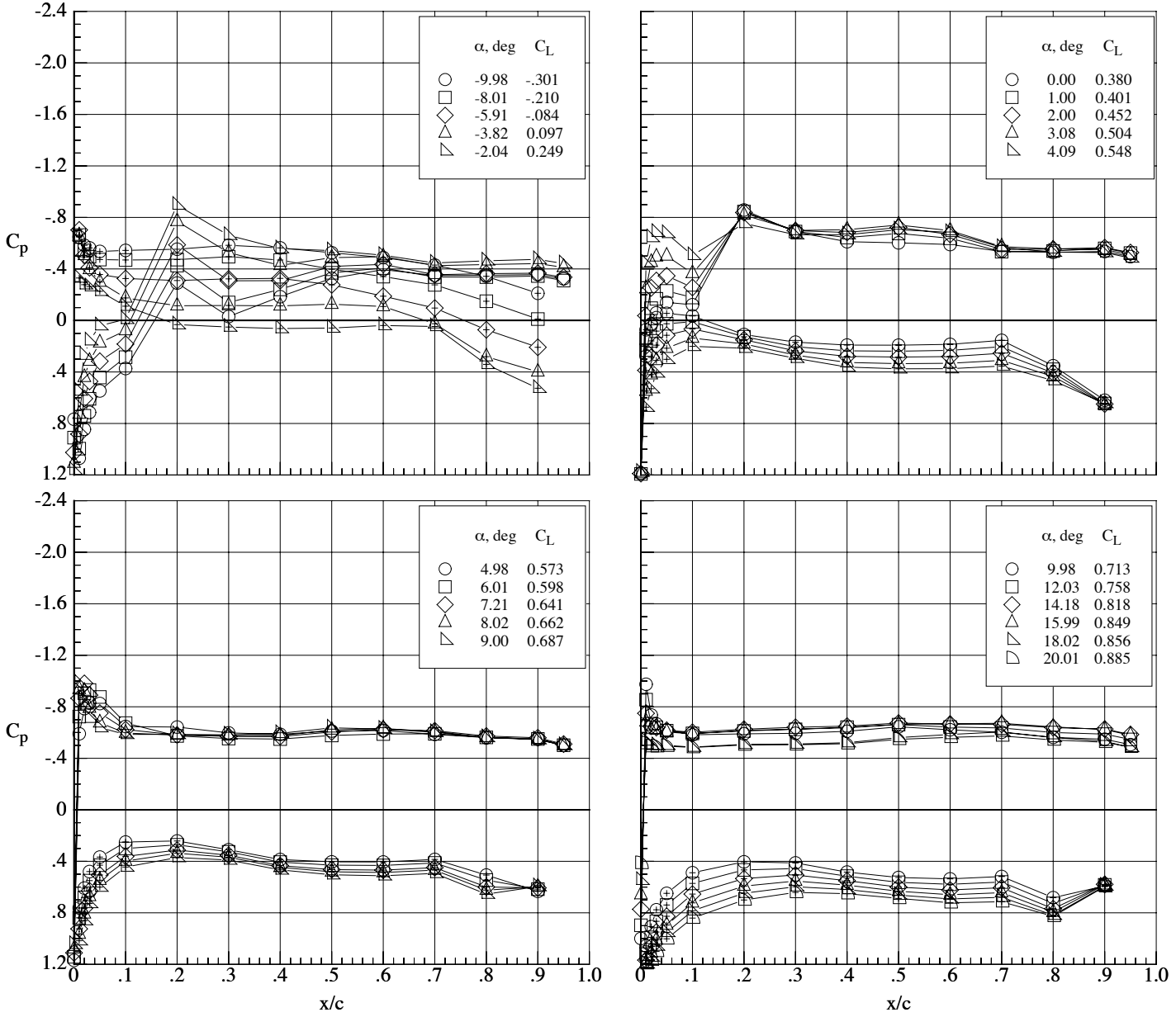

(b) Mach number 0.80.

Figure 111. Concluded.

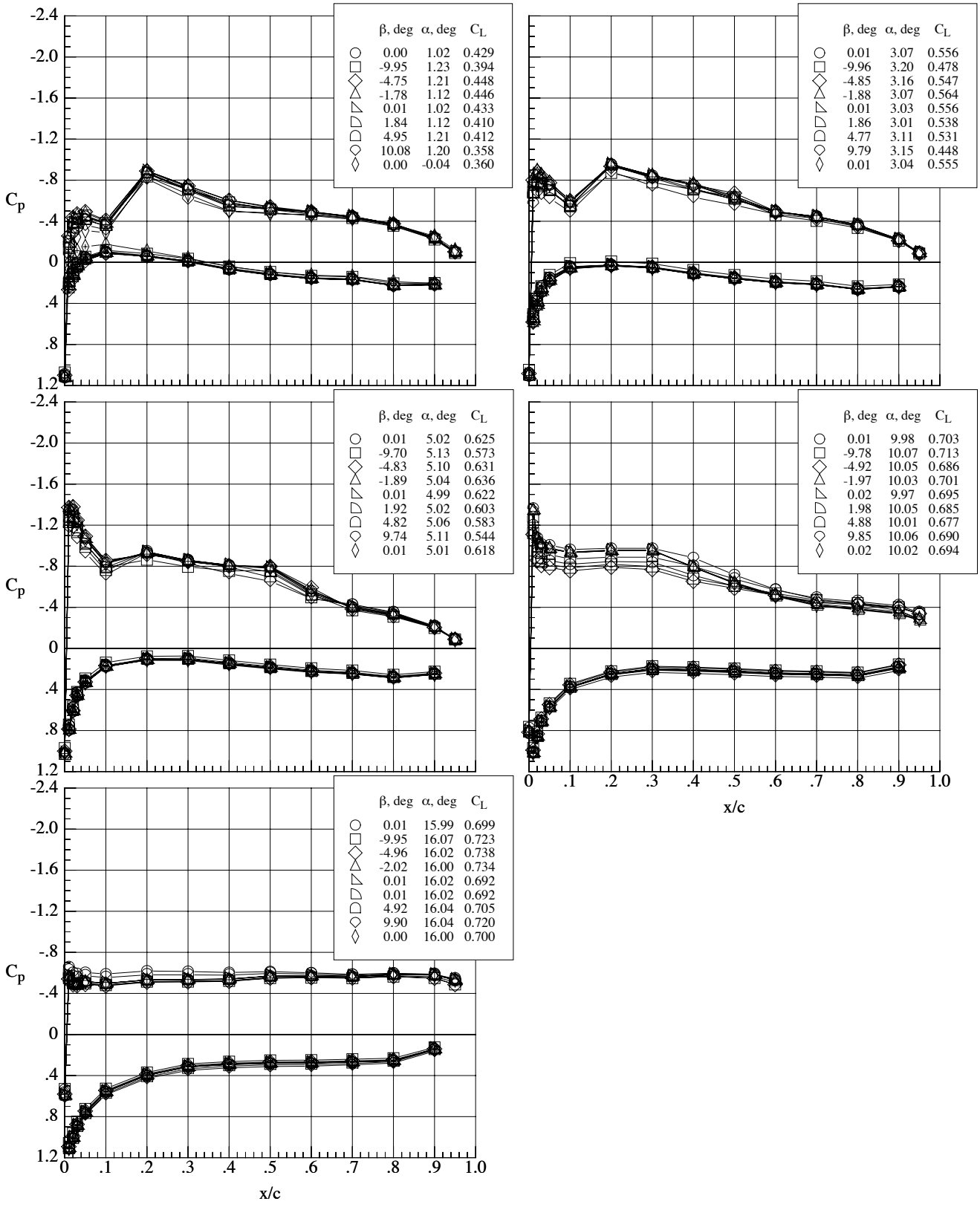

(a) Mach number 0.65.

Figure 112. Chordwise pressure coefficient distributions on the MA-SC-1 wing (bump on) at a Reynolds number of 60,000 over a range of sideslip angles. $\delta_h = 0°$ and $\delta_f = 0°$.

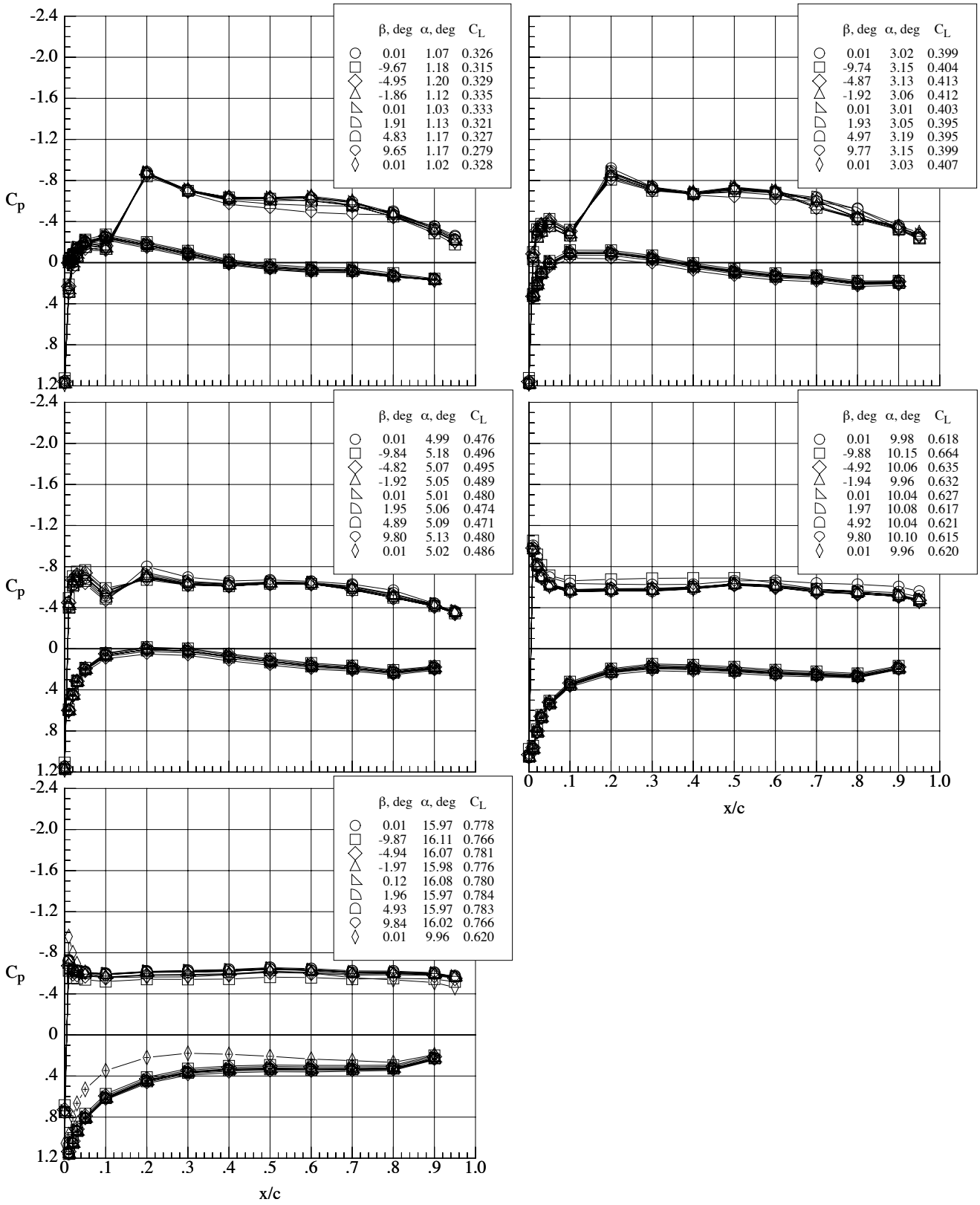

(b) Mach number 0.80.

Figure 112. Concluded.

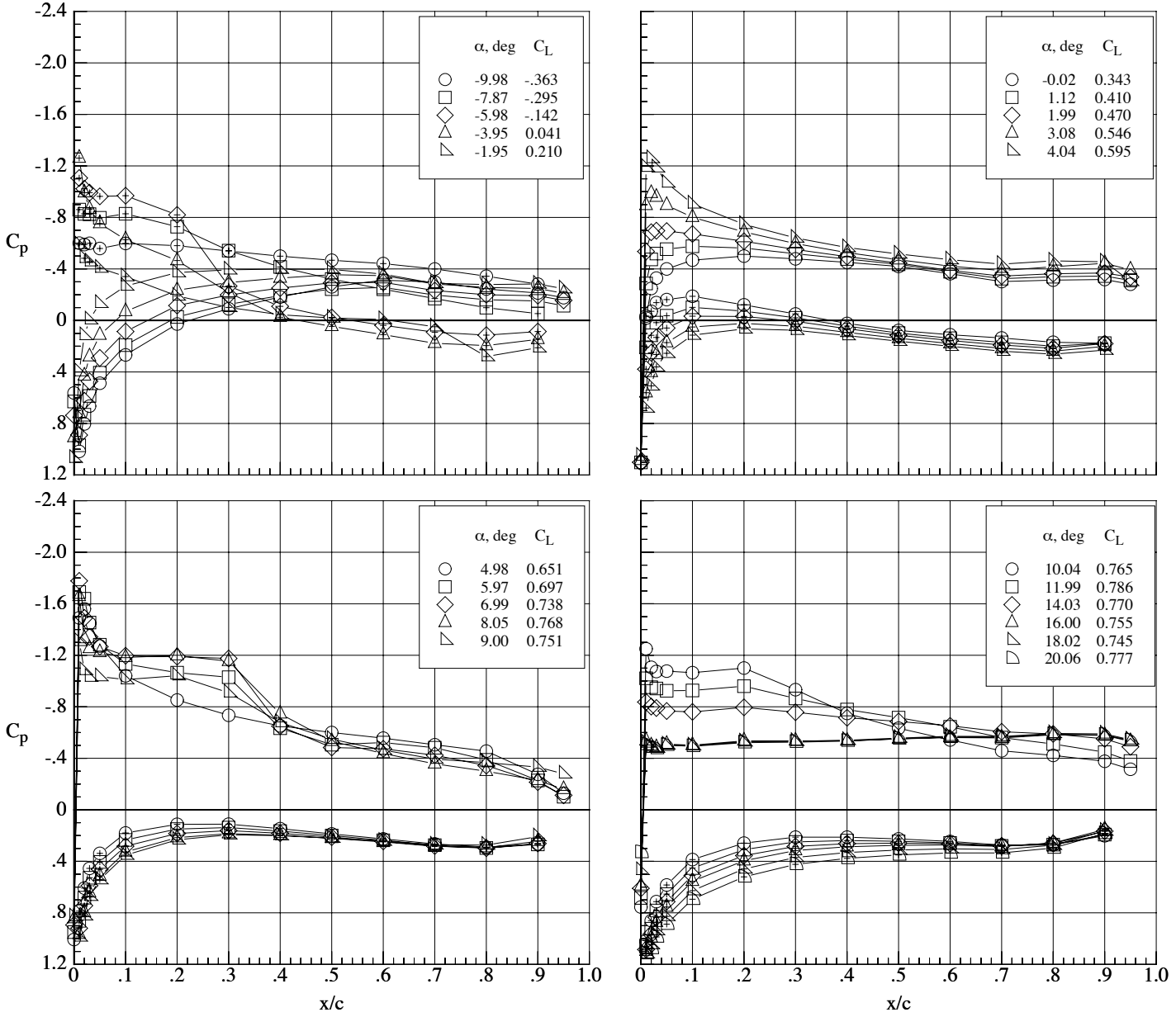

(a) Mach number 0.65.

Figure 113. Chordwise pressure coefficient distributions on the MA-SC-1 wing (bump off) at a Reynolds number of 100,000. $\delta_h = 0°$ and $\delta_f = 0°$.

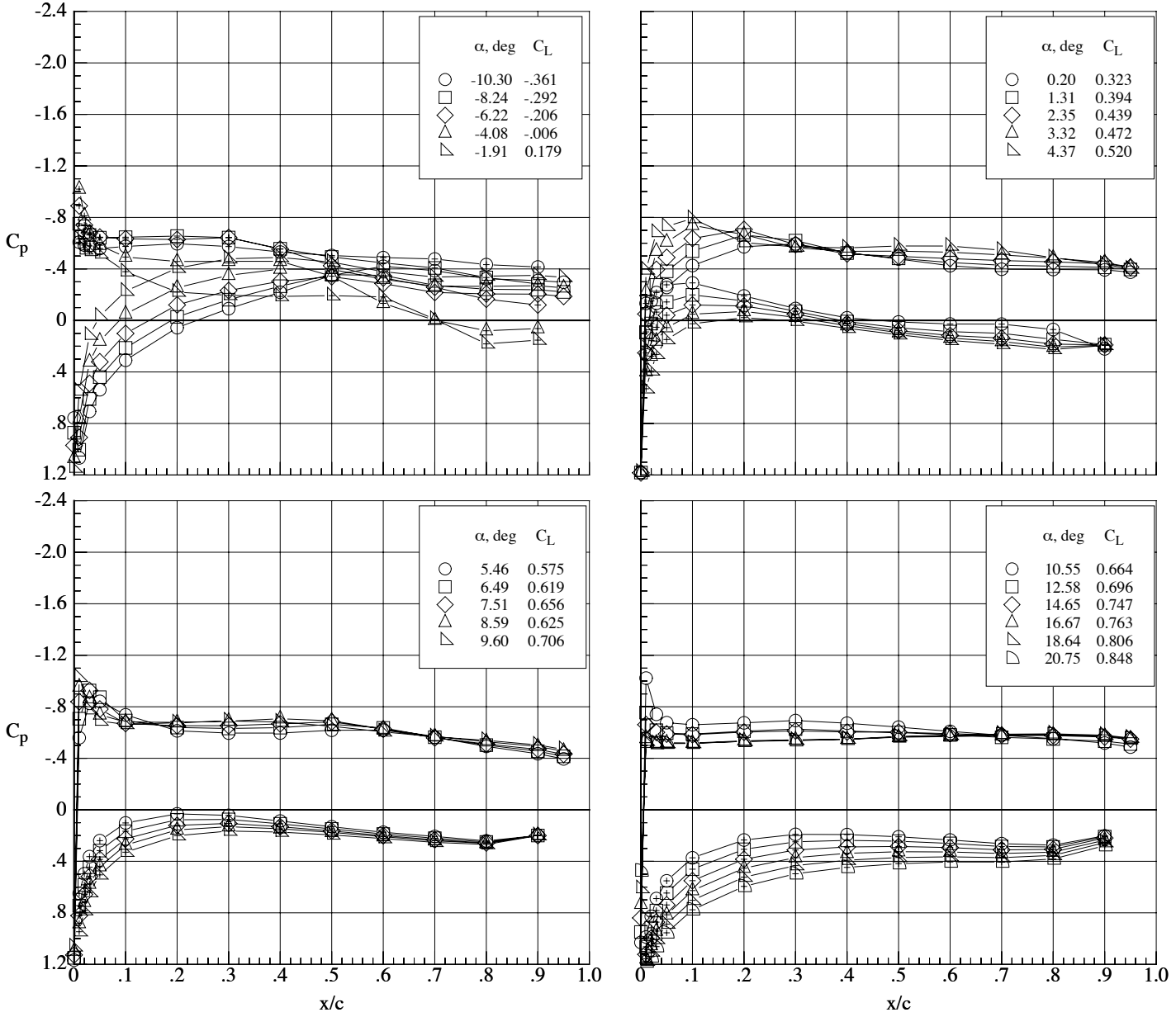

(b) Mach number 0.80.

Figure 113. Concluded.

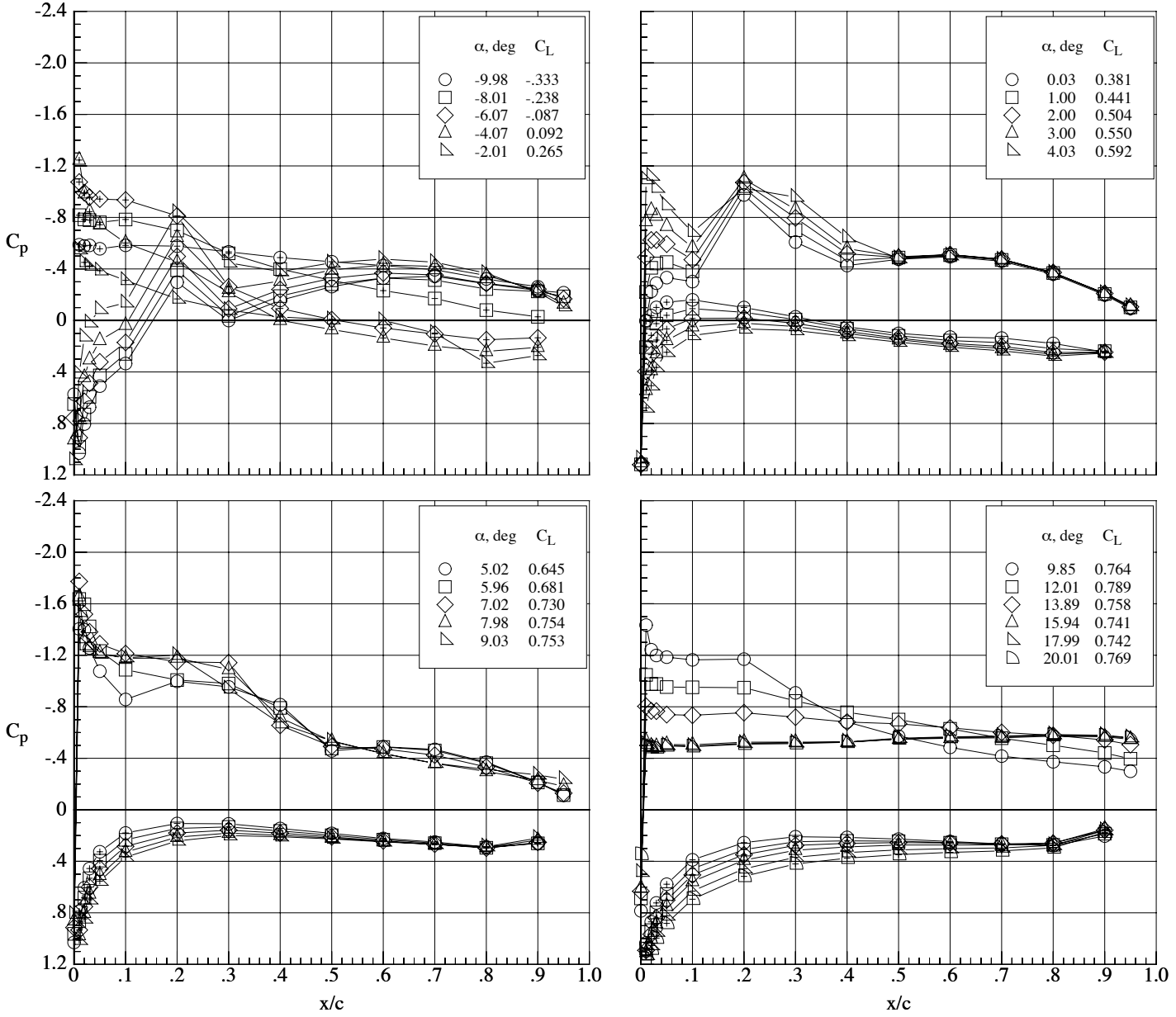

(a) Mach number 0.65.

Figure 114. Chordwise pressure coefficient distributions on the MA-SC-1 wing (bump on) at a Reynolds number of 100,000. $\delta_h = 0°$ and $\delta_f = 0°$.

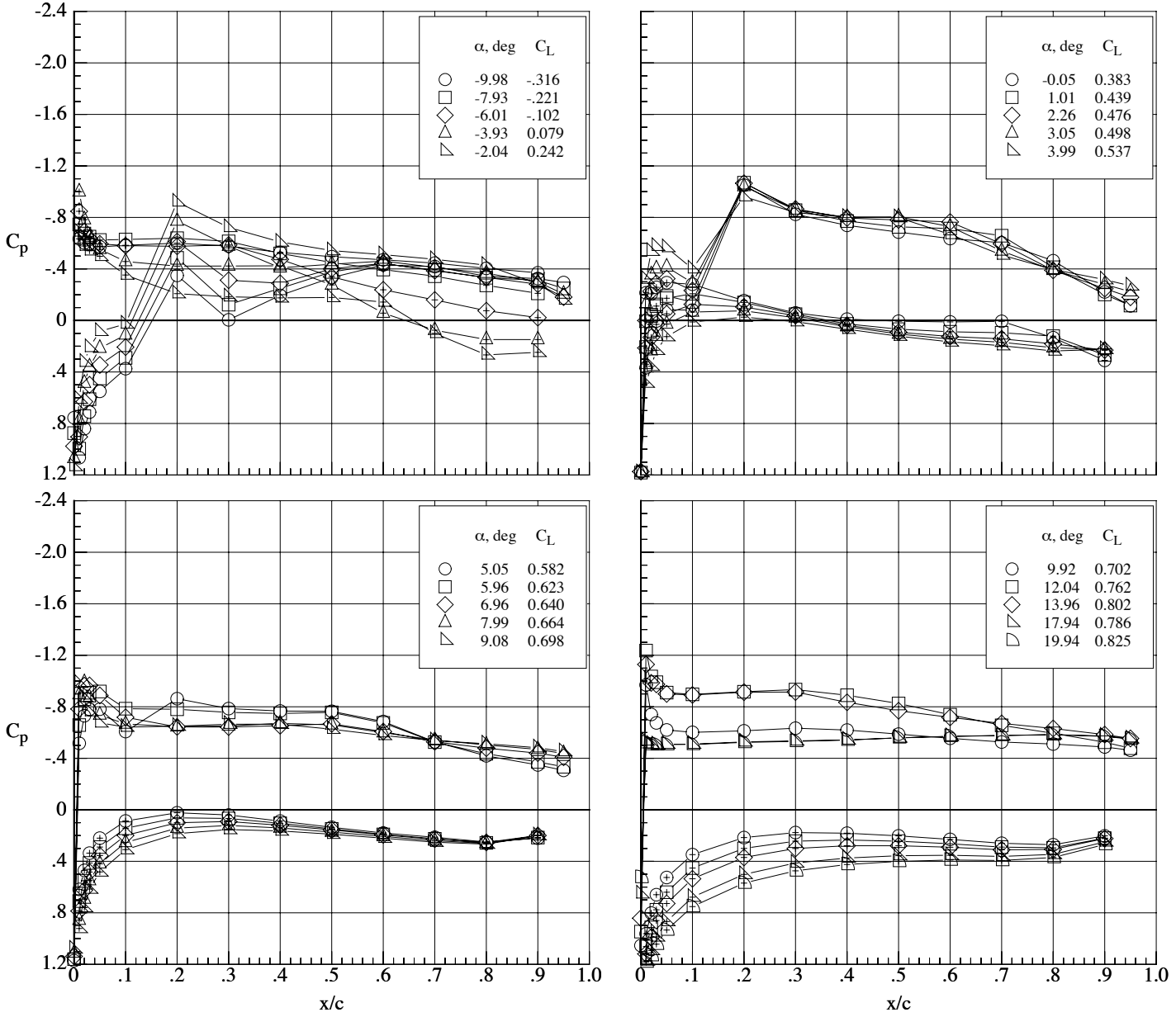

(b) Mach number 0.80.

Figure 114. Concluded.

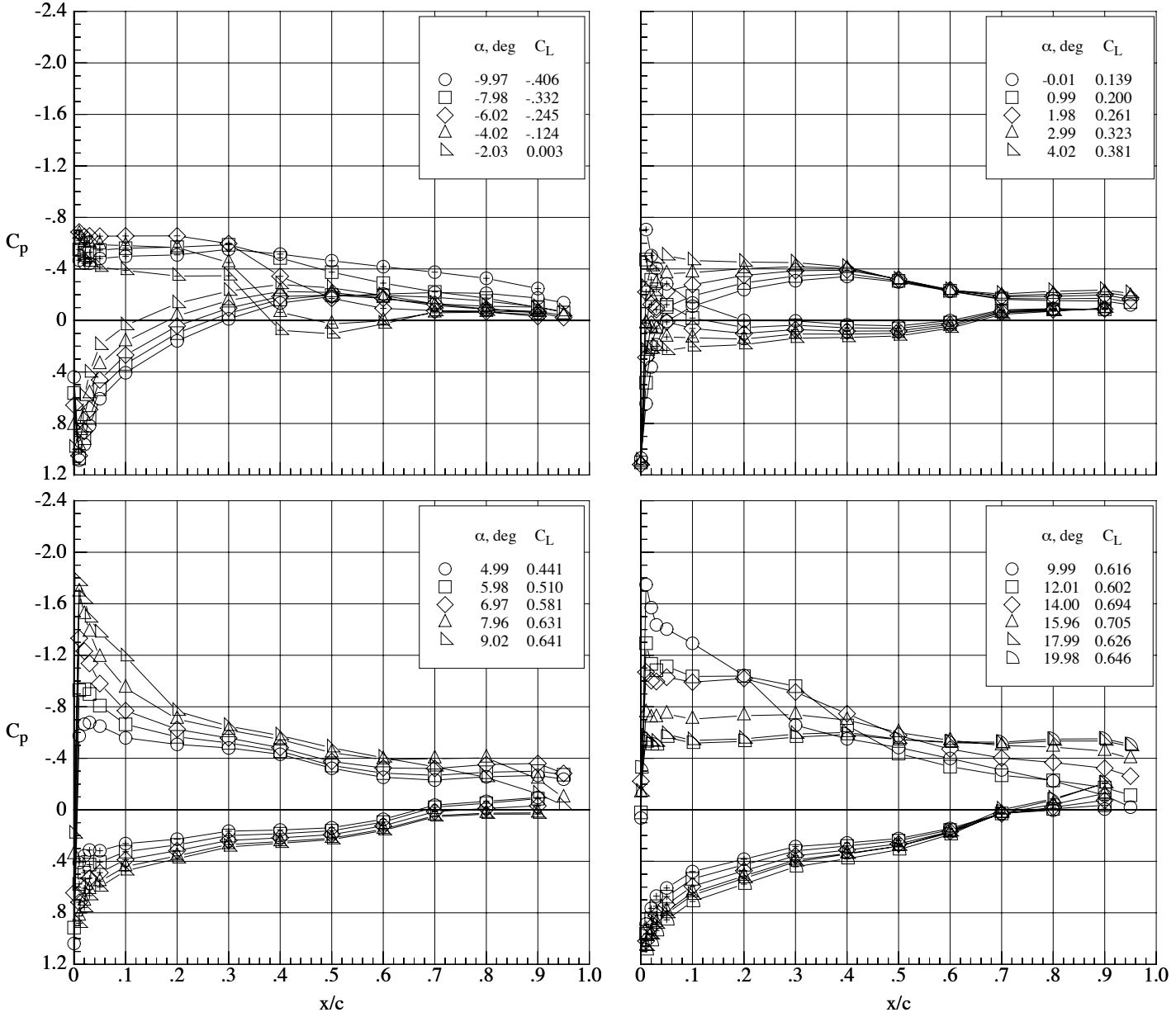

(a) Mach number 0.50.

Figure 115. Chordwise pressure coefficient distributions on the MA-SF-1 wing (bump off) at a Reynolds number of 40,000. $\delta_h = 0°$ and $\delta_f = 0°$.

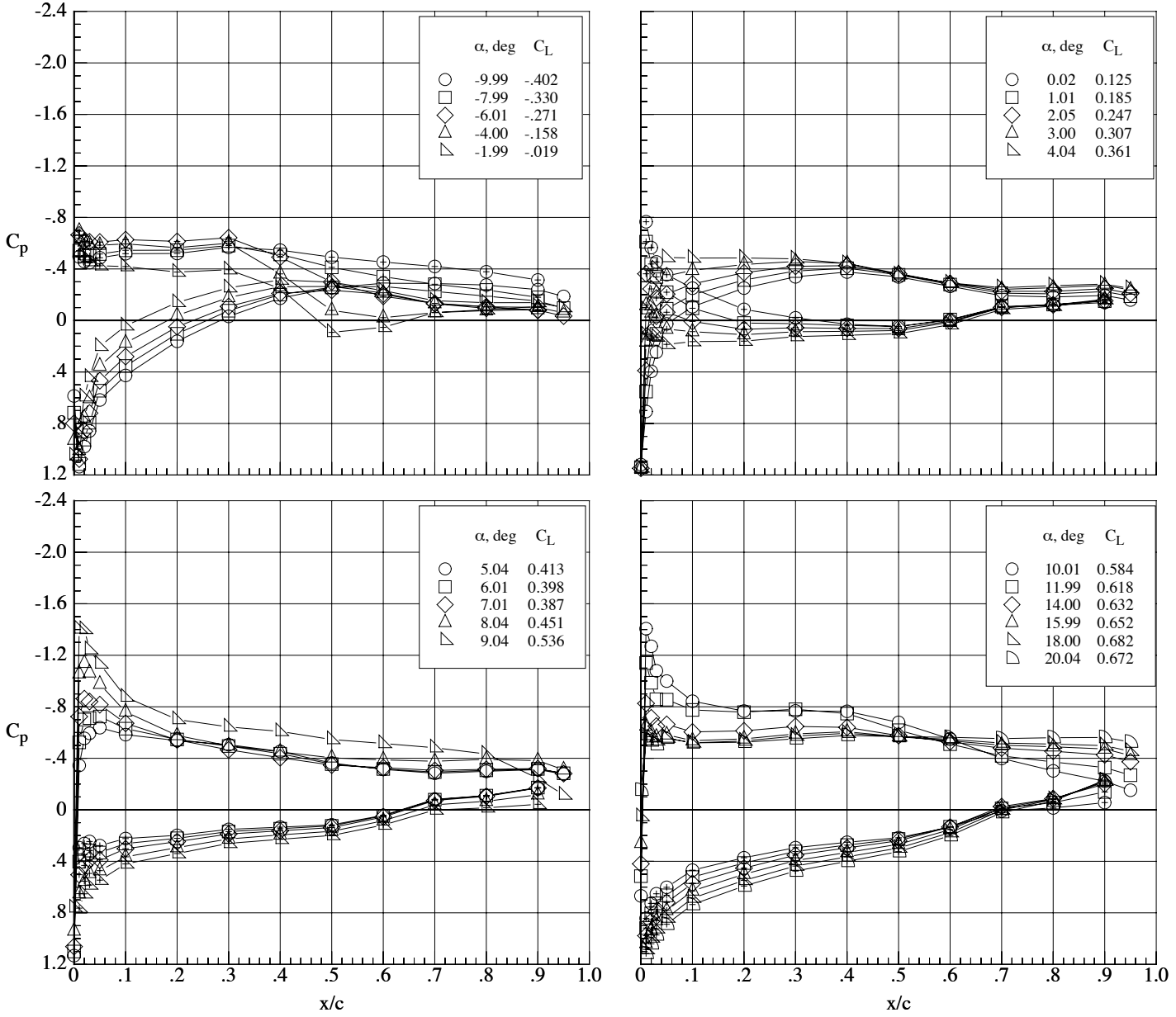

(b) Mach number 0.65.

Figure 115. Continued.

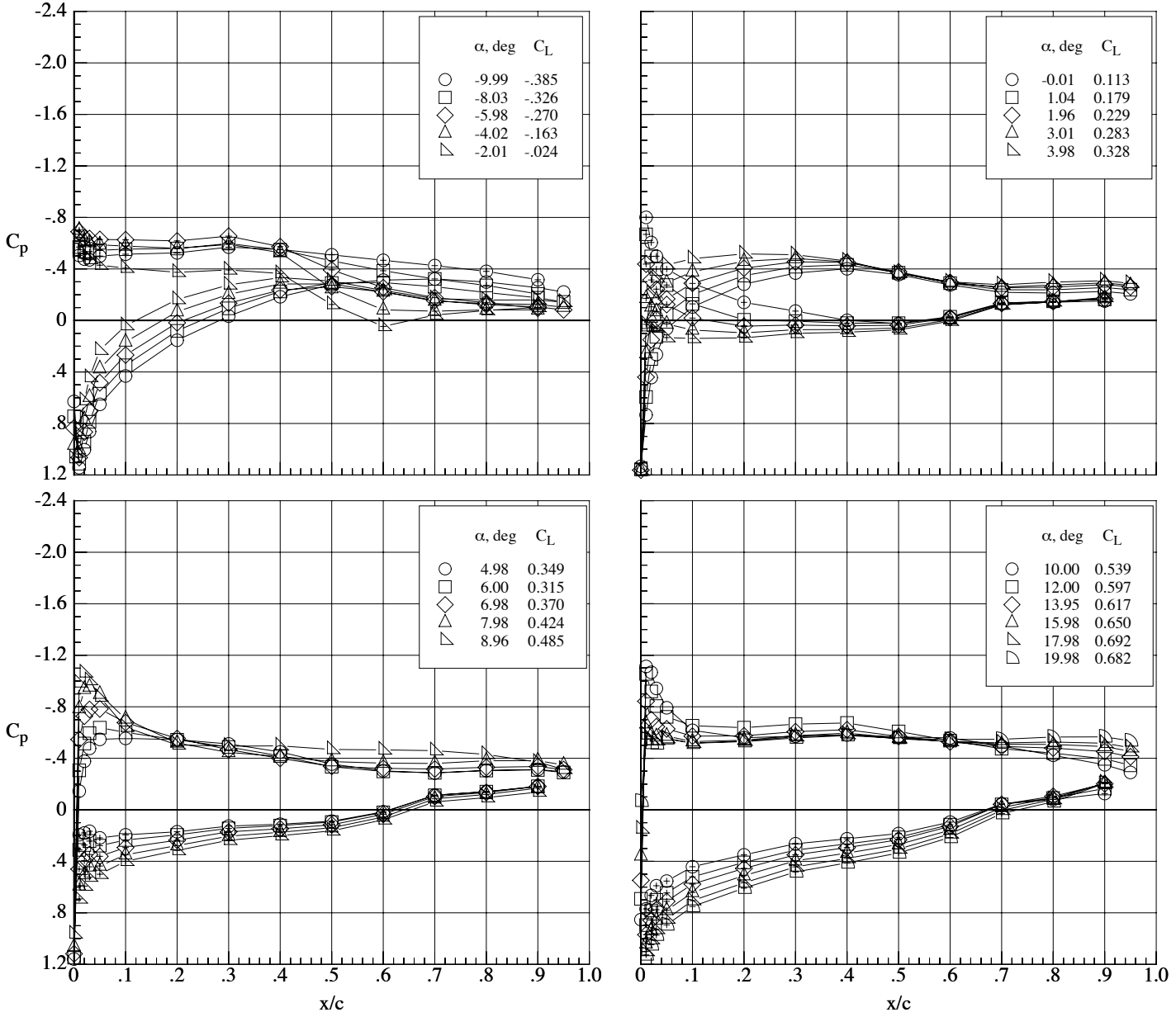

(c) Mach number 0.70.

Figure 115. Continued.

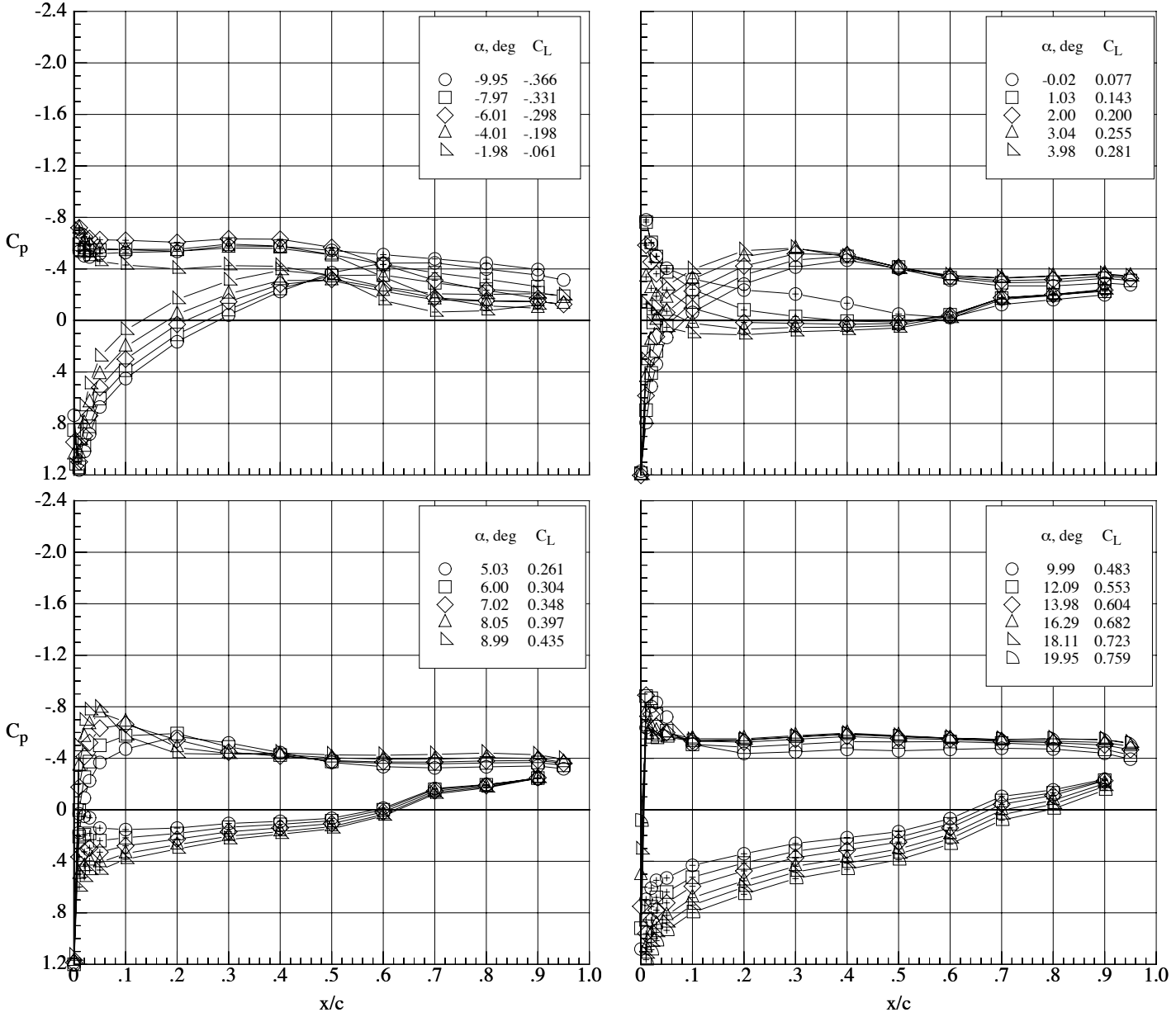

(d) Mach number 0.80.

Figure 115. Continued.

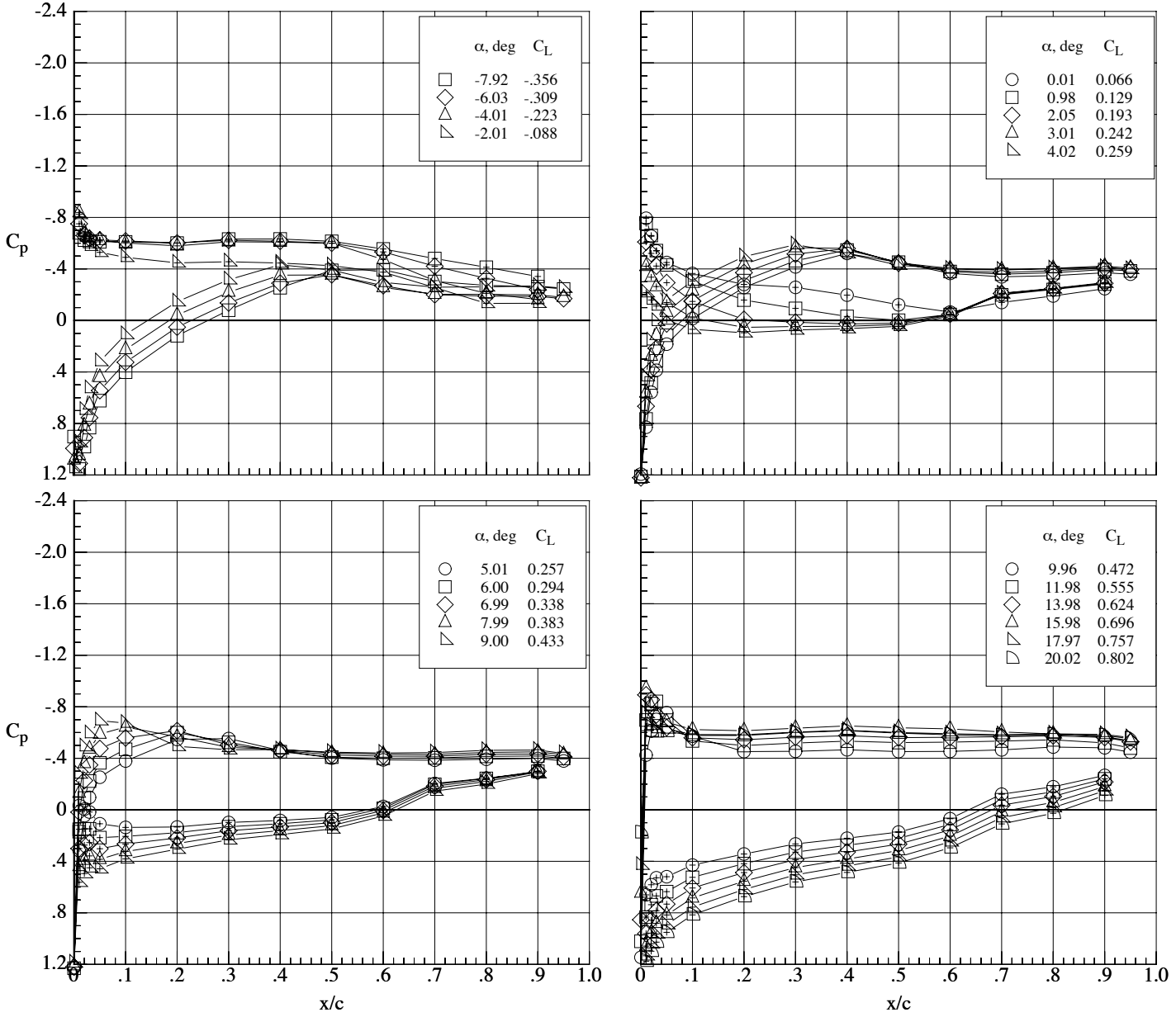

(e) Mach number 0.85.

Figure 115. Continued.

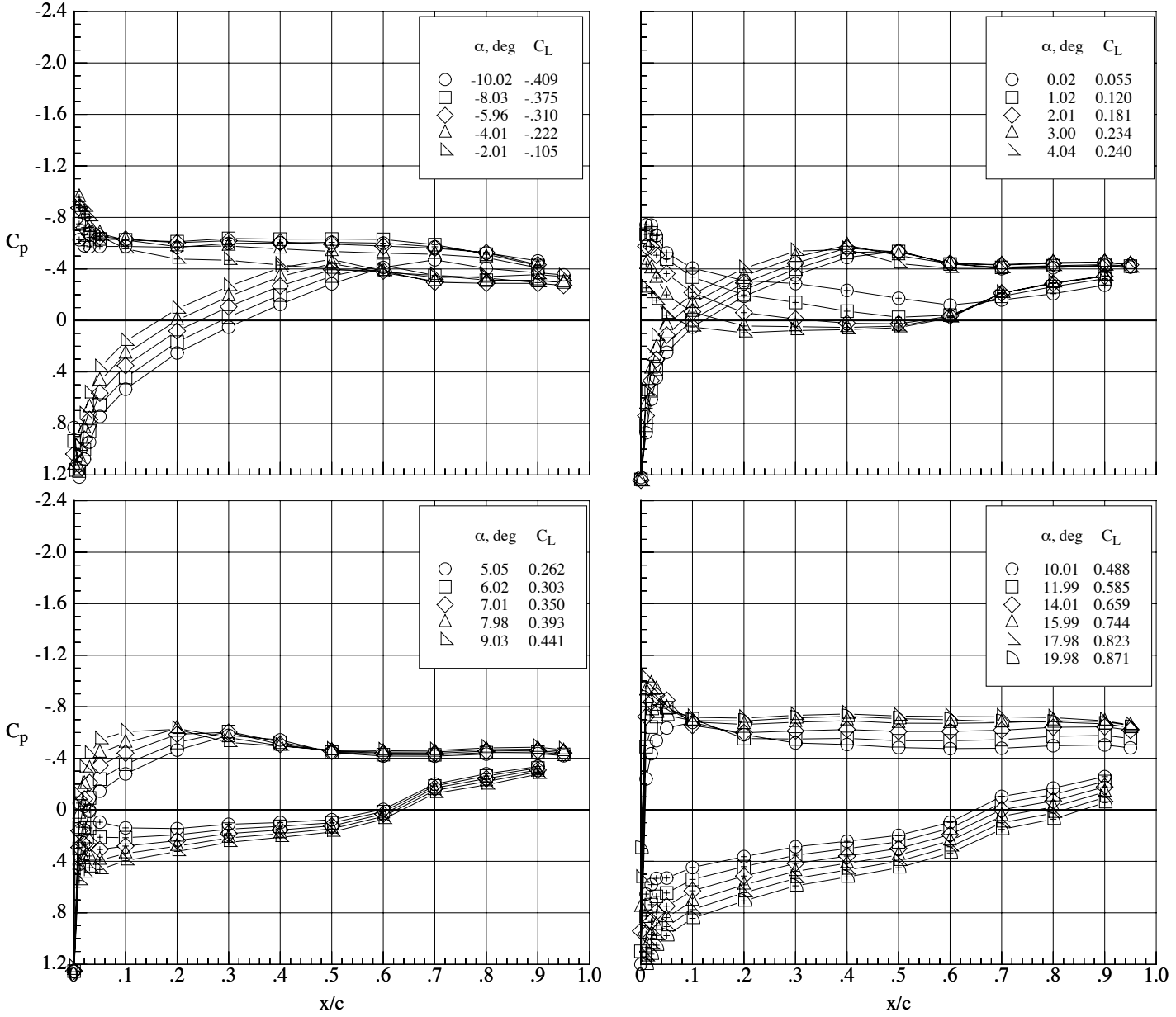

(f) Mach number 0.90.

Figure 115. Concluded.

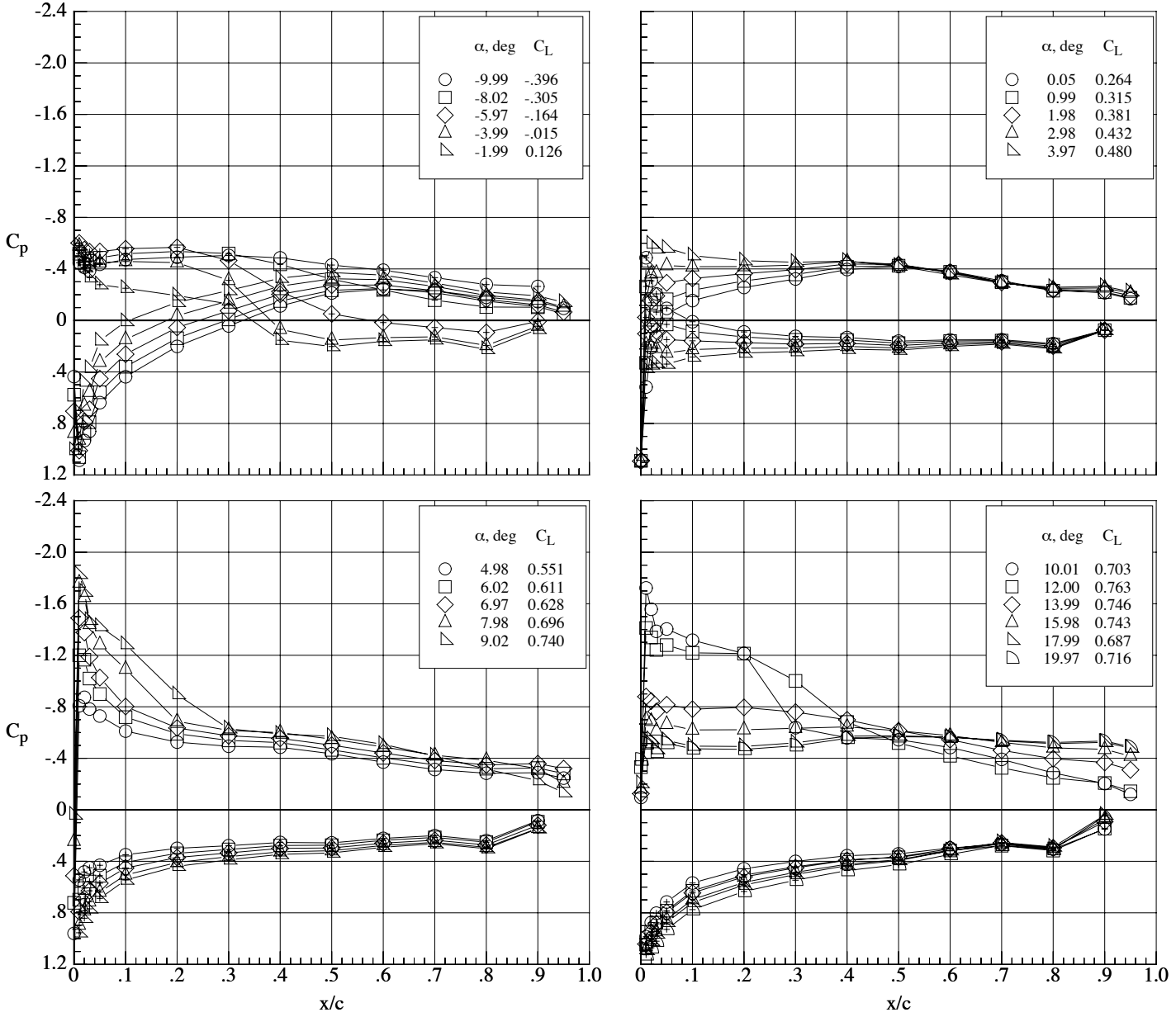

(a) Mach number 0.50.

Figure 116. Chordwise pressure coefficient distributions on the MA-SF-1 wing (bump off) at a Reynolds number of 40,000. $\delta_h = 0°$ and $\delta_f = 10°$.

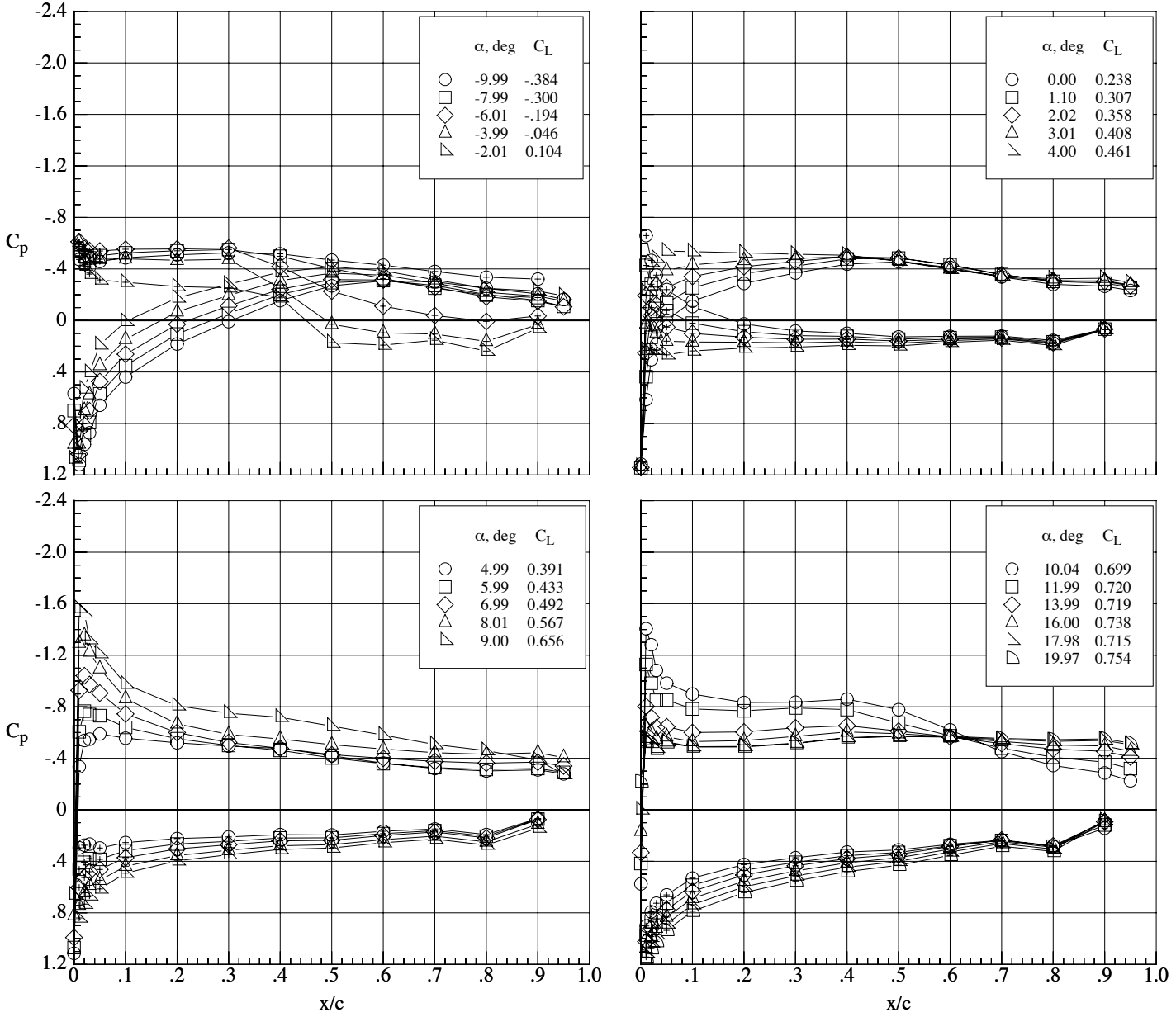

(b) Mach number 0.65.

Figure 116. Continued.

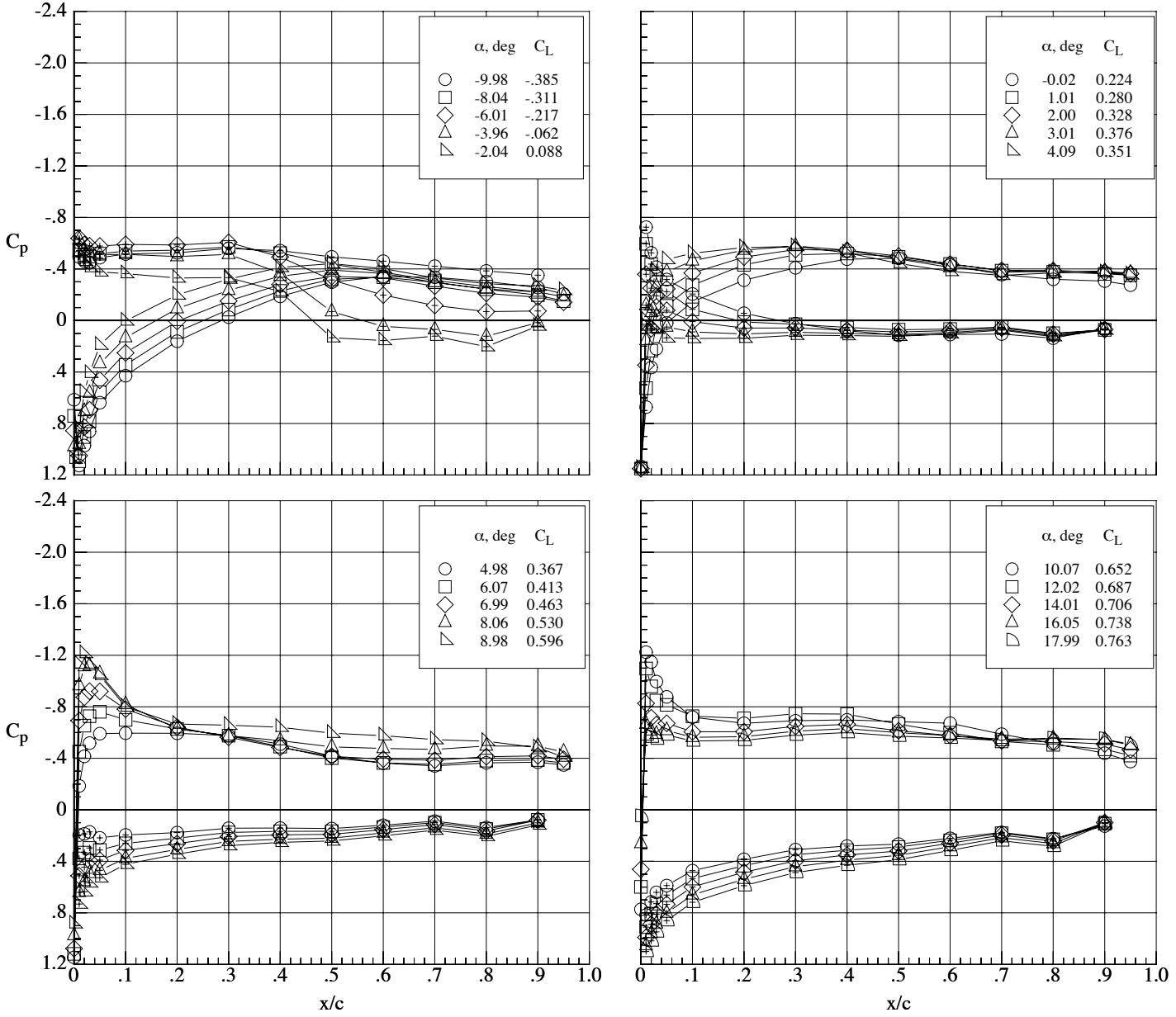

(c) Mach number 0.70.

Figure 116. Continued.

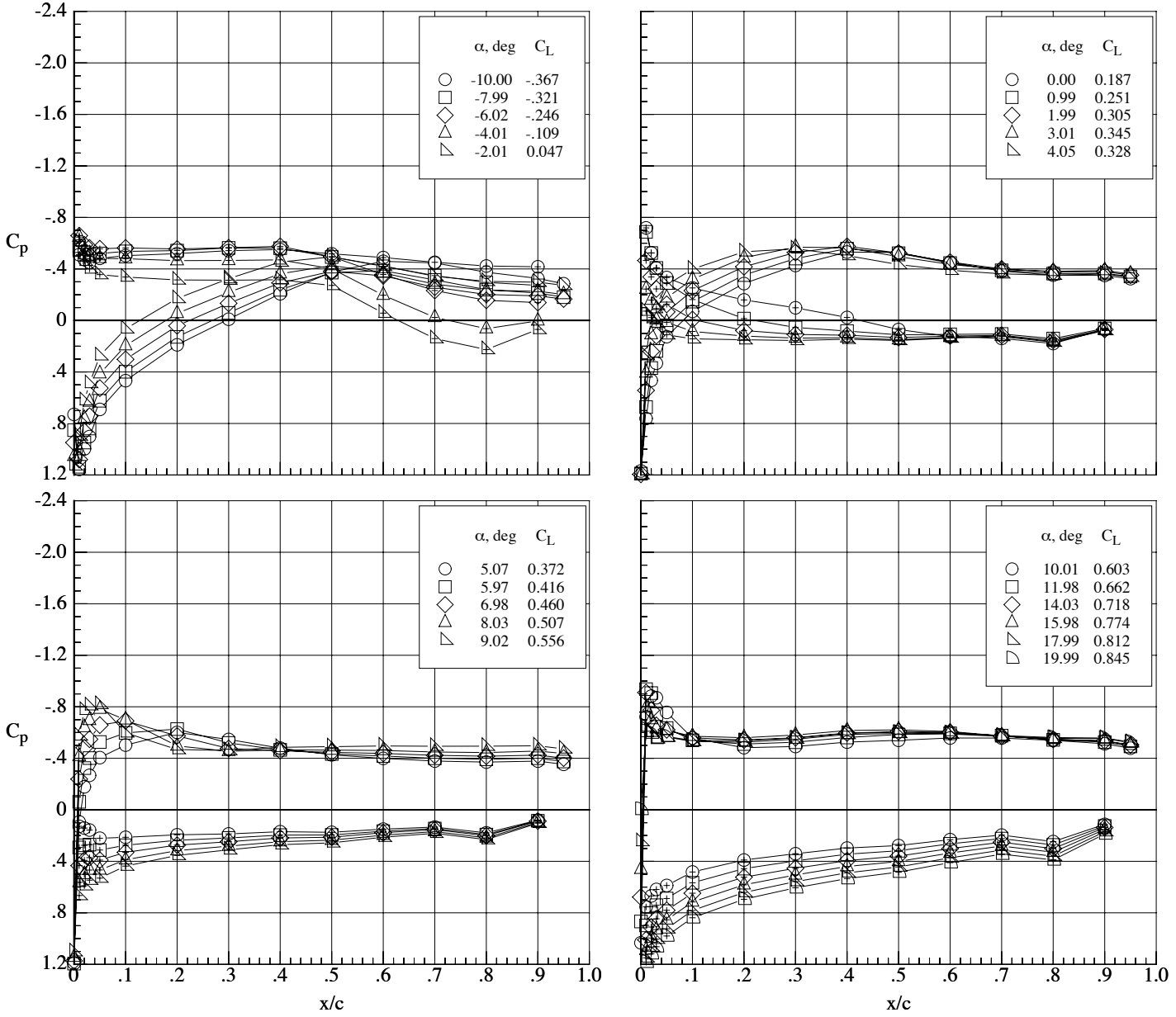

(d) Mach number 0.80.

Figure 116. Continued.

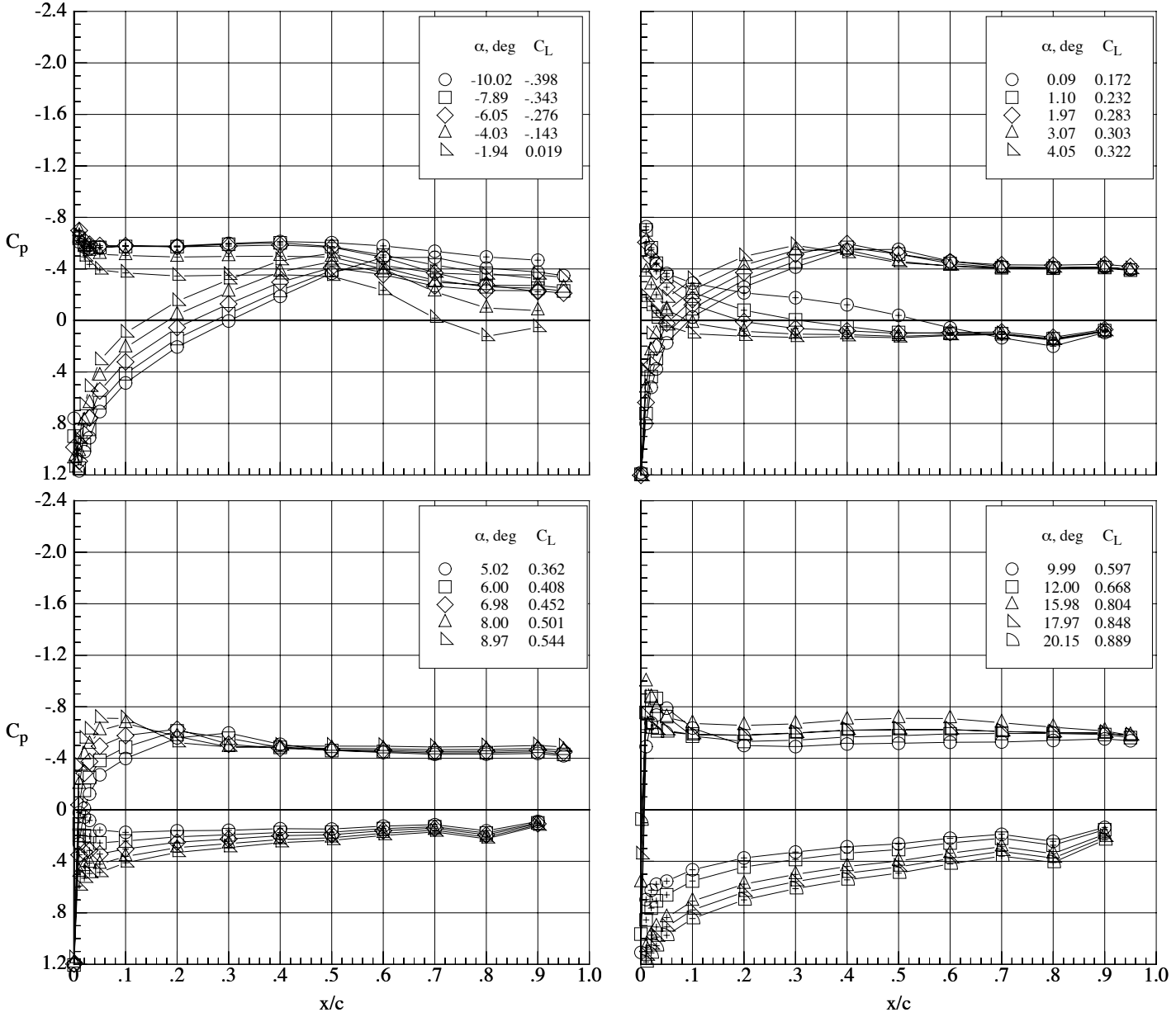

(e) Mach number 0.85.

Figure 116. Continued.

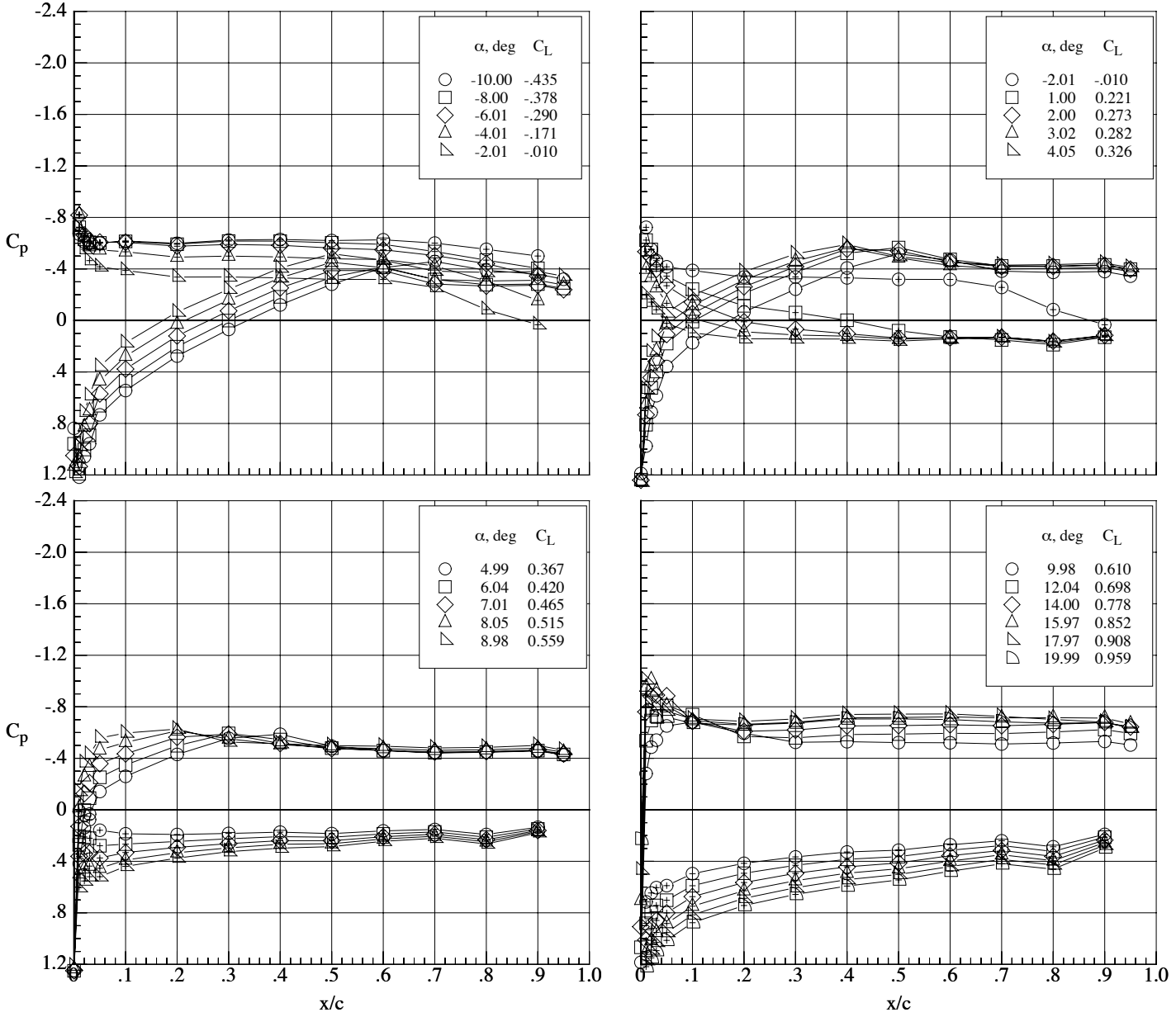

(f) Mach number 0.90.

Figure 116. Concluded.

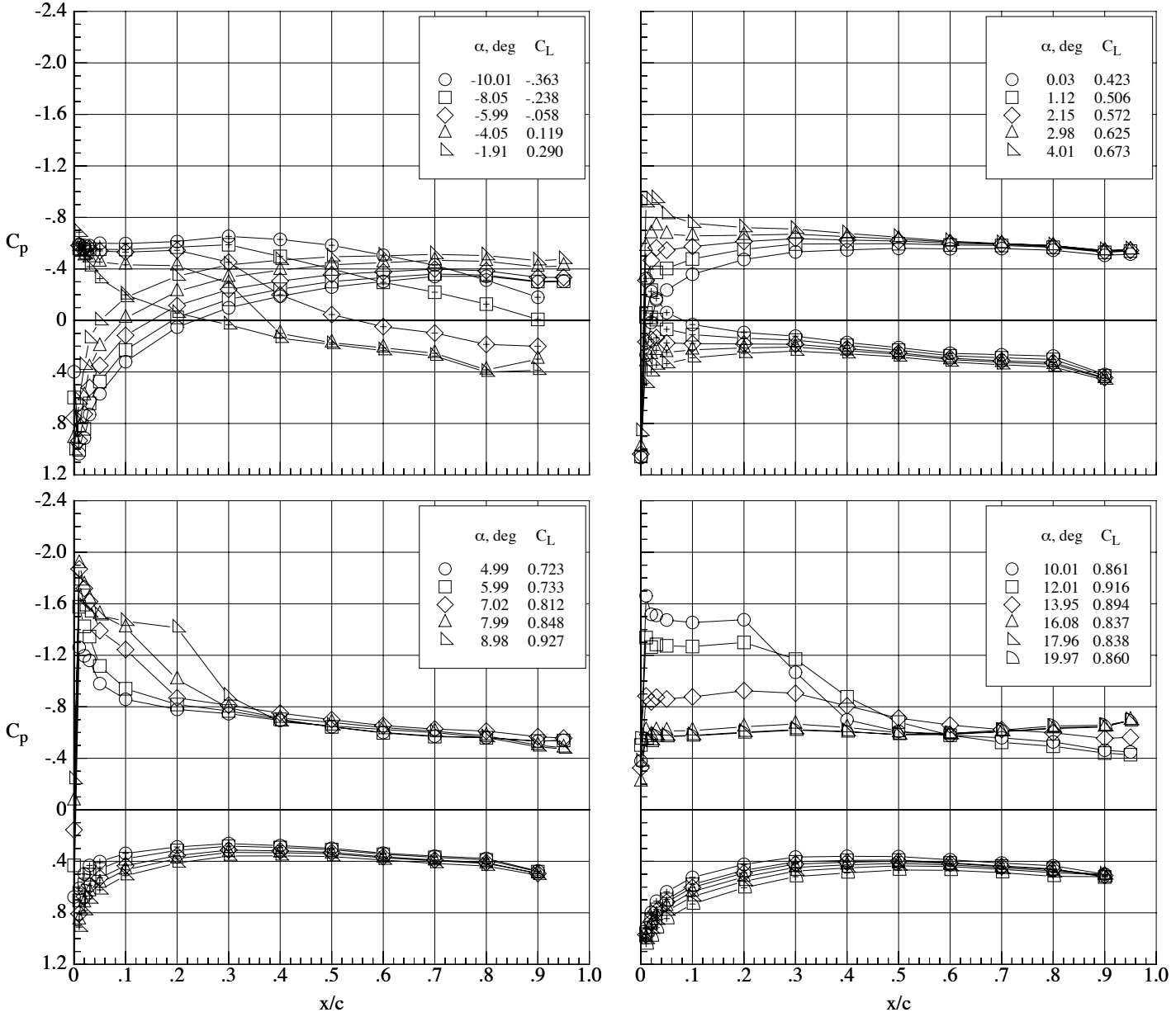

(a) Mach number 0.50.

Figure 117. Chordwise pressure coefficient distributions on the MA-SF-1 wing (bump off) at a Reynolds number of 40,000. $\delta_h = 0°$ and $\delta_f = 30°$.

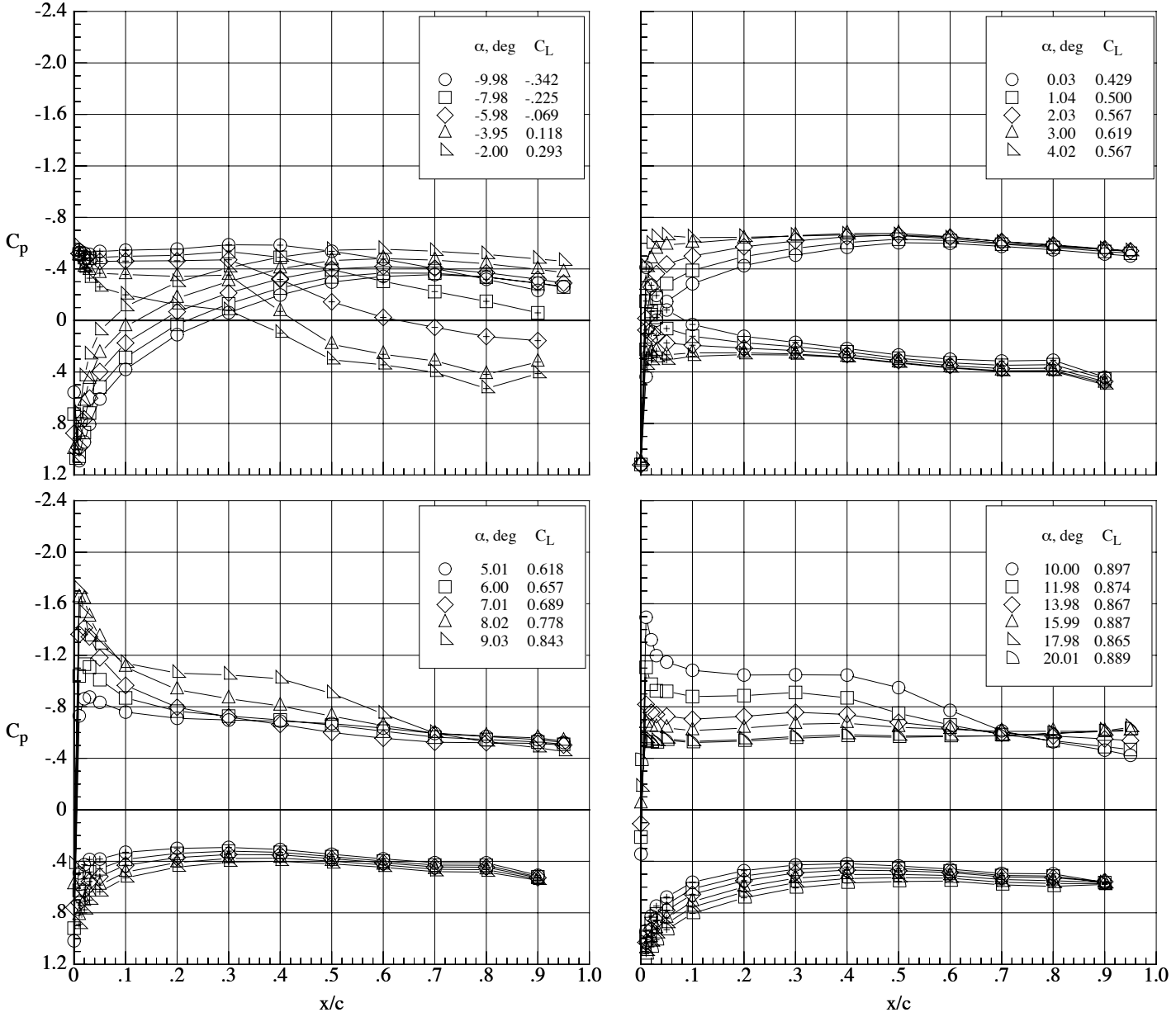

(b) Mach number 0.65.

Figure 117. Continued.

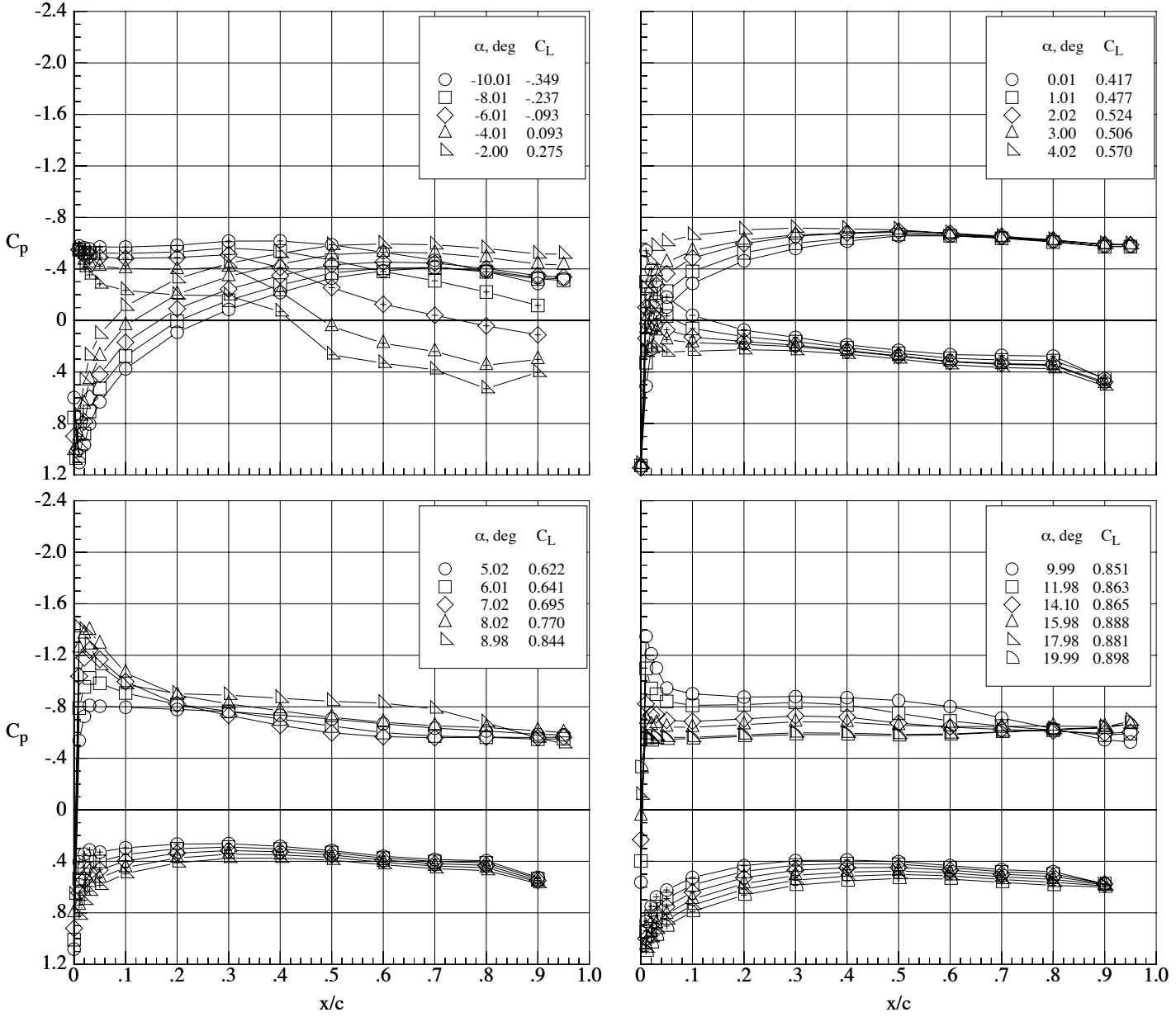

(c) Mach number 0.70.

Figure 117. Continued.

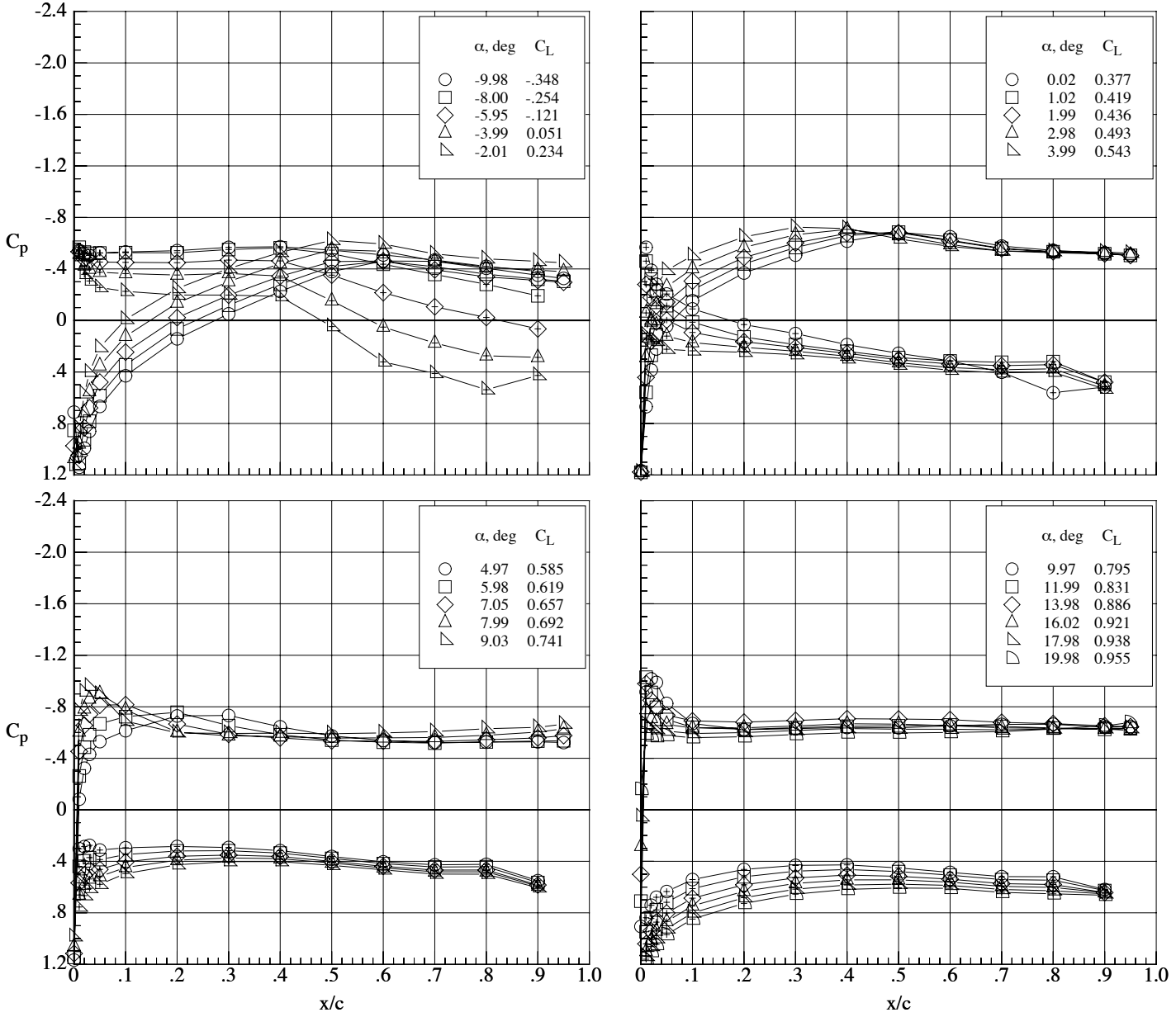

(d) Mach number 0.80.

Figure 117. Continued.

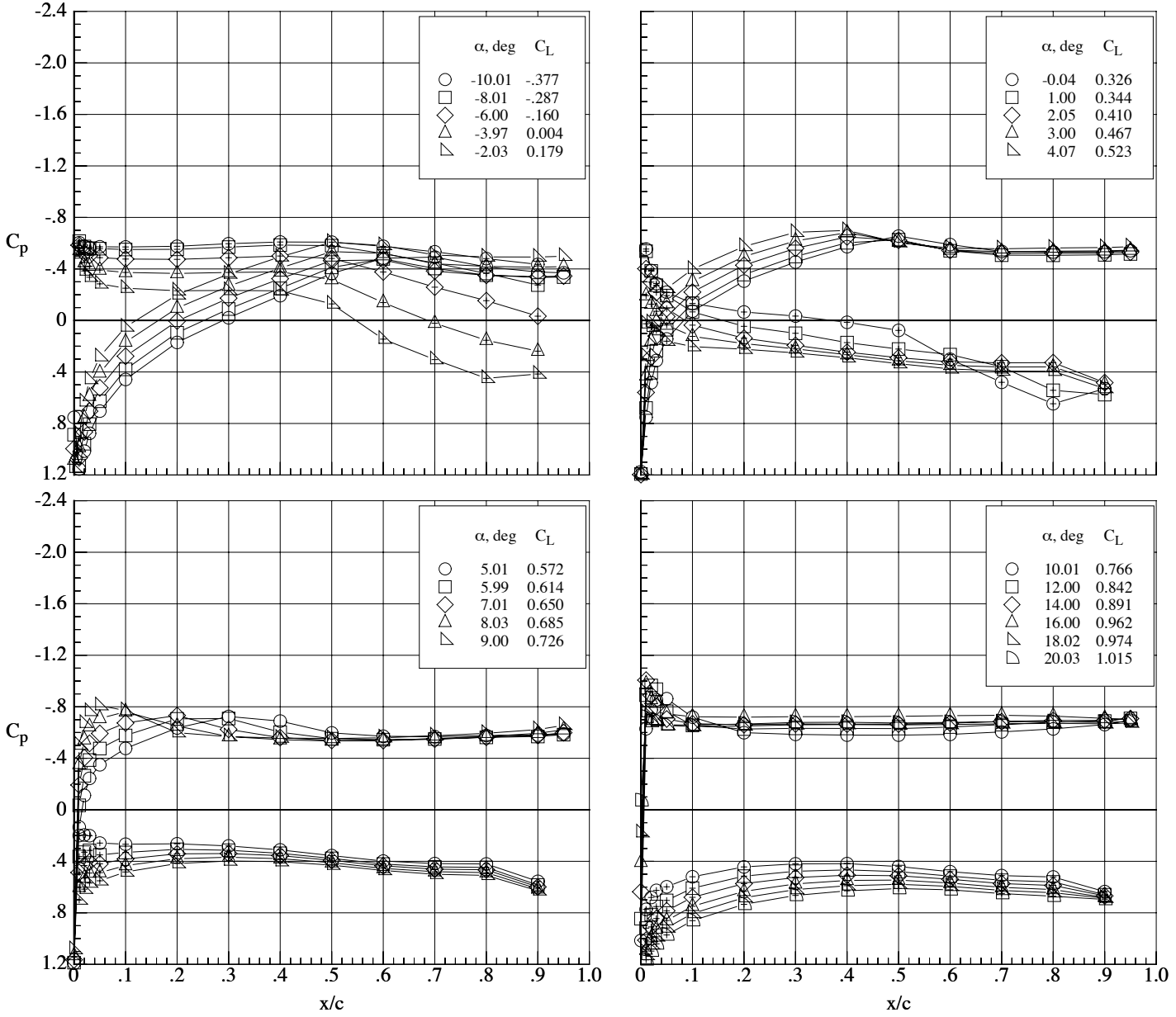

(e) Mach number 0.85.

Figure 117. Continued.

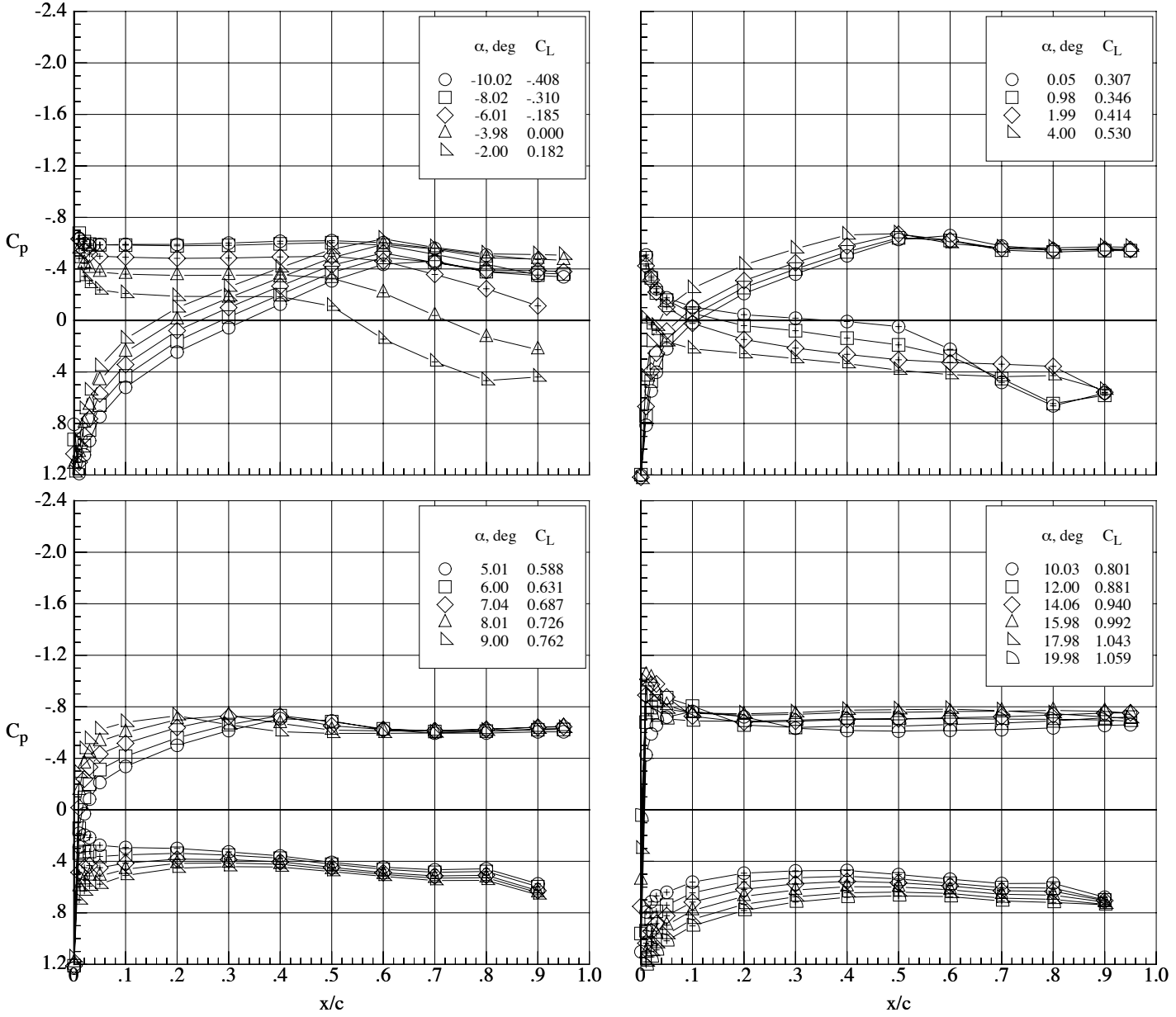

(f) Mach number 0.90.

Figure 117. Concluded.

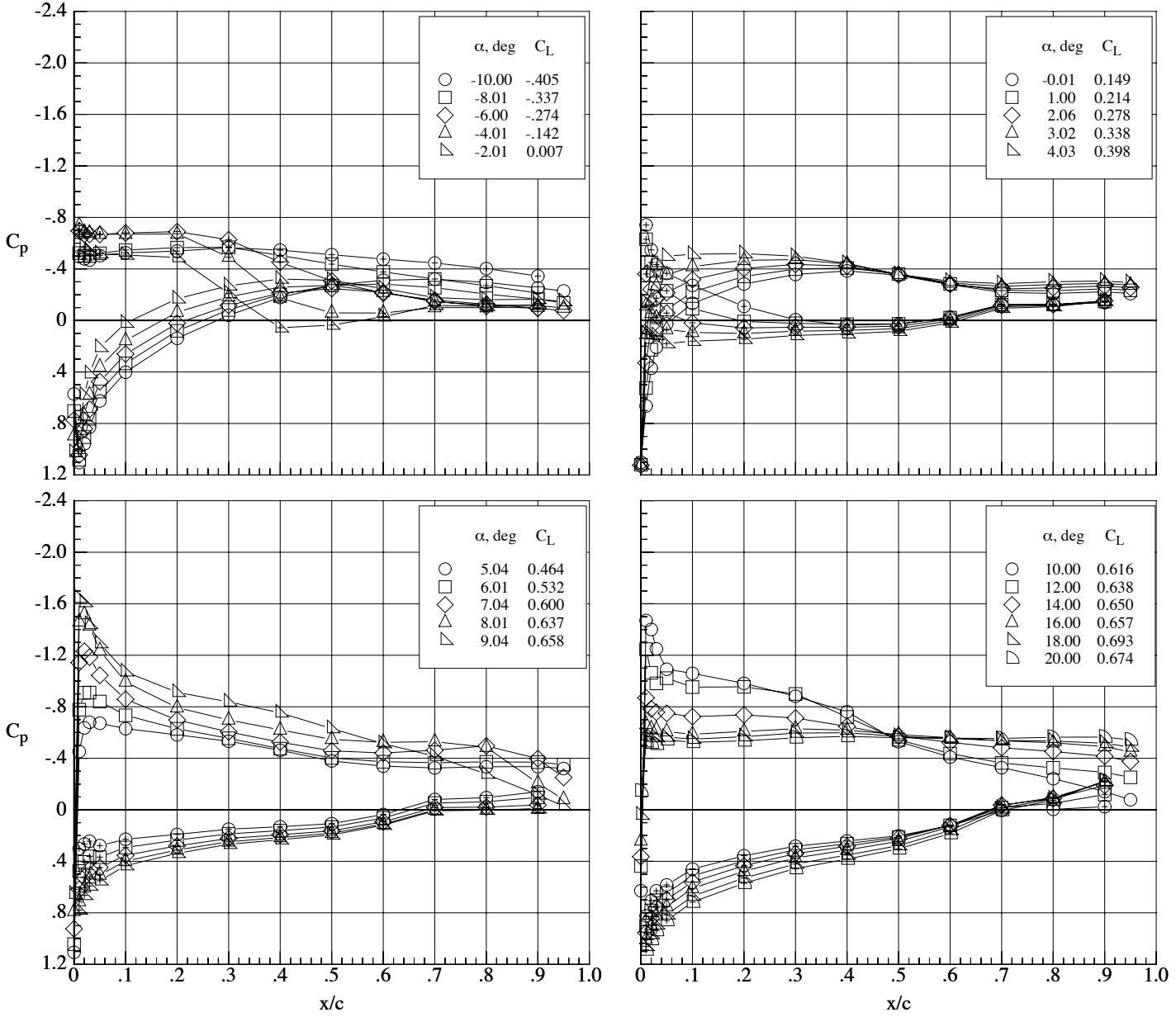

(a) Mach number 0.65.

Figure 118. Chordwise pressure coefficient distributions on the MA-SF-1 wing (bump off) at a Reynolds number of 60,000. $\delta_h = 0°$ and $\delta_f = 0°$.

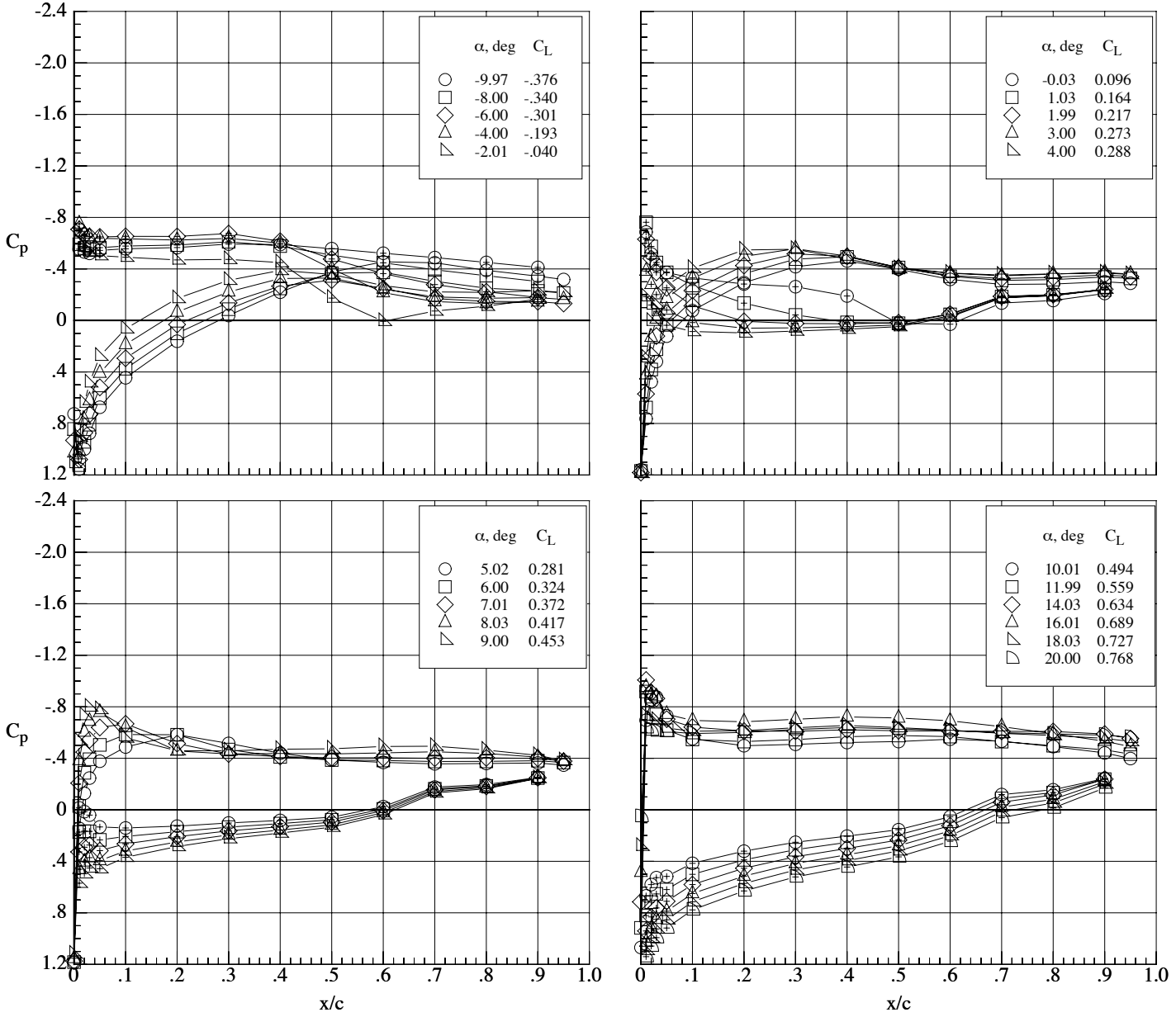

(b) Mach number 0.80.

Figure 118. Concluded.

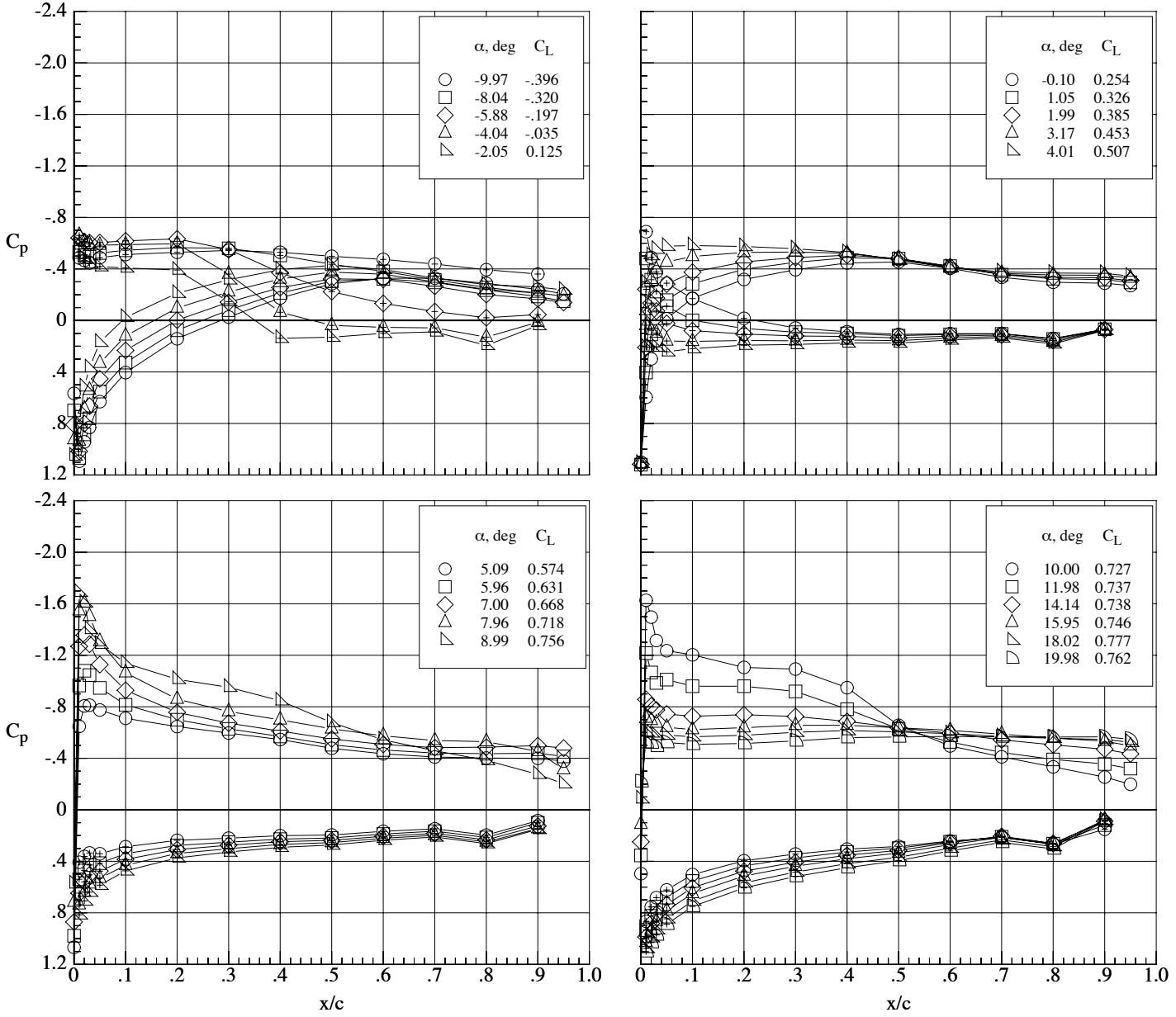

(a) Mach number 0.65.

Figure 119. Chordwise pressure coefficient distributions on the MA-SF-1 wing (bump off) at a Reynolds number of 60,000. $\delta_h = 0°$ and $\delta_f = 10°$.

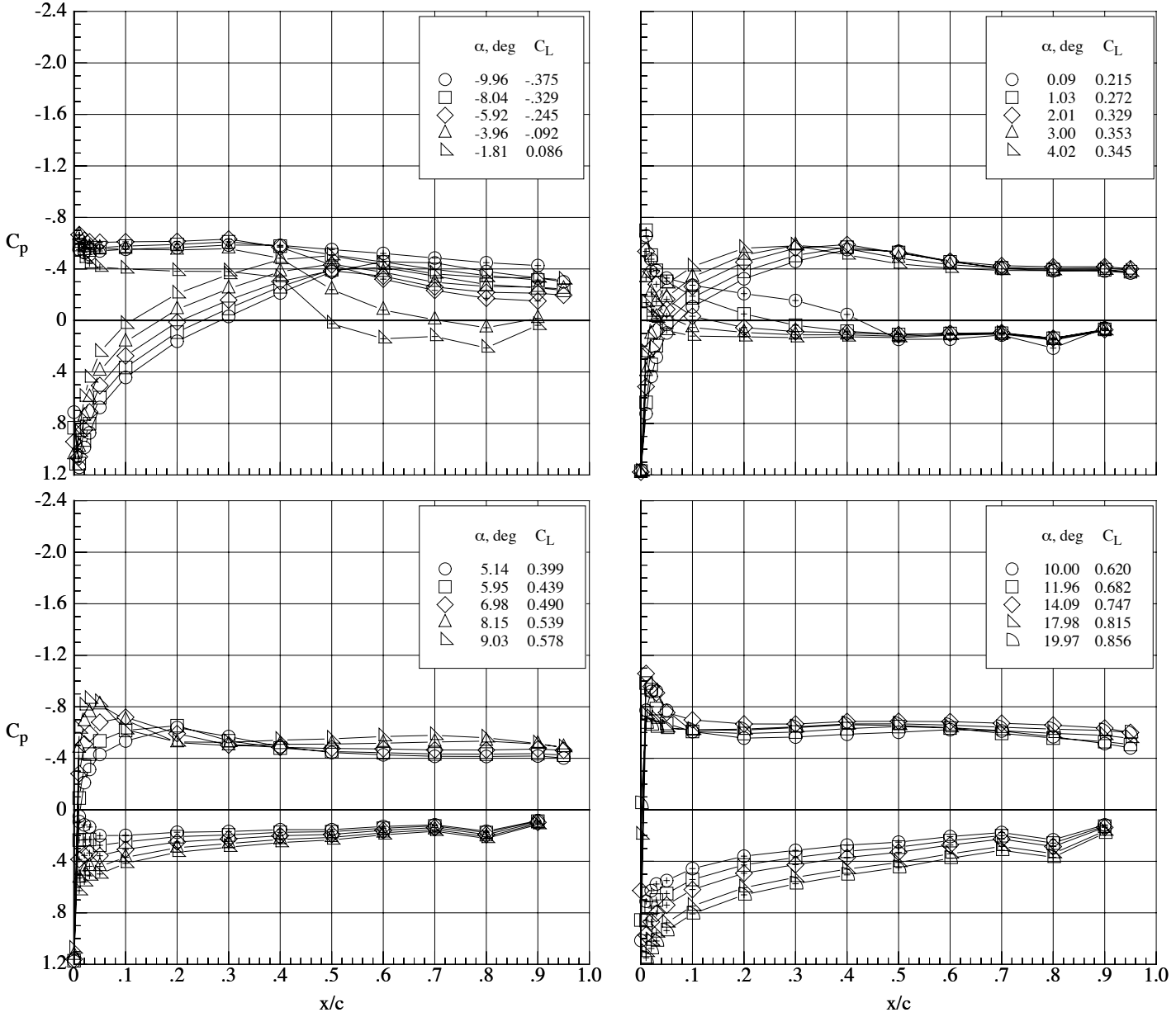

(b) Mach number 0.80.

Figure 119. Concluded.

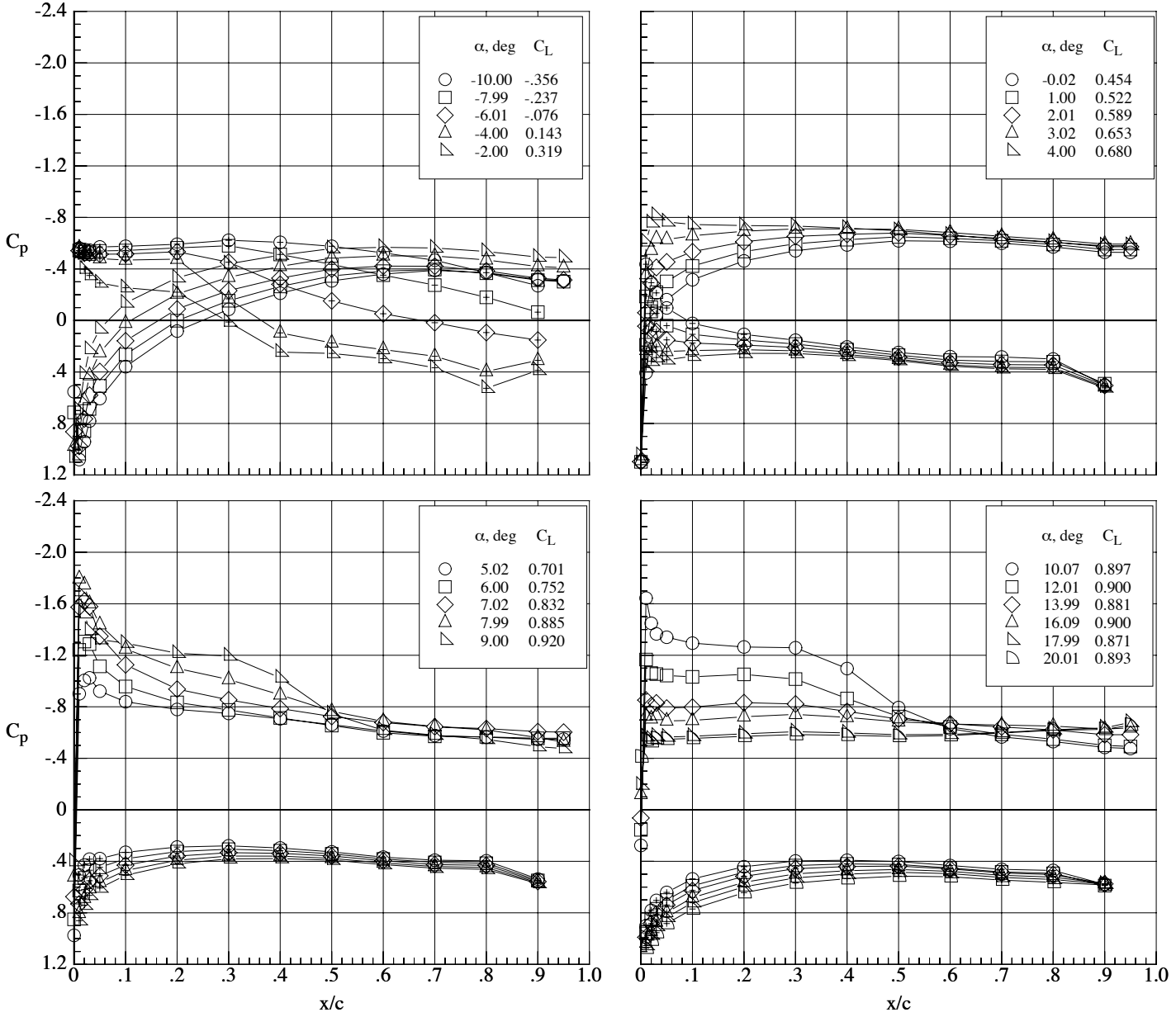

(a) Mach number 0.65.

Figure 120. Chordwise pressure coefficient distributions on the MA-SF-1 wing (bump off) at a Reynolds number of 60,000. $\delta_h = 0°$ and $\delta_f = 30°$.

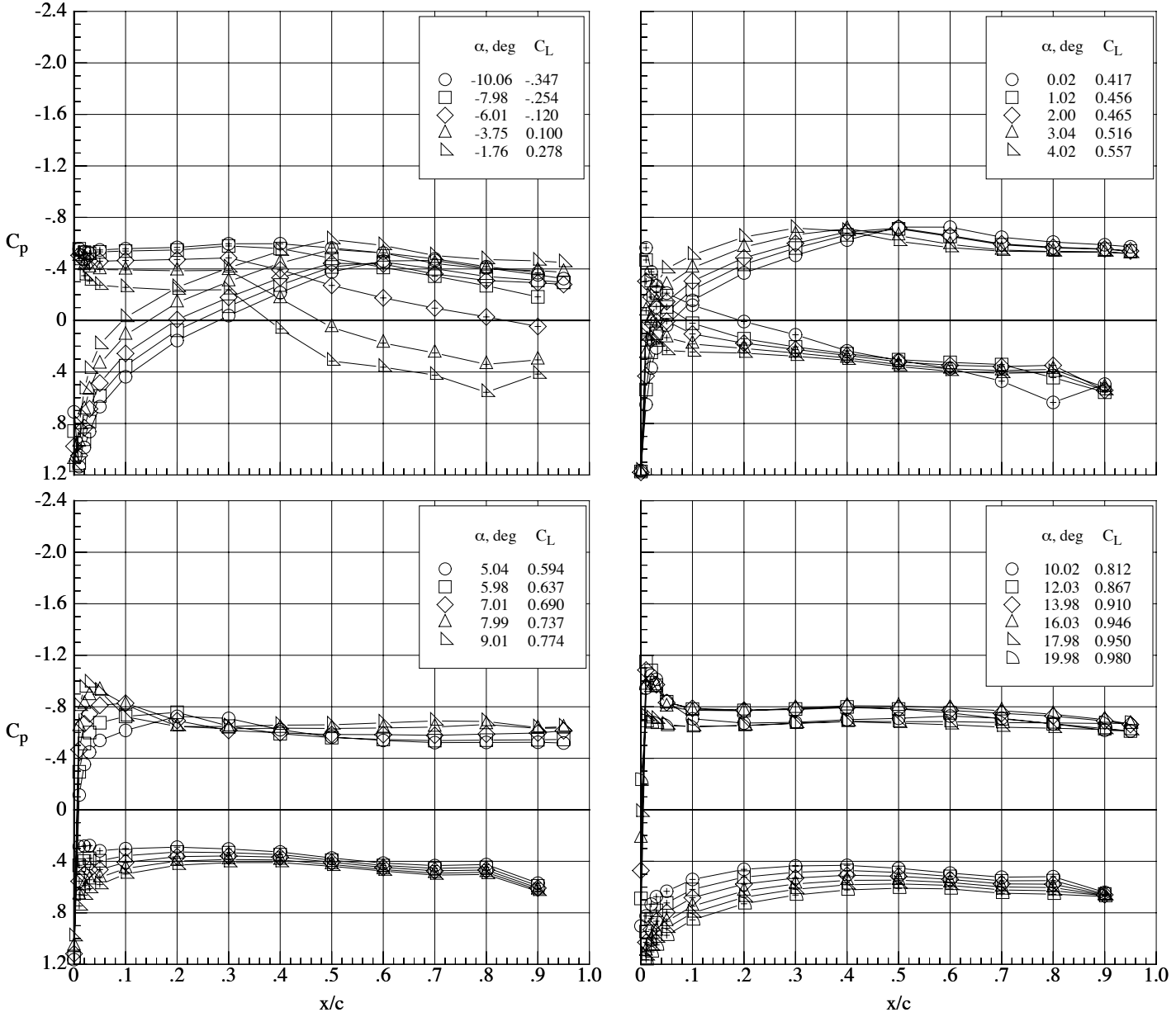

(b) Mach number 0.80.

Figure 120. Concluded.

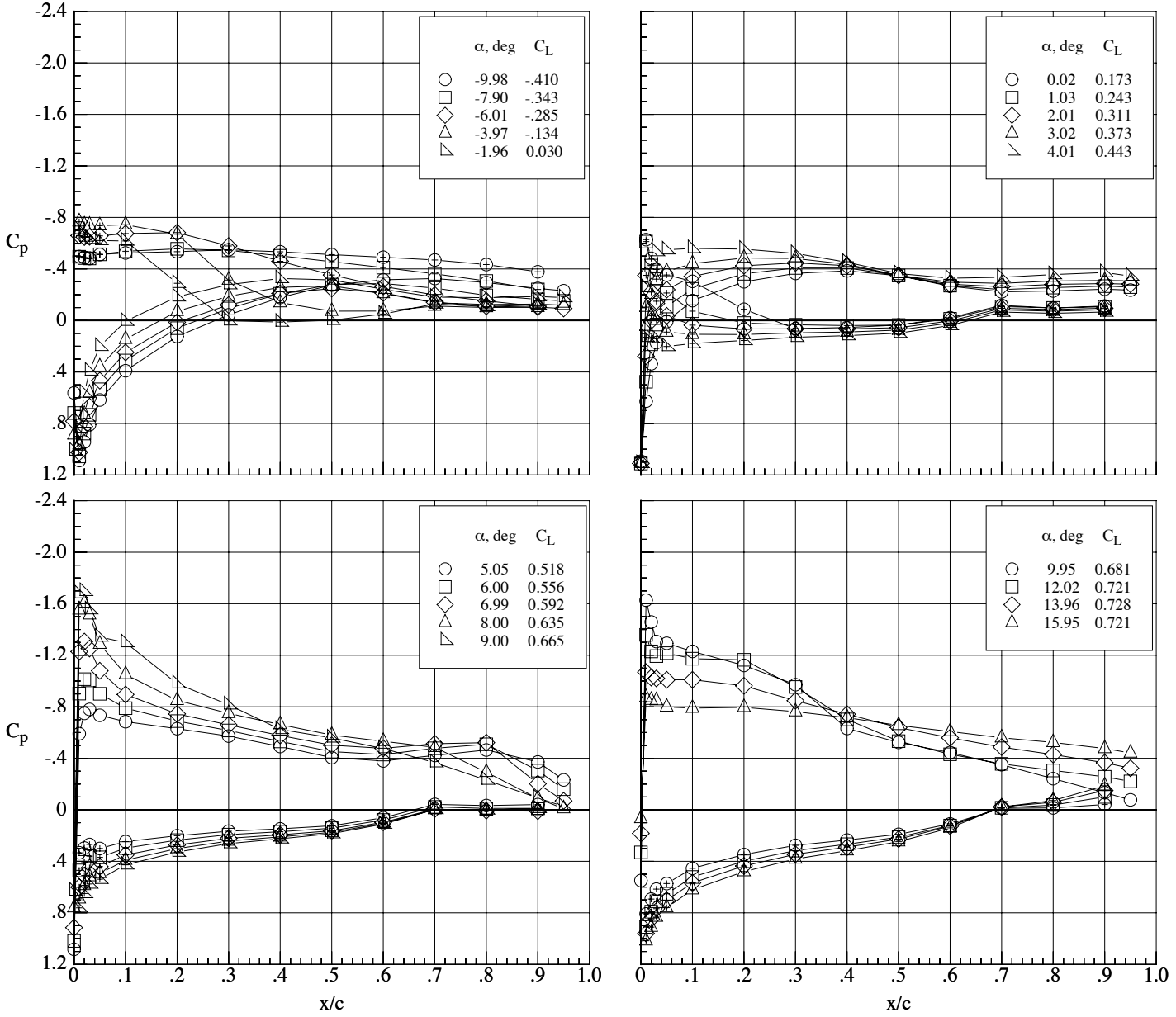

(a) Mach number 0.65.

Figure 121. Chordwise pressure coefficient distributions on the MA-SF-1 wing (bump off) at a Reynolds number of 100,000. $\delta_h = 0°$ and $\delta_f = 0°$.

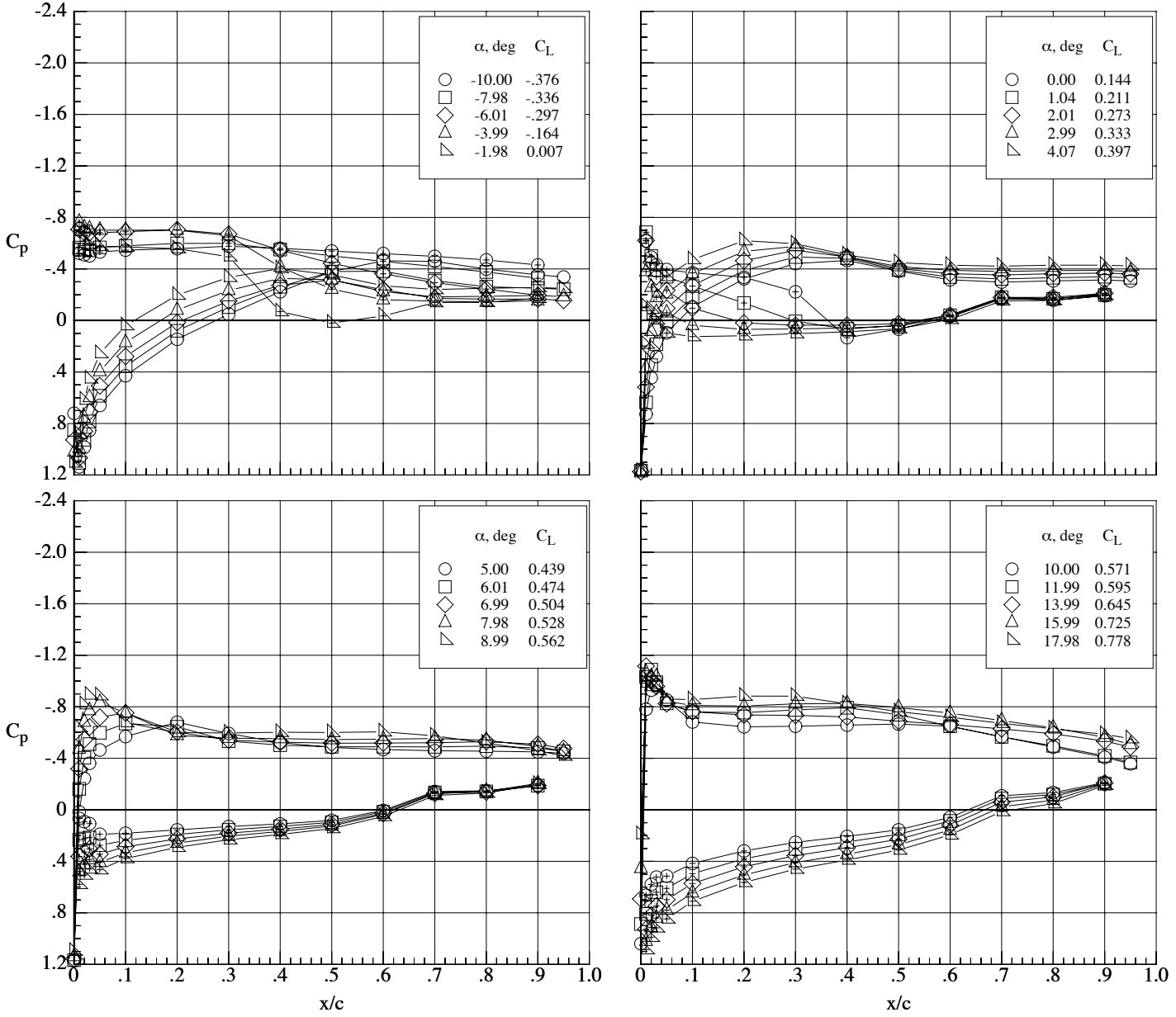

(b) Mach number 0.80.

Figure 121. Concluded.

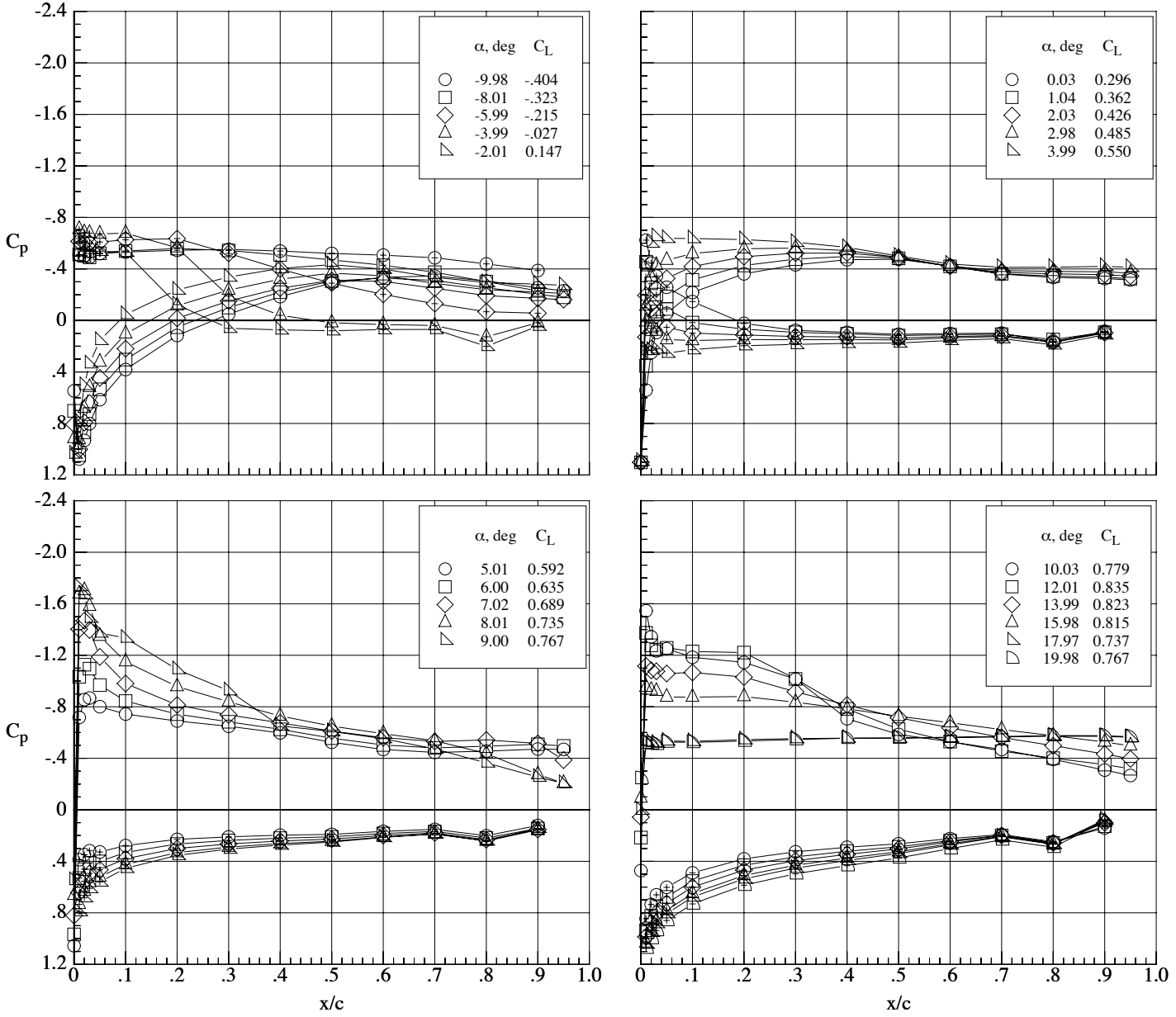

(a) Mach number 0.65.

Figure 122. Chordwise pressure coefficient distributions on the MA-SF-1 wing (bump off) at a Reynolds number of 100,000. $\delta_h = 0°$ and $\delta_f = 10°$.

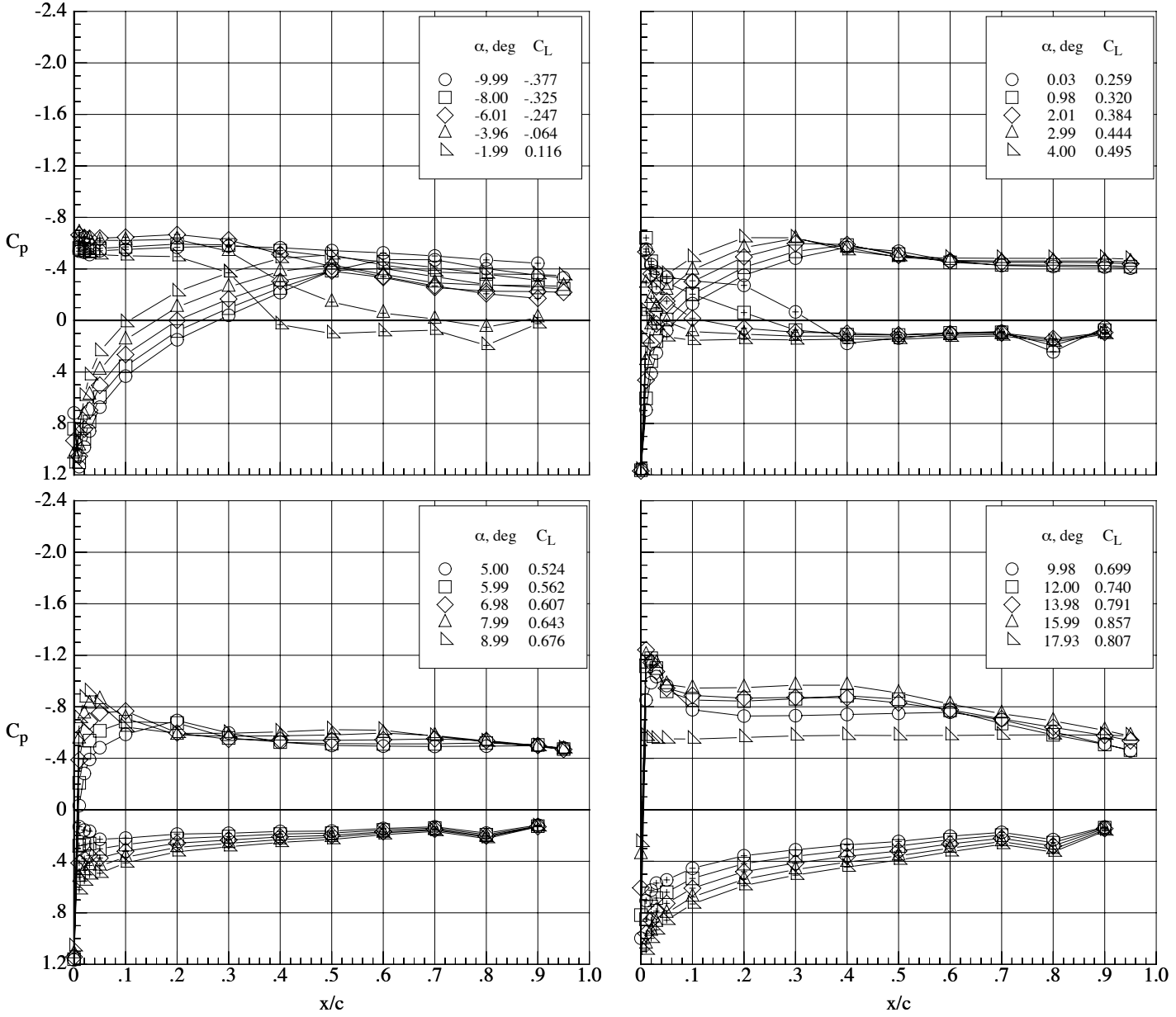

(b) Mach number 0.80.

Figure 122. Concluded.

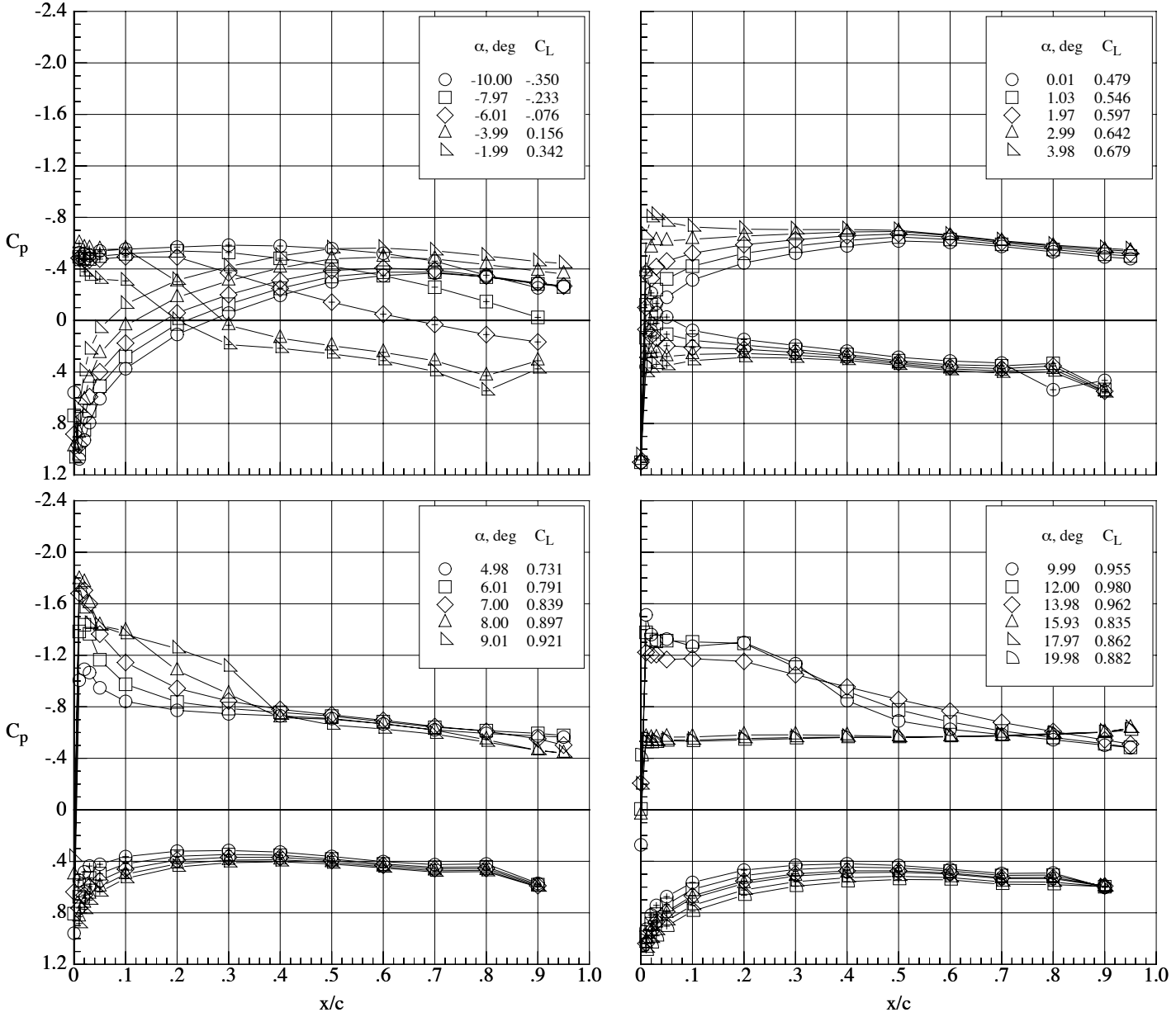

(a) Mach number 0.65.

Figure 123. Chordwise pressure coefficient distributions on the MA-SF-1 wing (bump off) at a Reynolds number of 100,000. $\delta_h = 0°$ and $\delta_f = 30°$.

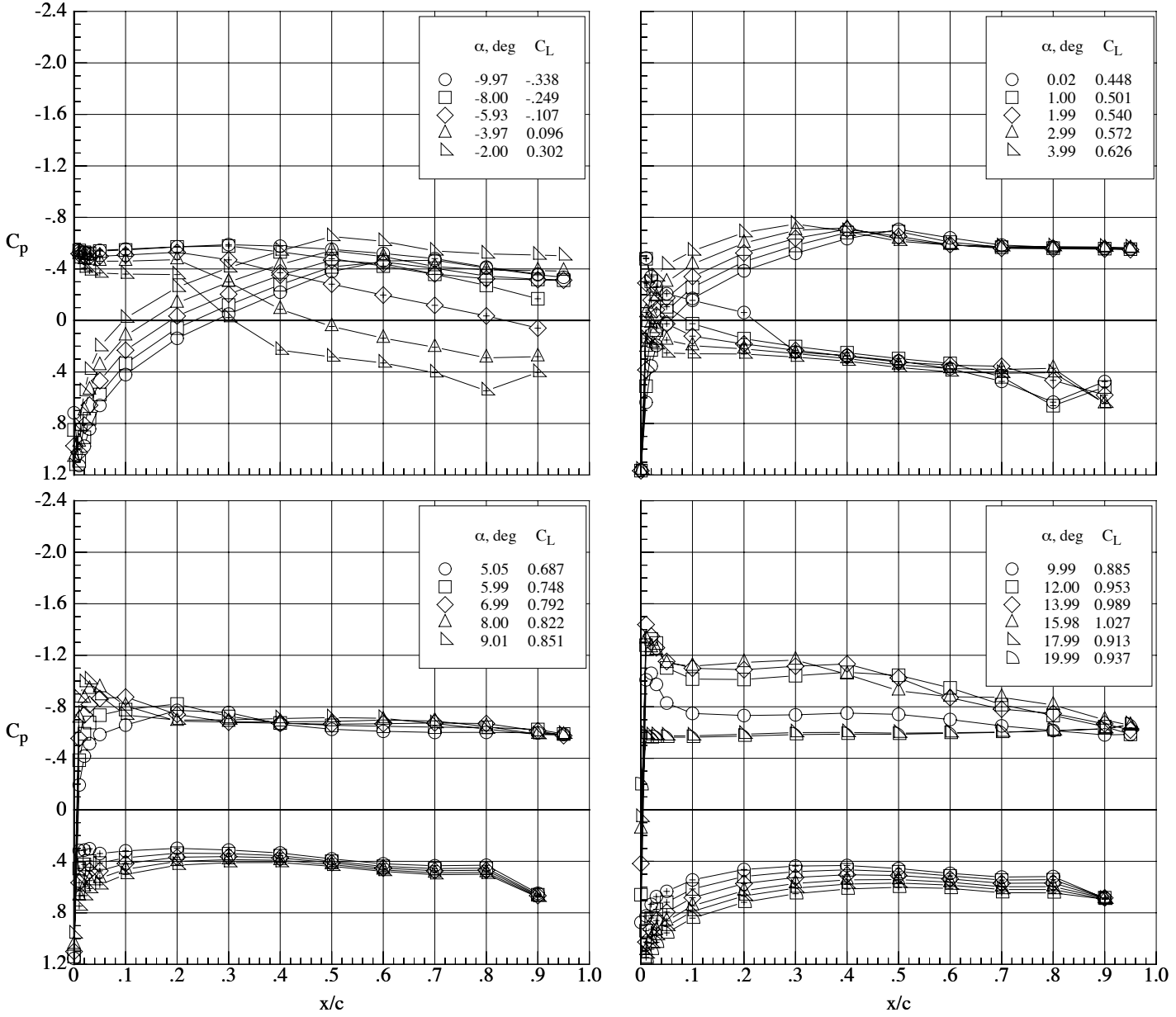

(b) Mach number 0.80.

Figure 123. Concluded.

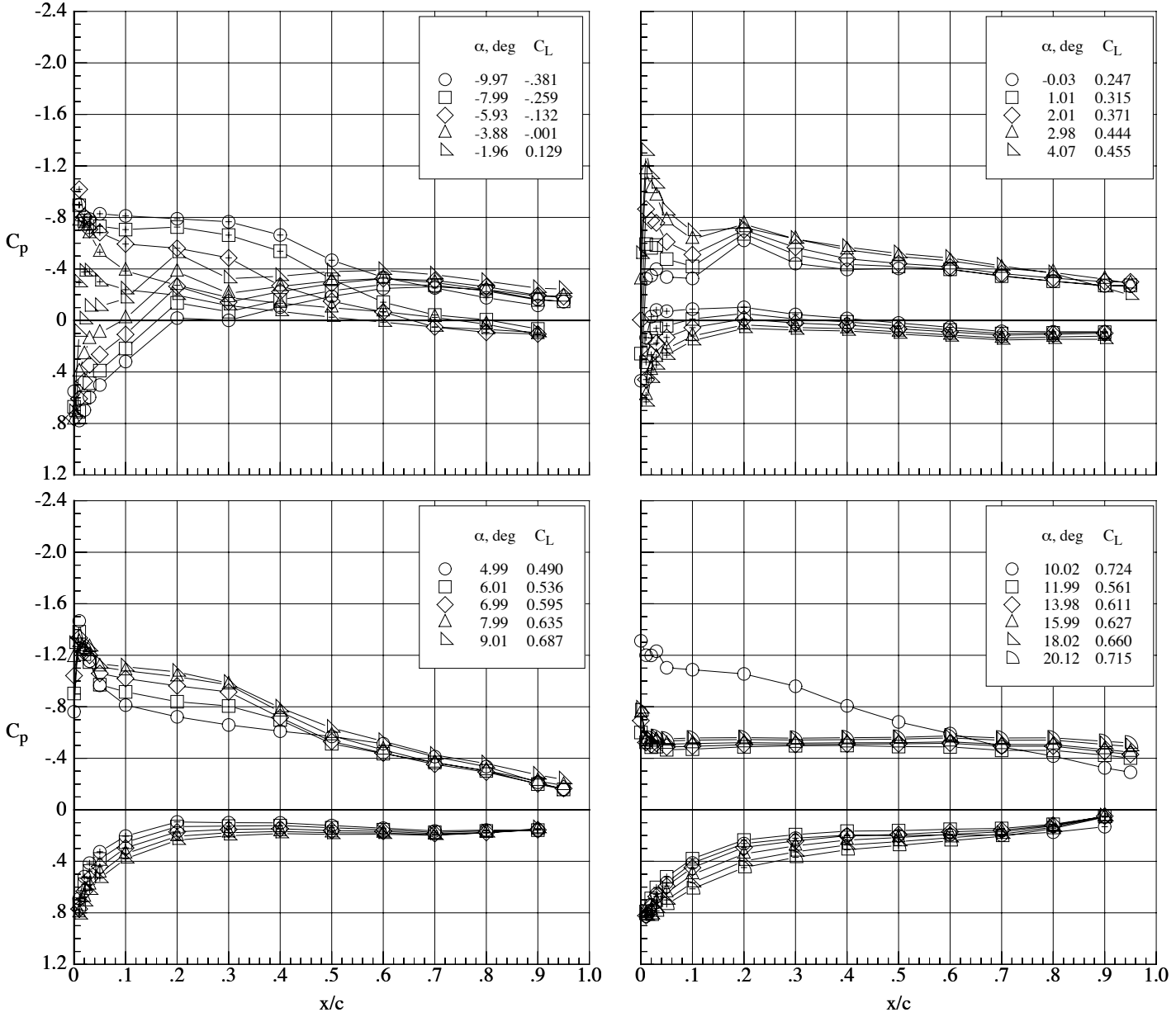

(a) Mach number 0.50.

Figure 124. Chordwise pressure coefficient distributions on the MA-SC-1t wing (bump on) at a Reynolds number of 40,000. $\delta_h = 0°$ and $\delta_f = 0°$.

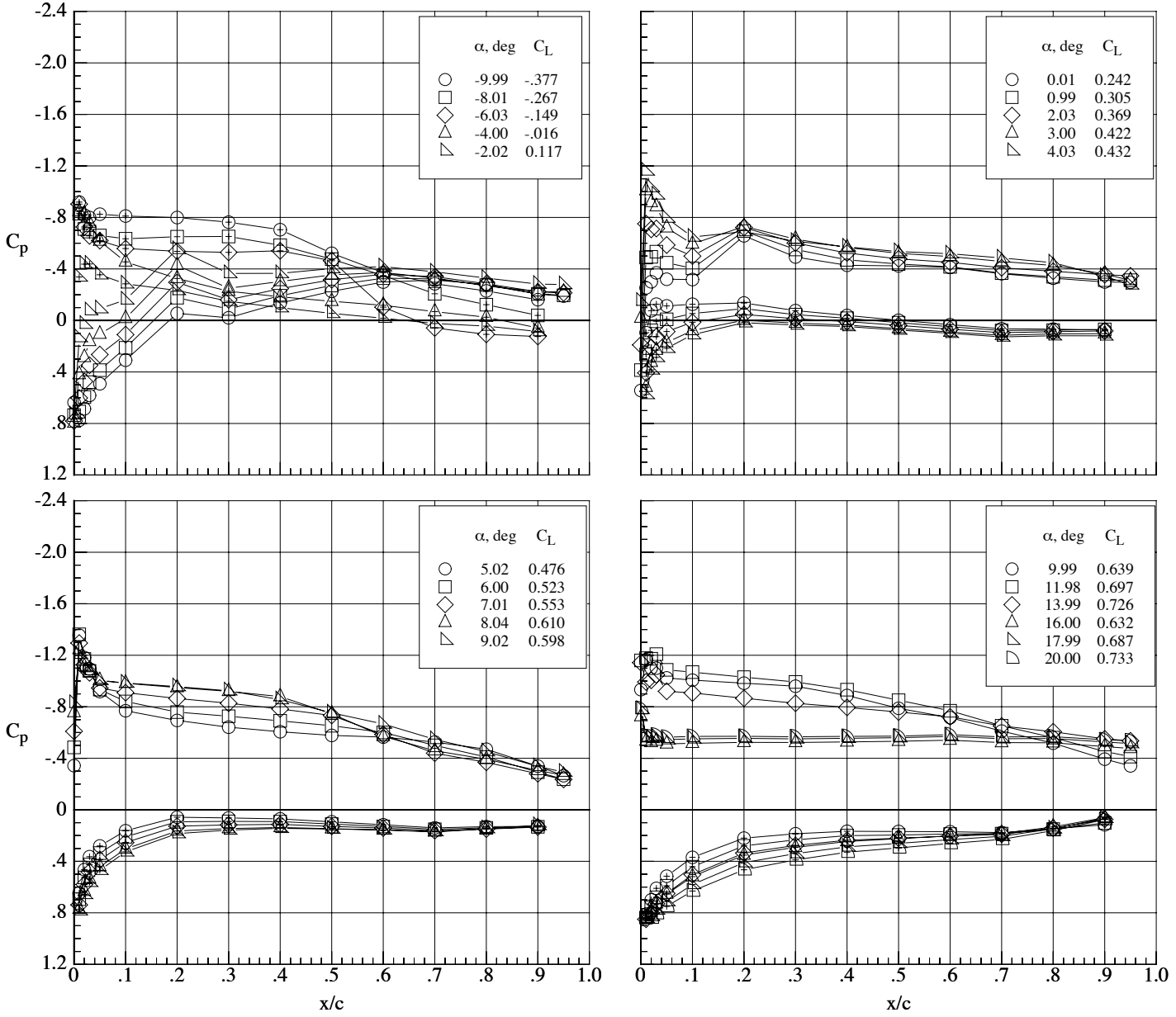

(b) Mach number 0.65.

Figure 124. Continued.

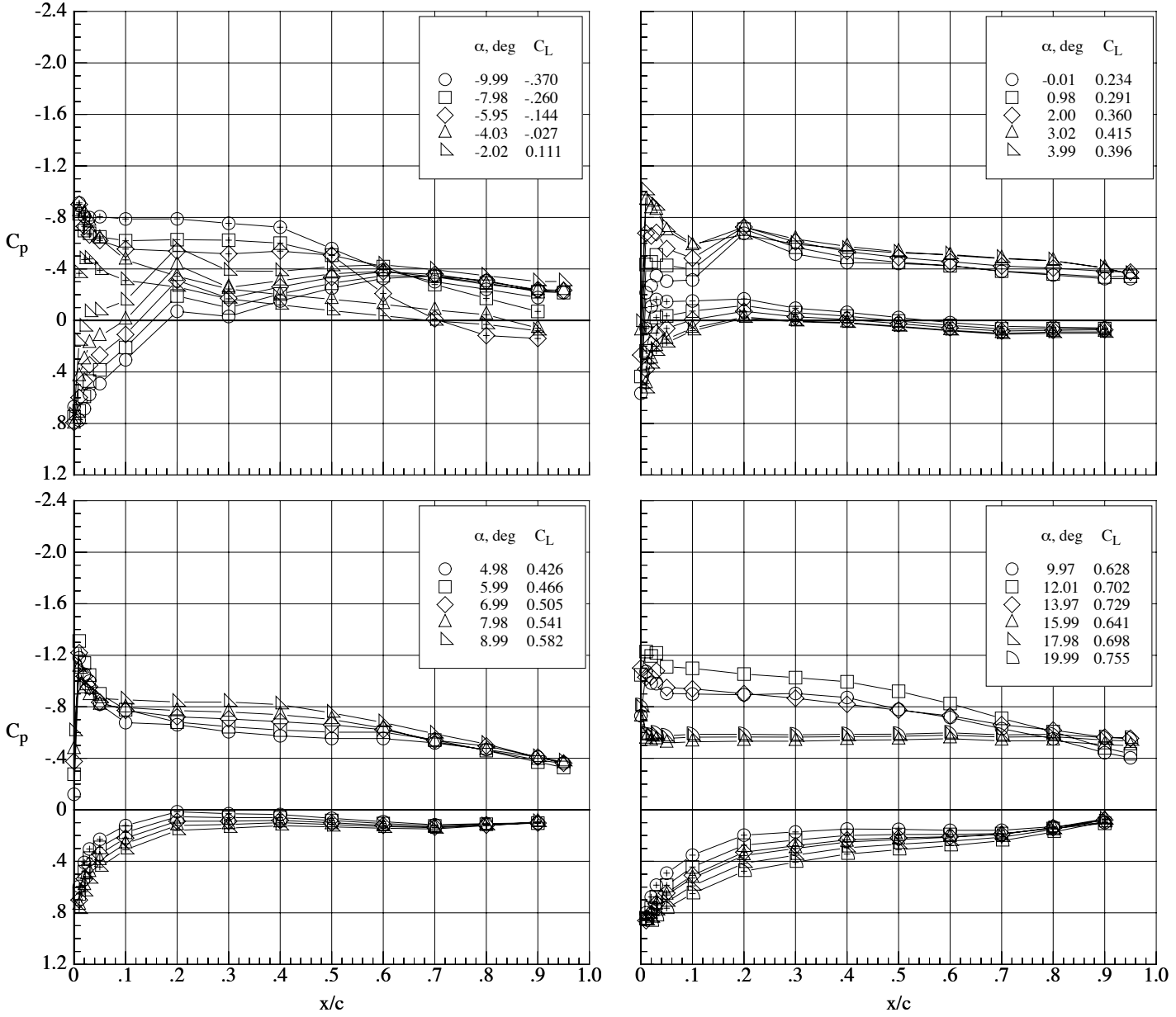

(c) Mach number 0.70.

Figure 124. Continued.

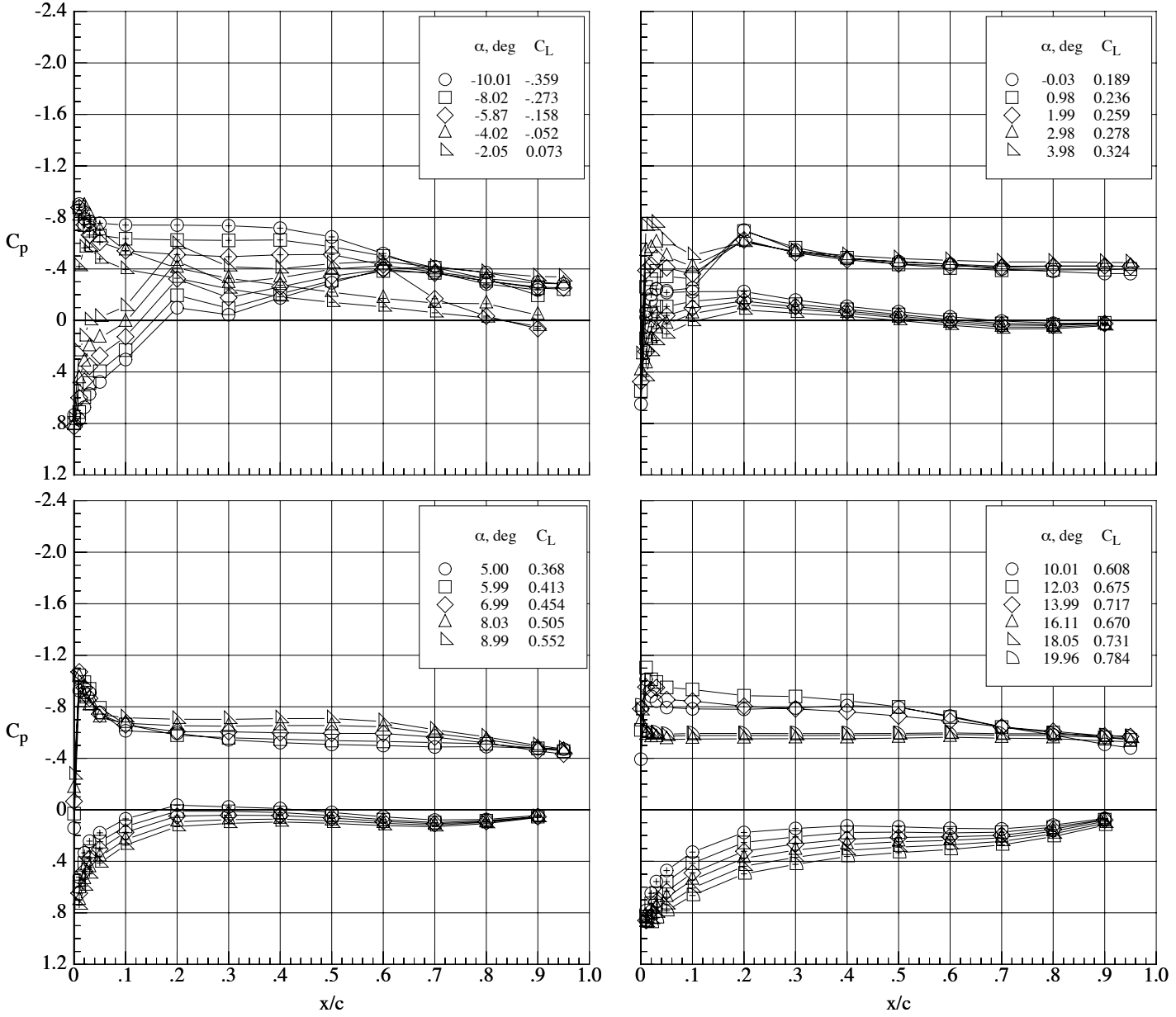

(d) Mach number 0.80.

Figure 124. Continued.

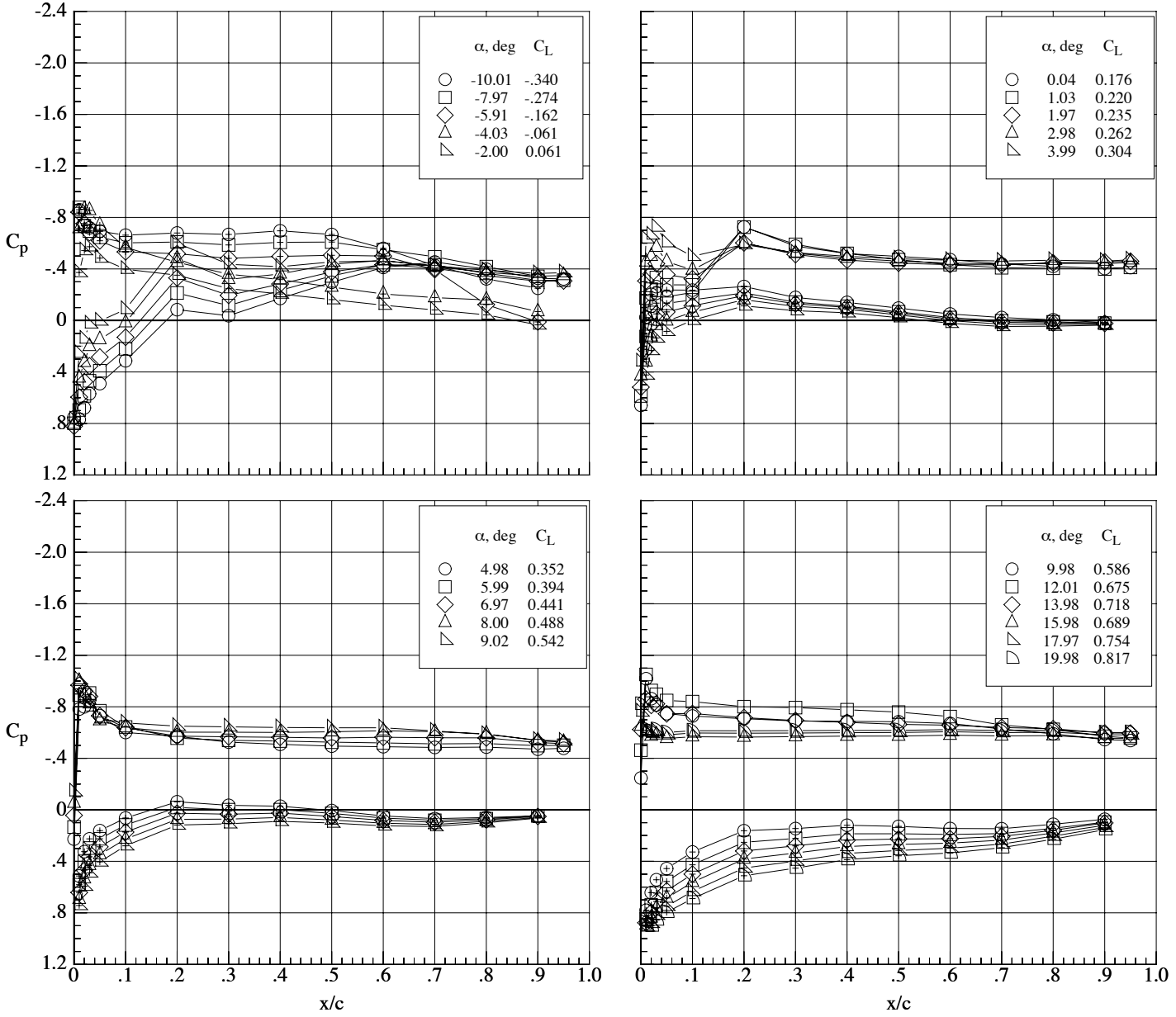

(e) Mach number 0.85.

Figure 124. Continued.

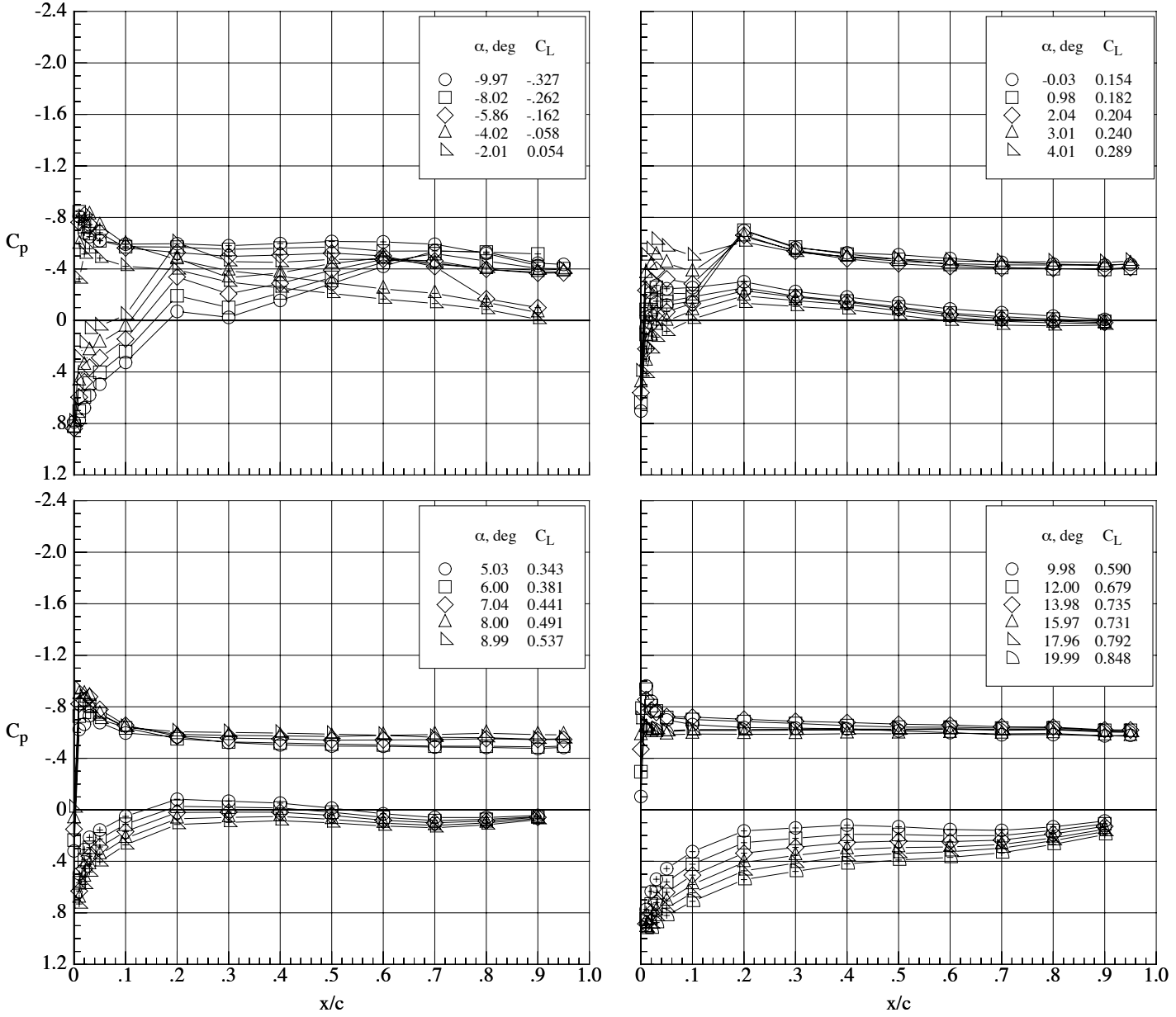

(f) Mach number 0.90.

Figure 124. Concluded.

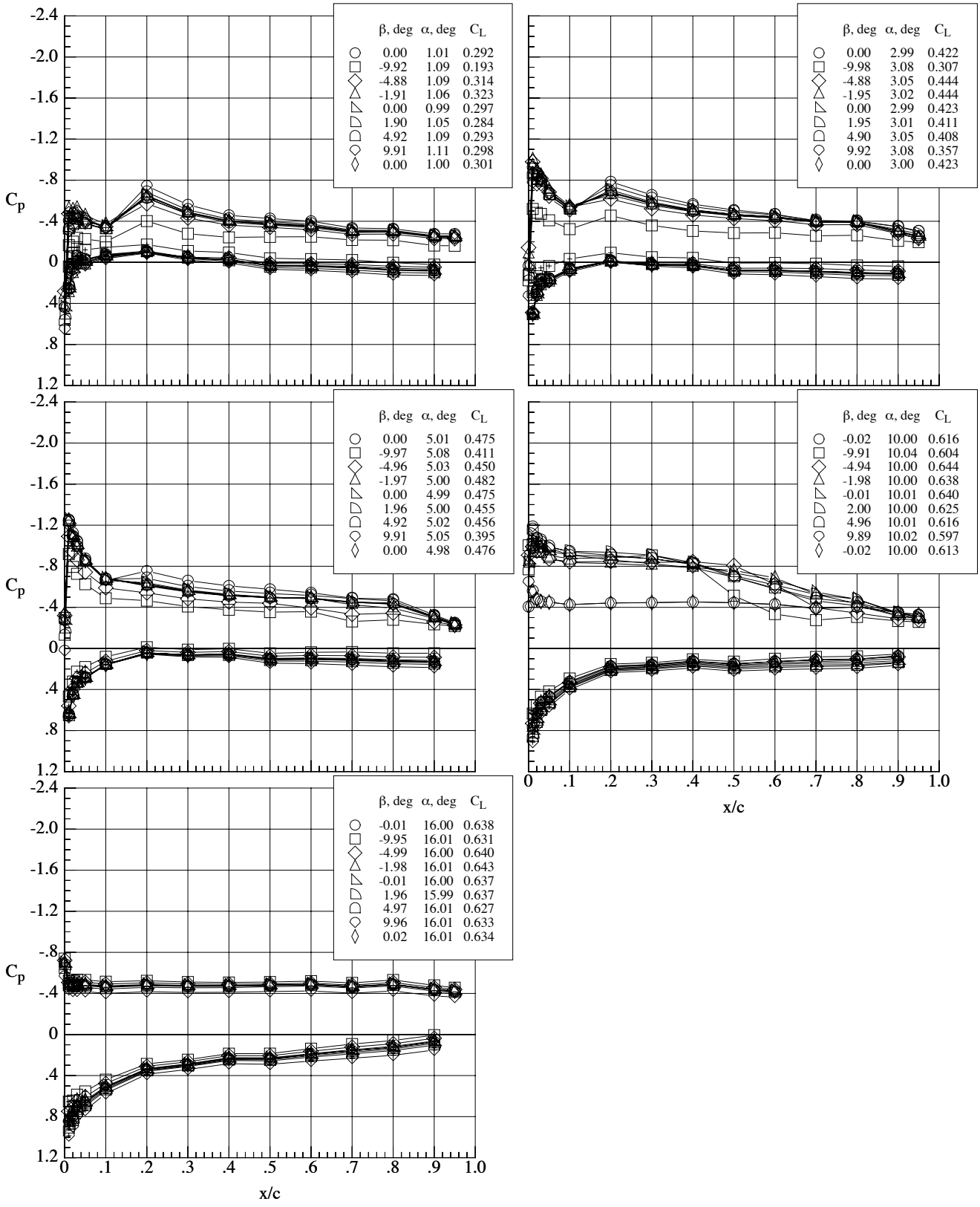

(a) Mach number 0.65.

Figure 125. Chordwise pressure coefficient distributions on the MA-SC-1t wing (bump on) at a Reynolds number of 40,000 over a range of sideslip angles. $\delta_h = 0°$ and $\delta_f = 0°$.

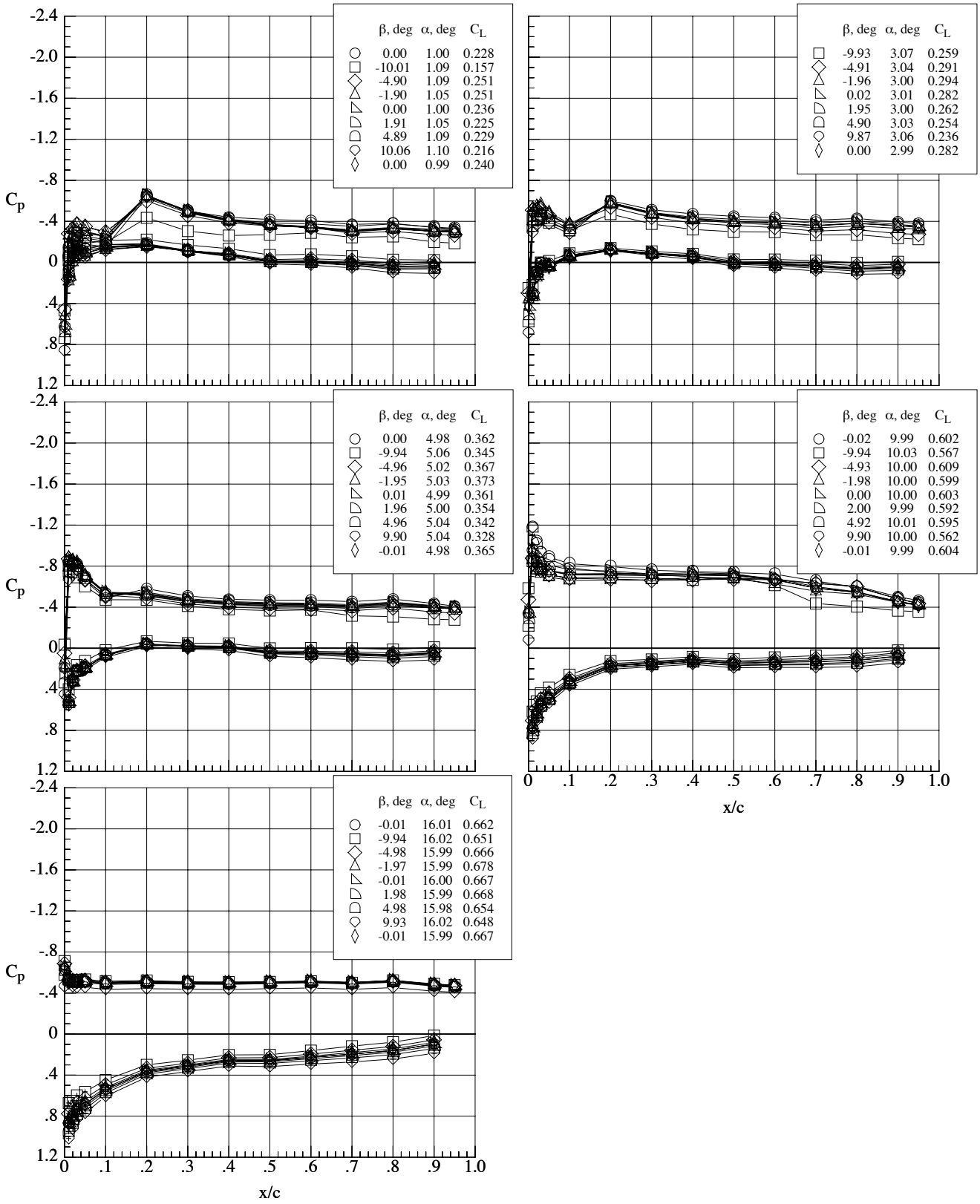

(b) Mach number 0.80.

Figure 125. Concluded.

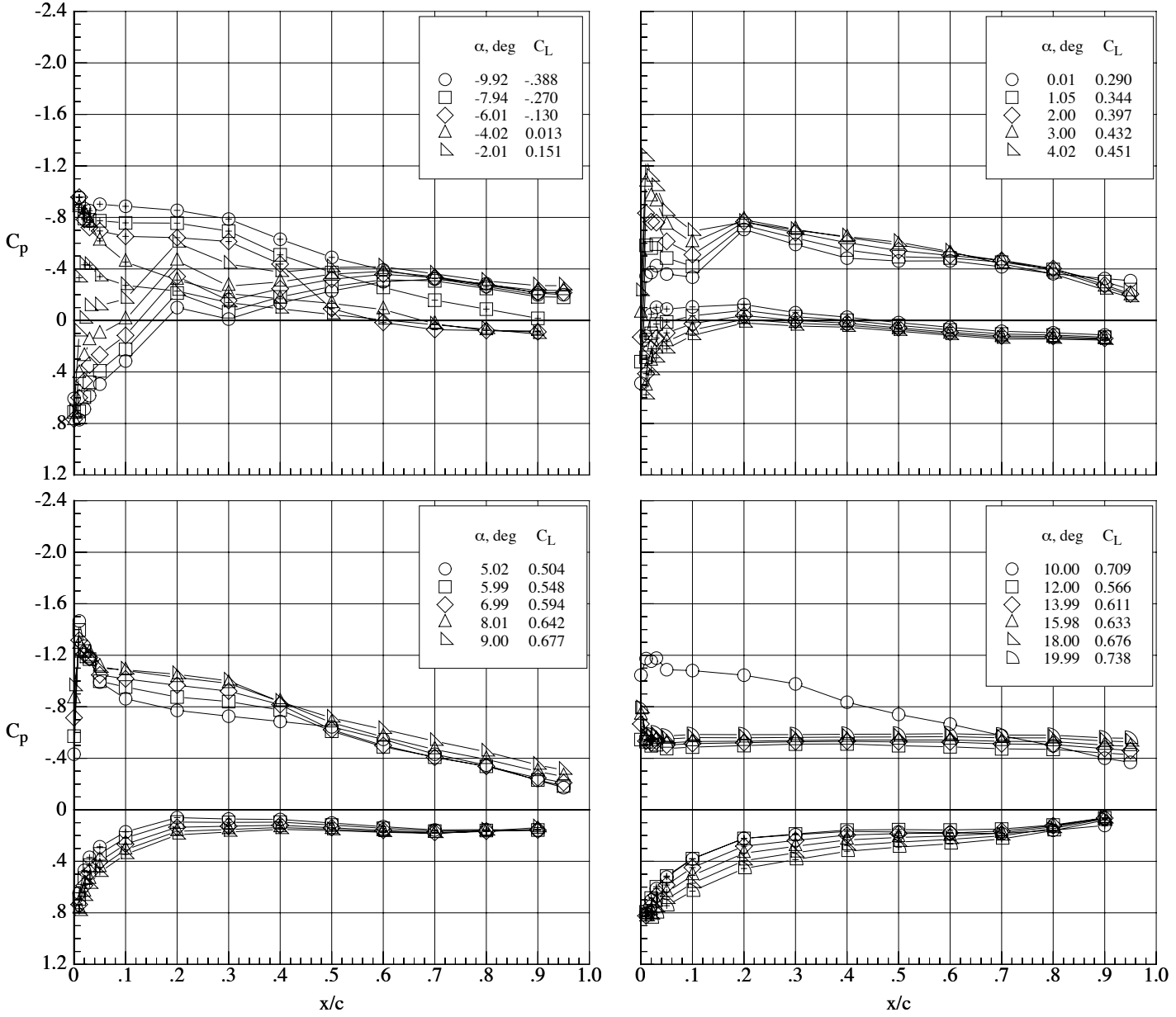

(a) Mach number 0.65.

Figure 126. Chordwise pressure coefficient distributions on the MA-SC-1t wing (bump on) at a Reynolds number of 60,000. $\delta_h = 0°$ and $\delta_f = 0°$.

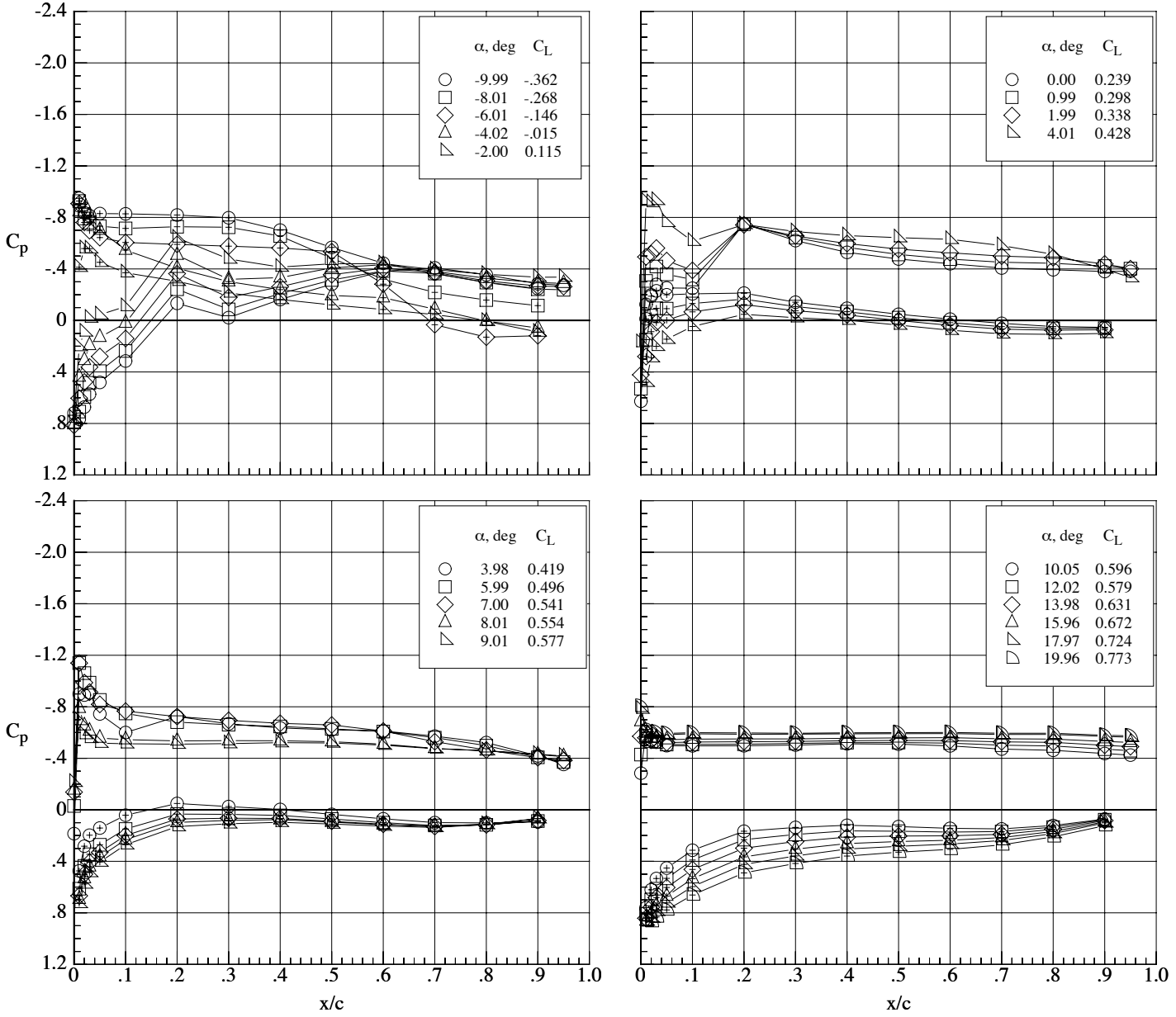

(b) Mach number 0.80.

Figure 126. Concluded.

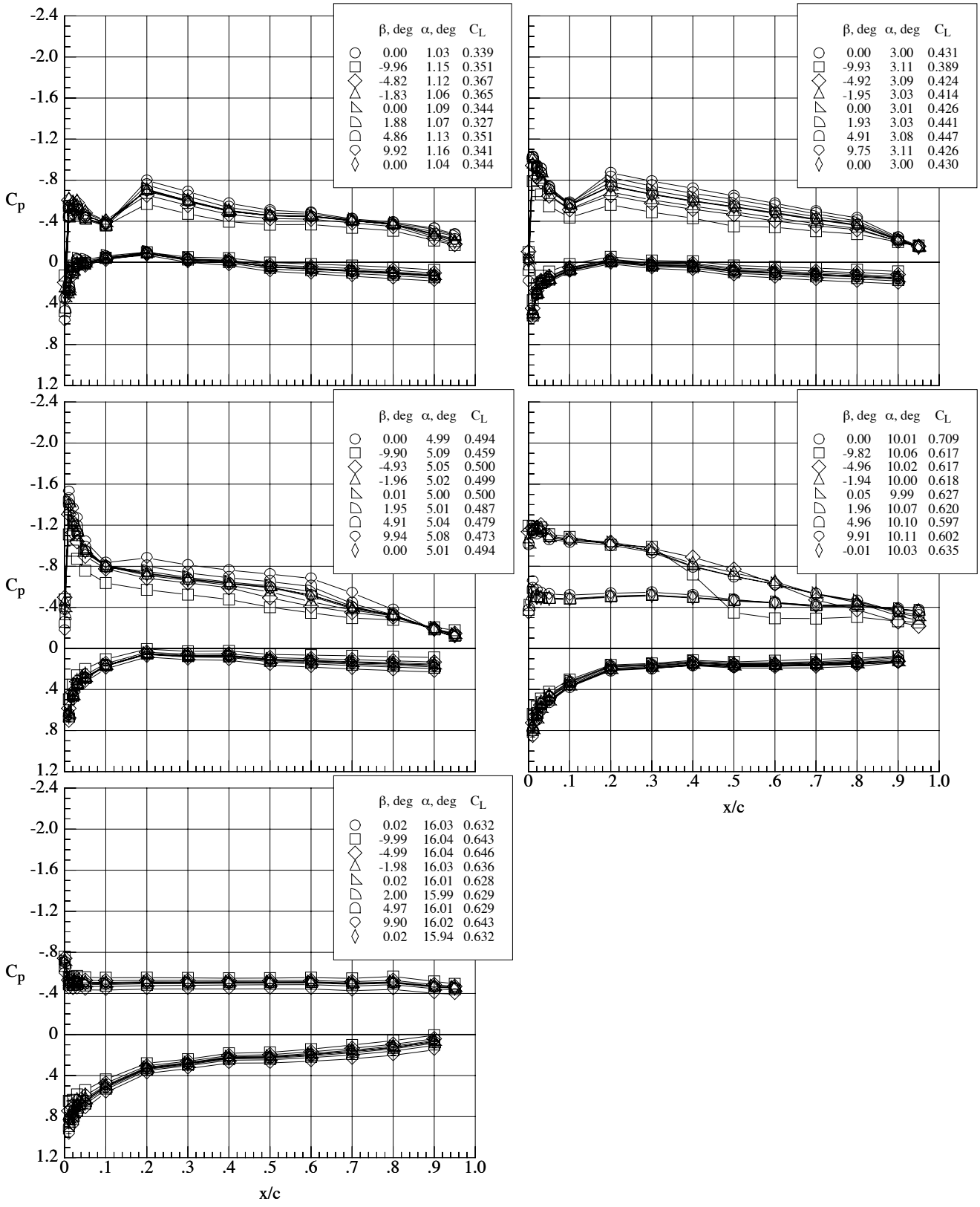

(a) Mach number 0.65.

Figure 127. Chordwise pressure coefficient distributions on the MA-SC-1t wing (bump on) at a Reynolds number of 60,000 over a range of sideslip angles. $\delta_h = 0°$ and $\delta_f = 0°$.

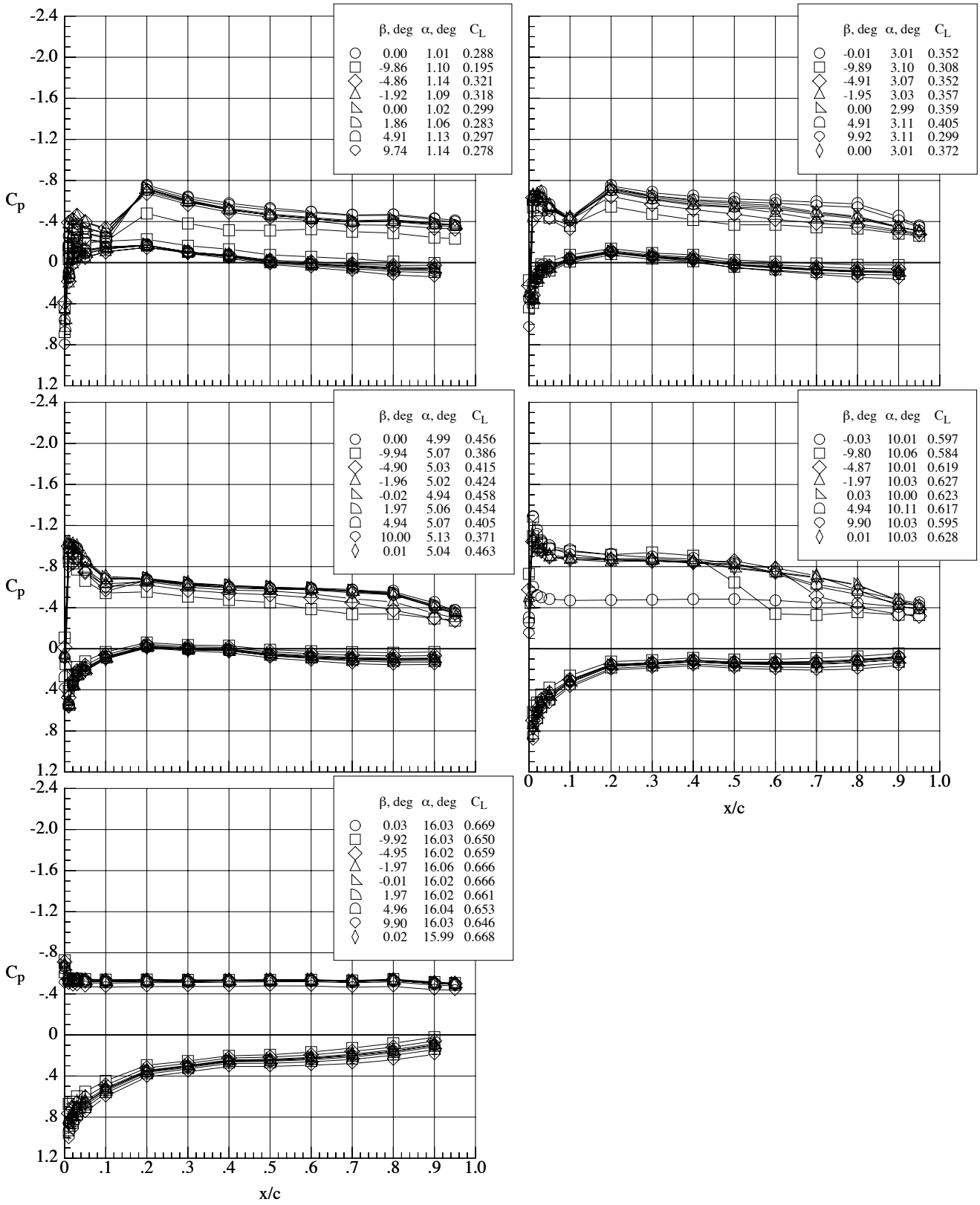

(b) Mach number 0.80.

Figure 127. Concluded.

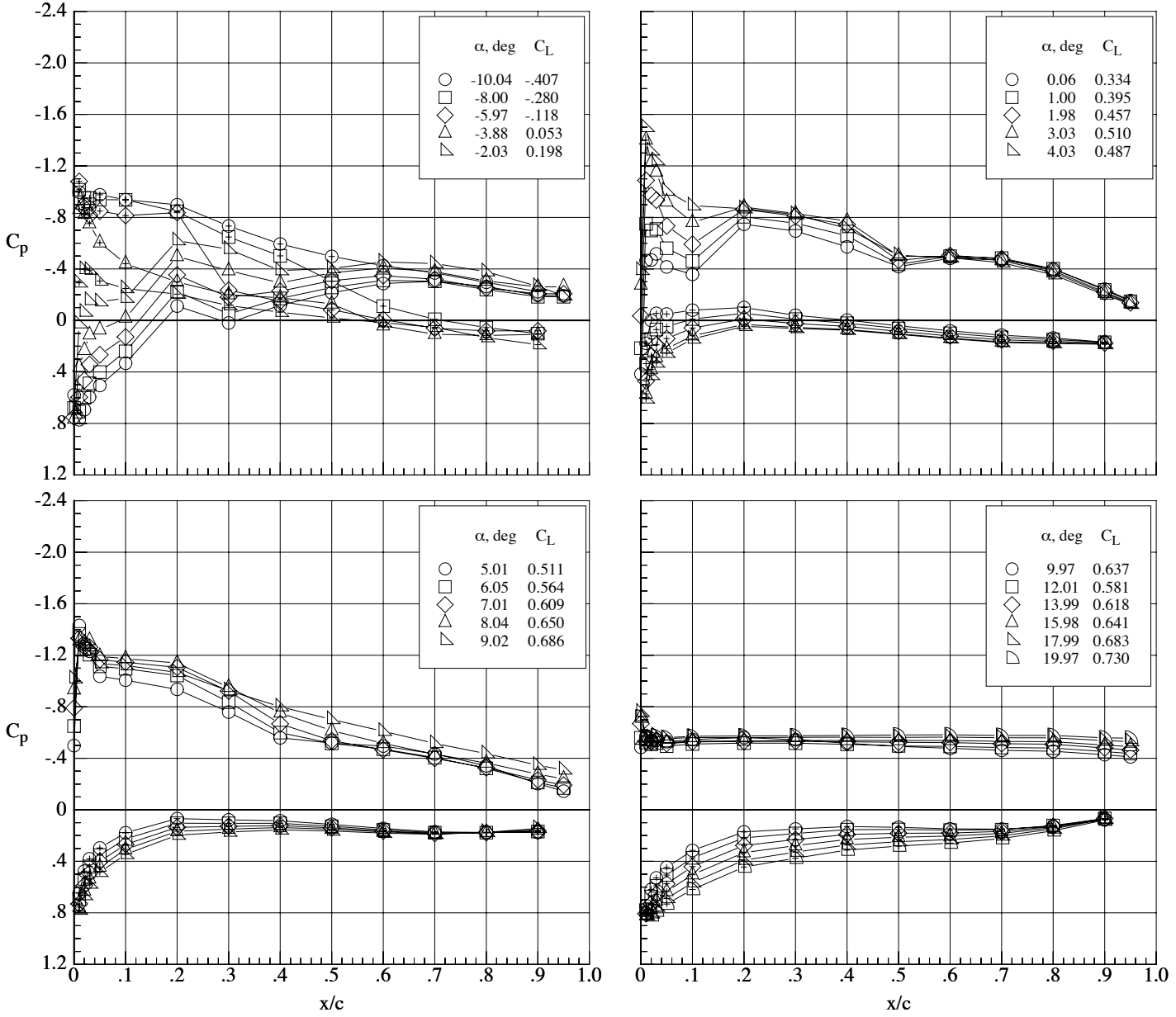

(a) Mach number 0.65.

Figure 128. Chordwise pressure coefficient distributions on the MA-SC-1t wing (bump on) at a Reynolds number of 100,000. $\delta_h = 0°$ and $\delta_f = 0°$.

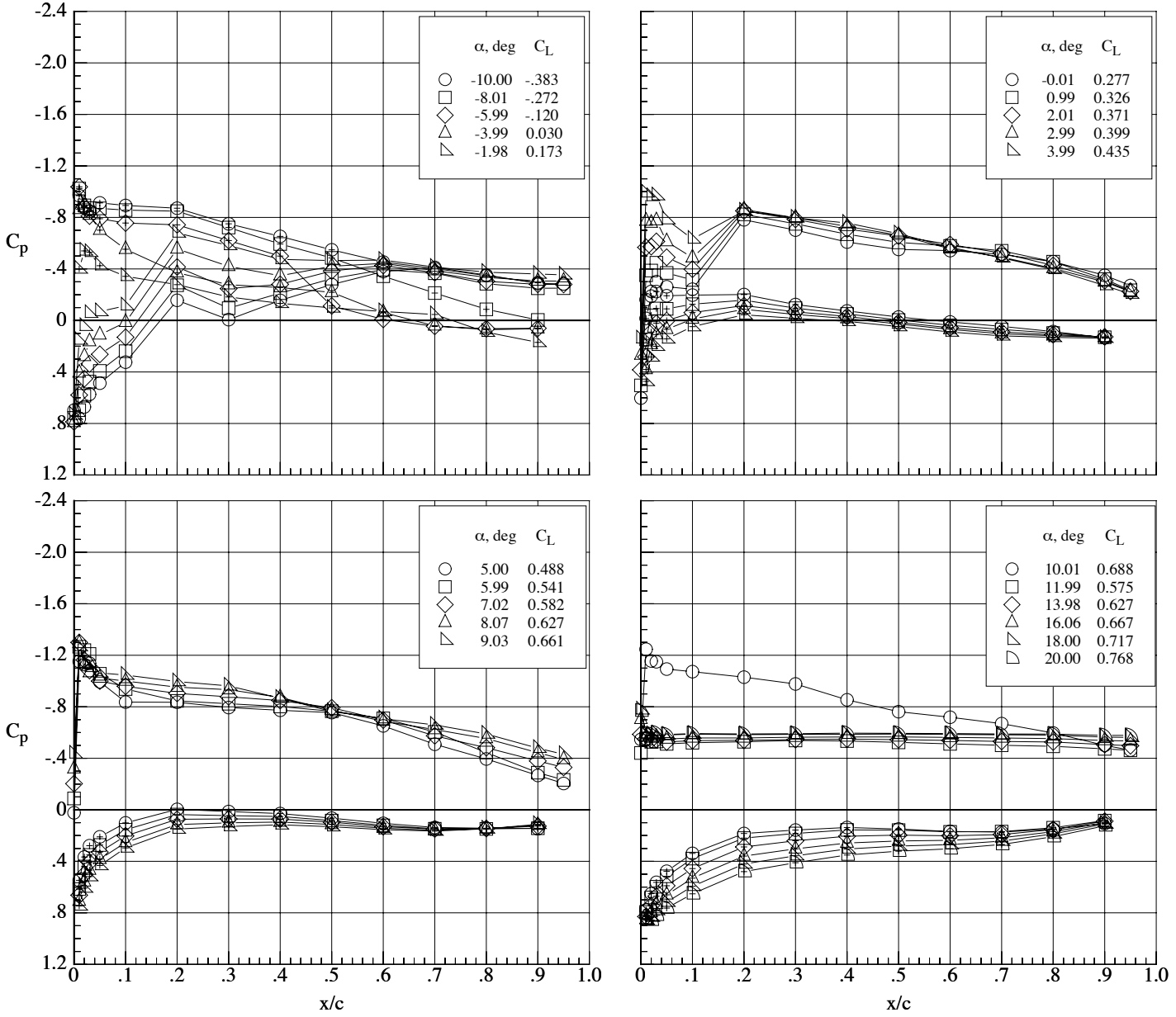

(b) Mach number 0.80.

Figure 128. Concluded.

REPORT DOCUMENTATION PAGE

Form Approved
OMB No. 0704-0188

1. REPORT DATE *(DD-MM-YYYY)*	2. REPORT TYPE	3. DATES COVERED *(From - To)*
01- 08 - 2006	Technical Memorandum	January 2004 - June 2005

4. TITLE AND SUBTITLE

Low Reynolds Number Aerodynamic Characteristics of Several Airplane Configurations Designed to Fly in the Mars Atmosphere at Subsonic Speeds

5a. CONTRACT NUMBER

5b. GRANT NUMBER

5c. PROGRAM ELEMENT NUMBER

6. AUTHOR(S)

Re, Richard J.; Pendergraft, Odis C., Jr.; and Campbell, Richard L.

5d. PROJECT NUMBER

5e. TASK NUMBER

5f. WORK UNIT NUMBER

561581.02.08.07

7. PERFORMING ORGANIZATION NAME(S) AND ADDRESS(ES)

NASA Langley Research Center
Hampton, VA 23681-2199

8. PERFORMING ORGANIZATION REPORT NUMBER

L-19252

9. SPONSORING/MONITORING AGENCY NAME(S) AND ADDRESS(ES)

National Aeronautics and Space Administration
Washington, DC 20546-0001

10. SPONSOR/MONITOR'S ACRONYM(S)

NASA

11. SPONSOR/MONITOR'S REPORT NUMBER(S)

NASA/TM-2006-214312

12. DISTRIBUTION/AVAILABILITY STATEMENT

Unclassified - Unlimited
Subject Category 02
Availability: NASA CASI (301) 621-0390

13. SUPPLEMENTARY NOTES

An electronic version can be found at http://ntrs.nasa.gov

14. ABSTRACT

A 1/4-scale wind tunnel model of an airplane configuration developed for short duration flight at subsonic speeds in the Martian atmosphere has been tested in the Langley Research Center Transonic Dynamics Tunnel. The tunnel was pumped down to extremely low pressures to represent Martian Mach/Reynolds number conditions. Aerodynamic data were obtained and upper and lower surface wind pressures were measured at one spanwise station on some configurations. Three unswept wings of the same planform but different airfoil sections were tested. Horizontal tail incidence was varied as was the deflection of plain and split trailing-edge flaps. One unswept wing configuration was tested with the lower part of the fuselage removed and the vertical/horizontal tail assembly inverted and mounted from beneath the fuselage. A sweptback wing was also tested. Tests were conducted at Mach numbers from 0.50 to 0.90. Wing chord Reynolds number was varied from 40,000 to 100,000 and angles of attack and sideslip were varied from -10° to 20° and -10° to 10°, respectively.

15. SUBJECT TERMS

Mars Flyer; Mars airplane; Low Reynolds number

16. SECURITY CLASSIFICATION OF:			17. LIMITATION OF ABSTRACT	18. NUMBER OF PAGES	19a. NAME OF RESPONSIBLE PERSON
a. REPORT	b. ABSTRACT	c. THIS PAGE			STI Help Desk (email: help@sti.nasa.gov)
					19b. TELEPHONE NUMBER *(Include area code)*
U	U	U	UU	332	(301) 621-0390